

# **Chemical Biology Applications of Photoresponsive DNA-Binding Agents**

Kumulative Dissertationsschrift

zur Erlangung des akademischen Grades eines  
Doktors der Naturwissenschaften  
(Dr. rer. nat.)

dem Fachbereich Chemie der Philipps-Universität Marburg  
(Hochschulkenziffer 1180)  
vorgelegt von

**Benedikt Heinrich, M.Sc.**  
aus Göttingen

Marburg an der Lahn 2019



Die vorliegende Arbeit wurde in der Zeit von November 2015 bis Dezember 2019 am Fachbereich Chemie der Philipps-Universität Marburg unter Leitung von Jun. Prof. Dr. Olalla Vázquez angefertigt.

Vom Fachbereich Chemie der Philipps-Universität Marburg (Hochschulkenziffer 1180) als Dissertation am 20.01.2020 angenommen.

Erstgutachterin: Jun. Prof. Dr. Olalla Vázquez

Zweitgutachter: Prof. Dr. Eric Meggers

Tag der mündlichen Prüfung: 24.01.2020





## Declaration

Ich erkläre, dass eine Promotion noch an keiner anderen Hochschule als der Philipps-Universität Marburg, Fachbereich Chemie, versucht wurde.

Ich versichere, dass ich meine vorgelegte Dissertation „*Chemical Biology Applications of Photoresponsive DNA-Binding Agents*“ selbst und ohne fremde Hilfe verfasst, nicht andere als die in ihr angegebenen Quellen oder Hilfsmittel benutzt, alle vollständig oder sinngemäß übernommenen Zitate als solche gekennzeichnet, sowie die Dissertation in der vorliegenden oder einer ähnlichen Form noch bei keiner anderen in- oder ausländischen Hochschule anlässlich eines Promotionsgesuchs oder zu anderen Prüfungszwecken eingereicht habe.

Marburg, den

Unterschrift:

Benedikt Heinrich



# Acknowledgements

At this point I like to thank ...

... Jun. Prof. Dr. Olalla Vázquez for the great collaboration and all we shared during the last years. It was a great experience to build up everything and see now, what we achieved together as a team. Especially this spirit and everything you taught us, is what I appreciated. You always inspired and motivated me to keep the passion for research and the unknown.

... Prof. Dr. Eric Meggers for being the second referee and the support during the last years. Especially in the beginning of this thesis and our young group it helped a lot to share space, equipment and experience, which we always appreciated. I further would like to thank your former and present group members for their support and the time we shared together in the lab.

... Prof. Dr. Armin Geyer and Prof. Dr. Nicole Graulich for being part of the thesis committee and teaching me the basics of bioorganic and peptide chemistry during my undergraduate and graduate studies and getting insights of educational research. It was often useful during the last years.

... my main collaborators Dr. Karim Bouazoune and Jun. Prof. Dr. Leon Schulte for everything you taught me and the great projects we achieved together. It was a pleasure to work with you.

... Dr. Uwe Linne and his team of the mass department for measuring several of my samples and having an open door for all kind of questions and Dr. Xiulan Xie and her team of the NMR department for measuring my samples and the good support.

... Greta, Lea and Lei for the unforgettable good (and sometimes hard) time we had together during the last years. You are a great team to work with and I enjoyed sharing this long time with you three. I especially appreciated the support we could give to each other and share together.

... Frank for being our general device assistant and all beyond. It was of good help to discuss several research aspects with you and enjoyable to share a coffee or candies from our draws.

... Nathalie, Sabine and Sabrina for introducing me into basic biochemical working methods and discussing several aspects of my work. I always felt home in your lab and enjoyed the time we spent together

... my internship students Andreas, Anna, Christoph, Duc, Dzung, Erik, Johanna, Kristine, Lukas, Max, Merle, Peter, Phuong, Rouzbeh, Steffen, Stephan, Valeska and Yassine, my master student Abbas as well as Magdalena and Robert, my bachelor student Benjamin and my postdocs Rashmi and Gaurav for your contribution to this work or smaller side projects, we worked on together.

... Greta, Lea, Nathalie and Sabine for correcting parts of my thesis.

... Ina and Andrea for the organizational help during the last years.

... our former master students Mathias, Laura and Andreas. Even though the time we spent together seems ages ago, I still have it good in mind.

... my friends for everything besides the lab during the last years. It was a great time we had together in Marburg. A special thanks to my numerous flat mates. It is great to still keep in touch and share the good memories.

... my family for your infinite support for any situation I and we went through together the last years. I know that I can always trust in you. A special thanks to Anna for being there, your support and all beyond.

# Contents

<b>1</b>	<b>Introduction</b>	<b>1</b>
1.1	Chemical Biology and its Educational Challenges	1
1.2	Photosensitive Molecules in Chemical Biology	2
1.2.1	Photoactivatable Molecules	3
1.2.2	Photocaged Molecules	6
1.2.2.1	Classes of Photolabile Protecting Groups	7
1.2.2.2	Applications of Photolabile Protecting Groups	8
1.2.3	Photoswitchable Molecules	10
1.2.3.1	Concepts	10
1.2.3.2	Classes of Photoswitches	11
1.2.3.3	Azobenzenes	13
1.2.3.4	Applications of Azobenzenes	14
1.2.4	Fluorophores	16
1.2.4.1	Concept of Fluorescence	17
1.2.4.2	Classes of Fluorophores	17
1.2.4.3	Small-Molecule Fluorophores	18
1.2.4.4	Fluorescent Proteins	20
1.2.4.5	dsDNA Sensors	22
1.3	References	24
<b>2</b>	<b>Motivation</b>	<b>39</b>
<b>3</b>	<b>Summaries</b>	<b>41</b>
3.1	English Summary	41
3.2	Zusammenfassung in deutscher Sprache	43
<b>4</b>	<b>Cumulative Part</b>	<b>45</b>
4.1	A Far-Red Fluorescent DNA Binder for Interaction Studies of Live Multidrug-Resistant Pathogens and Host Cells	45
4.1.1	Conclusion	95
4.1.2	Further Developments and Outlook	95
4.1.3	Author Contribution	100
4.1.4	References	100
4.2	<i>ortho</i> -Fluoroazobenzene Derivatives as DNA Intercalators for Photocontrol of DNA and Nucleosome Binding by Visible Light	102
4.2.1	Conclusion	158
4.2.2	Further Developments and Outlook	158
4.2.3	Author Contribution	160

4.2.4	References .....	161
4.3	4-Methyltrityl (Mtt)-Protected Pyrrole and Imidazole Building Blocks for Solid Phase Synthesis of DNA-Binding Polyamides .....	162
4.3.1	Conclusion.....	223
4.3.2	Further Developments and Outlook.....	223
4.3.3	Author Contribution .....	226
4.3.4	References .....	227
4.4	Spicing up an Interdisciplinary Chemical Biology Course with the Authentic Big Picture of Epigenetic Research.....	228
4.4.1	Conclusion.....	304
4.4.2	Author Contribution .....	304
4.4.3	References .....	305
<b>A List of Publications.....</b>		<b>306</b>
<b>B Curriculum Vitae .....</b>		<b>307</b>
<b>C Permissions for the Reprint of Publications.....</b>		<b>310</b>

## Abbreviations

A	adenine
a.u.	arbitrary unit
AIDS	acquired immune deficiency syndrome
ATP	adenosin triphosphate
Boc	<i>tert</i> -butyloxycarbonyl
BODIPY	boron-dipyrromethene
C	cytosine
calcd	calculated
cAMP	cyclic adenosine monophosphate
CD	circular dichroism
cm	centimeter
cRAF	cellular-induced rapidly accelerated fibrosarcoma
Cy	sulfoindocyanine
D	debye
DAPI	4',6'-diamidino-2-phenylindole dihydrochloride hydrate
DLS	dynamic light scattering
DNA	deoxyribonucleic acid
ds	double stranded
E.coli	escherichia coli
EDTA	ethylenediaminetetraacetic acid
Em	emission
eq	equivalent
ESI	electrospray ionization
EtBr	ethidium bromide
FACS	fluorescence-activated cell sorting
Fmoc	fluorenylmethoxycarbonyl
FP	fluorescent protein
FRET	Förster resonance energy transfer
G	guanine
GFP	green fluorescent protein
GSH	glutathione
h	hour
HeLa	Henrietta Lacks
HpD	haematoporphyrins derivatives
HRMS	high resolution mass spectrometry
Im	imidazole

IPTG	isopropyl $\beta$ -D-1-thiogalactopyranoside
kDa	kilo dalton
LUMO	lowest unoccupied molecular orbital
M	molar
<i>m</i>	mass
max	maximum
MCF	Michigan cancer foundation
MD	molecular dynamics
mM	milimolar
mRNA	messenger ribonucleic acid
Mtt	4-methyltrityl
NIR	near infrared
nm	nanometer
NMR	nuclear magnetic resonance
ns	nanosecond
OD	optical density
PCR	polymerase chain reaction
PDT	photodynamic therapy
PNA	peptide nucleic acid
PPG	photolabile protecting group
PS	photosensitizer
Py	pyrrole
Q	quencher
rmsd	root-mean-square deviation
ROS	reactive oxygen species
RP-HPLC	reverse phase high performance liquid chromatography
s	second
SEC	size-exclusion chromatography
SPPS	solid phase peptide synthesis
T	thymine, temperature
TO	thiazole orange
Tris	tris(hydroxymethyl)aminomethane
tRNA	transfer ribonucleic acid
UV	ultra violet
Vis	visible
YOYO	oxazole yellow dimer
z	charge
$\Delta G$	Gibbs energy
$^{\circ}\text{C}$	degree celsius



$\mu\text{M}$

mikromolar

$\lambda$

wavelength

$\Phi$

quantum yield



# 1 Introduction

## 1.1 Chemical Biology and its Educational Challenges

Chemical biology applies chemical strategies to address biological questions at the molecular level. Importantly, the interaction between both disciplines must be understood synergistically.<sup>[1]</sup> Despite that this field is relatively young in many chemistry departments, in the 18<sup>th</sup> century Joseph Priestley performed first chemical biological experiments by studying the influence of different gases on plants and mice.<sup>[2]</sup> The characteristic interdisciplinary approach of working at the interface of chemistry and biology has a high potential to solve the complex modern problems, which remain untackable from the traditional single approach. To face these vital dilemmas, it is necessary to train the new-student generations by the implementation of interdisciplinary courses.<sup>[3]</sup> Chemical biology is the perfect field to tear the classical borders down and prepare the students for future challenges (Figure 1.1).<sup>[1,4]</sup> Over the last years, more and more courses in chemical biology are part of the curricula of the chemistry departments.<sup>[1,5]</sup> There are a handful of cohorts that additionally include research experiences increasing the motivation of the students and leading to positive learning outcomes.<sup>[6]</sup> However, such combination of research experiences in chemical biology are still rare and focus on single experiments. Through this, the whole picture of research is not clearly seen by the students. Consequently, a course, which combines all of these features is highly necessary.

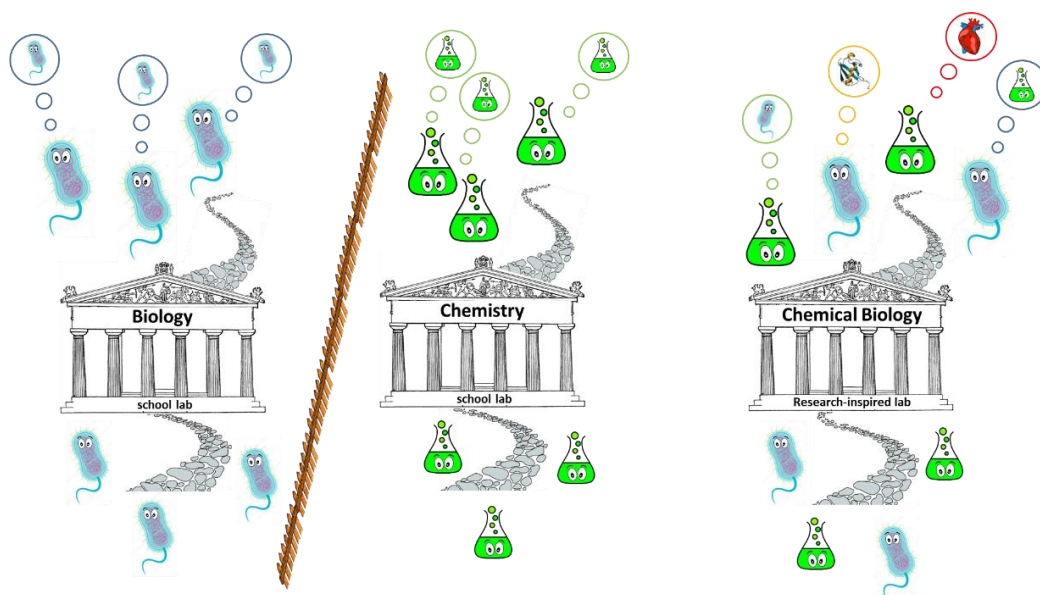


**Figure 1.1.** Schematic representation of the classical separated disciplines and taught subjects biology and chemistry in comparison to the approach in chemical biology, which combines the methods of both disciplines to result in an outcome which has the potential to solve complex modern problems.

Still, cultural differences between biology and chemistry departments challenge the offer of joint chemical biology courses for both disciplines as well as the implementation of chemical biology educational programs. Thus, apart of organizational and administrative issues, which become complex between different faculties, many students are not well-prepared to enter interdisciplinary study

## 1. Introduction

programs. Although chemistry and biology students successfully graduated in their field, few are familiar with concepts from both disciplines. Therefore, the instructors must be aware of these barriers and find a clever strategy to address and support both students at a similar extent, keeping the motivation high. Emerging from this approach, a new generation of students will be able to speak the language of chemistry and biology with equal fluency.<sup>[7,8]</sup>

Following the crucial need of encouraging more students to be open to face future challenges and think more interdisciplinary, the implementation of new courses in chemical biology could help to push the university education system forward, sponsor the critical thinking of students and yield in successful and enhanced positive learning outcomes.

### 1.2 Photosensitive Molecules in Chemical Biology

At the beginning of life, there was light. Light was the energy for the first primitive reactions on earth<sup>[9]</sup>, and it is still the power source involved in essential developmental biological processes such as photosynthesis.<sup>[10,11]</sup> The crucial role of photosensitive molecules in biological<sup>[10,12,13]</sup> and non-biological processes<sup>[14,15]</sup> serve as inspiration for further innovative developments. In particular, the complexity of the biological processes cannot only be understood by the study of single separated components, but it requires to have tools at our disposal that allow the dynamic study of living systems itself as well as the relationship between each component. Spatial and temporal control would serve as key instruments to deepen our knowledge in complex biological systems. Light as a tool serves a fast, precise, controllable and inexpensive form of energy. Even in nature, light is the ideal trigger: for billions of years it has been used in photosynthesis and phenomena such as vision and the biological clock.<sup>[10,12,13]</sup> Today, not only chemists use the tool of light for numerous reactions<sup>[16,17]</sup>, material science,<sup>[18,19]</sup> molecular motors<sup>[20,21,22]</sup> and photopharmacology,<sup>[23,24,25,26]</sup> but also to understand the complexity of biological systems and modulate their functions. Therefore, innovative tools controlled by light, allow to study where, when and to what extent a biological process is started and stopped, to decipher the living systems at molecular level.<sup>[11,27]</sup> In the following chapters, different optochemical tools: photoactivatable (chapter 1.2.1), photocaged (chapter 1.2.2) and photoswitchable molecules (chapter 1.2.3) as well as fluorophores (chapter 1.2.4) used for the study of biological functions are introduced.

Activation of samples can be performed at different wavelengths. Light with shorter wavelengths (e.g. UV-light) has a short penetration depth and is high in energy, which is often harmful for biological systems. Light with longer wavelengths (visible light) serves an increasing penetration depth and decreases in energy, which makes it more suitable for biological samples.<sup>[28]</sup> Most known optochemical transducers — converters of signals into different outputs<sup>[29]</sup> — still rely on irradiation with UV-light limiting their application particularly for in vivo studies.<sup>[27]</sup> The demand on visible light probes is, therefore, high and was faced within this work.

## 1. Introduction

### 1.2.1 Photoactivatable Molecules

The term 'photodynamic action' dates back more than 100 years<sup>[30]</sup> and is, today, the key concept in photodynamic therapy (PDT),<sup>[31]</sup> which became a well-studied form of therapy against cancer and various non-malignant diseases including infections. Around 1900 in Munich, the medical student Oscar Raab discovered that when microorganisms were incubated with certain dyes, they could be killed by irradiation. He later discovered that apart of light, oxygen was necessary to observe the death of the microorganisms (Figure 1.2).

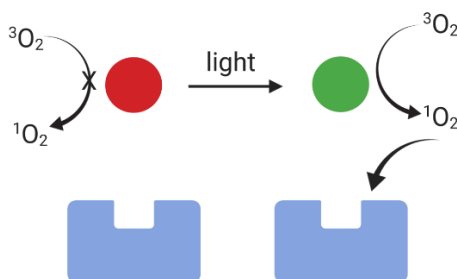


**Figure 1.2.** Photodynamic therapy uses compounds capable of transforming molecular oxygen into toxic singlet oxygen upon irradiation, illustrated using a receptor.<sup>[25]</sup>

Soon thereafter, similar approaches were used in cancer therapy.<sup>[30,31]</sup> In the 1970s the modern era of PDT started with the intense research efforts by Dougherty and co-workers.<sup>[31]</sup> He introduced a water-soluble mixture of porphyrins called haematoporphyrin derivatives (HpD)<sup>[32]</sup> and porfimer sodium, a more purified form, known as photofrin.<sup>[33]</sup> Although having many disadvantages such as skin photosensitivity and inefficiency, photofrin is still the most often used photosensitizer (PS) today.<sup>[31,33]</sup> Mechanistically, PSs are excited by UV (280-400 nm) or visible light (> 400 nm)<sup>[34]</sup> into an orbital with higher energy. By intersystem crossing, the energy is transferred to molecular oxygen to form reactive oxygen species, which are cytotoxic to several biomolecules and cause cell death (chapter 1.2.4.1).<sup>[35]</sup> The most common PS scaffolds are tetrapyrrole-based such as porphyrins (Figure 1.3, compound **1**) and similar derivatives like phthalocyanines (Figure 1.3, compound **2**). Other examples entail both natural products such as hypericin (Figure 1.3, compound **3**) and synthetic dyes like boron-dipyrromethene dyes (BODIPY, Figure 1.3, compound **4**) and 4,5,6,7-tetrachloro-2',4',5',7'-tetraiodofluorescein (rose bengal, Figure 1.3, compound **5**).<sup>[31]</sup> The ideal PS should absorb between 600 nm and 800 nm to ensure deep cell penetration and bearing enough energy to produce singlet oxygen and reactive oxygen species (ROS). They should further exhibit low dark toxicity and a fast clearance from tissues to minimize side effects due to phototoxicity. An additional advantage of many PS is their high fluorescence quantum yield, which turn them into suitable 'theranostic' agents, a combination of diagnostics and therapeutics. It allows to visualize a tumor (by fluorescence) and destroy it (by PDT) using the same agent.<sup>[31,35]</sup>

## 1. Introduction

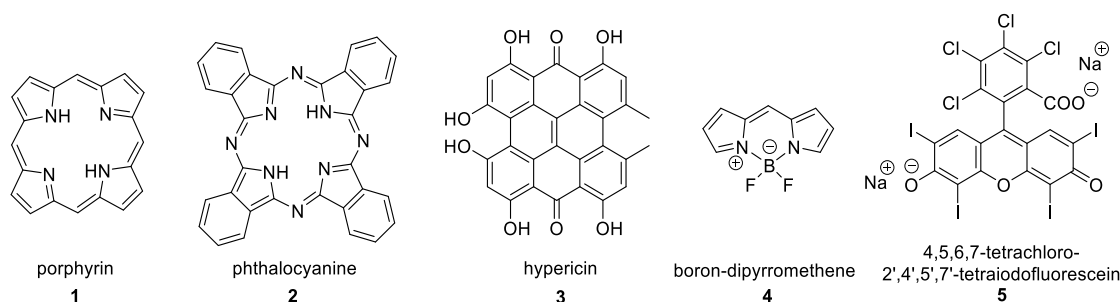


**Figure 1.3.** Most common scaffolds of photosensitizers (PS): porphyrin, phthalocyanine, hypericin, boron-dipyrromethene, 4,5,6,7-tetrachloro-2',4',5',7'-tetraiodofluorescein.<sup>[31,36]</sup>

Recent research approaches strive to develop innovative PS agents to reduce side effects, such as dark toxicity, and ensure selectivity.<sup>[37]</sup> These compounds have been classified depending on their mode of activation into environment-, enzyme- and nucleic acid-activatable photosensitizers.<sup>[38]</sup>

**Environment-activatable photosensitizers:** A unique phenomenon of tumor cells is their low pH (6.5 to 7.2) in extracellular tissues compared to normal tissues (pH ~7.4).<sup>[39]</sup> This is due to the high activity of cancer cells. Thus, both glycolysis and plasma membrane proton pumps's activity are enhanced, resulting in an enriched production of lactic acid, which, in turn, leads to the slightly acidic surrounding.<sup>[40]</sup> Therefore, PS with high fluorescence and singlet oxygen and ROS production at lower pH values, but a decreased activity at pH 7.4, would be appropriate for specific PDT and cancer imaging.<sup>[35]</sup> For example, Ju and co-workers designed a pH-sensitive aniline- based bromo-substituted aza-BODIPY-PS, which displayed fluorescence properties and sufficient singlet oxygen production for near-infrared cancer theranostics under acidic conditions (pH 4.5-5.0).<sup>[41,42]</sup> Thus, upon 808 nm laser irradiation of a mouse model, the direct monitoring of fluorescence of such compound allowed to observe a drastically decrease in tumor size. Whereas untreated tumor tissue displayed a fluorescence ratio at tumor to normal tissue of more than 10 fold, it decreased after the treatment down to a ratio of 1.4 fold. In addition, Wang and co-workers designed a water soluble supramolecular vesicle containing an iodinated BODIPY derivative, which underwent disassembly and consequently successfully released the chemotherapeutic selectively in the acidic surrounding of tumor cells.<sup>[43]</sup> This work suggested a promising drug nanocarrier, combining chemo- and photodynamic activities. A different strategy to initiate apoptotic cell death of cancer cells, using environment activatable PS, is the activation through glutathione (GSH).<sup>[44,45]</sup> GSH-levels are much higher in intracellular (10 mM) than in extracellular (2  $\mu$ M) environments<sup>[46]</sup> and even higher in tumor tissues.<sup>[47]</sup> By cleaving disulfide bonds to caging groups,<sup>[44]</sup> or reduction or addition of the GSH to styryl double bonds,<sup>[45]</sup> the described quenched photosensitizers are reactivated.

**Enzyme-activatable photosensitizers:** Overexpression of specific enzymes is often correlated to specific diseases,<sup>[48]</sup> so they can be used as PS activators. Whereas the PS will be active in tissues with the overexpressed enzyme, normal tissues will not be harmed. Especially high levels of proteases are

## 1. Introduction

connected to numerous diseases, and the use of protease inhibitor therapeutics has been clinically approved for cancers, hypertension, myocardial infarction, periodontitis, AIDS, thrombosis, respiratory disease and pancreatitis.<sup>[38,49]</sup> One example using this approach in the context of PDT was described by Zheng and co-workers. They used a short peptide linker, which is caspase-3 cleavable, to connect a PS and a quencher. Their photoactivatable PS consisted of pyropheophorbide- $\alpha$ , a chlorophyll analogue, as the photosensitizer and a carotenoid as its quencher, connected through a specific bioactive peptide sequence. As the PS and quencher are held in close proximity by the peptide sequence,  $^1\text{O}_2$  generation and lifetime is decreased. Upon incubation with caspase 3, the linker was cleaved and singlet oxygen production enhanced.<sup>[50]</sup> It was demonstrated that through a modular approach by connecting the same PS and quencher through different protease cleavable peptide sequences, different targets could be easily addressed.<sup>[51,52]</sup> To circumvent the dependency on natural peptide folding for the efficiency of the quenching, a zipper molecular beacon was designed, bearing a polyarginine / polyglutamate electrostatic sequence close to the PS and the quencher. The formation of a zipper hairpin-linked fluorophore-quencher pair brings both functionalities close to each other and ensures an efficient quenching.<sup>[53]</sup>

Nucleic acid-activatable photosensitizers: Nucleic acids have successfully served to activate photosensitizers. Numerous diseases are connected to altered gene expression due to mutations in the DNA and besides nucleic acids are easily accessible by solid-phase synthesis. Therefore, precise control over nucleic acid-based processes bears a high potential. Nucleic acid activatable photosensitizers are able to recognize even single-base mutations and discriminate cells, expressing these specific genes.<sup>[38]</sup> Direct DNA binding by small molecule photosensitizers such as methylene blue display sequence-selectivity in the singlet oxygen production with AT preference due to the quenching effects of the GC sequences.<sup>[54]</sup> Apart of this approach, different strategies for the sequence-specific targeting are known: one is the use of target hybridization strand displacement (Figure 1.4 A).<sup>[55]</sup> In this approach, a photosensitizer is linked to a nucleic acid sequence complementary to a target sequence, such as a mRNA linked to an overexpressed protein in cancer cells. Hybridization of this probe with a complementary sequence bearing a PS quencher results in an inactivated PS. However, in the presence of the specific RNA sequence, the sequence, linked to the photosensitizer is displaced and released, and the production of singlet oxygen is turned on. For precise control of this process, a well-chosen length of the oligonucleotides is necessary, whereas it is essential that the target strand has a higher affinity to the quencher oligonucleotide than to the one of the photosensitizer.<sup>[55]</sup> Another strategy applies molecular beacons (Figure 1.4 B).<sup>[56]</sup> These oligonucleotide approach consists of a short hybridized stem region, bearing both the photosensitizer and the quencher at its ends. These two strands are connected by a loop region, which is longer than the stem region and complementary to a specific target sequence.<sup>[56]</sup> Upon binding to the target sequence, the stem is dehybridized, and consequently, the PS activated. An example was applied for specifically targeting the cRAF-1 oncogene.<sup>[57]</sup> Incubation of cRAF-1 expressing cells with a molecular beacon, connected to a pyropheophorbide- $\alpha$  photosensitizer and a carotenoid quencher by a loop portion specific for the cRaf-1 oncogene, resulted in reduced viability of  $38.0 \pm 5.8\%$ , which is in agreement with the positive control. Importantly, significant less efficacy ( $81.0 \pm 4.6\%$

## 1. Introduction

viability) was observed with an analogue scrambled loop-region. Aptamers are short oligonucleotides (< 100 bases), capable of binding to many types of different targets, such as small molecules (amino acids, antibiotics), proteins or nucleic acid structures, in the same high specificity and affinity range as antibodies.<sup>[58]</sup> They have been used for drug delivery and nanotechnology applications by targeting cancer-associated molecules.<sup>[59]</sup> Tan and coworkers designed a thrombin specific PS aptamer which is deactivated by carbon nanotubes. The carbon nanotubes can bind the aptamer through ionic interactions and is further able to quench the fluorescence of the PS. In the presence of the target, the nanotube dissociates from the aptamer, and the fluorescence increased up to 20-fold (Figure 1.4 C).<sup>[60]</sup> Further activation mechanisms for photosensitizers besides environmental effects, enzymes and nucleic acids, are the use of quantum dots<sup>[61]</sup> and nanoparticles.<sup>[62]</sup>

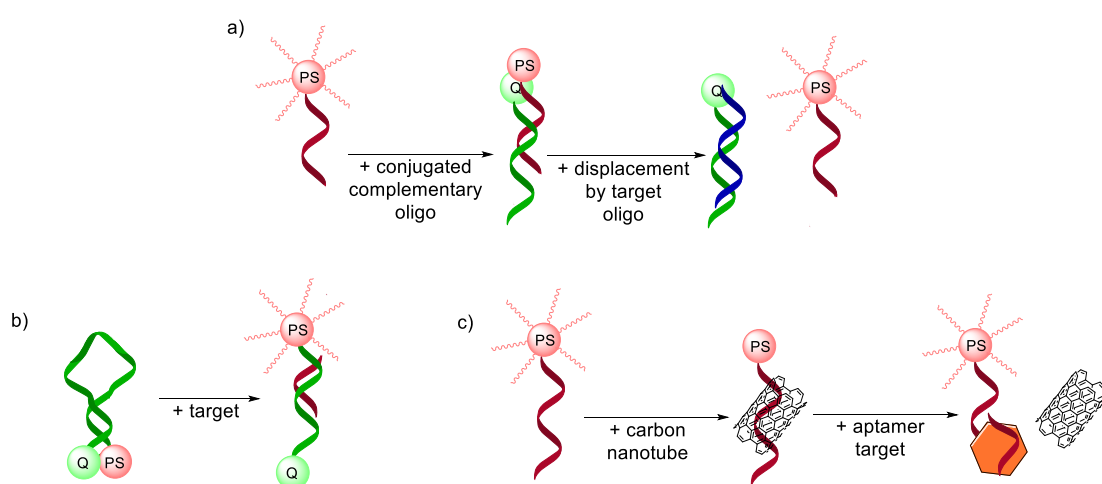


**Figure 1.4.** Activatable photosensitizers based on a) reverse hybridization systems, b) molecular beacons and c) aptamers.<sup>[38,55,57,60,62]</sup>

### 1.2.2 Photocaged Molecules

One strategy for the controlled release of biologically active compounds is the utilization of photolabile protecting groups (PPGs), which can be removed in a photoreaction/photolysis by irradiation with light. PPGs were first described in the early 1960s by Barton,<sup>[63]</sup> Barltrop,<sup>[64]</sup> and Sheehan<sup>[65]</sup> and applied in organic synthesis. Their use for biological applications was introduced in 1976 by Engels and Schlaeger,<sup>[66]</sup> who synthesized a photoprotected cyclic adenosine monophosphate (cAMP), and successfully tested their ability to activate the cAMP-dependent protein kinase under irradiation. One year later, the word “caged” compound was coined by Hoffman and coworkers when they reactivated a sodium-potassium pump upon release of photoprotected ATP.<sup>[67]</sup> The definition of “caged compound” is controversial as it can easily be misinterpreted. The name itself reminds on a compound trapped inside of an actual cage, which is opened by light, instead of the covalently linked photolabile protecting group. Furthermore, literature searches can be complicated, as varying expressions such as “photoactivatable”, “light-triggered” or “photocaged” are used, the protecting groups have structural similarity to many other



## 1. Introduction

contexts, and the term “caged” is used in many different perspectives.<sup>[27, 68]</sup> There are several requirements for a suitable PPG depending on their application:<sup>[27,69]</sup>

- strong absorbance at least over 300 nm, preferably in the visible light region, to not harm any biological components
- the photoreaction should be fast, clean and with a high quantum yield for an efficient photoactivation
- low intrinsic activity and stability under physiological conditions prior and during the photolysis
- solubility in physiological conditions and capable of crossing biological barriers
- its photolytical byproducts should be both transparent at the irradiation wavelength and non-toxic
- ideally, kinetic values are known and the released compounds detectable, e.g. by fluorescence

Since the introduction of “caged” compounds for biological applications 40 years ago, many different classes of photosensitive protecting groups with varying modifications were developed and applied to numerous systems.<sup>[68,69,70,71,72]</sup> In this chapter the existing classes and some examples are presented.

### 1.2.2.1. Classes of Photolabile Protecting Groups

The first and one of the most commonly used PPG for biological applications is the *ortho*-nitrobenzyl group (Figure 1.5, compound **6**) and its derivatives, which are deprotected at  $\lambda_{\text{max}} \approx 400$  nm with a release rate of  $10^2$  to  $10^4$  s<sup>-1</sup>. The main drawback of this PPG is the formation of a harmful nitrosoaldehyde as a byproduct after photolysis, whose aldehyde functionality can react with amines and its brown-colored degradation product acts as an internal filter.<sup>[68,69,73,74]</sup> Further modifications on the substituents of the *ortho*-nitrobenzyl facilitated absorbance over 400 nm<sup>[75,76]</sup> or could trap the formed nitrosoaldehyde.<sup>[77]</sup> Derivatives such as the *ortho*-nitrophenylethyl group (Figure 1.5, compound **7**) were developed to speed up the reaction due to a differing release mechanism, forming a nitrosoketone upon deprotection.<sup>[68]</sup> Another common class of PPGs are coumarin derivatives (Figure 1.5, compound **8**). They are deprotected at  $\lambda_{\text{max}} \approx 320$ -330 nm and characterized by fast release rates up to  $10^{10}$  s<sup>-1</sup>,<sup>[78]</sup> improved stability and the possibility of monitoring the fluorescent byproduct.<sup>[68,79,80]</sup> Substituents on the coumarin core (Figure 1.5, compound **8**, R<sup>3</sup> = Br, R<sup>4</sup> = OMe, R<sup>5</sup> = O) improved the solubility of the first generation compounds (Figure 1.5, compound **8**, R<sup>3</sup> = H, R<sup>4</sup> = OMe, R<sup>5</sup> = O).<sup>[69]</sup> Thiocoumarins (Figure 1.5, compound **8**, R<sup>3</sup> = H, R<sup>4</sup> = NEt<sub>2</sub>, R<sup>5</sup> = S) enable uncaging in the 470-500 nm wavelength range.<sup>[81]</sup> Other examples for visible light PPGs are photolabile ruthenium complexes.<sup>[82,83]</sup> Quinones (Figure 1.5, compound **9**)<sup>[84,85]</sup> and BODIPYs (Figure 1.5, compound **10**)<sup>[86]</sup> are groups, which even allow the release of the protected compounds by application of far-red and red light.

## 1. Introduction

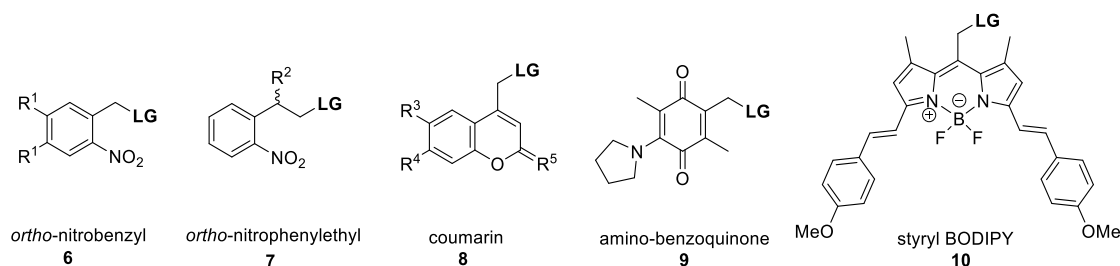


**Figure 1.5.** Structural scaffold of common photosensitive protecting groups. LG = leaving group/compound of interest.  $R^1 = H, OMe$ ;  $R^2 = H, Me$ ;  $R^3 = H, Br$ ;  $R^4 = OMe, NEt_2$ ;  $R^5 = O, S$ .

As mentioned before, the in vivo application of most photosensitive protecting groups is often restricted, because the photolysis involved harmful UV irradiation, and is, therefore, not fully biocompatible. The two-photon excitation uncaging strategy provides a suitable alternative to the normal single-photon excitation.<sup>[27]</sup> At high wavelengths, chromophores can simultaneously absorb two photons, resulting in a higher energetic state, which is about twice the frequency and often falls into the UV-region.<sup>[87,88]</sup> The resulting ability to apply red or near-infrared (NIR) light, allows the use of the phototherapeutic window between 650 and 950 nm,<sup>[69, 89]</sup> which is characterized by deep tissue penetration and low phototoxicity.<sup>[69]</sup>

Having a large variety of different PPGs with different absorbance properties depending on their substituents allows designing orthogonal protection strategies. More recently, orthogonally addressing multiple PPGs were introduced in one single system, allowing to deprotect two functionalities independently by irradiation at different wavelengths. In 2000, Bochet described the first example of orthogonal release of PPGs, in which two carboxylic acids were protected with a 3,5-dimethoxybenzyl alcohol and a 2-nitro-4,5-dimethoxybenzyl alcohol.<sup>[90]</sup> Bochet studied their different deprotection speed in mixed solutions upon irradiation with 254 nm and 350 nm. A perfect selective deprotection was not achieved, due to partial overlapping of the two absorbance spectra. To overcome this limitation, the deprotection should be applied sequentially. As most compounds absorb in the UV-region, one must start with irradiation of the protecting group bearing the absorbance maximum at the higher wavelength. After complete uncaging of the first protecting group, the shorter wavelength can be applied to deprotect the second protecting group.<sup>[91]</sup> This approach was successful in several examples.<sup>[92,93,94]</sup>

### 1.2.2.2. Applications of Photolabile Protecting Groups

The application of photolabile protecting groups is nowadays spread over the whole field of chemical biology. Numerous examples are known to protect small molecules, peptides and proteins, or oligonucleotides:

**Small molecules:** In particular, the pioneering caged ATP is the most common photocaged small molecule and even commercially available.<sup>[68,95]</sup> Young and Deiters developed a caged IPTG-version (Figure 1.6, compound **11**) to control gene expression.<sup>[96]</sup> In a similar approach, Cambridge et al. used a caged

## 1. Introduction

cyanodoxycycline (Figure 1.6, compound **12**) in eukaryotes.<sup>[97]</sup> The use of the protected amino acid glutamate (Figure 1.6, compound **13**) is an example of a small molecule in neurobiology and signaling pathways. Glutamate is responsible for the communication between neurons. Its commercially available version already allowed several investigations in neurosciences.<sup>[98,99]</sup> In combination with photocaged gamma-aminobutyric acid, an inhibitory neurotransmitter, it was possible to multimodular control the membrane potential of a single synapse.<sup>[100]</sup> Further examples are cyclic nucleotides,<sup>[101]</sup> phosphoinositols<sup>[102,103]</sup> or calcium, caged with photolabile chelators, as one of the most important carriers of chemical information.<sup>[104]</sup> One example of a photoactivatable small molecule interacting with DNA, is a photo-caged platinum(II) complex (Figure 1.6, compound **14**) described by Franz and coworkers.<sup>[105]</sup> A nitrophenyl group is built into the backbone of a tetradentate ligand. The complexed platinum is unreactive towards ligand exchange. Upon UV-light irradiation, the ligand backbone is cleaved and the Pt<sup>II</sup> complex can exchange ligands in a similar approach to cisplatin. In the dark, the caged complex showed no cytotoxicity towards human breast cancer MCF-7 cells, whereas upon irradiation it increased by 65%. Sugiyama and coworkers were able to introduce photocontrol into sequence-specific DNA alkylation.<sup>[106]</sup> By caging an alkylating group on a pyrrole and imidazole containing polyamide, which is known to target the DNA sequence-specifically, they were able to demonstrate their selective activation by UV irradiation both in vitro and in vivo.

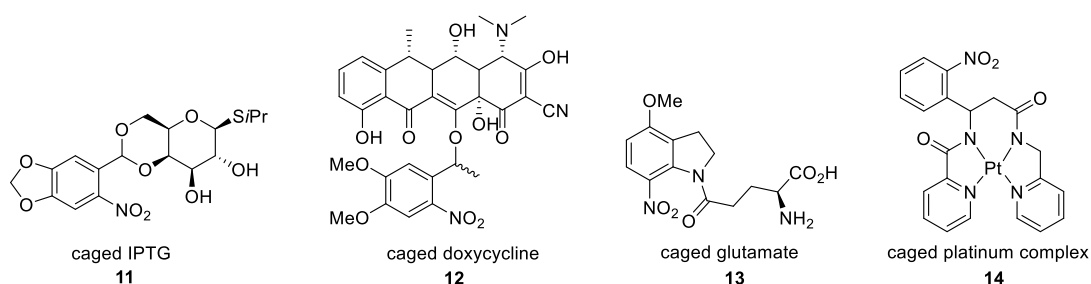


**Figure 1.6.** Examples of photocaged small molecules: caged IPTG, caged doxycycline, caged glutamate and caged platinum complex.

**Peptides and Proteins:** The introduction of cages in peptides and proteins can affect their function, and consequently provides biological control.<sup>[27]</sup> For example, photoactivatable peptides and enzymes were used to control kinase activity,<sup>[107,108]</sup> liposomes<sup>[109]</sup> and neurotransmitters.<sup>[110]</sup> A different approach focused on photodegradable peptides, where an unnatural photolabile amino acid is introduced into the backbone of a bioactive peptide. Upon light irradiation, the peptide is cleaved which results in loss of activity.<sup>[111, 112]</sup> By now, it is possible to introduce different photocages on many amino acids functionalities: the N-terminus,<sup>[113]</sup> acid-functionalities,<sup>[114]</sup> amides,<sup>[115]</sup> alcohols,<sup>[116,117]</sup> thiols<sup>[118]</sup> and amines.<sup>[109]</sup> On the level of proteins, there are different strategies to introduce the cages. The simplest one is to take advantage of the reactivity of a functional groups of the amino acid side chains, such as thiols due to their low abundance (<2%) in proteins and the highest nucleophilicity upon the amino acid side chain functionalities. Another possibility to address cages, are amines. They are also good reactants in nucleophilic substitutions, but rather common in proteins. Additional strategies apply unnatural amino

## 1. Introduction

acids.<sup>[119]</sup> Another approach uses the multimeric properties of proteins. The chemical synthesis of one subunit of the protein allows the introduction of a caged moiety at a desired position. This subunit can then be used to replace the wild-type counterpart to yield the caged protein.<sup>[68]</sup> To introduce caged amino acids into larger proteins, Schultz et al. established a method, using a nonsense-codon and a corresponding tRNA, loaded with the caged amino acid.<sup>[118]</sup>

Oligonucleotides: To introduce caging groups in oligonucleotides, they can be connected to the nucleobases to prevent Watson-Crick base pairing, on the ribose, the phosphodiester backbone or as an internal photocleavable linker.<sup>[27]</sup> Photocaged oligonucleotides can be used to regulate gene expression,<sup>[120,121]</sup> regulate aptamer activity<sup>[122]</sup> or cage molecular beacons.<sup>[123]</sup>

### 1.2.3 Photoswitchable Molecules

Photoswitchable molecules are compounds, which are able to isomerize between two or more different forms upon irradiation with a specific wavelength leading to different absorption spectra of their photostationary states.<sup>[29,124]</sup> Azobenzenes, stilbenes, diarylethenes and spiropyrans belong to the most common photoswitches and are described in more detail below. Due to the often non-invasive nature of light, they have been widely applied in the reversible photochemical regulation of biological systems<sup>[29]</sup> and serve as a scaffold for the field of photopharmacology.<sup>[25]</sup> Photopharmacology aims to face and improve pharmacological problems such as poor specificity, resulting in severe side effects, environmental toxicity and the growing problematic of resistance by introducing photoswitchable groups into the scaffold of the bioactive compounds to achieve control over the applied compounds.<sup>[26]</sup> The lack of controlling the activity of the drugs in space and time leads to those issues.

#### 1.2.3.1 Concepts

To achieve the before mentioned selectivity, several strategies can be applied:<sup>[25]</sup> 1) by avoiding cross-interactions to targets, which are absent in the human body,<sup>[125]</sup> 2) reducing off-target effects by selecting only targets, which are present in specific organs or overexpressed in a specific diseases, as immunotherapy;<sup>[126]</sup> or 3) local application, as it is performed in ophthalmology.<sup>[127]</sup> However, many diseases are difficult to combat, as their targets are expressed all over the body, in healthy and unhealthy cells.<sup>[126]</sup> To reduce side effects and to avoid off-targeting, photopharmacologists use light as the external trigger to control the activity of the bioactive molecule. Photoswitchable groups, introduced in the scaffold of the bioactive compound, can change its conformation upon irradiation. As the structure is most often directly linked to the dynamic and kinetic properties of the bioactive compounds, this approach allows a direct regulation of their therapeutic effect. As illustrated in Figure 1.7, photopharmacology is inspired by the more established photodynamic therapy, with the unique difference that the existence of the active compound can be regulated reversibly. Changing the conformation upon irradiation and thereby increasing the effective concentration of the active compound, has a direct and selective effect in the interaction with the receptor. Although, not yet being

## 1. Introduction

clinically approved, like the PDT, photopharmacology has a high potential as a new technique in medical treatment.<sup>[25,128]</sup>

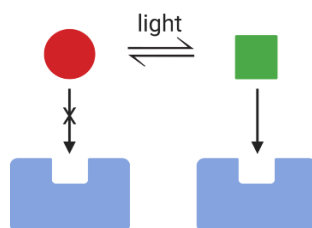


**Figure 1.7.** Photopharmacology uses light to photocontrol the conformation of a drug that can only bind to the target in one state, illustrated using a receptor.<sup>[25]</sup>

The dynamic regulation of the drug is obtained due to a reversible change in the structure of the photoswitch, resulting in the control of its properties. Photoswitches have already been incorporated into nucleic acids, the backbone of peptides, receptors and channels and were used to photoregulate enzyme activity as well as ligand binding to soluble proteins.<sup>[129]</sup>

The design approach for photocontrollable tools to modulate biomacromolecular function was nicely summarized by Trauner et al.<sup>[130,131,132]</sup> In a first attempt, the right photoswitch is selected. It is necessary to avoid phototoxicity and ensure a reliable isomerization over several cycles without affecting the integrity of the molecular transducer. Depending on the application, it might be advantageous to use a thermally instable photoswitch, which turns itself off in the absence of irradiation. In other cases, a thermodynamically stable photoregulator, whose activity is regulated by applying one specific wavelength, might be more suitable. Still, in the ideal case the conformation of the photoswitch changes completely between the two states. This is possible for those with areas of no spectral overlap for each conformation. These specific wavelengths can be used for irradiation to achieve high ratios for each isomer. Although this case is rare, it needs to be noted that even photoregulators with low isomer ratios in the 40/60 range can have pronounced biological effects.<sup>[130]</sup> Ideally, the photocontrollable moiety is introduced into the scaffold of the bioactive molecule giving the largest biological impact between the two conformers. Preferably, the isomerization changes completely between active and inactive. Furthermore, both states of the photoregulator must be soluble in the necessary media and efficient membrane permeability may be desirable, too. The new compound should not interfere with the applied assays, such as quench fluorescence, when needed. For in vivo application the cell penetration depth of the applied wavelengths needs to be considered.<sup>[130]</sup> Still, it needs to be noted that even photocontrollable compounds with a low penetration depth can have a pronounced effect in in vivo applications.<sup>[24]</sup>

### 1.2.3.2 Classes of Photoswitches

The most commonly used photoswitches are azobenzenes, stilbenes, spiropyranes, diarylethenes, thiophenefulgids and hemithioindigos (Figure 1.8). Each class of photoswitch has different properties, which are shortly summarized below. For all photoswitches, the influence of substituents on the

## 1. Introduction

absorbance wavelength is strong.<sup>[129]</sup> The applications of azobenzenes, in the context of nucleic acids, are discussed in more detail below (chapter 1.2.3.3 and 1.2.3.4).

**Azobenzenes:** Azobenzenes (Figure 1.8, compound **15**) belong to the most commonly used photoswitches for oligonucleotide modification and biological application in general.<sup>[124]</sup> Functionalization of the aromatic rings allow ligation to different bioactive molecules, which is applied in this work for DNA binding molecules.

**Stilbenes:** Structurally, stilbenes (Figure 1.8, compound **16**) are closely related to azobenzenes and possess similar photochemistry.<sup>[133]</sup> The *cis* conformation is more stable and thermal *cis/trans* isomerization negligible at room temperature.<sup>[129]</sup> A major drawback is the tendency of stilbenes to undergo irreversible cyclization / oxidation of the *cis* isomer.<sup>[134]</sup> Whereas in the past, stilbenes were used for the photoregulation of oligonucleotides,<sup>[129]</sup> more recent examples are, due to the before mentioned drawbacks, relatively rare.<sup>[124]</sup>

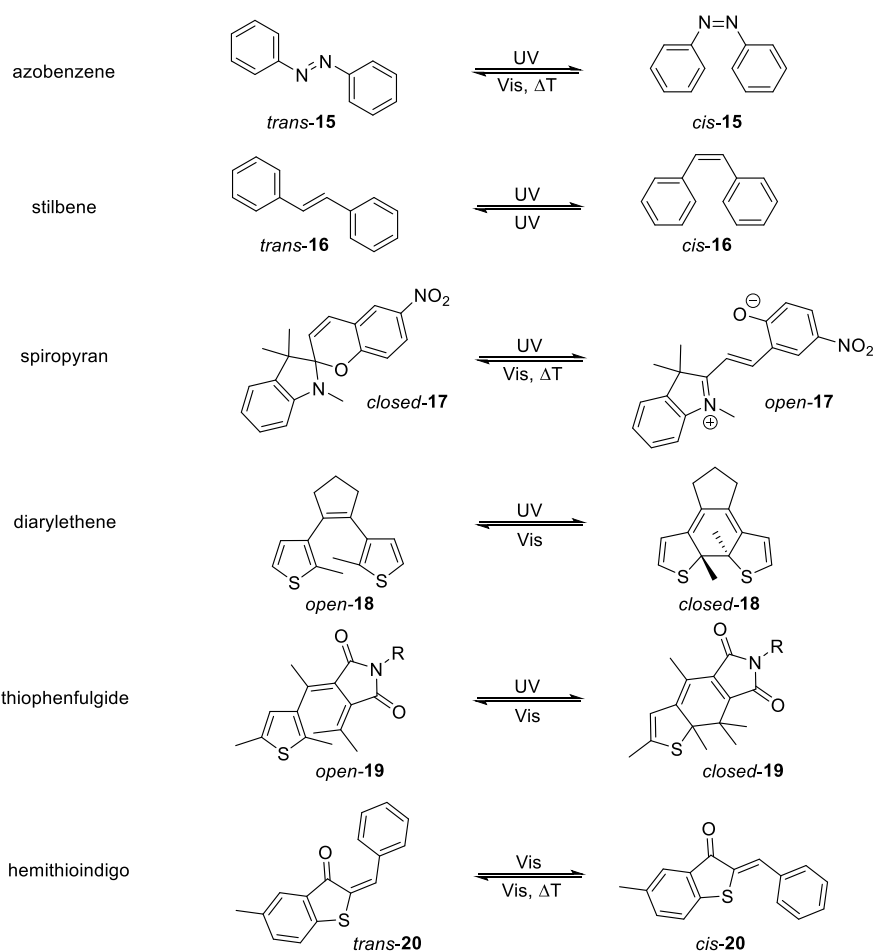


**Figure 1.8.** Molecular structures of the most commonly used photoswitches in their *cis/trans* or *open/closed* form: azobenzenes, stilbenes, spiropyrans, diarylethenes, thiophenfulgides and hemithioindigos.<sup>[124,129,135]</sup>

## 1. Introduction

***Spiropyrans***: Upon irradiation with UV-light, the C<sub>spiro</sub>-O bond of spiropyrans (Figure 1.8, compound **17**) undergoes heterolytic cleavage and results in the open zwitterionic form, known as merocyanine. Irradiation with visible light or thermal energy leads back to the closed form.<sup>[136,137]</sup> Substitution of the spiropyrans and the used solvent have a high influence to the equilibrium of the two states.<sup>[138,139]</sup> Apart of the structural change, the polarity of the compound changes drastically upon ring opening, which influences the hydrophilicity / hydrophobicity.<sup>[140,141]</sup> Both forms exhibit a dramatic difference in DNA binding. Whereas the closed form is nonbinding, ring opening by UV irradiation leads to the form which is able to intercalate into the DNA bases.<sup>[142]</sup>

***Diarylethenes***: The closed form of diarylethenes (Figure 1.8, compound **18**) is caused by reversible, photochemically induced cyclization<sup>[129]</sup> of the hexatriene moiety in the open form. They are thermally stable, until electron-withdrawing groups are introduced on the aromatic rings.<sup>[143]</sup> Furthermore, they feature an immense resistance to fatigue with repetitions of switching cycles up to 1000 times.<sup>[144]</sup>

***Fulgides***: The photochromic behavior of fulgides (Figure 1.8, compound **19**, shown with thiophenes) equals the one of diarylethenes: reversible cyclization upon irradiation transforms the hexatriene into a cyclohexadiene ring.<sup>[145,146]</sup> Presence of a heteroaromatic ring or substitution on the C-atoms, forming the C-C-double bond, induces thermal irreversibility.<sup>[147,148]</sup>

***Hemithioindigos***: Hemithioindigos (Figure 1.8, compound **20**) undergo *cis* to *trans* isomerization of their olefinic bond, which changes the dipole moment of the molecule significantly.<sup>[149]</sup> The isomerization upon irradiation at 400-410 nm (*cis* to *trans*) and 480-490 nm (*trans* to *cis*) is reversible and stable over thousands of switching cycles.<sup>[149,150]</sup> Whereas the photoisomerization is a very fast process, the thermal *trans* to *cis* reversion, especially in organic solvents, is very slow.<sup>[129,150]</sup>

### 1.2.3.3 Azobenzenes

For the classical, unsubstituted azobenzene (Figure 1.8, compound **15**), the *trans* isomer is the thermodynamically most stable form. It is a planar molecule with zero dipole moment. By irradiation with near-UV light, it can be isomerized into the *cis* form, which is nonplanar and has a dipole moment of ~ 3 D. The *cis/trans* ratio in the photostationary state is approximately 80/20.<sup>[124]</sup> Back isomerization is achieved by irradiation with light >460 nm or thermally resulting in a *cis/trans* ratio of approximately 20/80.<sup>[124, 151]</sup> The UV-vis spectrum of azobenzene is characterized by two absorption bands corresponding to the  $\pi \rightarrow \pi^*$  and  $n \rightarrow \pi^*$  electronic transitions. The  $\pi \rightarrow \pi^*$  transition is usually in the UV region and the  $n \rightarrow \pi^*$  transition in the visible region. Whereas for the *trans*-isomer the  $\pi \rightarrow \pi^*$  absorption band is very intense, the  $n \rightarrow \pi^*$  band is much weaker, as this transition is not allowed due to symmetry rules. For the *cis*-isomer the  $\pi \rightarrow \pi^*$  absorption band is shifted to shorter wavelengths with decreased intensity and the allowed  $n \rightarrow \pi^*$  band shows increased intensity with respect to the *trans*-isomer (Figure 1.9 B).<sup>[152]</sup> Aromatic ring substitution or expansion of the aromatic system, allows to shift these

## 1. Introduction

wavelengths into the visible light region,<sup>[153,154,155,156,157]</sup> which makes them suitable for even in vivo applications.<sup>[158]</sup> The wavelength shifts were based in splitting the  $n \rightarrow \pi^*$  absorption bands of the *cis* and *trans* isomer, which usually overlap in the 400-500 nm region (Figure 1.9 C). The separation of these two bands enables the irradiation of both forms with visible light.<sup>[157]</sup>

However, as explained before (chapter 1.2), there is an interest in developing novel visible-light/NIR derivatives. The first examples were described by Herges and co-workers, who used an ethylene linker to covalently bridge the *ortho*-positions.<sup>[155]</sup> Through this modification, they achieved photoisomerization in both directions by the use of visible light and an almost complete photoconversion (100% *trans* to *cis* and 92% *cis* to *trans*).<sup>[155]</sup> Woolley and co-workers described, soon after that, a modification, bearing four methoxy-groups in the *ortho*-position of the azobenzene.<sup>[153]</sup> Their new azo-derivative was regulated in the visible-light region, but possesses lower photoconversions (80% *trans* to *cis* and 85% *cis* to *trans*).<sup>[153]</sup> In 2012, Hecht and co-workers applied fluorine in *ortho*-positions of the azobenzene (*oF*<sub>4</sub>-Azo, Figure 1.9 A, compound **21**). The electron withdrawing group reduced the electron density in the N=N bond and consequently lowered the n-orbital. In contrast to the before mentioned examples, the fluorine substituents are relatively small, which barely distort the planar geometry of the *trans*-azobenzene.<sup>[154]</sup> The modification leads to an overall blue-shift of the  $n \rightarrow \pi^*$  transition band of the *cis*-*oF*<sub>4</sub>Azo and a red-shift for the one of *trans*-*oF*<sub>4</sub>-Azo. The bands are now well separated (Figure 1.9 B) and the *cis*-conformation shows an immense thermal stability in DMSO at 25 °C with a half-life of 2 years. Further modifications in the *para*-position resulted in a  $n \rightarrow \pi^*$  band separation of 50 nm and high ratios of the photostationary state of 92% and 97%.<sup>[157]</sup>

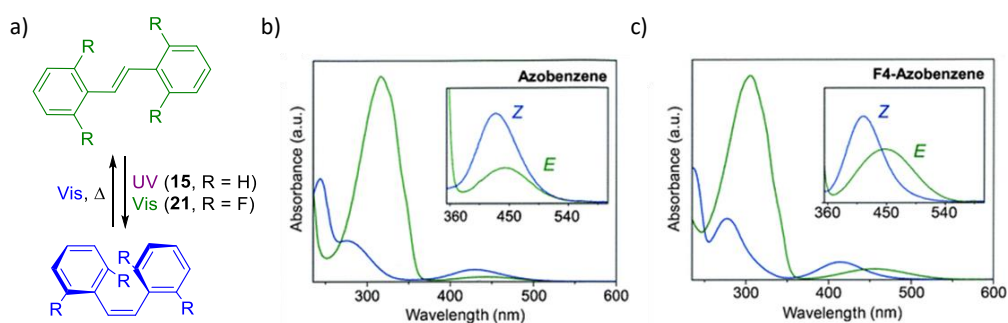


**Figure 1.9.** a) Molecular structure of azobenzene ( $R = H$ ) and  $F_4$ -azobenzene ( $R = F$ ), including their type of irradiation needed to switch between the two isomers. b) Absorbance spectra of *trans* (green) and *cis* (blue) azobenzene. c) Absorbance spectra of *trans* (green) and *cis* (blue)  $oF_4$ -azobenzene.<sup>[157]</sup>

### 1.2.3.4 Applications of Azobenzenes

In this section the application of azobenzene-derivatives is limited to nucleic acids (DNA and RNA). This overview is clustered in different types of oligonucleotide modifications since the azobenzene moiety can be implemented as a nucleoside surrogate, attached to the nucleoside, as phosphate backbone linker or through interactions via non-covalent interaction (Figure 1.10).<sup>[124]</sup>



## 1. Introduction

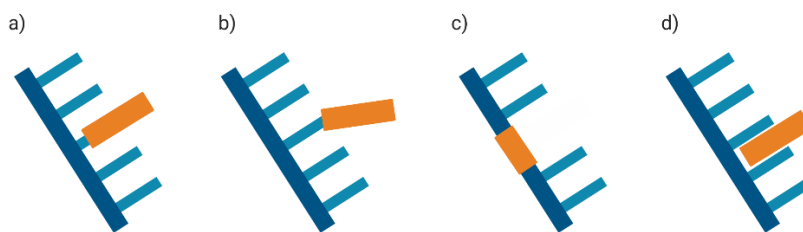


**Figure 1.10.** Schematic representation of azobenzene-derivative implementation in different types of oligonucleotides: a) Azobenzenes as nucleoside surrogate, b) Azobenzenes attached to the nucleoside, c) Azobenzene as phosphate backbone linker and d) Azobenzene in non-covalent interaction with oligonucleotides.<sup>[124]</sup>

Azobenzenes as nucleoside surrogates: The application of azobenzenes as nucleoside surrogates (Figure 1.10 A) is the most successful and frequently applied method. In this approach, the azobenzene is attached to a linker molecule, which is introduced into the backbone of the oligonucleotide and replaces the nucleobase in this position. Depending on the conformation of the switch and the flexibility of the linker, the photoswitch can either intercalate between the neighboring bases or hang out of the strand.<sup>[124]</sup> The insertion of the photoswitchable nucleoside surrogate has a large impact in the stability of the formed duplex and was applied to influence enzyme regulation,<sup>[159]</sup> DNA<sup>[160,161]</sup> and RNA cleavage,<sup>[162]</sup> and peptide nucleic acid (PNA) activity.<sup>[163,164]</sup> Structurally, the azobenzene is usually connected to a diol linker in the solid-phase synthesis of oligonucleotides. For biological applications, the introduction of azobenzenes as nucleoside surrogates are limited to short oligonucleotides, as the implementation by PCR is limited until now.<sup>[124,165]</sup> Asanuma and co-workers found that the introduction of a thiol group in *para* and two methyl groups in *ortho* position of the azobenzene nucleoside surrogate shifts the absorption maximum into the visible light ( $\lambda_{\text{max}} = 398 \text{ nm}$ ) and improves the thermal stability of the *cis*-isomer by 8-times.<sup>[166,167]</sup> This building block was introduced into a T7 promoter region involved in GFP expression. By controlling the melting of this region by light, the transcription by RNA polymerase could be photocontrolled.<sup>[168,169]</sup>

Azobenzenes attached to the nucleoside: Here, the azobenzene is connected through a linker to a modified nucleoside before or after the oligonucleotide synthesis (Figure 1.10 B).<sup>[124]</sup> The length and type of the linker regulates, where the photoswitch is positioned. Connection to the C5-position of pyrimidine bases by linkers such as triazole and phenylacetylene for example, usually places the photoswitch into the major groove,<sup>[170,171,172]</sup> causing a relative low effect on the melting temperature. However, the exact mode of interaction is unknown and computational studies are rare.<sup>[124]</sup>

Azobenzenes as phosphate backbone linkers: In this approach, the azobenzene is introduced into the backbone of the oligonucleotide (Figure 1.10 C). Most of these attempts aim to photocontrol the formation of oligonucleotide hairpins. Due to stacking of the photoswitch, melting temperatures are high and applications are, therefore, limited.<sup>[124]</sup> The azobenzene moiety is preferentially introduced as a diol. Since the *trans*-azobenzene is planar, the hairpins are usually built up that this isomer slides perfectly between the strands, whereas the *cis* conformation leads to destabilization.<sup>[173]</sup> One example of this

## 1. Introduction

application was described by Wu, He and Tang, who prepared several light-switchable dumbbells for the regulation of RNA digestion. The dumbbells were formed from antisense oligonucleotides and two short inhibitory sense strands, connected with an azobenzene linker. Whereas the hairpin is stabilized in the *trans* state, destabilization melting occurs in the *cis* form, and consequently hybridization to target RNA and its following digestion.<sup>[174]</sup>

***Azobenzenes in non-covalent nucleotide interactions:*** In a similar approach to photopharmacology, non-covalent binding photoswitches allow an on/off reversibility (Figure 1.10 D). Whereas in the *trans*-form, the planar conformation of azobenzenes result in  $\pi$ -stacking with the bases of the oligonucleotides, the bent *cis*-conformation leads to steric hindrance and lower binding affinities. To enhance double-stranded (ds) DNA binding, azobenzenes are usually functionalized with cationic ends, to increase electrostatic interaction with the phosphate backbone of the DNA.<sup>[124]</sup> The cationic azobenzene AzoDiGua (Figure 1.11, compound **22**) has been used to influence duplex stability.<sup>[175]</sup> The terminal guanidinium functionalized azobenzene intercalates as *trans*-AzoDiGua into the DNA, strongly stabilizes the DNA double helix and increased its melting temperature by several ten degrees. Upon UV-irradiation, which leads to the *cis*-isomer, ejection of AzoDiGua is induced, which results in a significant decrease of the melting temperature of up to 18 °C.<sup>[175]</sup> Azobenzene molecules have also been employed as DNA/RNA condensation agents.<sup>[176]</sup> The azobenzene trimethylammonium bromide surfactant AzoTAB (Figure 1.11, compound **23**) is a well-studied photoswitchable compacting agent, whose hydrophobic *trans*-form triggers ten times more compacted DNA. Irradiation with UV-light and the formation of the *cis*-isomer relaxes the DNA again.<sup>[176]</sup> AzoTAB was further demonstrated to reversibly inhibit RNA production, resulting in a photoreversible GFP production<sup>[177]</sup> and was used for gene silencing.<sup>[178]</sup>

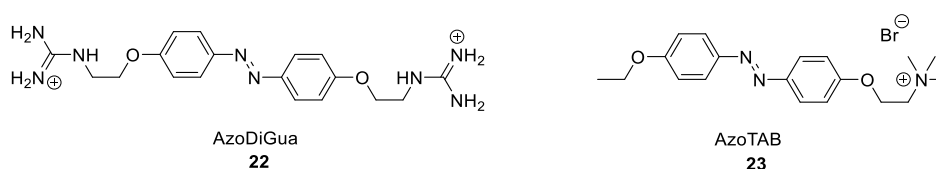


**Figure 1.11.** Molecular structure of AzoDiGua<sup>[175]</sup> and AzoTAB.<sup>[176]</sup>

### 1.2.4 Fluorophores

Photosensitive molecules can be used to visualize biological processes apart from controlling biological functions as in the case of photoactivatable, photocaged and photoswitchable compounds. These type of molecules are known as fluorophores. Fluorophores are compounds capable to emit fluorescence upon irradiation with a specific wavelength.<sup>[179]</sup> In this chapter, the concept of fluorescence (chapter 1.2.4.1), the classes of the main fluorophores (chapter 1.2.4.2) small-molecule fluorophores (chapter 1.2.4.3), fluorescent proteins (chapter 1.2.4.4) and common dsDNA sensors (chapter 1.2.4.5) are introduced.

## 1. Introduction

### 1.2.4.1 Concept of Fluorescence

The phenomenon of fluorescence can best be described in a Jablonski diagram (Figure 1.12). It is divided into three different stages: the excitation, the internal conversion and the fluorescence emission. During the excitation, energy in form of a photon supplied by an external source such as a lamp or a laser is absorbed by the fluorophore. This process creates an excited electronic singlet state ( $S_1'$ ), which in the next step undergoes an internal conversion to yield in the relaxed singlet excited state ( $S_1$ ). In the last step, the fluorophore returns back to its ground state ( $S_0$ ), by emitting a photon, which is observed as fluorescence. Due to the energy difference of the  $S_1'$  and  $S_1$  state, the energy of this photon is lower than the absorbed one, resulting in a longer wavelength. The difference in energy or wavelength between the excited and the emitted photon is called Stokes shift. Apart from returning to the ground state by fluorescence, the relaxed singlet excited state ( $S_1$ ) can undergo non-radiative decay, transfer its energy to another molecule in a Förster Resonance Energy Transfer (FRET) or perform an intersystem crossing to emit phosphorescence or transform molecular oxygen into singlet oxygen (chapter 1.2.1).<sup>[180,181]</sup>

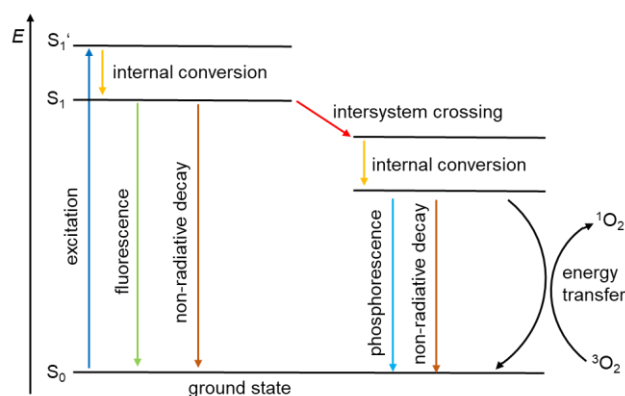


**Figure 1.12.** Jablonski diagram showing the process of fluorescence and other energy emitting phenomena after excitation of a photon by a fluorophore.

### 1.2.4.2 Classes of Fluorophores

The first studies in the field of fluorescence were performed on the molecule quinine (Figure 1.13, compound **24**). Later, such compound did not only become an important molecule in organic chemistry but also in medicinal chemistry. Thus, quinine is a drug against malaria.<sup>[182,183]</sup> Interestingly, William Perkin's attempt to synthesize quinine by oxidative dimerization of *N*-allyltoluidine in 1856, and similarly oxidizing aniline, accidentally resulted in the first synthetic dye: mauveine<sup>[183]</sup> (Figure 1.13, compound **25**). His initial studies laid the basis for the discovery of the main fluorophore classes during the next decades (Figure 1.13 and Figure 1.3): xanthenes (compound **26**) such as fluorescein (ca. 1871, compound **27**) and rhodamines (ca. 1887, compound **28**); coumarins (ca. 1884, compound **29**); phenoxazines (ca. 1903, compound **30**), cyanines (ca. 1924, compound **31**) and BODIPYs (ca. 1968, compound **4**).<sup>[182,184]</sup> Since then, there have been intense efforts to overcome the problems of these first generation fluorophores such as low photostability and intensity, as well as high hydrophobicity. The improvements resulted in excellent stains like the highly used "Alexa Fluor" dyes developed by Molecular Probes<sup>[185]</sup>

## 1. Introduction

and sulfoindocyanine succinimidyl esters (CyDyes) from Alan Waggoner.<sup>[186]</sup> These modern compounds can be modified to specifically target organelles, indicate ions or be used for imaging studies in living cells.<sup>[182]</sup> Apart from small molecules, fluorescent proteins are widely used in biological and medical imaging approaches. Having fluorescent-labeled proteins at the disposal, allowed biologists to synthesize fluorophore fusions. Subsequent advances in fluorescent proteins have replicated many of the properties once unique for small-molecule stains.<sup>[182]</sup> In the following chapters, the main classes of small-molecule fluorophores and the class of fluorescent proteins are described in detail.

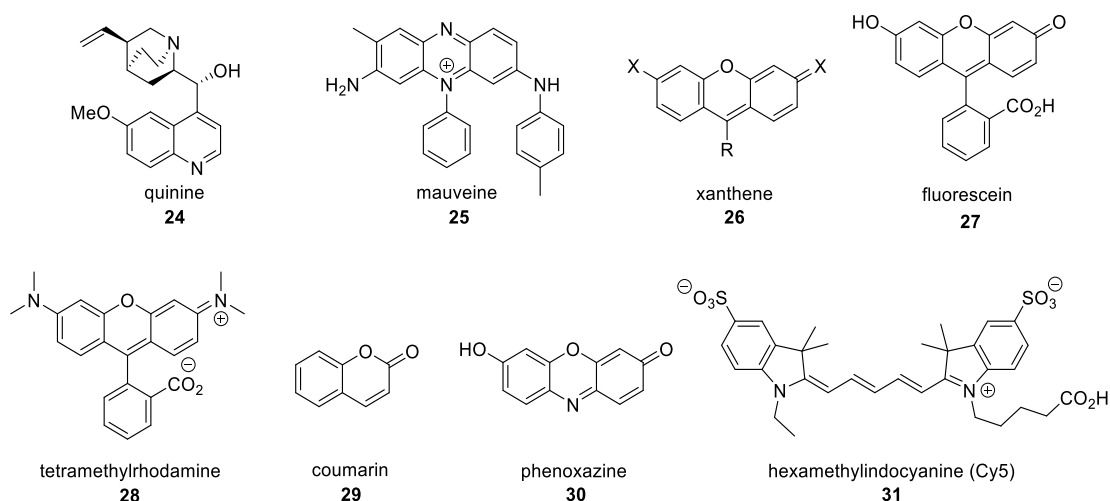


**Figure 1.13.** Molecular structure of the first fluorescent dye quinine (**24**), the first synthetic dye mauveine (**25**) and examples for the main classes of present fluorophores: xanthenes (**26**,  $X = O$ ,  $X = NR_2$ ), fluorescein (**27**), rhodamine (**28**), coumarin (**29**), phenoxazine (**30**) and cyanine (**31**).<sup>[182]</sup>

### 1.2.4.3 Small-Molecule Fluorophores

Several fluorophores were already introduced in the previous chapters, as some additionally function as photosensitizers or caging groups. Here, the main dye classes and their key characteristics are presented:

**Coumarins:** Coumarins (Figure 1.13, compound **29**) are a large class of natural products and pharmaceuticals,<sup>[187]</sup> which further present a suitable photolabile group. Derivatives as the thiocoumarin afford red-shifted cages (chapter 1.2.2).<sup>[81,188]</sup> Heteroatom substitution of the coumarin core on the phenolic ring yields highly fluorescent molecules.<sup>[179]</sup> 7-hydroxy-4-methylcoumarin (4-MU), for example, absorbs UV- and emits blue light under basic conditions, because the deprotonated hydroxyl group enlarged the conjugated  $\pi$ -system.<sup>[189]</sup> Halogenation of 4-MU<sup>[189]</sup> on the phenolic ring, which lowers the  $pK_a$  of the hydroxyl group, or the related 7-amino derivative are less pH sensitive.<sup>[190]</sup> *N*-acylation or *N*-alkylation of 7-amino-coumarins cause hypsochromic and bathochromic shifts and serve compounds with new properties. Coumarins find broad applications in chemical biology from assaying enzyme functions to imaging methods, self-labeling substrates or effective photolabile groups.<sup>[179]</sup>

## 1. Introduction

**Xanthenes:** Fluorescent compounds containing the xanthene moiety, a three membered ring structure bearing an oxygen in the central ring (Figure 1.13, compound **26**), serve a large class of fluorophores. Fluoresceins, rhodamines and phenoxazines are common members and described in more detail.<sup>[179]</sup>

Fluorescein (Figure 1.13, compound **27**) remains the dye of choice in modern biochemical, biological and medicinal research laboratories. In its dianionic open form it is highly fluorescent, bearing a  $pK_a$  of 6.4 and an immense quantum yield of 0.95.<sup>[179,188,191]</sup> Fluorination of fluorescein reduces the  $pK_a$ , while keeping good quantum yields, which results in more photostable and less pH sensitive derivatives.<sup>[192]</sup> Other modifications such as the replacement of the xanthene oxygen of fluorescein ( $\lambda_{max} = 490$  nm;  $\Phi = 0.95$ ) with a *gem*-dimethyl (carbofluorescein:  $\lambda_{max} = 567$  nm;  $\Phi = 0.62$ ) or a dimethylsilyl group (silafluorescein:  $\lambda_{max} = 598$  nm;  $\Phi = 0.42$ ) results in a red-shifted emission, but comes along with a decrease in quantum yield.<sup>[179]</sup> The introduction of locking groups on the phenolic oxygen connected as esters or ethers can modulate the equilibrium between open and closed form of fluoresceins. This strategy is used to prepare “caged” probes (chapter 1.2.2) or fluorogenetic substrates for many enzymes.<sup>[188,193]</sup> Several indicators for biological relevant ions were developed by modification of the fluorescein scaffold with chelating ligands.<sup>[194,195]</sup> One example is the calcium indicator Fluo-3, which is widely used in high-throughput screening to measure calcium ion fluxes in live cells.<sup>[196]</sup>

Rhodamines, the amino derivatives of fluoresceins (Figure 1.13, compound **28**), display a low pH sensitivity ( $pK_a$  4-5)<sup>[197]</sup> and tunable properties depending on the *N*-alkylation pattern.<sup>[179]</sup> Rhodamine 110, the simplest member of the class, exhibits similar fluorescence properties as fluorescein and is broadly used as fluorescent label.<sup>[198]</sup> The locked *N*-acyl rhodamine 110 is applied for measuring enzyme activity<sup>[199]</sup> and as activatable label in advanced fluorescence microscopy.<sup>[200]</sup> Replacement of the xanthene oxygen with carbon, silicon, germanium or tin shifts the spectral properties to higher wavelength due to the stabilization of the  $\pi$ -system LUMO and was applied in cells and whole animals.<sup>[201,202]</sup> Introduction of morpholine and piperidine substituents allow the access to cell type-specific fluorescent stains.<sup>[203]</sup> By pairing the rhodamine with the fluorescein dye, FRET-based experiments are possible and commonly applied in DNA sequencing.<sup>[179]</sup>

Phenoxazines (Figure 1.13, compound **30**) possess next to the xanthene oxygen an additional nitrogen atom in the central ring. This additional nitrogen atom results in a bathochromic shift compared to xanthene.<sup>[188]</sup> They are sensitive to the polarity of the medium and find applications as histochemical stains, lasers and fluorescent probes.<sup>[188,204]</sup> One representative of this class is resorufin, which is pH sensitive with a  $pK_a$  of 5.8.<sup>[205]</sup> Its locked derivatives serve as enzyme substrates<sup>[206]</sup> and photoactivatable compounds.<sup>[207]</sup> As it also undergoes facile redox chemistry and as well the reduced as also the oxidized form are non-fluorescent, it can be applied as a substrate for e.g. peroxidases<sup>[208]</sup> or as a cell-viability stain. Resazurin, another phenoxazine derivative, is reduced to its fluorescent analog inside living cells.<sup>[209]</sup>

**BODIPYs:** BODIPYs, (Figure 1.3, compound **4**) possess characteristics such as neutral charge, a small stokes shift, lipophilicity and an environment independent fluorescence.<sup>[184]</sup> Especially their halogenated derivatives further serve as good photosensitizers. Its higher photostability compared to fluorescein

## 1. Introduction

turns it into a suitable dye for many applications.<sup>[184,188]</sup> Especially as a fluorescent label, it serves highly useful in several analysis techniques.<sup>[210]</sup> To adjust its spectral properties it can be modified in numerous positions.<sup>[179]</sup>

**Cyanines:** Cyanine dyes (Figure 1.13, compound **31**) are molecules bearing a polymethine chain between two heterocyclic nitrogens (e.g.  $R_2N-(CH=CH)_n-CH=N^+R_2$ ).<sup>[179]</sup> Numerous examples of cyanine dyes were developed during the last decades, offering emission properties over the whole visible spectra (Figure 1.14).<sup>[211]</sup> They usually have high extinction coefficients (e.g. Cy3:  $\epsilon = 130000 \text{ M}^{-1}\text{cm}^{-1}$ ), excellent photostability<sup>[188]</sup> and are used as labels,<sup>[212]</sup> DNA stains<sup>[213]</sup> and membrane potential sensors.<sup>[214,215]</sup> The most common examples are the CyDyes, which are based on a sulfoindocyanine structure. Their different derivatives are named after their number of carbon atoms between the dihydroindole units. A higher number of methine carbons enlarge the  $\pi$ -system, which results in higher emission wavelength. For example, Cy3 emits at 568 nm, Cy5 at 672 nm and Cy7 at 788 nm. Further fine tuning of the spectral properties can be performed by changing the type of aromatic rings or its substituents.<sup>[179]</sup> The combination of CyDyes can be used as FRET pairs.<sup>[216]</sup>

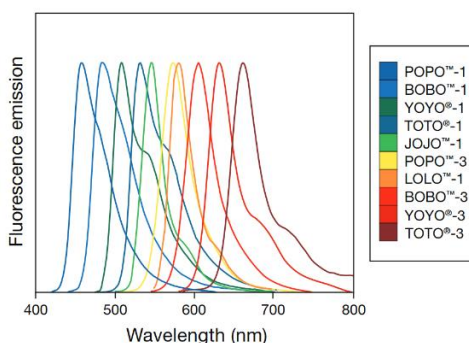
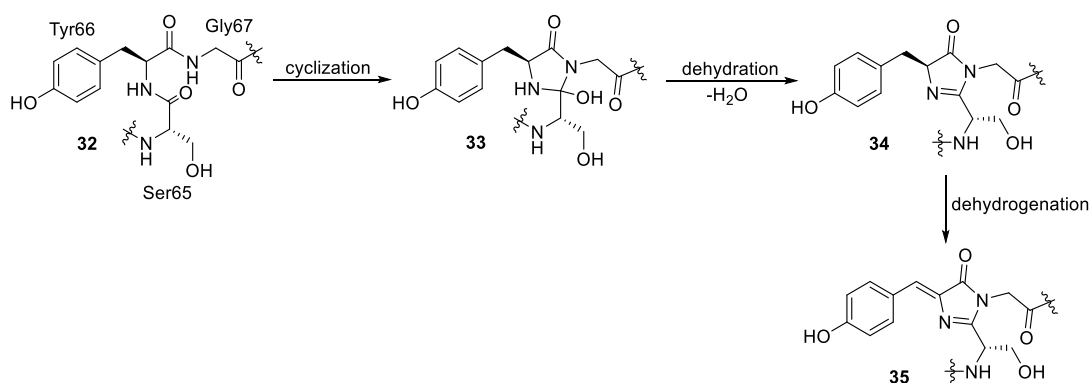


**Figure 1.14.** Emission spectra of different cyanine dye dimer derivatives, displaying their broad application range with emission spectra over the whole visible spectrum.<sup>[211]</sup>

### 1.2.4.4 Fluorescent Proteins

The first discovered fluorescent protein was the green fluorescent protein (GFP) in the 1960s during studies on the bioluminescent properties of *aequorea victoria* jellyfish. Shimomura and coworkers isolated the bioluminescent protein aequorin, which was named green fluorescent protein.<sup>[217]</sup> The fluorescent proteins (FP) are  $\sim 25 \text{ kDa}$  in size.<sup>[224]</sup> Whereas the whole protein consists out of an extreme rigid  $\beta$ -barrel-fold of 11  $\beta$ -sheets and a central  $\alpha$ -helix,<sup>[218]</sup> the principle chromophore is formed out of few crucial amino acids in the center of the  $\beta$ -barrel: after folding of the protein, the amide-nitrogen of glycine at the position 67 forms in a nucleophilic attack to the carbonyl of serine at the position 65 an imidazolinone, followed by dehydration. Dehydrogenation of the  $\alpha$ - $\beta$ -bond of tyrosine at position 66 sets the aromatic ring of the tyrosine into conjugation with the imidazolinone, which leads to the chromophore *p*-hydroxybenzylideneimidazolinone responsible for the green fluorescence (Scheme 1.1).<sup>[219]</sup>

## 1. Introduction



**Scheme 1.1.** Mechanism for the formation of *p*-hydroxybenzylideneimidazolinone out of the amino acid residues Ser65, Tyr66 and Gly67. These residues undergo cyclization, dehydration and a final dehydrogenation.<sup>[219]</sup>

Analysis of over 100 naturally occurring chromophore variants demonstrated that only four amino acids are highly conserved: glycine at the position 67 and tyrosine at the position 66 to form the chromophore itself and arginine at the position 96 and glutamic acid at the position 222 as catalytic residues located in close proximity to the formed chromophore.<sup>[220]</sup>

It was 30 years later when GFP had been cloned<sup>[221]</sup> and used as a fluorescent tag in bacteria gene expression,<sup>[222]</sup> when it became a unique tool for biological and medical imaging approaches. Since then, protein engineering based on GFP assisted in improving and varying the biochemical properties. Nowadays, fluorescent proteins cover the emission range over the whole visible spectrum.<sup>[223,224]</sup> These achievements were recognized by the Noble Prize in 2008.<sup>[225]</sup> Protein engineering of the remaining residues of the protein changed the local surrounding of the chromophore, yielding in broad variations in spectral characteristics, photostability, acid resistance and other physical properties.<sup>[224]</sup> Further explorations of marine organisms such as the mushroom anemone *discosoma striata* and the sea anemone *entacmaea quadricolor* even resulted in orange, red and far-red FPs.<sup>[223]</sup> The FP fused to another protein allows its own study of localization, movement and turnover. By addressing specific cell organelles it further enables visualization of their morphology, fusion and fission and segregation during cell division. They are applied for cell and tissue labeling and are used to label whole organisms, which allows the discrimination between transgenic and wild-type organisms. They enable visualization of enzymatic activity (e.g. kinases) or measurements for ion, metabolite and messenger concentrations (e.g. H<sup>+</sup>, Ca<sup>2+</sup>, Cl<sup>-</sup>, H<sub>2</sub>O<sub>2</sub>, cAMP).<sup>[224]</sup> By the use of different FP, FRET experiments<sup>[226]</sup> open further possibilities to study phenomena such as protein-protein-interactions.<sup>[226]</sup> Even though brighter fluorescent proteins were found in sharks,<sup>[227]</sup> the need for genetic manipulation and factors such as brightness and stability, still make the use of small-molecule fluorophores more appealing.<sup>[182,224]</sup>

## 1. Introduction

### 1.2.4.5 dsDNA Sensors

Many fluorescent sensors are based on environment sensitive fluorophores capable to interact with the dsDNA. They display low intrinsic fluorescence in aqueous media and a large fluorescence increase (fluorogenic dyes) or color change (solvatochromic dyes) upon DNA binding due to changes in the microenvironment such as polarity, viscosity and molecular order.<sup>[228]</sup> The dependence of fluorescence intensity on the surrounding environment can be reasoned by charge-transfer, intramolecular proton transfer, conformational changes, ground-state isomerization or aggregation effects of the fluorescent probe.<sup>[228]</sup> In the case of most dsDNA sensors, aggregation is often the reason for the decreased fluorescence in aqueous solution. The flat aromatic  $\pi$ -system of the sensors has a high tendency to form non-fluorescent H-aggregates.<sup>[229]</sup> In polar solvents, such as water, the aggregation-based quenching is favored. In contrast, in apolar solvents or environments such as inside the DNA, the dyes can disassemble, to yield fluorescence. The aggregation can be intramolecular as seen for the cyanine dye oxazole yellow dimer (YOYO-1) or intermolecular in monomeric dyes such as thiazole orange (TO).<sup>[228,230]</sup> One of the most popular and widely used dsDNA sensors is ethidium bromide (EtBr, Figure 1.15, compound **36**). It was one of the first commercially available dyes and is comparably inexpensive. By intercalating into the DNA, the microenvironment of the stain is changed and its fluorescence turned-on. This property is mainly used in gel electrophoresis to visualize dsDNA. In addition, the low intrinsic fluorescence allows the use without gel destaining. The toxicity for living systems reasoned the use of pretended safer, but more expensive DNA stains. However, it was shown that ethidium bromide is not a human mutagen and alternatives are sometimes even more toxic.<sup>[231,232]</sup>

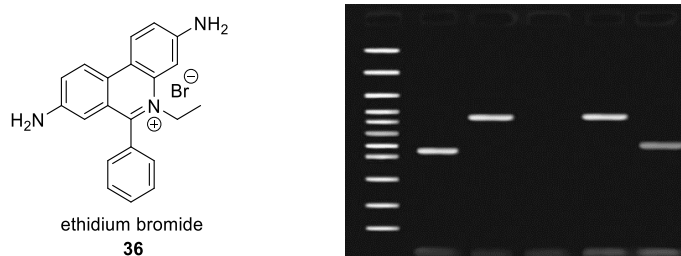


**Figure 1.15.** Left: Molecular structure of ethidium bromide. Right: agarose gel after gel electrophoresis stained with ethidium bromide. Stained lanes are a 100 bp ladder (Fermentas, Germany) and 494 bp and 734 bp PCR product samples.<sup>[233]</sup>

4',6'-diamidino-2-phenylindole dihydrochloride hydrate (DAPI, Figure 1.16, compound **37**) is a blue emitting stain that binds into the minor groove of the DNA and allows in vitro and in vivo staining. It often finds application to stain the cell nucleus in fluorescence microscopy.<sup>[231]</sup>



## 1. Introduction

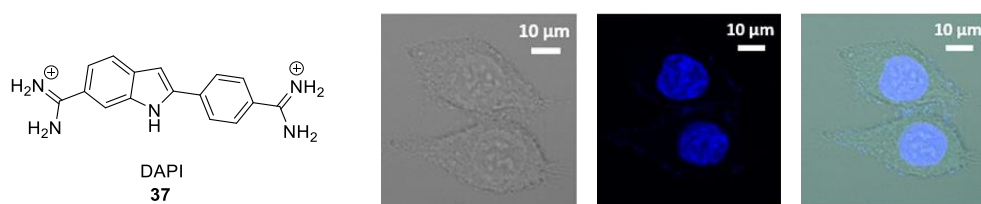


**Figure 1.16.** Left: Molecular structure of DAPI. Right: Confocal image of DAPI stained HeLa cells as bright field, DAPI-stained and merge picture.<sup>[234]</sup>

A rather modern DNA stain is represented by SYBR Green, a thiazole orange derived compound.<sup>[235]</sup> Its manufacturer Molecular Probes offers two different versions for DNA and RNA staining. It stains gels more sensitive than EtBr and reveals a supposed lower mutagenicity. These advantages come along with a high increase in costs.<sup>[231]</sup>

SyTO-9, a different dye manufactured by Molecular Probes, is a green-fluorescent nucleic acid stain for live and dead eukaryotic cells, as well as gram-positive and gram-negative bacteria. It displays a low intrinsic fluorescence with a quantum yield less than 0.01, which is strongly enhanced upon nucleic acid binding with quantum yields higher than 0.4.<sup>[236,237]</sup> All structural features of the compound are strongly protected by a patent. SyTO-9 was used to label live bacteria for macrophage uptake assays.<sup>[238,239]</sup> However, reduced colony formation was observed.<sup>[238]</sup>

### 1.3 References

---

- [1] van Dyke, A. R.; Gatazka, D. H.; Hanania, M. M. Innovations in Undergraduate Chemical Biology Education. *ACS Chem. Biol.* **2018**, *13*, 1, 26-35.
- [2] Willeford, B. F.; Das Portrait: Joseph Priestley (1733-1804). *Chem. Unserer Zeit* **1979**, *13*, 4, 111-117.
- [3] Tripp, B.; Shortlidge, E. E. A Framework to Guide Undergraduate Education in Interdisciplinary Science. *CBE Life Sci. Educ.* **2019**, *18*, 2, 1-12.
- [4] Orgill, M.; Cooper, M. M. Teaching and Learning about the Interface between Chemistry and Biology. *Chem. Educ. Res. Pract.* **2015**, *16*, 711-713.
- [5] Kean, K. M.; van Zee, K.; Mehl, R. A. Unnatural Chemical Biology: Research-Based Laboratory Course Utilizing Genetic Code Expansion. *J. Chem. Educ.* **2019**, *96*, 1, 66-74.
- [6] Auchincloss, L. C.; Laursen, S. L.; Branchaw, J. L.; Eagan, K.; Graham, M.; Hanauer, D. I.; Lawrie, G.; McLinn, C. M.; Pelaez, N.; Rowland, S.; Towns, M.; Trautmann, N. M.; Varma-Nelson, P.; Weston, T. J.; Dolan, E. L. Assessment of Course-Based Undergraduate Research Experiences: A Meeting Report. *CBE Life Sci. Educ.* **2014**, *13*, 1, 29-40.
- [7] Back to school. *Nat. Chem. Biol.* **2005**, *1*, 4, 175.
- [8] Begley, T. P. Chemical Biology: an Educational Challenge for Chemistry Departments. *Nat. Chem. Biol.* **2005**, *1*, 5, 236-238.
- [9] Miller, B. L. A Production of Amino Acids Under Possible Primitive Earth Conditions. *Science* **1953**, *117*, 3046, 528-529.
- [10] J. M. Berg, J. L. Tymoczko, L. Stryer, *Biochemie*, Elsevier GmbH, München, 6th edition, 2007, pp.603-605.
- [11] Ahmed, I.; Fruk, L. The Power of Light: Photosensitive Tools for Chemical Biology. *Mol. BioSyst.* **2013**, *9*, 565-570.
- [12] Sadave. D.; Hillis, D. M.; Heller, H. C.; Berenbaum, M. R. *Purves Biologie*, Spektrum Akademischer Verlag, Heidelberg, 9<sup>th</sup> edition, 2011, pp. 1292-1293.
- [13] Sadave. D.; Hillis, D. M.; Heller, H. C.; Berenbaum, M. R. *Purves Biologie*, Spektrum Akademischer Verlag, Heidelberg, 9<sup>th</sup> edition, 2011, p. 1045.
- [14] Zhang, N.-N.; Wang M.-S.; Guo G.-C. Photoresponsive Sulfone-Based Molecules: Photoinduced Electron Transfer and Heat/Air-Stable Radicals in the Solid State. *New J. Chem.* **2019**, *43*, 4506-4510.
- [15] Amirjalayer, S.; Buma, W. J. Light on the Structural Evolution of Photoresponsive Molecular Switches in Electronically Excited States. *Chem. Eur. J.* **2019**, *25*, 6252-6258.
- [16] Clayden, L.; Greeves, N.; Warren, S. *Organic Chemistry*, Oxford University Press, New York, 2012, 2<sup>nd</sup> edition, pp. 897, 927, 985-986.
- [17] de Assis, F. F.; Huang, X.; Akiyama, M.; Pilli, R. A.; Meggers, E. Visible-Light-Activated Catalytic Enantioselective  $\beta$ -Alkylation of  $\alpha,\beta$ -Unsaturated 2-Acyl Imidazoles Using Hantzsch Esters as Radical Reservoirs. *J. Org. Chem.* **2018**, *83*, 10922-10932.

## 1. Introduction

- 
- [18] Russew, M.-M.; Hecht, S. Photoswitches: From Molecules to Materials. *Adv. Mater.* **2010**, *22*, 31, 3348-3360.
- [19] Karcher, J.; Pianowski, Z. L. Photocontrol of Drug Release from Supramolecular Hydrogels with Green Light. *Chem. Eur. J.* **2018**, *24*, 45, 11605-11610.
- [20] Huber, L. A.; Hoffmann, K.; Thumser, S.; Böcher, N.; Mayer, P.; Dube, H. Direct Observation of Hemithioindigo-Motor Unidirectionality. *Angew. Chem. Int. Ed.* **2017**, *56*, 46, 14536-14539.
- [21] Lubbe, A. S.; Liu, Q.; Smith, S. J.; de Vries, J. W.; Kistemaker, J. C. M.; de Vries, A. H.; Faustino, I.; Meng, Z.; Szymanski, W.; Herrmann, A.; Feringa, B. L. Photoswitching of DNA Hybridization Using a Molecular Motor. *J. Am. Chem. Soc.* **2018**, *140*, 15, 5069-5076.
- [22] van Leeuwen, T.; Lubbe, A. S.; Stacko, P.; Wezenberg, S. J.; Feringa, B. L. Dynamic Control of Function by Light-Driven Molecular Motors. *Nat. Rev. Chem.* **2017**, *1*, 12, 1-7.
- [23] Broichhagen, J.; Frank, J. A.; Trauner, D. A Roadmap to Success in Photopharmacology. *Acc. Chem. Res.* **2015**, *48*, 7, 1947-1960.
- [24] Hüll, K.; Morstein, J.; Trauner, D. *In Vivo* Photopharmacology. *Chem. Rev.* **2018**, *118*, 21, 10710-10747.
- [25] Lerch, M. M.; Hansen, M. J.; van Dam, G. M.; Szymanski, W.; Feringa, B. L. Emerging Targets in Photopharmacology. *Angew. Chem. Int. Ed.* **2016**, *55*, 37, 10978-10999.
- [26] Velema, W. A.; Szymanski, W.; Feringa, B. L. Photopharmacology: Beyond Proof of Principle. *J. Am. Chem. Soc.* **2014**, *136*, 6, 2178-2191.
- [27] Brieke, C.; Rohrbach, F.; Gottschalk, A.; Mayer, G.; Heckel, A. Light-Controlled Tools. *Angew. Chem. Int. Ed.* **2012**, *51*, 34, 8446-8476
- [28] Ash, C.; Dubec, M.; Donne, K.; Bashford, T. Effect of Wavelength and Beam Width on Penetration in Light-Tissue Interaction Using Computational Methods. *Lasers Med. Sci.* **2017**, *32*, 8, 1909-1918.
- [29] Albert, L.; Vázquez, O. Photoswitchable Peptides for Spatiotemporal Control of Biological Functions. *Chem Commun.* **2019**, *55*, 10192-10213.
- [30] Moan, J.; Peng, Q. An Outline of the Hundred-Year History of PDT. *Anticancer Res.* **2003**, *23*, 3591-3600.
- [31] Abrahamse, H.; Hamblin, M. R. New Photosensitizers for Photodynamic Therapy. *Biochem. J.* **2016**, *473*, 347-364.
- [32] Dougherty, T. J.; Kaufman, J. E.; Goldfarb, A.; Weishaupt, K. R.; Boyle, D.; Mittleman, A. Photoradiation Therapy for the Treatment of Malignant Tumors. *Cancer Res.* **1978**, *38*, 8, 2628-2635.
- [33] Agostinis, P.; Berg, K.; Cengel, K. A.; Foster, T. H. Girotti, A. W.; Gollnick, S. O.; Hahn, S. M.; Hamblin, M. R.; Juzeniene, A.; Kessel, D.; Korbek, M.; Moan, J.; Mroz, P.; Nowis, D.; Piette, J.; Wilson, B. C.; Golab, J. Photodynamic Therapy of Cancer: An Update. *CA Cancer J. Clin.* **2011**, *61*, 4, 250-281.

## 1. Introduction

- 
- [34] Lawrence, K. P.; Douki, T.; Sarkany, R. P. E.; Acker, S.; Herzog, B.; Young, A. R. The UV/Visible Radiation Boundary Region (385-405 nm) Damages Skin Cells and Induces "Dark" Cyclobutane Pyrimidine Dimers in Human Skin *in vivo*. *Sci. Rep.* **2018**, *8*, 12722, 1-12.
- [35] Li, X.; Kolemen, S.; Yoon, J.; Akkaya, E. U. Activatable Photosensitizers: Agents for Selective Photodynamic Therapy. *Adv. Funct. Mater.* **2017**, *27*, 1604053.
- [36] Ludivíková, L.; Friš. P.; Heger, D.; Šebej, P.; Wirz, J.; Klán, P. Photochemistry of Rose Bengal in Water and Acetonitrile: a Comprehensive Kinetic Analysis. *Phys. Chem. Chem. Phys.* **2016**, *18*, 16266-16273.
- [37] Linden, G.; Zhang, L.; Pieck, F.; Linne, U.; Kosenkov, D.; Tonner, R.; Vázquez, O. Conditional Singlet Oxygen Generation through a Bioorthogonal DNA-targeted Tetrazine Reaction. *Angew. Chem. Int. Ed.* **2019**, *58*, 37, 12868-12873.
- [38] Lovell, J. F.; Liu, T. W. B.; Chen, J.; Zheng, G. Activatable Photosensitizers for Imaging and Therapy. *Chem. Rev.* **2010**, *110*, 2839-2857.
- [39] Gerweck, L. E.; Seetharaman, K. Cellular pH Gradient in Tumor versus Normal Tissue: Potential Exploitation for the Treatment of Cancer. *Cancer Res.* **1996**, *56*, 6, 1194-1198.
- [40] Montcourrier, P.; Silver, I.; Farnoud, R.; Bird, I.; Rochefort, H. Breast Cancer Cells Have a High Capacity to Acidify Extracellular Milieu by a Dual Mechanism. *Clin. Exp. Metastasis* **1997**, *15*, 4, 382-392.
- [41] Tian, J.; Zhou, J.; Shen, Z.; Ding, L.; Yu, J.-S.; Ju, H. A pH-Activatable and Aniline-Substituted Photosensitizer for Near-Infrared Cancer Theranostics. *Chem. Sci.* **2015**, *6*, 5969-5977.
- [42] Gallagher, W. M.; Allen, L. T.; O'Shea, C.; Kenna, T.; Hall, M.; Gorman, A.; Killoran, J.; O'Shea, D. F. A Potent Nonporphorin Class of Photodynamic Therapeutic Agent: Cellular Localisation, Cytotoxic Potential and Influence of Hypoxia. *Br. J. Cancer* **2005**, *92*, 9, 1702-1710.
- [43] Meng, L.-B.; Zhang, W.; Li, D.; Li, Y.; Hu, X.-Y.; Wang, L.; Li, G. pH-Responsive Supramolecular Vesicles Assembled by Water-Soluble Pillar[5]arene and a BODIPY Photosensitizer for Chemo-Photodynamic Dual Therapy. *Chem. Commun.* **2015**, *51*, 14381-14384.
- [44] Zhao, J.; Huang, L.; Cui, X.; Li, S.; Wu, H. Maximizing the Thiol-Activated Photodynamic and Fluorescence Imaging Functionalities of Theranostic Reagents by Modularization of Bodipy-Based Dyad Triplet Photosensitizers. *J. Mater. Chem. B* **2015**, *3*, 9194-9211.
- [45] Kolemen, S.; Işık, M.; Kim, G. M.; Kim, D.; Geng, H.; Buyuktemiz, M.; Karatas, T.; Zhang, X.-F.; Dede, Y.; Yoon, J.; Akkaya, E. U. Intracellular Modulation of Excited-State Dynamics in a Chromophore Dyad: Differential Enhancement of Photocytotoxicity Targeting Cancer Cells. *Angew. Chem. Int. Ed.* **2015**, *54*, 18, 5340-5344.
- [46] Cheng, R.; Feng, F.; Meng, F.; Deng, C.; Feijen, J.; Zhong, Z. Glutathione-Responsive Nano-Vehicles as a Promising Platform for Targeted Intracellular Drug and Gene Delivery. *J. Control. Release* **2011**, *152*, 1, 2-12.
- [47] Gamcsik, M. P.; Kasibhatla, M. S.; Teeter, S. D.; Colvin, O. M. Glutathione Levels in Human Tumors. *Biomarkers* **2012**, *17*, 8, 671-691.

## 1. Introduction

- 
- [48] Prelich, G. Gene Overexpression: Uses, Mechanisms, and Interpretation. *Genetics* **2012**, *190*, 3, 841-854.
- [49] Turk, B. Targeting Proteases: Successes, Failures and Future Prospects. *Nat. Rev. Drug Discovery* **2006**, *5*, 9, 785-799.
- [50] Chen, J.; Stefflova, K.; Niedre, M. J.; Wilson, B. C.; Chance, B.; Glickson, J. D.; Zheng, G. J. Protease-Triggered Photosensitizing Beacon Based on Singlet Oxygen Quenching and Activation. *J. Am. Chem. Soc.* **2004**, *126*, 37, 11450-11451.
- [51] Zheng, G.; Chen, J.; Stefflova, K.; Jarvi, M.; Li, H.; Wilson, B. C. Photodynamic Molecular Beacon as an Activatable Photosensitizer based on Protease-Controlled Singlet Oxygen Quenching and Activation. *Proc. Natl. Acad. Sci. U. S. A.* **2007**, *104*, 21, 8989-8994.
- [52] Lo, P.; Chen, J.; Stefflova, K.; Warren, M. S.; Navab, R.; Bandarchi, B.; Mullins, S.; Tsao, M.; Cheng, J. D.; Zheng, G. J. Photodynamic Molecular Beacon Triggered by Fibroblast Activation Protein on Cancer-Associated Fibroblasts for Diagnosis and Treatment of Epithelial Cancers. *J. Med. Chem.* **2009**, *52*, 2, 358-368.
- [53] Chen, J.; Liu, T. W. B.; Lo, P.; Wilson, B. C.; Zheng, G. "Zipper" Molecular Beacons: A Generalized Strategy to Optimize the Performance of Activatable Protease Probes. *Bioconjugate Chem.* **2009**, *20*, 10, 1836-1842.
- [54] Kelly, J. M., van der Putten, W. J.; McConnell, D. J. Laser Flash Spectroscopy of Methylene Blue with Nucleic Acids. *Photochem. Photobiol.* **1987**, *45*, 2, 167175.
- [55] Cló, E.; Snyder, J. W.; Voigt, N. V.; Ogilby, P. R.; Gothelf, K. V. DNA-Programmed Control of Photosensitized Singlet Oxygen Production. *J. Am. Chem. Soc.* **2006**, *128*, 13, 4200-4201.
- [56] Tyagi, S.; Kramer, F. R. Molecular Beacons: Probes that Fluoresce upon Hybridization. *Nat. Biotechnol.* **1996**, *14*, 3, 303-308.
- [57] Chen, J.; Lovell, J. F.; Lo, P.; Stefflova, K.; Niedre, M.; Wilson, B. C.; Zheng, G. A Tumor mRNA-Triggered Photodynamic Molecular Beacon based on Oligonucleotide Hairpin Control of Singlet Oxygen Production. *Photochem. Photobiol. Sci.* **2008**, *7*, 7, 775-781.
- [58] Pestourie, C.; Tavitian, B.; Duconge, F. Aptamers against Extracellular Targets for in vivo Applications. *Biochimie* **2005**, *87*, 9-10, 921-930.
- [59] Levy-Nissenbaum, E.; Radovic-Moreno, A. F.; Wang, A. Z.; Langer, R.; Farokhzad, O. C. Nanotechnology and Aptamers: Applications in Drug Delivery. *Trends Biotechnol.* **2008**, *26*, 8, 442-449.
- [60] Zhu, Z.; Tang, Z.; Phillips, J. A.; Yang, R.; Wang, H.; Tan, W. Regulation of Singlet Oxygen Generation Using Single-Walled Carbon Nanotubes. *J. Am. Chem. Soc.* **2008**, *130*, 33, 10856-10857.
- [61] Shi, L.; Hernandez, B.; Selke, M. Singlet Oxygen Generation from Water-Soluble Quantum Dot-Organic Dye Nanocomposites. *J. Am. Chem. Soc.* **2006**, *128*, 19, 6278-6279.
- [62] Lucky, S. S.; Soo, K. C.; Zhang, Y. Nanoparticles in Photodynamic Therapy. *Chem. Rev.* **2015**, *115*, 4, 1990-2042.

## 1. Introduction

- 
- [63] Barton, D. H. R.; Chow, Y. L.; Cox, A.; Kirby, G. W. Photosensitive Protection of Functional Groups. *Tetrahedron Lett.* **1962**, *23*, 1055-1057.
- [64] Barltrop, J. A.; Schofield, P. Photosensitive Protecting Groups *Tetrahedron Lett.* **1962**, *16*, 697-699.
- [65] Sheehan, J. C.; Wilson, R. M. Photolysis of Desyl Compounds. A New Photolytic Cyclization *J. Am. Chem. Soc.* **1964**, *86*, 23, 5277-5281.
- [66] Engels, J.; Schlaeger, E. J. Synthesis, Structure, and Reactivity of Adenosine Cyclic 3',5'-Phosphate-benzyltriesters *J. Med. Chem.* **1977**, *20*, 7, 907-911.
- [67] Kaplan, J. H.; Forbush, B.; Hoffman, J. F. Rapid Photolytic Release of Adenosine 5'-triphosphate from a Protected Analog: Utilization by the Sodium:Potassium Pump of Human Red Blood Cell Ghosts. *Biochemistry* **1978**, *17*, 10, 1929-1935.
- [68] Mayer, G.; Heckel, A. Biologically Active Molecules with a „Light Switch“. *Angew. Chem. Int. Ed.* **2006**, *45*, 30, 4900-4921.
- [69] Klán, P.; Šolomek, T.; Bochet, C. G.; Blanc A.; Givens, R.; Rubina, M.; Popik, V.; Kostikov, A.; Wirz, J. Photoremovable Protecting Groups in Chemistry and Biology: Reaction Mechanisms and Efficacy. *Chem. Rev.* **2013**, *113*, 119-191.
- [70] Yu, H.; Li, J.; Wu, D.; Qiu, Z.; Zhang, Y. Chemistry and Biological Applications of Photo-Labile Organic Molecules. *Chem. Soc. Rev.* **2010**, *39*, 2, 464-473.
- [71] Lee, H.-M.; Larson, D. R.; Lawrence, D. S. Illuminating the Chemistry of Life: Design, Synthesis, and Applications of “Caged” and Related Photosensitive Compounds. *ACS Chem. Biol.* **2009**, *4*, 6, 409-427.
- [72] Hansen, M. J.; Velema, W. A.; Lerch, M. M.; Szymanski, W.; Feringa, B. L. Wavelength-Selective Cleavage of Photoprotecting Groups: Strategies and Applications in Dynamic Systems. *Chem. Soc. Rev.* **2015**, *44*, 11, 3358-3377.
- [73] Pelliccioli, A. P.; Wirz, J. Photoremovable Protecting Groups: Reaction Mechanisms and Applications. *Photochem. Photobiol. Sci.* **2002**, *1*, 7, 441-458.
- [74] Corrie, J. E. T.; Barth, A.; Munasinghe, V. R. N.; Trentham, D. R.; Hutter, M. C. Photolytic Cleavage of 1-(2-Nitrophenyl)ethyl Ethers Involves Two Parallel Pathways and Product Release Is Rate-Limited by Decomposition of a Common Hemiacetal Intermediate. *J. Am. Chem. Soc.* **2003**, *125*, 28, 8546-8554.
- [75] Bochet, C. G. Wavelength-Selective Cleavage of Photolabile Protecting Groups. *Tetrahedron Lett.* **2000**, *41*, 6341-6346.
- [76] Stanton-Humphreys, M. N.; Taylor, R. D. T.; McDougall, C.; Hart, M. L.; Brown, C. T. A.; Emptage, N. J.; Conway, S. J. Wavelength-Orthogonal Photolysis of Neurotransmitters *in vivo*. *Chem. Commun.* **2012**, *48*, 657-659.
- [77] Pirrung, M. C.; Lee, Y. R.; Park, K.; Springer, J. B. Pentadienylnitrobenzyl and Pentadienylnitropiperonyl Photochemically Removable Protecting Groups. *J. Org. Chem.* **1999**, *64*, 5042-5047.

## 1. Introduction

- 
- [78] Hagen, V.; Frings, S.; Wiesner, B.; Helm, S.; Kaupp, U. B.; Bending, J. [7-(Dialkylamino)coumarin-4-yl]methyl-Caged Compounds as Ultrafast and Effective Long-Wavelength Phototriggers of 8-Bromo-Substituted Cyclic Nucleotides. *ChemBioChem* **2003**, *4*, 434-442.
- [79] Givens, R. S.; Rubina, M.; Wirz, J. Applications of *p*-Hydroxyphenacyl (*p*HP) and Coumarin-4-ylmethyl Photoremovable Protecting Groups. *Photochem. Photobiol. Sci.* **2012**, *11*, 3, 472- 488.
- [80] Schultz, C. Molecular Tools for Cell and Systems Biology. *HFSP J.* **2007**, *1*, 4, 230- 248.
- [81] Fournier, L.; Gauron, C.; Xu, L.; Aujard, I.; Le Saux, T.; Gagey-Eilstein, N.; Maurin, S.; Dubrulle, S.; Baudin, J.-B.; Bensimon, D.; Volovitch, M.; Vríz, S.; Jullien, L. A Blue-Absorbing Photolabile Protecting Group for *in Vivo* Chromatically Orthogonal Photoactivation. *ACS Chem. Biol.* **2013**, *8*, 7, 1528-1536.
- [82] Howerton, B. S.; Heidary, D. K.; Glazer, E. C. Strained Ruthenium Complexes Are Potent Light-Activated Anticancer Agents. *J. Am. Chem. Soc.* **2012**, *134*, 20, 8324-8327.
- [83] Filevich, O.; Etchenique, R. RuBiGABA-2: a Hydrophilic Caged GABA with Long Wavelength Sensitivity. *Photochem. Photobiol. Sci.* **2013**, *12*, 1565-1570.
- [84] Carling, C.-J.; Olejniczak, J.; Foucault-Collet, A.; Collet, G.; Viger, M. L.; Huu, V. A. N.; Duggan, B. M.; Almutairi, A. Efficient Red Light Photo-Uncaging of Active Molecules in Water upon Assembly into Nanoparticles. *Chem. Sci.* **2016**, *7*, 2392-2398.
- [85] Wang, X.; Kalow, J. A. Rapid Aqueous Photouncaging by Red Light. *Org. Lett.* **2018**, *20*, 7, 1716-1719.
- [86] Peterson, J. A.; Wijesooriya, C.; Gehrman, E. J.; Mahoney, K. M.; Goswami, P. P.; Albright, T. R.; Syed, A.; Dutton, A. S.; Smith, E. A.; Winter, A. H. Family of BODIPY Photocages Cleaved by Single Photons of Visible/Near-Infrared Light. *J. Am. Chem. Soc.* **2018**, *140*, 23, 7343-7346.
- [87] Göppert-Mayer, M. Elementary Processes with Two Quantum Transitions. *Ann. Phys.* **2009**, *18*, 466-479.
- [88] Kauffman, J. F.; Turner, J. M.; Alabugin, I. V.; Breiner B.; Kovalenko, S. V.; Badaeva, E. A.; Masunov, A.; Tretiak, S. Two-Photon Excitation of Substituted Eneidyne. *J. Phys. Chem. A* **2006**, *110*, 1, 241-251.
- [89] König, K. J. Multiphoton Microscopy in Life Sciences. *J. Microsc.* **2000**, *200*, 83- 104.
- [90] Bochet, C. G. Wavelength-Selective Cleavage of Photolabile Protecting Groups. *Tetrahedron Lett.* **2000**, *41*, 6341-6346.
- [91] Hansen, M. J.; Velema, W. A.; Lerch, M. M.; Szymanski, W.; Feringa, B. L. Wavelength-Selective Cleavage of Photoprotecting Groups: Strategies and Applications in Dynamic Systems. *Chem Soc. Rev.* **2015**, *44*, 3358-3377.
- [92] Rodrigues-Correia, A.; Weyel, X. M. M.; Heckel, A. Four Levels of Wavelength-Selective Uncaging for Oligonucleotides. *Org. Lett.* **2013**, *15*, 21, 5500-5503.
- [93] Priestman, M. A.; Sun, L.; Lawrence, D. S. Dual Wavelength Photoactivation of cAMP- and cGMP-Dependent Protein Kinase Signaling Pathways. *ACS Chem. Biol.* **2011**, *6*, 4, 377-384.
- [94] Kotzur, N.; Briand, B.; Beyermann, M.; Hagen, V. Wavelength-Selective Photoactivatable Protecting Groups for Thiols. *J. Am. Chem. Soc.* **2009**, *131*, 46, 16927-16931.

## 1. Introduction

- 
- [95] See for example <http://www.molecularprobes.com>
- [96] Young, D. D.; Deiters, A. Photochemical Activation of Protein Expression in Bacterial Cells. *Angew. Chem. Int. Ed.* **2007**, *46*, 23, 4290-4292.
- [97] Cambridge S. B.; Geissler D.; Calegari F.; Anastassiadis K.; Hasan, M. T.; Stewart, A. F. Huttner, W. B.; Hagen, V.; Bonhoeffer, T. Doxycycline-Dependent Photoactivated Gene Expression in Eukaryotic Systems. *Nat. Methods* **2009**, *6*, 527-531.
- [98] Asrican, B.; Lisman, J.; Otmakhov, N. Synaptic Strength of Individual Spines Correlates with Bound Ca<sup>2+</sup>-Calmodulin-Dependent Kinase II. *J. Neurosci.* **2007**, *27*, 51, 14007-14011.
- [99] Shankar, G. M.; Bloodgood, B. L.; Townsend, M.; Walsh, D. M.; Selkoe, D. J.; Sabatini, B. L. Natural Oligomers of the Alzheimer Amyloid- $\beta$  Protein Induce Reversible Synapse Loss by Modulating an NMDA-Type Glutamate Receptor-Dependent Signaling Pathway. *J. Neurosci.* **2007**, *27*, 11, 2866-2875.
- [100] Kantevari, S.; Matsuzaki, M.; Kanemoto, Y.; Kasai, H.; Ellis-Davies, G. C. R. Two-Color, Two-Photon Uncaging of Glutamate and GABA. *Nat. Methods* **2010**, *7*, 2, 123-125.
- [101] Bönigk, W.; Loogan, A.; Seiffert, R.; Kashikar, N.; Klemm, C.; Krause, E.; Hagen, V.; Kremmer, E.; Strünker, T.; Kaupp, U. B. An Atypical CNG Channel Activated by a Single cGMP Molecule Controls Sperm Chemotaxis. *Science Signaling* **2009**, *94*, 2, 1-8.
- [102] Kantevari, S.; Hoang, C. J.; Ogrodnik, J.; Egger, M.; Niggli, E.; Ellis-Davies, G. C. R. Synthesis and Two-Photon Photolysis of 6-(*ortho*-Nitroveratryl)-Caged IP<sub>3</sub> in Living Cells. *ChemBioChem* **2006**, *7*, 174-180.
- [103] Kantevari, S.; Buskila, Y.; Ellis-Davies, G. C. R. Synthesis and Characterization of Cell-Permeant 6-Nitrodibenzofuranyl-caged IP<sub>3</sub>. *Photochem. Photobiol. Sci.* **2012**, *11*, 508-513.
- [104] Ellis-Davies, G. C. R. Neurobiology with Caged Calcium. *Chem. Rev.* **2008**, *108*, 1603-1613.
- [105] Ciesienki, K. L.; Hyman, L. M.; Yang, D. T.; Haas, K. L.; Dickens, M. G.; Holbrook, R. J.; Franz, K. J. A Photo-Caged Platinum(II) Complex That Increases Cytotoxicity upon Light Activation. *Eur. J. Inorg. Chem.* **2010**, *15*, 2224-2228.
- [106] Park, S.; Bando, T.; Shinohara, K.-I.; Nishijima, S.; Sugiyama, H. Photocontrollable Sequence-Specific DNA Alkylation by a Pyrrole-Imidazole Polyamide *seco*-CBI Conjugate. *Bioconjugate Chem.* **2011**, *22*, 2, 120-124.
- [107] Dai, Z.; Dulyaninova, N. G.; Kumar, S.; Bresnick, A. R.; Lawrence, D. S. Visual Snapshot of Intracellular Kinase Activity at the Onset of Mitosis. *Chem. Biol.* **2007**, *14*, 11, 1254-1260.
- [108] Lee, H.-M.; Xu, W.; Lawrence, D. S. Construction of a Photoactivatable Profluorescent Enzyme Via Proximity Labeling. *J. Am. Chem. Soc.* **2011**, *133*, 8, 2331-2333.
- [109] Mizukami, S.; Hosoda, M.; Satake, T.; Okada, S.; Hori, Y.; Furuta, T.; Kikuchi, K. Photocontrolled Compound Release System Using Caged Antimicrobial Peptide. *J. Am. Chem. Soc.* **2010**, *132*, 28, 9524-9525.
- [110] Kuner, T.; Li, Y.; Gee, K.R.; Bonewald, L. F.; Augustine, G. J. Photolysis of a Caged Peptide Reveals Rapid Action of *N*-ethylmaleimide Sensitive Factor before Neurotransmitter Release. *Proc. Natl. Acad. Sci. USA* **2008**, *105*, 1, 347-352.



## 1. Introduction

- 
- [111] Parker, L. L.; Kurutz, J. W.; Kent, S. B. H.; Kron, S. J. Control of the Yeast Cell Cycle with a Photocleavable  $\alpha$ -Factor Analogue. *Angew. Chem. Int. Ed.* **2006**, *45*, 38, 6322-6325.
- [112] Toebe, M.; Coccoris, M.; Bins, A.; Rodenko, B.; Gomez, R.; Nieuwkoop, N. J.; van de Kastele, W.; Rimmelzwaan, G. F.; Haanen, J. B. A. G.; Ovaa, H.; Schumacher, T. N. M. Design and Use of Conditional MHC Class I Ligands. *Nat. Med.* **2006**, *12*, 2, 246-251.
- [113] Gatterdam, V.; Stoess, T.; Menge, C.; Heckel, A. Tampé, R. Caged Glutathione – Triggering Protein Interaction by Light. *Angew. Chem. Int. Ed.* **2012**, *51*, 16, 3960-3963.
- [114] Shembekar, V. R.; Chen, Y.; Carpenter, B. K.; Hess, G. P. A Protecting Group for Carboxylic Acids That Can Be Photolyzed by Visible Light. *Biochemistry* **2005**, *44*, 19, 7107-7114.
- [115] Nandy, S.K.; Agnes, R. S.; Lawrence, D. S. Photochemically-Activated Probes of Protein-Protein Interactions. *Org. Lett.* **2007**, *9*, 12, 2249-2252.
- [116] Tatsu, Y.; Shigeri, Y.; Sogabe, S.; Yumoto, N.; Yoshikawa, S. Solid-Phase Synthesis of Caged Peptides Using Tyrosine Modified with a Photocleavable Protecting Group: Application to the Synthesis of Caged Neuropeptides Y. *Biochem. Biophys. Res. Commun.* **1996**, *227*, 3, 688-693.
- [117] Wang, Q.; Dai, Z.; Cahill, S. M.; Blumenstein, M.; Lawrence, D. S. Light-Regulated Sampling of Protein Tyrosine Kinase Activity. *J. Am. Chem. Soc.* **2006**, *128*, 43, 14016-14017.
- [118] Wu, N.; Deiters, A.; Cropp, T. A.; King, D.; Schultz, P. G. A Genetically Encoded Photocaged Amino Acid. *J. Am. Chem. Soc.* **2004**, *126*, 44, 14306-14307.
- [119] Spicer, C. D.; Davis, B. G. Selective Chemical Protein Modification. *Nat. Commun.* **2014**, *5*, 4740, 1-14.
- [120] Tang, X.; Dmochowski, I. J. Regulating Gene Expression with Light-Activated Oligonucleotides. *Mol. Biosyst.* **2007**, *3*, 100-110.
- [121] Deiters, A.; Garner, R. A.; Lusic, H.; Govan, J. M.; Dush, M.; Nascone-Yoder, N. M.; Yoder, J. A. Photocaged Morpholino Oligomers for the Light-Regulation of Gene Function in Zebrafish and *Xenopus* Embryos. *J. Am. Chem. Soc.* **2010**, *132*, 44, 15644-15650.
- [122] Famulok, M.; Hartig, J. S.; Mayer, G. Functional Aptamers and Aptazymes in Biotechnology, Diagnostics, and Therapy. *Chem. Rev.* **2007**, *107*, 9, 3715-3743.
- [123] Wang, C.; Zhu, Z.; Song, Y.; Lin, H.; Yang, C. J.; Tan, W. Caged Molecular Beacons: Controlling Nucleic Acid Hybridization with Light. *Chem. Commun.* **2011**, *47*, 5708-5710.
- [124] Lubbe, A. S.; Szymanski, W.; Feringa, B. L. Recent Developments in Reversible Photoregulation of Oligonucleotide Structure and Function. *Chem. Soc. Rev.* **2017**, *46*, 1052-1079.
- [125] Lewis, K. Platforms for Antibiotic Discovery. *Nat. Rev. Drug Discovery* **2013**, *12*, 5, 371-387.
- [126] Hanahan, D.; Weinberg, R. A. Hallmarks of Cancer: the Next Generation. *Cell* **2011**, *144*, 5, 646-674.
- [127] Gaudana, R.; Ananthula, H. K.; Parenky, A.; Mitra, A. K. Ocular Drug Delivery. *AAPS J.* **2010**, *12*, 3, 348-360.
- [128] Brazil, R. Photopharmacology: Using Light to Activate Drugs. *The Pharmaceutical Journal* **2017**, *298*, 7898, 1-9.

## 1. Introduction

- 
- [129] Szymański, W.; Beierle, J. M.; Kistemaker, H. A. V.; Velema, W. A.; Feringa, B. L. Reversible Photocontrol of Biological Systems by the Incorporation of Molecular Photoswitches. *Chem. Rev.* **2013**, *113*, 8, 6114-6178.
- [130] Broichhagen, J.; Frank, J. A.; Trauner, D. A Roadmap to Success in Photopharmacology. *Acc. Chem. Res.* **2015**, *48*, 7, 1947-1960.
- [131] Mart, R. J.; Allemann, R. K. Azobenzene Photocontrol of Peptides and Proteins. *Chem. Commun.* **2016**, *52*, 83, 12262-12277.
- [132] Morstein, J.; Awale, M.; Reymond, J.-L.; Trauner, D. Mapping the Analog Space Enables the Optical Control of New Biological Targets. *ACS Cent. Sci.* **2019**, *5*, 4, 607-618.
- [133] Waldeck, D. H. Photoisomerization Dynamics of Stilbenes in Polar Solvents. *J. Mol. Liq.* **1993**, *57*, 127-148.
- [134] Cammenga, H. K.; Emel'yanenko, V. N.; Verevkin, S. P. Re-investigation and Data Assessment of the Isomerization and 2,2'-Cyclization of Stilbenes and Azobenzenes. *Ind. Eng. Chem. Res.* **2009**, *48*, 22, 10120-10128.
- [135] Wiedbrauk, S.; Dube, H. Hemithioindigo – an Emerging Photoswitch. *Tetrahedron Lett.* **2015**, *56*, 29, 4266-4274.
- [136] Berkovic, G.; Krongauz, V.; Weiss, V. Spiropyrans and Spirooxazines for Memories and Switches. *Chem. Rev.* **2000**, *100*, 5, 1741-1754.
- [137] Lukyanov, B. S.; Lukyanova, M. B. Spiropyran: Synthesis, Properties, and Application. (Review). *Chem. Heterocycl. Compd.* **2005**, *41*, 3, 281-311.
- [138] Flannery J. B. Photo- and Thermochromic Transients from Substituted 1',3',3'-Trimethylindolinobenzospiropyrans. *J. Am. Chem. Soc.* **1968**, *90*, 21, 5660-5671.
- [139] Chibisov, A. K.; Görner, H. Photoprocesses in Spiropyran-Derived Merocyanines. *J. Phys. Chem. A* **1997**, *101*, 24, 4305-4312.
- [140] Levitus, M.; Glaser, G.; Neher, D.; Aramendía, P. F. Direct Measurement of the Dipole Moment of a Metastable Merocyanine by Electromechanical Interferometry. *Chem. Phys. Lett.* **1997**, *277*, 1-3, 118-124.
- [141] Bletz, M.; Pfeifer-Fukumura, U.; Kolb, U.; Baumann, W. Ground- and First-Excited-Singlet-State Electric Dipole Moments of Some Photochromic Spirobenzopyrans in Their Spiropyran and Merocyanine Form. *J. Phys. Chem. A* **2002**, *106*, 10, 2232-2236.
- [142] Andersson, J.; Li, S.; Lincoln, P.; Andréasson, J. Photoswitched DNA-Binding of a Photochromic Spiropyran. *J. Am. Chem. Soc.* **2008**, *130*, 36, 11836-11837.
- [143] Gilat, S. L.; Kawai, S. H.; Lehn, J. M. Light-Triggered Molecular Devices: Photochemical Switching of Optical and Electrochemical Properties in Molecular Wire Type Diarylethene Species. *Chem. Eur. J.* **1995**, *1*, 5, 275-284.
- [144] Irie, M. Diarylethenes for Memories and Switches. *Chem. Rev.* **2000**, *100*, 5, 1685-1716.
- [145] Santiago, A.; Becker, R. S. Photochromic Fulgides. Spectroscopy and Mechanism of Photoreactions. *J. Am. Chem. Soc.* **1968**, *90*, 14, 3654-3658.
- [146] Yokoyama, Y. Fulgides for Memories and Switches. *Chem. Rev.* **2000**, *100*, 5, 1717-1740.

## 1. Introduction

- 
- [147] Heller, H. G.; Oliver, S. J. Photochromic Heterocyclic Fulgides. Part 1. Rearrangement Reactions of (E)- $\alpha$ -3-furylethylidene(isopropylidene)succinic Anhydride. *J. Chem. Soc., Perkin Trans. 1* **1981**, 197-201.
- [148] Darcy, P. J.; Heller, H. G.; Strydom, P. J.; Whittall, J. Photochromic Heterocyclic Fulgides. Part 2. Electrocyclic Reactions of (E)- $\alpha$ -2,5-dimethyl-3-furylethylidene(alkyl-substituted methylene)succinic Anhydride. *J. Chem. Soc., Perkin Trans. 1* **1981**, 202-201.
- [149] Lougheed, T.; Borisenko, V., Hennig, T.; Rück-Braun, K.; Woolley, G. A. Photomodulation of Ionic Current through Hemithioindigo-Modified Gramicidin Channels. *Org. Biomol. Chem.* **2004**, *2*, 2798-2801.
- [150] Yamaguchi, T.; Seki, T.; Tamaki, T.; Ichimura, K. Photochromism of Hemithioindigo Derivatives. I. Preparation and Photochromic Properties in Organic Solvents. *Bull. Chem. Soc. Jpn.* **1992**, *65*, 3, 649-656.
- [151] Fischer, E. Temperature Dependence of Photoisomerization Equilibria. Part I. Azobenzene and the Azonaphthalenes. *J. Am. Chem. Soc.* **1960**, *82*, 13, 3249-3252.
- [152] Merino, E.; Ribagorda, M. Control over Molecular Motion using the *cis-trans* Photoisomerization of the Azo Group. *Beilstein J. Org. Chem.* **2012**, *8*, 1071-1090.
- [153] Beharry, A. A.; Sadovski, O.; Woolley, G. A. Azobenzene Photoswitching without Ultraviolet Light. *J. Am. Chem. Soc.* **2011**, *133*, 49, 19684-19687.
- [154] Bléger, D.; Schwarz, J.; Brouwer, A. M.; Hecht, S. *o*-Fluoroazobenzenes as Readily Synthesized Photoswitches Offering Nearly Quantitative Two-Way Isomerization with Visible Light. *J. Am. Chem. Soc.* **2012**, *134*, 51, 20597-20600.
- [155] Siewertsen, R.; Neumann, H.; Buchheim-Stehn, B.; Herges, R.; Näther, C.; Renth, F.; Temps, F. Highly Efficient Reversible *Z-E* Photoisomerization of a Bridged Azobenzene with Visible Light through Resolved  $S_1(n\pi^*)$  Absorption Bands. *J. Am. Chem. Soc.* **2009**, *131*, 43, 15594-15595.
- [156] Dong, M.; Babalhavaeji, A.; Collins, C. V. Jarrah, K.; Sadovski, O.; Dai, Q.; Woolley, G. A. Near-Infrared Photoswitching of Azobenzenes under Physiological Conditions. *J. Am. Chem. Soc.* **2017**, *139*, 38, 13483-13486.
- [157] Knie, C.; Utecht, M.; Zhao, F.; Kulla, H.; Kovalenko, S.; Brouwer, A. M.; Saalfrank, P.; Hecht, S.; Bléger, D. *ortho*-Fluoroazobenzenes: Visible Light Switches with Very Long-Lived *Z* Isomers. *Chem. Eur. J* **2014**, *20*, 50, 16492-16501.
- [158] Samanta, S.; Beharry, A. A.; Sadovski, O.; McCormick, T. M.; Babalhavaeji, A.; Tropepe, V.; Woolley, G. A. Photoswitching Azo Compounds in Vivo with Red Light. *J. Am. Chem. Soc.* **2013**, *135*, 26, 9777-9784.
- [159] Kim, Y.; Phillips, J. A.; Liu, H.; Kang, H.; Tan, W. Using Photons to Manipulate Enzyme Inhibition by an Azobenzene-Modified Nucleic Acid Probe. *Proc. Natl. Acad. Sci. U. S. A.* **2009**, *106*, 16, 6489-6494.
- [160] Zou, Y.; Chen, J.; Zhu, Z.; Lu, L.; Huang, Y.; Song, Y.; Zhang, H.; Kang, H.; Yang, C. J. Single-Molecule Photon-Fueled DNA Nanoscissors for DNA Cleavage Based on the Regulation of Substrate Binding Affinity by Azobenzene. *Chem. Commun.* **2013**, *49*, 8716-8718.

## 1. Introduction

- 
- [161] Carmi, N.; Balkhi, S. R.; Breaker, R. R. Cleaving DNA with DN. *Proc. Natl. Acad. Sci. U. S. A.* **1998**, *95*, 5, 2233-2237.
- [162] Liu, Y.; Sen, D. Light-Regulated Catalysis by an RNA-Cleaving Deoxyribozyme. *J. Mol. Biol.* **2004**, *341*, 4, 887-892.
- [163] Stafforst, T.; Hilvert, D. Modulating PNA/DNA Hybridization by Light. *Angew. Chem. Int. Ed.* **2010**, *49*, 51, 9998-10001.
- [164] Zhang, L.; Linden, G.; Vázquez, O. In Search of Visible-Light Photoresponsive Peptide Nucleic Acids (PNAs) for Reversible Control of DNA Hybridization. *Beilstein J. Org. Chem.* **2019**, *15*, 2500-2508.
- [165] Liang, X.; Fujioka, K.; Asanuma, H. Nick Sealing by T4 DNA Ligase on a Modified DNA Template: Tethering a Functional Molecule on D-Threoninol. *Chem. Eur. J.* **2011**, *17*, 37, 10388-10396.
- [166] Nishioka, H.; Liang, X.; Kashida, H.; Asanuma, H. 2',6'-Dimethylazobenzene as an Efficient and Thermo-Stable Photo-Regulator for the Photoregulation of DNA Hybridization. *Chem. Commun.* **2007**, 4354-4356.
- [167] Fujii, T.; Kashida, H.; Asanuma, H. Analysis of Coherent Heteroclustering of Different Dyes by Use of Threoninol Nucleotides for Comparison with the Molecular Exciton Theory. *Chem. Eur. J.* **2009**, *15*, 39, 10092-10102.
- [168] Liu, M.; Asanuma, H.; Komiyama, M. Azobenzene-Tethered T7 Promoter for Efficient Photoregulation of Transcription. *J. Am. Chem. Soc.* **2006**, *128*, 3, 1009-1015.
- [169] Kamiya, Y.; Takagi, T.; Ooi, H.; Ito, H.; Liang, X.; Asanuma, H. Synthetic Gene Involving Azobenzene-Tethered T7 Promoter for the Photocontrol of Gene Expression by Visible Light. *ACS Synth. Biol.* **2015**, *4*, 4, 365-370.
- [170] Mayer-Enthart, E.; Wagenknecht, H.-A. Structure-Sensitive and Self-Assembled Helical Pyrene Array Based on DNA Architecture. *Angew. Chem. Int. Ed.* **2006**, *45*, 20, 3372-3375.
- [171] Kočalka, P.; Andersen, N. K.; Jensen, F.; Nielsen, P. Synthesis of 5-(1,2,3-Triazol-4-yl)-2'-deoxyuridines by a Click Chemistry Approach: Stacking of Triazoles in the Major Groove Gives Increased Nucleic Acid Duplex Stability. *ChemBioChem* **2007**, *8*, 17, 2106-2116.
- [172] Nguyen, T.; Brewer, A.; Stulz, E. Duplex Stabilization and Energy Transfer in Zipper Porphyrin-DNA. *Angew. Chem. Int. Ed.* **2009**, *48*, 11, 1974-1977.
- [173] Wu, L.; Koumoto, K.; Sugimoto, N. Reversible Stability Switching of a Hairpin DNA via a Photo-Responsive Linker Unit. *Chem. Commun.* **2009**, *14*, 1915-1917.
- [174] Wu, L.; He, Y.; Tang, X. Photoregulating RNA Digestion Using Azobenzene Linked Dumbbell Antisense Oligodeoxynucleotides. *Bioconjugate Chem.* **2015**, *26*, 6, 1070-1079.
- [175] Bergen, A.; Rudiuk, S.; Morel, M.; Le Saux, T.; Ihmels, H.; Baigl, D. Photodependent Melting of Unmodified DNA Using a Photosensitive Intercalator: A New and Generic Tool for Photoreversible Assembly of DNA Nanostructures at Constant Temperature. *Nano Lett.* **2016**, *16*, 1, 773-780.
- [176] Le Ny, A.-L. M.; Lee, C. T. Photoreversible DNA Condensation Using Light-Responsive Surfactants. *J. Am. Chem. Soc.* **2006**, *128*, 19, 6400-6408.

## 1. Introduction

- 
- [177] Estévez-Torres, A.; Crozatier, C.; Diguët, A.; Hara, T.; Saito, H.; Yoshikawa, K.; Baigl, D. Sequence-Independent and Reversible Photocontrol of Transcription/Expression Systems using a Photosensitive Nucleic Acid Binder. *Proc. Natl. Acad. Sci. U. S. A.* **2009**, *106*, 30, 12219-12223.
- [178] Rudiuk, S.; Saito, H. Hara, T.; Inoue, T.; Yoshikawa, K.; Baigl, D. Light-Regulated mRNA Condensation by a Photosensitive Surfactant Works as a Series Photoswitch of Translation Activity in the Presence of Small RNAs. *Biomacromolecules* **2011**, *12*, 11, 3945-3951.
- [179] Lavis, L. D.; Raines, R. T. Bright Ideas for Chemical Biology. *ACS Chem. Biol.* **2008**, *3*, 3, 142-155.
- [180] Johnson, I.; Spence, M. (eds.), *The Molecular Probes Handbook. A Guide to Fluorescent Probes and Labeling Technologies*, Life Technologies Corporation, Eugene, 11th edition, 2010, p. 3.
- [181] Jablonski, A. Efficiency of Anti-Stokes Fluorescence in Dyes. *Nature* **1993**, *131*, 839-840.
- [182] Lavis, L. D. Chemistry is Dead. Long Live Chemistry! *Biochemistry* **2017**, *56*, 39, 5165-5170.
- [183] Kaufman, T. S.; Rúveda, E. A. The Quest for Quinine: Those Who Won the Battles and Those Who Won the war. *Angew. Chem. Int. Ed.* **2005**, *44*, 6, 854-885.
- [184] Loudet, A.; Burgess, K. BODIPY Dyes and Their Derivatives: Syntheses and Spectroscopic Properties. *Chem. Rev.* **2007**, *107*, 11, 4891-4932.
- [185] Panchuk-Voloshina, N.; Haugland, R. P.; Bishop-Stewart, J.; Bhalgat, M. K.; Millard, P. J.; Mao, F.; Leung, W.-Y.; Haugland, R. P. Alexa Dyes, a Series of New Fluorescent Dyes that Yield Exceptionally Bright, Photostable Conjugates. *J. Histochem. Cytochem.* **1999**, *47*, 9, 1179-1188.
- [186] Mujumdar, R. B.; Ernst, L. A.; Mujumdar, S. R.; Lewis, C. J.; Waggoner, A. S. Cyanine Dye Labeling Reagents: Sulfoindocyanine succinimidyl Esters. *Bioconjugate Chem.* **1993**, *4*, 2, 105-111.
- [187] Riveiro, M.; De Kimpe, N.; Moglioni, A.; Vázquez, R.; Monczur, F.; Shayo, C.; Davio, C. Coumarins: Old Compounds with Novel Promising Therapeutic Perspectives. *Curr. Med. Chem.* **2010**, *17*, 13, 1325-1338.
- [188] Lavis, L. D.; Raines, R. T. Bright Building Blocks for Chemical Biology. *ACS Chem. Biol.* **2014**, *9*, 4, 855-866.
- [189] Sun, W.-C.; Gee, K. R.; Haugland, R. P. Synthesis of Novel Fluorinated Coumarins: Excellent UV-light Excitable Fluorescent Dyes. *Bioorg. Med. Chem.* **1998**, *8*, 22, 3107-3110.
- [190] Jin, X.; Uttamapinant, C.; Ting, A. Y. Synthesis of 7-Aminocoumarin by Buchwald-Hartwig Cross Coupling for Specific Protein Labeling in Living Cells. *ChemBioChem* **2011**, *12*, 1, 65-70.
- [191] Lavis, L. D. Rutkoski, T. J.; Raines, R. T. Tuning the pK<sub>a</sub> of Fluorescein to Optimize Binding Assays. *Anal. Chem.* **2007**, *79*, 17, 6775-6782.
- [192] Sun, W.-C.; Gee, K. R.; Klaubert, D. H.; Haugland, R. P. Synthesis of Fluorinated Fluoresceins. *J. Org. Chem.* **1997**, *62*, 19, 6469-6475.
- [193] Tian, L.; Yang, Y.; Wysocki, L. M.; Arnold, A. C.; Hu, A.; Ravichandran, B.; Sternson, S. M.; Looger, L. L.; Lavis, L. D. A Selective Esterase-Ester Pair for Targeting Small Molecules with Cellular Specificity. *Proc. Natl. Acad. Sci. U. S. A.* **2012**, *109*, 13, 4756-4761.
- [194] Minta, A.; Kao, J. P.; Tsien, R. Y. Fluorescent Indicators for Cytosolic Calcium Based on Rhodamine and Fluorescein Chromophores. *J. Biol. Chem.* **1989**, *264*, 14, 8171-8178.

## 1. Introduction

- 
- [195] Martin, V. V.; Rothe, A.; Gee, K. R. Fluorescent Metal Ion Indicators Based on Benzoannelated Crown Systems: A Green Fluorescent Indicator for Intracellular Sodium Ions. *Bioorg. Med. Chem. Lett.* **2005**, *15*, 7, 1851-1855.
- [196] Inglese, J.; Johnson, R. L.; Simenov, A.; Xia, M.; Zheng, W.; Austin, C. P.; Auld, D. S. High-Throughput Screening Assays for the Identification of Chemical Probes. *Nat. Chem. Biol.* **2007**, *3*, 8, 466-479.
- [197] Stratton, S. G.; Taumoefolau, G. H.; Purnell, G. E.; Rasooly, M.; Czaplinski, W. L.; Harbron, E. J. Tuning the pK<sub>a</sub> of Fluorescent Rhodamine pH Probes through Substituent Effects. *Chem. Eur. J.* **2017**, *23*, 56, 14064-14072.
- [198] Lavis, L. D.; Chao, T.-Y.; Raines, R. T. Fluorogenic Label for Biomolecular Imaging. *ACS Chem. Biol.* **2006**, *1*, 4, 252-260.
- [199] Levine, M. N.; Raines, R. T. Sensitive Fluorogenic Substrate for Alkaline Phosphatase. *Anal. Biochem.* **2011**, *418*, 2, 247-252.
- [200] Wysocki, L. M.; Grimm, J. B.; Tkachuk, A. N.; Brown, T. A.; Betzig, E.; Lavis, L. D. Facile and General Synthesis of Photoactivatable Xanthene Dyes. *Angew. Chem. Int. Ed.* **2011**, *50*, 47, 11206-11209.
- [201] Koide, Y.; Urano, Y.; Hanaoka, K.; Terai, T.; Nagano, T. Evolution of Group 14 Rhodamines as Platform for Near-Infrared Fluorescence Probes Utilizing Photoinduced Electron Transfer. *ACS Chem. Biol.* **2011**, *6*, 6, 600-608.
- [202] Lukinavičius, G.; Umezawa, K.; Olivier, N.; Honigmann, A.; Yang, G.; Plass, T.; Mueller, V.; Reymond, L.; Corrêa, I. R.; Luo, Z.-G.; Schultz, C.; Lemke, E. A.; Heppenstall, P.; Eggeling, C. Manley, S.; Johnsson, K. A Near-Infrared Fluorophore for Live-Cell Super-Resolution Microscopy of Cellular Proteins. *Nat. Chem.* **2013**, *5*, 132-139.
- [203] Im, C.-N.; Kang, N.-Y.; Ha, H.-H.; Bi, X.; Lee, J. J.; Park, S.-J.; Lee, S.-Y.; Vendrell, M.; Kim, Y. K.; Lee, J.-S.; Li, J.; Ahn, Y.-H.; Feng, B.; Ng, H.-H.; Yun, S.-W.; Chang, Y.-T. A Fluorescent Rosamine Compound Selectively Stains Pluripotent Stem Cells. *Angew. Chem. Int. Ed.* **2010**, *49*, 41, 7497-7500.
- [204] Jose, J.; Burgess, K. Benzophenoxazine-Based Fluorescent Dyes for Labeling Biomolecules. *Tetrahedron* **2006**, *62*, 48, 11021-11037.
- [205] Bueno, C.; Villegas, M. L.; Bertolotti, S. G.; Previtali, C. M.; Neumann, M. G.; Encinas, M. V. The Excited-State Interaction of Resazurin and Resorufin with Amines in Aqueous Solutions. Photophysics and Photochemical Reaction. *Photochem. Photobiol.* **2002**, *76*, 4, 385-390.
- [206] Hofmann, J.; Sernetz, M. Immobilized Enzyme Kinetics Analyzed by Flow-Through Microfluorimetry: Resorufin- $\beta$ -galactopyranoside as a New Fluorogenic Substrate for  $\beta$ -galactosidase. *Anal. Chim. Acta* **1984**, *163*, 67-72.
- [207] Theriot, J. A.; Mitchison, T. J. Actin Microfilament Dynamics in Locomoting Cell. *Nature* **1991**, *352*, 126-131.
- [208] Zhou, M.; Diwu, Z.; Panchuk-Voloshina, N.; Haugland, R. P. A Stable Nonfluorescent Derivative of Resorufin for the Fluorometric Determination of Trace Hydrogen Peroxide: Applications in

## 1. Introduction

---

- Detecting the Activity of Phagocyte NADPH Oxidase and other Oxidases. *Anal. Biochem.* **1997**, *253*, 2, 162-168.
- [209] O'Brien, J.; Wilson, I.; Orton, T.; Pognan, F. Investigation of the Alamar Blue (resazurin) Fluorescent Dye for the Assessment of Mammalian Cell Cytotoxicity. *Eur. J. Biochem.* **2000**, *267*, 17, 5421-5426.
- [210] Banks, P.; Gosselin, M.; Prystay, L. Impact of a Red-Shifted Dye Label for High Throughput Fluorescence Polarization Assays of G Protein-Coupled Receptors. *J. Biomol. Screening* **2000**, *5*, 5, 329-334.
- [211] Johnson, I.; Spence, M. (eds.), *The Molecular Probes Handbook. A Guide to Fluorescent Probes and Labeling Technologies*, Life Technologies Corporation, Eugene, 11th edition, 2010, p. 307.
- [212] Buschmann, V.; Weston, K. D.; Sauer, M. Spectroscopic Study and Evaluation of Red-Absorbing Fluorescent Dyes. *Bioconjugate Chem.* **2003**, *14*, 1, 195-204.
- [213] Cosa, G.; Focsaneanu, K. S.; McLean, J. R. N.; McNamee, J. P.; Scaiano, J. C. Photophysical Properties of Fluorescent DNA-Dyes Bound to Single- and Double-Stranded DNA in Aqueous Buffered Solution. *Photochem. Photobiol.* **2001**, *73*, 6, 585-599.
- [214] Smith, J. C. Potential-Sensitive Molecular Probes in Membranes of Bioenergetics Relevance. *Biochim. Biophys. Acta* **1990**, *1016*, 1, 1-28.
- [215] Plasek, J.; Sigler, K. Slow Fluorescent Indicators of Membrane Potential: A Survey of Different Approaches to Probe Response Analysis. *J. Photochem. Photobiol. B.* **1996**, *33*, 2, 101-124.
- [216] Schobel, U.; Egelhaaf, H. J.; Brecht, A.; Oelkrug, D.; Gauglitz, G. New Donor-Acceptor Pair for Fluorescent Immunoassays by Energy Transfer. *Bioconjugate Chem.* **1999**, *10*, 6, 1107-1114.
- [217] Shimomura, O.; Johnson, F. H.; Saiga, Y. Extraction, Purification and Properties of Aequorin, a Bioluminescent Protein from the Luminous Hydromedusan, Aequorea. *J. Cell Comp. Physiol.* **1962**, *59*, 3, 223-239.
- [218] Ormo, M.; Cubitt, A. B.; Kallio, K.; Gross, L. A.; Tsien, R. Y.; Remington, S. J. Crystal Structure of the Aequorea Victoria Green Fluorescent Protein. *Science* **1996**, *273*, 5280, 1392-1395.
- [219] Tsien, R. Y. The Green Fluorescent Protein. *Annu. Rev. Biochem.* **1998**, *67*, 509-544.
- [220] Remington, S. J. Fluorescent Proteins: Maturation, Photochemistry and Photophysics. *Curr. Opin. Struct. Biol.* **2006**, *16*, 6, 714-721.
- [221] Prasher, D. C.; Eckenrode, V. K.; Ward, W. W.; Prendergast, F. G.; Cormier, M. J. Primary Structure of the Aequorea Victoria Green-Fluorescent Protein. *Gene* **1992**, *111*, 2, 229-233.
- [222] Chalfie, M.; Tu, Y.; Euskirchen, G.; Ward, W. W.; Prasher, D. C. Green Fluorescent Protein as a Marker for Gene Expression. *Science* **1994**, *263*, 5148, 802-805.
- [223] Rodriguez, E. A.; Campbell, R. E.; Lin, J. Y.; Lin, M. Z.; Miyawaki, A.; Palmer, A. E.; Shu, X.; Zhang, J.; Tsien, R. Y. The Growing and Glowing Toolbox of Fluorescent and Photoactive Proteins. *Trends Biochem. Sci.* **2017**, *42*, 2, 111-129.
- [224] Kremers, G.-J.; Gilbert, S. G.; Cranfill, P. J.; Davidson, M. W.; Piston, D. W. Fluorescent Proteins at a Glance. *J. Cell Sci.* **2011**, *124*, 157-160.

## 1. Introduction

- 
- [225] Chudakov, D. M.; Matz, M. V.; Lukyanov, S.; Lukyanov, K. A. Fluorescent Proteins and Their Applications in Imaging Living Cells and Tissues. *Physiol. Rev.* **2010**, *90*, 3, 1103-1163.
- [226] Piston, D. W.; Kremers, G. J. Fluorescent Protein FRET: the Good, the Bad and the Ugly. *Trends Biochem. Sci.* **2007**, *32*, 9, 407-414.
- [227] Park, H. B.; Lam, Y. C.; Gaffney, J. P.; Weaver, J. C.; Krivoschik, S. R.; Hamchand, R.; Pieribone, V.; Gruber, D. F.; Crawford, J. M. Bright Green Biofluorescence in Sharks Derives from Bromo-Kynurenine Metabolism. *iScience* **2019**, *19*, 1277-1286.
- [228] Klymchenko, A. S. Solvatochromic and Fluorogenic Dyes as Environment-Sensitive Probes: Design and Biological Applications. *Acc. Chem. Res.* **2017**, *50*, 2, 366-375.
- [229] Würthner, F.; Kaiser, T. E.; Saha-Möllner, C. R. J-Aggregates: From Serendipitous Discovery to Supramolecular Engineering of Functional Dye Materials. *Angew. Chem. Int. Ed.* **2011**, *50*, 15, 3376-3410.
- [230] Okamoto, A. ECHO Probes: a Concept of Fluorescence Control for Practical Nucleic Acid Sensing. *Chem. Soc. Rev.* **2011**, *40*, 12, 5815-5828.
- [231] Bourzac, K. M.; LaVine L. J.; Rice, M. S. Analysis of DAPI and SYBR Green I as Alternatives to Ethidium Bromide for Nucleic Acid Staining Agarose Gel Electrophoresis. *J. Chem. Educ.* **2003**, *80*, 11, 1292-1296.
- [232] Lowe, D. The Myth of Ethidium Bromide. *Biological News* **2016**, 18 april.
- [233] Khamesipour, F.; Rahimi, E.; Shakerian, A.; Doosti, A.; Momtaz, H. Molecular Study of the Prevalence of *Brucella Abortus* and *Brucella Melitensis* in the Blood and Lymph Node Samples of Slaughtered Camels by Polymerase Chain Reaction (PCR) in Iran. *Acta Veterinaria-Beograd* **2014**, *64*, 2, 245-256.
- [234] Tang, Q.; Xiao, W.; Huang, C.; Si, W.; Shao, J.; Huang, W.; Chen, P.; Zhang, Q.; Dong, X. pH-Triggered and Enhanced Simultaneous Photodynamic and Photothermal Therapy Guided by Photoacoustic and Photothermal Imaging. *Chem. Mater.* **2017**, *29*, 12, 5216-5224.
- [235] Dragan, A. I.; Pavlovic, R.; McGivney, J. B.; Casas-Finet, J. R.; Bishop, E. S.; Strouse, R. J.; Schenerman, M. A.; Geddes, C. D.; SYBR Green I: Fluorescence Properties and Interaction with DNA. *J. Fluoresc.* **2012**, *22*, 4, 1189-1199.
- [236] Stiefel, P.; Schmidt-Emrich, S.; Maniura-Weber, K.; Ren, Q. Critical Aspects of Using Bacterial Cell Viability Assays with the Fluorophores SYTO9 and Propidium Iodide. *BMC Microbiol.* **2015**, *15*, 36, 1-9.
- [237] Johnson, I.; Spence, M. (eds.), *The Molecular Probes Handbook. A Guide to Fluorescent Probes and Labeling Technologies*, Life Technologies Corporation, Eugene, 11th edition, 2010, p. 313.
- [238] Atwal, S.; Giengkam, S.; VanNieuwenhze, M.; Salje, J. Live Imaging of the Genetically Intractable Obligate Intracellular Bacteria *Orientia Tsutsugamushi* Using a Panel of Fluorescent Dyes. *J. Microbiol. Methods* **2016**, *130*, 169-176.
- [239] Pitz, A. M.; Perry, G. A.; Jensen-Smith, H. C.; Gentry-Nielsen, M. J. A Flow Cytometric Assay to Quantify *in Vivo* Bacterial Uptake by Alveolar Macrophages. *J. Microbiol. Methods* **2010**, *81*, 194-196.



## 2 Motivation

Photosensitive molecules have revolutionized Molecular Biology since they allow the visualization, control and manipulation of biological functions by a non-invasive source: light. Nowadays photoresponsive compounds are spread over many fields of life science research. Their importance was further highlighted by several Noble Prizes: in 2016 Sauvage, Stoddart and Feringa were awarded for the design and synthesis of molecular machines, in 2014 Betzig, Hell and Moerner for the development of super-resolved fluorescence microscopy and in 2008 Shimomura, Chalfie and Tsien for the discovery, development and implementation of the green fluorescent protein (GFP). Despite many different strategies using photoactivatable, photocaged and photoswitchable molecules have been established for both optochemical control of biological processes and their visualization over the last decades, there are still limitations (chapter 1.2). Consequently, there is a "call to arms" for chemical biologists to synthesize novel improved molecules and develop innovative tools to understand biology at molecular level and, therefore, move life science research into a new era. In this thesis we aim to synthesize novel photosensitive molecules capable of opening new venues to visualize and control biological phenomena, which to date were not accessible. In different projects we intent to develop novel fluorophores for the study of multidrug resistant bacteria, engineer visible-light photoswitches to control epigenetic processes (Figure 2.1) and transfer these interdisciplinary approaches into the class room.

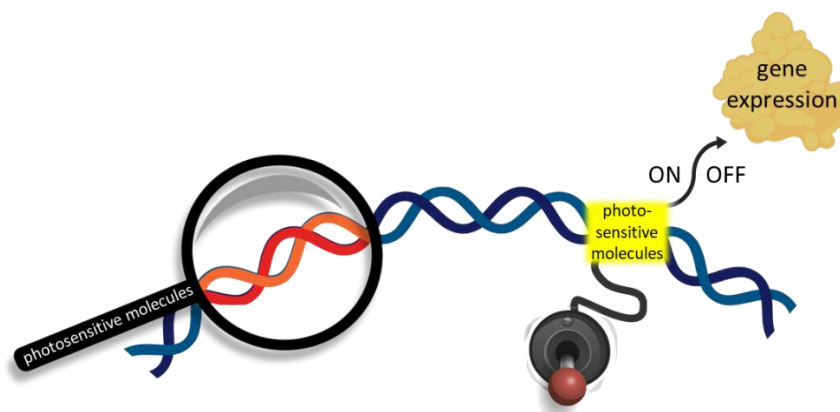


**Figure 2.1.** Photosensitive tools for the visualization, control and manipulation of biological functions by light. In the context of this thesis, photosensitive molecules were used to target nucleic-acid based processes.

- 1) Synthesis and study of new fluorophores capable of labeling multidrug-resistant bacteria with low cytotoxicity to enable real-time assays

The growing number of multidrug-resistant bacteria has become a significant problem and received the highest research priority by the World Health Organization. New solutions to combat against them, are urgently required, and research is lagging. Fluorescence labeling studies would provide more in-depth knowledge and will help to find solutions to fight back. The most established method to visualize biological functions in biomedical research is the implementation of GFP and its derivatives. However,

## 2. Motivation

many important organisms have been difficult to modify, including many multidrug-resistant bacteria due to the impossibility of select their transformants carrying the GFP-coding transgene with antibiotics. Therefore, studies with fluorescence tagged multidrug-resistant bacteria, especially in the host cell interplay are rare. The implementation of small-molecule nucleic acid stains to avoid the need for genetic manipulation has been so far limited to compounds with high cytotoxicity, or a low labeling efficiency in antibiotic sensitive bacteria (chapter 1.2.4.5). In this project we aimed at the design, synthesis and study of novel fluorophores to label multidrug-resistant bacteria efficiently without affecting their viability to allow real-time studies.

### 2) Synthesis and study of visible-light photoswitches for the control of DNA-based epigenetic processes

The lack of specificity is a big issue in pharmacology, which often results in severe side effects, environmental toxicity and drug-resistance. Photopharmacology aims to overcome this challenge by using photoswitchable molecules. Additionally, these compounds will help to better understand biological pathways as the reversible control in space and time allows precise activation/deactivation of the desired targets. The reversible regulation of DNA-based biological processes were, so far, mainly accessed by the use of classical azobenzenes. Their implementation demands the use of UV light, which is harmful. To evade this great problem, we planned to introduce new visible-light photoregulators to control nucleic acid binding. They would allow to reversibly regulate the exposure of DNA and, in turn, study and control genome functions in physiological as well as disease contexts. In this thesis, we aim to develop specific methodologies to access and study these regulators to get deeper insights into photopharmacology of nucleic-acid based processes.

### 3) Bringing the big picture of epigenetic research into an interdisciplinary chemical biology course

Chemical biology is a highly interdisciplinary area. Despite such approaches are more and more common in research, the implementation in education is still rare. Therefore, we planned to extrapolate the intrinsic nature of chemical biology to an interdisciplinary course for chemistry and biology master students to give them the real-world picture of science and highlight the importance of collaborative work to succeed.

## 3 Summaries

### 3.1 English Summary

This thesis presents the synthesis of novel photoresponsive DNA-binding agents as well as their application for both visualization and control of biological processes. In addition, the implementation of an innovative course to transfer the interdisciplinary research culture of chemical biology to education is reported. This cumulative dissertation is mainly composed of four chapters, each of them dealing with either published or submitted articles under revision. An introduction, motivation and outlook are included, too.

The first article is published in *Angewandte Chemie International Edition*, and describes the development of a new far-red fluorescent DNA binder, 6-TramTO-3, as an alternative chemical tool to the green fluorescent protein (GFP) for interaction studies of live multidrug-resistant pathogens and host cells. Thus, the derivatization of thiazole orange (TO) resulted in a new cyanine dye, 6-TramTO-3, whose spectroscopic properties were analyzed. DNA binding analysis by UV-vis, fluorescence and CD spectroscopy was performed to study the interaction mode upon addition to DNA. Initially, fluorescence confocal microscopy, FACS and growth curve analysis with live *E. coli* displayed an efficient staining of more than 90% and no effect on the bacterial viability. Importantly, 6-TramTO-3 overcomes common limitations of other frequently used fluorophores like ethidium bromide, carboxyfluorescein succinimidyl ester and SyTO-9, such as low staining efficiency and cytotoxicity without genetic manipulation. Encouraged by these unique properties, we tested 6-TramTO-3 with antibiotic-sensitive and multidrug-resistant *Klebsiella pneumoniae* strains. 6-TramTO-3 conferred both strains a highly specific red-fluorescent shift with 91% and 87% in the 652-671 nm red2 channel without observable cytotoxic effects. Next, we performed phagocytosis assays with human macrophages, which revealed a different strain behavior for the first time. Besides the publication, an European patent was filed (18174086.1 – 1011) and numerous collaborations with universities, research institutes and companies were initiated to apply 6-TramTO-3 in different contexts.

The second article is published in *Organic & Biomolecular Chemistry*, and presents *ortho*-tetra-fluoroazobenzene derivatives as DNA intercalators for photocontrol of DNA and nucleosome binding upon visible-light irradiation. Its use is less harmful to biological systems and therefore, preferred over UV-light, which is needed for the most known nucleic acid targeting photoswitchable systems. Thus, the introduction of such moiety in the backbone of the minor groove binder netropsin added dynamic control and changed the recognition mode. UV-vis, HPLC and NMR analysis demonstrated the photoisomerization of the new compounds by visible light. DNA-binding analysis conducted by UV-vis, fluorescence and CD spectroscopy revealed an intercalating binding mode in the low nM-region with differences between isomers. Finally, the use of the new derivative as a light-controllable nucleosome binder was explored. The different binding affinities observed on free DNA were corroborated for the

### 3. Summaries

nucleosomal DNA. Interestingly, electromobility shift assays and dynamic light scattering experiments proved that when the compound is in its *trans*-form, it intercalated into the nucleosomal DNA, induced distortion, which further led to disruption of the nucleosomes. These findings will help to introduce photochemical control to pave the way to altering nucleosome-based processes by light.

The third chapter of this thesis is a submitted manuscript to the journal *Organic Letters* under revision and deals with a novel synthetic approach to access pyrrole-imidazole (Py-Im) DNA binding polyamides based on 4-methyltrityl (Mtt) solid-phase peptide synthesis (SPPS). Commonly Py-Im polyamide hairpins are synthesized by Boc- and Fmoc- SPPS. New Mtt-protected pyrrole and imidazole building blocks were synthesized with higher yields than the Boc- and Fmoc-analogues. Their implementation could successfully be shown by the synthesis and study of a DNA-binding polyamide applying all Mtt-building blocks. Our methodology is orthogonal to Fmoc and will allow the implementation of base labile compounds and other sensitive groups in Py-Im polyamide chemistry affording novel polyamide conjugates. In a further attempt, it was already possible to use the new building blocks for the introduction of a photoswitchable compound into the polyamide-hairpin backbone, which will access the introduction of dynamic and spatial control in the level of sequence specific DNA binding in biological assays.

The fourth chapter is a submitted manuscript to the *Journal of Chemical Education* under replied revision, in which a novel course for master students in chemistry and biology is introduced to fill the missing gap between cutting-edge interdisciplinary research and education of future scientists. In other words, our course aimed at bringing the authentic “big picture” of science by the combination of lectures, a discovery-based research laboratory and science communication. The students experienced the advantages of collaborative work, wrote a short article and were guided in the design and defense of their own research proposals in chemical biology. Evaluation of the course clearly proved that the course fosters cooperative research relationships between biology and chemistry students, provides a unique and genuine research experience and increased the students’ interest in interdisciplinary approaches and collaborative work. The course and assessment material was accessible to inspire other interdisciplinary fields

#### 3.1 Zusammenfassung in deutscher Sprache

In der vorliegenden Thesis werden die Synthese innovativer photoregulierbarer DNA-bindender Verbindungen sowie deren Anwendung zur Visualisierung und Steuerung biologischer Prozesse vorgestellt. Darüber hinaus wird über die Implementierung eines neuartigen Kurses zur Übertragung der interdisziplinären Forschungskultur der Chemischen Biologie auf die Lehre berichtet. Diese kumulative Dissertation besteht hauptsächlich aus vier Kapiteln, die sich jeweils mit veröffentlichten oder in Revision stehenden Artikeln befassen. Zudem umfasst die Arbeit eine Einleitung, eine Motivation und je Kapitel einen Ausblick.

Der erste Artikel wurde in der *Angewandten Chemie International Edition* veröffentlicht und beschreibt die Entwicklung einer neuen tiefrot fluoreszierenden DNA-bindenden Verbindung 6-TramTO-3 als alternatives chemisches Instrument zum Grün-Fluoreszierenden-Protein (GFP) für Interaktionsstudien mit lebenden multiresistenten Krankheitserregern und Wirtszellen. Basierend auf der Grundstruktur des Thiazoloranges (TO) wurde ein neuer Cyaninfarbstoff, 6-TramTO-3, entwickelt, dessen spektroskopische Eigenschaften untersucht wurden. Eine DNA-Bindungsanalyse durch UV-vis-, Fluoreszenz- und CD-Spektroskopie wurde durchgeführt, um den Bindungsmodus nach Zugabe von DNA zu untersuchen. Konfokale Fluoreszenzmikroskopie, FACS und Wachstumskurvenanalyse mit lebenden *E. coli* zeigten eine effiziente Färbung von 93% und keinen Einfluss auf die Lebensfähigkeit der Bakterien. Entscheidend dabei ist, dass 6-TramTO-3 die üblichen Problematiken anderer häufig verwendeter chemischer Fluorophore wie Ethidiumbromid, Carboxyfluorescein-Succinimidylester und SyTO-9, wie geringe Färbungseffizienz und Zytotoxizität ohne genetische Manipulation überwindet. Aufgrund dieser herausragenden Eigenschaften haben wir 6-TramTO-3 im Weiteren mit Antibiotika-sensitiven wie auch multiresistenten *Klebsiella pneumoniae*-Stämmen getestet. 6-TramTO-3 verlieh beiden Stämme eine hochspezifische rot-fluoreszierende Verschiebung mit 91% und 87% in den 652-671 nm roten Kanal, ohne die Viabilität zu beeinflussen. Als nächstes führten wir Phagozytostests mit menschlichen Makrophagen durch, wobei erstmalig ein unterschiedliches Wirtsverhalten gezeigt werden konnte. Neben der Veröffentlichung des Fachartikels wurden ein europäisches Patent angemeldet (18174086.1 - 1011) und zahlreiche Kooperationen mit Universitäten, Forschungsinstituten und Unternehmen initiiert, um 6-TramTO-3 in diversen Zusammenhängen anzuwenden.

Der zweite Artikel wurde in *Organic & Biomolecular Chemistry* veröffentlicht und stellt *ortho*-Tetrafluorazobenzolderivate als DNA-Interkalatoren für die photokontrollierbare Bindung an der DNA und den Nukleosomen durch Bestrahlung mit sichtbarem Licht vor. Dieses ist für biologische Systeme weniger schädlich und daher UV-Licht vorzuziehen, welches für die die Regulierung der bekanntesten photoschaltbaren nukleinsäurebindenden Systeme benötigt wird. Die Einführung einer solchen Einheit in das Grundgerüst des kleine Furchen bindenden Netropsins führt zu einer dynamischen Kontrolle und änderte den Erkennungsmodus. UV-Vis-, HPLC- und NMR-Analyse zeigten die Photoisomerisierung der neuen Verbindungen. Eine DNA-Bindungsanalyse mittels UV-Vis-, Fluoreszenz- und CD-Spektroskopie ergab einen interkalierenden Bindungsmodus mit Affinitäten im niedrigen nM-Bereich und Unterschieden zwischen den Isomeren. Schließlich wurde die Verwendung des neuen Derivats als

### 3. Summaries

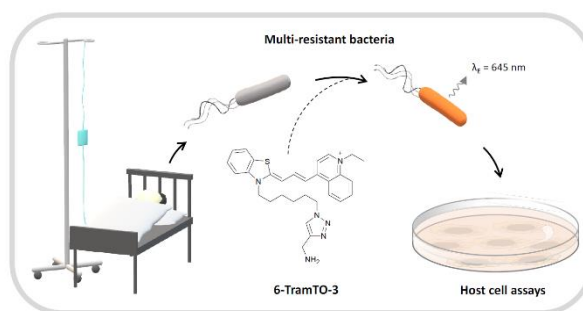
lichtkontrollierbare nukleosomenbindende Substanz untersucht. Die bei freier DNA beobachteten unterschiedlichen Bindungsaffinitäten wurden für die nukleosomale DNA bestätigt. Interessanterweise zeigten Elektromobilitäts-Shift-Untersuchungen und dynamische Lichtstreuungsexperimente, dass die *trans*-Form der Verbindung eine Aufweitung der nukleosomalen DNA induzierte, die zur Entwindung der Nukleosomen führte. Diese Erkenntnisse werden dazu beitragen, eine photochemische Kontrolle einzuführen, um den Weg zur Veränderung von nukleosomenbasierten Prozessen durch Licht zu ebnet.

Das dritte Kapitel dieser Arbeit ist ein in Revision stehendes Manuskript im Journal *Organic Letters* und befasst sich mit einem neuartigen Syntheseansatz der Pyrrol-Imidazol (Py-Im)-DNA-bindende Polyamide auf der Basis von 4-Methyltrityl (Mtt) Festphasenpeptidsynthese (SPPS) zugänglich macht. Üblicherweise werden Py-Im-Polyamid-Haarnadeln durch Boc- und Fmoc-SPPS synthetisiert. Neue Mtt-geschützte Pyrrol- und Imidazol-Bausteine wurden mit höheren Ausbeuten als die entsprechenden Boc- und Fmoc-Analoga synthetisiert. Ihre Anwendung konnte durch die Synthese und Untersuchung eines DNA-bindenden Polyamids unter Einsatz der Mtt-Bausteine erfolgreich gezeigt werden. Unsere Methode ist orthogonal zu Fmoc und ermöglicht die Implementierung basenlabiler Verbindungen und anderer empfindlicher Gruppen in der Py-Im-Polyamidchemie, wodurch neue Polyamidkonjugate erhalten werden können. In einem weiteren Versuch war es bereits möglich, die neuen Bausteine für die Einführung einer photoschaltbaren Verbindung in das Polyamid-Haarnadel-Rückgrat zu verwenden, die die Einführung von dynamischer und räumlicher Kontrolle der sequenzspezifischen DNA-Bindung in biologischen Untersuchungen ermöglicht.

Das vierte Kapitel ist ein in bearbeiteter Revision stehendes Manuskript im *Journal of Chemical Education*, welches einen neuartigen Kurs für Masterstudenten in den Fächern Chemie und Biologie vorstellt, um die vorhandene Lücke zwischen interdisziplinärer Spitzenforschung und der Ausbildung künftiger Wissenschaftler zu schließen. Mit anderen Worten, der Kurs zielte darauf ab, durch die Kombination von Vorlesungen, einem entdeckungsbasierten Forschungslaborkurses und wissenschaftlicher Kommunikation das authentische „Gesamtbild“ der Wissenschaft zu vermitteln. Die Studierenden erlebten die Vorteile von Kollaborationen, verfassten einen kurzen Artikel und wurden bei der Konzeption und Präsentation ihrer eigenen Forschungsvorschläge in der Chemischen Biologie angeleitet. Die Evaluation des Kurses zeigte eindeutig, dass die Lehrveranstaltung kooperative Forschungsbeziehungen zwischen Biologie- und Chemiestudenten fördert, ein einzigartiges und echtes Forschungserlebnis bietet und das Interesse der Studierenden an interdisziplinären Ansätzen und gemeinsamer Arbeit erhöht. Das Kurs- und Bewertungsmaterial wird zugänglich sein, um andere interdisziplinäre Wissenschaftsbereiche zu inspirieren ähnliche Kurse durchzuführen.

## 4 Cumulative Part

### 4.1 A Far-Red Fluorescent DNA Binder for Interaction Studies of Live Multidrug-Resistant Pathogens and Host Cells



Turning the light on: The fluorescent labeling agent 6-TramTO-3 was developed for real-time analysis of bacterial infection. This far-red fluorescent nucleic acid stain efficiently labeled bacteria through DNA binding without affecting their growth or viability. Staining of *Klebsiella pneumoniae*, a major threat to hospitalized patients, uncovered different interaction strategies of antibiotic-resistant and antibiotic-sensitive *Klebsiella* strains with immune cells.

This chapter was published as: Schulte, L. N.<sup>†</sup>; Heinrich, B.<sup>†</sup>; Janga, H.; Schmeck, B. T.; Vazquez, O.\* A Far-Red Fluorescent DNA Binder for Interaction Studies of Live Multidrug-Resistant Pathogens and Host Cells, *Angew. Chem. Int. Ed.* **2018**, *57*, 36, 11564-11568; and *Angew. Chem.* **2018**, *130*, 36, 11738-11742. Copyright John Wiley & Sons, Inc. The license for reprinting this article is attached at the end of the thesis.

<sup>†</sup> these authors contributed equally.

The results were further used to file a European patent: patent no. 18174086.1 - 1011: Cyanine dyes and their usage for in vivo staining of microorganisms.

Our findings were additionally recognized by the local (Oberhessische Presse, 28.07.2019, p. 3) and national (G.I.T Laboratory Journal, volume 23, april 2019, pp. 20-22) press. Olalla Vázquez and Leon Schulte received the MarBiNa Research Award 2018 by Initiative Biotechnologie und Nanotechnologie (Oberhessische Presse, 12.04.2019, p. 4) for this project.

## Fluorescence Labeling

International Edition: DOI: 10.1002/anie.201804090  
German Edition: DOI: 10.1002/ange.201804090

## A Far-Red Fluorescent DNA Binder for Interaction Studies of Live Multidrug-Resistant Pathogens and Host Cells

Leon N. Schulte<sup>+</sup>, Benedikt Heinrich<sup>+</sup>, Harshavardhan Janga, Bernd T. Schmeck, and Olalla Vázquez\*

**Abstract:** Transgene expression of green fluorescent protein (GFP) has facilitated the spatiotemporal investigation of host–pathogen interactions; however, introduction of the GFP gene remains challenging in drug-resistant bacteria. Herein, we report a novel far-red fluorescent nucleic acid stain, **6-TramTO-3**, which efficiently labels bacteria through a DNA binding mode without affecting growth and viability. Exemplarily, we stained *Klebsiella pneumoniae*, a major threat to hospitalized patients, and deciphered divergent interaction strategies of antibiotic-resistant and antibiotic-sensitive *Klebsiella* strains with immune cells. **6-TramTO-3** constitutes an off-the-shelf reagent for real-time analysis of bacterial infection, including strains for which the use of genetically encoded reporters is not feasible. Eventually, our approach may aid the development of strategies to combat a major worldwide health threat: multidrug-resistant bacteria.

The discovery, characterization, and implementation of the green fluorescent protein (GFP) has unquestionably revolutionized modern molecular cell biology, and was recognized by the Nobel Prize in Chemistry in 2008.<sup>[1]</sup> Nowadays, GFP derivatives are widely used as fluorescent reporters to study biological processes at the cellular and molecular level. In the case of bacterial infection, we and others have used GFP for fluorescence labeling of bacteria to study host–pathogen interactions with unprecedented sensitivity down to single-cell resolution.<sup>[2]</sup> These novel approaches have the potential to transform our understanding of bacterial strategies to override host immunity but currently rely on genetic manipulation. Unfortunately, several important organisms have remained difficult to modify for fluorescent-protein expression, in particular the growing number of multidrug-resistant bacteria posing an emerging threat to patients in clinics worldwide. Specifically, these strains may acquire resistance to the antibiotics used to select transformants carrying the

fluorescent-protein transgene. Thus, the investigation of host-cell interplay with drug-resistant bacteria by means of fluorescence labeling has lagged behind.

Excessive use of antibiotics has propelled the spread of multidrug-resistant bacteria at alarming rates.<sup>[3]</sup> As a consequence, incremental failure of antimicrobial treatment in patients leads to increased fatality rates due to the systemic spread of bacteria and organ failure. Among a number of major disease-causing agents, *Klebsiella pneumoniae* has received highest research priority by the World Health Organization owing to rapid acquisition of novel resistances.<sup>[4]</sup> New research tools compatible with resistant bacteria, such as fluorescence-labeling approaches, are urgently required. Detailed investigation of the disease-causing strategies of drug-resistant bacteria interacting with their hosts will assist rational drug design<sup>[5]</sup> and may eventually reduce fatality rates of infected patients.

Herein, we report the synthesis and applicability of novel far-red fluorescent DNA cyanine dyes for straightforward live bacterial cell labeling, allowing subsequent infection studies. We identified **6-TramTO-3** as a vital dye, conferring bacterial fluorescence staining without compromising microbial growth. We exemplify our approach with *Escherichia coli* as well as antibiotic-resistant and antibiotic-sensitive *K. pneumoniae* strains. Importantly, our results reveal differential strategies of the examined strains in their interaction with primary human host cells.

In the past decades, chemical biology has made great strides towards the development of fluorescent small molecules as alternatives to genetically encoded fluorescent reporters. Particularly in the context of inflammation, fluorophores have recently been shown to selectively track<sup>[6]</sup> or report the activity<sup>[7]</sup> of phagocytic immune cells, such as macrophages. These cells play a major role in the clearance of bacteria in a process referred to as phagocytosis. For the study of bacteria–phagocyte interactions,<sup>[8]</sup> fluorescein derivatives have been used in bacteria uptake assays,<sup>[9]</sup> though they tend to suffer from quenching in environments with low pH values. Nanospheres may fluorescently label living bacteria, although the consequences for bacterial viability are unclear.<sup>[10]</sup> BODIPY derivatives have been used to stain obligate intracellular bacteria, however with high background due to host-cell co-staining<sup>[11]</sup> and continuous fluorescence emission independent of target structure binding. Light-up DNA binders have been used instead, but at the expense of compromising bacteria viability.<sup>[12]</sup> For example, live bacterial cells have been labeled for macrophage uptake assays with the nucleic acid stain SyTO-9<sup>TM</sup>.<sup>[9e,13]</sup> However, reduced colony formation by the stained bacteria was observed,<sup>[9e]</sup>

[\*] B. Heinrich,<sup>[†]</sup> Jun.-Prof. Dr. O. Vázquez  
Fachbereich Chemie, Philipps-Universität Marburg  
Hans-Meerwein-Strasse 4, 35043, Marburg (Germany)  
E-mail: olalla.vazquez@staff.uni-marburg.de  
Jun.-Prof. Dr. L. N. Schulte,<sup>[†]</sup> H. Janga, Prof. Dr. B. T. Schmeck  
Institute for Lung Research, Philipps-Universität Marburg  
Hans-Meerwein-Strasse 2, 35043, Marburg (Germany)  
Prof. Dr. B. T. Schmeck  
Member of the German Center for Lung Research (DZL) (Germany)

[†] These authors contributed equally.

Supporting information and the ORCID identification number(s) for the author(s) of this article can be found under:  
<https://doi.org/10.1002/anie.201804090>.



indicative of toxicity, which compromises the use of SyTO-9<sup>TM</sup> as a vital dye for pathogen–host investigations. Taking SyTO-9<sup>TM</sup> as a starting point, and due to the excellent spectroscopic properties of such cyanine compounds,<sup>[14]</sup> we aimed at the synthesis of a versatile azide-functionalized unsymmetrical NIR cyanine dye, **6-AzTO-3**, based on classical thiazole orange (TO) and related compounds.<sup>[15]</sup> To increase both solubility and affinity, we also prepared two amino derivatives: **6-NH<sub>2</sub>TO-3** and **6-TramTO-3** (Figure 1; see the Supporting Information for compound synthesis).

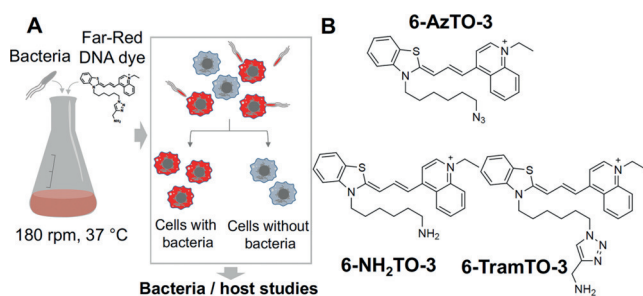


**Figure 1.** A) Schematic representation of growth-compatible bacterial labeling for host–pathogen studies: Live bacteria cells are labeled with far-red fluorescent dyes and subsequently added to host-cell cultures. Host cells containing bacteria may be identified by FACS or microscopy for detailed host–pathogen interaction analysis. B) Chemical structure of the synthesized and tested far-red dyes.

Initially, we evaluated whether our compounds and other common fluorophores for biological research, such as ethidium bromide (EtBr), carboxyfluorescein succinimidyl ester (CFSE), or SyTO-9<sup>TM</sup>, could enable fluorescent labeling of live *E. coli* without affecting viability. The bacterial culture medium was supplemented directly with the candidate compounds, and *E. coli* growth was monitored over time (Figure 2; see also Figure S43 A in the Supporting Information). At mid-exponential growth phase, fluorescence labeling was determined by fluorescence-activated cell sorting (FACS) analysis. Importantly, none of the standard fluorophores (EtBr and CFSE) was found eligible for bacterial vital

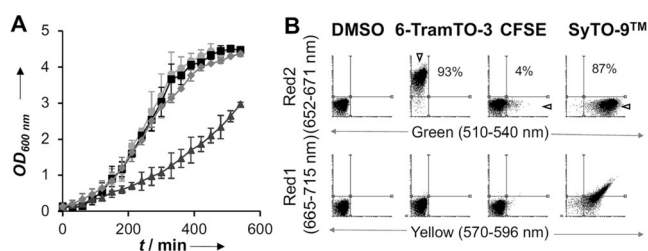


**Figure 2.** A) Optical density ( $OD_{600\text{nm}}$ ) of *E. coli* LB cultures supplemented with dimethyl sulfoxide (DMSO; light-gray line with dots), **6-TramTO-3** (black line with squares), CFSE (gray line with rhombuses), or Syto-9<sup>TM</sup> (gray line with triangles) over time. Mean data points and standard deviations are derived from three independent experiments. B) Representative dot plots of bacteria, including quantification from three independent experiments (see Figure S48 C), from (A) sampled at  $OD_{600\text{nm}} = 2.0$  and analyzed by FACS in the red1, red2, green, and yellow channels.

staining at 2.5  $\mu\text{M}$ : Despite being compatible with bacterial growth, CFSE hardly labeled bacteria at all, whereas EtBr did not confer a pronounced fluorescence shift in the red/green/yellow emission bands commonly used in FACS (see Figure S43 B). As a possible explanation, EtBr displays intrinsic membrane impermeability in living cells at low concentrations.<sup>[14b]</sup> Interestingly, SyTO-9<sup>TM</sup>, which conferred efficient green-fluorescence labeling, delayed bacterial growth substantially. Moreover, cross-emission into the yellow and red spectrum was observed, rendering combination of SyTO-9<sup>TM</sup> with other fluorophores difficult. Importantly, all our novel cyanine dyes conferred a highly specific red-fluorescence shift of live bacteria in the 652–671 nm red2 channel, as determined by FACS (Figure 2; see also Figure S43 B) and microscopy (see Figure S41). Notably, the compound **6-TramTO-3** was fully compatible with normal bacterial growth in liquid medium (Figure 2) and on solid medium (see Figure S44 B), thus suggesting no effects on viability. Importantly, **6-TramTO-3** fluorescence labeling remained stable over several hours after shifting the bacteria into dye-free media (see Figure S45). Consequently, we selected **6-TramTO-3** as the most promising candidate for further spectroscopic characterization as well as DNA-binding-affinity, sequence-selectivity, and activity studies with antibiotic-sensitive and antibiotic-resistant bacteria.

In aqueous solution, **6-TramTO-3** shows long-wavelength maxima of excitation and emission (633 and 645 nm, respectively; see Figure S24 B) and low intrinsic fluorescence ( $\Phi_F = 0.005$ ). Remarkably, upon the addition of double-stranded calf thymus DNA (dsDNA<sub>CT</sub>), the fluorescence emission intensity increased dramatically (> 25-fold;  $\Phi_F = 0.27$ ), and emission was stable over several hours (see Figures S27–S29). Interestingly, this fluorescence increase outcompetes that observed for EtBr under the same conditions (Figure 3 A). Furthermore, the **6-TramTO-3** emission maximum was found to be shifted to the far-red part of the spectrum, which enabled **6-TramTO-3** detection in the FACS red2 fluorescence channel. Our results also suggest the implementation of

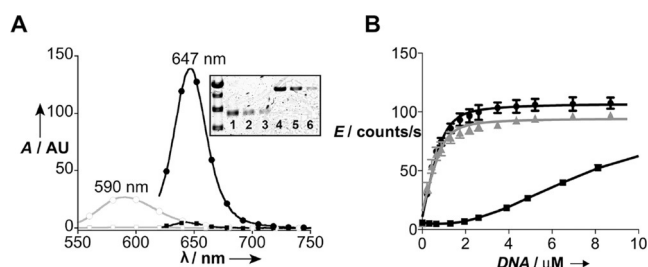


**Figure 3.** A) Fluorescence emission spectra in Tris buffer (pH 7.6) and 50 mM KCl at 20°C of a 1  $\mu\text{M}$  solution of: **6-TramTO-3** alone (black line with black squares), **6-TramTO-3** in the presence of dsDNA<sub>CT</sub> (15 equiv; black line with black dots), EtBr alone (gray line with white squares), and EtBr in the presence of dsDNA<sub>CT</sub> (15 equiv; gray line with white dots). Insert shows gel staining of different dsDNAs with **6-TramTO-3**; lines 1–3: circular bacterial dsDNA; lines 4–6: linearized bacterial dsDNA; both in amounts of 1000, 500, and 100 ng. B) Emission profiles at 647 nm for titrations of **6-TramTO-3** with: dsDNA<sub>CT</sub> (black line with squares), dsDNA<sub>hCC</sub> (gray line with triangles), and dsDNA<sub>hAT</sub> (black line with dots). All data are mean values derived from three independent measurements.

**6-TramTO-3** as a replacement for EtBr to post-stain DNA in gel electrophoresis (Figure 3A; see also Figure S39).

To obtain more information on the affinity and selectivity of **6-TramTO-3**–DNA binding, we performed fluorescence titrations with dsDNA<sub>CT</sub> and hairpin oligonucleotides containing either the sequence ATTA (dsDNA<sub>hAT</sub>) or GGCC (dsDNA<sub>hGC</sub>). In all cases, the addition of DNA resulted in a progressive increase in fluorescence emission (Figure 3B). The rise in the emission at 647 nm could be fitted to a simplified 1:1 binding model, resulting in the corresponding apparent dissociation constants. The calculated affinity of **6-TramTO-3** for dsDNA<sub>CT</sub> ( $K_D = (19.5 \pm 2.6) \mu\text{M}$ ) is reminiscent of previously obtained results for DNA intercalators, such as EtBr ( $K_D = 15 \mu\text{M}$ ), methylene blue ( $K_D = 46 \mu\text{M}$ ), and acridine orange ( $K_D = 36 \mu\text{M}$ ) with the same DNA.<sup>[16]</sup> Furthermore, thermal melting experiments showed significant dsDNA<sub>CT</sub> stabilization upon **6-TramTO-3** binding ( $\Delta T_m = 5^\circ\text{C}$ ). **6-TramTO-3** displays a higher affinity for both hairpin oligonucleotides than for dsDNA<sub>CT</sub>. Analysis of the apparent dissociation constants of **6-TramTO-3** for dsDNA<sub>hAT</sub> and dsDNA<sub>hGC</sub> ( $K_D = (0.114 \pm 0.03) \mu\text{M}$ ,  $K_D = (0.104 \pm 0.054) \mu\text{M}$ , respectively) indicates non-sequence-specific binding, further supporting the intercalation binding mode.<sup>[17]</sup> The slightly lower fluorescence intensity observed with dsDNA<sub>hGC</sub> might be explained by photoinduced electron transfer (PET) in GC-rich sequences.<sup>[18]</sup> Next, to better understand the binding mode of **6-TramTO-3**, we carried out absorbance titrations (Figure 4a). The addition of dsDNA<sub>CT</sub> (< 2.5 equiv of DNA)

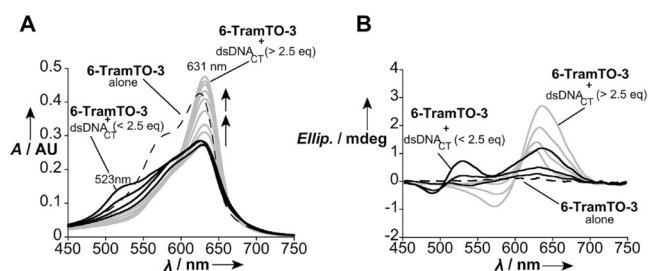


**Figure 4.** A) UV/Vis spectra of 12.3  $\mu\text{M}$  solutions and B) CD spectra of 36.9  $\mu\text{M}$  solutions of: **6-TramTO-3** alone (black dotted line), **6-TramTO-3** in the presence of increasing amounts of dsDNA<sub>CT</sub> (< 2.5 equiv; black lines), and **6-TramTO-3** in the presence of increasing amounts of dsDNA<sub>CT</sub> (> 2.5 equiv; gray lines) in Tris buffer (pH 7.6) with 50 mM KCl at 20 °C. All data are mean values derived from three independent measurements.

caused a dramatic change in the absorption spectrum: A 102 nm blue shift of the absorption maximum of **6-TramTO-3** was observed, and was also found to be temperature-dependent (see Figure S37). Further increments in the number of equivalents of DNA promoted a new response: a red-shifted transition with a maximum intensity at 631 nm. This result points to a half-intercalating binding mode. Circular dichroism (CD) experiments corroborated the suggested binding modes (Figure 4B). Taken together, our findings show that **6-TramTO-3** behaves as a novel DNA-intercalating dye compatible with bacterial cell growth, conferring fluorescence labeling at an emission wavelength suitable for routine FACS analysis.

Having established an assay for fluorescence labeling of live *E. coli* cells, we tested the applicability of **6-TramTO-3** for the staining of clinically relevant bacteria that are hard to modify genetically owing to resistance to selection antibiotics. A lack of genetic tools has hampered studies on the interaction of such strains with host cells by standard methods, such as fluorescence microscopy or FACS. To test whether our dye could overcome this current limitation, we focused on the major human pathogen *K. pneumoniae*. To this end, antibiotic-resistant and antibiotic-sensitive *K. pneumoniae* were cultured and compared with *E. coli*. Resistance to standard antibiotics was confirmed by spotting bacterial dilutions onto solid medium (Figure 5A). Whereas multi-

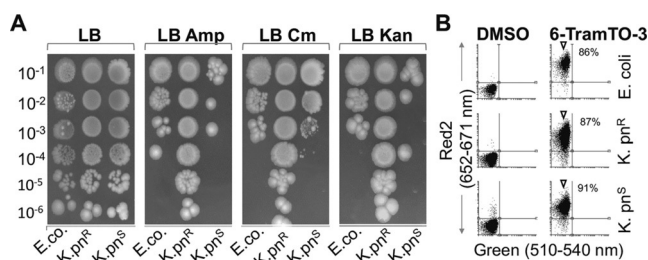


**Figure 5.** A) Indicated dilutions of bacteria sampled at  $\text{OD}_{600\text{nm}} = 2.0$  were spotted onto LB solid medium without antibiotics (LB) or supplemented with ampicillin (LB Amp), kanamycin (LB Kan), or chloramphenicol (LB Cm), followed by outgrowth for 48 h. E.co. = *E. coli*; K.pn<sup>R</sup> = multiresistant *K. pneumoniae*; K.pn<sup>S</sup> = antibiotic-sensitive *K. pneumoniae*. B) Representative dot plots of FACS analysis (red2 and green channel) of all three strains in the presence of DMSO or **6-TramTO-3**, sampled at  $\text{OD}_{600\text{nm}} = 2.0$ , including quantification from three independent experiments (see Figure S48A).

resistant *K. pneumoniae* were insensitive to kanamycin, ampicillin, and chloramphenicol, both *E. coli* and the other *K. pneumoniae* strain were sensitive to all three antibiotics. All bacterial strains were successfully fluorescently labeled (Figure 5B; see also Figure S44A) and grew normally in the presence of **6-TramTO-3** (see Figure S44B,C). Thus, **6-TramTO-3** does not disturb bacterial growth and overcomes the current lack of a universal fluorescence-labeling approach for multidrug-resistant pathogenic bacteria.

After demonstrating the successful fluorescence labeling of multiresistant microbes, we sought to evaluate the use of **6-TramTO-3** in studies addressing the interaction of these bacteria with host cells. Bacterial infections typically occur through ingestion or inhalation and subsequent colonization of the mucosal surfaces of the lung or gastrointestinal tract. Resident immune cells, such as macrophages, may phagocytose and neutralize bacteria or signal to the environment to prevent them from causing disease.<sup>[19]</sup> In a proof-of-principle experiment we examined the interaction of *E. coli* and both *Klebsiella* strains with primary human macrophages through bacterial labeling with **6-TramTO-3**. Nonpathogenic *E. coli* have previously been shown to be readily phagocytosed by macrophages.<sup>[20]</sup> Consequently, the *E. coli* strain used in this study was readily taken up in coculture experiments, as indicated by a red shift of approximately 26% of the macrophages (Figure 6A,B). Importantly, phagocytosis rates

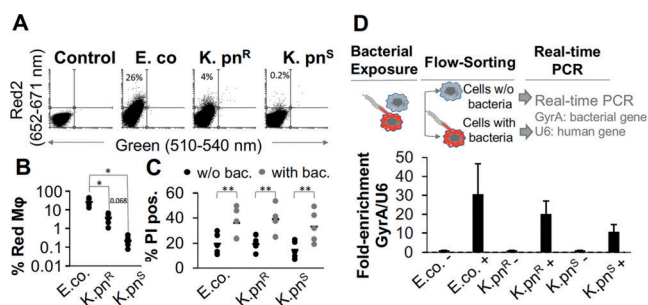


**Figure 6.** A) Representative dot plots of human macrophages exposed to **6-TramTO-3**-labeled bacteria; the observed shift in the red channel is indicative of bacterial uptake. B) Quantification of red-shifted macrophages. Data are derived from five independent experiments. C) Quantification of propidium iodide (PI)-positive macrophages with (red-shifted) or without bacteria (unshifted). D) Experimental scheme and qRT-PCR using RNA from both fractions to determine the relative abundance of human U6 snRNA versus bacterial housekeeper RNA GyrA. E.co. = *E. coli*; K.pn<sup>R</sup> = multiresistant *K. pneumoniae*; K.pn<sup>S</sup> = antibiotic-sensitive *K. pneumoniae*. Statistical significances were evaluated using a one-way Anova (B) or a two-tailed Student *t*-test (C). \*  $P \leq 0.05$ ; \*\*  $P \leq 0.01$ .

obtained with **6-TramTO-3**-labeled *E. coli* matched results obtained with yellow fluorescent protein (YFP) expressing *E. coli* (see Figure S46), thus confirming the reliability of our cyanine dye approach.

Separation of **6-TramTO-3**-positive from **6-TramTO-3**-negative (unstained) macrophages by FACS and subsequent quantitative real-time PCR (qRT-PCR; Figure 6D) confirmed that the red-shifted population comprised macrophages that had taken up bacteria. Interestingly, in *Klebsiella*-exposure experiments only approximately 4% of the macrophages took up the antibiotic-resistant strain, whereas approximately 0.2% took up the antibiotic-sensitive strain (Figure 6A,B), as confirmed by FACS and qRT-PCR. Intriguingly, the antibiotic-resistant strain was found to be encapsulated, whereas the antibiotic-sensitive strain does not possess a capsule (see Figure S47). This result implies that besides the capsule, *Klebsiella* may employ further means to prevent phagocytic uptake.

To trace the fate of macrophages with phagocytosed bacteria, co-staining with the yellow-fluorescent cell-death stain propidium iodide was performed. As compared to the macrophage subpopulation without intracellular bacteria (lower-left quadrants in Figure 6A), the macrophage subpopulation with phagocytosed *E. coli* or sensitive and multiresistant *K. pneumoniae* (upper-left quadrants in Figure 6A) in the same culture dish preferentially entered cell death (Figure 6C). This result is in line with the reported role of macrophages in digestion and subsequent self-degradation as part of bacterial clearance.<sup>[21]</sup>

Together these observations suggest that the examined *Klebsiella* strains adopt different virulence strategies: Whereas the encapsulated, multidrug-resistant strain evades clearance by antimicrobial compounds, but only partially evades phagocytosis, the antibiotic-sensitive strain has learned to cope with clearance by immune cells, such as macrophages. Follow-up investigations using **6-TramTO-3** to

screen uptake rates of non-encapsulated *K. pneumoniae* strains by macrophages may reveal novel virulence factors involved in the evasion of phagocytosis by this major pathogen. To the best of our knowledge, no direct comparison of the interaction of antibiotic-resistant and antibiotic-sensitive pathogens with human immune cells has been provided previously by means of fluorescence labeling (Figure 7).

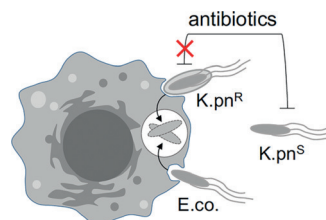


**Figure 7.** Model illustrating the observed interaction of antibiotic-sensitive and antibiotic-resistant bacteria with human macrophages.

In conclusion, we synthesized and studied a novel far-red fluorescent cyanine derivative, **6-TramTO-3**, for live bacterial-cell tracking. **6-TramTO-3** is a fluorescent light-up probe with an up to 27-fold signal increase in the presence of dsDNA and no apparent effects on bacteria viability. We demonstrated efficient labeling of multidrug-resistant bacteria, the fluorescence tagging of which by genetic manipulation is not feasible. Thereby, our exemplary investigations with pathogenic microbes revealed divergent interaction modes of multiresistant and antibiotic-sensitive *Klebsiella* bacteria with human macrophages. We anticipate that our approach will open the door to further advanced applications, such as dual RNA-Seq<sup>[2b]</sup> or single-cell RNA-Seq<sup>[2c]</sup> to understand the disease strategies of antibiotic-resistant bacteria, an emerging worldwide threat.

## Acknowledgements

We gratefully acknowledge: Dr. Gabriele Malengo for microscopy image acquisition; Dr. Daniela Kiekebusch and Andrea Harms for their initial assistance with the Typhoon device and ISS PC1 spectrofluorometer, respectively; Prof. Dr. Reinier Mutters for providing clinical isolates of *K. pneumoniae*; Prof. Dr. Concepción González-Bello and Prof. Dr. Olga García-Mancheno for critical feedback on the manuscript. Financial support was obtained from the Fulbright Commission (Fulbright-Cottrell Award 2016 to O.V.), the von Behring-Röntgen Stiftung (vBR project 63-0036 to L.N.S.), the German Research Foundation, and the Hessen State Ministry of Higher Education, Research, and the Arts (SFB/TR-84, LOEWE Medical RNomics—FKZ 519/03/00.001-(0003) to B.T.S.).

## Conflict of interest

The authors declare no conflict of interest.



**Keywords:** antibiotics · DNA recognition · fluorescence-activated cell sorting · far-red cyanine dyes · multidrug-resistant bacteria

**How to cite:** *Angew. Chem. Int. Ed.* **2018**, *57*, 11564–11568  
*Angew. Chem.* **2018**, *130*, 11738–11742

- [1] a) O. Shimomura, *Angew. Chem. Int. Ed.* **2009**, *48*, 5590–5602; *Angew. Chem.* **2009**, *121*, 5698–5710; b) J. K. M. Sanders, S. E. Jackson, *Chem. Soc. Rev.* **2009**, *38*, 2821–2822; M. Zimmer, *Chem. Soc. Rev.* **2009**, *38*, 2823–2832.
- [2] a) R. H. Valdivia, A. E. Hromockyj, D. Monack, L. Ramakrishnan, S. Falkow, *Gene* **1996**, *173*, 47–52; b) A. J. Westermann, K. U. Fröstner, F. Amman, L. Barquist, Y. Chao, L. N. Schulte, L. Müller, R. Reinhardt, P. F. Stadler, J. Vogel, *Nature* **2016**, *529*, 496–501; c) A.-E. Saliba, L. Li, A. J. Westermann, S. Appenzeller, D. A. C. Stapels, L. N. Schulte, S. Helaine, J. Vogel, *Nat. Microbiol.* **2016**, *2*, 16206–16214.
- [3] a) S. B. Levy, B. Marshall, *Nat. Med.* **2004**, *10*, S122–S129; b) A. Y. Peleg, D. C. Hooper, *N. Engl. J. Med.* **2010**, *362*, 1804–1813; c) D. van Duin, D. L. Paterson, *Infect. Dis. Clin. North Am.* **2016**, *30*, 377–390.
- [4] a) R. Podschun, U. Ullmann, *Clin. Microbiol. Rev.* **1998**, *11*, 589–603; b) WHO, **2014**, Antimicrobial Resistance: Global Report on Surveillance.
- [5] a) K. M. O’Connell, J. T. Hodgkinson, H. F. Sore, M. Welch, G. P. Salmond, D. R. Spring, *Angew. Chem. Int. Ed.* **2013**, *52*, 10706–10733; *Angew. Chem.* **2013**, *125*, 10904–10932; b) M. F. Chellat, L. Raguž, R. Riedl, *Angew. Chem. Int. Ed.* **2016**, *55*, 6600–6626; *Angew. Chem.* **2016**, *128*, 6710–6738.
- [6] a) A. Vázquez-Romero, N. Kielland, M. J. Arévalo, S. Preciado, R. J. Mellanby, Y. Feng, R. Lavilla, M. Vendrell, *J. Am. Chem. Soc.* **2013**, *135*, 16018–16021; b) N.-Y. Kang, S.-J. Park, X. Wei, E. Ang, A. Samanta, W. H. P. Driessen, V. Ntziachristos, K. O. Vasquez, J. D. Peterson, S.-W. Yun, Y.-T. Chang, *Chem. Commun.* **2014**, *50*, 6589–6591.
- [7] a) A. Fernández, M. Vermeren, D. Humphries, R. Subiros-Funosas, N. Barth, L. Campana, A. MacKinnon, Y. Feng, M. Vendrell, *ACS Cent. Sci.* **2017**, *3*, 995–1005; b) A. Fernández, M. Vendrell, *Chem. Soc. Rev.* **2016**, *45*, 1182–1196, and references therein.
- [8] A. E. Smartt, S. Ripp, *Anal. Bioanal. Chem.* **2011**, *400*, 991–1007.
- [9] a) D. A. Drevets, P. A. Campbell, *J. Immunol. Methods* **1991**, *142*, 31–38; b) A. K. Lehmann, A. Halstensen, C. F. Bassøe, *Cytometry* **1998**, *33*, 406–413; c) C. L. Weingart, G. Broitman-Maduro, G. Dean, S. Newman, M. Peppler, A. A. Weiss, *Infect. Immun.* **1999**, *67*, 4264–4267; d) M. E. Fuller, S. H. Streger, R. K. Rothmel, B. J. Mailloux, J. A. Hall, T. C. Onstott, J. K. Fredrickson, D. L. Balkwill, M. F. DeFlaun, *Appl. Environ. Microbiol.* **2000**, *66*, 4486–4496; e) S. Atwal, S. Giengkama, M. Van Nieuwenhze, J. Salje, *J. Microbiol. Methods* **2016**, *130*, 169–176; f) E. A. Vander Top, G. A. Perry, M. J. Gentry-Nielsen, *BMC Microbiol.* **2006**, *6*, 61–70.
- [10] I. Roy, D. Shetty, R. Hota, K. Baek, J. Kim, C. Kim, S. Kappert, K. Kim, *Angew. Chem. Int. Ed.* **2015**, *54*, 15152–15155; *Angew. Chem.* **2015**, *127*, 15367–15370.
- [11] H. Boleti, D. M. Ojcius, A. Dautry-Varsat, *J. Microbiol. Methods* **2000**, *40*, 265–274.
- [12] a) E. Ortega, I. Algarra, M. J. Serrano, G. Alvarez de Cienfuegos, J. J. Gaforio, *J. Immunol. Methods* **2001**, *253*, 189–193; b) J. J. Gaforio, M. J. Serrano, E. Ortega, I. Algarra, G. Alvarez de Cienfuegos, *Cytometry* **2002**, *48*, 93–96.
- [13] A. M. Pitz, G. A. Perry, H. C. Jensen-Smith, M. J. Gentry-Nielsen, *J. Microbiol. Methods* **2010**, *81*, 194–203.
- [14] a) A. Tárnok, *Cytometry Part A* **2008**, *73*, 477–479; b) *Molecular Probes: Handbook of Fluorescent Probes and Research Chemicals*, 11th ed., Molecular Probes, Eugene, **2010**, chap. 8, pp. 311–314.
- [15] a) A. Mishra, R. K. Behera, P. K. Behera, B. K. Mishra, G. B. Behera, *Chem. Rev.* **2000**, *100*, 1973–2012; b) J. Ghasemi, S. H. Ahmadi, A. L. Ahmad, S. Ghobadi, *Appl. Biochem. Biotechnol.* **2008**, *149*, 9–22; c) X. Peng, T. Wu, J. Fan, J. Wang, S. Zhang, F. Song, S. Sun, *Angew. Chem. Int. Ed.* **2011**, *50*, 4180–4183; *Angew. Chem.* **2011**, *123*, 4266–4269.
- [16] S. Nafisi, A. A. Saboury, N. Keramat, J.-F. Neault, H.-A. Tajmir-Riahi, *J. Mol. Struct.* **2007**, *827*, 35–43.
- [17] a) B. A. Armitage, *Top. Curr. Chem.* **2005**, *253*, 55–76; b) T. G. Deligeorgiev, S. Kaloyanova, J. J. Vaquero, *Recent Pat. Mater. Sci.* **2009**, *2*, 1–26.
- [18] a) S. O. Kelley, J. K. Barton, *Science* **1999**, *283*, 375–381; b) A. Erve, Y. Saoudi, S. Thiro, C. Guetta-Landras, J.-C. Florent, C.-H. Nguyen, D. S. Grierson, A. V. Popov, *Nucleic Acids Res.* **2006**, *34*, e43.
- [19] S. H. E. Kaufmann, A. Dorhoi, *Immunity* **2016**, *44*, 476–491.
- [20] C. Gille, B. Spring, L. Tewes, C. F. Poets, T. Orlikowsky, *Cytometry Part A* **2006**, *69*, 152–154.
- [21] T. Frankenberg, S. Kirschnek, H. Häcker, G. Häcker, *Eur. J. Immunol.* **2008**, *38*, 204–215.

Manuscript received: April 6, 2018

Accepted manuscript online: July 4, 2018

Version of record online: August 6, 2018

Supporting Information  
©Wiley-VCH 2016  
69451 Weinheim, Germany

**Abstract:** Transgene expression of green fluorescent protein (GFP) has facilitated the spatio-temporal investigation of host-pathogen interactions; however, the introduction of the GFP gene remains challenging in drug-resistant bacteria. Herein, we report a novel far-red fluorescent nucleic acid stain, **6-TramTO-3**, which efficiently labels bacteria through a DNA binding mode without affecting growth and viability. Exemplarily, we stained *Klebsiella pneumoniae*, a major threat to hospitalized patients, and deciphered for the first time, divergent interaction strategies of antibiotic-resistant and -sensitive *Klebsiella* strains with immune cells. **6-TramTO-3** constitutes an off-the-shelf-reagent for real-time analysis of bacterial infection, including strains where the use of genetically-encoded reporters is not feasible. Eventually, our approach may support the development of therapeutics to combat a major worldwide health threat: multidrug-resistant bacteria.

**DOI:** [10.1002/anie.201804090](https://doi.org/10.1002/anie.201804090)

## SUPPORTING INFORMATION

## Table of Contents

<b>Abbreviations .....</b>	<b>54</b>
<b>Experimental Procedures .....</b>	<b>55</b>
Materials and Experimental Procedures .....	55
High-Performance Liquid Chromatography (HPLC) .....	55
Nuclear Magnetic Resonance Spectroscopy (NMR) .....	56
Mass Spectrometry .....	56
Fluorescence Measurements .....	56
Fluorescence Quantum Yield .....	56
UV-VIS Measurements .....	57
CD Measurements .....	57
Thermal Melting Analysis .....	57
Gel Electrophoresis .....	57
Bacteria and Host Cell Culture .....	57
<i>Bacteria Culture and Staining / Destaining Experiments</i> .....	58
<i>Bacteria Capsule Staining</i> .....	58
<i>Host Cell Culture and Exposure to Bacteria</i> .....	58
Fluorescence Microscopy .....	58
<i>Cell Preparation</i> .....	58
<i>Microscope Settings</i> .....	58
Flow Cytometry .....	59
<i>Analysis</i> .....	59
<i>Cell Sorting</i> .....	59
Quantitative Real-Time PCR .....	59
Bacterial DNA Preparation .....	59
<b>Synthesis .....</b>	<b>60</b>
Synthesis of the Quinolinium Iodide (5) .....	61
Synthesis of the <i>N</i> -alkylated Benzothiazolium Intermediate (8) .....	62
Synthesis of the Azido Cyanine Dye Derivative 6-AzTO-3 (1) .....	66
Synthesis of the Amine Cyanine Dyes: 6-TramTO-3 (2) and 6-NH <sub>2</sub> TO-3 (3) .....	71
<b>Results and Discussion .....</b>	<b>80</b>
Excitation and Emission Spectra of the NIR Cyanine Dye Derivatives .....	80
Fluorescence Emission of the NIR Cyanine Dye Derivatives with(out) dsDNA <sub>CT</sub> .....	80
Fluorescence Titrations of 6-TramTO-3 .....	80
Binding Affinity Determination by DynaFit .....	82
Fluorescence Quantum Yield .....	83
Concentration Determination .....	84
UV-Vis Titrations .....	86
CD Measurements .....	87
Gel Electrophoresis .....	87

## SUPPORTING INFORMATION

---

Thermal Melting Analysis .....	87
Fluorescence Microscopy .....	88
Additional Cell-Based Assays .....	90
<b>References.....</b>	<b>94</b>

## SUPPORTING INFORMATION

## Abbreviations

A	absorbance
CD	circular dichroism
CFSE	carboxyfluorescein <i>N</i> -succinimidyl ester
COSY	correlation spectroscopy
dsDNA <sub>CT</sub>	double-stranded <i>calf thymus</i> DNA
dsDNA <sub>hAT</sub>	double-stranded DNA hairpin with the consensus sequence <i>ATTA</i>
dsDNA <sub>hGC</sub>	double-stranded DNA hairpin with the consensus sequence <i>GGCCC</i>
d	doublet
DMSO	dimethylsulfoxide
ECL	enhanced chemiluminescence
EI	electron ionisation, emission intensity
eq	equivalent
ESI	electrospray ionisation
EtBr	Ethidium bromide
HPLC	high performance liquid chromatography
HSQC	heteronuclear single quantum correlation spectroscopy
Hz	hertz
$K_D$	apparent dissociation constant
m	multiplet
<i>m</i>	mass
MeCN	acetonitrile
MS	mass spectrometry
NIR	Near infrared
NMR	nuclear magnetic resonance
PBS	phosphate buffered saline
PMT	photomultiplier tube
ppm	part per million
q	quartet
r.t.	room temperature
s	singlet
t	triplet
TCEP	tris(2-carboxyethyl)phosphine
TAE	tris-acetate-EDTA
TFA	trifluoroacetic acid
$T_m$	melting temperature
Tris	tris(hydroxymethyl)aminomethane
UV	ultraviolet
Vis	visible
z	charge
$\epsilon$	molar extinction coefficient
$\eta$	refractive index
$\lambda$	wavelength
$\Phi_F$	quantum yield



## SUPPORTING INFORMATION

## Experimental Procedures

## Materials and Experimental Procedures

All commercially purchased reagents were used without further purification as delivered from the corresponding company. The respective reagents were purchased from the following companies: lepidine, *N,N*-diphenylformamidine, 2-methylbenzothiazole, ethyliodide, copper powder, triphenylphosphine, DMSO for molecular biology, ethidium bromide, potassium chloride, 2,6-lutidine and DNA hairpins from Sigma Aldrich (USA), tris(2-carboxyethyl)phosphine (TCEP), acetic anhydride, copper(II) sulfate, Tris(hydroxymethyl)aminomethane (Tris) and sodium chloride from Carl Roth (Germany), nigrosin and crystal violet from Merck (Germany), sodium azide, and propargylamine from Acros Organics (Belgium), triethylamine and acetonitrile (MeCN) from VWR (USA), dibromohexane from Alfa Aesar (USA), copper(I) bromide from Santa Cruz Biotechnology (USA), trifluoroacetic acid (TFA) from abcr (Germany), Atto 655 NHS-ester from Atto-tec (Germany), SYTO-9™ nucleic acid stain from Life Technologies (USA), carboxyfluorescein *N*-succinimidyl ester (CFSE) from Thermo Fisher (Germany), CSL 1kb DNA ladder from Cleaver Scientific (UK) and calf thymus DNA (dsDNA<sub>CT</sub>) and Alexa Fluor® 647 C<sub>2</sub>-maleimide was purchased from Invitrogen (USA). Water was purified with a Milli-Q Ultra Pure Water Purification System (TKA, Germany).

## High-Performance Liquid Chromatography (HPLC)

For preparative purposes, a PLC 2020 Personal Purification System (Gilson) with a preparative Nucleodur C18 HTec-column (5 μm, 250 x 16 mm; Macherey & Nagel) using an isocratic regime during the first five minutes for column equilibration, followed by a linear gradient 5% to 75% B in 30 min, for both compounds: **6-TramTO-3 (2)** and **6-NH<sub>2</sub>TO-3 (3)**, with a flow rate of 10 mL/min at 25°C was used. The detection was carried out by measuring the absorption at wavelengths: 220 nm and 300 nm. Milli-Q water (A) and MeCN (B) were employed as eluents with an addition of 0.1% of TFA for both solvents.

For analytical purposes, an Agilent 1260 Infinity II HPLC-System (Agilent Technologies) with an EC 125/2 Nucleodur 100-C18 ec column (Macherey & Nagel) using an isocratic regime during the first five minutes for column equilibration, followed by a linear gradient 5% to 75% B in 30 min with a flow rate of 0.2 mL/min at 55°C was used. The detection was carried out by measuring the absorbance at a wavelength of 660 nm for the NIR cyanine dye derivatives **1**, **2** and **3**. In all cases, milli-Q water (A) and MeCN (B) were employed as eluents with an addition of 0.05% of TFA for A and 0.03% for B.

Below the HPLC chromatograms of the synthesized NIR cyanine dyes used in the bacteria cell-based experiments:

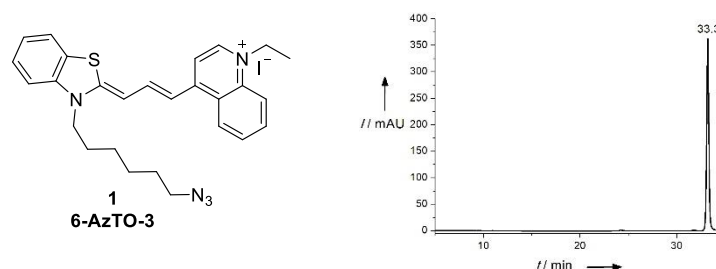


**Figure S1:** Structure of **6-AzTO-3 (1)** used in the bacteria cell-based assays and its corresponding HPLC chromatogram.

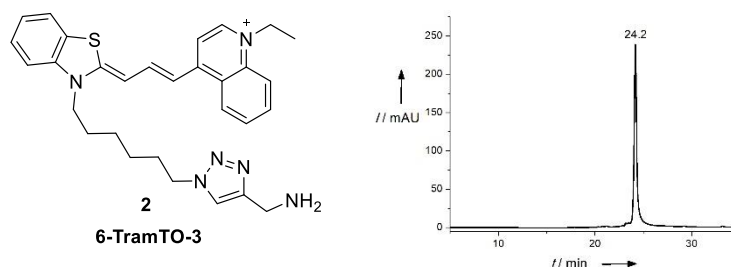


**Figure S2:** Structure of **6-TramTO-3 (2)** used in the bacteria cell-based assays and its corresponding HPLC chromatogram.

## SUPPORTING INFORMATION

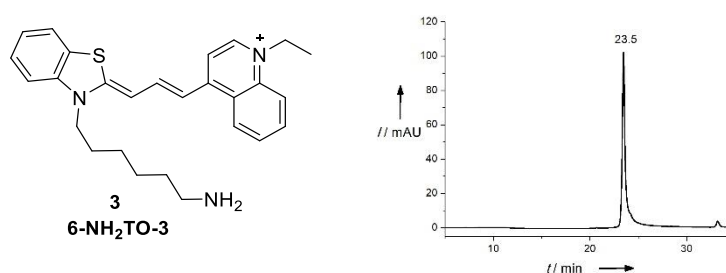


**Figure S3:** Structure of **6-NH<sub>2</sub>TO-3 (3)** used in the bacteria cell-based assays and its corresponding HPLC chromatogram.

### Nuclear Magnetic Resonance Spectroscopy (NMR)

All NMR spectra were automatically measured at 300 K either in a Bruker AV III HD 300 MHz at a frequency of 300 MHz (<sup>1</sup>H) or 75 MHz (<sup>13</sup>C) or in a Bruker AV III HD 500 MHz at a frequency of 500 MHz (<sup>1</sup>H) or 125 MHz (<sup>13</sup>C). All chemical shifts ( $\delta$ ) are relative to tetramethylsilane (TMS), i.e.  $\delta(\text{TMS}) = 0$  ppm. As internal standards, deuterated chloroform (CDCl<sub>3</sub>), dimethyl sulfoxide (DMSO) with TMS were used. Solvent shifts (ppm):  $\delta(\text{CHCl}_3) = 7.26$  ppm (<sup>1</sup>H),  $\delta(\text{CHCl}_3) = 77.16$  ppm (<sup>13</sup>C),  $\delta(\text{DMSO}) = 2.50$  ppm (<sup>1</sup>H),  $\delta(\text{DMSO}) = 39.52$  ppm (<sup>13</sup>C).<sup>[1]</sup> The assignment of each signal was based on two-dimensional nuclear magnetic resonance spectroscopy (2D NMR), i.e. heteronuclear single quantum coherence (HSQC), heteronuclear multiple bond correlation spectroscopy (HMBC) and correlation spectroscopy (COSY).

### Mass Spectrometry

Electrospray ionization mass spectrometry (ESI-MS) was performed on a Finnigan LTQ-FT (Thermo Fischer Scientific). EI-MS was performed on an AccuTOF GCv (JEOL).

### Fluorescence Measurements

Fluorescence measurements and titrations were performed on a Jasco FP-6500 spectrofluorometer equipped with a Thermo Haake WKL 26 water recirculator at 20°C. Unless otherwise noted, a 1400  $\mu\text{L}$  fluorescence cuvette of HellmaAnalytics (104F-QS) was used and the measurements were performed with the following settings: increment: 1.0 nm; integration time: 0.2 s; speed: 500 nm/min; sensitivity: medium; excitation slit width: 3 nm; emission slit width: 3 nm; excitation wavelength 610 nm. The emission spectra were recorded from 625 to 750 nm at 20°C. From all spectra, the corresponding background signal was subtracted.

The used hairpin double-stranded DNAs: dsDNA<sub>hAT</sub> and dsDNA<sub>hGC</sub> had the following sequences:

**Table S1.** Binding sites and sequences of DNA hairpins, which were used for fluorescence titrations experiments.

DNA	binding site	sequence (5' – 3')
dsDNA <sub>hAT</sub>	ATTA	GGCGATTACAGCTTTTTGCTGTAATCGCC
dsDNA <sub>hGC</sub>	GGCCC	GGCAGGCCAGCTTTTTGCTGGGCCTGCC

### Fluorescence Quantum Yield

Fluorescence intensity values for the quantum yields were determined on an ISS PC1 spectrofluorometer with an ISS 11650 lamp connected to an ISS Simpson model 109 and an ISS 80011 photomultiplier connected to a MGW Lauda K2R D and an Amherst Scientific Corp. 7600F for cooling. A VWR Refrigerated Circ 1160S was connected for the cooling of the cuvette chamber. It was measured in a 1400  $\mu\text{L}$  fluorescence cuvette of HellmaAnalytics (104F-QS) at 25°C using the following settings: increment: 2.0 nm; integration time: 1.0 s; excitation slit width: 0.25 mm; emission slit width: 0.5 mm; excitation wavelength 590 nm. The emission spectra were recorded from 610 to 750 nm. From all spectra the corresponding background signal was subtracted. Absorbance values were

## SUPPORTING INFORMATION

measured on a Jasco V-650 UV-Vis Spectrophotometer equipped with a Jasco PAC-743 temperature controlled cell holder and a Julabo F250 cooling system. UV-Vis titration measurements were performed in a 1400  $\mu\text{L}$  quartz cuvette with a pathlength of 1 cm at 25°C using the following settings: increment: 1.0 nm; bandwidth: 1.0 nm; scanning speed: 1000 nm/min; scanning mode: continuous. From all values, the corresponding background signal was subtracted. The values for the reference compounds were measured in duplicates, the ones for **6-TramTO-3** with and without dsDNA<sub>CT</sub> in triplicates. The quantum yields of **6-TramTO-3** with (30 eq) and without dsDNA<sub>CT</sub> were determined in 10 mM Tris pH 7.6 and 50 mM KCl. All measurement were following the procedure of Horiba<sup>[2]</sup> and using the equation:

$$\phi_X = \phi_{ST} \left( \frac{\text{Grad}_X}{\text{Grad}_{ST}} \right) \left( \frac{\eta_X^2}{\eta_{ST}^2} \right) \quad (\text{S1})$$

where  $\Phi$  = fluorescence quantum yield,  $\eta$  = refractive index of the used solvent, Grad = gradient from the plot of integrated fluorescence intensity vs absorbance and the subscripts ST and X denote standard and tested sample.

As reference compounds, Atto 655 in PBS pH 7.4 ( $\Phi = 0.30$ )<sup>[3]</sup> and Alexa Fluor® 647 in 50 mM potassium phosphate pH 7.2 and 150 mM NaCl ( $\Phi = 0.33$ )<sup>[4]</sup> were used. All solvents were degassed before use.

### UV-VIS Measurements

UV-Vis titration measurements were performed on a Jasco V-650 UV-Vis spectrophotometer equipped with a Jasco PAC-743 temperature controlled cell holder and a Julabo F250 cooling system to maintain the temperature constant at 20°C during the measurements. UV-Vis titration measurements were performed in a 500  $\mu\text{L}$  quartz cuvette with a pathlength of 1 cm at 20°C. The absorbance spectra were recorded from 400 nm to 800 nm.

The concentration determination and measurement of full UV-Vis spectra were performed on a Tecan 20M at room temperature. The measurements were performed in a 1400  $\mu\text{L}$  quartz cuvette with a pathlength of 1 cm in a volume of 1 mL.

### CD Measurements

CD titration measurements were performed on a Jasco J-810 Spectropolarimeter equipped with a Jasco CDF-426S peliter controller and a Thermo Haake WKL 26 water recirculator at 20°C using a 350  $\mu\text{L}$  CD cuvette of HellmaAnalytics (110-QS) at a concentration of 36.9  $\mu\text{M}$  of **6-TramTO-3** in 10 mM Tris pH 7.6 and 50 mM KCl. The settings were: range from 750-450 nm, speed of 100 nm/min, response of 4 s, band width of 10 nm and a data pitch of 1 nm. The measurement was performed 2 min after the addition of dsDNA<sub>CT</sub>. Each measurement consisted of a mean of 5 measurements. Three independent measurements were performed.

### Thermal Melting Analysis

Thermal melting analysis was performed on a Jasco J-810 spectropolarimeter equipped with a Jasco CDF-426S peliter controller and a Thermo Haake WKL 26 water recirculator. It was measured at a concentration of 45  $\mu\text{M}$  of dsDNA<sub>CT</sub> with and without 1.8  $\mu\text{M}$  of **6-TramTO-3** in 10 mM Tris pH 7.5. The measurement was performed at 260 nm, with a response of 2 s, a band width of 10 nm, from 40-95°C, a slope of 2°C/min. Three independent measurements were recorded and the intensity normalized.

### Gel Electrophoresis

Gel electrophoresis was performed with a Mini-Sub® Cell GT Cell (Biorad, USA) system with a power supply: MP-300V (Major Science, USA), for 75 min at 25°C with constant 80 V. For the experiments, 6  $\mu\text{L}$  of 1000 ng, 500 ng and 100 ng of dsDNA<sub>bc</sub> and dsDNA<sub>bl</sub> in TAE, containing 10% glycerol were loaded. As DNA ladder, CSL 1kb ladder was used. The gel was resolved in 1% agarose gel using TAE as a running buffer and analyzed by post-staining with either 1  $\mu\text{M}$  of **6-TramTO-3**, or 1  $\mu\text{M}$  ethidium bromide in TAE buffer. The gel was visualized using a Typhoon TRIO Variable Mode Imager (Amersham Biosciences, UK). To visualize the gel stained by **6-TramTO-3**, we used: the emission filter 670 BP 30 Cy5, the red laser (633 nm), PMT 400, pixel size 25 microns and normal sensitivity. For the case of the gel stained ethidium bromide, we used: no filter, an ECL + Excitation, PMT 400, pixel size 25 microns and a normal sensitivity.

### Bacteria and Host Cell Culture

## SUPPORTING INFORMATION

Bacteria Culture and Staining / Destaining Experiments

*Escherichia coli* (*E. coli*) NEB5 $\alpha$  (New England Biolabs) and antibiotic-resistant (Prof. Jörg Vogel, Würzburg) and  $\beta$ -sensitive (Prof. Reinier Mutter, Marburg) *Klebsiella pneumoniae* (*K. pneumoniae*) were cultured in Luria-Bertani (LB) solid medium (LB-Agar) overnight at 37°C. For staining, growth curve analysis and replating experiments bacteria were suspended in LB liquid medium at an OD<sub>600 nm</sub> of 1.0 and 800  $\mu$ L were transferred into a culture tube containing 7.2 mL of LB liquid medium supplemented with DMSO or candidate dyes (2.5  $\mu$ M final concentration) followed by continuous shaking at 180 rpm and 37 °C. Density of bacterial cultures was measured using an Ultraspec 10 Cell Density Meter with 600 nm LED source (Amersham Biosciences). To address destaining of **6-TramTO-3** labelled bacteria over time cells grown till an OD<sub>600 nm</sub> of 2 in the presence of the dye (2.5  $\mu$ M final concentration) were washed five times with phosphate buffered saline (PBS) and resuspended in 8 ml fresh LB medium (without **6-TramTO-3**) or added into X-Vivo15 host cell medium (without **6-TramTO-3**) in 6-well culture dishes as described below (host cell culture). LB-cultures were placed back into the shaking incubator and X-vivo15 medium cultures were placed into the host cell incubator for the remainder of the experiment. For bacterial re-plating experiments bacteria were sampled at OD<sub>600 nm</sub> = 2.0 and 5  $\mu$ L of indicated dilutions in LB-medium were spotted onto LB-agar plates (Fig. 5) or 100  $\mu$ L were plated onto LB-agar plates followed by incubation at 37°C until colonies became visible. For generation of YFP-expressing *Escherichia coli* cells the strain introduced above (NEB5 $\alpha$ ) was chemically transformed with the pUCP20-eYFP plasmid (a gift from Mariette Barbier (Addgene plasmid # 78466) using the CaCl<sub>2</sub>-method.

Bacteria Capsule Staining

5  $\mu$ L bacteria suspension grown till OD<sub>600 nm</sub> of 2 were placed on a microscopy slide and mixed with 1  $\mu$ L nigrosin solution (100 mg nigrosin + 5  $\mu$ L formalin per ml H<sub>2</sub>O). Bacteria/nigrosin mixture was spread out into a film and air-dried. The slide was then saturated with crystal violet solution (5 mg crystal violet + 200  $\mu$ L methanol per 1 ml H<sub>2</sub>O) and after 1 min of incubation carefully rinsed with water. The slide was again air-dried and analyzed on an AXIO Vert.A1 wide-field microscope (Zeiss) at 63x magnification.

Host Cell Culture and Exposure to Bacteria

For primary human macrophage cultures buffy coats from blood donations were loaded onto Lymphoprep™ gradient medium (Fresenius Kabi) followed by centrifugation. The peripheral blood mononuclear cell band was isolated from the gradient and monocytes were enriched using CD14 MACS beads (Miltenyi) according to the manufacturer's instructions. To differentiate monocytes into macrophages cells were cultured in 6-well plates (800.000 cells/mL) in 2 mL X-Vivo 15 medium (Lonza) supplemented with 5 % fetal bovine serum (Biochrom) and 15 ng/mL recombinant human GM-CSF (Preprotech).

On day 7 macrophages were considered terminally differentiated and treated with stained bacteria. To this end bacteria stained as described above or modified for YFP expression were sampled at an OD<sub>600 nm</sub> = 2.0 and washed five times with phosphate buffered saline (PBS). After the last wash bacteria were brought to an OD<sub>600 nm</sub> of 2.0 and 16  $\mu$ L, equivalent to 16.000.000 bacteria were added to each well to achieve a multiplicity of infection of 20. Culture plates were then centrifuged for 10 min at 250 g and 37°C to establish physical contact between macrophages and bacteria. Subsequently, culture plates were transferred back into a 37°C incubator with CO<sub>2</sub> atmosphere for the remainder of the stimulation period.

**Fluorescence Microscopy**Cell Preparation

For microscopic analysis, bacterial cells cultures were taken up in PBS and added onto an IBIDI 8-wells glass bottom plate pre-coated with poly-L-lysine. After 10 min of incubation non-adherent bacteria were washed away with PBS and remaining bacteria were layered with a film of PBS, followed by microscopic analysis.

Macrophage cells were grown and stimulated with bacteria as described above but grown in 35 mm IBIDI  $\mu$ -Dish (800.000 cells per dish in 2 mL of culture medium).

Microscope Settings

For acquisition of confocal images, we used an LSM880 Laser Scanning Confocal Microscope (Zeiss, Germany). Images were acquired with a 63X 1.4 oil immersion objective, fluorescence excitation was obtained using the 633 nm laser line, fluorescence emission was detected in the 633-695 nm range. For the images of bacteria alone, pixel size is 0.05 microns and image size is 27.1X27.1 microns. For the images of macrophages co-incubated with bacteria, pixel size is 0.13 microns and image size is 135.0X135.0 microns, z-scaling is 0.5 microns.

## SUPPORTING INFORMATION

## Flow Cytometry

Analysis

Bacteria and macrophages were washed with PBS prior to flow cytometry and analysed using a Guava easyCyte flow cytometer (Millipore). FCS3.0 files were analysed using Flowing Software (<http://flowingsoftware.btk.fi/>). Cells were first gated in the forward- / side-scatter plot to exclude debris, followed by quadrant gating in plots using the fluorescence channels as shown. For live/dead cell discrimination cells in PBS were supplemented with 0.4  $\mu\text{L}/\text{mL}$  propidium-iodide (5 mg/ml solution) followed by 5 min incubation on ice. Propidium iodide signal was recorded in the yellow channel.

Cell Sorting

For separation of macrophages containing or not containing bacteria cells were washed twice with PBS, removed from the culture dishes using a rubber scraper and sorted using an Aria III Fluorescence Activated Cell Sorter (BD) with 100  $\mu\text{m}$  nozzle and cooling. Sorting was performed with no more than 1000 events per second and 'Single Cell' purity setting.

**Quantitative Real-Time PCR**

For quantitative real-time PCR (qRT-PCR) analysis cell pellets were dissolved in Trizol reagent (Thermo Fisher) and RNA was extracted with chloroform. RNA from the aqueous phase was precipitated with isopropanol and washed once with 70% ethanol. Air-dried RNA was resuspended in water and treated with DNaseI (Thermo Fisher) according to the manufacturer's instructions. RNA was extracted with 25:24:1 phenol, chloroform, isoamylalcohol (Roth) and precipitated with 30:1 ethanol, sodium-acetate (3M, pH5.5). RNA-pellet was washed once with 70% ethanol, air-dried and resuspended in double-distilled water. Nucleic acid concentration was determined using a Nanodrop-2000 spectrometer.

To determine U6 and GyrA gene expression RNA samples were subjected to qRT-PCR analysis using the POWER SYBR Green RNA-to-CT kit (Thermo Fisher) according to the manufacturer's instructions and a QuantStudio3 device (Applied Biosystems). Primer sequences (ordered from Metabion) were: U6 forward: GCTTCGGCAGCACATATACTAAAAT, U6 reverse: ATATGGAACGCTTCACGAATTTG, GyrA forward: TTACACCGGTCAACATTGAGG, GyrA reverse: TTCATGGCGTAAAGTACGCG. Gene expression differences were calculated based on the Threshold-Cycle (CT) values according to the  $2^{-\Delta\Delta\text{CT}}$  formula.<sup>[5]</sup>

**Bacterial DNA Preparation**

To obtain pure DNA for staining experiments chemically competent *E. coli* NEB5 $\alpha$  cells were transformed with pUC18 plasmid DNA by heat-shock (42°C, 120 seconds) and subsequently shifted to LB medium containing Ampicillin (100  $\mu\text{g}/\text{ml}$ ). After shaking for 12 h at 37°C and 180 rpm bacteria were pelleted by centrifugation and pUC18 plasmid DNA was isolated using the Plasmid Pure column purification kit (Macherey Nagel) according to the manufacturer's instructions. For experiments with linearized bacterial DNA pUC18 plasmid DNA was incubated overnight with KpnI restriction enzyme (Thermo Fisher) at 37°C, followed by purification using the GeneJet PCR purification kit (Thermo Fisher) according to the manufacturer's instructions. Linearized DNA was eluted from the purification column with double-distilled water.

## SUPPORTING INFORMATION

## Synthesis

Below, it is shown the followed retrosynthetic approach for the preparation of the cyanine dye derivatives: **6-AzTO-3** (**1**), **6-TramTO-3** (**2**) and **6-NH<sub>2</sub>TO-3** (**3**). The building block compounds (**5**), (**6**), (**9**) were synthesized according to the literature. Their analytical data were consistent with such literature. Compounds (**7**), (**10**) and (**11**) were commercially available. Other intermediates and finals compounds were synthesized following the procedures described below.

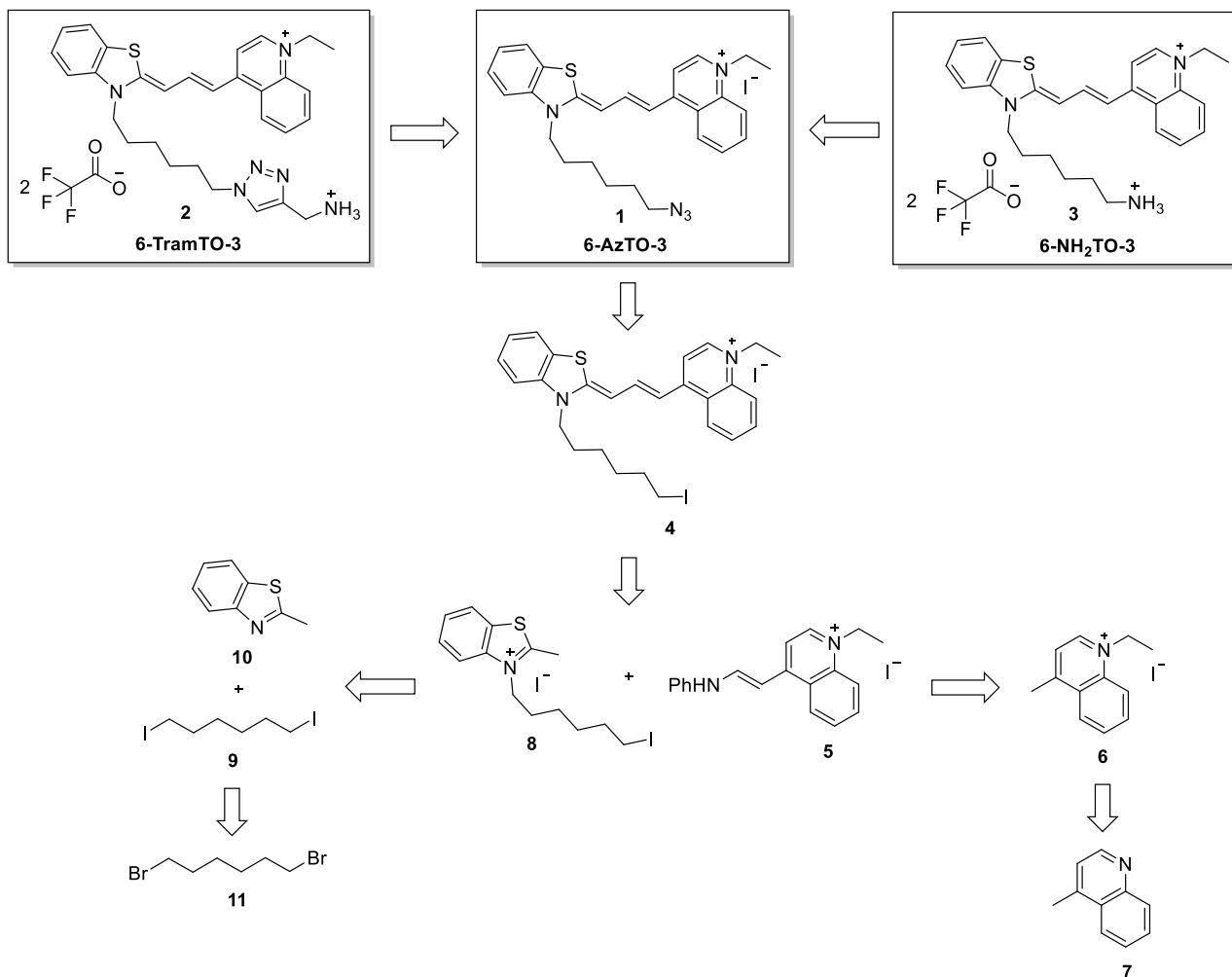


**Figure S4.** Retrosynthetic approach for the preparation of the cyanine dye derivatives **6-AzTO-3** (**1**), **6-TramTO-3** (**2**) and **6-NH<sub>2</sub>TO-3** (**3**).

## SUPPORTING INFORMATION

## Synthesis of the Quinolinium Iodide (5)

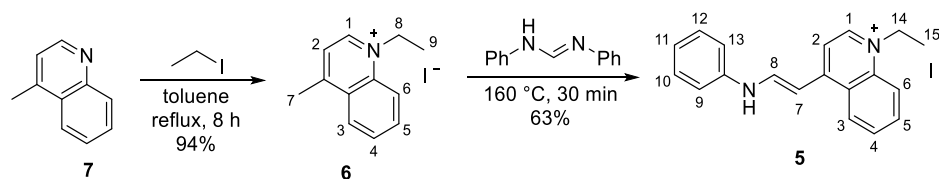
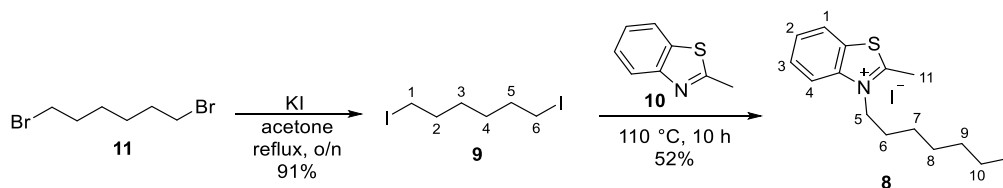


Figure S5. Synthesis route of quinolinium iodide (5) starting from lepidine (7).

**1-ethyl-4-methylquinolin-1-ium iodide (6):** Following the procedure of PENG et al.,<sup>[6]</sup> lepidine (7, 143 mg, 1.00 mmol) was dissolved in toluene (1 mL) and ethyl iodide (0.10 mL, 1.25 mmol) was added. The mixture was refluxed in a sealed tube for 8 h. The resulting solid was crushed, washed several times with ethyl ether and dried under vacuum to yield the desired product **6** without further purification (280 mg, 0.94 mmol, 94%) as a green solid.  $R_f=0.35$  ( $\text{CH}_2\text{Cl}_2/\text{MeOH}$  10:1);  $^1\text{H NMR}$  (300 MHz,  $[\text{D}_6]\text{DMSO}$ , 25°C):  $\delta=9.42$  (d, 1H,  $^3J(\text{H,H})=6.0$  Hz; H-1), 8.60 (d, 1H,  $^3J(\text{H,H})=8.9$  Hz; H-6), 8.55 (d, 1H,  $^3J(\text{H,H})=8.6$  Hz; H-3), 8.26 (dd, 1H,  $^3J(\text{H,H})=8.9$  Hz,  $^3J(\text{H,H})=8.6$  Hz; H-5), 8.01 – 8.11 (m, 2H; H-1 and H-4), 5.05 (q, 2H,  $^3J(\text{H,H})=7.2$  Hz; H-8), 3.01 (s, 3H; H-7), 1.59 (t, 3H,  $^3J(\text{H,H})=7.2$  Hz; H-9);  $^{13}\text{C NMR}$  (75 MHz,  $[\text{D}_6]\text{DMSO}$ , 25°C):  $\delta=158.3$  ( $\text{C}_q$ ), 148.1 (CH), 136.5 ( $\text{C}_q$ ), 135.1 (CH), 129.5 (CH), 128.9 ( $\text{C}_q$ ), 127.1 (CH), 122.8 (CH), 119.2 (CH), 52.5 ( $\text{CH}_2$ ), 19.6 ( $\text{CH}_3$ ), 15.2 ( $\text{CH}_3$ ); **HRMS-ESI<sup>+</sup> ( $m/z$ ):**  $[\text{M}]^+$  calcd for  $\text{C}_{12}\text{H}_{14}\text{N}$ , 172.1121; found, 172.1122.

**(E)-1-ethyl-4-(2-(phenylamino)vinyl)quinolin-1-ium iodide (5):** Following a procedure of KISHINO et al.,<sup>[7]</sup> the iminium salt **6**, (200 mg, 0.67 mmol) and *N,N*-diphenylformamidinium iodide (131 mg, 0.67 mmol) were mixed under vigorous stirring at 160°C for 30 min. The mixture was allowed to cool down to 25°C. The resulting solid was crushed and washed several times with ethyl ether. The crude product was recrystallized from ethanol. The crystallization was completed within one night at 0°C. The precipitate was filtered off and washed with ethanol and ethyl ether to yield the desired product **5** (169 mg, 0.42 mmol, 63%) as a brown solid.  $R_f=0.33$  ( $\text{CH}_2\text{Cl}_2/\text{MeOH}$  10:1);  $^1\text{H NMR}$  (300 MHz,  $[\text{D}_6]\text{DMSO}$ , 25°C):  $\delta=10.94$  (s, 1H; NH), 8.89 (d, 1H,  $^3J(\text{H,H})=12.5$  Hz; H-8), 8.69 (d, 1H,  $^3J(\text{H,H})=7.1$  Hz; H-1), 8.32 (d, 1H,  $^3J(\text{H,H})=8.6$  Hz; H-6), 8.22 (d, 1H,  $^3J(\text{H,H})=8.7$  Hz; H-3), 8.15 (d, 1H,  $^3J(\text{H,H})=7.1$  Hz; H-2), 8.05 (dd, 1H,  $^3J(\text{H,H})=8.7$  Hz,  $^3J(\text{H,H})=7.3$  Hz; H-4), 7.81 (dd, 1H,  $^3J(\text{H,H})=7.3$  Hz,  $^3J(\text{H,H})=8.6$  Hz; H-5), 7.39 – 7.48 (m, 4H; H-9, H-10, H-12 and H-13), 7.13 (dd, 1H,  $^3J(\text{H,H})=7.2$  Hz,  $^3J(\text{H,H})=7.2$  Hz; H-11), 6.74 (d, 1H,  $^3J(\text{H,H})=12.5$  Hz; H-7), 4.70 (q, 2H,  $^3J(\text{H,H})=7.2$  Hz; H-14), 1.48 (t, 3H,  $^3J(\text{H,H})=7.2$  Hz; H-15);  $^{13}\text{C NMR}$  (75 MHz,  $[\text{D}_6]\text{DMSO}$ , 25°C):  $\delta=153.9$  ( $\text{C}_q$ ), 145.8 (CH), 143.3 (CH), 139.9 ( $\text{C}_q$ ), 137.4 ( $\text{C}_q$ ), 134.0 (CH), 129.6 (3C; CH), 127.3 (CH), 125.0 (CH), 123.8 (CH), 123.8 ( $\text{C}_q$ ), 118.3 (CH), 116.6 (CH), 109.9 (CH), 95.9 (CH), 49.8 ( $\text{CH}_2$ ), 14.8 ( $\text{CH}_3$ ); **HRMS-ESI<sup>+</sup> ( $m/z$ ):**  $[\text{M}]^+$  calcd for  $\text{C}_{19}\text{H}_{19}\text{N}_2$ , 275.1543; found, 275.1545.

## SUPPORTING INFORMATION

Synthesis of the *N*-alkylated Benzothiazolium Intermediate (**8**)

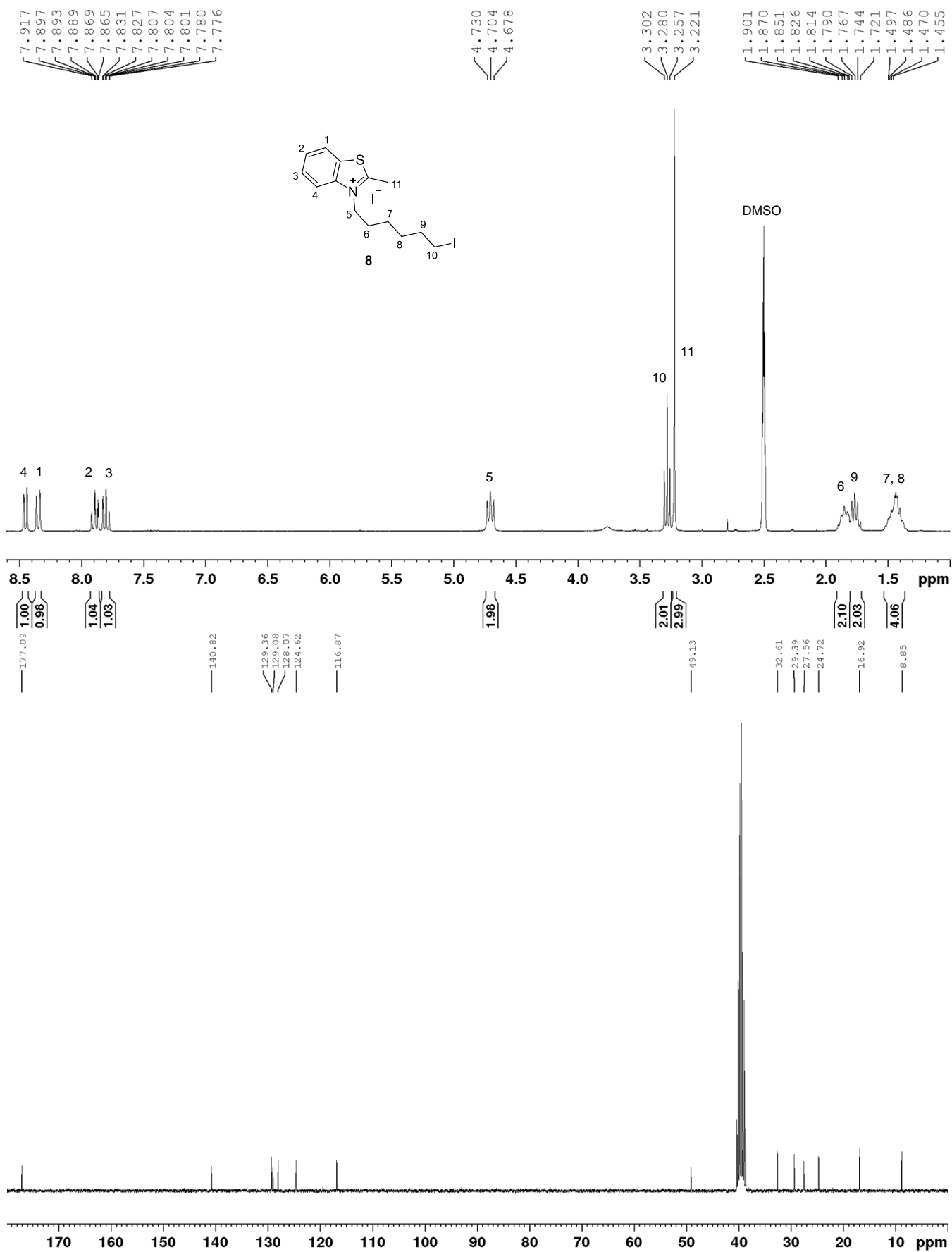
**Figure S6.** Synthesis route of *N*-alkylated benzothiazolium intermediate (**8**) starting from 1,6-dibromohexane (**11**) and 2-methylbenzothiazole (**10**).

**1,6-diiodohexane (9):** Following the procedure of SCHEUFFLER et al.<sup>[8]</sup> 1,6-dibromohexane (**11**, 20.0 mL, 130 mmol) was dissolved in acetone (500 mL) and potassium iodide (65.7 g, 396 mmol) was added. The suspension was refluxed overnight. After full conversion of the starting material the solvent was removed under reduced pressure. The remaining solid was resuspended in chloroform and filtered. The resulting solution was washed with distilled water; the aqueous layer was extracted once more with chloroform. The combined organic layers were dried over magnesium sulfate and the solvent was removed under reduced pressure to yield the desired product **9** without further purification (39.8 g, 118 mmol, 91%) as a pale orange liquid.  $R_f=0.86$  (*n*-pentane);  $^1\text{H NMR}$  (300 MHz,  $\text{CDCl}_3$ , 25°C):  $\delta=3.19$  (t, 4H,  $^3J(\text{H,H})=7.0$  Hz; H-1 and H-6), 1.79 – 1.89 (m, 4H; H-2 and H-5), 1.39 – 1.47 (m, 4H; H-3 and H-4);  $^{13}\text{C NMR}$  (75 MHz,  $\text{CDCl}_3$ , 25°C):  $\delta=33.3$  (2C;  $\text{CH}_2$ ), 29.5 (2C;  $\text{CH}_2$ ), 6.8 (2C;  $\text{CH}_2$ ); **HRMS-ESI<sup>+</sup> (*m/z*):**  $[\text{M}]^+$  calcd for  $\text{C}_6\text{H}_{12}\text{I}_2$ , 337.90284; found, 337.90185.

**3-(6-iodohexyl)-2-methylbenzo[d]thiazol-3-ium (8):** Under inert atmosphere, 2-methylbenzothiazole (**10**, 500  $\mu\text{L}$ , 3.93 mmol) was added to 1,6-diiodohexane (**9**, 3.24 mL, 19.7 mmol) and stirred at 110°C for 21.5 h. The reaction mixture was cooled to 25°C over 30 min and cooled for another 1 h at 4°C. The precipitate was filtered off and washed with cold ethyl ether to yield the desired product **8** (730 mg, 2.03 mmol, 52%) as pale orange solid.  $R_f=0.39$  ( $\text{CH}_2\text{Cl}_2/\text{MeOH}$  10:1);  $^1\text{H NMR}$  (300 MHz,  $[\text{D}_6]\text{DMSO}$ , 25°C):  $\delta=8.45$  (d, 2H,  $^3J(\text{H,H})=8.0$  Hz; H-4), 8.35 (d, 2H,  $^3J(\text{H,H})=8.5$  Hz; H-1), 7.89 (dd, 2H,  $^3J(\text{H,H})=8.5$  Hz,  $^3J(\text{H,H})=7.2$  Hz; H-2), 7.80 (dd, 2H,  $^3J(\text{H,H})=8.0$  Hz,  $^3J(\text{H,H})=7.2$  Hz; H-3), 4.70 (t, 2H,  $^3J(\text{H,H})=7.8$  Hz; H-5), 3.28 (t, 2H,  $^3J(\text{H,H})=6.8$  Hz; H-10), 3.22 (s, 3H; H-11), 1.80 – 1.91 (m, 2H; H-6), 1.71 – 1.80 (m, 2H; H-9), 1.36 – 1.53 (m, 4H; H-7 and H-8);  $^{13}\text{C NMR}$  (75 MHz,  $[\text{D}_6]\text{DMSO}$ , 25°C):  $\delta=177.1$  ( $\text{C}_q$ ), 140.8 ( $\text{C}_q$ ), 129.4 (CH), 129.1 ( $\text{C}_q$ ), 128.1 (CH), 124.6 (CH), 116.9 (CH), 49.1 ( $\text{CH}_2$ ), 32.6 ( $\text{CH}_2$ ), 29.4 ( $\text{CH}_2$ ), 27.6 ( $\text{CH}_2$ ), 24.7 ( $\text{CH}_2$ ), 16.9 ( $\text{CH}_3$ ), 8.8 ( $\text{CH}_2$ ); **HRMS-ESI<sup>+</sup> (*m/z*):**  $[\text{M}]^+$  calcd for  $\text{C}_{14}\text{H}_{19}\text{INS}$ , 360.0277; found, 360.0275.



## SUPPORTING INFORMATION

Figure S7. <sup>1</sup>H NMR and <sup>13</sup>C NMR spectra of the compound (**8**).

## SUPPORTING INFORMATION

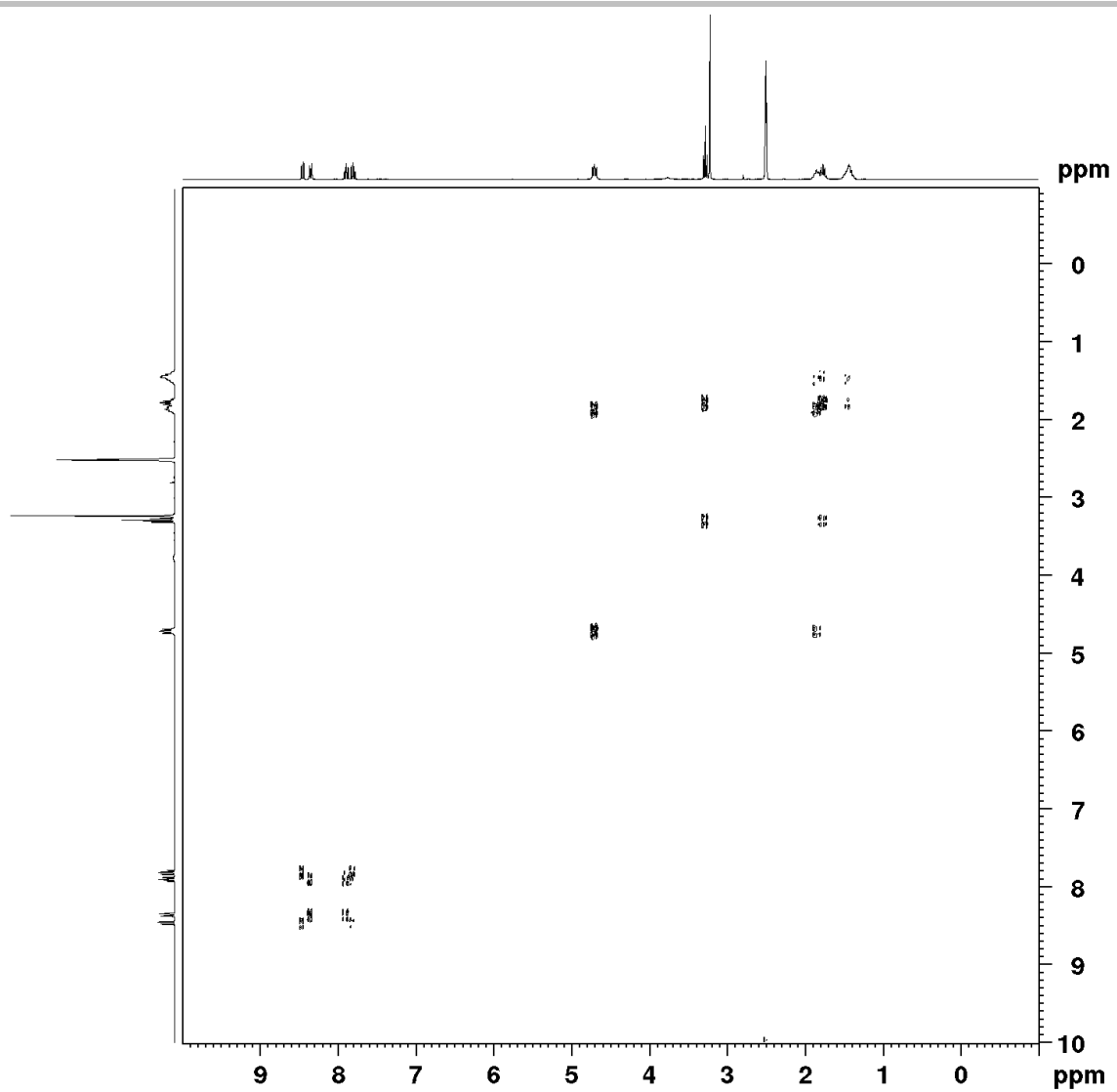


Figure S8. COSY-NMR spectra of the compound (8).

## SUPPORTING INFORMATION

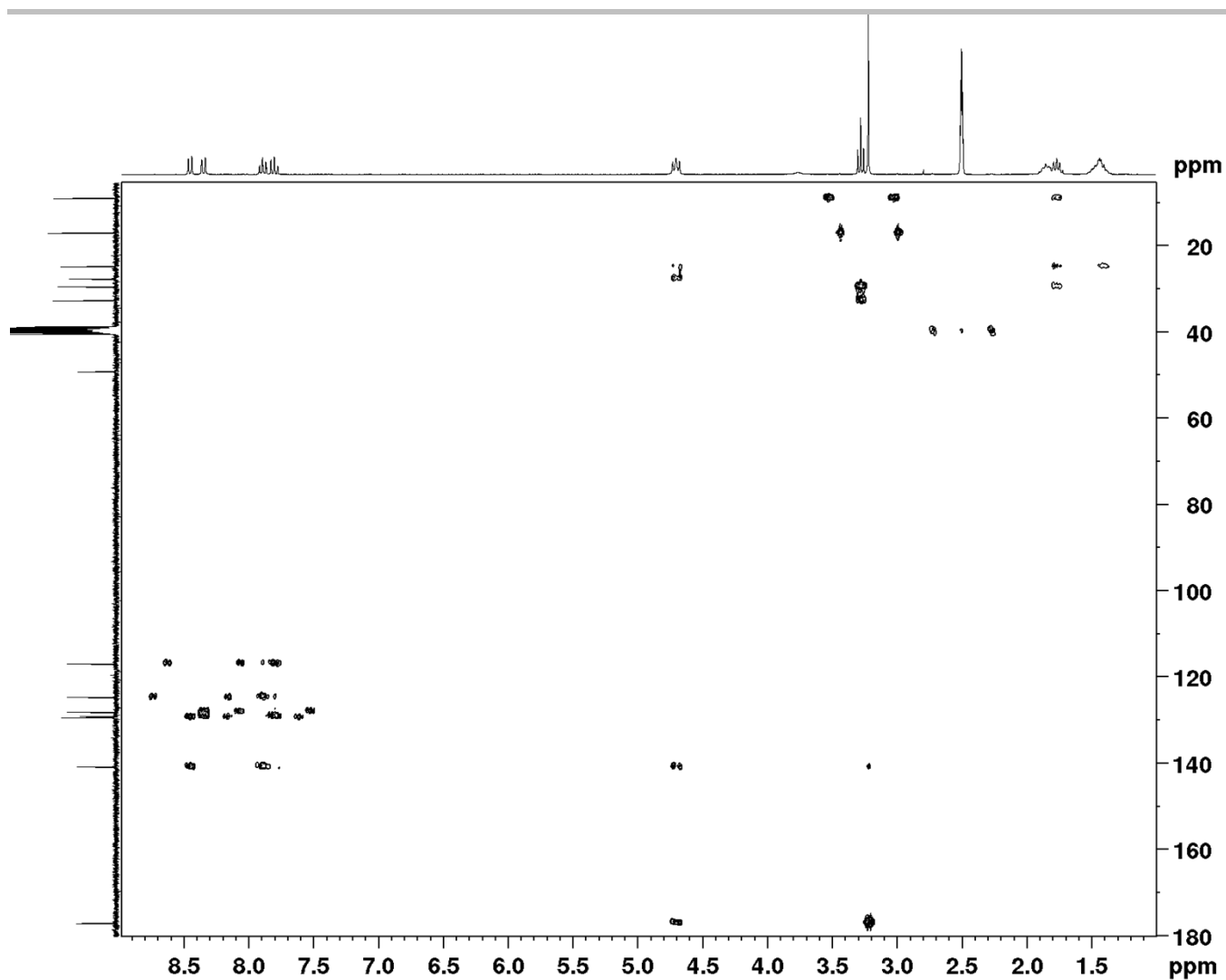
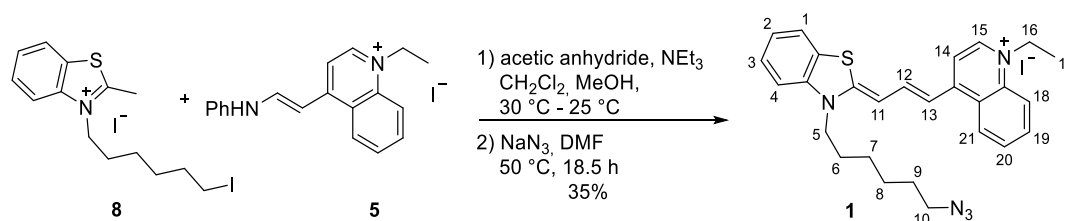


Figure S9. HMBC-NMR spectra of the compound (8).

## SUPPORTING INFORMATION

## Synthesis of the Azido Cyanine Dye Derivative 6-AzTO-3 (1)



**Figure S10.** Synthesis route of azido cyanine dye **6-AzTO-3 (1)** starting from *N*-alkylated benzothiazolium intermediate (**8**) and quinolinium iodide (**5**).

**4-((1E,3Z)-3-(3-(6-azidohexyl)benzo[d]thiazol-2(3H)-ylidene)prop-1-en-1-yl)-1-ethylquinolin-1-ium iodide (1):** The quinolinium (**5**, 250 mg, 0.62 mmol) and thiazolium (**8**, 303 mg, 0.62 mmol) were dissolved in dichloromethane (1.5 mL) and methanol (1.5 mL). Acetic anhydride (585  $\mu$ L, 6.20 mmol) and triethylamine (605  $\mu$ L, 4.36 mmol) were added and the resulting mixture was heated at 30°C for one min. Afterwards, the reaction flask was wrapped in aluminum foil and stirring in the dark at 25°C for another 1.5 h, then the solvent was removed. The crude was washed with distilled water, dissolved in dichloromethane, dried over magnesium sulfate and purified by flash column chromatography (allox, MeOH in  $\text{CH}_2\text{Cl}_2$ : 0%  $\rightarrow$  0.1%  $\rightarrow$  0.2%  $\rightarrow$  0.3%  $\rightarrow$  0.4%). Under inert atmosphere, the obtained product was dissolved in DMF (3 mL) and sodium azide (53.0 mg, 0.82 mmol) was added. The resulting mixture was heated at 50°C for 18.5 h. The solvent was removed and the product purified by flash column chromatography (allox, MeOH in  $\text{CH}_2\text{Cl}_2$ : 0%  $\rightarrow$  0.1%  $\rightarrow$  0.2%  $\rightarrow$  0.3%  $\rightarrow$  0.4%) to yield the desired product (**1**, 130 mg, 0.22 mmol, 35%) as blue solid.  $R_f=0.37$  ( $\text{CH}_2\text{Cl}_2/\text{MeOH}$  10:1);  **$^1\text{H NMR}$  (300 MHz, [D4]MeOD, 25°C):**  $\delta=8.32$  (d, 1H,  $^3J(\text{H,H})=8.4$  Hz; H-18), 8.05 (d, 1H,  $^3J(\text{H,H})=7.2$  Hz; H-15), 7.96 (dd, 1H,  $^3J(\text{H,H})=12.3$  Hz,  $^3J(\text{H,H})=13.3$  Hz; H-12), 7.75 – 7.78 (m, 2H; H-20 and H-21), 7.51 – 7.56 (m, 2H; H-4 and H-19), 7.49 (d, 1H,  $^3J(\text{H,H})=7.2$  Hz; H-14), 7.26 (dd, 1H,  $^3J(\text{H,H})=8.2$  Hz,  $^3J(\text{H,H})=7.2$  Hz; H-2), 7.16 (d, 1H,  $^3J(\text{H,H})=8.2$  Hz; H-1), 7.12 (dd, 1H,  $^3J(\text{H,H})=7.9$  Hz,  $^3J(\text{H,H})=7.2$  Hz; H-3), 6.95 (d, 1H,  $^3J(\text{H,H})=13.3$  Hz; H-13), 6.43 (d, 1H,  $^3J(\text{H,H})=12.3$  Hz; H-11), 4.40 (q, 2H,  $^3J(\text{H,H})=7.2$  Hz; H-16), 4.10 (t, 2H,  $^3J(\text{H,H})=7.8$  Hz; H-5), 3.30 – 3.33 (m, 2H; H-10), 1.73 – 1.79 (m, 2H; H-6), 1.58 - 1.65 (m, 2H; H-9), 1.46 – 1.53 (m, 7H; H-7, H-8 and H-17);  **$^{13}\text{C NMR}$  (75 MHz, [D4]MeOD, 25°C):**  $\delta=163.2$  ( $\text{C}_q$ ), 152.4 ( $\text{C}_q$ ), 145.1 (CH), 142.8 ( $\text{C}_q$ ), 142.4 (CH), 139.3 ( $\text{C}_q$ ), 134.4 (CH), 128.7 (CH), 127.6 (CH), 126.8 (CH), 126.4 ( $\text{C}_q$ ), 126.0 ( $\text{C}_q$ ), 125.3 (CH), 123.4 (CH), 118.2 (CH), 113.1 (CH), 110.6 (2C; CH), 99.8 (CH), 52.4 ( $\text{CH}_2$ ), 50.9 ( $\text{CH}_2$ ), 47.0 ( $\text{CH}_2$ ), 29.8 ( $\text{CH}_2$ ), 28.3 ( $\text{CH}_2$ ), 27.6 ( $\text{CH}_2$ ), 27.3 ( $\text{CH}_2$ ), 15.0 ( $\text{CH}_3$ );  $t_R=33.3$  min (5% to 75% B in 30 min); **HRMS-ESI $^+$  ( $m/z$ ):** [ $\text{M}$ ] $^+$  calcd for  $\text{C}_{27}\text{H}_{30}\text{N}_5\text{S}$ , 456.2216; found, 456.2215.

## SUPPORTING INFORMATION

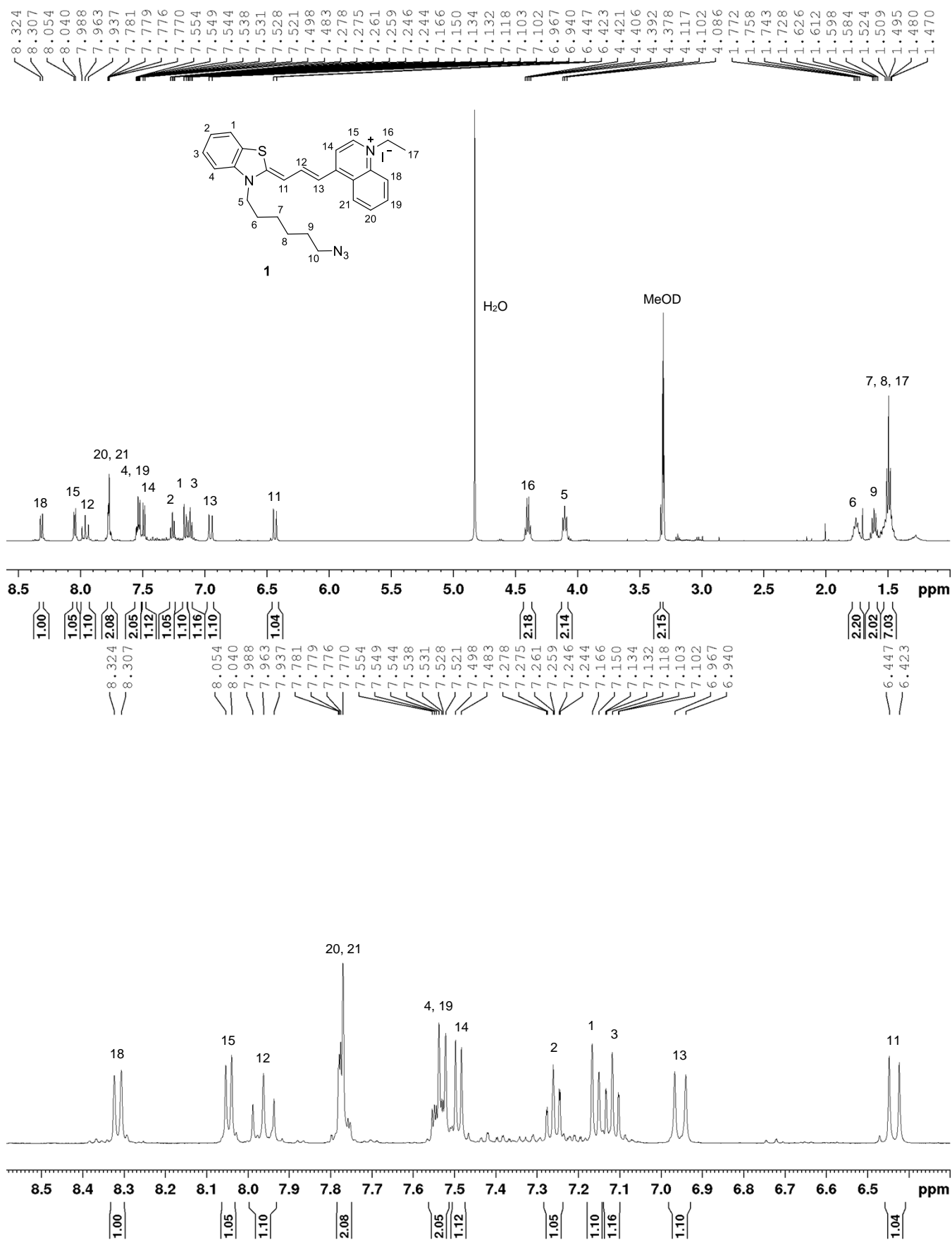


Figure S11. <sup>1</sup>H-NMR spectrum of 6-AzTO-3 (1) and zoom in the region between 6.3 and 8.6 ppm.

## SUPPORTING INFORMATION

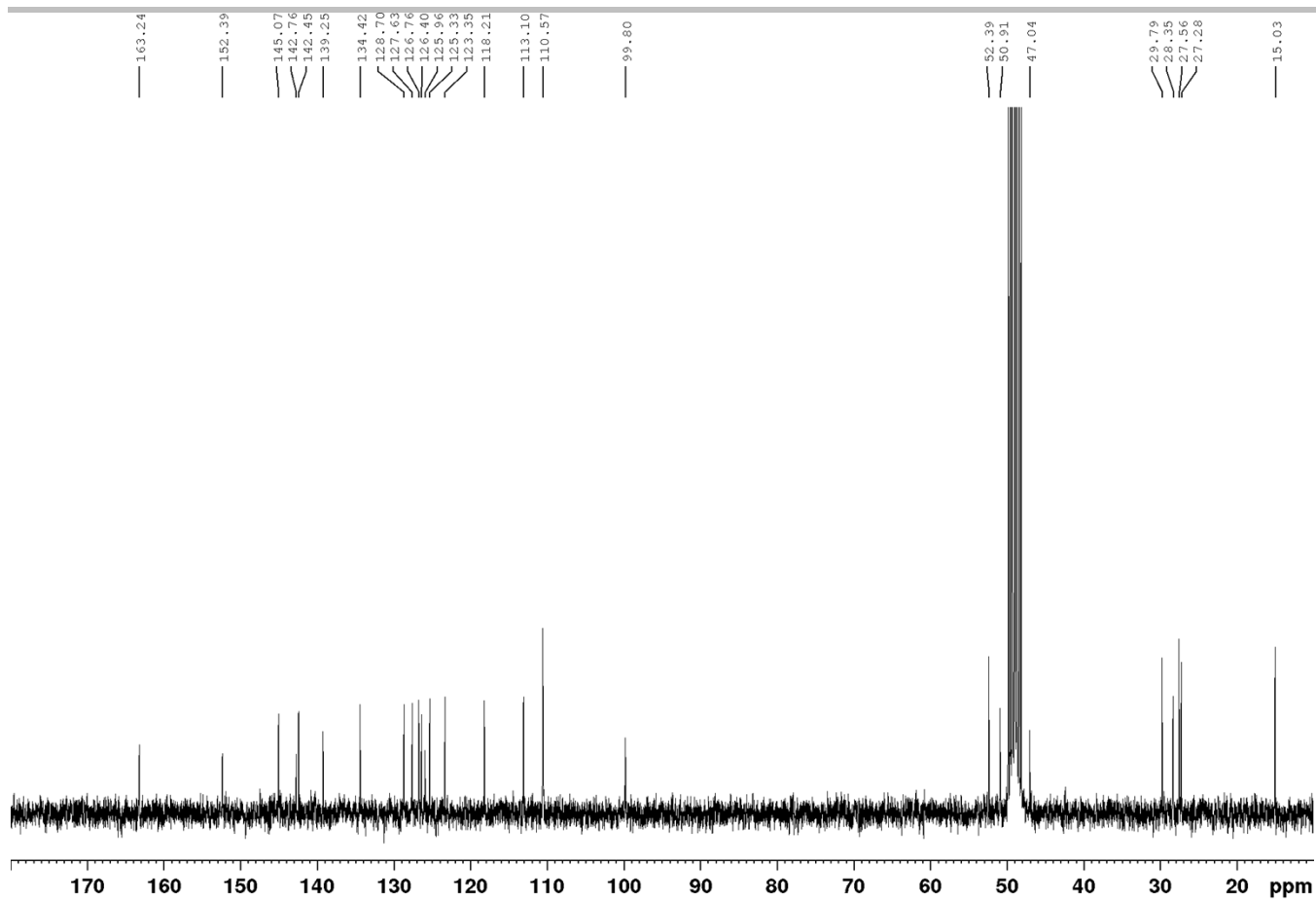


Figure S12.  $^{13}\text{C}$ -NMR spectrum of 6-AzTO-3 (1).

## SUPPORTING INFORMATION

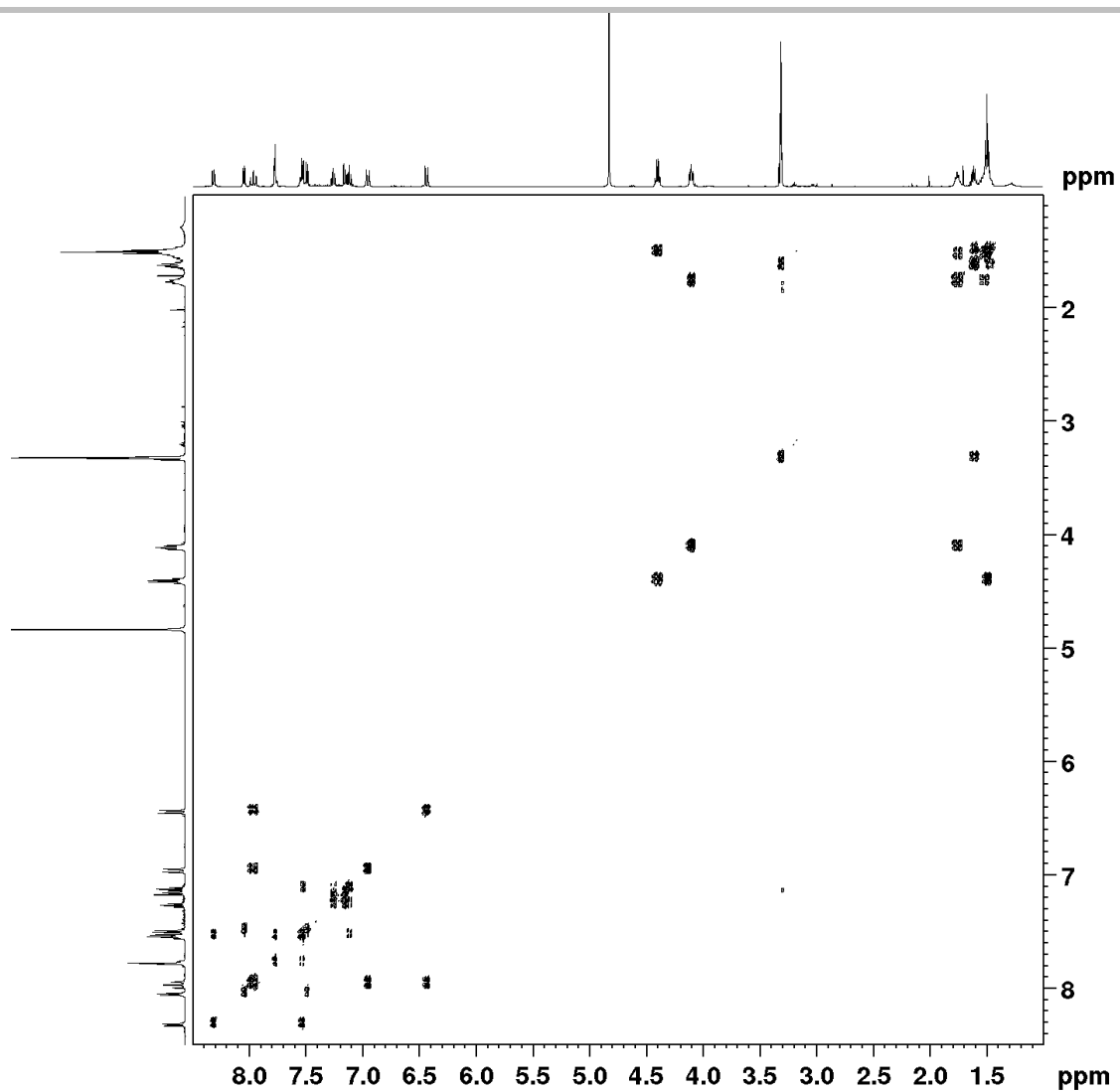


Figure 13. COSY-NMR spectrum of 6-AzTO-3 (1)

## SUPPORTING INFORMATION

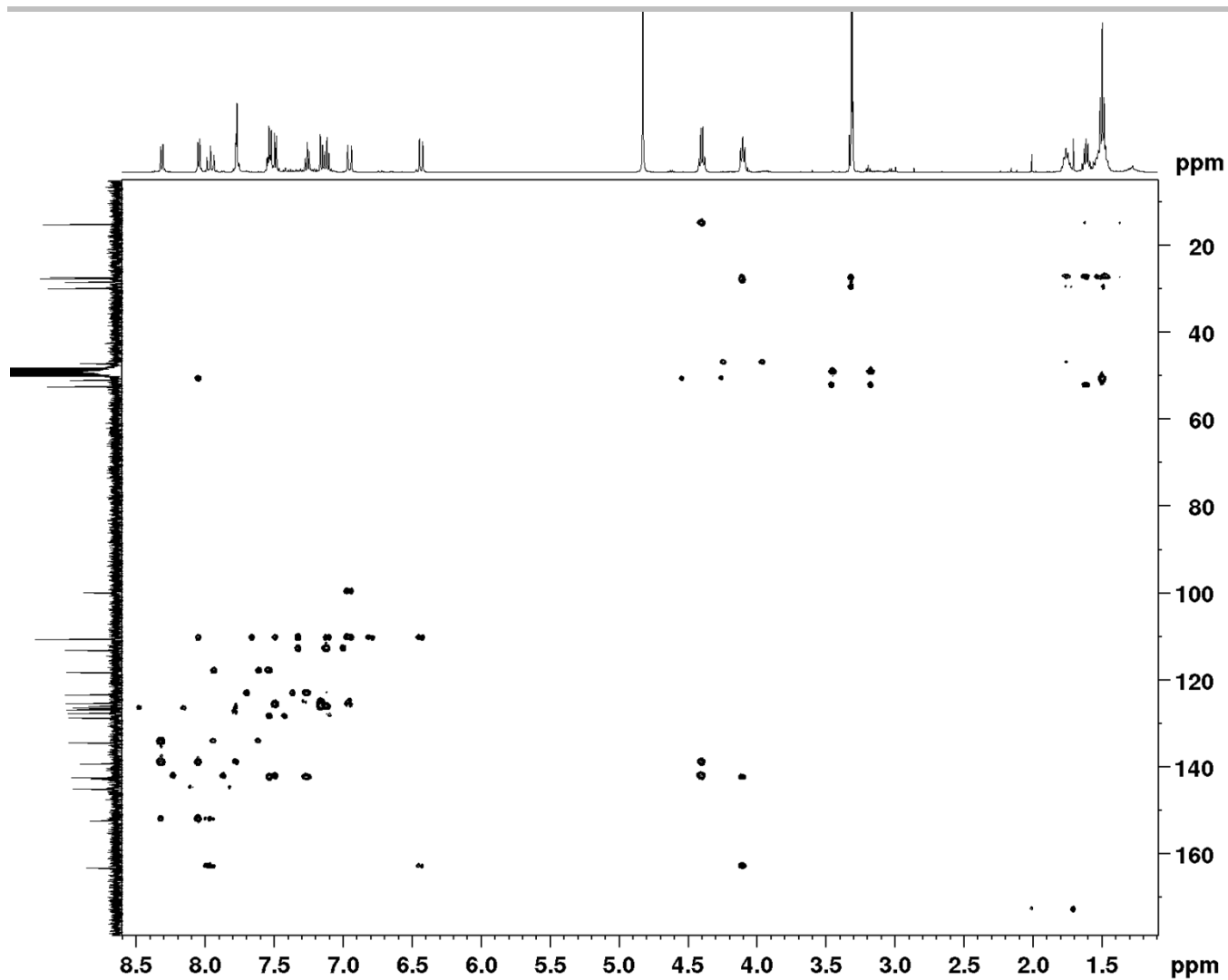


Figure S14. HMBC-NMR spectrum of 6-AzTO-3 (1).



## SUPPORTING INFORMATION

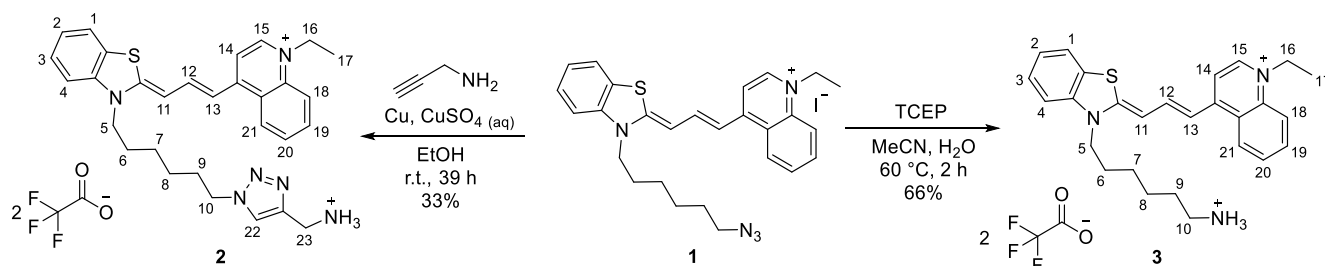
Synthesis of the Amine Cyanine Dyes: 6-TramTO-3 (2) and 6-NH<sub>2</sub>TO-3 (3)

Figure S15. Synthesis route of the amine cyanine dyes 6-TramTO-3 (2) and 6-NH<sub>2</sub>TO-3 (3) starting from azido cyanine dye 6-AzTO-3 (1).

**4-((1E,3Z)-3-(3-(6-(4-(aminomethyl)-1H-1,2,3-triazol-1-yl)hexyl)benzo[d]thiazol-2(3H)-ylidene)prop-1-en-1-yl)-1-ethylquinolin-1-ium iodide (6-TramTO-3):** Under inert atmosphere, azido derivative cyanine dye 6-AzTO-3 (3, 49.0 mg, 84.0  $\mu$ mol) was dissolved in ethanol (415  $\mu$ L) and propargylamine (10.7  $\mu$ L, 168  $\mu$ mol), copper powder (6.4 mg, 101  $\mu$ mol) and copper sulfate (100 mM, 42  $\mu$ L, 4.20  $\mu$ mol) were added. The resulting mixture was stirred for 39 h, filtered and the solvent was removed. The product was purified by preparative HPLC (5 - 75%) to yield the desired product (2, 20.5 mg, 27.8  $\mu$ mol, 33%) as blue solid.  $R_f=0.08$  (CH<sub>2</sub>Cl<sub>2</sub>/MeOH 10:1); **<sup>1</sup>H NMR (300 MHz, [D6]DMSO, 25 °C):**  $\delta=8.48$  (d, 1H, <sup>3</sup>J(H,H)=8.4 Hz; H-18), 8.45 (d, 1H, <sup>3</sup>J(H,H)=7.2 Hz; H-15), 8.31 (s, 2H; NH<sub>2</sub>), 8.09 – 8.18 (m, 3H; H-12, H-21 and H-22), 7.97 (dd, 1H, <sup>3</sup>J(H,H)=8.4 Hz, <sup>3</sup>J(H,H)=7.3 Hz; H-20), 7.86 – 7.88 (m, 2H; H-4 and H-14), 7.71 (dd, 1H, <sup>3</sup>J(H,H)=8.4 Hz, <sup>3</sup>J(H,H)=7.3 Hz; H-19), 7.58 (d, 1H, <sup>3</sup>J(H,H)=8.2 Hz; H-1), 7.48 (dd, 1H, <sup>3</sup>J(H,H)=8.2 Hz, <sup>3</sup>J(H,H)=7.2 Hz; H-2), 7.31 (dd, 1H, <sup>3</sup>J(H,H)=8.0 Hz, <sup>3</sup>J(H,H)=7.2 Hz; H-3), 7.13 (d, 1H, <sup>3</sup>J(H,H)=13.2 Hz; H-13), 6.50 (d, 1H, <sup>3</sup>J(H,H)=12.3 Hz; H-11), 4.61 (q, 2H, <sup>3</sup>J(H,H)=7.2 Hz; H-16), 4.40 (t, 2H, <sup>3</sup>J(H,H)=7.1 Hz; H-10), 4.22 (t, 2H, <sup>3</sup>J(H,H)=7.6 Hz; H-5), 4.09 – 4.13 (m, 2H; H-23), 1.79 – 1.86 (m, 2H; H-6), 1.68 – 1.76 (m, 2H; H-9), 1.44 – 1.49 (m, 5H; H-8 and H-17), 1.29 – 1.36 (m, 2H; H-7); **<sup>13</sup>C NMR (75 MHz, [D6]DMSO, 25 °C):**  $\delta=160.9$  (C<sub>q</sub>), 150.5 (C<sub>q</sub>), 144.0 (CH), 142.3 (CH), 141.5 (C<sub>q</sub>), 140.1 (C<sub>q</sub>), 137.7 (C<sub>q</sub>), 133.5 (CH), 127.7 (CH), 126.7 (CH), 125.3 (CH), 124.8 (C<sub>q</sub>), 124.3 (C<sub>q</sub>), 124.2 (2C; CH), 122.7 (CH), 117.9 (CH), 112.5 (CH), 110.0 (CH), 109.5 (CH), 98.5 (CH), 49.4 (2C; CH<sub>2</sub>), 45.5 (CH<sub>2</sub>), 34.0 (CH<sub>2</sub>), 29.7 (CH<sub>2</sub>), 26.9 (CH<sub>2</sub>), 25.6 (CH<sub>2</sub>), 25.5 (CH<sub>2</sub>), 14.8 (CH<sub>3</sub>);  $t_R=24.2$  min (5% to 75% B in 30 min); **HRMS-ESI<sup>+</sup> (m/z):** [M]<sup>+</sup> calcd for C<sub>30</sub>H<sub>35</sub>N<sub>6</sub>S, 511.2638; found, 511.2641.

**mono(4-((1E,3Z)-3-(3-(6-ammoniohexyl)benzo[d]thiazol-2(3H)-ylidene)prop-1-enyl)-1-ethylquinolinium) mono(2,2,2-trifluoroacetate) (6-NH<sub>2</sub>TO-3):** Azido derivative cyanine dye (3, 40 mg, 87.6  $\mu$ mol) was dissolved in acetonitrile (600  $\mu$ L) and a solution of TCEP in milli-Q water (0.44 M, 600  $\mu$ L, 263  $\mu$ mol) was added. The resulting mixture was stirred for 2 h at 60 °C afterwards it was purified by preparative HPLC (5 - 75%) to yield the desired product (3, 31.5 mg, 57.8  $\mu$ mol, 66%) as blue solid.  $R_f=0.05$  (CH<sub>2</sub>Cl<sub>2</sub>/MeOH 10:1); **<sup>1</sup>H NMR (500 MHz, [D6]DMSO, 25 °C):**  $\delta=8.43$  – 8.52 (m, 2H; H-15 and H-18), 8.13 – 8.20 (m, 1H; H-12), 8.10 (d, 1H, <sup>3</sup>J(H,H)=8.6 Hz; H-21), 7.97 (dd, 1H, <sup>3</sup>J(H,H)=7.7 Hz, <sup>3</sup>J(H,H)=8.6 Hz; H-20), 7.86 – 7.92 (m, 2H; H-4 and H-14), 7.67 – 7.79 (m, 4H; H-19 and NH<sub>3</sub>), 7.60 (d, 1H, <sup>3</sup>J(H,H)=8.0 Hz; H-1), 7.49 (dd, 1H, <sup>3</sup>J(H,H)=7.3 Hz, <sup>3</sup>J(H,H)=8.0 Hz; H-2), 7.31 (dd, 1H, <sup>3</sup>J(H,H)=7.3 Hz, <sup>3</sup>J(H,H)=7.5 Hz; H-3), 7.14 (d, 1H, <sup>3</sup>J(H,H)=13.2 Hz; H-13), 6.52 (d, 1H, <sup>3</sup>J(H,H)=12.2 Hz; H-11), 4.61 (q, 2H, <sup>3</sup>J(H,H)=7.2 Hz; H-16), 4.24 (t, 2H, <sup>3</sup>J(H,H)=7.1 Hz; H-5), 2.75 – 2.82 (m, 2H; H-10), 1.69 – 1.78 (m, 2H; H-6), 1.52 – 1.58 (m, 2H; H-9), 1.37 – 1.50 (m, 7H; H-7, H-8 and H-17); **<sup>13</sup>C NMR (125 MHz, [D6]DMSO, 25 °C):**  $\delta=158.1$  (C<sub>q</sub>), 150.5 (C<sub>q</sub>), 144.0 (CH), 142.3 (CH), 141.5 (C<sub>q</sub>), 137.7 (C<sub>q</sub>), 133.5 (CH), 127.7 (CH), 126.7 (CH), 125.3 (CH), 124.7 (C<sub>q</sub>), 124.3 (C<sub>q</sub>), 124.2 (CH), 122.7 (CH), 118.0 (CH), 112.5 (CH), 110.3 (CH), 109.5 (CH), 98.4 (CH), 49.4 (CH<sub>2</sub>), 45.5 (CH<sub>2</sub>), 38.7 (CH<sub>2</sub>), 26.9 (CH<sub>2</sub>), 26.9 (CH<sub>2</sub>), 25.6 (2C; CH<sub>2</sub>), 14.8 (CH<sub>3</sub>);  $t_R=23.5$  min (5% to 75% B in 30 min); **HRMS-ESI<sup>+</sup> (m/z):** [M]<sup>+</sup> calcd for C<sub>27</sub>H<sub>32</sub>N<sub>3</sub>S, 430.2311; found, 430.2302.

## SUPPORTING INFORMATION

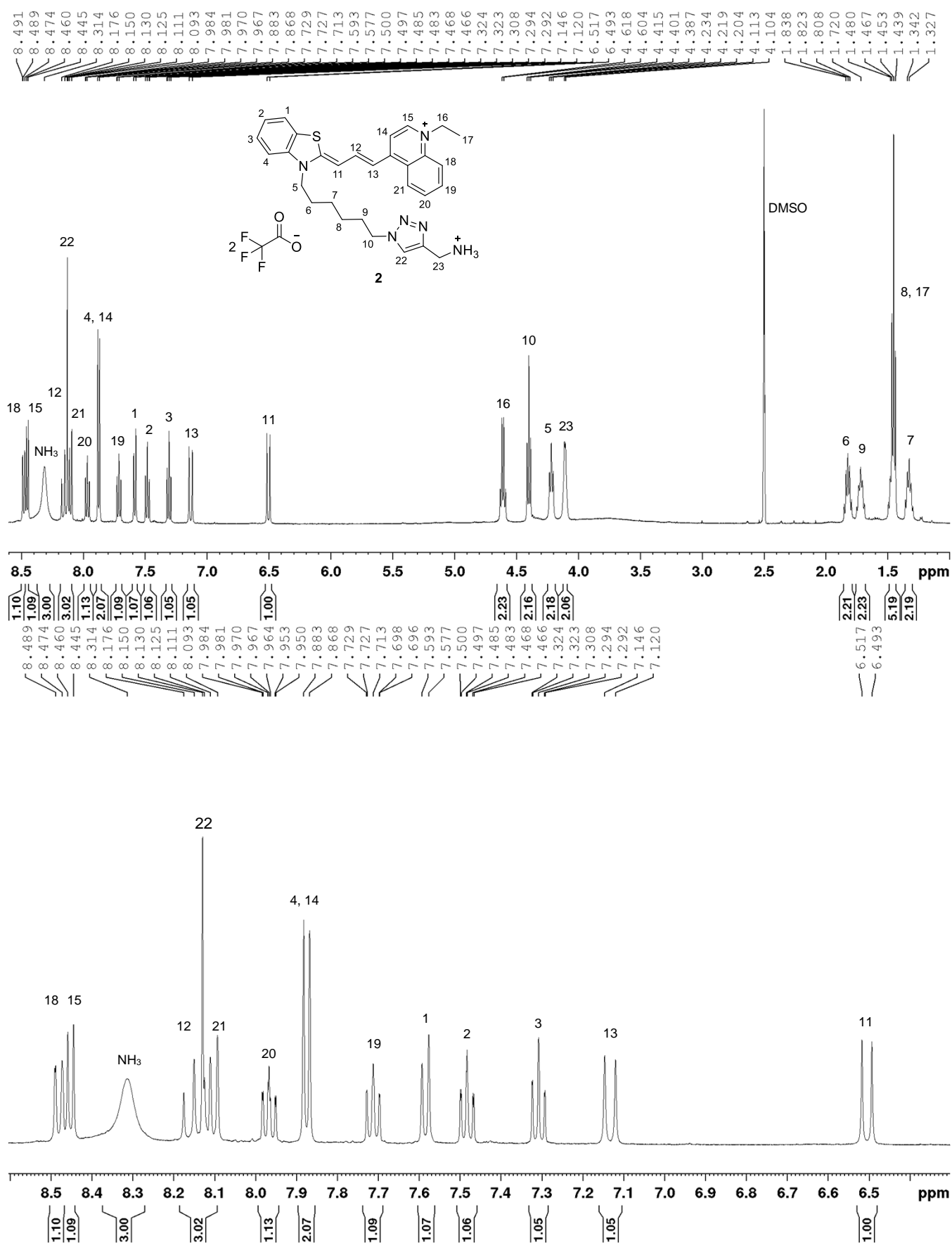


Figure S16.  $^1\text{H-NMR}$  spectrum of 6-TramTO-3 (2) and zoom in the region between 6.3 and 8.6 ppm.

## SUPPORTING INFORMATION

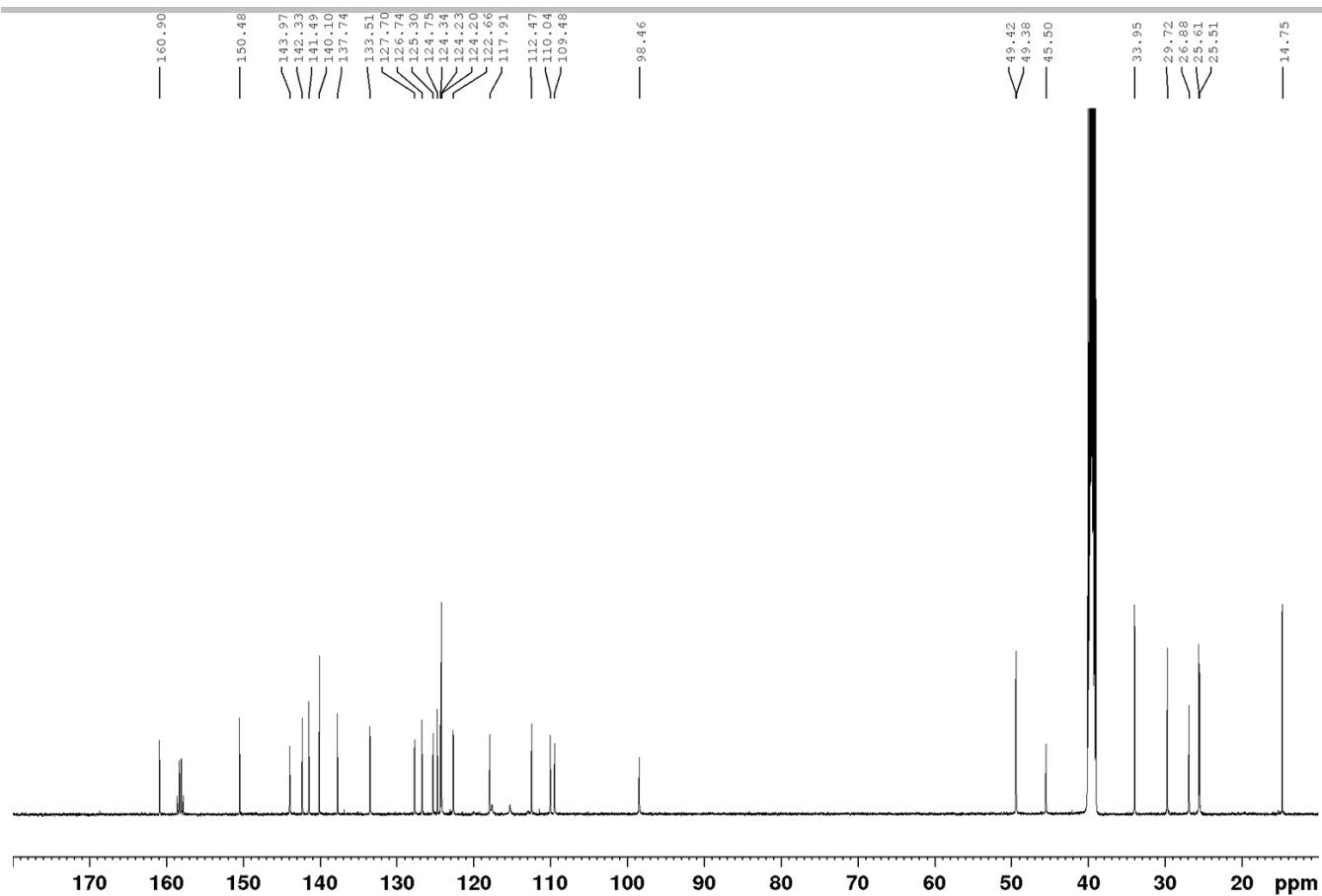


Figure S17. <sup>13</sup>C-NMR spectrum of 6-TramTO-3 (2).



## SUPPORTING INFORMATION

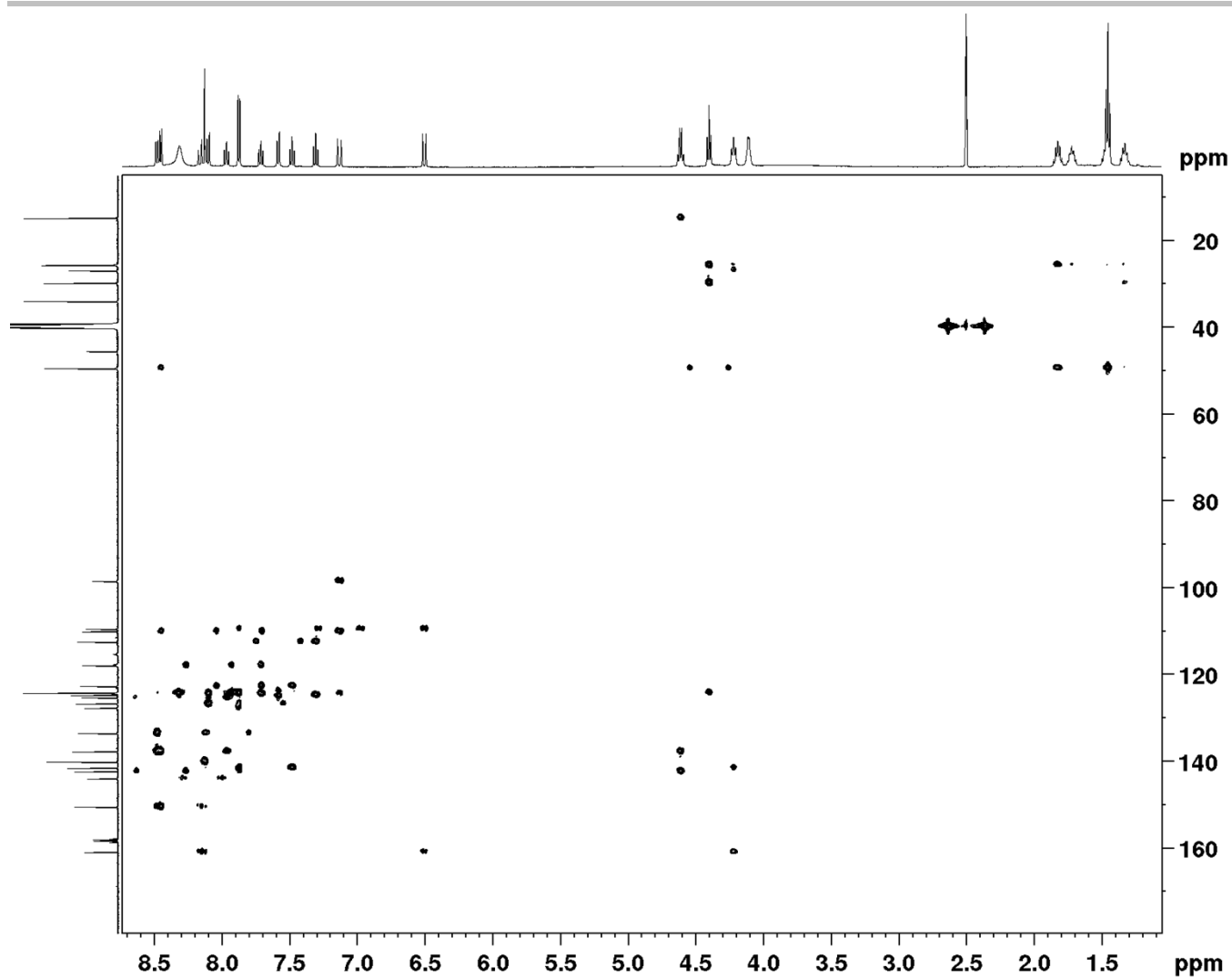


Figure S19. HMBC-NMR spectrum of the 6-TramTO-3 (2).

## SUPPORTING INFORMATION

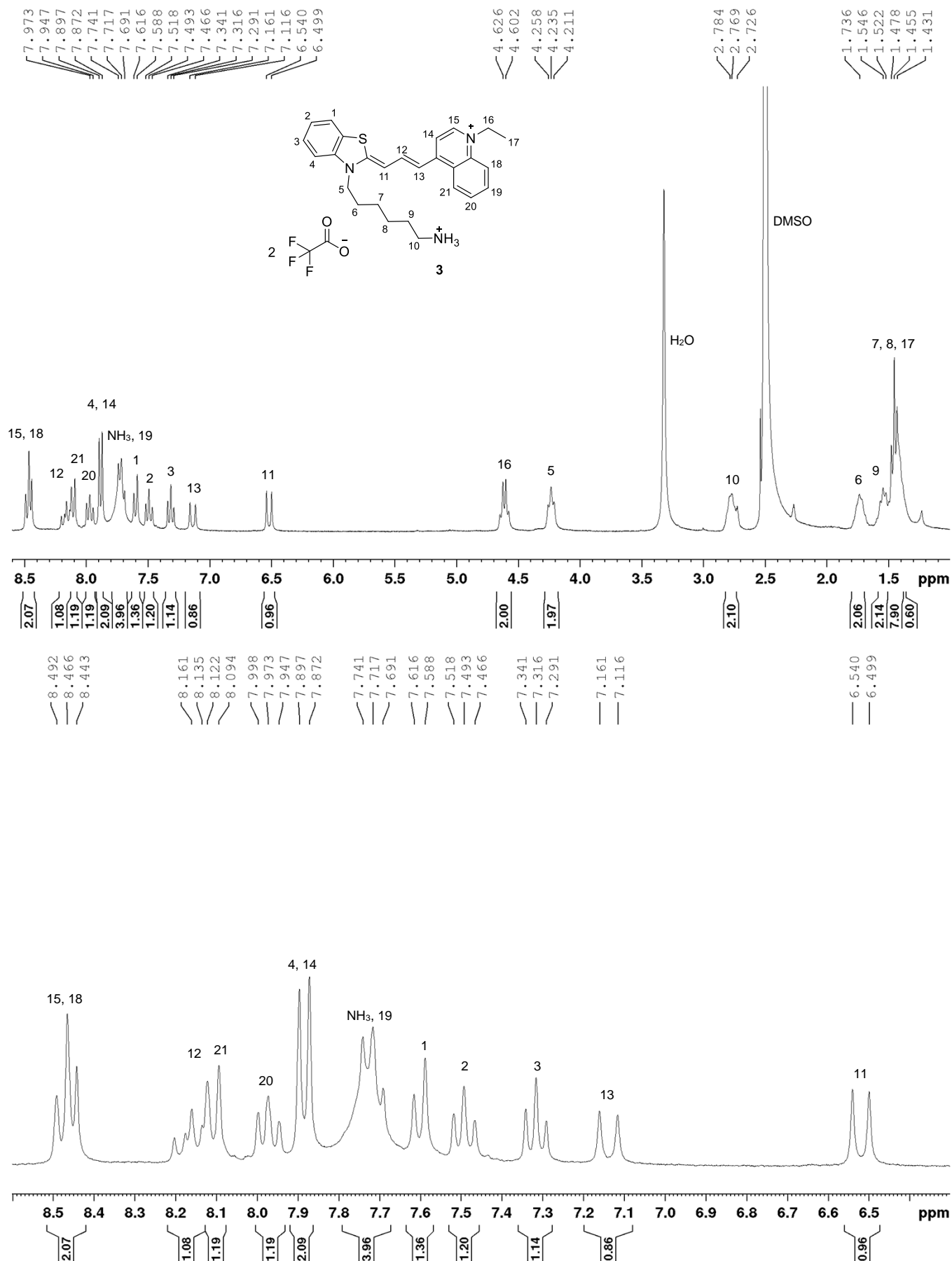


Figure S20 <sup>1</sup>H-NMR spectrum of 6-NH<sub>2</sub>TO-3 (3) and zoom in the region between 6.3 and 8.6 ppm.

## SUPPORTING INFORMATION

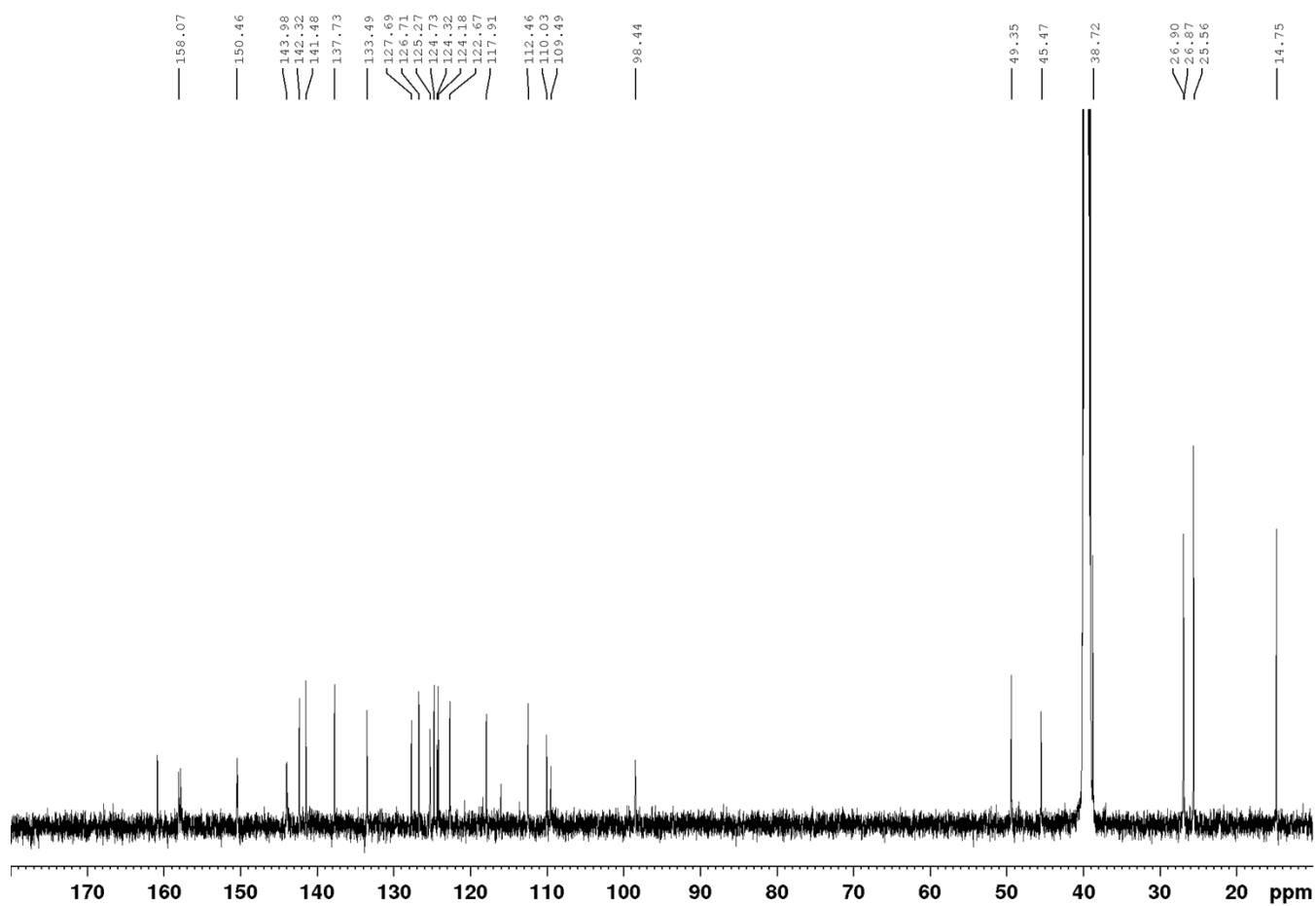


Figure S21.  $^{13}\text{C}$ -NMR spectrum of 6-NH<sub>2</sub>TO-3 (3).

## SUPPORTING INFORMATION

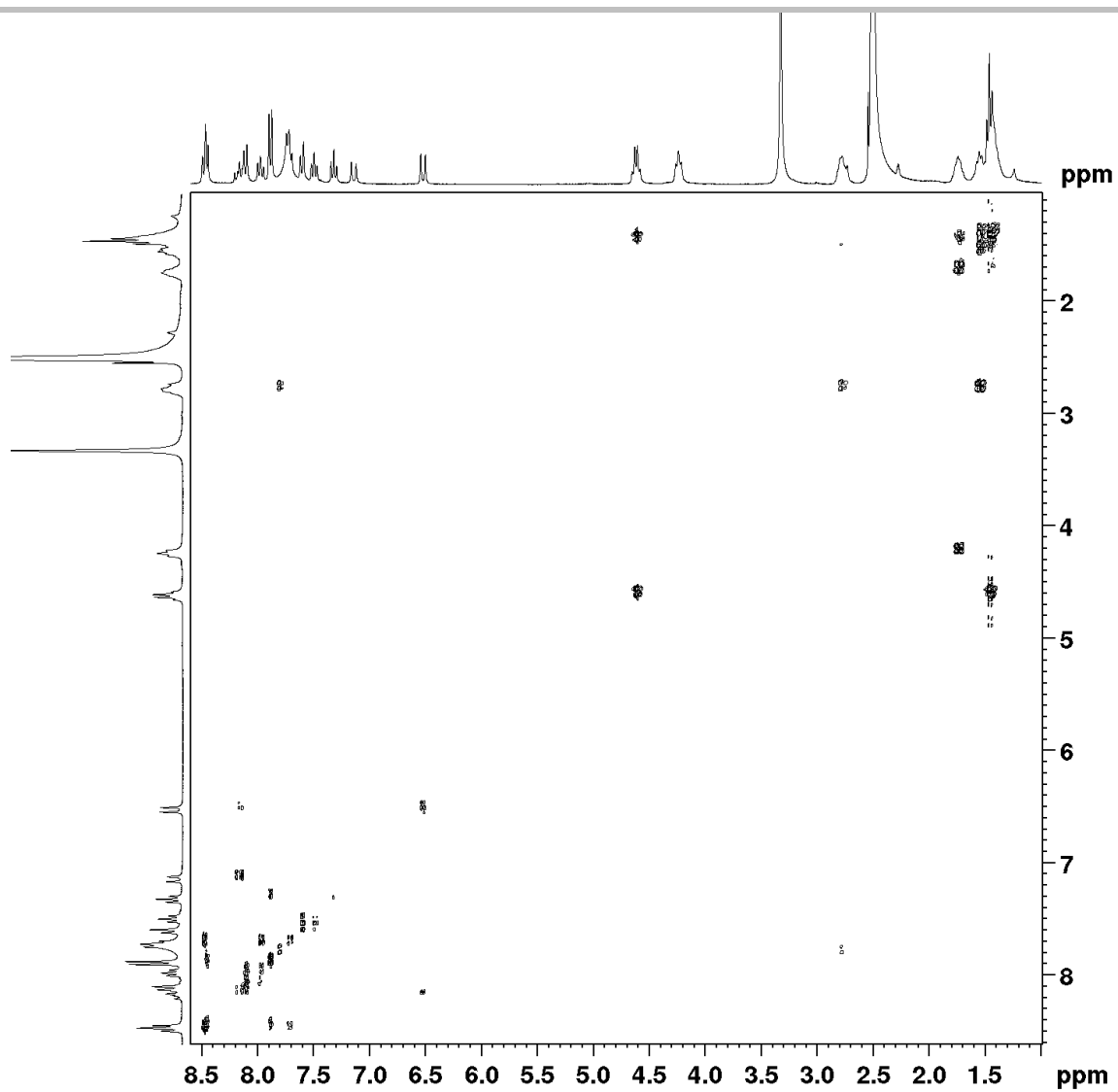


Figure S22. COSY-NMR spectra of 6-NH<sub>2</sub>TO-3 (3).



## SUPPORTING INFORMATION

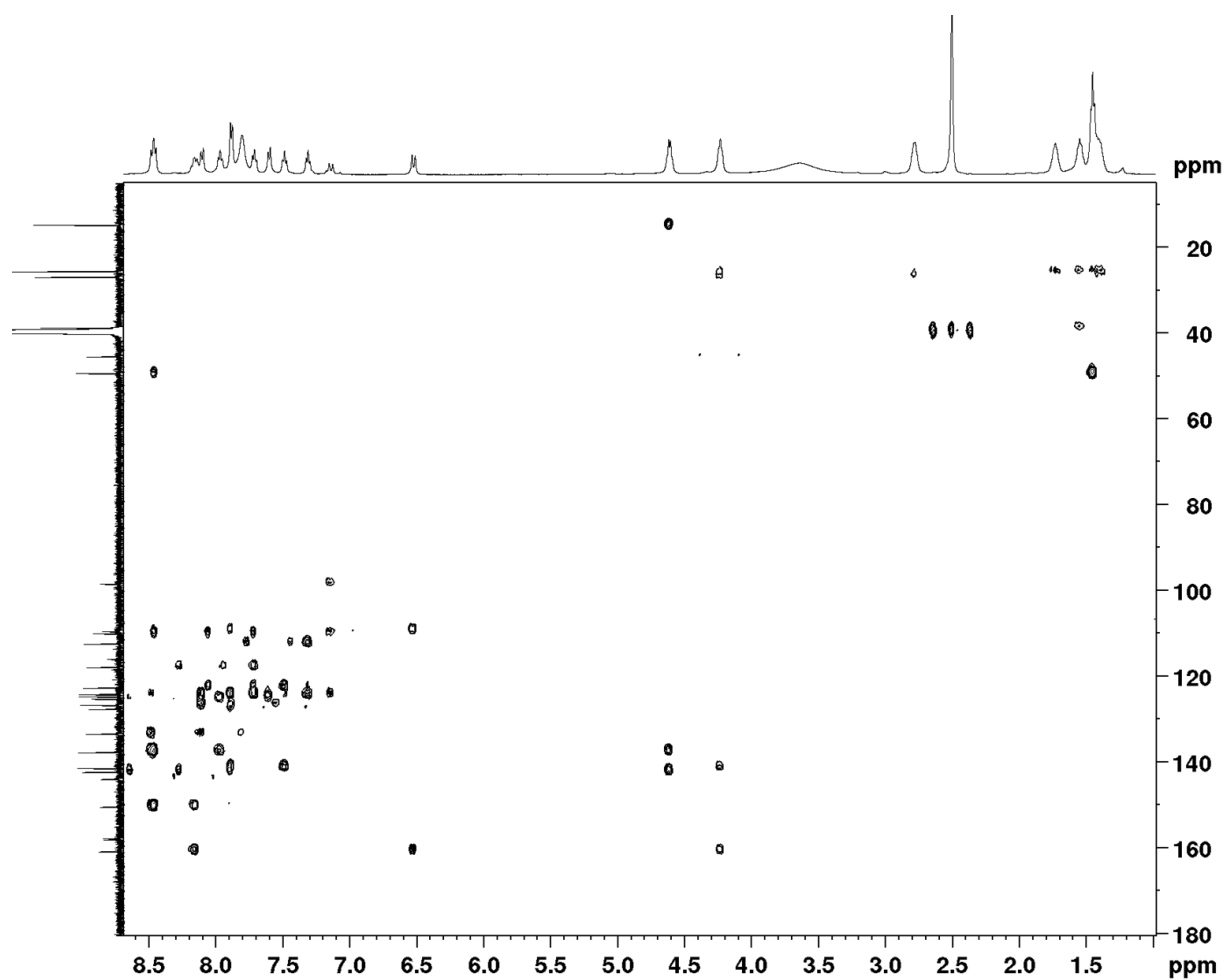


Figure S23. HMBC-NMR spectra of 6-NH<sub>2</sub>TO-3 (3).

## SUPPORTING INFORMATION

## Results and Discussion

## Excitation and Emission Spectra of the NIR Cyanine Dye Derivatives

For each cyanine dye derivative: **6-AzTO-3**, **6-TramTO-3** and **6-NH<sub>2</sub>TO-3**, the excitation and emission spectra of a 10  $\mu\text{M}$  solution of the corresponding compound in 1 mL of 10 mM Tris pH 7.6 and 50 mM KCl were measured. The excitation spectra were recorded at an emission of 670 nm in a range from 500 – 660 nm (slit 5/10 nm), while the emission spectra were measured at an excitation of 590 nm in a range from 600 – 750 nm (slit 5/10 nm).

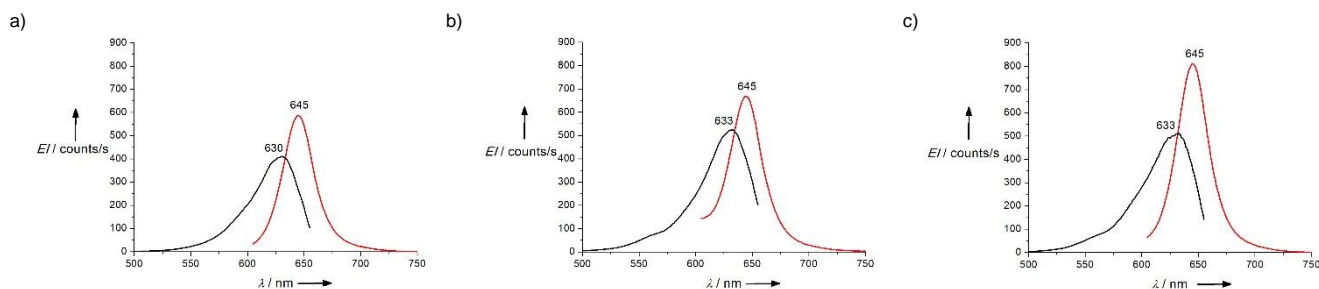


**Figure S24.** Excitation (black line) and emission (red line) spectra of 10  $\mu\text{M}$  solution of cyanine dye: a) **6-AzTO-3**; b) **6-TramTO-3** and c) **6-NH<sub>2</sub>TO-3** in 1 mL 10 mM Tris pH 7.6 mM and 50 mM KCl at 20°C.

Fluorescence Emission of the NIR Cyanine Dye Derivatives with(out) dsDNA<sub>CT</sub>

We compared the fluorescence properties of different cyanine dyes: **6-AzTO-3**, **6-TramTO-3** and **6-NH<sub>2</sub>TO-3** in presence of double-stranded calf thymus DNA (dsDNA<sub>CT</sub>). The emission spectra of a 1  $\mu\text{M}$  solution of the corresponding compound in 120  $\mu\text{L}$  of 10 mM Tris pH 7.6 and 50 mM KCl were measured in presence and absence of 15  $\mu\text{M}$  dsDNA<sub>CT</sub>. A 100  $\mu\text{L}$  fluorescence cuvette of HellmaAnalytics (105.250-QS) was used. The spectra were measured using an excitation and emission slits of 5 nm.

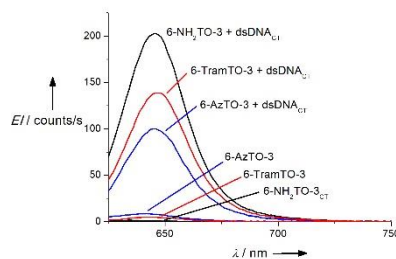


**Figure S25.** Emission spectra of 1  $\mu\text{M}$  solution of cyanine dye in presence and absence of 15  $\mu\text{M}$  dsDNA<sub>CT</sub>. All spectra were measured in 120  $\mu\text{L}$  10 mM Tris pH 7.6 and 50 mM KCl at 20°C: **6-AzTO-3** is shown in blue; **6-TramTO-3** is shown in red and **6-NH<sub>2</sub>TO-3** is shown in black.

## Fluorescence Titrations of 6-TramTO-3

All fluorescence titrations followed the same procedure: to 1 mL of 1  $\mu\text{M}$  solution of corresponding cyanine dye derivative in 10 mM Tris pH 7.6 and 50 mM KCl aliquots of a stock solution of the corresponding annealed DNA (dsDNA<sub>hAT</sub> and dsDNA<sub>hGC</sub> = 435  $\mu\text{M}$ ; dsDNA<sub>CT</sub> = 0.65 mM) were successively added and the fluorescence spectra were recorded in a range from 625-750 nm after 1 min of each addition. For each compound three independent measurements were carried out. The fluorescence emission plotted is the resulting mean of the three independent measurements.

## SUPPORTING INFORMATION

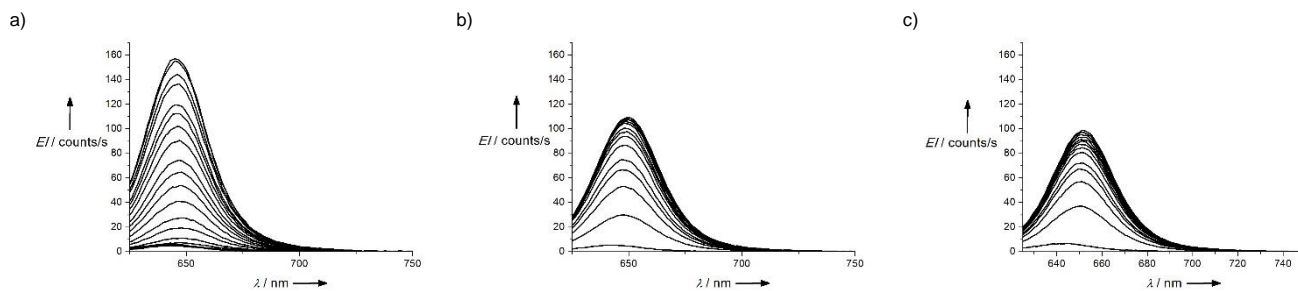


**Figure S26.** Fluorescence spectra of the titration of **6-TramTO-3** with a) dsDNA<sub>CT</sub>; b) dsDNA<sub>HAT</sub>; c) dsDNA<sub>HGC</sub>. All spectra were measured of a 1  $\mu\text{M}$  solution of cyanine dye in 10 mM Tris pH 7.6 mM and 50 mM KCl at 20°C.

The stability of **6-TramTO-3** fluorescence signal was studied in presence and absence of dsDNA<sub>CT</sub>. Emission spectra of a 2.5  $\mu\text{M}$  solution of **6-TramTO-3** in 10 mM Tris pH 7.6 and 50 mM KCl (total volume 1 mL) were measured in presence and absence of 37.5  $\mu\text{M}$  dsDNA<sub>CT</sub>. The fluorescence spectra were recorded in a range from 625-750 nm with slits of 3/5 nm for the sample without dsDNA<sub>CT</sub> and slits of 3/3 nm for the sample with dsDNA<sub>CT</sub> and measuring at one hour intervals for 5 hours. Incubation of the samples was performed at both 20°C and 37°C in the dark. Three independent measurements were carried out for each experiment.

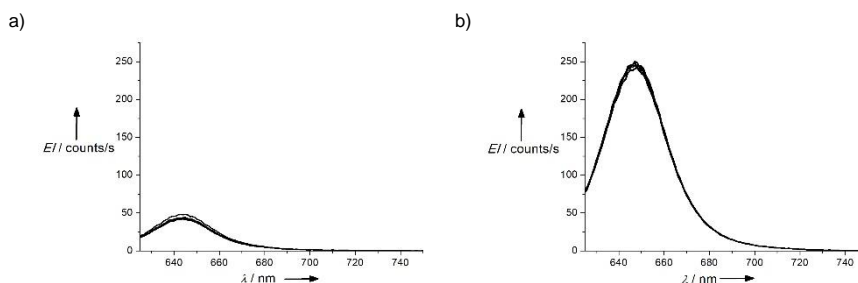


**Figure S27.** Fluorescence spectra of **6-TramTO-3** a) alone; b) with 37.5  $\mu\text{M}$  dsDNA<sub>CT</sub> after incubation at 20°C. All spectra were measured of a 2.5  $\mu\text{M}$  solution of **6-TramTO-3** in 10 mM Tris pH 7.6 and 50 mM KCl.

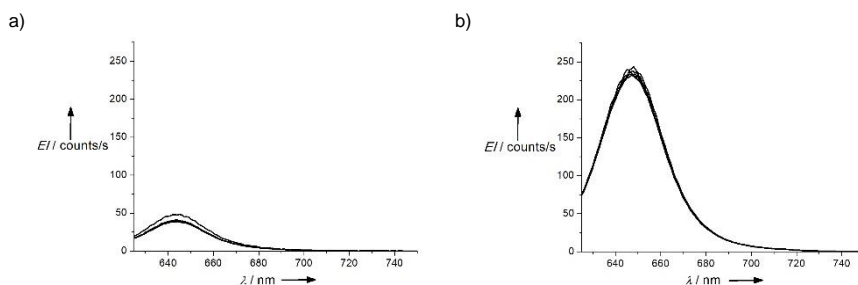
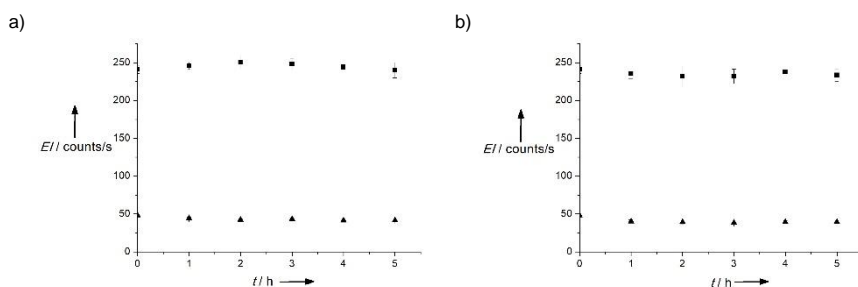


**Figure S28.** Fluorescence spectra of **6-TramTO-3** a) alone; b) with 37.5  $\mu\text{M}$  dsDNA<sub>CT</sub> after incubation at 37°C. All spectra were measured of a 2.5  $\mu\text{M}$  solution of **6-TramTO-3** in 10 mM Tris pH 7.6 and 50 mM KCl.

The fluorescence intensity at the maximum (647 nm) of each spectrum was plotted against the time intervals. Mean values from three independent measurements with its standard deviation are shown below.



## SUPPORTING INFORMATION

**Figure S29.** Fluorescence stability of **6-TramTO-3**: alone (black triangles) or with 37.5  $\mu\text{M}$  dsDNA<sub>CT</sub> (black squares) after incubation at a) 20°C and b) 37°C.

### Binding Affinity Determination by DynaFit

For the determination of the binding affinity, the maximum of each fluorescence spectrum (647 nm in the case of dsDNA<sub>CT</sub>, 647 nm in the case of dsDNA<sub>HAT</sub> and 650 nm in the case of dsDNA<sub>HGC</sub>) was plotted against the added dsDNA concentration. The mean values from three independent measurements with its standard deviation is shown. The  $K_D$ -value and its standard deviation was determined using the program DynaFit. Table S2 shows the determined  $K_D$ -values.

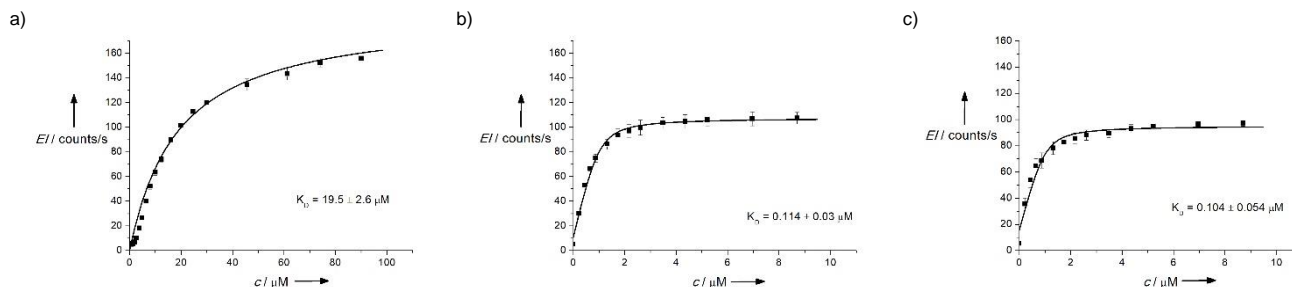


**Figure S30.** Calculated binding affinities from the fluorescence spectra of the titration of **6-TramTO-3** with a) dsDNA<sub>CT</sub>; b) dsDNA<sub>HAT</sub>; c) dsDNA<sub>HGC</sub>.

**Table S2.** Determined binding constants of **6-TramTO-3** with dsDNA<sub>CT</sub>, dsDNA<sub>HAT</sub> and dsDNA<sub>HGC</sub>.

DNA	binding affinity [ $\mu\text{M}$ ]
dsDNA <sub>CT</sub>	$19.5 \pm 2.6$
dsDNA <sub>HAT</sub>	$0.114 \pm 0.03$
dsDNA <sub>HGC</sub>	$0.104 \pm 0.054$

All binding affinities were determined by fitting the obtained experimental data in the *DynaFit 4.0* software. The program is available free of charge for academical use at <http://www.biokin.com/dynafit/><sup>[9]</sup> In this program it is necessary to create scripts containing information about the chemical model underlying the experimental data, the concentration of the fixed component, determined spectroscopic data of the titration and information about the location of files. An example of a script is shown below with comments (in italic) about the purpose of the keywords.

```
[task]
  task = fit           nature of the calculation performed by Dynafit
  data = equilibria

[mechanism]
  P + LL <=> P.LL    :    KdL  dissociation  simple 1:1 binding model
                                     indicates that it is a dissociation constant

[constants]
  KdL = 2 ?          initial KD-value for iteration
                                     the ? indicates that this value will be optimized

[concentrations]
  LL = 1             fixed concentration of the cyanine dye derivative

[responses]
  LL = 5.8 ?        contribution to the spectroscopic signal (adjustable parameters, as is specified
  P.LL = 155.8 ?   by the question mark after the numerical value)
                                     fluorescence intensity of the dye alone
                                     fluorescence intensity of the saturated DNA / dye signal

[data]
  variable P        location of files and information about the data
  file ./Measurements/data/BH574_mean.txt  indicates the species that changes its concentration
                                     path of the experimental data file

[output]
  directory ./Measurements/output/BH574_mean  path indicating the location of the output file

[end]
```

## SUPPORTING INFORMATION

## Fluorescence Quantum Yield

The slopes for the determination of the quantum yields and their calculated quantum yield values are summarized in table S3.

**Table S3.** Determined slopes and corresponding quantum yields for the two reference compounds Alexa Fluor® 647 and Atto 655 and for **6-TramTO-3** with and without dsDNA<sub>CT</sub>.

dye	slope	mean	reference dye	quantum yield	quantum yield (lit.)
Alexa Fluor® 647	52937300				
		51185000	Atto 655	0.32	0.33 <sup>[4]</sup>
Alexa Fluor® 647	49432700				
Atto 655	48486000				
		47618300	Alexa Fluor® 647	0.31	0.30 <sup>[3]</sup>
Atto 655	46750600				
<b>6-TramTO-3</b> alone	792132				
<b>6-TramTO-3</b> alone	822593	809683	Alexa Fluor® 647	0.0052	
<b>6-TramTO-3</b> alone	814323				
<b>6-TramTO-3</b> + DNA	41583400				
<b>6-TramTO-3</b> + DNA	41800000	42097433	Alexa Fluor® 647	0.27	
<b>6-TramTO-3</b> + DNA	42908900				

## SUPPORTING INFORMATION

## Concentration Determination

For the accurate determination of our compounds **6-TramTO-3** the extinction coefficient was calculated. A specific amount ( $< 2.00$  mg) of the compound was weighted on a Mettler Toledo XP6 and dissolved in a known amount of milli-Q water. Increasing amounts of such stock solution were added into a 1 mL cuvette filled with 1 ml of milli-Q water. The corresponding absorbance of each addition was measured on a Tecan Spark 20M at the maximum at 625 nm and without exceeding 10% of the initial volume. In all the cases the absorbance was between 0.1 and 1 AU to be in concordance with Lambert-Beer law.<sup>[10]</sup>

$$A = \epsilon l c \quad (\text{S2})$$

In this equation: A = absorbance of the solution; l = length of the cuvette; c = concentration;  $\epsilon$  = molar extinction coefficient.

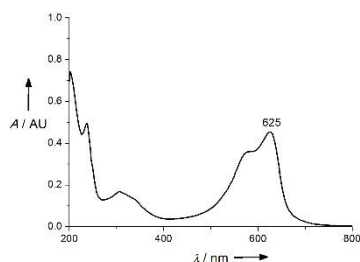


**Figure S31.** UV-Vis spectrum of a 10  $\mu\text{M}$  solution of **6-TramTO-3** in 1 mL 10 mM Tris pH 7.6 and 50 mM KCl.

The lineal regression of the obtained absorbance measurements versus the concentrations of **6-TramTO-3** allowed us to obtain the molar extinction coefficient. These measurements were repeated three times independently i.e. from three different stock solutions. The mean extinction coefficient and the standard deviation of **6-TramTO-3** at a wavelength of 625 nm in milli-Q water was  $59403 \pm 646 \text{ M}^{-1}\text{cm}^{-1}$ .

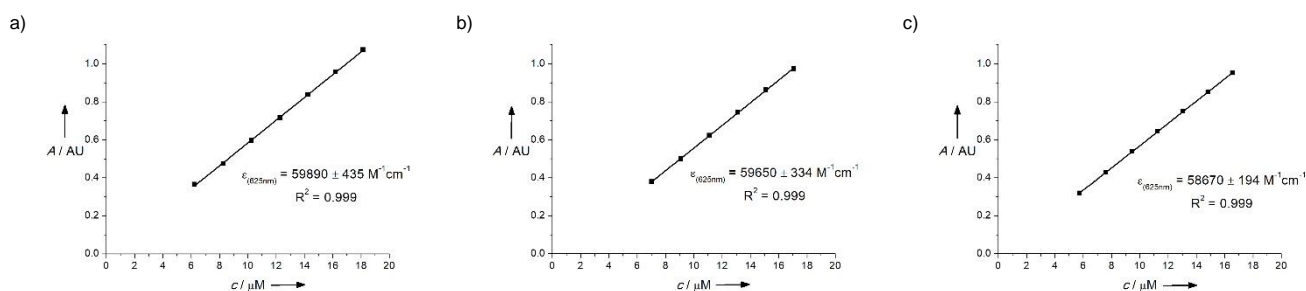


**Figure S32.** Determination of the extinction coefficient of compound **6-TramTO-3** in milli-Q water. The absorbance maximum at 625 nm was plotted against the dye concentration. Three independent measurements are shown with the calculated extinction coefficient and their corresponding regression value ( $R^2$ ). The mean extinction coefficient and the standard deviation of **6-TramTO-3** is  $59403 \pm 646 \text{ M}^{-1}\text{cm}^{-1}$ .

The mean extinction coefficient and the standard deviation of **6-NH<sub>2</sub>TO-3** and **6-AzTO-3** were determined following the above described procedure. The extinction coefficient of **6-NH<sub>2</sub>TO-3** was determined in milli-Q water, whereas the extinction coefficient of **6-AzTO-3** was determined in DMSO due to its low aqueous solubility. Figure S30 shows the corresponding UV-Vis spectra in 1 mL 10 mM Tris pH 7.6 and 50 mM KCl at a dye concentration of 10  $\mu\text{M}$ . For the spectrum of **6-AzTO-3** 1% of DMSO was added for a better solubility. Figure S31 and Figure S32 show the lineal regressions from the three independent measurements. Table 4 summarized the molar extinction coefficient obtained.

## SUPPORTING INFORMATION

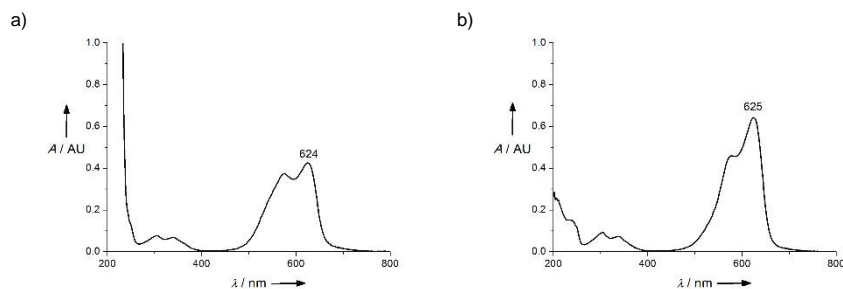


**Figure S33.** a) UV-Vis spectra of compound **6-AzTO-3** in 1 mL 10 mM Tris pH 7.6 and 50 mM KCl at a dye concentration of 10  $\mu\text{M}$  and 1% DMSO. b) UV-Vis spectra of compound **6-NH<sub>2</sub>TO-3** in 1 mL 10 mM Tris pH 7.6 and 50 mM KCl at a dye concentration of 10  $\mu\text{M}$ .

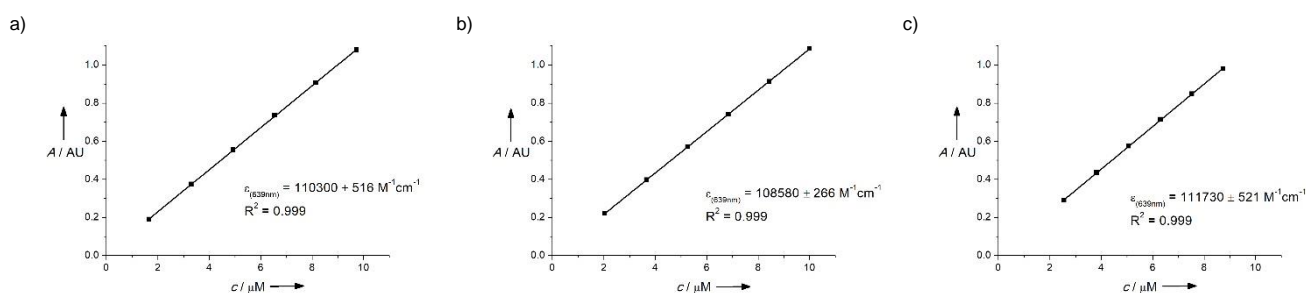


**Figure S34.** Determination of the extinction coefficient of compound **6-AzTO-3** in DMSO. The absorbance maximum at 639 nm was plotted against the dye concentration. Three independent measurements are shown with the calculated extinction coefficient and their corresponding regression value ( $R^2$ ). The mean extinction coefficient and the standard deviation of **6-AzTO-3** is  $110203 \pm 1577 \text{ M}^{-1}\text{cm}^{-1}$ .

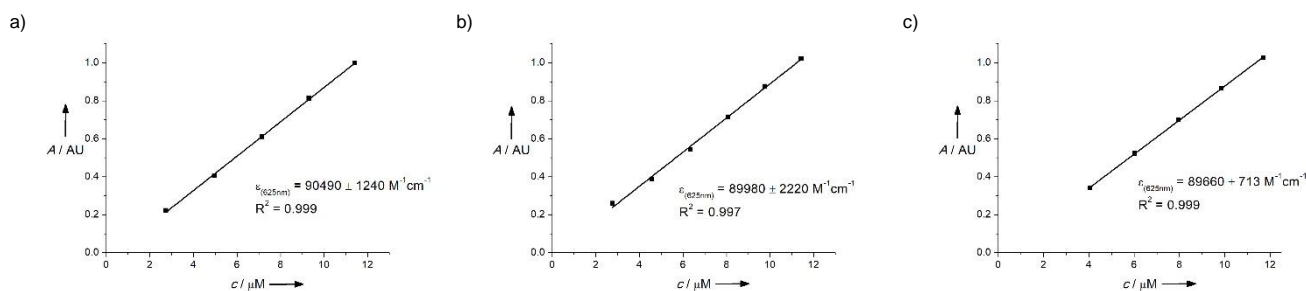


**Figure S35.** Determination of the extinction coefficient of compound **6-NH<sub>2</sub>TO-3** in milli-Q water. The absorbance maximum at 625 nm was plotted against the dye concentration. Three independent measurements are shown with the calculated extinction coefficient and their corresponding regression value ( $R^2$ ). The mean extinction coefficient and the standard deviation of **6-NH<sub>2</sub>TO-3** is  $90043 \pm 418 \text{ M}^{-1}\text{cm}^{-1}$ .

**Table S4.** Determined mean extinction coefficients and standard deviations of **6-AzTO-3** in DMSO and **6-TramTO-3** and **6-NH<sub>2</sub>TO-3** in water.

	<b>6-AzTO-3</b> in DMSO	<b>6-TramTO-3</b> in water	<b>6-NH<sub>2</sub>TO-3</b> in water
mean	$110203 \pm 1577 \text{ M}^{-1}\text{cm}^{-1}$	$59403 \pm 646 \text{ M}^{-1}\text{cm}^{-1}$	$90043 \pm 418 \text{ M}^{-1}\text{cm}^{-1}$

Syto-9<sup>TM</sup> was used as a 3.34 mM DMSO stock commercial solution. For EtBr the extinction coefficient  $\epsilon_{480\text{nm}} = 5600 \text{ M}^{-1}\text{cm}^{-1}$ <sup>[11]</sup> was used. dsDNA<sub>CT</sub> was purchased as a solution of 15.4 mM solution.

## SUPPORTING INFORMATION

For the determination of the concentration of the hairpin DNAs, the purchased lyophilized DNA was dissolved in milli-Q water, heated to 95°C for 10 min and slowly cooled down to r.t. Their molar extinction coefficients were determined by using the following formula:<sup>[12]</sup>

$$\epsilon_{260nm} = \{(8.8 * \#T) + (7.3 * \#C) + (11.7 * \#G) + (15.4 * \#A)\} * 0.8 * 10^3 M^{-1}cm^{-1} \quad (S3)$$

In the formula # = number of nucleobases determined throughout the DNA sequence, T = thymine, C = cytosine, G = guanine, A = adenine

## UV-Vis Titrations

UV-Vis titration measurements were performed at a concentration of 12.3  $\mu$ M of the dye in 10 mM Tris pH 7.6 and 50 mM KCl. Increasing aliquots of a 1.54 mM and 15.4 mM stock solutions of dsDNA<sub>CT</sub> were successively added and the absorbance spectra were recorded in a range from 400-800 nm after 1 min of each addition. Three independent measurements were carried out. The presented spectra are the resulting mean of the three independent measurements.

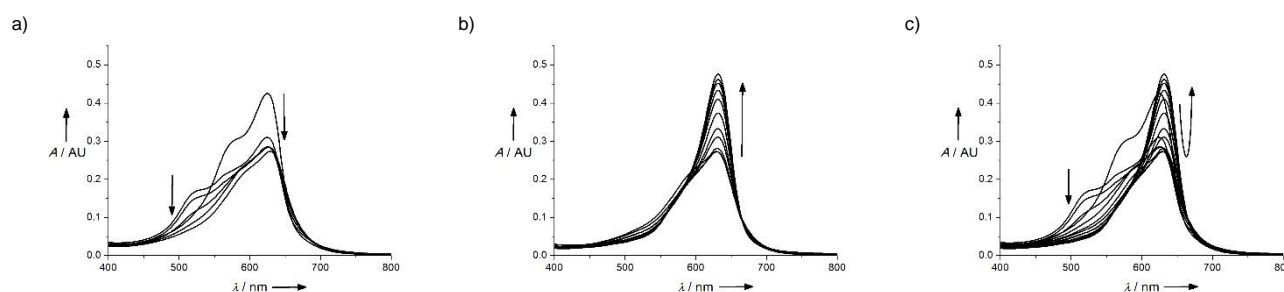


**Figure S36.** UV-Vis spectra of the titrations of a 12.3  $\mu$ M solution of **6-TramTO-3** in 10mM Tris pH 7.6 and 50mM KCl with increasing amounts of dsDNA<sub>CT</sub> where a) the equivalents of dsDNA<sub>CT</sub> are: 0, 0.4, 0.7, 1.1, 1.5, 2.3; b) the equivalents of dsDNA<sub>CT</sub> are: 2.3, 3.0, 3.8, 5.3, 6.8, 10.5, 18.0, 25.5, 40.6, 55.6, 70.6 and c) is the combined titration of a and b.

We recorded the temperature dependence of the sample: to get a strong signal at 523 nm, a 12.3  $\mu$ M solution of **6-TramTO-3** in 10 mM Tris pH 7.6 and 50 mM KCl was prepared and 7.5  $\mu$ M dsDNA<sub>CT</sub> added. The measurement was started at a temperature at 2°C and the temperature increased in 4°C steps. After the device reached the set temperature we waited for 2 min before measurement. Figure S34 shows the change of the UV-Vis spectra with increasing temperature. Further, the signal at 523 nm and 625 nm were plotted against the temperature.

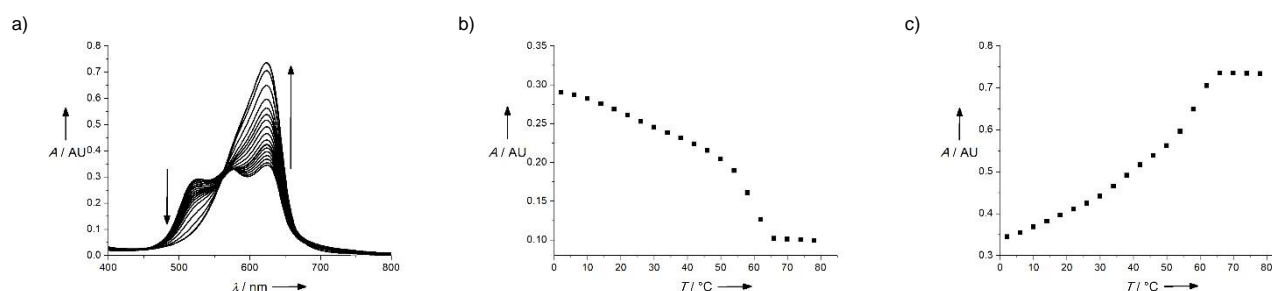


**Figure S37.** Temperature dependence of the UV-Vis signal of **6-TramTO-3** in 10 mM Tris pH 7.6 and 50 mM KCl with 7.5  $\mu$ M dsDNA<sub>CT</sub>. a) full UV-Vis spectra with increasing temperature from 2°C to 78°C; b) plot of the absorbance at 523 nm against the temperature; c) plot of the absorbance at 635 nm against the temperature.



## SUPPORTING INFORMATION

## CD Measurements

The shown CD-Spectra in figure 38 represent the mean of the three independent measurements.

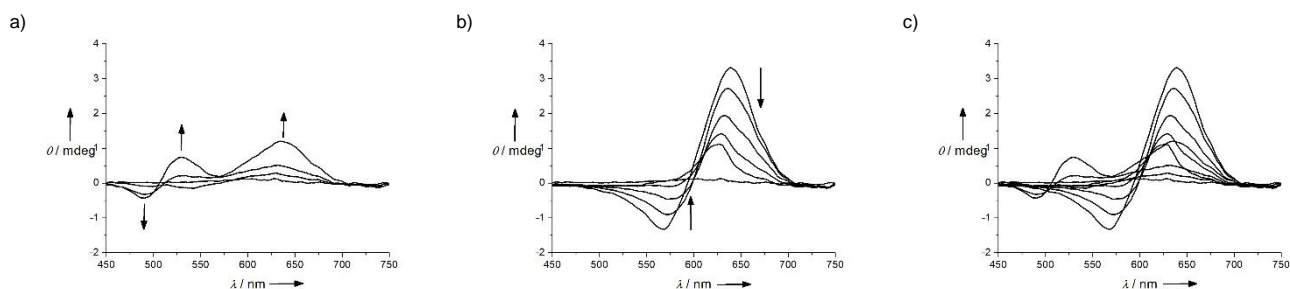


**Figure S38.** CD spectra of the titrations of a 36.9  $\mu\text{M}$  solution of **6-TramTO-3** in 10mM Tris pH 7.6 and 50 mM KCl with increasing amounts of dsDNA<sub>CT</sub> where a) the equivalents of dsDNA<sub>CT</sub> are: 0, 0.4, 0.8, 1.2; b) the equivalents of dsDNA<sub>CT</sub> are 2.4, 4.9, 9.8, 20.3 and 40.7 c) is the complete titration

## Gel Electrophoresis

Figure S39 shows the two gels with different amounts of dsDNA<sub>bl</sub> and dsDNA<sub>bc</sub> stained with **6-TramTO-3** or ethidium bromide.

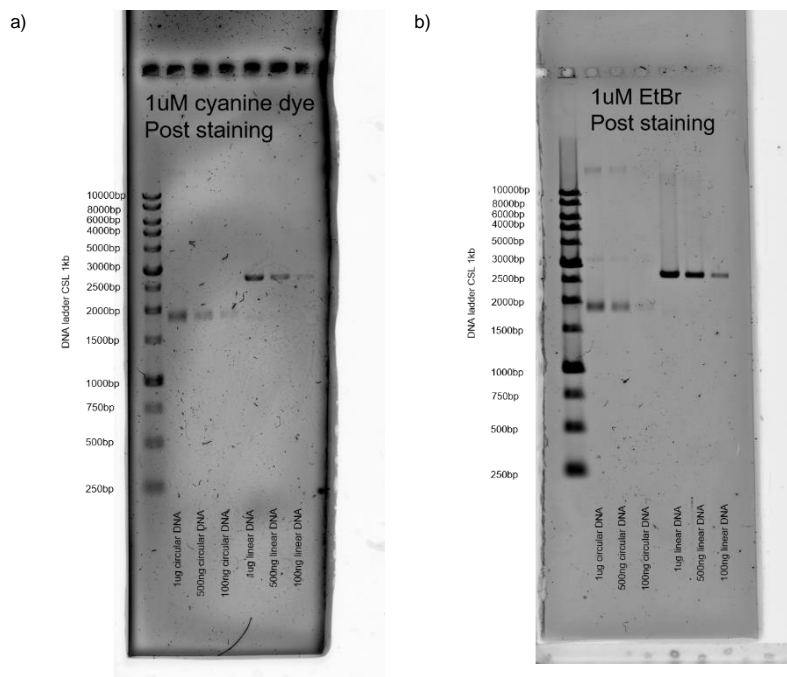


**Figure S39.** 1% agarose gel electrophoresis with 1000 ng, 500 ng and 100 ng of dsDNA<sub>bc</sub> and dsDNA<sub>bl</sub>. CSL 1kb DNA ladder was used as a reference. The gel was run for 75 min at 25°C at 80 V and post stained with either a) 1  $\mu\text{M}$  of **6-TramTO-3** in TAE buffer or b) 1  $\mu\text{M}$  ethidium bromide in TAE buffer.

## Thermal Melting Analysis

Figure S40 shows the determined melting point for dsDNA<sub>CT</sub> with and without addition of **6-TramTO-3**.

## SUPPORTING INFORMATION

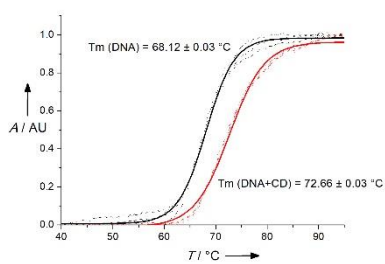


**Figure S40.** Melting temperature measurements of 45  $\mu\text{M}$  dsDNA<sub>CT</sub> with and without addition of 1.8  $\mu\text{M}$  **6-TramTO-3** in 10 mM Tris pH 7.5. The melting points were calculated to be 68.12°C for dsDNA<sub>CT</sub> alone and 72.66°C for dsDNA<sub>CT</sub> with addition of **6-TramTO-3**.

### Fluorescence Microscopy

Figure S41 shows confocal microscopy pictures of **6-TramTO-3** labeled *E. coli* bacteria attached on an IBIDI 8-wells glass-bottom plate coated with poly-L-lysine (bright field, red channel, merged image).

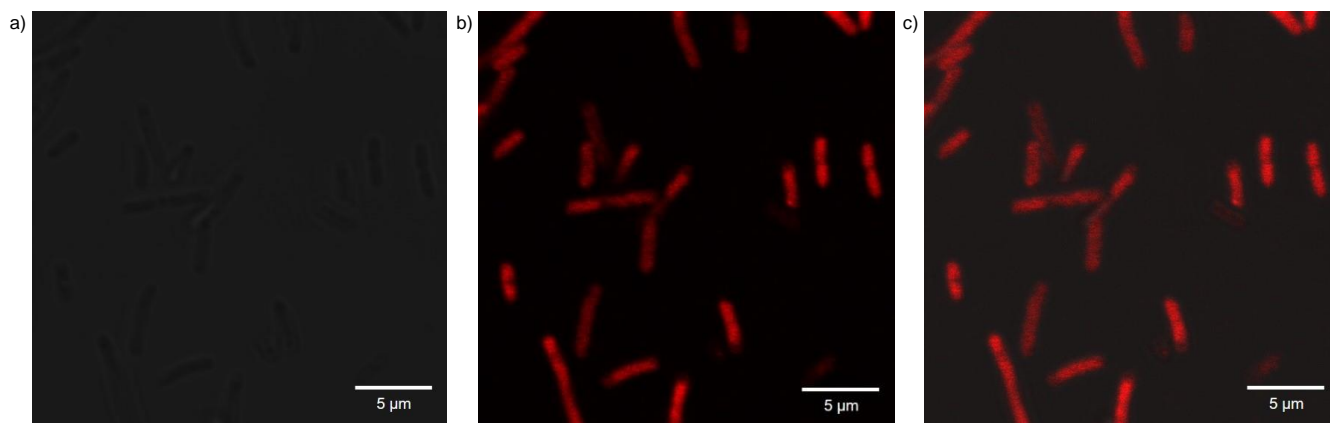
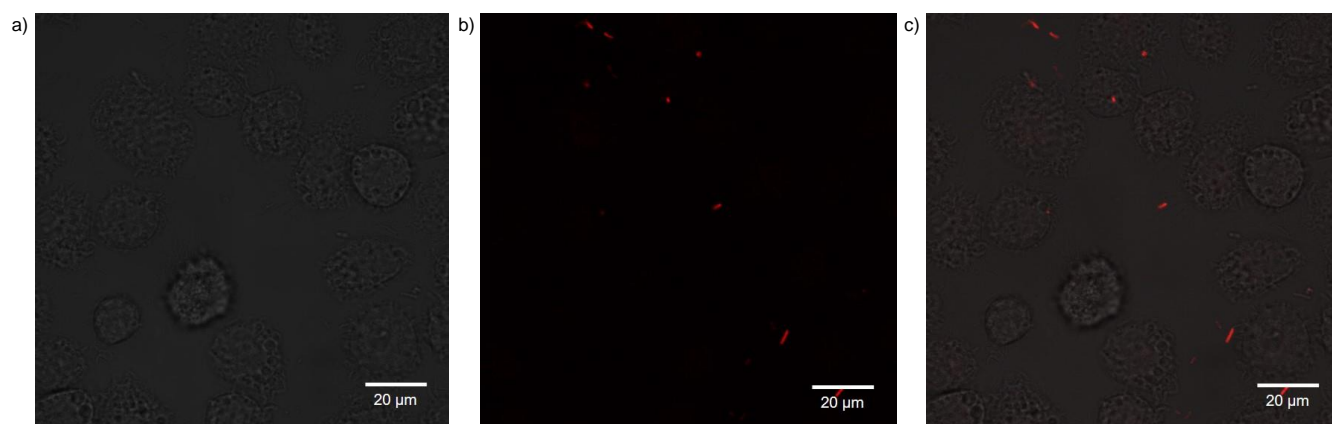


**Figure S41.** Microscopy of *E. coli* bacteria stained with **6-TramTO-3** and attached on a poly-L-lysine coated plate. Shown are a) bright field; b) red channel; c) merged image.

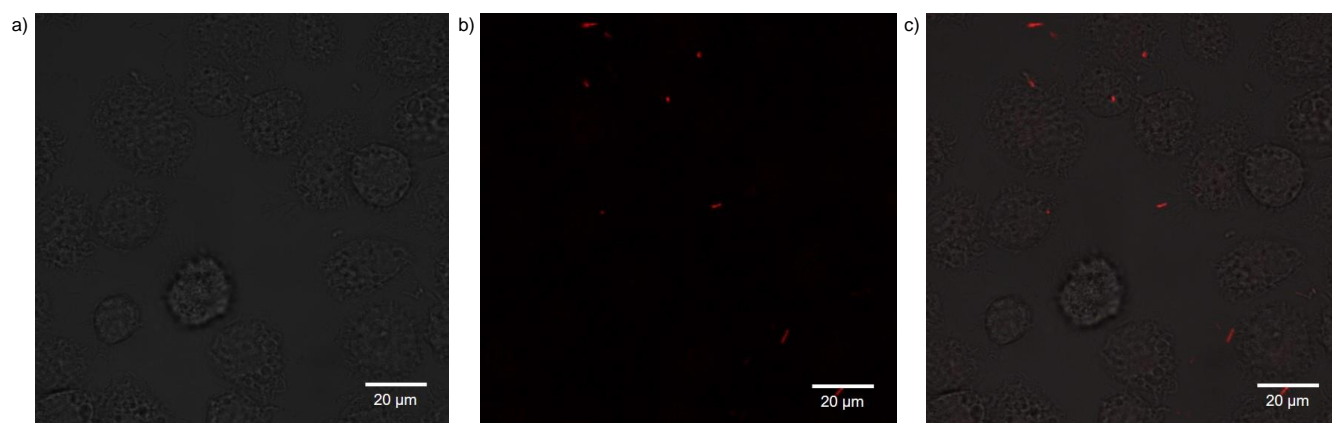
## SUPPORTING INFORMATION

Figure S42 shows confocal microscopy pictures of macrophages exposed to bacteria stained with 6-TramTO-3 (bright field, red channel, merged image), including z-stacks (Z).

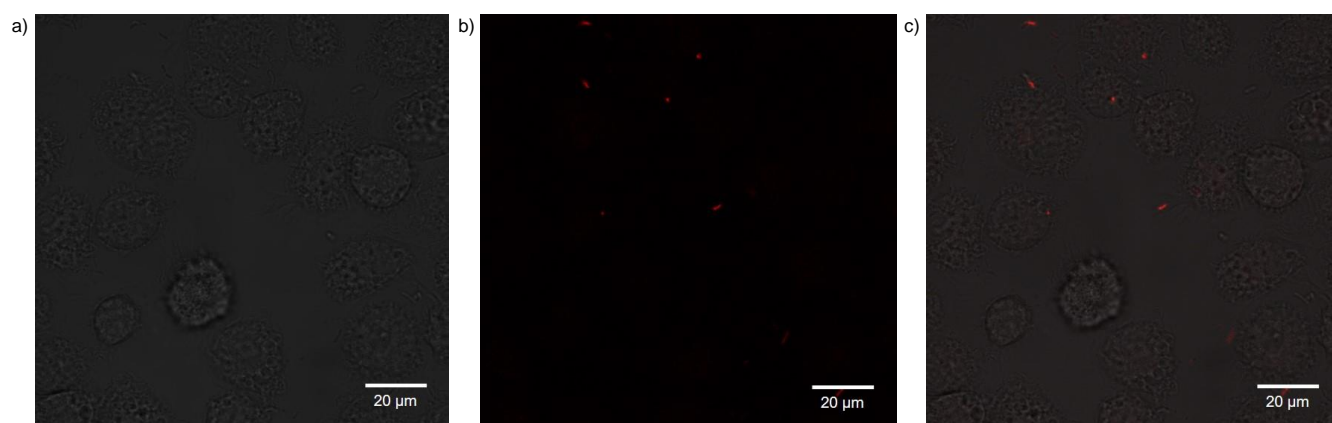
Z1



Z2

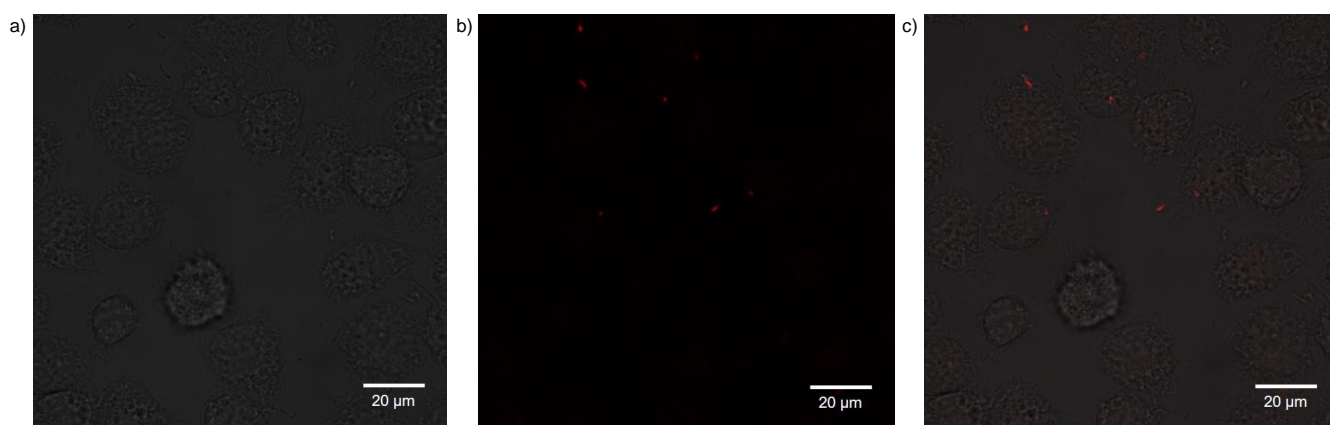


Z3

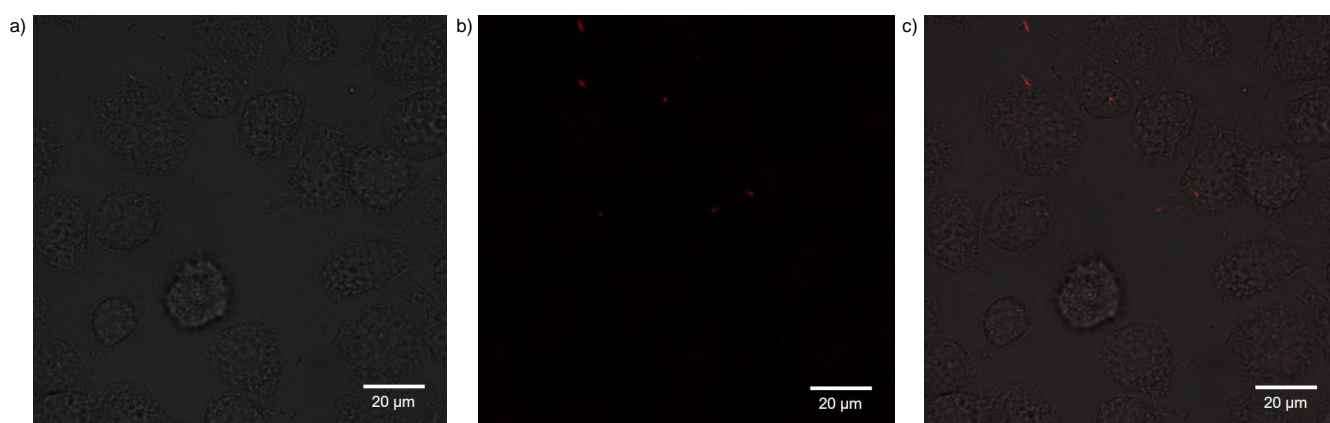


## SUPPORTING INFORMATION

Z4



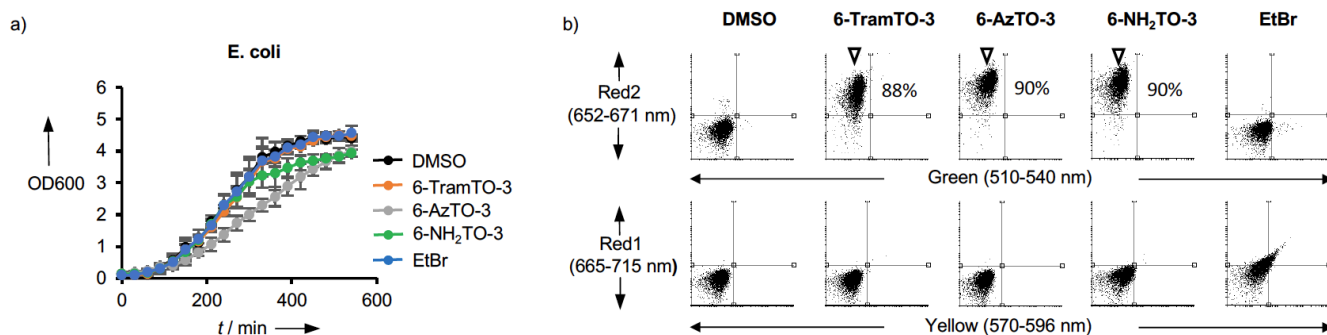
Z5



**Figure S42.** Confocal microscopy of bacteria and macrophages stained with **6-TramTO-3**. Shown are a) bright field; b) red channel; c) merged image at different Z-stacks

### Additional Cell-Based Assays

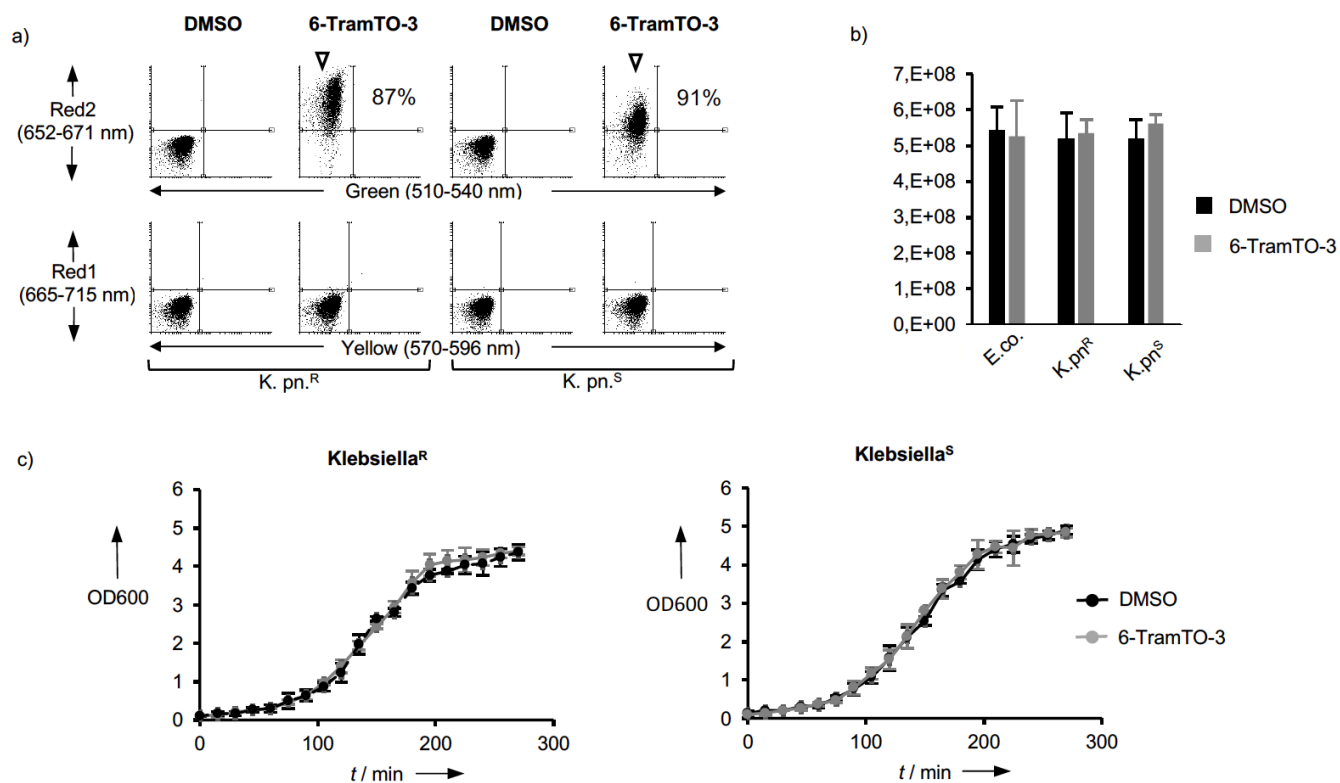
Figure S43 shows the growth of *E. coli* in the presence of the indicated fluorescence dyes (a) and the fluorescence shift of the bacteria in the indicated FACS channels (b).



**Figure S43.** a) *E. coli* was grown in the presence of the indicated dyes and the optical density (OD600) was determined at various time-points. Mean values and standard-deviations from three independent experiments are shown. b) Fluorescence shift of *E. coli* cells grown in the presence of the indicated dyes was recorded by flow-cytometry at an optical density of 2.0 in the indicated channels, including quantification from independent experiments (Figure S48).

## SUPPORTING INFORMATION

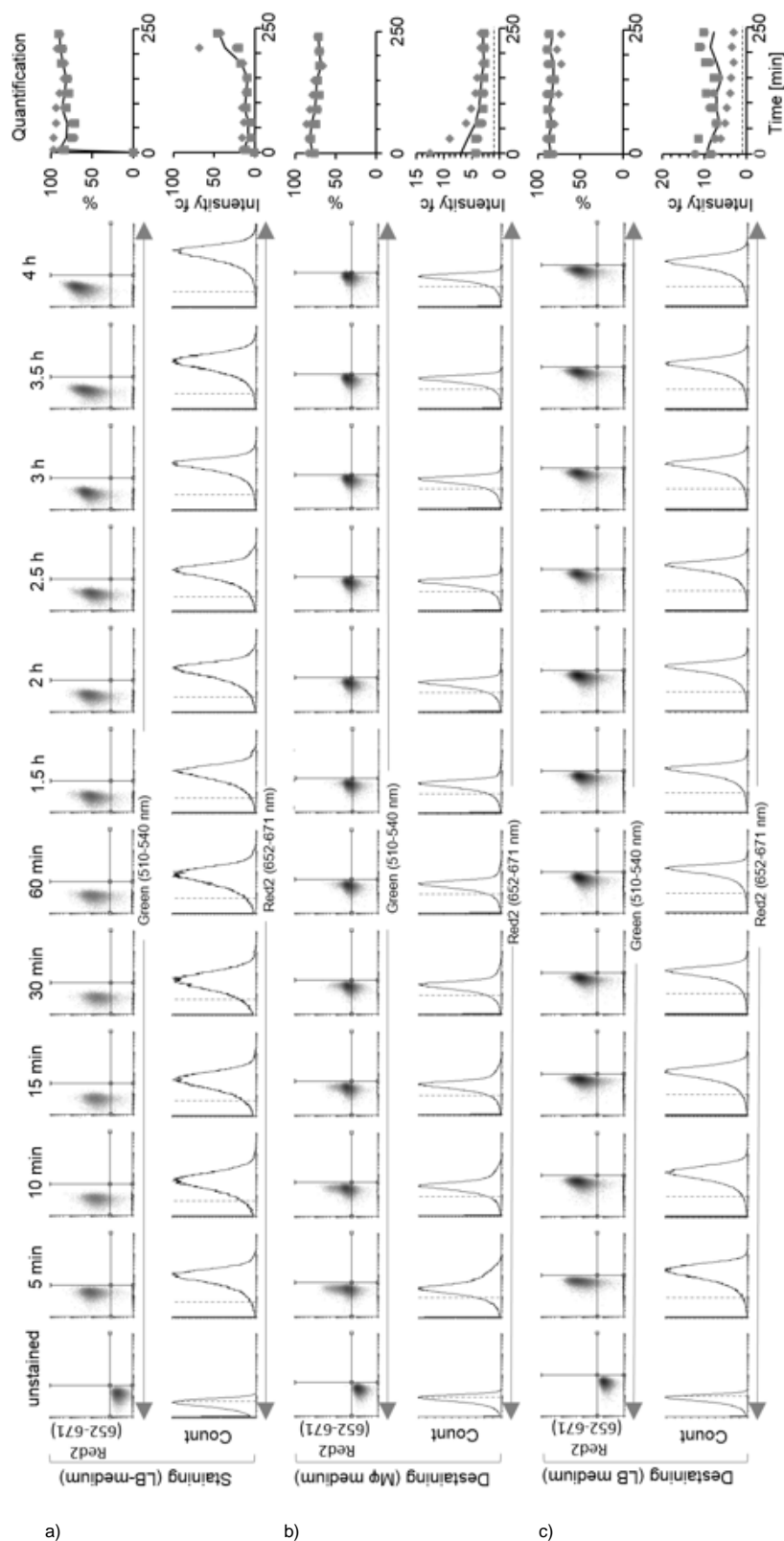
Figure S44 shows the labelling of antibiotic-resistant and -sensitive *Klebsiella pneumoniae* strains with **6-TramTO-3** (a), the quantification of colonies formed by DMSO- or **6-TramTO-3** labeled bacteria on solid agar (b) and *Klebsiella* growth in the presence of **6-TramTO-3** or DMSO.



**Figure S44.** a) *Klebsiella pneumoniae* strains (R = resistant, S = sensitive) were grown in the presence of DMSO or **6-TramTO-3** and fluorescence shift of cells in the indicated channels at an optical density of 2.0, including quantification from independent experiments (Figure S48), was recorded by flow-cytometry. b) 24 h after plating of *E. coli* and *K. pneumoniae* strains sampled at an optical density of 2.0, grown in the presence of DMSO or **6-TramTO-3**, onto LB solid agar plates colony forming units per ml of culture were determined (Y-axis). Error bars represent the standard deviation derived from three independent experiments. c) *K. pneumoniae* (R = resistant, S = sensitive) was grown in the presence of DMSO or **6-TramTO-3** and the optical density (OD<sub>600nm</sub>) was determined at various time-points. Mean values and standard-deviations from three independent experiments are shown.

## SUPPORTING INFORMATION

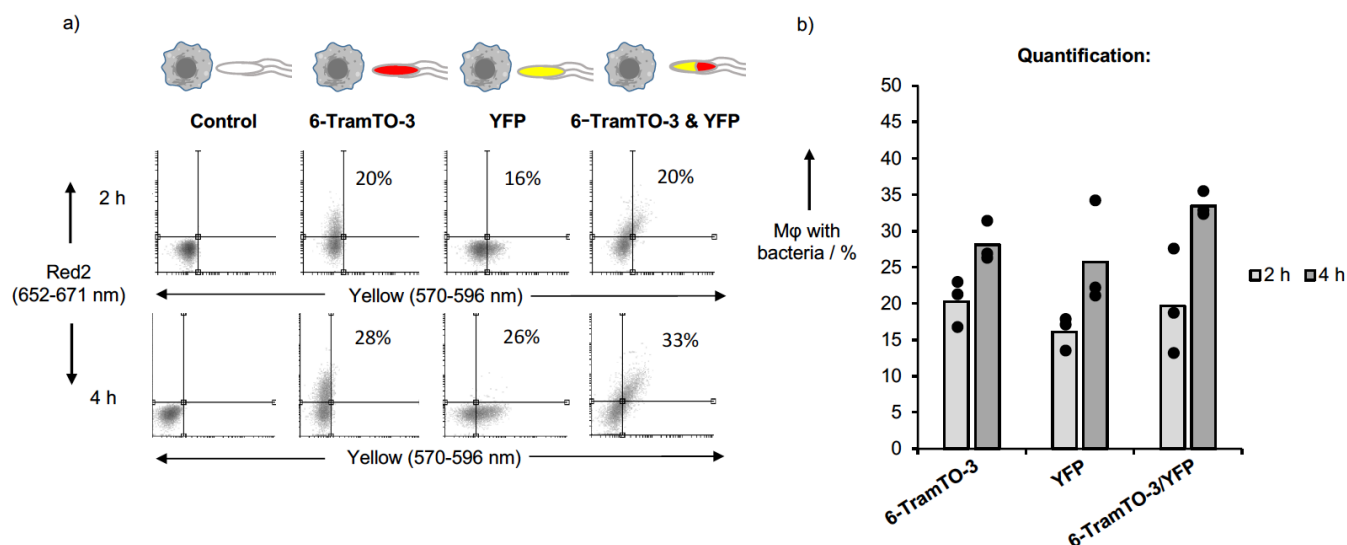
Figure S45 shows the change in fluorescence intensity and percentage of red-shifted bacteria during staining of *Escherichia coli* with **6-TramTO-3** and upon shift into dye-free LB-medium or X-Vivo-15 macrophage medium.



**Figure S45.** a) *Escherichia coli* cultures were grown for 4 h ( $\approx OD_{600nm} = 2.0$ ) in the presence of  $2.5 \mu M$  **6-TramTO-3** and bacterial red fluorescence staining was determined at the indicated time-points by FACS (upper row: Red2 vs Green channel scatter plots; lower row: histogram plots with cell number vs Red2 fluorescence). Quantification of the percentage of bacteria in the red gate and the fold-change in fluorescence intensity compared to unstained bacteria is provided on the right hand side. b) Same as a) but upon shift of **6-TramTO-3** labelled *E. coli* at  $OD_{600nm} = 2.0$  into dye-free X-Vivo-15 macrophage culture medium. c) Same as a) but upon shift of **6-TramTO-3** labelled *E. coli* at  $OD_{600nm} = 2.0$  into dye-free LB medium. Mean values and individual data points from three independent experiments are shown.

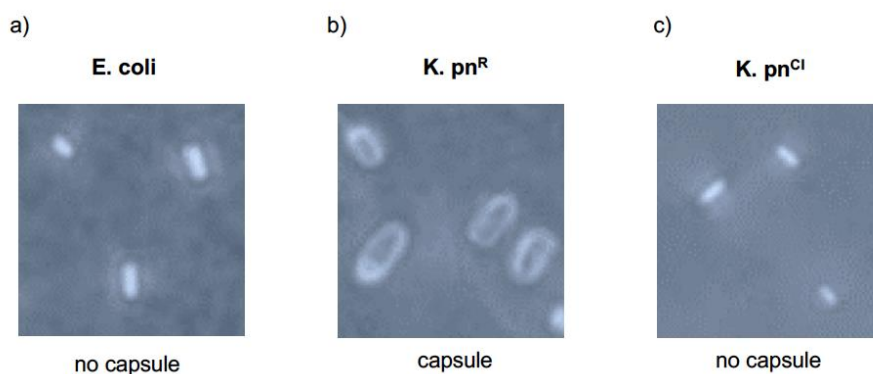
## SUPPORTING INFORMATION

Figure S46 shows the development of a fluorescent macrophage side-population upon exposure to 6-TramTO-3-, YFP- or 6-TramTO-3/YFP double-positive bacteria.



**Figure S46.** a) Macrophages were stimulated with un-labeled, 6-TramTO-3 labeled, YFP-expressing or 6-TramTO-3/YFP double-positive *Escherichia coli* for 2 and 4 h. Samples of stimulated macrophage cultures were recorded by FACS and representative dot-plots (Red2 versus Yellow channel) are shown. b) Quantification of the percentage of macrophages with phagocytosed bacteria as reported using 6-TramTO-3-, YFP- or 6-TramTO-3/YFP-labeled bacteria at 2 and 4 h post onset of the co-culture experiment. Mean values and individual data points from three independent experiments are shown.

Figure S47 shows the presence of a capsule in the antibiotics-resistant *K. pneumoniae* strain but not in the *E. coli* or antibiotics-sensitive strain.



**Figure S47.** Bacteria were stained with nigrosin and crystal violet and pictures were recorded at 63x magnification by widefield microscopy a) *E. coli* = *E. coli*; b) *K. pn<sup>R</sup>* = multiresistant *K. pneumoniae*; c) *Kpn<sup>S</sup>* = antibiotic-sensitive *K. pneumoniae*



## SUPPORTING INFORMATION

Figure S48 shows the quantification plots of independent measurements of the FACS experiments

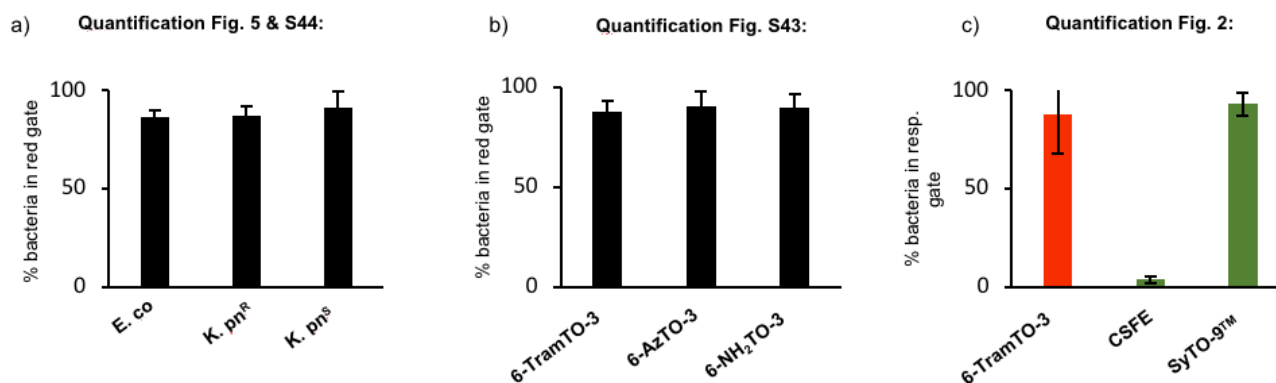


**Figure S48.** a) Quantification of bacterial **6-TramTO-3** labeling data from Fig. 5 (panel B, right hand side) and Fig. S44 (panel A, upper row). b) Quantification of bacterial labeling data from Fig. S43 (panel B). c) Quantification of bacterial labeling data from Fig. 2 (panel B, upper row). **6-TramTO-3** was detected in the red2 channel, CSFE and SyTO9<sup>TM</sup> in the green channel. All data represent mean values and standard deviations derived from three independent experiments.

## References

- [1] H. E. Gottlieb, V. Kotlyar, A. Nudelman, *J. Org. Chem.* **1997**, *62*, 7512–7515.
- [2] Horiba Scientific: A Guide to Recording Fluorescence Quantum Yields, <http://www.horiba.com/fileadmin/uploads/Scientific/Documents/Fluorescence/quantumyieldstrad.pdf>, 2018.
- [3] Atto Tec GmbH, [https://www.atto-tec.com/fileadmin/user\\_upload/Katalog\\_Flyer\\_Support/ATTO\\_655.pdf](https://www.atto-tec.com/fileadmin/user_upload/Katalog_Flyer_Support/ATTO_655.pdf), 2018.
- [4] <https://www.thermofisher.com/de/de/home/references/molecular-probes-the-handbook/tables/fluorescence-quantum-yields-and-lifetimes-for-alexa-fluor-dyes.html>, 2018.
- [5] K. J. Livak, T. D. Schmittgen, *Methods.* **2001**, *25*, 402–408.
- [6] X. Peng, T. Wu, J. Fan, J. Wang, S. Zhang, F. Song, S. Sun, *Angew. Chem. Int. Ed.* **2011**, *50*, 4180–4183.
- [7] S. Kishino, S. Yasui, K. Takahata, M. U. S. Ohkawa, United States Patent, Pat. No.: US 4386146 1983.
- [8] F. Asinger, B. Scheuffler, *J. Prakt. Chem.* **1960**, *4*, 265–289.
- [9] P. Kuzmic, *Anal. Biochem.* **1996**, *237*, 260–273.
- [10] D. F. Swinehart, *J. Chem. Educ.* **1962**, *39*, 333–335.
- [11] L. Feng, A. Zhao, J. Ren, X. Qu, *Nucl. Acids Res.* **2013**, *41*, 7987–7996.
- [12] G. Kallansrud, B. Ward, *Anal. Biochem.* **1996**, *236*, 134–138



## 4. Cumulative Part

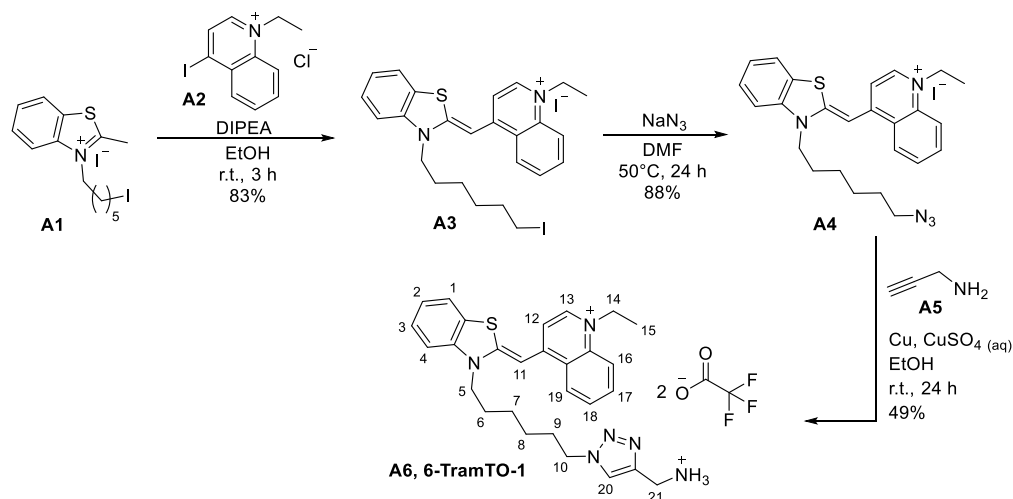
### 4.1.1 Conclusion

A new far-red fluorescent DNA stain, 6-TramTO-3, was synthesized and studied as a vital dye for bacteria tracking in host-cell interaction studies. 6-TramTO-3 is a cyanine dye derivative, which labels bacteria fast and efficiently without the need for genetic manipulation or effects on their viability. So far, neither fluorescent proteins, nor commercial dyes were able to stain multidrug-resistant bacteria. We demonstrated the applicability of 6-TramTO-3 in FACS analysis and confocal fluorescence microscopy and, for the first time, showed different interaction behavior of multidrug-resistant and antibiotic-sensitive *Klebsiella* strains during phagocytosis by human macrophages. Our new off-the-shelf reagent may help to identify unknown disease-causing strategies, permitting improved drug-design against multidrug-resistant bacteria. We believe that future developments will show the utility of 6-TramTO-3 in many different microorganisms allowing phagocytosis studies with other hosts. The synthesis and study of new TramTO-derivatives could enable multicolor labeling and grant deeper understanding of its mode of action and the reason for its lack of toxicity in our bacterial experiments.

### 4.1.2 Further Developments and Outlook

Additional experiments with 6-TramTO-3 were performed, and supplementary biological and chemical approaches are currently under investigations. We were interested in exploring new green and yellow emitting TramTO derivatives to provide multiple color staining. We further aimed to gain insights into the nontoxic behavior of the dye in bacterial labeling experiments by derivatization of the triazole group of 6-TramTO-3. To access a green fluorescent version of TramTO, we designed the analogue bearing only one instead of three carbons in the methine-bridge. We expected to observe a change in the spectroscopic properties as the one reported from thiazole orange-3 (TO-3) to TO-1.<sup>[1,2]</sup> At the same time, we wanted to verify the role of the side-chain triazole moiety in the non-toxic behavior. Scheme 4.1.1 illustrates the synthetic pathway for the new green-fluorescent dye 6-TramTO-1. In a nucleophilic aromatic substitution of benzothiazole **A1** to the quinoline **A2**, the TO-1 backbone was formed. In a S<sub>N</sub>2-reaction, the side chain iodine was replaced by an azide. The azide derivative **A4** serves as the starting material in a click reaction with propargylamine, to yield the final compound 6-TramTO-1 **A6**.

#### 4. Cumulative Part



**Scheme 4.1.1.** Synthesis path for the green emitting TramTO derivative 6-TramTO-1 (**A6**).

Analytical data and a figure of the  $^1\text{H-NMR}$  spectra of 6-TramTO-1 (Figure 4.1.1) are given below:

**$^1\text{H-NMR}$**  (500 MHz,  $\text{DMSO-}d_6$ ,  $\delta$ ): 8.75 (d, 1H,  $J = 8.8$  Hz, H-16), 8.67 (d, 1H,  $J = 7.2$  Hz, H-13), 8.29 (br s, 3H,  $\text{NH}_3^+$ ), 8.17 (d, 1H,  $J = 8.8$  Hz, H-19), 8.10 (s, 1H, H-20), 8.05 (dd, 1H,  $J = 7.9$  Hz,  $J = 0.9$  Hz, H-4), 8.01 (m, 1H, H-17), 7.80 – 7.75 (m, 2H, H-1, H-18), 7.61 (m, 1H, H-2), 7.45 – 7.41 (m, 2H, H-3, H-12), 6.94 (s, 1H, H-11), 4.66 (q, 2H,  $J = 7.2$  Hz, H-14), 4.63 (t, 2H,  $J = 7.4$  Hz, H-10), 4.37 (t, 2H,  $J = 7.0$  Hz, H-5), 4.12 – 4.06 (m, 2H, H-21), 1.83 – 1.75 (m, 4H, H-6, H-9), 1.54 – 1.46 (m, 5H, H-8, H-15), 1.36 – 1.28 (m, 2H, H-7).

**$^{13}\text{C-NMR}$**  (125 MHz,  $\text{DMSO-}d_6$ ,  $\delta$ ): 159.4 ( $\text{C}_q$ ), 148.7 ( $\text{C}_q$ ), 144.0 (CH), 140.0 ( $\text{C}_q$ ), 136.9 ( $\text{C}_q$ ), 133.3 (CH), 128.2 (CH), 126.9 (CH), 125.7 (CH), 124.5 (CH), 124.3 ( $\text{C}_q$ ), 124.1 (2C, CH,  $\text{C}_q$ ), 123.9 ( $\text{C}_q$ ), 123.0 (CH), 118.0 (CH), 113.0 (CH), 108.3 (CH), 87.6 (CH), 49.5 ( $\text{CH}_2$ ), 49.3 ( $\text{CH}_2$ ), 45.6 ( $\text{CH}_2$ ), 33.9 ( $\text{CH}_2$ ), 29.6 ( $\text{CH}_2$ ), 26.8 ( $\text{CH}_2$ ), 25.6 ( $\text{CH}_2$ ), 25.4 ( $\text{CH}_2$ ), 14.7 ( $\text{CH}_3$ ). **HRMS-ESI $^+$**  ( $m/z$ ): [ $\text{M}$ ] $^+$  calcd for  $\text{C}_{28}\text{H}_{33}\text{N}_6\text{S}^+$ , 485.2482; found, 485.2487.

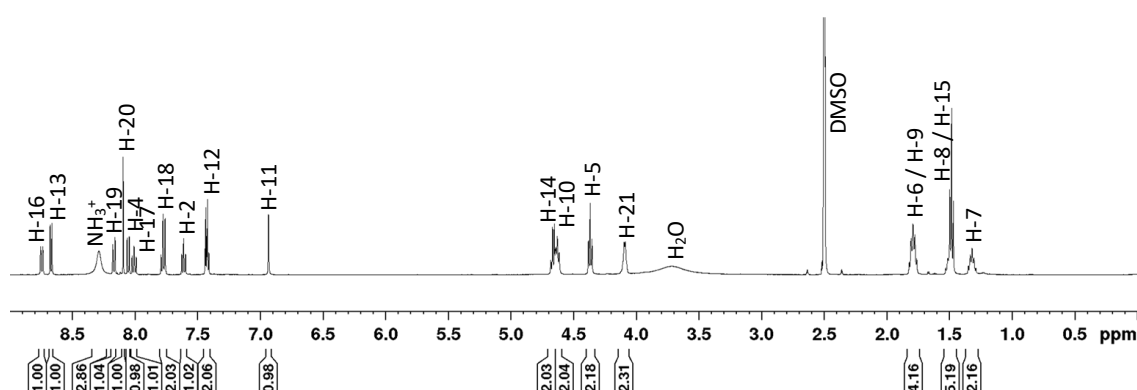


**Figure 4.1.1.**  $^1\text{H-NMR}$  spectra of the green emitting TramTO derivative 6-TramTO-1.

#### 4. Cumulative Part

Next, we preliminary investigated growth, viability and labeling efficiency studies with 6-TramTO-1 in *E. coli* and *Klebsiella* strains.<sup>1</sup> For both strains and as already observed for 6-TramTO-3 the growth curves overlay the ones of the negative DMSO control with just a very slight growth delay, suggesting the same non-toxic behavior (Figure 4.1.2).

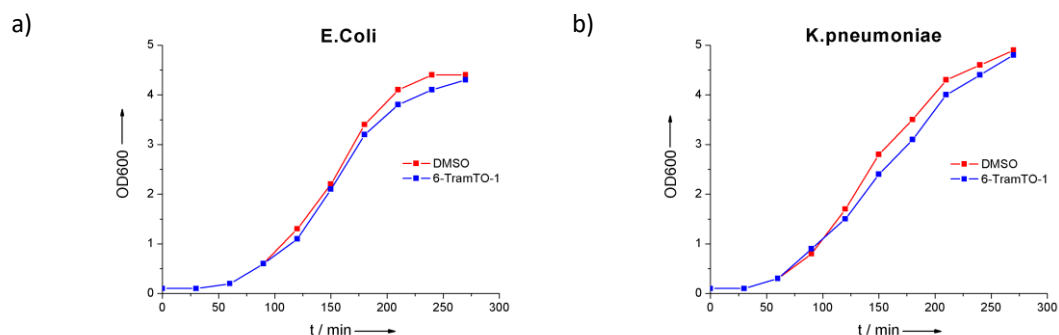


**Figure 4.1.2.** Optical density ( $OD_{600\text{ nm}}$ ) of a) *E. coli* and b) *K. pneumoniae* LB cultures supplemented with DMSO (red line with dots) and 6-TramTO-1 (blue line with dots) over time. These preliminary results were obtained once.

Regarding the labeling efficiency, under the same conditions as with 6-TramTO-3 in FACS analysis, incubation with 6-TramTO-1 resulted in a shift of *E. coli* population in all channels, except the Red2-channel (652-671 nm), but only 59% of the cells into the yellow channel (570-596 nm). This observation is in agreement with previous results from the green emitting dye SyTO-9. Unfortunately, in the case of *Klebsiella*, hardly any labeling could be observed with 6-TramTO-1 (Figure 4.1.3 and Figure 4.1.4). Further experiments need to be performed to explain the lack of labeling.

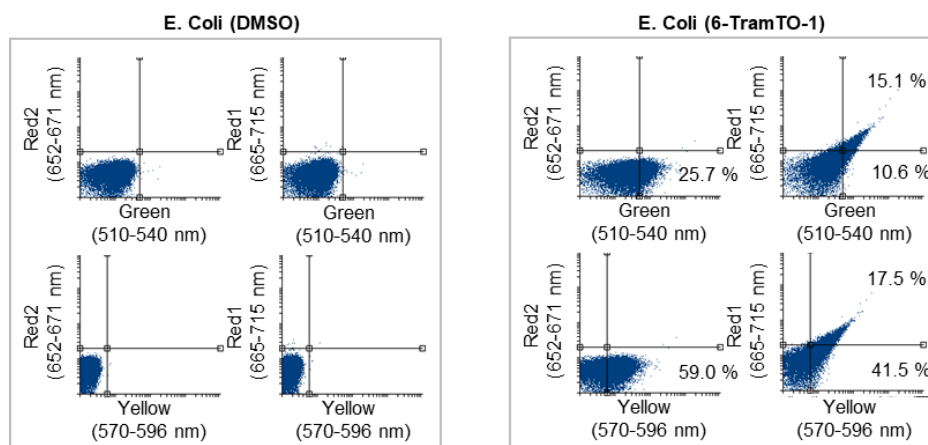


**Figure 4.1.3.** Representative dot plots of *E. coli* after incubation with DMSO (left) and 6-TramTO-1 (right), including quantification from one experiment. Bacteria were sampled at  $OD_{600\text{ nm}} = 2.0$  and analyzed by FACS in the red1, red2, green and yellow channels.

<sup>1</sup> FACS and growth curve analysis were performed by Jun.-Prof. Dr. Leon Schulte, iLung Institute for Lung Research, Marburg.

#### 4. Cumulative Part

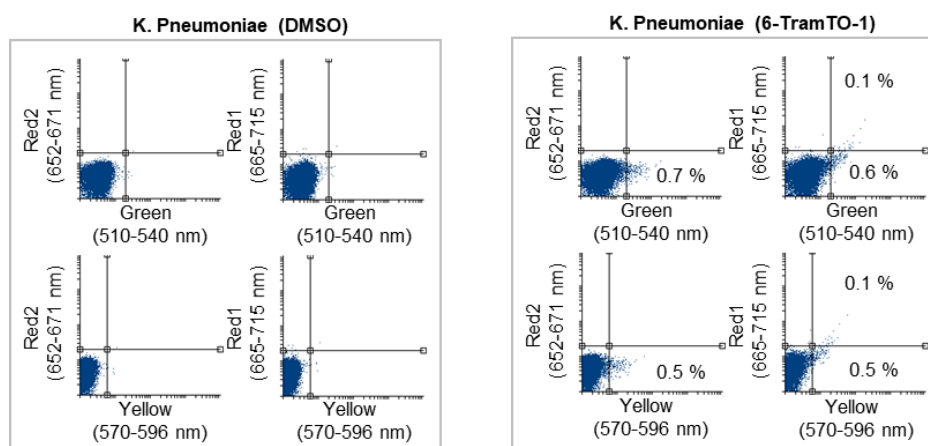


**Figure 4.1.4.** Representative dot plots of *K. pneumoniae* after incubation with DMSO (left) and 6-TramTO-1 (right), including quantification from one experiment. Bacteria were sampled at  $OD_{600\text{ nm}} = 2.0$  and analyzed by FACS in the red1, red2, green and yellow channels.

Preliminary staining experiments with fixed HeLa cells<sup>II</sup> (Figure 4.1.5) revealed comparable good labeling results of the green fluorescent dye 6-TramTO-1 in comparison to the far-red labeling dye 6-TramTO-3. As expected, both dyes stain the nucleus of the HeLa cells. Present studies focus on the verification by confocal microscopy and the determination of binding affinities for comparison.

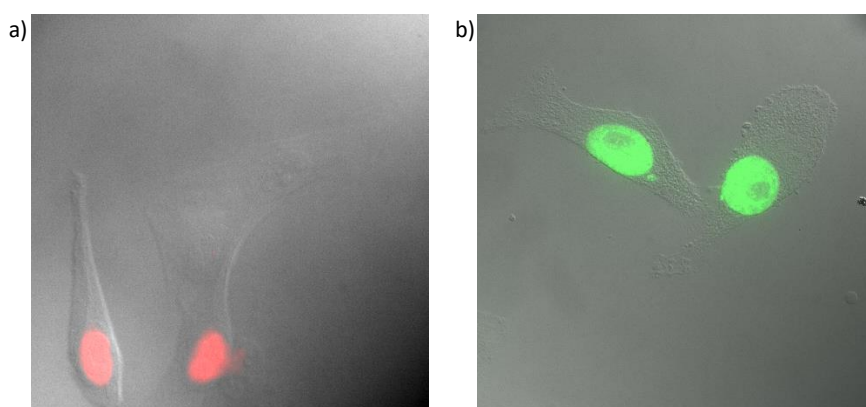


**Figure 4.1.5.** Fluorescence microscopy images of fixed HeLa cells, incubated with 5  $\mu\text{M}$  a) 6-TramTO-3 and b) 6-TramTO-1 in DPBS.

Inspired by the described findings, current investigations target the decoding of the role of the triazole in the binding mode and especially the non-toxic behavior of the TramTO derivatives. We, therefore, plan to synthesize various 6-TramTO-1 and 6-TramTO-3 versions with a short ( $C_n$  with  $n = 2$ ) and a long ( $C_n$  with  $n = 6$ ) side chain, connecting different functional groups (Figure 4.1.6). Additionally, an expected yellow emitting triazole-dye (Figure 4.1.6, compound **A8**, expected  $\lambda_{Em}$  emission = 601 nm)<sup>[3]</sup> was designed and will be synthesized. Further attempts face the specific targeting of mitochondria by connecting a triphenylphosphine moiety<sup>[4]</sup> or a mitochondria-penetrating peptide<sup>[5]</sup> to the TramTO-derivatives. All of these compounds, including 6-TramTO-1, will be analyzed in spectroscopic binding

<sup>II</sup> Cell preparation and fluorescence microscopy were performed by Greta Linden, AK Vázquez, Philipps-Universität Marburg.

## 4. Cumulative Part

studies, towards their cytotoxicity and in labeling studies with fixed HeLa cells in fluorescence microscopy.

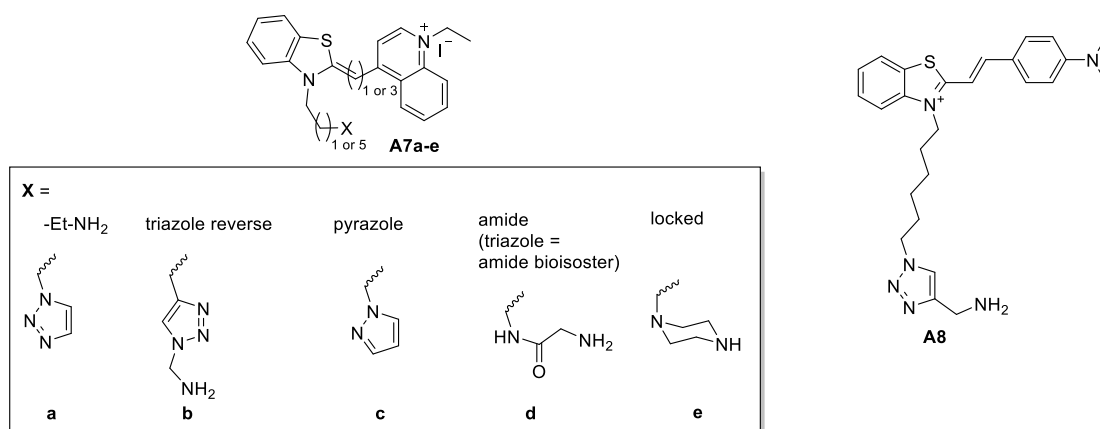


**Figure 4.1.6.** Planned scaffolds for in-depth understanding of triazole role in the TramTO dyes. Compound **A8** represents a planned expected yellow emitting version.

To broaden the field of applications of 6-TramTO-3, several collaborations have been established. All collaborators plan to test our compounds in different systems. The following list gives an overview of the present collaborators and their planned research projects:

- 1) Roy Gross, Julius-Maximilians-University Würzburg: “Characterization of the interaction of the etiological agent of whooping cough *Bordetella pertussis* with human 3D airways models.”
- 2) Mariana Pinho, University NOVA de Lisboa: “Use of far-red fluorescent nucleic acid staining compound 6-TramTO-3 to label DNA in live *Staphylococcus aureus* cells.”
- 3) Rolf Müller, Helmholtz Institute for Pharmaceutical Research Saarland: “Labeling of different bacterial species with 6-TramTO-3 for the use in host cell and zebrafish embryo infection models.”
- 4) Ralf Ehrlich, Leibniz-Institute of Photonic Technology Jena: “Live staining of gram-negative antibiotic-resistant bacteria.”
- 5) Pierre Cosson, Centre Médical Universitaire Geneva: “Fluorescence labeling of different bacteria (*Klebsiella*, *E. coli*, *P.aeruginosa*, *B.subtilis*) and their application in phagocytosis studies.”
- 6) Raphaël Georges Duval, Nanogalenix (company) in Switzerland: “Labeling of harmful bacteria; targeting specific tissues such as solid tumors or cells; labeling parasites or other types of living species in the  $\mu\text{m}/\text{mm}$  range.”
- 7) Peter Graumann, Philipps-University Marburg: “Spatial distribution of the signal recognition particle in bacteria.”
- 8) Torsten Waldminghaus, Max Planck Institute for Terrestrial Microbiology Marburg: “Quantification of DNA in gram-negative bacteria with Flow Cytometry.”
- 9) Pierre Stallforth, Leibniz-Institute for Natural Product Research and Infection Biology Jena: “Labeling of various bacteria that interact with soil amoebae for monitoring the transition to the fruiting bodies.”

## 4. Cumulative Part

- 10) Cynthia Sharma, Julius-Maximilians-University Würzburg: "Investigation of host-pathogen interactions using fluorescence-based sorting and imaging techniques."
- 11) Knut Drescher: Philipps-University Marburg: "6-TramTO-3 as a fluorescent dye for the investigation of bacterial biofilm studies."

### 4.1.3 Author Contribution

The initial idea of 6-TramTO-3 resulted from an azide functionalized version 6-AzTO-3, I was preparing to selectively mark the nucleosome by click reaction. I synthesized and fully characterized 6-AzTO-3, and also the two amine derivatives 6-NH<sub>2</sub>TO-3 and 6-TramTO-3, including all previous synthetic intermediates. I performed their spectroscopic analysis (absorbance and fluorescence spectra) and determined their extinction coefficients. Of the most promising compound 6-TramTO-3, I determined the quantum yields and melting temperature with and without DNA, and fully characterized its complex binding mode to DNA by fluorescence titrations with calf thymus, AT- and GC-rich DNA, circular dichroism and absorbance spectroscopy. I further evaluated temperature-dependent DNA binding. Additionally, I demonstrated the application of 6-TramTO-3 as a DNA stain in gel electrophoresis.

Fluorescence microscopy measurements were assisted by Dr. Gabriele Malengo (Synmikro, Marburg). Bacterial labeling studies with multidrug resistant and sensitive strains, and following phagocytosis studies were performed by Jun.-Prof. Dr. Leon Schulte and Harshavardhan Janga (iLung Institute for Lung Research, Marburg). Jun.-Prof. Dr. Olalla Vázquez had the role of corresponding author, was leading or involved in all the 14-role taxonomy for author-contribution assignment.<sup>[6]</sup>

Under the supervision of Jun.-Prof. Dr. Olalla Vázquez, I further developed the project after the publication, such as the design, synthesis and study of new TramTO derivatives or guided students into the topic. The initial synthetic derivatization of 6-TramTO-1 was performed together with Dr. Rashmi Sharma (DAV University, Jalandhar, Punjab, India; DFG-project VA 1002/3-1).

Finally, some of the named collaborations were the result of discussions after my flash communication at the 6<sup>th</sup> European Chemical Biology Symposium in Madrid in April 2019 and a talk I gave within the Synmikro cluster in July 2019 in Marburg.

Marburg,

Jun. Prof. Dr. Olalla Vázquez

Benedikt Heinrich

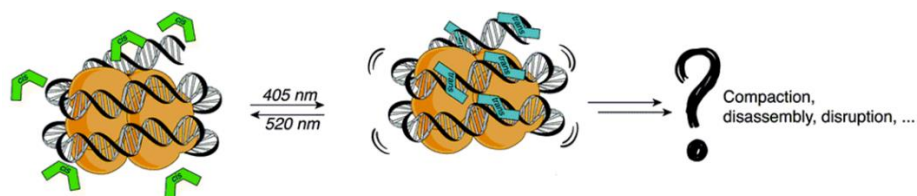
### 4.1.4 References

- [1] Sovenyhazi, K. M.; Bordelon, J. A.; Petty, J. T. Spectroscopic studies of the multiple binding modes of a trimethine-bridged cyanine dye with DNA. *Nucleic Acids Res.* **2003**, *31*, 15, 2561-2569.
- [2] Petty, J. T.; Bordelon, J. A.; Robertson, M. E. Thermodynamic Characterization of the Association of Cyanine Dyes with DNA. *J. Phys. Chem. B.* **2000**, *104*, 30, 7221-7227.

#### 4. Cumulative Part

- [3] Ikeda, S.; Kubota, T.; Yuki, M.; Okamoto, A. Exciton-Controlled Hybridization-Sensitive Fluorescent Probes: Multicolor Detection of Nucleic Acids. *Angew. Chem. Int. Ed.* **2009**, *48*, 35, 6480-6484.
- [4] Zielonka, J.; Joseph, J.; Sikora, A.; Hardy, M.; Ouari, O.; Vasquez-Vivar, J.; Cheng, G.; Lopez, M.; Kalyanaraman, B. Mitochondria-Targeted Triphenylphosphonium-Based Compounds: Syntheses, Mechanisms of Action, and Therapeutic and Diagnostic Applications. *Chem. Rev.* **2017**, *117*, 15, 10043-10120.
- [5] Horton, K. L.; Stewart, K. M.; Fonseca, S. B.; Guo, Q.; Kelley, S. O. Mitochondria-Penetrating Peptides. *Chem. Biol.* **2008**, *15*, 4, 375-382.
- [6] Allen, L.; Scott, J.; Brand, A.; Hlava, M.; Altman, M. Publishing: Credit where credit is due. *Nature* **2014**, *508*, 7496, 312-313.

## 4.2 *ortho*-Fluoroazobenzene Derivatives as DNA Intercalators for Photocontrol of DNA and Nucleosome Binding by Visible Light



We report a high-affinity photoswitchable DNA binder, which displays different nucleosome-binding capacities upon visible-light irradiation. By electromobility shift assay and dynamic light scattering experiments, the following nucleosome disassembly was analyzed.

This chapter was published as: [Heinrich, B.](#); Bouazoune, K.; Wojcik, M.; Bakowsky, U.; Vázquez, O.\* *ortho*-Fluoroazobenzene derivatives as DNA intercalators for photocontrol of DNA and nucleosome binding by visible light. *Org. Biomol. Chem.* **2019**, *17*, 1827-1833. Copyright Royal Society of Chemistry 2019. Material in this chapter was reproduced from the above mentioned reference with permission from The Royal Society of Chemistry. This article was a contribution to the Special New Talent Themed Issue 2019 in *Organic & Biomolecular Chemistry Journal*.



# *ortho*-Fluoroazobenzene derivatives as DNA intercalators for photocontrol of DNA and nucleosome binding by visible light†

Received 20th September 2018,  
Accepted 19th December 2018

DOI: 10.1039/c8ob02343c

Benedikt Heinrich,<sup>a</sup> Karim Bouazoune,<sup>b</sup> Matthias Wojcik,<sup>c</sup>  
Udo Bakowsky,<sup>c</sup> and Olalla Vázquez\*<sup>a</sup>

rsc.li/obc

**We report a high-affinity photoswitchable DNA binder, which displays different nucleosome-binding capacity upon visible-light irradiation. Both photochemical and DNA-recognition properties were examined by UV-Vis, HPLC, CD spectroscopy, NMR, FID assays, EMSA and DLS. Our probe sets the basis for developing new optoepigenetic tools for conditional modulation of nucleosomal DNA accessibility.**

Over the last decades, a large number of studies have established that the organization of eukaryotic DNA, by proteins and RNAs, into a nucleoprotein complex referred to as chromatin is key to regulate genome functions.<sup>1</sup> The most abundant chromatin proteins are the histones. These proteins tightly wrap DNA into a “beads-on-a-string”-like structure. Each ‘bead’ is referred to as a nucleosome and comprises a histone octamer around which about 150 base pairs (bp) of DNA are wrapped. On average, nucleosomes are separated by about 50 bp of free (also called “linker”) DNA.<sup>2</sup> This entails that about 75% of our DNA is wrapped around histones. This nucleosomal organization restricts access to DNA considerably. As a result, nuclear processes such as DNA repair, replication and transcription largely depend on enzymes that can change nucleosomal DNA accessibility.<sup>3–5</sup>

Hence, the ability to control chromatin compaction and, in turn, DNA accessibility using small molecules may provide us with means to study and, conceivably, control (at least some) genome functions, in physiological as well as disease contexts. So far, the use of small-molecule probes as complementary tools to classic chromatin biochemical approaches has strongly contributed to deciphering epigenetic mechanisms

and strengthened our understanding of genome regulation. However, this approach has mainly been limited to enzyme inhibitors<sup>6–9</sup> and altering nucleosome accessibility has largely been disregarded. Indeed, while there is just a handful of examples of compounds capable of targeting nucleosomal DNA, to our knowledge, none of these molecules allow spatio-temporal control of nucleosome binding.<sup>10–15</sup>

Reversible photoresponsive molecules, which have demonstrated their potential in diverse areas (material science,<sup>16–17</sup> molecular motors<sup>18–20</sup> photopharmacology,<sup>21–24</sup> molecular containers,<sup>25</sup> *etc.*) represent a very promising chemical alternative to optogenetics.<sup>26,27</sup> However, the implementation of photoswitchable genome regulators has been very scarce and again only focused on histone-modifying enzymes, so far.<sup>28–30</sup> Therefore, we designed and synthesized a novel photoswitch, which allows light-driven DNA and nucleosome binding and we studied the consequences of this interaction (Fig. 1a).

The ability of externally controlling DNA-associated processes by switching the state of a photochromic DNA binder has previously been demonstrated.<sup>31,32</sup> However, such examples are mainly restricted to the use of azo-modified DNA binders, which involve undesirable UV irradiation.<sup>33–38</sup> There are several strategies to synthesize azobenzene photoswitches that undergo isomerization upon visible-light irradiation.<sup>39–42</sup> For example, the Hecht group has recently optimized the properties of the classical azobenzenes by introducing  $\sigma$ -electron-withdrawing fluorine atoms in *ortho* position to the azobenzene unit. Such substitution leads to visible-light switches with high photoconversions and very long-lived *cis*-isomers.<sup>43,44</sup> Furthermore, to our knowledge, photoswitchable DNA binders have never been used in the context of the nucleosome. Consequently, inspired by the natural DNA minor groove binder netropsin (**1**), we synthesized and studied two water-soluble photosensitive pyrrole hybrids that have identical number of *N*-methyl pyrrole rings as netropsin, but incorporate an *ortho*-fluoroazobenzene scaffold between the pyrrole backbone and also vary in terms of their net charge at physiologi-

<sup>a</sup> Fachbereich Chemie, Philipps-Universität Marburg, Hans-Meerwein-Straße 4, 35043 Marburg, Germany. E-Mail: olalla.vazquez@staff.uni-marburg.de

<sup>b</sup> Institut für Molekularbiologie und Tumorforschung, Philipps-Universität Marburg, Hans-Meerwein-Straße 2, 35043 Marburg, Germany.

<sup>c</sup> Institut für Pharmazeutische Technologie & Biopharmazie, Philipps-Universität Marburg Robert-Koch-Straße 4, 35037 Marburg, Germany.

Electronic Supplementary Information (ESI) available: See DOI: 10.1039/c8ob02343c

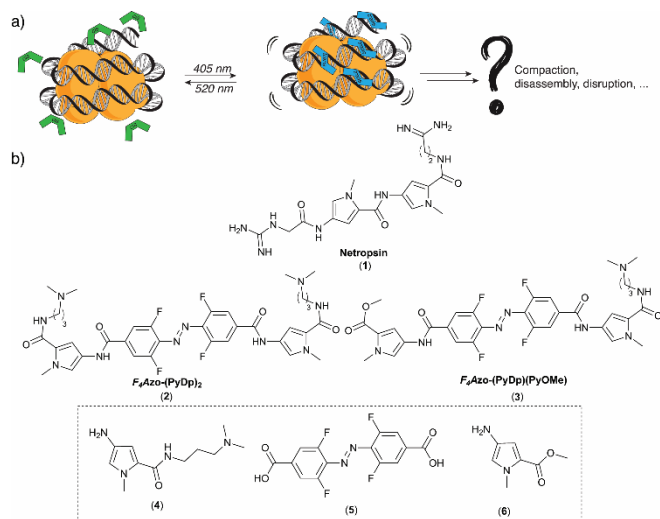


**Fig. 1** (a) Outline of the photocontrollable nucleosome targeting approach based on light-visible photoswitchable DNA binders. (b) Structure of the studied molecules, highlighting the key synthetic building blocks.

cal conditions:  $F_4\text{Azo}-(\text{PyDp})_2$  (**2**) and  $F_4\text{Azo}-(\text{PyDp})(\text{PyOMe})$  (**3**) (Fig. 1b).

The synthesis of  $F_4\text{Azo}-(\text{PyDp})_2$  (**2**) and  $F_4\text{Azo}-(\text{PyDp})(\text{PyOMe})$  (**3**) was straightforward through one-pot condensation between the previously reported building blocks: **4**,<sup>45</sup> **5**,<sup>43,44</sup> and **6**.<sup>46</sup> (Fig. 1 & Schemes S1-S4†). Once synthesized, their photochemical behaviour was investigated in detail. Thus, the *ortho*-fluoroazobenzene building block **5** alone and also in presence of the pyrrole moieties showed the expected absorption bands: intense band at  $\lambda_{\text{max}} = 319$  nm assigned to the  $\pi \rightarrow \pi^*$  transition together with a weaker one due to a  $n \rightarrow \pi^*$  and significant intensity decrease of the  $\pi \rightarrow \pi^*$  band with a slight increase of the  $n \rightarrow \pi^*$  one under 405 nm and 520 nm irradiation, respectively (Fig. S21b†). Nevertheless, the direct insertion of the azophenyl derivative into the pyrrole backbone affected the parental spectra, as observed for related compounds.<sup>47</sup> Irradiation of  $F_4\text{Azo}-(\text{PyDp})_2$  (**2**) entails fast spectroscopic changes.<sup>48</sup> Thus, upon irradiation with 520 nm there is a clear intensity decrease between 287 nm and 500 nm, the  $\lambda_{\text{max}}$  is slightly shifted to 278 nm and a new partly overlapping band at  $\lambda_{\text{max}} = 420$  nm can be detected (Fig. 2a). The photostationary state is reached after just 2 minutes of irradiation. We also demonstrated the reversibility of the photoisomerization for up to 16 cycles without any significant photobleaching (Fig. 2b).

We next determined the isomer ratios at the photostationary state as well as the lifetime of the isomers by integrating the peak area of the HPLC chromatograms at the isosbestic point (287 nm). As expected, the *trans*-isomer was the thermodynamically stable species (*trans/cis* ratio 92:8; Fig. S23a†) Importantly, the thermal relaxation of the *cis*-isomer was slow (*cis/trans* ratio 77:23, after 9 hours stored in the dark, Fig. 3), which enabled both DNA and nucleosome binding experiments.

Unfortunately,  $F_4\text{Azo}-(\text{PyDp})(\text{PyOMe})$  (**3**) did not show any major change by neither UV-Vis spectroscopy nor HPLC

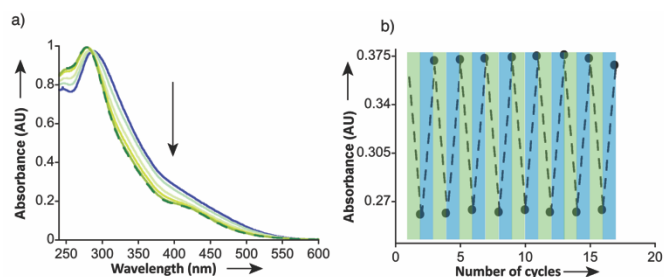


**Fig. 2** (a) UV-Vis spectra of a 20  $\mu\text{M}$  solution of  $F_4\text{Azo}-(\text{PyDp})_2$  (**2**) in 10 mM Tris buffer pH 7.6, 50 mM KCl and DMSO (98:2), initially at the thermodynamic state (blue) and after successive irradiation intervals at 520 nm (green). (b) Reversible photochromism upon alternating irradiation at 520 nm (green) and 405 nm (blue) measured at 335 nm. Represented data are calculated from three independent experiments.

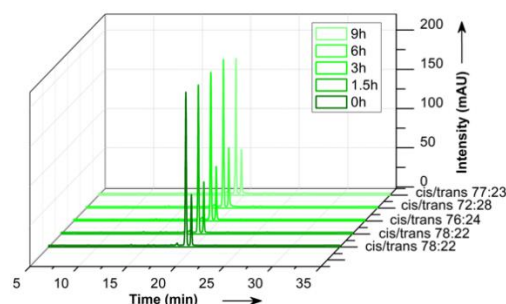


**Fig. 3** Evaluation of the *cis*-isomer stability of  $F_4\text{Azo}-(\text{PyDp})_2$  (**2**) in 10 mM Tris buffer pH 7.4, 10 mM NaCl and DMSO (95:5) by HPLC after initial irradiation at 520 nm for 2 min (time 0h). Samples were stored in total darkness. HPLC chromatograms were recorded after the listed times. Represented data are a set, which is representative of the measurements from three independent experiments.

(Fig. S20 & S23b†). This forced us to use <sup>1</sup>H-NMR analysis for further investigations (Fig. 4). Thus, the *trans/cis* ratios were calculated by the integration of the aromatic proton signals (6.8 ppm–8.1 ppm). Gratifyingly, in the case of  $F_4\text{Azo}-(\text{PyDp})_2$  (**2**) we corroborated the same ratio as the one obtained by HPLC (*trans/cis* ratio 93:7 and 30:70 for the *trans*- and *cis*-state, respectively). In addition, <sup>1</sup>H-NMR studies revealed that, indeed, the photochemical behaviour of  $F_4\text{Azo}-(\text{PyDp})(\text{PyOMe})$  (**3**) is analogue to  $F_4\text{Azo}-(\text{PyDp})_2$  (**2**) (*trans/cis* ratio 97:3 and 27:73 for the *trans*- and the *cis*-state, respectively).

Once the photoisomerization was fully characterized, we explored whether the two compounds are able to interact with DNA and whether their isomers displayed any differences in DNA-binding affinity. Thermal melting experiments are the most common methodology used for the evaluation of DNA interactions; however, we observed decomposition at high temperatures (Fig. S36†). Consequently, we performed a fluorescent intercalator displacement (FID) assay<sup>49</sup> compatible with the isomerization. We also compared our results with the minor groove binder netropsin (**1**). Thiazole orange (TO) was chosen as intercalator since its excitation and emission hardly affect the *trans/cis* isomerization (Fig. S34†). This experiment relies on a decrease of fluorescence due to the displacement of

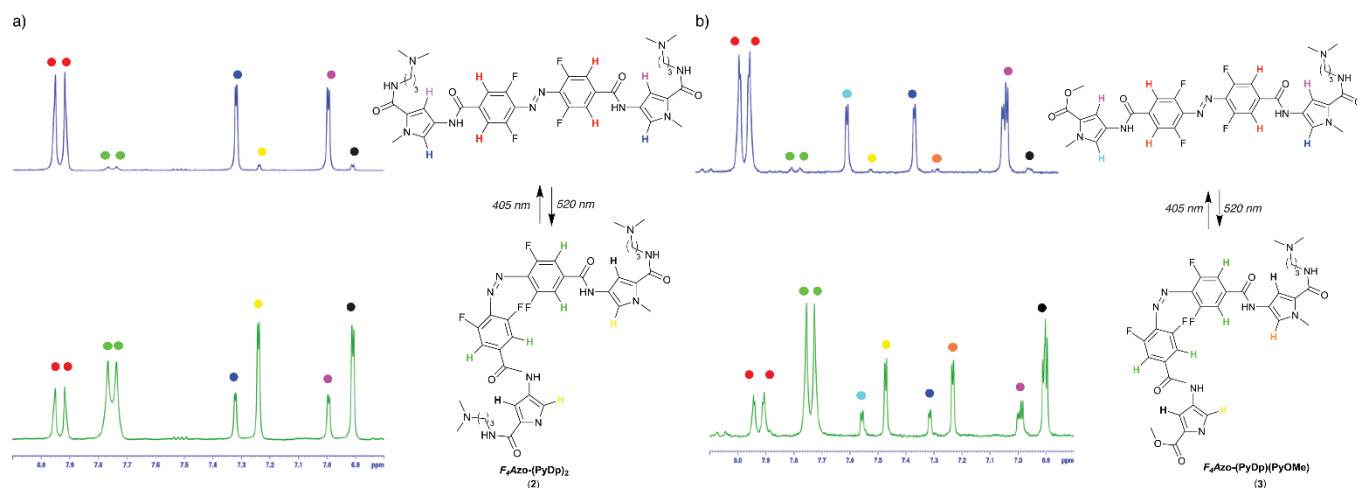


**Fig. 4** Selected aromatic region of the  $^1\text{H-NMR}$  spectra (300 MHz) of a 4 mM solution of (a)  $F_4\text{Azo-(PyDp)}_2$  (**2**) and (b)  $F_4\text{Azo-(PyDp)(PyOMe)}$  (**3**) in  $\text{DMSO-d}_6$  after irradiation to the *trans*- (top) and *cis*-isomer (bottom). Aromatic protons are marked in colours in the spectra and molecules.

DNA-bound TO by the competitive binder. Therefore, we first determined the apparent binding constant of TO in presence of a hairpin oligonucleotide, which contains the sequence *ATTA* ( $\text{dsDNA}_{\text{hAT}}$ ) with the HypSpec software. Subsequently we simulated the species distribution for the obtained binding constant ( $K_D = 59.8 \pm 13.1$  nM) by using the HySS software. The affinity of TO to  $\text{dsDNA}_{\text{hAT}}$  enabled FID experiments at low  $\mu\text{M}$  range with more than 95% of TO-DNA complex in our experimental conditions (Table S4 $\dagger$ ), which assures the reliability of the assay. Typical fluorescence quenchers such as DABCYL or BHQ-1 are provided with the diazenyl functional group ( $\text{R-N=N-R'}$ ), therefore we initially performed control competition assays in presence of increasing amounts of **5** to rule out artefacts due to quenching effects (Fig. S38 $\dagger$ ). As showed in Fig. 5, both  $F_4\text{Azo-(PyDp)}_2$  (**2**) and  $F_4\text{Azo-(PyDp)}$

(**PyOMe**) (**3**) were able to efficiently replace the bound TO from the DNA. The obtained data suggested binding modes beyond the 1:1 stoichiometry. For the mathematical analysis of the FID assays, the experimental data were fitted globally (all wavelengths simultaneously) with HypSpec. These experimental data fitted the model adequately (Fig. S33 $\dagger$ ).

The analysis of the apparent dissociation constants indicated that both photoswitchable compounds have high DNA-binding affinity in the nM range (Table 1). Importantly, for both azobenzene derivatives (**2** and **3**), the binding capacity of their isomers is different. This demonstrates a conformation-dependent binding mode. In each pair, the *trans*-isomer is always the best binder, which is in agreement with other previous examples of azobenzene derivatives.<sup>33–38</sup> Furthermore, upon addition of the netropsin (**1**) control, the emission intensity of DNA-Bound TO also decreased significantly. The faster saturation of the netropsin (**1**) in comparison with our photoswitchable binders, together with the fact that its binding curve does not also appear to follow a standard isotherm may be indicative of different binding modes. It was expected that netropsin (**1**), as a minor groove binder, could not fully displace the intercalator TO and reach saturation.<sup>50</sup> The binding curve of netropsin (**1**) with a hairpin oligonucleotide containing the sequence *GGCCC* ( $\text{dsDNA}_{\text{hGC}}$ ) displayed the standard

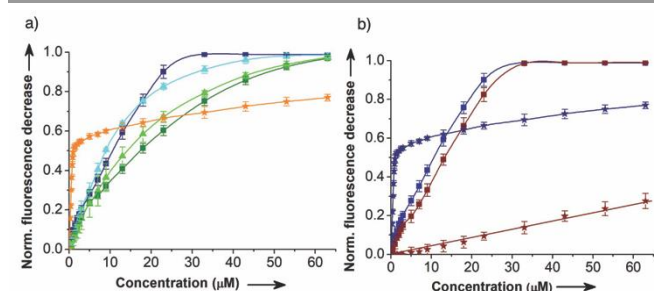


**Fig. 5** (a) Competitive displacement analysis of a 6  $\mu\text{M}$  TO solution in 20 mM  $\text{NaH}_2\text{PO}_4$  pH 7.4, 100 mM  $\text{NaCl}$  and 1  $\mu\text{M}$  of  $\text{dsDNA}_{\text{hAT}}$  with: netropsin (**1**, orange stars);  $F_4\text{Azo-(PyDp)}_2$  isomers (*trans*-**2** dark blue squares; *cis*-**2** dark green squares) and  $F_4\text{Azo-(PyDp)(PyOMe)}$  (*trans*-**3** light blue triangles; *cis*-**3** light green triangles); (b) sequence-selectivity analysis of netropsin (**1**, stars) *trans*- $F_4\text{Azo-(PyDp)}_2$  (*trans*-**2**, squares) in presence 6  $\mu\text{M}$  TO solution in 20 mM  $\text{NaH}_2\text{PO}_4$  pH 7.4, 100mM  $\text{NaCl}$  and 1  $\mu\text{M}$  of  $\text{dsDNA}_{\text{hAT}}$  (blue) or  $\text{dsDNA}_{\text{hGC}}$  (brown). Represented data and standard deviations are mean values calculated from three independent experiments. Data points were fitted with HypSpec, using multi-variant factor analysis to obtain globally optimized parameters. Lines are “eye-guides” for assistance in visualizing the binding curves.

**Table 1** Binding affinities derived from FID experiments with selected hairpin oligonucleotide ( $\text{dsDNA}_{\text{h}}$ ).

Compound	$\text{dsDNA}_{\text{h}}$ site	$K_D$ (nM)
Netropsin ( <b>1</b> )	<i>ATTA</i>	$10 \pm 1$
Netropsin ( <b>1</b> )	<i>GGCCC</i>	n. c.
<i>cis</i> - $F_4\text{Azo-(PyDp)(PyOMe)}$ ( <i>cis</i> - <b>3</b> )	<i>ATTA</i>	$82 \pm 6$
<i>trans</i> - $F_4\text{Azo-(PyDp)(PyOMe)}$ ( <i>trans</i> - <b>3</b> )	<i>ATTA</i>	$54 \pm 3$
<i>cis</i> - $F_4\text{Azo-(PyDp)}_2$ ( <i>cis</i> - <b>2</b> )	<i>ATTA</i>	$108 \pm 14$
<i>trans</i> - $F_4\text{Azo-(PyDp)}_2$ ( <i>trans</i> - <b>2</b> )	<i>ATTA</i>	$60 \pm 1$
<i>trans</i> - $F_4\text{Azo-(PyDp)}_2$ ( <i>trans</i> - <b>2</b> )	<i>GGCCC</i>	$13 \pm 1$

n.c. represents not calculated.

isotherm for non-specific interaction *i.e.* proportional to the concentration of added ligand (Fig. 5b).

To get additional insight into its binding mode, we performed exemplarily selectivity experiments with  $F_4\text{Azo}-(\text{PyDp})_2$  (**2**) and the additional hairpin  $\text{dsDNA}_{hGC}$  (Fig. 5b) as well as circular dichroism (CD) experiments (Fig. 6).

Regarding selectivity,  $F_4\text{Azo}-(\text{PyDp})_2$  (**2**) showed a slight preference for  $\text{dsDNA}_{hGC}$ . Of note, all the obtained binding constants were derived from indirect assessments, based on the TO affinity to the corresponding dsDNA and its loss of fluorescence when it is displaced by a new binder. Therefore, the technique is limited to compounds with binding affinities in the same range. In addition, ligand-induced condensation or interference with the fluorescence could not be discriminated from the actual fluorescence loss due to displacement, which may explain non-standard isotherms. Consequently, these values are, strictly speaking, estimations. Despite these inherent drawbacks, the FID assay is a straightforward method for the comparative characterization of DNA-recognition by the azobenzene derivatives on the one hand, and on the other hand, by the netropsin (and compounds with similar binding modes).

The CD experiments of  $F_4\text{Azo}-(\text{PyDp})_2$  (**2**) with the double-stranded *calif thymus* DNA ( $\text{dsDNA}_{CT}$ ) confirmed a non-covalent interaction beyond the external non-specific electrostatic association with the DNA phosphates. Therefore, the observed interaction differs from the cationic polyamines such as spermine and spermidine.<sup>51</sup> The CD spectra of the  $\text{dsDNA}_{CT}$  alone showed the characteristic bands of the canonical B-DNA conformation (Fig. 6, grey line): a positive band at 275 nm and a negative one at 245 nm of similar intensity.<sup>52</sup>  $F_4\text{Azo}-(\text{PyDp})_2$  (**2**) is achiral and, hence, optically inactive (Fig. 6, black line). However, when increasing amounts of  $F_4\text{Azo}-(\text{PyDp})_2$  (**2**) were added to the  $\text{dsDNA}_{CT}$ , induced circular dichroic (ICD) signals were detected, as expected from DNA binders.

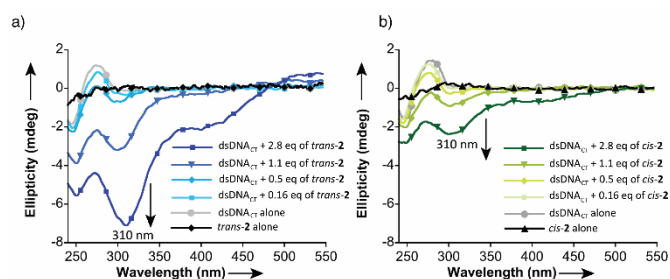


**Fig. 6** CD spectra of a 50  $\mu\text{M}$  solution of  $\text{dsDNA}_{CT}$  in 20 mM  $\text{NaH}_2\text{PO}_4$  pH 7.4, 100 mM NaCl with increasing amounts of the  $F_4\text{Azo}-(\text{PyDp})_2$  isomers: (a) *trans*-**2**, blue; (b) *cis*-**2**, green.  $F_4\text{Azo}-(\text{PyDp})_2$  amounts: 0 eq (grey circles); 0.16 eq (light squares); 0.5 eq (diamonds); 1.1 eq (triangles) and 2.8 eq (dark squares). Black line represents the CD spectra of a 142  $\mu\text{M}$  (equivalent to 2.8 eq in the titration) solution of  $F_4\text{Azo}-(\text{PyDp})_2$  isomers under the same conditions: (a) *trans*-**2** (diamonds); (b) *cis*-**2** (triangles). Represented data are mean values calculated from two independent experiments; buffer subtracted; eq means equivalents: mol of compound **2** per mol of  $\text{dsDNA}_{CT}$ .

Intriguingly, the addition of  $F_4\text{Azo}-(\text{PyDp})_2$  (**2**) induced a remarkable dose-dependent increase in magnitude of the signal in the region of 240–480 nm with a clear negative peak at 310 nm. Importantly, the two isomers *cis*-**2** and *trans*-**2** behaved differently in the CD experiments under the same conditions. In particular, the ICD signals are more pronounced with *trans*-**2** than with *cis*-**2**, which is concurrent with our previous FID experiments (as described above).

To understand the observed CD signature, we performed UV-Vis titrations (Fig. 7). We observed that the addition of  $F_4\text{Azo}-(\text{PyDp})_2$  (**2**) promoted a red shift of the absorbance maximum of the  $\text{dsDNA}_{CT}$  and a new partly overlapped band at 420 nm, as in the CD spectra. However, the CD band at 310 nm was not clearly detected in our UV-Vis measurements. Other azo-modified polyamines displayed CD signals at  $\sim 310$  nm in presence of DNA but, to our knowledge, always with positive ellipticity.<sup>34,53</sup> However, it has been reported that strong insertion of intercalators into the DNA causes a red-shifted band with high negative CD signals between 240 nm and 340 nm,<sup>54</sup> which is consistent with our observations.

All together our results have shown that  $F_4\text{Azo}-(\text{PyDp})_2$  (**2**) is a photoswitchable molecule capable of interacting with the DNA through a conformation-dependent binding mode.

Finally, we explored the possibility of using  $F_4\text{Azo}-(\text{PyDp})_2$  (**2**) as a controllable nucleosome binder using visible light. For this endeavour, we first reconstituted nucleosome core particles (NCP) using chicken erythrocyte histones<sup>55</sup> and the Widom 601 DNA, which forms a stably positioned nucleosomes.<sup>56</sup> We next used native gel electrophoretic mobility shift assays (EMSA) to analyse nucleosome reconstitution efficiency. We also used EMSA to assess nucleosome integrity after incubating nucleosomes with increasing amounts of either netropsin (**1**) or  $F_4\text{Azo}-(\text{PyDp})_2$  (**2**) for three hours. As shown in Fig. 8, low concentrations of the minor groove binder netropsin (up to 4 eq) do not affect the nucleosome integrity. In the presence of high netropsin concentrations, the bands became very diffuse and consequently barely detectable. This phenomenon may be due to the formation of many different species through unspecific electrostatic interactions<sup>57,58</sup> and/or aggre-

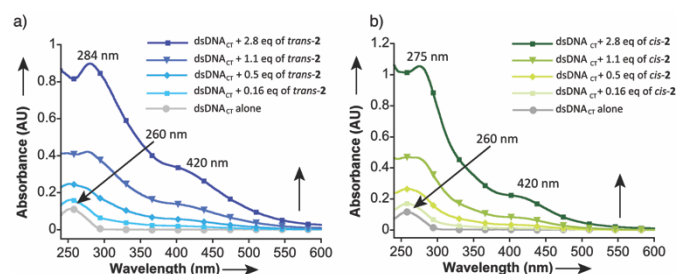


**Fig. 7** UV-Vis spectra of a 12.5  $\mu\text{M}$  solution of  $\text{dsDNA}_{CT}$  in 20 mM  $\text{NaH}_2\text{PO}_4$  pH 7.4, 100 mM NaCl with increasing amounts of the  $F_4\text{Azo}-(\text{PyDp})_2$  isomers: (a) *trans*-**2**, blue; (b) *cis*-**2**, green.  $F_4\text{Azo}-(\text{PyDp})_2$  amounts: 0 eq (grey circles); 0.16 eq (light squares); 0.5 eq (diamonds); 1.1 eq (triangles) and 2.8 eq (dark squares). Represented data are calculated from three independent experiments; buffer was subtracted; eq means equivalents: mol of compound **2** per mol of  $\text{dsDNA}_{CT}$ .



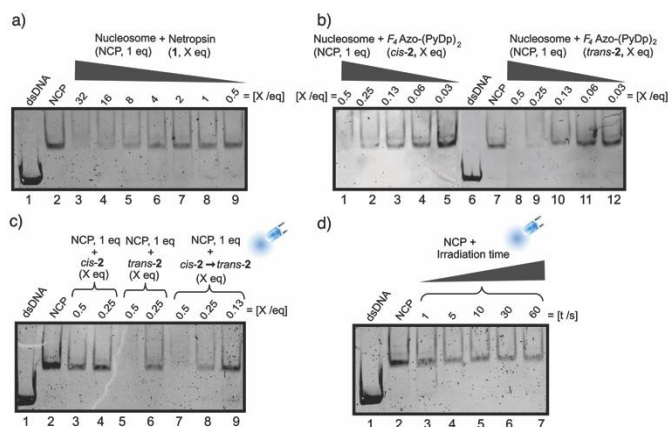


**Fig. 8** Evaluation of the interaction of DNA binders with Widom 601 nucleosome core particle (NCP). All experiments were performed with 300 nM NCP and 55 nM dsDNA as control in 10 mM Tris buffer pH 8, 1 mM EDTA, 50 mM NaCl and DMSO (90:10) and analyzed by ethidium bromide staining, after electrophoresis: (a) netropsin interaction: lane 1: dsDNA; lanes 2-9: NCP + [netropsin] = 0, 32, 16, 8, 4, 2, 1, 0.5 eq.; (b)  $F_4$ Azo-(PyDp) $_2$  (2) interaction: lane 7: NCP; lane 6: dsDNA; lane 1-5: NCP + [*cis*-2] = 0.5, 0.25, 0.13, 0.06, 0.03 eq.; lane 8-12: NCP + [*trans*-2] = 0.5, 0.25, 0.13, 0.06, 0.03 eq. DMSO stocks of  $F_4$ Azo-(PyDp) $_2$  (2) were irradiated before EMSA; (c)  $F_4$ Azo-(PyDp) $_2$  (2) interaction with *in situ* irradiation: lane 1: dsDNA; lane 2: NCP; lane 3-4: control with previous irradiation of NCP + [*cis*-2] = 0.5, 0.25 eq.; lane 5-6: control with previous irradiation of NCP + [*trans*-2] = 0.5, 0.25; lane 7-9 *in situ* irradiation at 405 nm for 10 s of NCP + [*cis*-2] = 0.5, 0.25, 0.13 eq.; (d) effect of irradiation at 405 nm on NCP: lane 1: dsDNA; lane 2: NCP; lane 3-7: NCP after 1 s, 5 s, 10 s, 30 s, 60 s irradiation. Eq. means equivalents: mol of compound per mol of base pair; NCP means nucleosome core particle.

gates, which may be too big to enter the gel. Interestingly, the binding of our molecule  $F_4$ Azo-(PyDp) $_2$  (2) apparently triggered this effect at lower concentrations than netropsin, despite having the same net charge (Fig. 8a & b). Importantly, there was a noticeable difference between isomers. In particular, the intensity of the nucleosome band abruptly ceased to be detectable in the presence of 0.5 eq. of the *trans*-2, while at the same concentration, the *cis*-2 failed to fully alter the nucleosome band. Furthermore, the fact that we circumvented the use of strong UV light, for the isomerization, facilitated the *in situ* application. Thus, the same procedure was repeated but now performing the irradiation *in situ*: after incubating the *cis*-2 for 1 h with the nucleosome, the samples were irradiated at 405 nm for 10 s, in a single isomerization cycle. As a control, we also included both isomers irradiated prior to the nucleosome incubation. Gratifyingly, we observed that the *in situ* formed *trans*-2 showed a higher impact than the parental *cis*-2. Of note, no irradiation effect on the nucleosome was detectable (Fig. 8d).

To complement the EMSA studies and gain preliminary insights into the effect of  $F_4$ Azo-(PyDp) $_2$  (2) on the NCPs, we performed dynamic light scattering (DLS) measurements. Nucleosomes are colloidal particles of 11 nm wide,<sup>59</sup> and alterations in their hydrodynamic size can assist in the characterization of the interaction with small molecules. In this ana-

lysis, we used NCP at 2  $\mu$ M concentration, employing plasmids containing multiple repeats of the Widom 601 sequence for large-scale DNA isolation.<sup>60</sup> As shown in Fig. 9, the particle size of the NCP is consistent with previous reports.<sup>61,62</sup> Increasing amounts of  $F_4$ Azo-(PyDp) $_2$  (2) clearly change the size distribution resulting in larger particles than the canonical NCP (Fig. 9a). This effect was reproducible and, interestingly, changes were already detectable from the first  $F_4$ Azo-(PyDp) $_2$  addition (0.06 eq.), although no alterations in the EMSA bands were observable under the same conditions at this concentrations (Fig. S46a†). This was also contrary to the case of the netropsin, where low concentrations did not affect the size of the particle (Fig. S42 & S46d†). Therefore, as expected, the insertion of  $F_4$ Azo-(PyDp) $_2$  (2) caused higher structural distortion than for the minor groove binder 1. To study the possibility that such distortion leads to aggregation

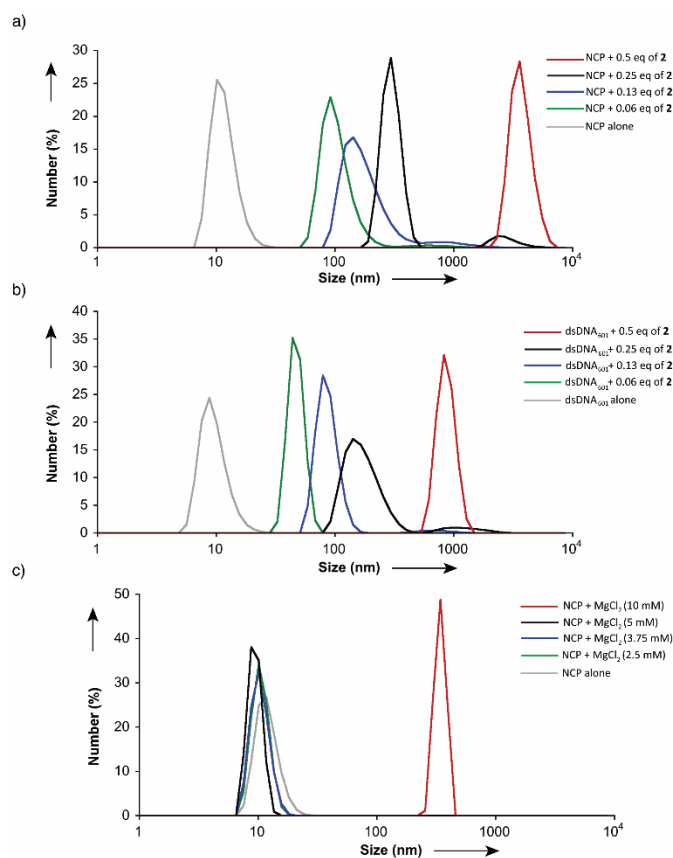


**Fig. 9** Effect of  $F_4$ Azo-(PyDp) $_2$  on: (a) nucleosome (NCP); (b) dsDNA<sub>601</sub> at 2  $\mu$ M concentration in 10 mM Tris 1 mM EDTA pH 8.0 and 50 mM NaCl monitored by dynamic light scattering (DLS).  $F_4$ Azo-(PyDp) $_2$  (2) amounts: 0 eq. (grey); 0.06 eq. (green); 0.13 eq. (blue); 0.25 eq. (black) and 0.5 eq. (red); (c) effect of MgCl<sub>2</sub> on NCP at 2  $\mu$ M concentration in 3.5 mM Tris 0.35 mM EDTA pH 8.0 monitored by DLS. MgCl<sub>2</sub> concentrations: 0 mM (grey); 2.5 mM (green); 3.75 mM (blue); 5 mM (black); 10 mM (red). Intensity statistics of 10 measurements. Represented data are a representative one of two measurements from independent experiments; eq means equivalents (mol of compound per mol of base pair) Represented data are a set, which is representative of the measurements from two independent experiments.

via nucleosome disassembly, we performed control experiments with the analogue set-up but using the dsDNA employed for the nucleosome assembly (dsDNA<sub>601</sub>) instead of the whole NCP, as well as, the precipitated NCP in presence of magnesium chloride; and histone octamer alone. However, the latter protein complex did not display any DLS signal under these conditions. 10 mM of magnesium chloride promoted the precipitation of the NCP (Fig. S43 & S46c†) and the appearance of single peak of higher size than the NCP alone but smaller than the one obtained with highest concentrations of *F*<sub>4</sub>Azo-(PyDp)<sub>2</sub> (**2**) (342 nm versus 3580 nm, respectively). Interestingly, the incubation of dsDNA<sub>601</sub> in presence of *F*<sub>4</sub>Azo-(PyDp)<sub>2</sub> (**2**) (Fig. 9b) displayed DNA-higher order structures, as reported with other cationic molecules<sup>63-65</sup> such as polyamines, surfactants, *etc.* Qualitatively, the distribution of the peaks obtained from this titration were similar to the one observed in the presence of NCP (Fig. 9a). Therefore, these DLS data suggest that, first, the *F*<sub>4</sub>Azo-(PyDp)<sub>2</sub> (**2**) intercalates into the nucleosomal DNA inducing distortions, which lead to the formation of high size aggregates. These observations are consistent with the hypothesis that nucleosome distortion subsequently leads to disruption. Future experiments will be required to fully characterize these alterations and their kinetics.

In summary, we have designed, synthesized and studied a novel photoswitchable *ortho*-fluoroazobenzene DNA binder: *F*<sub>4</sub>Azo-(PyDp)<sub>2</sub>. We also demonstrated that its DNA interaction depends on the conformation, which, importantly, can be controlled by visible-light. Furthermore, our study establishes the possibility of performing photocontrollable nucleosome binding. To our knowledge this is the first time that nucleosome targeting is externally modulated by visible-light photoswitches. We believe that this approach uncovers the possibility of using photosensitive chemical tools to alter nucleosome-based processes. At this point, it is impossible to predict whether our molecule can preferentially impact specific cell functions. It is more plausible that, if appropriately taken up by cells, the molecule would alter cell functions randomly, since *F*<sub>4</sub>Azo-(PyDp)<sub>2</sub> (**2**) only shows a slight sequence binding preference. Thus, future directions may include the development of sequence-specific nucleosome binders to potentially control cell functions specifically *via* modulation of DNA transcription and/or repair processes.

## Conflicts of interest

There are no conflicts to declare

## Acknowledgements

The authors gratefully acknowledge: Prof. E. Meggers (Phillips-Universität Marburg) for the accessibility to his S1 laboratory; Prof. P. Ballester (ICIQ) for the insight into the use of HypSpec and HySS software; Prof. S. Hecht (Humboldt-Universität zu

Berlin) for the discussions and suggestions regarding the initial isomerization irradiation experiments; Prof. A. Brehm (IMT Marburg) for critical advice and support; Prof. J-J Song (Korea Advanced Institute of Science and Technology) for supplying the plasmid pUC-19/16X601; M. Alawak and J. Schäfer (Phillips-Universität Marburg) for initial discussions regarding DLS; N. Frommknecht (Phillips-Universität Marburg) for design assistance and construction of LED lamps; COST action CM1406 (Epigenetic Chemical Biology EPICHEMBIO) for support in networking and mutual cooperation. O.V. thanks the SPP1926 for the Young Investigator Award and Fulbright Commission for the Fulbright-Cottrell Award 2016. Finally, this work was financially supported by Fulbright Commission and the DFG programs: SPP1926 'Next Generation Optogenetics', Young Investigator program (grant # GO1011/11-1) and TRR81: 'Chromatin Changes in Differentiation and Malignancies (TRR81/3, Z04)'.

## Notes and references

- G. Felsenfeld, *Cold Spring Harb Perspect. Biol.*, 2014, **6**(1), a018200.
- D. E. Schones, K. Cui, S. Cuddapah, T. Y. Roh, A. Barski, Z. Wang, G. Wei and K. Zhao, *Cell*, 2008, **132**(5), 887-898.
- K. Luger, *Chromosome Res.*, 2006, **14**(1), 5-16.
- C. R. Clapier and B. R. Cairns, *Annu. Rev. Biochem.*, 2009, **78**, 273-304.
- C. D. Allis and T. Jenuwein, *Nat. Rev. Genet.*, 2016, **17**(8), 487-500.
- C. D. Allis and T. W. Muir, *ChemBioChem*, 2011, **12** (2), 264-279.
- A. Huston, C. H. Arrowsmith, S. Knapp and M. Schapira, *Nat. Chem. Biol.*, 2015, **11**(8), 542-545.
- J. Shortt, C. J. Ott, R. W. Johnstone and J. E. Bradner, *Nat. Rev. Cancer*, 2017, **17**(4), 160-183.
- P. A. Cole, *Nat. Chem. Biol.*, 2008, **4**(10), 590-597.
- J. D. Trzuppek, J. M. Gottesfeld and D. L. Boger, *Nat. Chem. Biol.*, 2006, **2**(2), 79-82.
- E. Y. Chua, G. E. Davey, C. F. Chin, P. Droge, W. H. Ang and C. A. Davey, *Nucleic Acids Res.*, 2015, **43**(11), 5284-5296.
- R. K. Suto, R. S. Edayathumangalam, C. L. White, C. Melander, J. M. Gottesfeld, P. B. Dervan and K. Luger, *J. Mol. Biol.*, 2003, **326**(2), 371-380.
- R. S. Edayathumangalam, P. Weyermann, J. M. Gottesfeld, P. B. Dervan and K. Luger, *Proc. Natl. Acad. Sci. U. S. A.*, 2004, **101**(18), 6864-6869.
- C. T. McMurray and K. E. van Holde, *Proc. Natl. Acad. Sci. U. S. A.*, 1986, **83**(22), 8472-8476.
- M. E. Nunez, K. T. Noyes and J. K. Barton, *Chem. Biol.*, 2002, **9**(4), 403-415.
- M. M. Russew and S. Hecht, *Adv. Mater.*, 2010, **22**(31), 3348-3360.
- J. Karcher and Z. L. Pianowski, *Chem. Eur. J.*, 2018, **24**(45), 11605-11610.

- 18 L. A. Huber, K. Hoffmann, S. Thumser, N. Bocher, P. Mayer and H. Dube, *Angew. Chem. Int. Ed.*, 2017, **56**(46), 14536-14539.
- 19 A. S. Lubbe, Q. Liu, S. J. Smith, J. W. de Vries, J. C. M. Kistemaker, A. H. de Vries, I. Faustino, Z. Meng, W. Szymanski, A. Herrmann and B. L. Feringa, *J. Am. Chem. Soc.*, 2018, **140**(15), 5069-5076.
- 20 T. van Leeuwen, A. S. Lubbe, P. Stacko, S. J. Wezenberg and B. L. Feringa, *Nat. Rev. Chem.*, 2017, **1**(12), 96.
- 21 J. Broichhagen, J. A. Frank and D. Trauner, *Acc. Chem. Res.*, 2015, **48**(7), 1947-60.
- 22 K. Hull, J. Morstein and D. Trauner, *Chem. Rev.*, 2018, **118**(21), 10710-10747.
- 23 M. M. Lerch, M. J. Hansen, G. M. van Dam, W. Szymanski and B. L. Feringa, *Angew. Chem. Int. Ed.*, 2016, **55**(37), 10978-10999.
- 24 W. A. Velema, W. Szymanski and B. L. Feringa, *J. Am. Chem. Soc.*, 2014, **136**(6), 2178-2191.
- 25 A. Diaz-Moscoco and P. Ballester, *Chem. Commun.*, 2017, **53**(34), 4635-4652.
- 26 M. Banghart, K. Borges, E. Isacoff, D. Trauner and R. H. Kramer, *Nat. Neurosci.*, 2004, **7**(12), 1381-1386.
- 27 L. Fenno, O. Yizhar and K. Deisseroth, *Annu. Rev. Neurosci.*, 2011, **34**, 389-412.
- 28 L. Albert, J. Xu, R. W. Wan, V. Srinivasan, Y. L. Dou and O. Vazquez, *Chem. Sci.*, 2017, **8**(6), 4612-4618.
- 29 S. A. Reis, B. Ghosh, J. A. Hendricks, D. M. Szantai-Kis, L. Tork, K. N. Ross, J. Lamb, W. Read-Button, B. Zheng, H. Wang, C. Salthouse, S. J. Haggarty and R. Mazitschek, *Nat. Chem. Biol.*, 2016, **12**(5), 317-323.
- 30 W. Szymanski, M. E. Ourailidou, W. A. Velema, F. J. Dekker and B. L. Feringa, *Chemistry*, 2015, **21**(46), 16517-16524.
- 31 A. S. Lubbe, W. Szymanski and B. L. Feringa, *Chem. Soc. Rev.*, 2017, **46**(4), 1052-1079.
- 32 E. Pazos, J. Mosquera, M. E. Vazquez and J. L. Mascarenas, *ChemBioChem*, 2011, **12**(13), 1958-1973.
- 33 A. Bergen, S. Rudiuk, M. Morel, T. Le Saux, H. Ihmels and D. Baigl, *Nano Lett.*, 2016, **16**(1), 773-780.
- 34 M. Deiana, Z. Pokladek, J. Olesiak-Banska, P. Mlynarz, M. Samoc and K. Matczyszyn, *Sci. Rep.*, 2016, **6**, 28605-28611.
- 35 S. Ghosh, D. Usharani, A. Paul, S. De, E. D. Jemmis and S. Bhattacharya, *Bioconjugate Chem.*, 2008, **19**(12), 2332-2345.
- 36 C. Dohno, S. N. Uno and K. Nakatani, *J. Am. Chem. Soc.*, 2007, **129**(39), 11898-11899.
- 37 T. Stafforst and D. Hilvert, *Angew. Chem. Int. Ed.*, 2010, **49**(51), 9998-10001.
- 38 T. Goldau, K. Murayama, C. Brieke, S. Steinwand, P. Mondal, M. Biswas, I. Burghardt, J. Wachtveitl, H. Asanuma and A. Heckel, *Chem. Eur. J.*, 2015, **21**(7), 2845-2854.
- 39 J. Garcia-Amoros and D. Velasco, *Beilstein J. Org. Chem.*, 2012, **8**, 1003-1017.
- 40 H. M. Bandara and S. C. Burdette, *Chem. Soc. Rev.*, 2012, **41**(5), 1809-1825.
- 41 M. X. Dong, A. Babalhavaeji, S. Samanta, A. A. Beharry and G. A. Woolley, *Acc. Chem. Res.*, 2015, **48**(10), 2662-2670.
- 42 D. Bleger and S. Hecht, *Angew. Chem. Int. Ed.*, 2015, **54**(39), 11338-11349.
- 43 D. Bleger, J. Schwarz, A. M. Brouwer and S. Hecht, *J. Am. Chem. Soc.*, 2012, **134**(51), 20597-20600.
- 44 C. Knie, M. Utecht, F. Zhao, H. Kulla, S. Kovalenko, A. M. Brouwer, P. Saalfrank, S. Hecht and D. Bleger, *Chemistry*, 2014, **20**(50), 16492-16501.
- 45 C. Hotzel, A. Marotto and U. Pindur, *Eur. J. Med. Chem.*, 2002, **37**(5), 367-378.
- 46 N. R. Wurtz, J. M. Turner, E. E. Baird and P. B. Dervan, *Org. Lett.*, 2001, **3**(8), 1201-1203.
- 47 R. Sekiya, A. Diaz-Moscoco and P. Ballester, *Chemistry*, 2018, **24**(9), 2182-2191.
- 48 C. W. Ong, Y. T. Yang, M. C. Liu, K. R. Fox, P. H. Liu and H. W. Tung, *Org. Biomol. Chem.*, 2012, **10**(5), 1040-1046.
- 49 D. L. Boger, B. E. Fink, S. R. Brunette, W. C. Tse and M. P. Hedrick, *J. Am. Chem. Soc.*, 2001, **123**(25), 5878-5891.
- 50 Y. W. Ham, W. C. Tse and D. L. Boger, *Bioorg. Med. Chem. Lett.*, 2003, **13**(21), 3805-3807.
- 51 H. Deng, V. A. Bloomfield, J. M. Benevides and G. J. Thomas Jr., *Nucleic Acids Res.*, 2000, **28**(17), 3379-3385.
- 52 J. Kypr, I. Kejnovska, D. Renciuik and M. Vorlickova, *Nucleic Acids Res.*, 2009, **37**(6), 1713-1725.
- 53 M. Deiana, Z. Pokladek, K. Matczyszyn, P. Mlynarz, M. Buckle and M. Samoc, *J. Mater. Chem. B*, 2017, **5**(5), 1028-1038.
- 54 F. Livolant and M. F. Maestre, *Biochemistry*, 1988, **27**(8), 3056-3068.
- 55 C. L. Peterson and J. C. Hansen, *CSH Protoc.*, 2008, **3**(12), 1-8.
- 56 R. D. Makde, J. R. England, H. P. Yennawar and S. Tan, *Nature*, 2010, **467**(7315), 562-566.
- 57 E. K. Liebler and U. Diederichsen, *Org. Lett.*, 2004, **6**(17), 2893-2896.
- 58 O. Vazquez, J. B. Blanco-Canosa, M. E. Vazquez, J. Martinez-Costas, L. Castedo and J. L. Mascarenas, *ChemBioChem*, 2008, **9**(17), 2822-28229.
- 59 A. Bertin, S. Mangenot, M. Renouard, D. Durand and F. Livolant, *Biophys. J.*, 2007, **93**(10), 3652-3663.
- 60 P. N. Dyer, R. S. Edayathumangalam, C. L. White, Y. Bao, S. Chakravarthy, U. M. Muthurajan and K. Luger, *Methods Enzymol.*, 2004, **375**, 23-44.
- 61 A. Banerjee, P. Majumder, S. Sanyal, J. Singh, K. Jana, C. Das and D. Dasgupta, *FEBS Open Bio*, 2014, **4**, 251-259.
- 62 Y. Arimura, H. Kimura, T. Oda, K. Sato, A. Osakabe, H. Tachiwana, Y. Sato, Y. Kinugasa, T. Ikura, M. Sugiyama, M. Sato and H. Kurumizaka, *Sci. Rep.*, 2013, **3**, 3510.
- 63 D. Baigl and K. Yoshikawa, *Biophys. J.*, 2005, **88**(5), 3486-3493.
- 64 S. Rudiuk, S. Franceschi-Messant, N. Chouini-Lalanne, E. Perez and I. Rico-Lattes, *Langmuir*, 2008, **24**(16), 8452-8457.
- 65 A. Venancio-Marques, A. Bergen, C. Rossi-Gendron, S. Rudiuk and D. Baigl, *ACS Nano*, 2014, **8**(4), 3654-3663.

*ortho*-Fluoroazobenzene Derivatives as DNA Intercalators for Photocontrol  
of DNA and Nucleosome Binding by Visible Light

Benedikt Heinrich, Karim Bouazoune, Matthias Wojcik, Udo Bakowsky and Olalla Vázquez \*



## **Table of Contents**

<b>Abbreviations</b> .....	<b>112</b>
<b>Materials and Experimental Procedures</b> .....	<b>114</b>
<i>Nuclear Magnetic Resonance Spectroscopy (NMR)</i> .....	114
<i>High Performance Liquid Chromatography (HPLC)</i> .....	114
<i>Mass Spectrometry</i> .....	115
<i>UV-Vis Spectroscopy</i> .....	115
<i>Fluorescence Spectroscopy</i> .....	115
<i>Circular Dichroism</i> .....	115
<i>Dynamic Light Scattering</i> .....	115
<b>Synthesis</b> .....	<b>116</b>
<i>Synthesis of the Symmetrical ortho-fluorazobeneze-4,4'-dicarboxylic acid (<math>F_4</math>Azo-diacid, 5)</i> .....	116
<i>Synthesis of Pyrrole Monomers Py(Dp) (8) and Py(OMe) (7)</i> .....	118
<i>Synthesis of photoswitchable ortho-fluorazobenzene-pyrrole hybrids: <math>F_4</math>Azo-(PyDp)<sub>2</sub> (2) and <math>F_4</math>Azo-(PyDp)(PyOMe) (3)</i> .....	120
<b>Concentration Determination</b> .....	<b>136</b>
<b>Photoisomerization of <math>F_4</math>Azo-(PyDp)<sub>2</sub> (2) and <math>F_4</math>Azo-(PyDp)(PyOMe) (3)</b> .....	<b>138</b>
<i>UV-Vis Characterization</i> .....	138
<i>RP-HPLC Characterization</i> .....	140
<i>NMR Characterization</i> .....	140
<b>DNA Binding Experiments</b> .....	<b>140</b>
<i>Complex Formation Calculation by HySS2009</i> .....	143
<i>Binding Affinity Calculation by HypSpec</i> .....	145
<b>Control Experiments with <math>F_4</math>Azo-(PyDp)<sub>2</sub> (2)</b> .....	<b>147</b>
<b>CD Experiments</b> .....	<b>149</b>
<b>DLS Experiments</b> .....	<b>150</b>
<b>Nucleosome Assays</b> .....	<b>151</b>
<i>Nucleosomal DNA</i> .....	151
<i>Native Polyacrylamide Gel Electrophoresis</i> .....	153
<i>Histone Octamer Extraction</i> .....	153
<i>Reconstitution of Nucleosome Core Particles</i> .....	154
<i>Gel Electrophoresis Mobility Shift Assay (EMSA)</i> .....	155
<i>EMSA Controls of the DLS</i> .....	156
<b>References</b> .....	<b>157</b>

## Abbreviations

A	absorbance
APS	ammonium persulfate
AU	arbitrary unit
bp	base pair
CD	circular dichroism
d	doublet
DIPEA	<i>N, N</i> -diisopropylethylamine
DLS	dynamic light scattering
DMAP	4-(dimethylamino)pyridine
dNTP	deoxyribonucleotide triphosphate
Dp	<i>N, N</i> -dimethyl-1,3-diaminopropane
dsDNA <sub>CT</sub>	double-stranded <i>cal</i> f <i>thymus</i> DNA
dsDNA <sub>hAT</sub>	double-stranded DNA hairpin with the consensus sequence <i>ATTA</i>
dsDNA <sub>hGC</sub>	double-stranded DNA hairpin with the consensus sequence <i>GGCCC</i>
<i>E. coli</i>	<i>Escherichia coli</i>
EDTA	ethylenediaminetetraacetic acid
EGTA	ethylene glycol-bis( $\beta$ -aminoethyl ether)- <i>N, N, N', N'</i> -tetraacetic acid
EI	emission intensity, electron ionization
EMSA	electrophoretic mobility shift assay
ESI-MS	electrospray ionization mass spectroscopy
EtBr	ethidium bromide
FID	fluorescence intercalator displacement
HATU	hexafluorophosphate azobenzotriazole tetramethyl uronium
HF	high-fidelity
HMBC	heteronuclear multiple bond correlation spectroscopy
HRMS	high resolution mass spectroscopy
HSQC	heteronuclear single quantum correlation spectroscopy
$K_D$	binding affinity constant
kDa	kilodalton
m	multiplet
n.c.	non-calculated
NMR	nuclear magnetic resonance
PAGE	polyacrylamide gel electrophoresis
PCR	polymerase chain reaction
PMSF	phenylmethane sulfonyl fluoride
ppm	part per million
Py	pyrrole
$R_f$	retention factor
RP-HPLC	reverse phase-high performance liquid chromatography
s	singlet
t	triplet
TEA	triethylamine

TBE	tris/borate/EDTA buffer
TEMED	tetramethylethylenediamine
TMS	trimethylsilyl protecting group
TO	thiazole orange
Tris	tris(hydroxymethyl)aminomethane
UV	ultraviolet
Vis	visible
$\delta$	chemical shift
$\epsilon$	extinction coefficient
$\theta$	ellipticity
$\lambda$	wavelength

## Materials and Experimental Procedures

All commercially purchased reagents were used from the following companies without further purification: trichloroacetyl chloride, thionyl chloride, DMSO for molecular biology, potassium chloride, APS, Igepal CA630, EGTA, citric acid, CM-Sephadex, potassium acetate, primers and DNA hairpins from Sigma Aldrich (USA); iron(II) sulfate heptahydrate, acetic anhydride, Tris, boronic acid, 19 : 1 acrylamide : bisacrylamide, TEMED, sucrose, adenine, potassium dihydrogen phosphate and DIPEA from Carl Roth (Germany); sodium hydroxide, potassium hydroxide, EDTA, ethidium bromide, dipotassium hydrogen phosphate, ethanol absolute, PEG 6000, isoamyl alcohol and nitric acid from Merck (Germany); potassium permanganate, *N,N*-dimethyl-1,3-diaminopropane (Dp), spermidine, spermine, sodium citrate, calcium chloride and Pd/C from Alfa Aesar (USA); DMF peptide grade and HATU from Iris Biotech (Germany); phusion polymerase and 5X HF buffer from New England Biolabs (USA); 4-bromo-2,6-difluoroaniline from Fluorochem (UK); copper (I) cyanide and heparin sodium salt from TCI (Japan), *N*-methyl pyrrole (Py) and glycerol from Acros Organics (Belgium); DMAP and PMSF from Fluka (USA); agarose, dNTPs and *calif thymus* DNA from Invitrogen (USA); sodium chloride from VWR (USA); sodium dihydrogen phosphate from Grössing GmbH (Austria); netropsin from Santa Cruz Biotechnology (USA); MNase (LS004797) from Worthington (USA); phenol, sodium dodecyl sulfate, RNase (A3832,0050) and glucose monohydrate from PanReac Applichem ITW Reagents (USA); sodium acetate from Riedel de Haen (Germany); glacial acetic acid and EcoRV from Fisher Scientific (USA) and HT Gel from Biorad (USA). Water was purified with a milli-Q Ultra Pure Water Purification System (TKA, Germany).

### *Nuclear Magnetic Resonance Spectroscopy (NMR)*

All NMR spectra were automatically measured at 300 K either in a Bruker AV III HD 300 MHz at a frequency of 300 MHz ( $^1\text{H}$ ) or 75 MHz ( $^{13}\text{C}$ ) or in a Bruker AV III HD 500 MHz at a frequency of 500 MHz ( $^1\text{H}$ ) or 125 MHz ( $^{13}\text{C}$ ). All chemical shifts ( $\delta$ ) are relative to tetramethylsilane (TMS), i.e.  $\delta(\text{TMS}) = 0$  ppm. As internal standards, deuterated chloroform ( $\text{CDCl}_3$ ), dimethyl sulfoxide (DMSO) with TMS were used. Solvent shifts (ppm):  $\delta(\text{CHCl}_3) = 7.26$  ppm ( $^1\text{H}$ ),  $\delta(\text{CHCl}_3) = 77.16$  ppm ( $^{13}\text{C}$ ),  $\delta(\text{DMSO}) = 2.50$  ppm ( $^1\text{H}$ ),  $\delta(\text{DMSO}) = 39.52$  ppm ( $^{13}\text{C}$ ).<sup>[1]</sup> Coupling constants are given in Hz. The assignment of each signal was based on two-dimensional nuclear magnetic resonance spectroscopy (2D NMR), i.e. heteronuclear single quantum coherence (HSQC) and heteronuclear multiple bond correlation spectroscopy (HMBC). Unless otherwise noted, the NMR tubes were Wilmad NMR tubes (WG-5-7E; OD:  $4.947 \pm 0.019$  mm; ID: 4.1 mm; length 7). For analytical purposes the photoswitchable *ortho*-fluorazobenzene-pyrrole hybrids were fully characterized as their *E*-isomers. The symbol \* represents *Z*-isomer signals in the spectra. For the isomerization studies also the *Z*-isomer was analyzed.

### *High Performance Liquid Chromatography (HPLC)*

For preparative purposes, a PLC 2020 Personal Purification System (Gilson) with a preparative Nucleodur C18 HTec-column (5  $\mu\text{m}$ , 250 x 16 mm; Macherey & Nagel) using an isocratic regime during the first five minutes, for column equilibration, followed by a linear gradient 5% to 60% B in 40 min for compounds **2** and **17** and a linear gradient 5% to 75% B in 30 min for compound **3** with a flow rate of 10 mL/min at 25°C was used. The detection was carried out by measuring the absorption at wavelengths: 220 nm and 260 nm. Milli-Q water (A) and MeCN (B) were employed as eluents with an addition of 0.1% of TFA in both solvents.

For analytical purposes, an Agilent 1260 Infinity II HPLC-System (Agilent Technologies) with either an EC 125/2 Nucleodur 100-C18 ec column (Macherey & Nagel) with a flow rate of 0.2 mL/min for purity analysis or an eclipse XDB-C18 (5  $\mu\text{m}$ , 4.6 x 150 mm, Agilent) with a flow rate of 1.0 mL/min for switching studies using with an isocratic regime during the first five minutes, for column equilibration, followed by a linear gradient 5% to 75% B in 30 min at 55°C was used.

### *Mass Spectrometry*

Electrospray ionization mass spectrometry (ESI-MS) was performed on a Finnigan LTQ-FT (Thermo Fischer Scientific). EI-MS was performed on an AccuTOF GCv (JEOL).

### *UV-Vis Spectroscopy*

UV-Vis measurements were performed on a Tecan 20M at room temperature using a quartz cuvette (Hellma Analytics; 104-QS) with a pathlength of 1 cm in a volume of 1 mL. The represented measurements were always buffer subtracted.

### *Fluorescence Spectroscopy*

Fluorescence measurements were performed on a Jasco FP-6500 spectrofluorometer equipped with a Thermo Haake WKL 26 water recirculator at 20°C. Unless otherwise noted, fluorescence cuvette (Hellma Analytics; 104F-QS) was used. The measurements were performed with the following settings: increment: 1.0 nm; integration time: 0.2 s; speed: 500 nm/min; sensitivity: medium; excitation slit width: 3 nm; emission slit width: 5 nm; excitation wavelength 490 nm. The emission spectra were recorded from 510 to 700 nm at 20°C. From all spectra, the corresponding background signal was subtracted. Measurements were performed in triplicates. The represented measurements were always buffer subtracted.

### *Circular Dichroism*

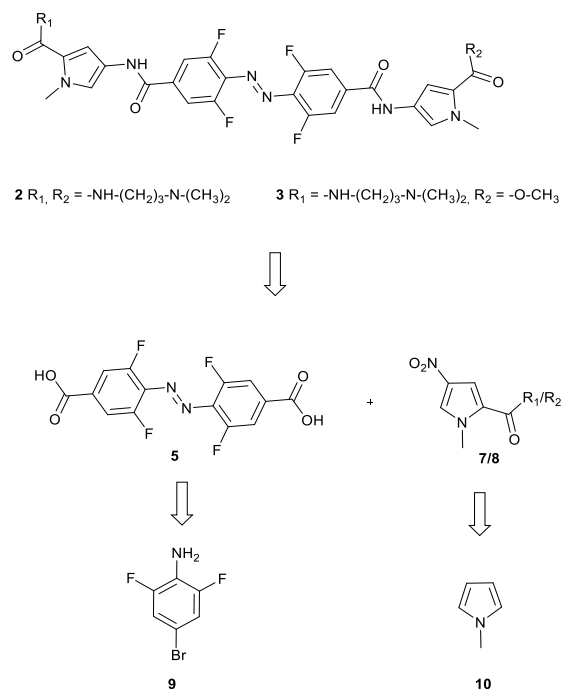
CD titration measurements were performed on a Jasco J-810 Spectropolarimeter equipped with a Jasco CDF-426S peliter controller and a Thermo Haake WKL 26 water recirculator at 20°C using a CD cuvette (Hellma Analytics; QS 0.200). The settings were: range from 550-230 nm, speed of 100 nm/min, response of 0.25 s, band width of 2 nm and a data pitch of 1 nm. The represented measurements were always buffer subtracted.

### *Dynamic Light Scattering*

Dynamic Light Scattering (DLS) measurements were performed on a Malvern Instruments (UK) Zetasizer Nano ZS equipped with a 10 mW HeNe laser at a wavelength of 633 nm. Measurements were performed at 25°C using an UVette (Eppendorf; 0030106300). The settings were: material: protein (RI 1.450, absorbance 0.001); dispersant: viscosity 0.8812 cP, RI 1.331; equilibration time: 180 s; cell: disposable cuvette ZEN0040; measurement: measurement angle: 173° backscatter (NIBS default), measurement duration: number of runs 10, run duration 10 s. The corresponding hydrodynamic diameter were then analyzed with respect to their number percentage by DLS.

## Synthesis

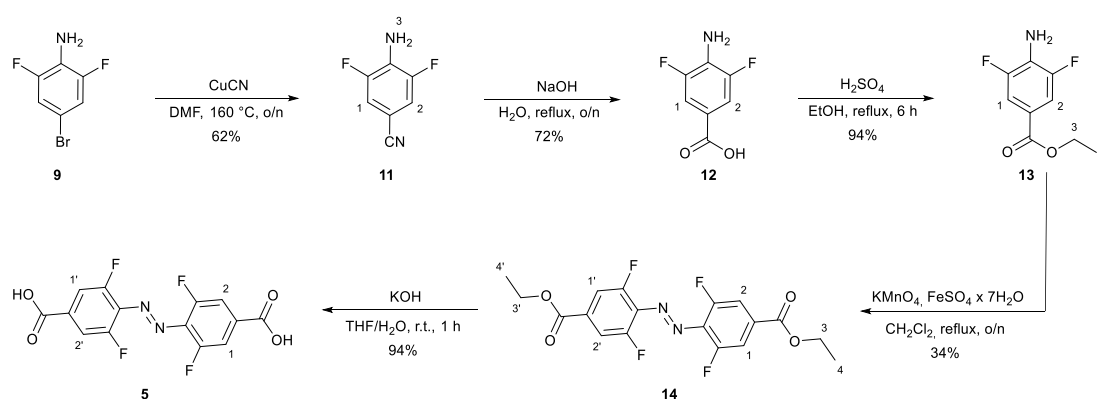
The retrosynthesis of the photoswitches is illustrated for the *E*-isomer because it is the most stable thermodynamically.



**Scheme S1:** Retrosynthetic approach for the preparation of the fluorazobenzene derivatives  $F_4$ Azo-(PyDp)<sub>2</sub> (**2**) and  $F_4$ Azo-(PyDp)(PyOMe) (**3**).

### Synthesis of the Symmetrical ortho-fluorazobenzene-4,4'-dicarboxylic acid ( $F_4$ Azo-diacid, **5**)

This synthesis was reported before by Hecht *et al.*<sup>[ii,iii]</sup> Such procedure is based in the preparation of the symmetrical ortho-fluorazobenzene-4,4'-diester ( $F_4$ -diester, **14**).<sup>[iii]</sup> We followed the same approach with minor modifications.



**Scheme S2:** Synthesis route of  $F_4$ Azo-diacid (**5**) starting from 4-bromo-2,6-difluoroaniline (**9**).

**4-amino-3,5-difluorobenzonitrile (11):** 4-bromo-2,6-difluoroaniline (**9**, 5.00 g, 24.0 mmol) and CuCN (6.45 g, 72.0 mmol) were dissolved in DMF (50 mL) and heated to 160°C for 16 h. The mixture was poured into saturated Na<sub>2</sub>CO<sub>3</sub> (250 mL), filtered and the precipitate washed with EtOAc. The organic phases were washed with NH<sub>3</sub> 12% aqueous solution and dried over MgSO<sub>4</sub>. The crude product was purified by column chromatography (CH<sub>2</sub>Cl<sub>2</sub>/*n*-pentane 2:1) to yield the desired product (**11**,

2.29 g, 14.9 mmol, 62 %) as a white solid.  $R_f = 0.39$  ( $\text{CH}_2\text{Cl}_2/n\text{-pentane 2:1}$ );  $\delta\text{H}$ (300 MHz;  $\text{CDCl}_3$ ;  $\text{Me}_4\text{Si}$ ) 7.13 (2 H, dd,  $^3J_{\text{HF}}$  6.0,  $^4J_{\text{HH}}$  2.3, H-1 and H-2), 4.29 (2 H, br s,  $\text{NH}_2$ );  $\delta\text{C}$  (75 MHz;  $\text{CDCl}_3$ ;  $\text{Me}_4\text{Si}$ ) 152.3 ( $\text{C}_{\text{arom.}}$ ), 149.0 ( $\text{C}_{\text{arom.}}$ ), 129.8 ( $\text{C}_{\text{arom.}}$ ), 118.0 (CN), 115.7 (CH), 115.4 (CH); 98.4 ( $\text{C}_{\text{arom.}}$ ) **HRMS-ESI<sup>+</sup> ( $m/z$ ):**  $[\text{M}]^+$  calcd for  $\text{C}_7\text{H}_4\text{F}_2\text{N}_2$ , 154.03425; found, 154.03252.

**4-amino-3,5-difluorobenzoic acid (12):** 4-amino-3,5-difluorobenzonitrile (**11**, 2.25 g, 14.6 mmol) was suspended in 1M NaOH (80 mL) and refluxed overnight. The reaction mixture was cooled to r.t. and acidified with 1M HCl. The resulting precipitate was dissolved in EtOAc, dried over  $\text{MgSO}_4$ , filtered and the solvent removed under reduced pressure to yield the desired product (**12**, 2.20 g, 12.7 mmol, 87 %) as a white solid.  $R_f = 0.93$  (EtOAc/formic acid 1:0.02);  $\delta\text{H}$ (300 MHz;  $[\text{D6}]\text{DMSO}$ ;  $\text{Me}_4\text{Si}$ ) 12.68 (1 H, s, COOH), 7.39 (2 H, dd,  $^3J_{\text{HF}}$  7.2,  $^4J_{\text{HH}}$  2.4, H-1 and H-2), 6.05 (2 H, s,  $\text{NH}_2$ );  $\delta\text{C}$  (75 MHz;  $[\text{D6}]\text{DMSO}$ ;  $\text{Me}_4\text{Si}$ ) 166.0 (COOH), 151.3 ( $\text{C}_{\text{arom.}}$ ), 148.2 ( $\text{C}_{\text{arom.}}$ ), 130.6 ( $\text{C}_{\text{arom.}}$ ), 115.7 ( $\text{C}_{\text{arom.}}$ ), 112.3 (CH), 112.1 (CH); **HRMS-ESI<sup>-</sup> ( $m/z$ ):**  $[\text{M}]^-$  calcd for  $\text{C}_7\text{H}_4\text{F}_2\text{N}_2\text{O}_2$ , 172.0216; found, 172.0217.

**ethyl 4-amino-3,5-difluorobenzoate (13):** 4-amino-3,5-difluorobenzoic acid (**12**, 1.90 g, 11.0 mmol) was dissolved in EtOH (40 mL) and conc.  $\text{H}_2\text{SO}_4$  (4 mL) and refluxed for 5 h. Conc.  $\text{H}_2\text{SO}_4$  was added and the reaction mixture refluxed for 1 h. The mixture was neutralized with sat.  $\text{NaHCO}_3$ , extracted with  $\text{CH}_2\text{Cl}_2$ , the organic phases dried over  $\text{MgSO}_4$ , filtered and the solvent removed under reduced pressure to yield the desired product (**13**, 2.07 g, 10.3 mmol, 94 %) as a pale brown solid.  $R_f = 0.29$  ( $\text{CH}_2\text{Cl}_2/n\text{-pentane 1:1}$ );  $\delta\text{H}$ (300 MHz;  $\text{CDCl}_3$ ;  $\text{Me}_4\text{Si}$ ) 7.53 (2 H, dd,  $^3J_{\text{HF}}$  7.2,  $^4J_{\text{HH}}$  2.1, H-1 and H-2), 4.33 (2 H, q,  $^3J_{\text{HH}}$  7.1 Hz, H-3), 3.86 (2 H, br s,  $\text{NH}_2$ ), 1.37 (3 H, t,  $^3J_{\text{HH}}$  7.1, H-4);  $\delta\text{C}$  (75 MHz;  $[\text{D6}]\text{DMSO}$ ;  $\text{Me}_4\text{Si}$ ) 165.3 (CO), 152.4 ( $\text{C}_{\text{arom.}}$ ), 149.3 ( $\text{C}_{\text{arom.}}$ ), 128.9 ( $\text{C}_{\text{arom.}}$ ), 118.8 ( $\text{C}_{\text{arom.}}$ ), 112.8 (CH), 112.6 (CH), 61.2 ( $\text{CH}_2$ ), 14.5 ( $\text{CH}_3$ ); **HRMS-ESI<sup>+</sup> ( $m/z$ ):**  $[\text{M}]^+$  calcd for  $\text{C}_9\text{H}_9\text{F}_2\text{N}_2\text{O}_2\text{H}$ , 202.0674; found, 202.0675.

**diethyl 4,4'-(diazene-1,2-diyl)-bis(3,5-difluorobenzoate) (14):** ethyl 4-amino-3,5-difluorobenzoate (**13**, 1.36 g, 6.76 mmol) was dissolved in  $\text{CH}_2\text{Cl}_2$  (115 mL) and  $\text{KMnO}_4$  (11.5 g, 73.0 mmol) and  $\text{FeSO}_4 \times 7\text{H}_2\text{O}$  (11.5 g, 41.2 mmol) were added. The reaction mixture was refluxed overnight and filtered over celite. The solvent was removed under reduced pressure and the crude purified by column chromatography ( $\text{CH}_2\text{Cl}_2/n\text{-pentane 1:1}$ ) to yield the desired product (**14**, 452 mg, 1.13 mmol, 34 %) as an orange solid.  $R_f = 0.75$  ( $\text{CH}_2\text{Cl}_2$ ); **HRMS-ESI<sup>+</sup> ( $m/z$ ):**  $[\text{M}]^+$  calcd for  $\text{C}_{18}\text{H}_{14}\text{F}_4\text{N}_2\text{O}_4\text{H}$ , 399.0962; found, 399.0963.

**E-isomer:**

$\delta\text{H}$ (300 MHz;  $\text{CDCl}_3$ ;  $\text{Me}_4\text{Si}$ ) 7.74 (4 H, d,  $^3J_{\text{HF}}$  8.9, H-1, H-1', H-2 and H-2'), 4.43 (4 H, q,  $^3J_{\text{HH}}$  7.1, H-3 and H-3'), 1.43 (6 H, t,  $^3J_{\text{HH}}$  7.1, H-4 and H-4');  $\delta\text{C}$  (75 MHz;  $\text{CDCl}_3$ ;  $\text{Me}_4\text{Si}$ ) 163.8 (2 C, CO), 156.9 (2 C,  $\text{C}_{\text{arom.}}$ ), 153.4 (2 C,  $\text{C}_{\text{arom.}}$ ), 134.0 (2 C,  $\text{C}_{\text{arom.}}$ ), 133.9 (2 C,  $\text{C}_{\text{arom.}}$ ), 114.2 (2 C, CH), 113.9 (2 C, CH), 62.3 (2 C,  $\text{CH}_2$ ), 14.3 (2 C,  $\text{CH}_3$ ).

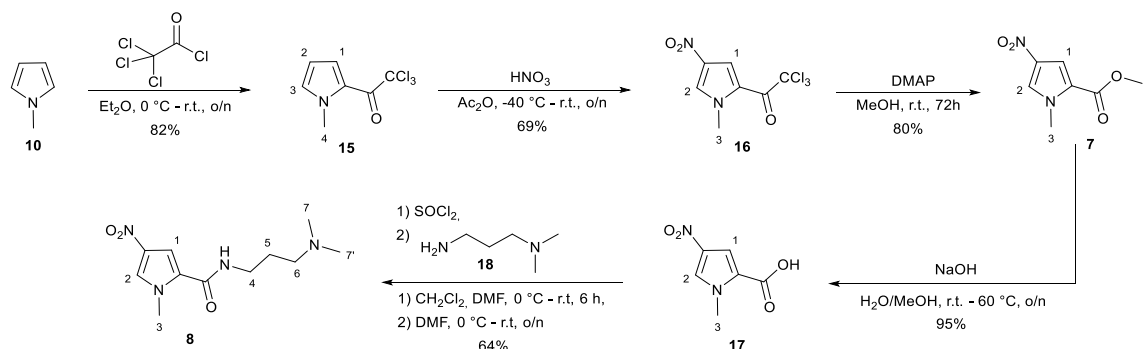
**4,4'-(diazene-1,2-diyl)-bis(3,5-difluorobenzoic acid) (5):** diethyl 4,4'-(diazene-1,2-diyl)-bis(3,5-difluorobenzoate) (**14**, 449 mg, 1.13 mmol) was dissolved in THF (25 mL) and KOH (228 mg, 4.06 mmol) dissolved in  $\text{H}_2\text{O}$  (13 mL) was added. The reaction mixture was stirred for 1 h and acidified with 1M HCl. The formed precipitate was filtered and dried on the freeze-dryer overnight to yield the desired product (**5**, 362 mg, 1.06 mmol, 94 %) as a pale orange solid.  $R_f = 0.63$  (EtOAc/formic acid 1:0.02); **HRMS-ESI<sup>-</sup> ( $m/z$ ):**  $[\text{M}]^-$  calcd for  $\text{C}_{14}\text{H}_5\text{F}_4\text{N}_2\text{O}_4$ , 341.0191; found, 341.0203.

**E-isomer:**

$\delta\text{H}$ (300 MHz;  $[\text{D6}]\text{DMSO}$ ;  $\text{Me}_4\text{Si}$ ) 13.84 (1 H, br s, COOH), 7.80 (4 H, d,  $^3J_{\text{HF}}$  9.3 Hz, H-1, H-1', H-2 and H-2');  $\delta\text{C}$  (75 MHz;  $[\text{D6}]\text{DMSO}$ ;  $\text{Me}_4\text{Si}$ ) 164.5 (2 C, CO), 156.0 (2 C,  $\text{C}_{\text{arom.}}$ ), 152.5 (2 C,  $\text{C}_{\text{arom.}}$ ), 135.2 (2 C,  $\text{C}_{\text{arom.}}$ ), 133.0 (2 C,  $\text{C}_{\text{arom.}}$ ), 114.0 (2 C, CH), 113.7 (2 C, CH).

## Synthesis of Pyrrole Monomers Py(Dp) (**8**) and Py(OMe) (**7**)

This synthesis was reported before by Dervan *et al.*,<sup>[iv]</sup> Lown *et al.*,<sup>[vi]</sup> and Pindur *et al.*,<sup>[vi]</sup> such procedure is based in the preparation of the nitro pyrrole methylester **7**.<sup>[iv]</sup> We followed the same approach with minor modifications.



**Scheme S3:** Synthesis route of O<sub>2</sub>N-Py-OMe (**7**) and O<sub>2</sub>N-Py-Dp (**8**) starting from *N*-methylpyrrole (**10**).

**2,2,2-trichloro-1-(1-methyl-1H-pyrrol-2-yl)ethan-1-one (15):** Under inert atmosphere, to a solution of trichloroacetyl chloride (2.80 mL, 25.0 mmol) in Et<sub>2</sub>O (5.00 mL), a solution of *N*-methylpyrrole (2.20 mL, 25.0 mmol) in Et<sub>2</sub>O (5.00 mL) was added at 0 °C over 1 h. The reaction mixture was stirred overnight at r.t. and neutralized with K<sub>2</sub>CO<sub>3</sub> solution. It was extracted with Et<sub>2</sub>O, dried over MgSO<sub>4</sub> and the solvent removed under reduced pressure to yield the desired product (**15**, 4.67 g, 20.6 mmol, 82 %) as brown solid. *R*<sub>f</sub> = 0.60 (*n*-pentane / EtOAc 1:1); **δ**H(300 MHz; [D4]MeOD; Me<sub>4</sub>Si) 7.46 - 7.42 (2 H, m, H-1 and H-3), 6.30 (1 H, dd, <sup>3</sup>J<sub>HH</sub> 4.3, <sup>3</sup>J<sub>HH</sub> 2.5, H-2), 3.91 (3 H, s, H-4); **δ**C (75 MHz; [D4]MeOD; Me<sub>4</sub>Si) 171.8 (CO), 135.3 (CH), 123.6 (CH), 120.7 (C<sub>q</sub>), 109.1 (CH), 96.0 (CCl<sub>3</sub>), 36.2 (CH<sub>3</sub>); **HRMS-EI**<sup>+</sup> (*m/z*): [M]<sup>+</sup> calcd for C<sub>7</sub>H<sub>6</sub>Cl<sub>3</sub>N<sub>1</sub>O<sub>1</sub>, 225.95932; found, 225.95978.

**2,2,2-trichloro-1-(1-methyl-4-nitro-1H-pyrrol-2-yl)ethan-1-one (16):** Under inert atmosphere, to a solution of 2,2,2-trichloro-1-(1-methyl-1H-pyrrol-2-yl)ethan-1-one (1.50 g, 6.62 mmol) in Ac<sub>2</sub>O (8.00 mL, 84.6 mmol), conc. HNO<sub>3</sub> (0.60 mL, 14.4 mmol) was added at -40 °C over 30 min. The reaction mixture was slowly warmed up to r.t. and stirred overnight. It was neutralized with Na<sub>2</sub>CO<sub>3</sub> solution, extracted with EtOAc, washed with *brine*, the organic phases dried over MgSO<sub>4</sub> and the solvent removed under reduced pressure to yield the desired product (**16**, 1.24 g, 4.56 mmol, 69 %) as brown solid. *R*<sub>f</sub> = 0.16 (*n*-pentane / EtOAc 10:1); **δ**H(300 MHz; [D6]DMSO; Me<sub>4</sub>Si) 8.56 (1 H, d, <sup>4</sup>J<sub>HH</sub> 1.6, H-2), 7.80 (1 H, d, <sup>4</sup>J<sub>HH</sub> 1.6, H-1), 4.00 (3 H, s, H-3); **δ**C (75 MHz; [D6]DMSO; Me<sub>4</sub>Si) 172.8 (CO), 134.2 (C<sub>q</sub>), 132.5 (CH), 120.6 (C<sub>q</sub>), 116.3 (CH), 94.5 (CCl<sub>3</sub>), 50.0 (CH<sub>3</sub>); **HRMS-EI**<sup>+</sup> (*m/z*): [M]<sup>+</sup> calcd for C<sub>7</sub>H<sub>6</sub>Cl<sub>3</sub>N<sub>2</sub>O<sub>3</sub>, 270.94440; found, 270.94291.

**methyl 1-methyl-4-nitro-1H-pyrrole-2-carboxylate (7):** To a solution of 2,2,2-trichloro-1-(1-methyl-4-nitro-1H-pyrrol-2-yl)ethan-1-one (**16**, 4.72 g, 17.4 mmol) in MeOH (58.0 mL) DMAP (212 mg, 1.74 mmol) was added and stirred at r.t. for 72 h. The solvent was removed and the crude product purified by column chromatography (*n*-pentane / EtOAc 4:1 → 1:1) to yield the desired product (**7**, 2.57 g, 14.0 mmol, 80%) as yellow solid. *R*<sub>f</sub> = 0.16 (*n*-pentane / EtOAc 10:1); **δ**H(300 MHz; [D6]DMSO; Me<sub>4</sub>Si) 8.27 (1 H, d, <sup>4</sup>J<sub>HH</sub> 2.0, H-2), 7.30 (1 H, d, <sup>4</sup>J<sub>HH</sub> 2.0, H-1), 3.92 (3 H, s, H-3), 3.80 (3 H, s, H-4); **δ**C (75 MHz; [D6]DMSO; Me<sub>4</sub>Si) 159.8 (CO), 134.2 (C<sub>q</sub>), 129.4 (CH), 122.6 (C<sub>q</sub>), 111.5 (CH), 51.7 (CH<sub>3</sub>), 37.4 (CH<sub>3</sub>); **HRMS-ESI**<sup>+</sup> (*m/z*): [M]<sup>+</sup> calcd for C<sub>7</sub>H<sub>8</sub>N<sub>2</sub>O<sub>4</sub>H, 185.05623; found, 185.05665.

**1-methyl-4-nitro-1H-pyrrole-2-carboxylic acid (17):** To a solution of methyl 1-methyl-4-nitro-1H-pyrrole-2-carboxylate (**7**, 2.00 g, 10.9 mmol) in MeOH (25.0 mL) 1M NaOH (15mL) was added and the reaction mixture stirred at r.t. overnight and heated at 60 °C for 1 h. Afterwards, it was extracted with EtOAc and washed with saturated NaHCO<sub>3</sub>. The aqueous phases

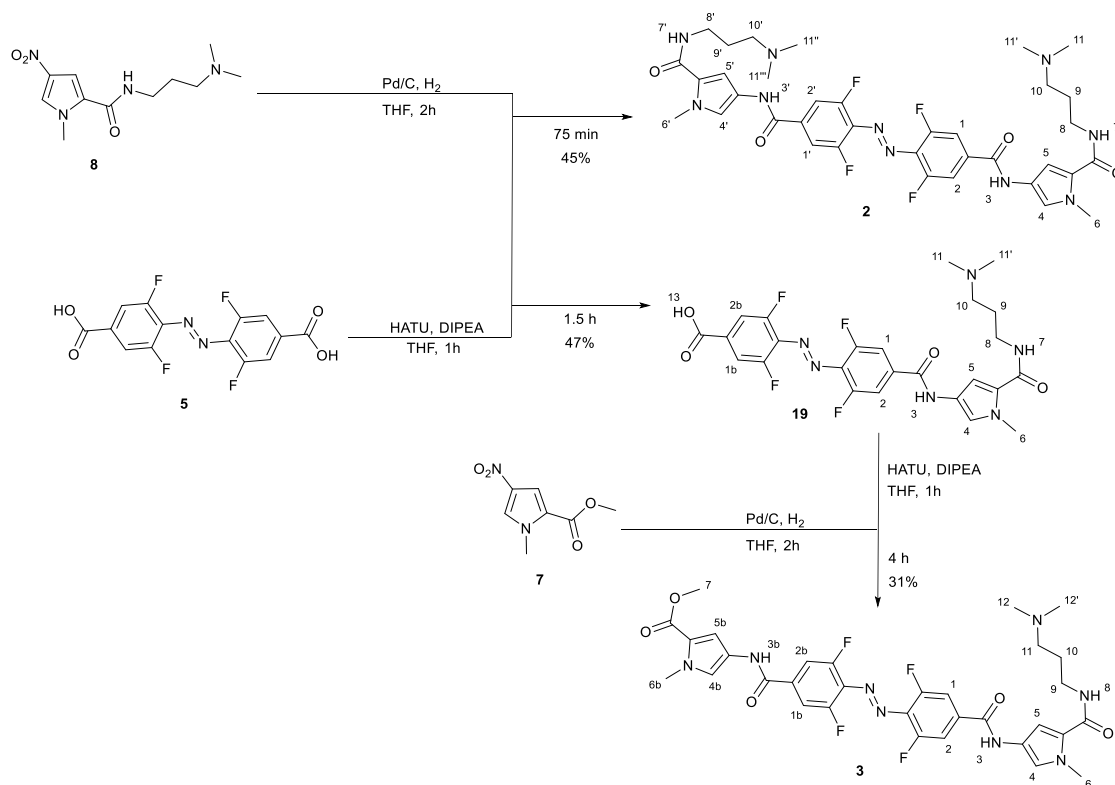


were acidified with 2M HCl, extracted with EtOAc, the organic phases dried over MgSO<sub>4</sub>, filtered and the solvent removed under reduced pressure to yield the desired product (**17**, 1.77 g, 10.4 mmol, 95%) as pale yellow solid. **R<sub>f</sub>**= 0.33 (EtOAc/formic acid 1:0.02); **δH**(300 MHz; [D6]DMSO; Me<sub>4</sub>Si) 13.11 (1 H, s, COOH), 8.21 (1 H, d, <sup>4</sup>J<sub>HH</sub> 2.1, H-2), 7.25 (1 H, d, <sup>4</sup>J<sub>HH</sub> 2.1, H-1), 3.91 (3 H, s, H-3); **δC** (75 MHz; [D6]DMSO; Me<sub>4</sub>Si) 160.9 (CO), 134.0 (C<sub>q</sub>), 129.1 (CH), 123.8 (C<sub>q</sub>), 111.4 (CH), 37.4 (CH<sub>3</sub>); **HRMS-ESI<sup>-</sup>** (**m/z**): [M]<sup>-</sup> calcd for C<sub>6</sub>H<sub>5</sub>N<sub>2</sub>O<sub>4</sub>, 169.0255; found, 169.0257.

***N*-(3-(dimethylamino)propyl)-1-methyl-4-nitro-1H-pyrrole-2-carboxamide (8)**: To a solution of 1-methyl-4-nitro-1H-pyrrole-2-carboxylic acid (**17**, 674 mg, 3.96 mmol) in CH<sub>2</sub>Cl<sub>2</sub> (13.5 mL) and DMF (112 μL), SOCl<sub>2</sub> (2.88 mL, 39.6 mmol) was added slowly at 0 °C. The reaction mixture was warmed up to r.t. and stirred for another 6 h. The solvent was removed under reduced pressure. At 0 °C under inert atmosphere, the crude was dissolved in DMF (2.70 mL) and *N,N*-dimethyl-1,3-diaminopropane (**18**, 1.10 mL, 8.71 mmol) added dropwise. The reaction mixture was warmed to up to r.t. and stirred for 16 h. Deionized water was added to be extracted with EtOAc. The organic phases were washed with saturated NaHCO<sub>3</sub>, dried over MgSO<sub>4</sub>, filtered and the solvent removed under reduced pressure. The crude product was purified by column chromatography (CH<sub>2</sub>Cl<sub>2</sub> / MeOH / TEA 10:1:0.5%) to yield the desired product (**8**, 642 mg, 2.52 mmol, 64%) as pale yellow solid. **R<sub>f</sub>**= 0.07 (CH<sub>2</sub>Cl<sub>2</sub> / MeOH / TEA 10:1:0.5%); **δH**(300 MHz; [D4]MeOD; Me<sub>4</sub>Si) 7.82 (1 H, d, <sup>4</sup>J<sub>HH</sub> 1.9, H-2), 7.27 (1 H, d, <sup>4</sup>J<sub>HH</sub> 1.9, H-1), 3.95 (3 H, s, H-3), 3.33 (2 H, t, <sup>3</sup>J<sub>HH</sub> 7.0, H-4), 2.41 (2 H, t, <sup>3</sup>J<sub>HH</sub> 7.6, H-6), 2.27 (6 H, s, H-7 and H-7'), 1.84 – 1.72 (2 H, m, H-5); **δC** (75 MHz; [D4]MeOD; Me<sub>4</sub>Si) 162.9 (CO), 136.2 (C<sub>q</sub>), 128.4 (CH), 127.9 (C<sub>q</sub>), 108.5 (CH), 58.2 (CH<sub>2</sub>), 45.4 (2C, CH<sub>3</sub>), 38.7 (CH<sub>3</sub>), 37.9 (CH<sub>2</sub>), 28.1 (CH<sub>2</sub>); **HRMS-ESI<sup>+</sup>** (**m/z**): [M]<sup>+</sup> calcd for C<sub>11</sub>H<sub>18</sub>N<sub>4</sub>O<sub>3</sub>H, 255.1452; found, 255.1457.

## Synthesis of photoswitchable ortho-fluorazobenzene-pyrrole hybrids: $F_4$ Azo-(PyDp) $_2$ (**2**) and $F_4$ Azo-(PyDp)(PyOMe) (**3**)

This synthesis relies on the condensation reactions between the  $F_4$ Azo-diacid (**5**) and the reduced pyrrole derivatives.



**Scheme S4:** Synthesis route of photoswitchable fluorazobenzene dimers  $F_4$ Azo-(PyDp) $_2$  (**2**) and  $F_4$ Azo-(PyDp)(PyOMe) (**3**) starting from  $F_4$ Azo-diacid (**5**), O<sub>2</sub>N-Py-Dp (**8**) and O<sub>2</sub>N-Py-OMe (**7**).

**4,4'-((4,4'-(ethene-1,2-diyl)bis(3,5-difluorobenzoyl))bis(azanediyl))bis(N-(3-(dimethylamino)propyl)-1-methyl-1H-pyrrole-2-carboxamide) (**2**):** Compound **8**, (78.1 mg, 0.31 mmol) and Pd/C 10% dry (50.0 mg, 64.0% w/w) was suspended in THF (3.0 mL) and stirred under H<sub>2</sub> atmosphere for 2 h. The reaction mixture was filtered over celite and the solvent removed under reduced pressure.  $F_4$ Azo-diacid (**5**, 50.0 mg, 0.15 mmol) and HATU (117 mg, 0.31 mmol) were dissolved in THF (400  $\mu$ L) and DIPEA (107  $\mu$ L, 0.61 mmol) added. The reaction mixture was stirred for 75 min before the reduced pyrrole **8** dissolved in THF (700  $\mu$ L) was added. After stirring for 4.5 h, the solvent was removed and the crude purified by preparative HPLC (5 - 60% over 40 min) to yield the desired product as its TFA salt (**2**, 68.8 mg, 0.07 mmol, 47%) as orange solid.  $t_R$  = 22.6 min (5% to 75% B in 30 min); **HRMS-ESI<sup>+</sup> (m/z):** [M]<sup>+</sup> calcd for C<sub>36</sub>H<sub>42</sub>F<sub>4</sub>N<sub>10</sub>O<sub>4</sub>H, 755.3399; found, 755.3428.

***E*-isomer:**

**$\delta$ H**(500 MHz; [D6]DMSO; Me<sub>4</sub>Si): 10.69 (2 H, s, NH-3 and NH-3'), 9.58 (2 H, br s, NH<sup>+</sup>-12 and NH<sup>+</sup>-12'), 8.26 (2 H, t, <sup>3</sup>J<sub>HH</sub> 5.9, NH-7 and NH-7'), 7.96 (2 H, s, H-1 and H-1' / H-2 and H-2'), 7.92 (2 H, s, H-1 and H-1' / H-2 and H-2'), 7.33 (2 H, d, <sup>4</sup>J<sub>HH</sub> 1.7, H-4 and H-4'), 6.99 (2 H, d, <sup>4</sup>J<sub>HH</sub> 1.7 Hz, H-5 and H-5'), 3.86 (6 H, s, H-6 and H-6'), 3.26 (4 H, dt, <sup>3</sup>J<sub>HH</sub> 6.3, <sup>3</sup>J<sub>HH</sub> 5.9, H-8 and H-8'), 3.04 – 3.14 (4 H, m, H-10 and H-10'), 2.79 (12 H, s, H-11, H-11', H-11'' and H-11'''), 1.79 – 1.92 (4 H, m, H-9 and H-9');  **$\delta$ C** (125 MHz; [D6]DMSO; Me<sub>4</sub>Si) 161.5 (2 C, CO), 160.0 (2 C, CO), 156.2 (2 C, C<sub>q</sub>), 152.7 (2 C, C<sub>q</sub>), 138.5 (2 C, C<sub>q</sub>), 131.9 (2 C, C<sub>q</sub>), 123.1 (2 C, C<sub>q</sub>), 121.5 (2 C, C<sub>q</sub>), 118.7 (2 C, CH), 112.5 (2 C, CH), 112.1 (2 C, CH), 104.5 (2 C, CH), 54.8 (2 C, CH<sub>2</sub>), 43.4 (4 C, CH<sub>3</sub>), 36.2 (2 C, CH<sub>3</sub>), 35.5 (2 C, CH<sub>2</sub>), 24.7 (2 C, CH<sub>2</sub>).

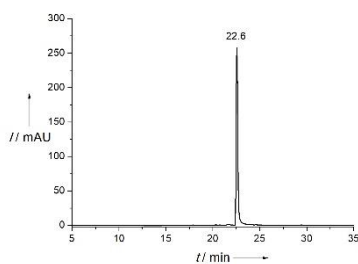


**Figure S1:** HPLC chromatogram of F<sub>4</sub>Azo-(PyDp)<sub>2</sub> (**2**).

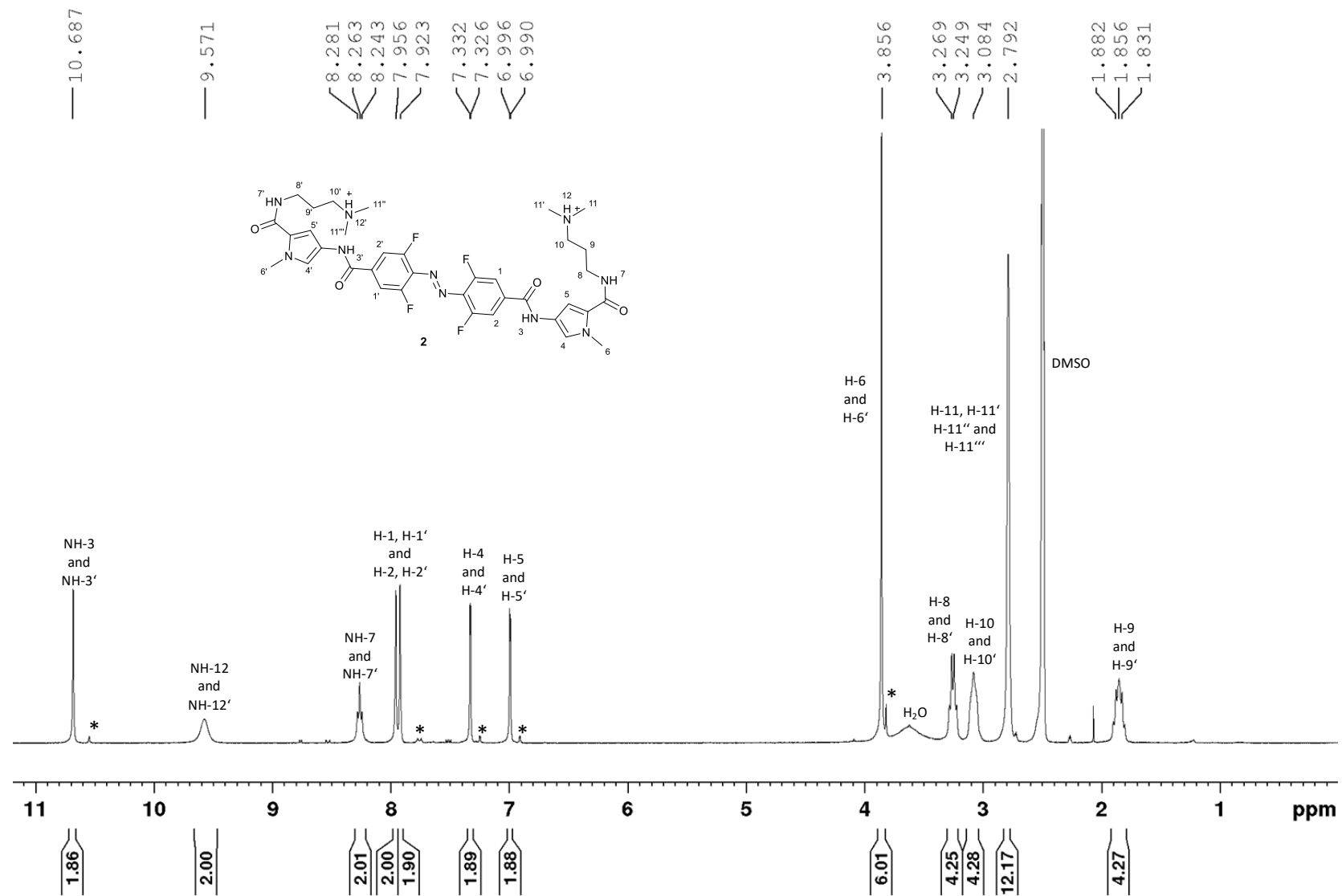


Figure S2: <sup>1</sup>H-NMR spectrum of *trans*-F<sub>4</sub>Azo-(PyDp)<sub>2</sub> (2).

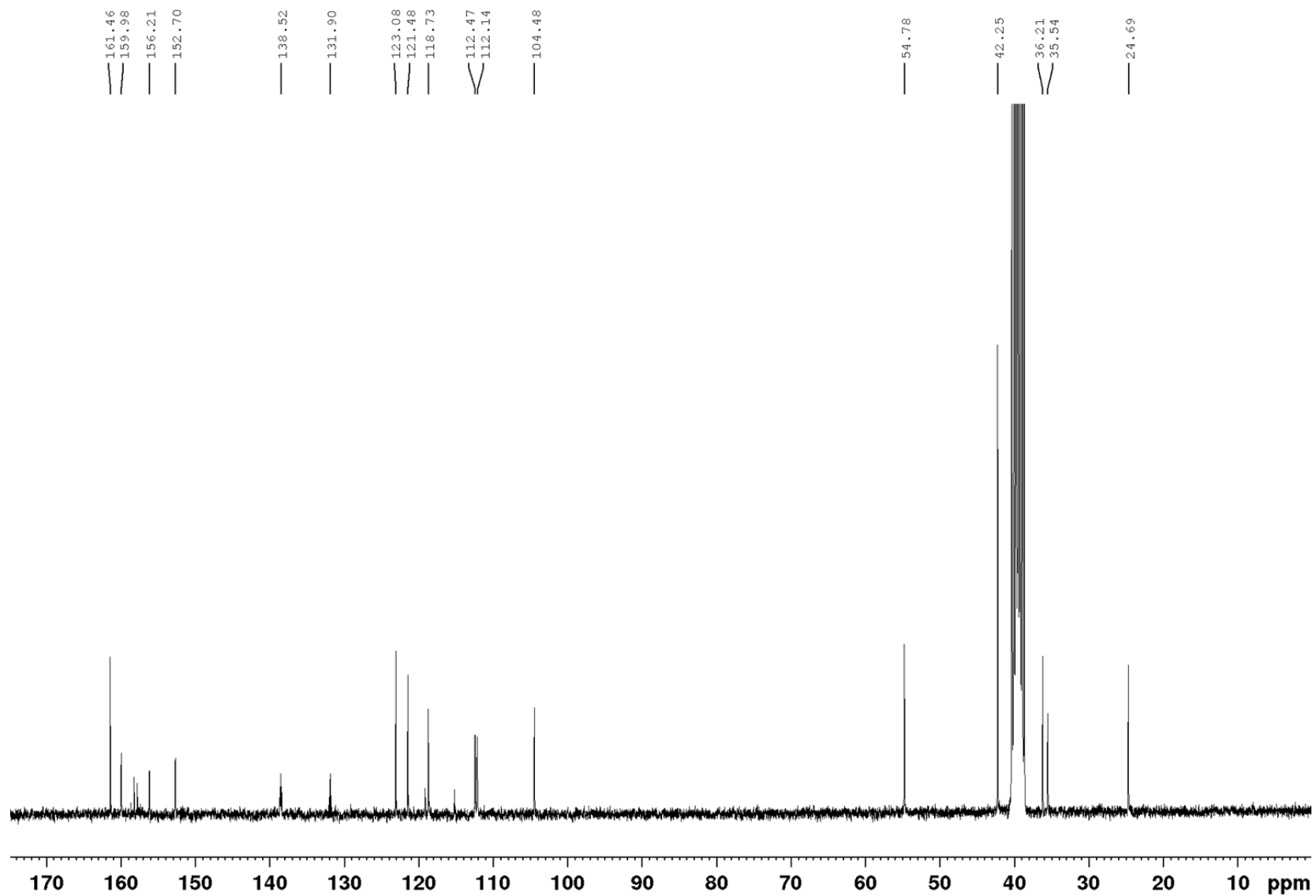


Figure S3:  $^{13}\text{C}$ -NMR spectrum of *trans*-F<sub>4</sub>Azo-(PyDp)<sub>2</sub> (**2**).

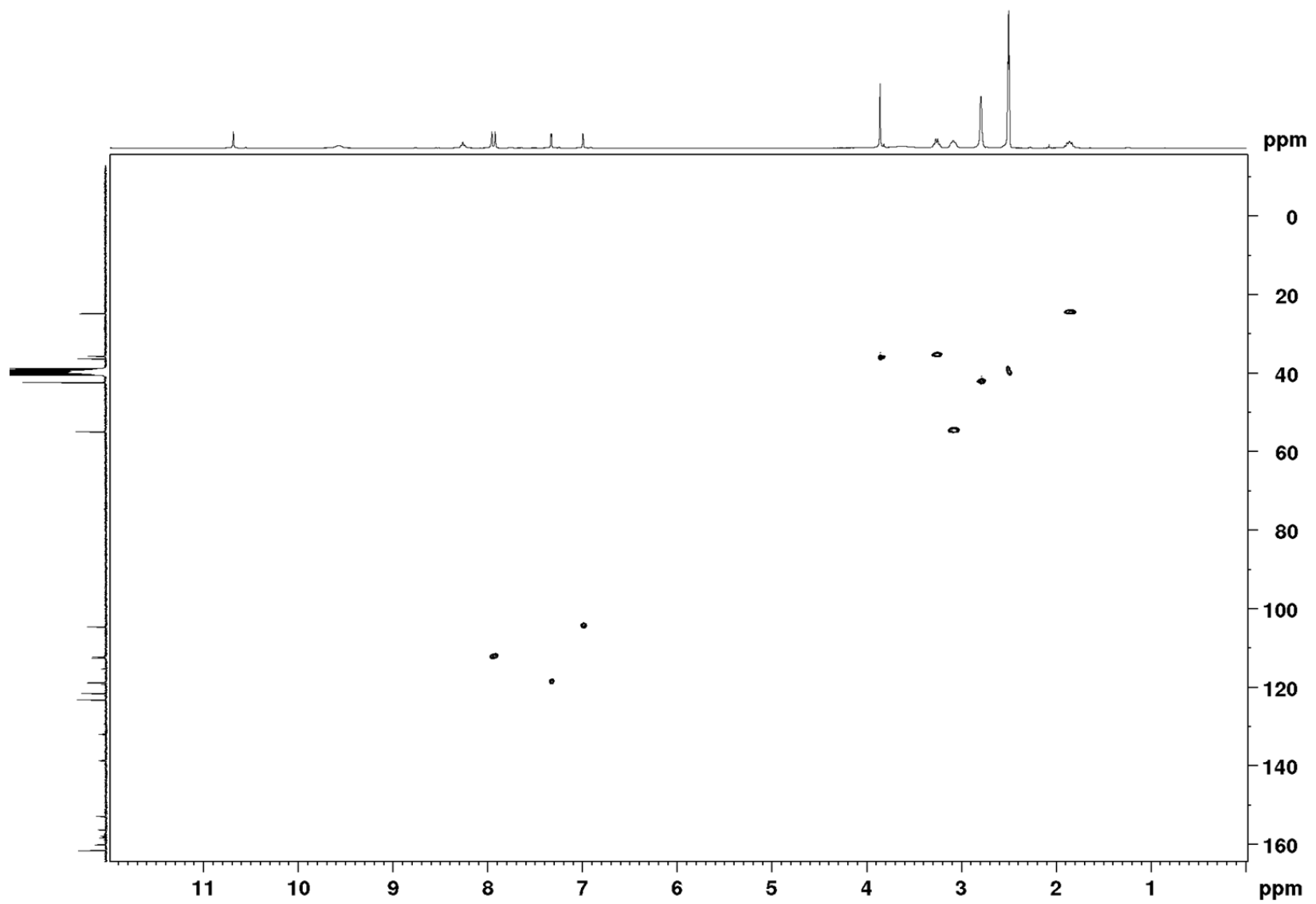


Figure S4: HSQC-NMR spectrum of *trans*-F<sub>4</sub>Azo-(PyDp)<sub>2</sub> (2).

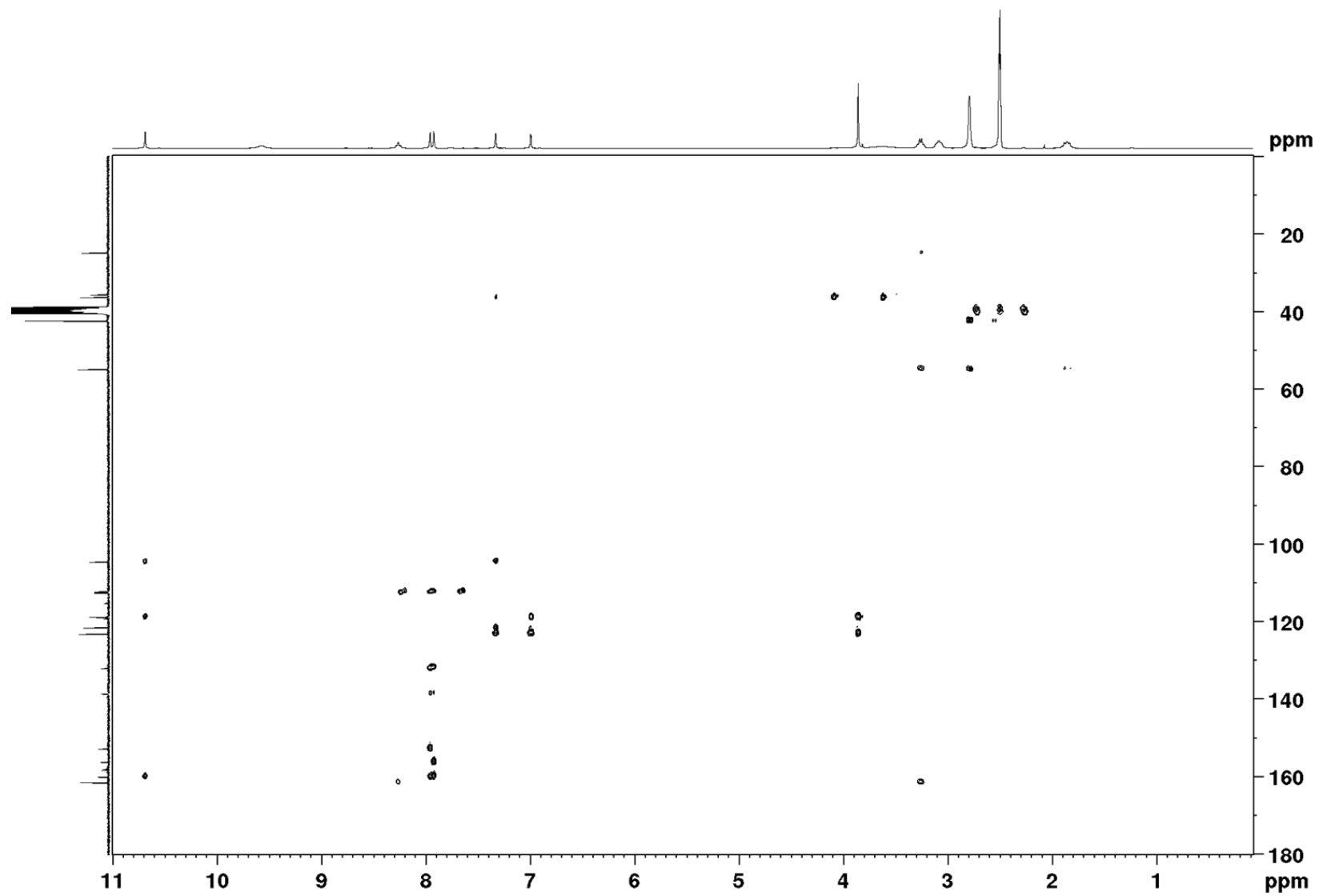
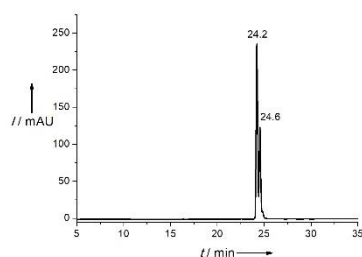


Figure S5: HMBC-NMR spectrum of *trans*-F<sub>4</sub>Azo-(PyDp)<sub>2</sub> (2).

**4-(4-(4-((5-((3-(dimethylamino)propyl)carbamoyl)-1-methyl-1H-pyrrol-3-yl)carbamoyl)-2,6-difluorostyryl)-3,5-difluorobenzamido)-1-methyl-1H-pyrrole-2-carboxylic acid (19):** Compound **6**, (16.2 mg, 0.06 mmol) and Pd/C 5% dry (20.0 mg, 123% w/w) was suspended in THF (3.0 mL) and stirred under H<sub>2</sub> atmosphere for 2 h. The reaction mixture was filtered over celite and the solvent removed under reduced pressure. F<sub>4</sub>Azo-diacid (**5**, 50.0 mg, 0.15 mmol) and HATU (33.5 mg, 0.09 mmol) were dissolved in THF (10 mL) and DIPEA (85.0 μL, 0.49 mmol) added. The reaction mixture was stirred for 50 min before the reduced pyrrole **8** dissolved in THF (1.50 mL) was added. After stirring for 1.5 h, the solvent was removed and the crude purified by preparative HPLC (5 - 60% over 40 min) to yield the desired product as its TFA salt (**19**), 19.7 mg, 0.03 mmol, 47%) as orange solid. *t<sub>R</sub>*=24.2 min (*cis*), 24.6 min (*trans*) (5% to 75% B in 30 min); HRMS-ESI<sup>+</sup> (*m/z*): [M]<sup>+</sup> calcd for C<sub>25</sub>H<sub>24</sub>F<sub>4</sub>N<sub>6</sub>O<sub>4</sub>H, 549.1868; found, 549.1883.

**E-isomer:**

**δH(500 MHz; [D<sub>6</sub>]DMSO; Me<sub>4</sub>Si)** 13.95 (1 H, s, COOH), 10.68 (1 H, s, NH-3), 9.48 (1 H, br s, NH<sup>+</sup>-12), 8.27 (1 H, t, <sup>3</sup>J<sub>HH</sub> 5.8, NH-7), 7.94 (1 H, s, H-1 / H-2), 7.92 (1 H, s, H-1 / H-2), 7.83 (1 H, s, H-1b / H-2b), 7.81 (1 H, s, H-1b / H-2b), 7.32 (1 H, d, <sup>4</sup>J<sub>HH</sub> 1.9, H-4), 6.99 (1 H, d, <sup>4</sup>J<sub>HH</sub> 1.9, H-5), 3.85 (3 H, s, H-6), 3.28 – 3.22 (2 H, m, H-8), 3.11 – 3.06 (2 H, m, H-10), 2.79 (6 H, s, H-11 and H-11'), 1.88 – 1.81 (2 H, m, H-9); **δC (125 MHz; [D<sub>6</sub>]DMSO; Me<sub>4</sub>Si)** 164.5 (COOH), 161.4 (CO), 159.9 (CO), 155.5 (C<sub>q</sub>), 155.3 (C<sub>q</sub>), 153.5 (C<sub>q</sub>), 153.3 (C<sub>q</sub>), 138.7 (C<sub>q</sub>), 134.9 (C<sub>q</sub>), 133.2 (C<sub>q</sub>), 131.8 (C<sub>q</sub>), 123.0 (C<sub>q</sub>), 121.4 (C<sub>q</sub>), 118.7 (CH), 114.1 (CH), 113.9 (CH), 112.4 (CH), 112.3 (CH), 104.4 (CH), 54.7 (CH<sub>2</sub>), 42.2 (2C, CH<sub>3</sub>), 36.2 (CH<sub>3</sub>), 35.4 (CH<sub>2</sub>), 24.7 (CH<sub>2</sub>).



**Figure S6:** HPLC chromatogram of F<sub>4</sub>Azo-(PyDp)(COOH) (**19**).



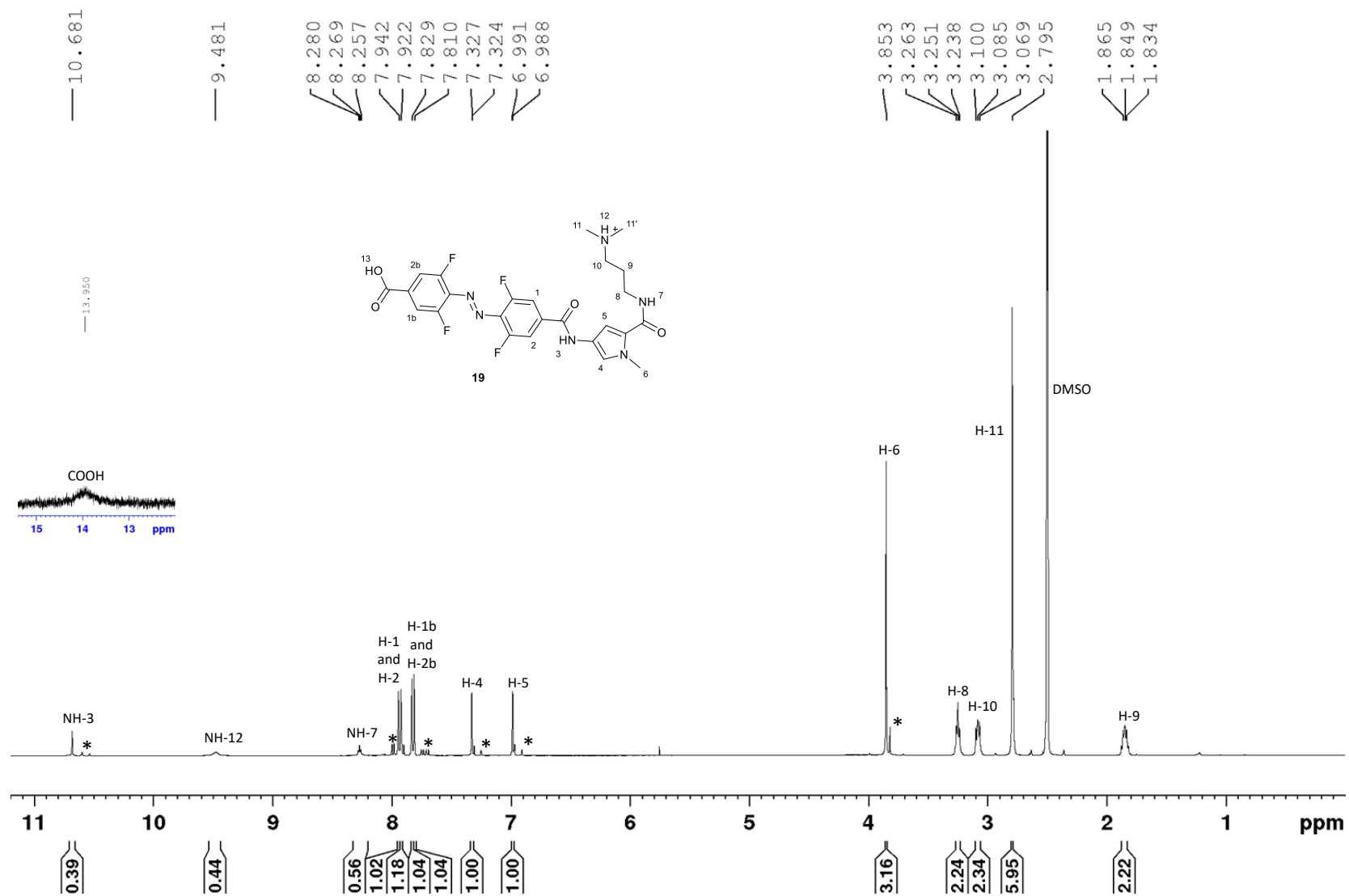


Figure S7: <sup>1</sup>H-NMR spectrum of *trans*-F<sub>4</sub>Azo-(PyDp)(COOH) (**19**). The inset shows the signal of the acid.

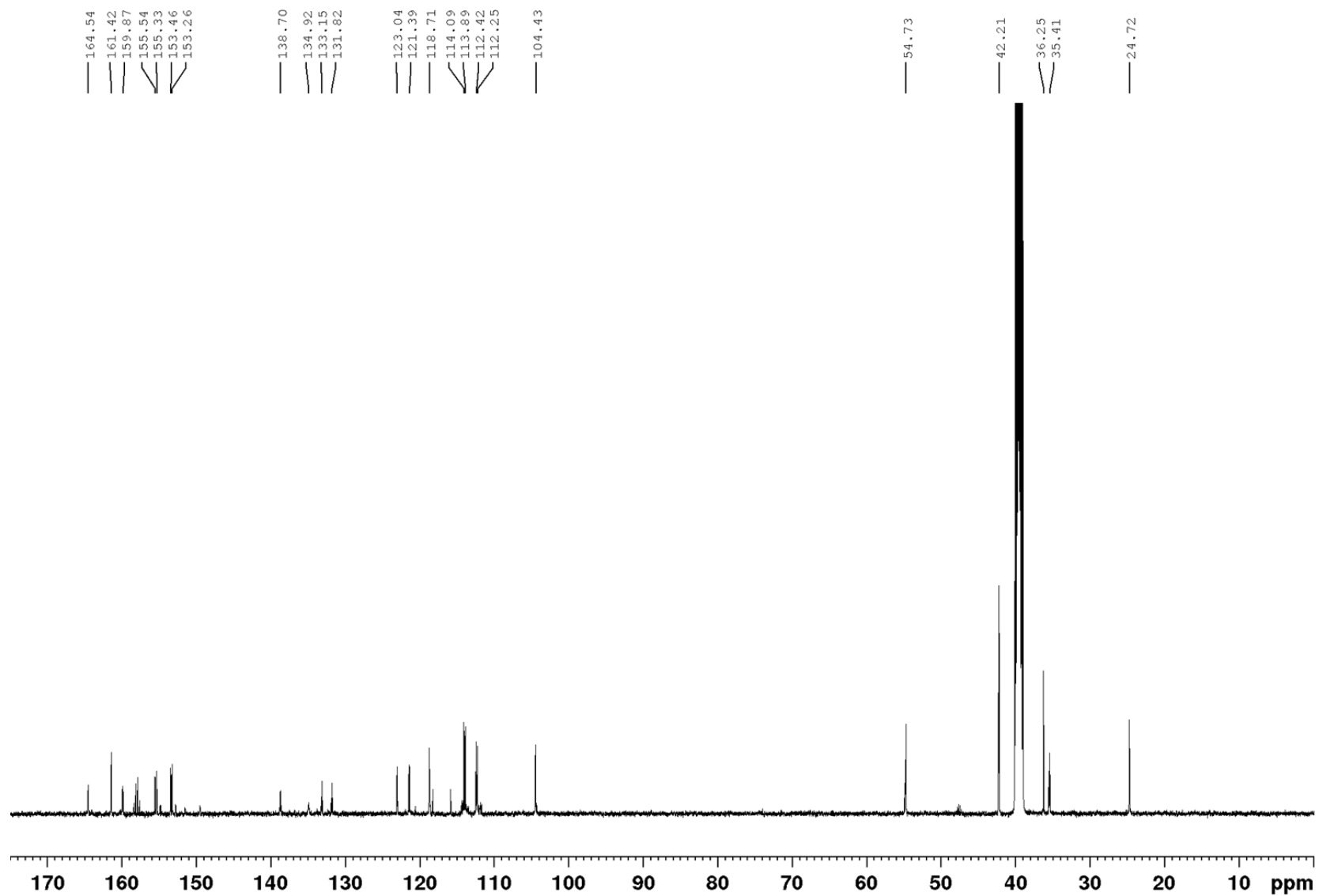


Figure S8:  $^{13}\text{C}$ -NMR spectrum of *trans*- $F_4\text{Azo}$ -(PyDp)(COOH) (**19**).

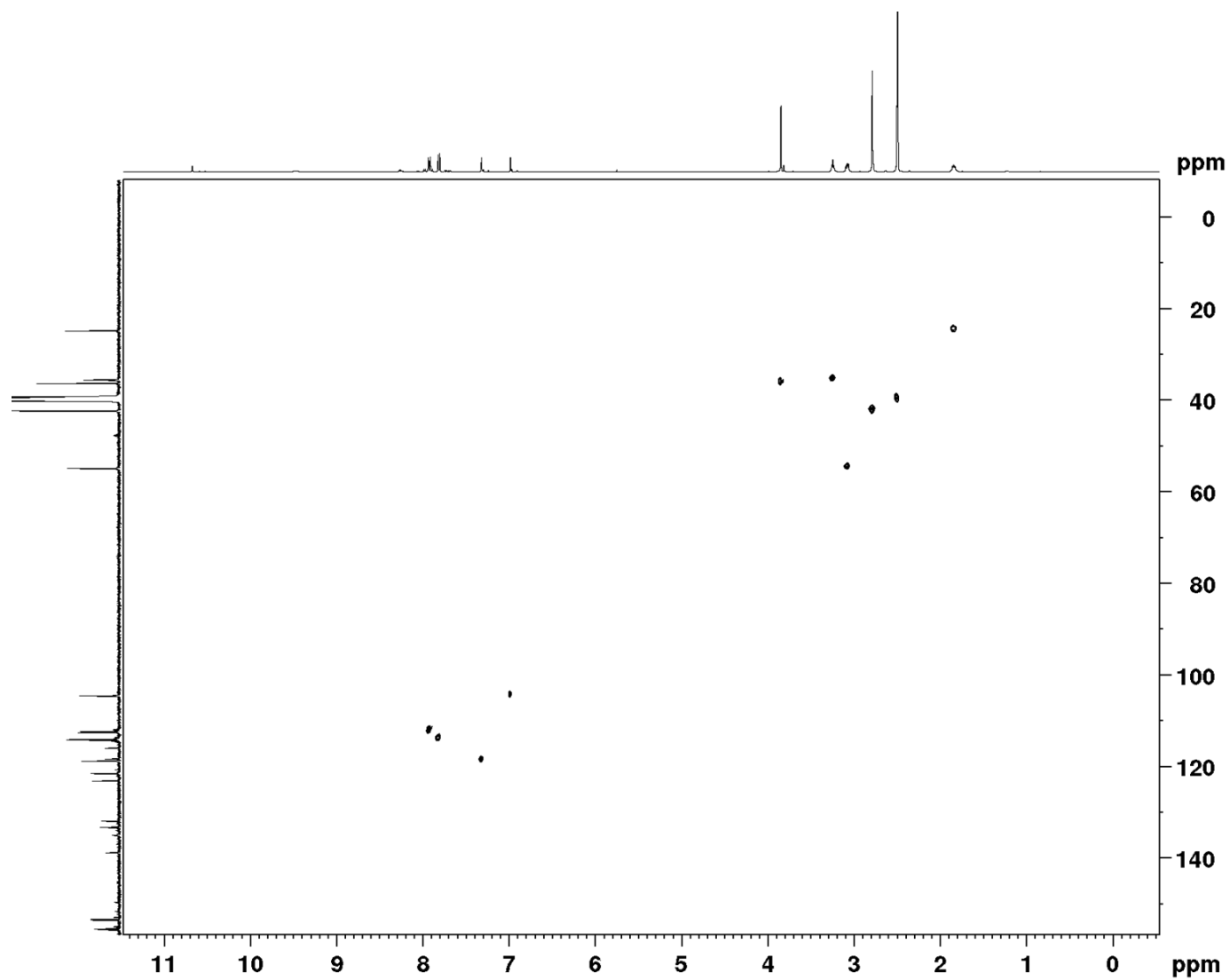


Figure S9: HSQC-NMR spectrum of *trans*- $F_4$ Azo-(PyDp)(COOH) (**19**).

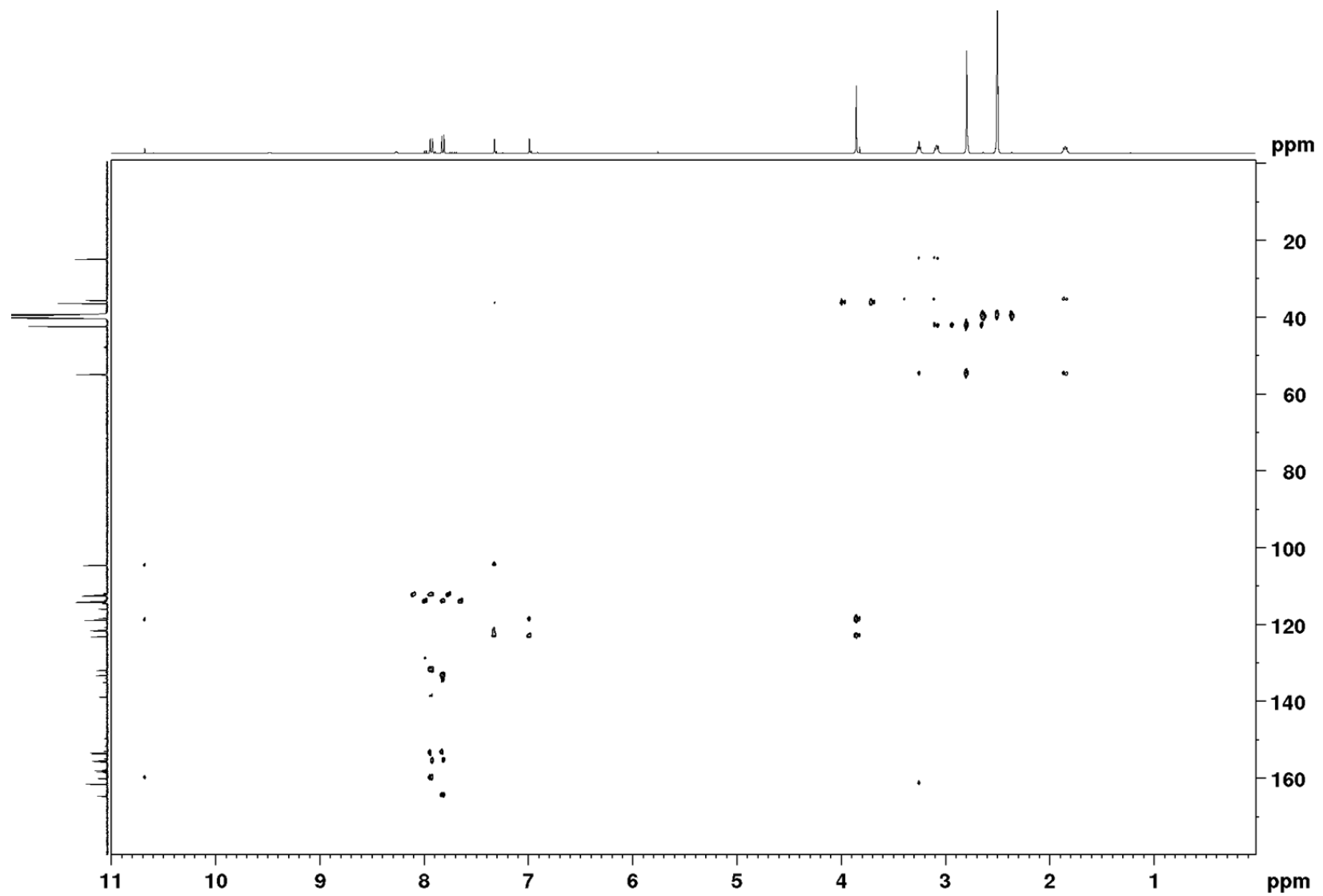
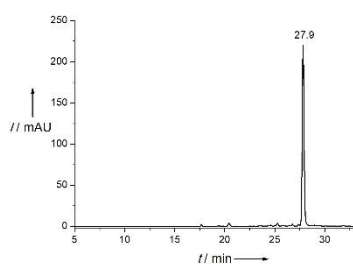


Figure S10: HMBC-NMR spectrum of *trans*-F<sub>4</sub>Azo-(PyDp)(COOH) (**19**).

**(E)-3-(4-(4-((2,6-difluoro-4-(5-(methoxycarbonyl)-1-methyl-1H-pyrrol-3-yl)carbamoyl)phenyl)diazenyl)-3,5-difluorobenzamido)-1-methyl-1H-pyrrole-2-carboxamido)-N,N-dimethylpropan-1-aminium (3):** Compound **7**, (4.40 mg, 24.1  $\mu$ mol) and Pd/C 5% dry (6.00 mg, 136% w/w) was suspended in THF (3.0 mL) and stirred under H<sub>2</sub> atmosphere for 2 h. The reaction mixture was filtered over celite and the solvent removed under reduced pressure. F<sub>4</sub>Azo-(PyDp)(COOH) (**19**, 12.0 mg, 21.9  $\mu$ mol) and HATU (9.16 mg, 24.1  $\mu$ mol) were dissolved in THF (400  $\mu$ L) and DIPEA (12.6  $\mu$ L, 72.3  $\mu$ mol) added. The reaction mixture was stirred for 4 h before the reduced pyrrole **7** dissolved in THF (600  $\mu$ L) was added. After stirring for 2.5 h, the solvent was removed and the crude purified by preparative HPLC (5 - 75% over 30 min) to yield the desired product as its TFA salt (**3**, 5.40 mg, 6.76  $\mu$ mol, 31%) as orange solid.  $t_R$ =27.9 min (5% to 75% B in 30 min); HRMS-ESI<sup>+</sup> (*m/z*): [M]<sup>+</sup> calcd for C<sub>32</sub>H<sub>32</sub>F<sub>4</sub>N<sub>8</sub>O<sub>5</sub>H, 685.2505; found, 685.2532.

**E-isomer:**

**$\delta$ H(500 MHz; [D<sub>6</sub>]DMSO; Me<sub>4</sub>Si)** 10.66 (1 H, s, NH-3 / NH-3b), 10.63 (1 H, s, NH-3 / NH-3b), 9.24 (1 H, br s, NH<sup>+</sup>-13), 8.25 (1 H, t, <sup>3</sup>J<sub>HH</sub> 5.7, NH-8), 7.94 (2 H, s, H-1 / H-2 / H-1b / H-2b), 7.91 (2 H, s, H-1 / H-2 / H-1b / H-2b), 7.56 (1 H, d, <sup>4</sup>J<sub>HH</sub> 1.8, H-4b), 7.31 (1 H, d, <sup>4</sup>J<sub>HH</sub> 1.8, H-4), 7.00 (1 H, d, <sup>4</sup>J<sub>HH</sub> 1.8, H-5 / H-5b), 6.99 (1 H, d, <sup>4</sup>J<sub>HH</sub> 1.8, H-5 / H-5b), 3.88 (3 H, s, H-6), 3.86 (3 H, s, H-6b), 3.76 (3 H, s, H-7), 3.30 – 3.22 (2 H, m, H-9), 3.13 – 3.03 (2 H, m, H-11), 2.80 (3 H, s, H-12 / H-12'), 2.79 (3 H, s, H-12 / H-12'), 1.91 – 1.78 (2 H, m, H-10);  **$\delta$ C (125 MHz; [D<sub>6</sub>]DMSO; Me<sub>4</sub>Si)** 161.9 (CO), 161.2 (CO), 160.5 (CO), 160.4 (CO), 156.0 (2C, C<sub>q</sub>), 153.9 (2C, C<sub>q</sub>), 138.8 (2C, C<sub>q</sub>), 132.4 (2C, C<sub>q</sub>), 123.5 (C<sub>q</sub>), 122.6 (C<sub>q</sub>), 122.0 (C<sub>q</sub>), 121.7 (CH), 119.6 (C<sub>q</sub>), 119.2 (CH), 112.9 (2C, CH), 112.7 (2C, CH), 109.0 (CH), 104.9 (CH), 55.3 (CH<sub>2</sub>), 51.6 (CH<sub>3</sub>), 42.7 (2C, CH<sub>3</sub>), 36.8 (CH<sub>3</sub>), 36.7 (CH<sub>3</sub>), 36.0 (CH<sub>2</sub>), 25.2 (CH<sub>2</sub>).



**Figure S11:** HPLC chromatogram of F<sub>4</sub>Azo-(PyDp)(PyOMe) (**3**).

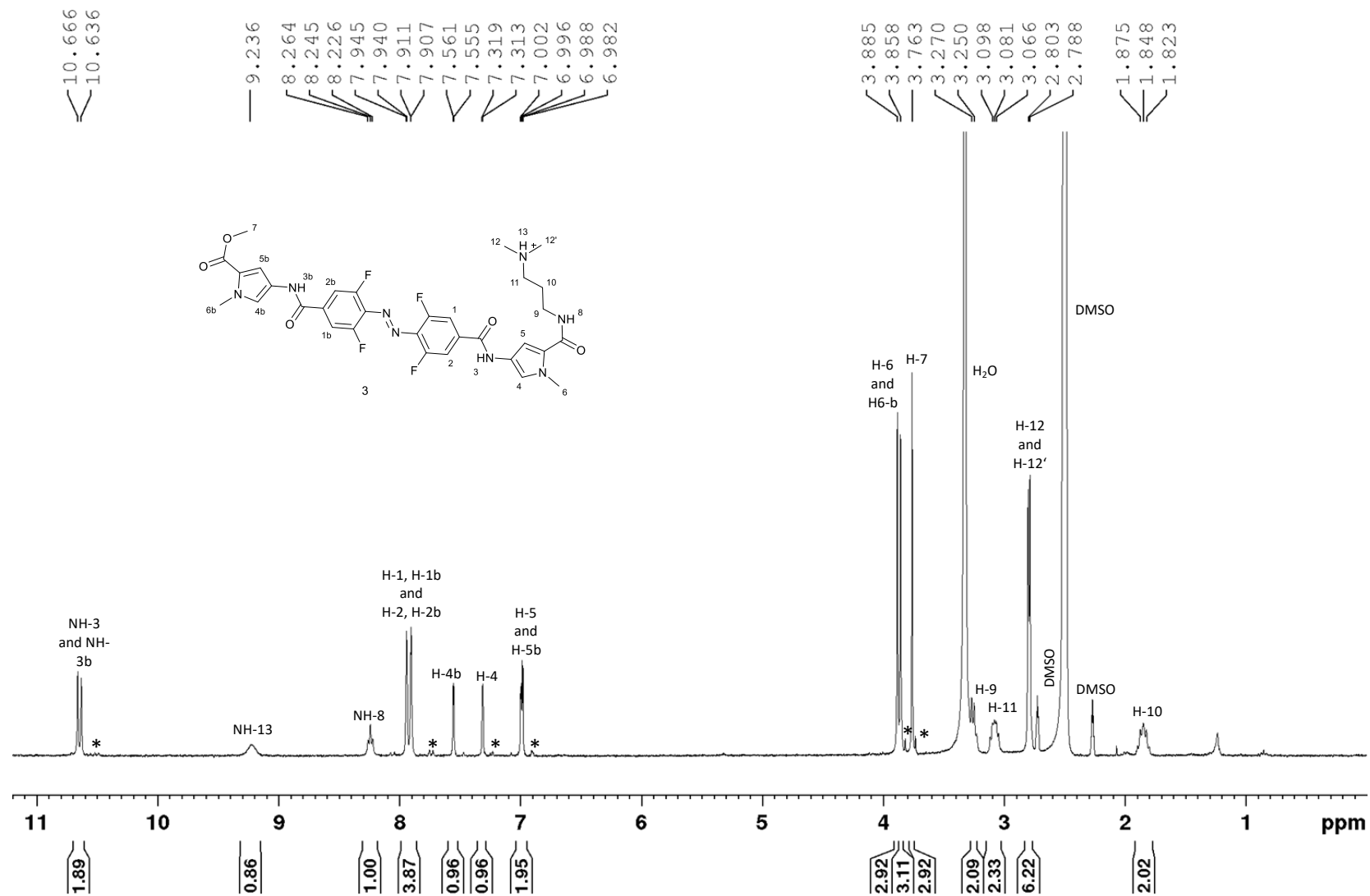


Figure S12: <sup>1</sup>H-NMR spectrum of *trans*-F<sub>4</sub>Azo-(PyDp)(PyOMe) (**3**).

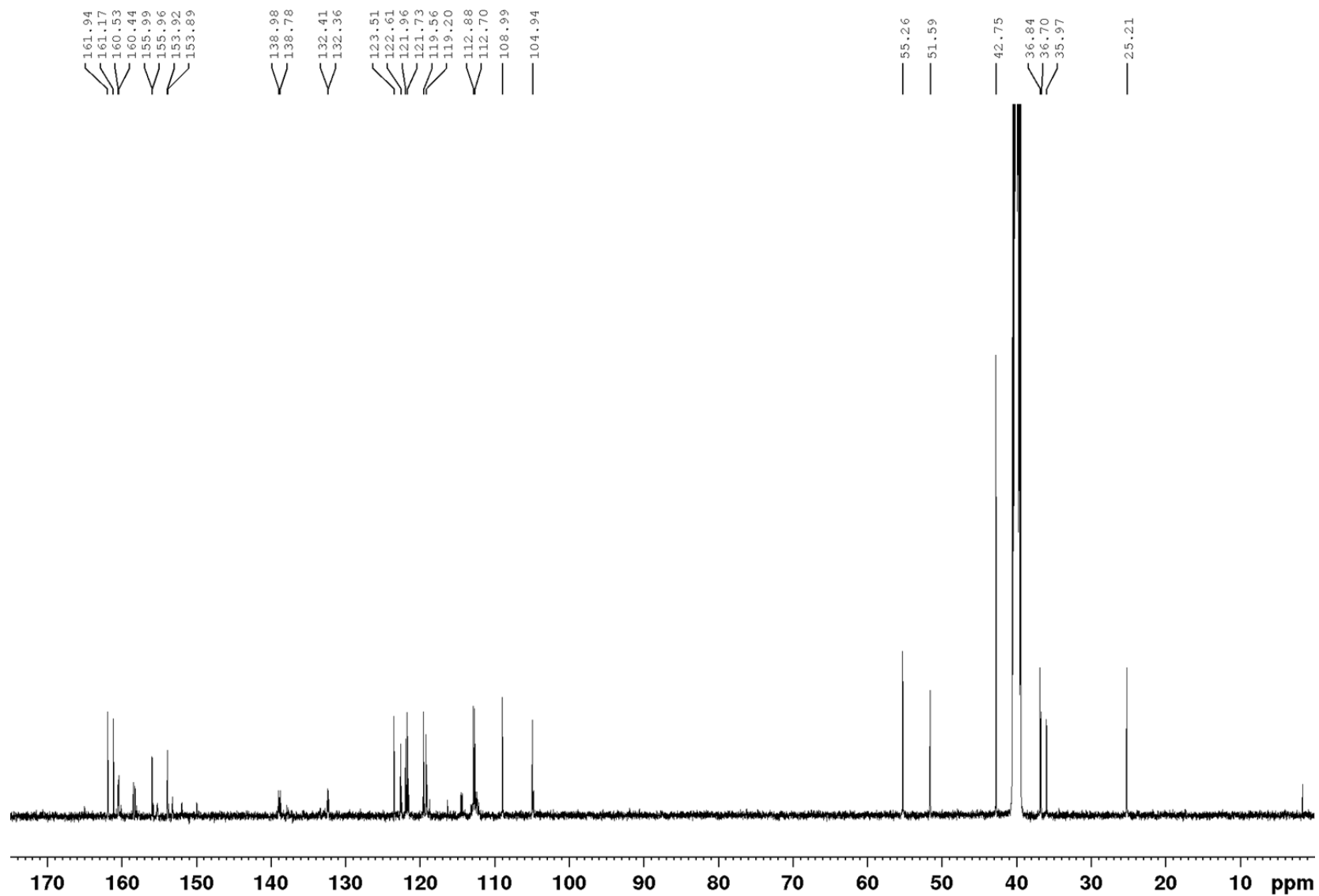


Figure S13:  $^{13}\text{C}$ -NMR spectrum of *trans-trans*- $F_4\text{Azo-(PyDp)(PyOMe)}$  (**3**).

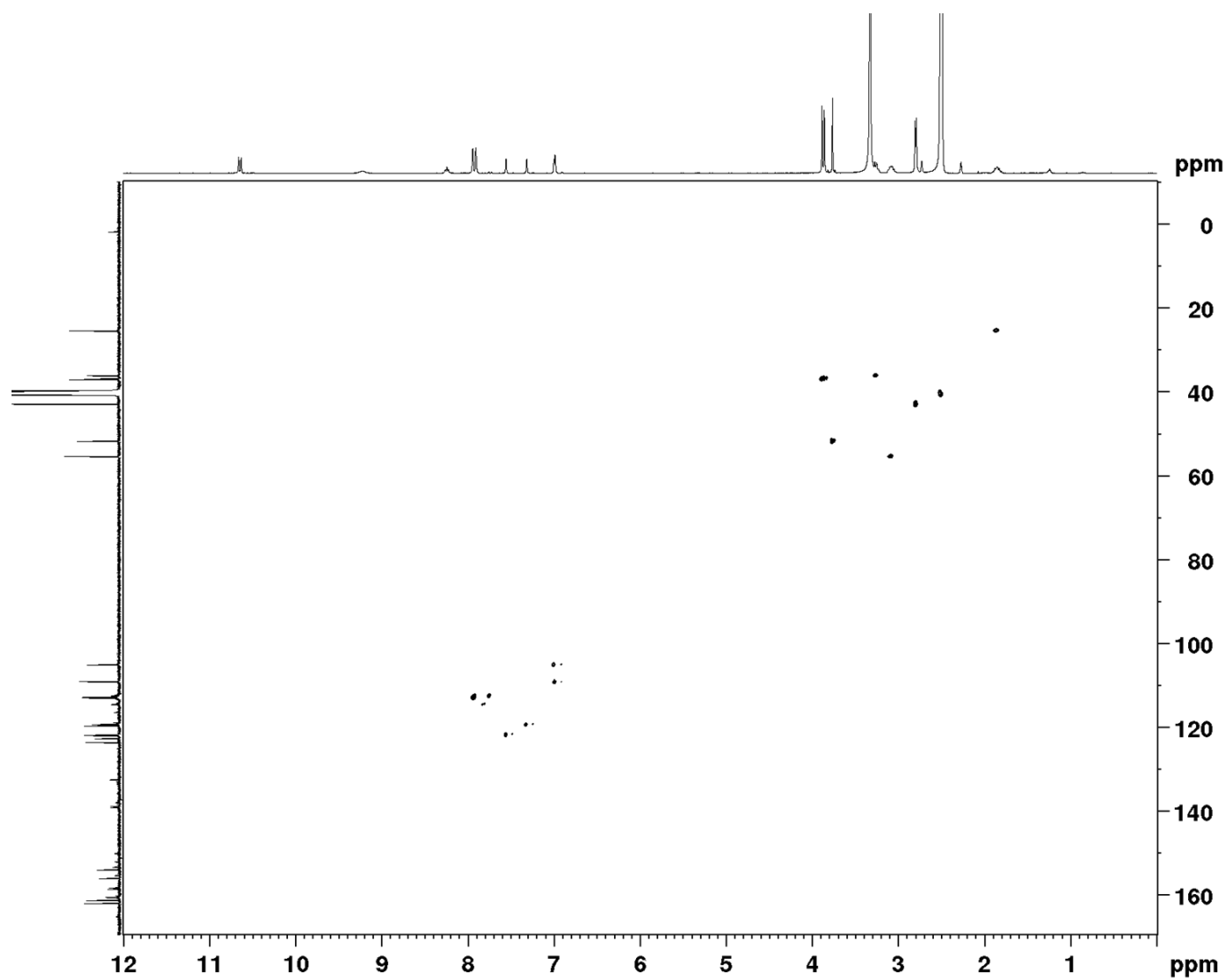


Figure S14: HSQC-NMR spectrum of *trans-trans*-F<sub>4</sub>Azo-(PyDp)(PyOMe) (3).



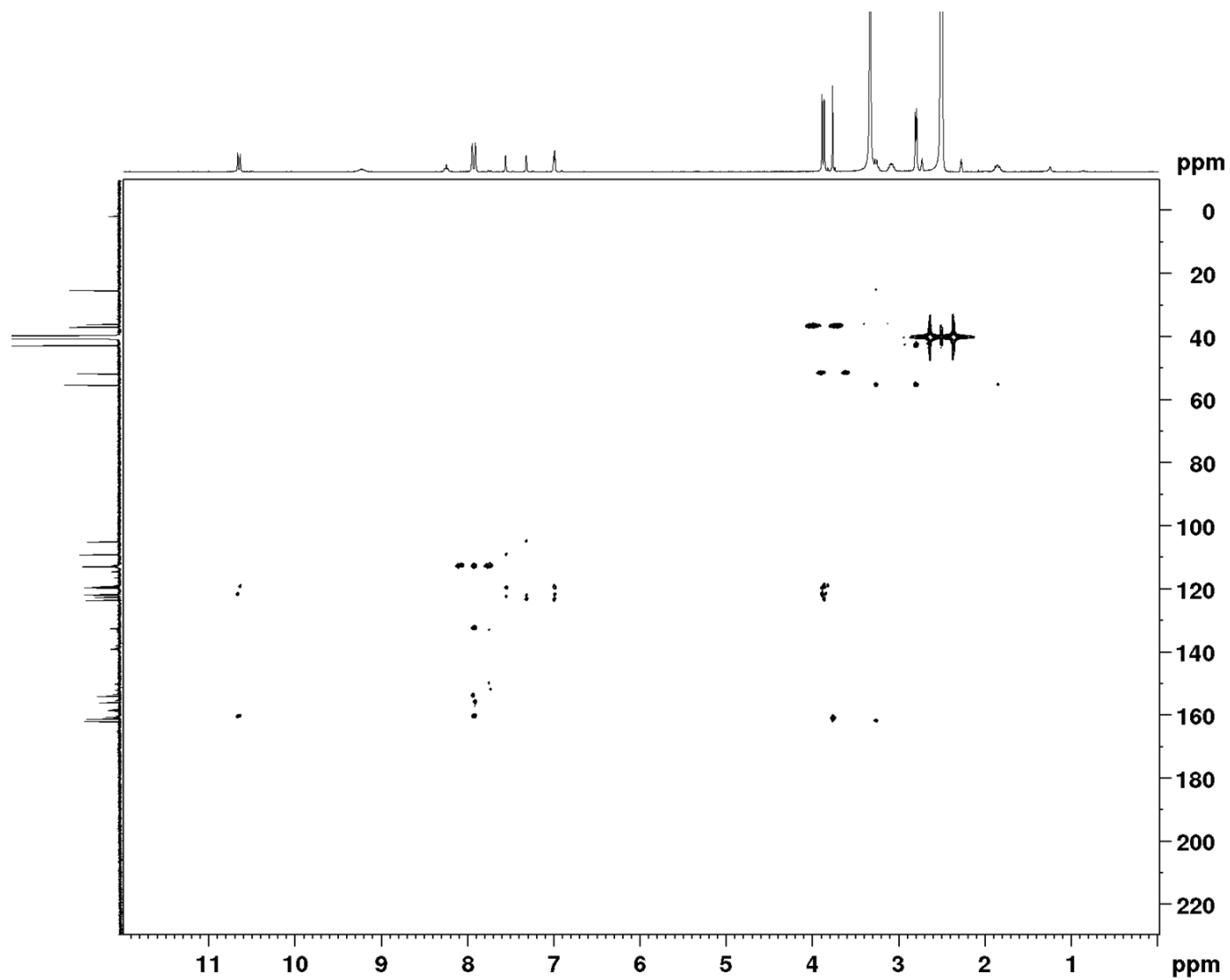


Figure S15: HMBC-NMR spectrum of *trans*-F<sub>3</sub>Azo-(PyDp)(PyOMe) (3).

## Concentration Determination

For the accurate concentration determination of the compounds:  $F_4\text{Azo}-(\text{PyDp})(\text{PyOMe})$  (**3**) and  $F_4\text{Azo}-(\text{PyDp})_2$  (**2**) their extinction coefficient in DMSO at room temperature was calculated. A specific amount (1.00 - 2.00 mg) of the corresponding compound was weighted on a Mettler Toledo XP6 micro balance and dissolved in a known volume of DMSO. Increasing amounts of such stock solution were added into a cuvette filled with 1 mL of DMSO. The corresponding absorbance of each addition was measured on a Tecan Spark 20M at the individual maximum and without exceeding 10% of the initial volume. In all the cases the absorbance was between 0.1 and 1 AU to be in concordance with Lambert-Beer law.<sup>[vii]</sup>

$$A = \epsilon l c \quad (\text{S1})$$

In this equation:  $A$  = absorbance of the solution;  $l$  = length of the cuvette;  $c$  = concentration;  $\epsilon$  = molar extinction coefficient. Below the UV-Vis spectrum of a 24  $\mu\text{M}$  concentration of the compound  $F_4\text{Azo}-(\text{PyDp})(\text{PyOMe})$  (**3**) in DMSO (Figure S16). The lineal regression of the obtained absorbance measurements versus the concentrations of the  $F_4\text{Azo}-(\text{PyDp})(\text{PyOMe})$  allowed us to obtain the molar extinction coefficient (Figure S17). This experiment was repeated three times independently i.e. from three different stock solutions.

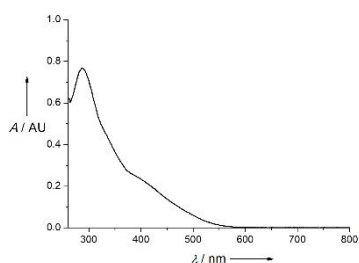


Figure S16: UV-Vis spectrum of a 24  $\mu\text{M}$  solution of compound  $F_4\text{Azo}-(\text{PyDp})(\text{PyOMe})$  (**3**) in DMSO.

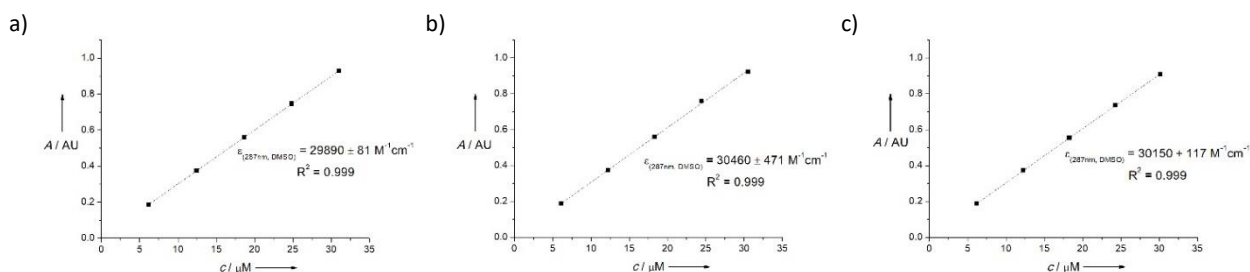
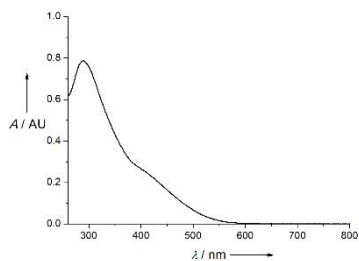
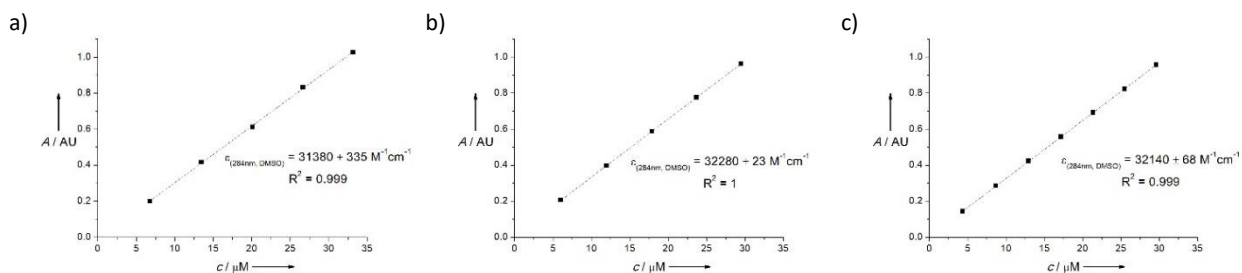


Figure S17: Determination of the extinction coefficient of compound  $F_4\text{Azo}-(\text{PyDp})(\text{PyOMe})$  (**3**) in DMSO. The absorbance maximum at 287 nm was plotted against the  $F_4\text{Azo}-(\text{PyDp})(\text{PyOMe})$  concentration. Three independent measurements are shown with the calculated extinction coefficient and their corresponding regression value ( $R^2$ ). The mean extinction coefficient and the standard deviation of  $F_4\text{Azo}-(\text{PyDp})(\text{PyOMe})$  (**3**) is  $30167 \pm 285 \text{ M}^{-1}\text{cm}^{-1}$ .

Below the UV-Vis spectrum of a 24  $\mu\text{M}$  concentration of the compound  $F_4\text{Azo}-(\text{PyDp})_2$  (**2**) in DMSO (Figure S18). The lineal regression of the obtained absorbance measurements versus the concentrations of  $F_4\text{Azo}-(\text{PyDp})_2$  (**2**) allowed us to obtain the molar extinction coefficient (Figure S19). This experiment was repeated three times independently i.e. from three different stock solutions.



**Figure S18:** UV-Vis spectrum of a 24  $\mu\text{M}$  solution of compound  $F_4\text{Azo}-(\text{PyDp})_2$  (**2**) in DMSO.



**Figure S19:** Determination of the extinction coefficient of compound  $F_4\text{Azo}-(\text{PyDp})_2$  (**2**) in DMSO. The absorbance maximum at 284 nm was plotted against the dimer concentration. Three independent measurements are shown with the calculated extinction coefficient and their corresponding regression value ( $R^2$ ). The mean extinction coefficient and the standard deviation of  $F_4\text{Azo}-(\text{PyDp})_2$  (**2**) is  $31933 \pm 484 \text{ M}^{-1}\text{cm}^{-1}$ .

Table S1 summarized the obtained molar extinction coefficient for both compounds.

**Table S1:** Determined mean extinction coefficients and standard deviations of  $F_4\text{Azo}-(\text{PyDp})(\text{PyOMe})$  (**3**) and  $F_4\text{Azo}-(\text{PyDp})_2$  (**2**) in DMSO at r.t.

	$F_4\text{Azo}-(\text{PyDp})_2$ in DMSO (284 nm)	$F_4\text{Azo}-(\text{PyDp})(\text{PyOMe})$ in DMSO (287 nm)
mean	$31933 \pm 484 \text{ M}^{-1}\text{cm}^{-1}$	$30167 \pm 285 \text{ M}^{-1}\text{cm}^{-1}$

In general during the concentration determination, the absorption values were subtracted against the corresponding buffer solution. For thiazole orange, we used the extinction coefficient from the literature in DMSO:  $\epsilon_{503\text{nm}} = 63000 \text{ M}^{-1}\text{cm}^{-1}$ <sup>[viii]</sup>.

For the concentration determination of the hairpin DNAs, the purchased lyophilized DNA was dissolved in Milli-Q water, heated to 95°C for 10 min and slowly cooled down to room temperature. Their molar extinction coefficients were determined by using the following formula:<sup>[ix]</sup>

$$\epsilon_{260\text{nm}} = \{(8.8 * \#T) + (7.3 * \#C) + (11.7 * \#G) + (15.4 * \#A)\} * 0.8 * 10^3 \text{ M}^{-1}\text{cm}^{-1} \quad (\text{S2})$$

In the formula # = number of nucleobases determined throughout the DNA sequence, T = thymine, C = cytosine, G = guanine, A = adenine. Table S2 summarizes the sequences and the determined extinction coefficients of the hairpin DNAs.

**Table S2.** Binding sites, sequences and extinction coefficients of DNA hairpins, which were used for fluorescence titrations experiments.

DNA	binding site	sequence (5' – 3')	extinction coefficient at 260 nm
dsDNA <sub>hAT</sub>	ATTA	GGCGATTACAGCTTTTGGCTGTAATCGCC	238400 M <sup>-1</sup> cm <sup>-1</sup>
dsDNA <sub>hGC</sub>	GGCCC	GGCAGGCCAGCTTTTGGCTGGGCCTGCC	225920 M <sup>-1</sup> cm <sup>-1</sup>

The nucleic acid concentration after the PCR was determined on a NanoDrop 2000 spectrometer (Thermo Scientific) by measuring the absorbance at 260 nm and using the extinction coefficient in water for double-stranded DNA (50 ng\*cm/ $\mu$ L).<sup>[x]</sup> dsDNA<sub>CT</sub> was purchased as a solution of 15.4 mM concentration.

The concentration of the nucleosomes in 10 mM Tris 1 mM EDTA pH 8.0 and 50 mM NaCl were also determined on the NanoDrop using the extinction coefficient from the literature:  $\epsilon_{260\text{nm}} = 1880000 \text{ M}^{-1}\text{cm}^{-1}$ .<sup>[xi]</sup>

### Photoisomerization of *F*<sub>4</sub>Azo-(PyDp)<sub>2</sub> (**2**) and *F*<sub>4</sub>Azo-(PyDp)(PyOMe) (**3**)

A 405 nm LED lamp (Roschwege Star UV 405-03-00-00, 405 nm, 700 mA, 3.5 V, P<sub>optisch</sub> = 670 mW) was used for the irradiation at 405 nm and a 520 nm LED lamp (Roschwege Star LSC-G 520 nm, 1A, 3.8 V, 87 lm, 130°) was used for irradiation at 520 nm. For the irradiation at 520 nm a filter (FGL515 –  $\varnothing$ 25 mm OG515 Colored Galss Filter, 515 nm longpass, Thorlabs) was further attached to the lamp.

For the *F*<sub>4</sub>Azo-derivatives, the *trans*-isomer is the thermodynamically most stable form,<sup>[iii]</sup> which was also yielded from the synthesis as the major product. The photostationary states were studied by UV-Vis spectroscopy, RP-HPLC and by NMR. All photoisomerization measurements were performed in the dark.

#### UV-Vis Characterization

For the characterization of the photoisomerization of the compound *F*<sub>4</sub>Azo-(PyDp)(PyOMe) (**3**) via UV-Vis measurements, a solution of 20  $\mu$ M of **3** in 10 mM Tris pH 7.6, 50 mM KCl and DMSO (98:2) (total volume 1 mL) was irradiated for 1 min at 405 nm to ensure complete conversion to the *trans* state. Afterwards, to obtain the *cis* isomer such solution was irradiated at 520 nm at different time intervals: 10 s / 30 s / 1 min / 2 min / 3 min / 5 min / 10 min. As seen in figure S20, after 10 min of continuous irradiation no significant spectroscopic changes could be observed. Afterwards this solution was irradiated at the time intervals: 5 s / 10 s / 30 s / 1 min / 1.5 min / 2 min / 2.5 min / 3 min at 405 nm, which brought the characteristic *trans*-isomer spectrum (Figure S20B). No significant spectroscopic changes were observed after 3 min. The represented data are the mean values calculated from three independent measurements.

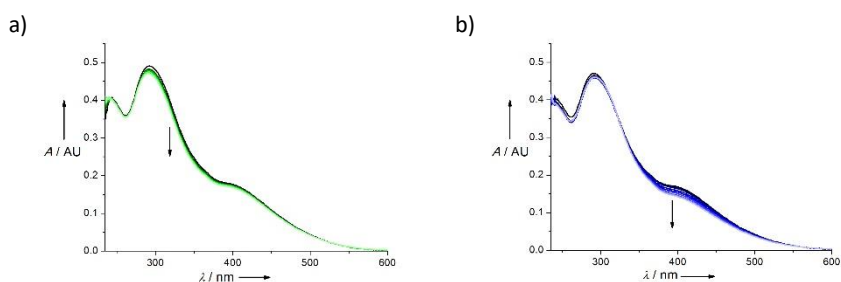


**Figure S20:** UV-Vis spectra of 20  $\mu\text{M}$  of  $F_4\text{Azo}-(\text{PyDp})(\text{PyOMe})$  (**3**) in 10 mM Tris, pH 7.6 50 mM KCl and DMSO (98:2). A) 1 min irradiation at 405 nm followed by successive time interval (10 s / 30 s / 1 min / 2 min / 3 min / 5 min / 10 min) irradiation at 520 nm. B) Final irradiation conditions of A, followed by successive time interval (5 s / 10 s / 30 s / 1 min / 1.5 min / 2 min / 2.5 min / 3 min) irradiation at 405 nm.

We further recorded DMSO subtracted absorbance spectrum of: a) a 40  $\mu\text{M}$  solution of  $\text{O}_2\text{N-Py-Dp}$  (**8**) in 10 mM Tris pH 7.6, 50 mM KCl and DMSO (98:2); b) 20  $\mu\text{M}$  solution of  $F_4\text{Azo}-(\text{COOH})_2$  (**5**) in the *trans* and the *cis*-state in 10 mM Tris 50 mM pH 7.6, KCl and DMSO (98:2) and c) the combined solutions in the *trans* and the *cis*-state. Figure S21 shows the described spectra.

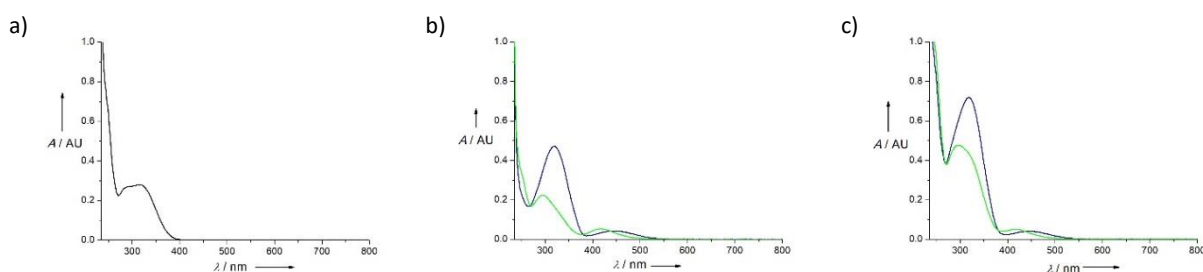


**Figure S21:** A) UV-Vis spectra of 40  $\mu\text{M}$   $\text{O}_2\text{N-Py-Dp}$  (**8**) in 10 mM Tris pH 7.6, 50 mM KCl and DMSO (98:2). B) UV-Vis spectra of 20  $\mu\text{M}$   $F_4\text{Azo}-(\text{COOH})_2$  (**5**) in 10 mM Tris pH 7.6, 50 mM KCl and DMSO (98:2). The green spectra shows the compound in the *cis*-state, which was achieved by irradiating the sample for 2 min at 520 nm. The blue spectra shows the compound in the *trans*-state, which was achieved by irradiating the sample for 10 s at 405 nm C) UV-Vis spectra of a mixture of 40  $\mu\text{M}$   $\text{O}_2\text{N-Py-Dp}$  (**8**) and 20  $\mu\text{M}$   $F_4\text{Azo}-(\text{COOH})_2$  (**5**) in 10 mM Tris pH 7.6, 50 mM KCl and DMSO (98:2). The green spectra shows the compound in the *cis*-state, which was achieved by irradiating the sample for 2 min at 520 nm. The blue spectra shows the compound in the *trans*-state, which was achieved by irradiating the sample for 10 s at 405 nm.

We further recorded the spectra of the *trans*- and the *cis*-isomer of a 20  $\mu\text{M}$  solution of  $F_4\text{Azo}-(\text{PyDp})_2$  (**2**) in DMSO under the same conditions, which spectra is shown in figure S22.

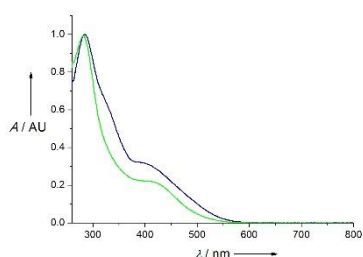


**Figure S22:** UV-Vis spectra of 20  $\mu\text{M}$  of  $F_4\text{Azo}-(\text{PyDp})_2$  (**2**) in DMSO. The blue spectra shows the spectra of the *trans*-isomer, which was achieved by 1 min irradiation at 405 nm. The green spectra shows the spectra of the *cis*-isomer, which was achieved by irradiation at 520 nm for 2 min.

The procedure of the absorbance titrations was: addition of increasing amounts of a 2.73 mM  $F_4\text{Azo}-(\text{PyDp})_2$  solution in DMSO to solution of 12.5  $\mu\text{M}$  dsDNA<sub>CT</sub> in 20 mM  $\text{NaH}_2\text{PO}_4$  pH 7.4, 100 mM NaCl in the corresponding cuvette. The stock solution of  $F_4\text{Azo}-(\text{PyDp})_2$  was irradiated for 10 s at 405 nm to measure the *trans*-derivative or 2 min at 520 nm to measure the *cis*-derivative. Solutions were kept in the dark and the measurement performed in the absence of light. Small aliquots of the compound stocks were stepwise added and the fluorescence spectra recorded after an incubation time of 3 min. The corresponding spectra are buffer subtracted and show the mean out of three measurements.

## RP-HPLC Characterization

For the characterization of the photoisomerization of the compounds via RP-HPLC measurements, a solution of 50  $\mu\text{M}$  of each compound in 10 mM Tris pH 7.4, 10 mM NaCl and DMSO (95:5) was irradiated for 10 s at 405 nm to obtain the *trans*-isomer and for 2 min at 520 nm to obtain the *cis*-isomer and 30  $\mu\text{L}$  were injected into the RP-HPLC. The photostationary states reached upon irradiation were determined by integration of the peak areas in the HPLC chromatogram at 287 nm (isosbestic point). In the case of  $F_4\text{Azo}-(\text{PyDp})_2$  (**2**) it was possible to detect both isomers by RP-HPLC, in the case of  $F_4\text{Azo}-(\text{PyDp})(\text{PyOMe})$  (**3**) it was not possible to separate both isomers by RP-HPLC and analyze their photoisomerization. The represented data shows a representative one of three measurements from independent experiments. Figure S23 shows the corresponding RP-HPLC chromatograms with their *trans/cis*-ratio after irradiation of the samples.

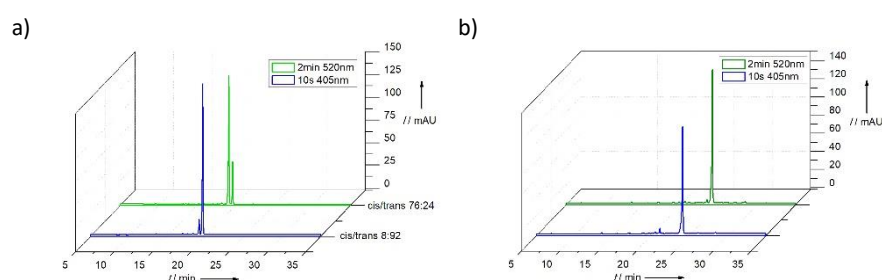


**Figure S23:** RP-HPLC chromatogram of A)  $F_4\text{Azo}-(\text{PyDp})_2$  (**2**) and B)  $F_4\text{Azo}-(\text{PyDp})(\text{PyOMe})$  (**3**) after irradiation at 405 nm for 10 s and 520 nm for 2 min and their corresponding *trans/cis*-ratio.

## NMR Characterization

For the characterization of the photoisomerization of the compounds via NMR, a solution of 2 mg of each compound was dissolved in  $\text{DMSO}_d6$  to give a 4 mM solution and their  $^1\text{H}$ -NMR spectra was measured in a brown NMR tube (Rotilabo-NMR tube, Carl Roth) to get the spectrum of the thermodynamically more stable *trans*-isomer. To get the spectrum of the *cis*-isomer the solution was irradiated for 2 min at 520 nm, transferred into the Rotilabo-NMR tube and its  $^1\text{H}$ -NMR spectra was measured. In the case of  $F_4\text{Azo}-(\text{PyDp})(\text{PyOMe})$  (**3**) another spectrum after irradiation for 4 min at 520 nm was recorded, to ensure the maximum conversion after 2 min of irradiation, which was determined for  $F_4\text{Azo}-(\text{PyDp})_2$  (**2**) as sufficient. The *trans/cis*-ratio was calculated by integration of the proton signals of the pyrroles and the aromatic protons of the tetra-ortho-fluorazobenzenes. The represented data shows a representative one of three measurements from independent experiments.

## DNA Binding Experiments

DNA binding affinities were determined via fluorescence intercalation displacement (FID) titrations. To a solution of hairpin DNA, thiazole orange (TO) was added yielding in a fluorescence increase upon binding to the DNA. Addition of our compounds led to a decrease of fluorescence due to the displacement of the fluorescent TO. The affinity of TO to the respective hairpin DNA, allows the determination of the binding affinity of our molecules through the fluorescence decrease measurements.<sup>[xii]</sup> We decided to use TO instead of EtBr, as it gives a much higher fluorescence increase upon DNA binding and therefore, allowed to use smaller slits sizes in our FID assay. This results in less light exposure of our samples and a lower probability of back-isomerization during the measurement.<sup>[xiii]</sup>

To determine the binding affinity of TO to the hairpin DNAs, titrations were performed in 20 mM  $\text{NaH}_2\text{PO}_4$  pH 7.4, 100 mM NaCl (total volume 1 mL) at a constant TO concentration of 1  $\mu\text{M}$ . Small aliquots of DNA stocks (50  $\mu\text{M}$  and 500  $\mu\text{M}$ ) were stepwise added and the fluorescence spectra recorded after an incubation time of 3 min. The corresponding spectra are buffer subtracted and show the mean out of three independent measurements. The maximum at 530 nm was plotted versus the added amount of DNA. Represented data are mean values calculated from three independent experiments. The binding affinity was calculated using the program HypSpec using the non-corrected measured spectra.

The following figures show the recorded mean fluorescence spectra of TO with  $\text{dsDNA}_{\text{hAT}}$  and  $\text{dsDNA}_{\text{hGC}}$  and its maximum plotted against the added amount of DNA.

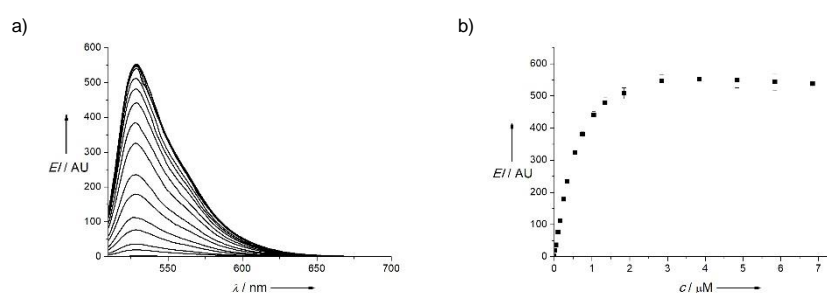


**Figure S24:** A) Mean fluorescence spectra of a 1  $\mu\text{M}$  solution of TO in 20 mM  $\text{NaH}_2\text{PO}_4$  pH 7.4, 100 mM NaCl with increasing amounts of  $\text{dsDNA}_{\text{hAT}}$ . B) Fluorescence intensity maximum at 530 nm plotted against the concentration of added DNA. Represented data are mean values and their standard deviation calculated from three independent experiments.

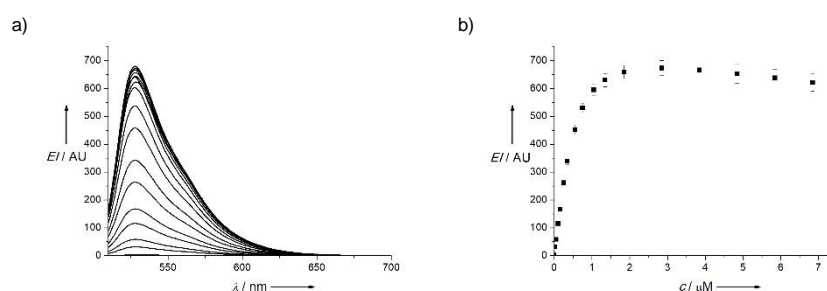


**Figure S25:** A) Mean fluorescence spectra of a 1  $\mu\text{M}$  solution of TO in 20 mM  $\text{NaH}_2\text{PO}_4$  pH 7.4, 100 mM NaCl with increasing amounts of  $\text{dsDNA}_{\text{hGC}}$ . B) Fluorescence intensity maximum at 530 nm plotted against the concentration of added DNA. Represented data are mean values and their standard deviation calculated from three independent experiments.

Using the program HypSpec and setting the number of reagents to 2, the corresponding binding affinities were calculated out of the non-corrected measured spectra and summarized in table S5 (Section Binding Affinity Calculation by HypSpec).

Once the  $K_D$  of TO to the hairpin DNAs was determined, we performed the FID titrations to determine the  $K_D$  of the compounds. Varying from the described procedure above, the slits for the displacement titrations were excitation slit width: 3 nm; emission slit width: 3 nm. Titrations were performed in 20 mM  $\text{NaH}_2\text{PO}_4$  pH 7.4, 100 mM NaCl (total volume 1 mL) at a TO concentration of 6  $\mu\text{M}$  and a hairpin concentration of 1  $\mu\text{M}$ , which equals the ideal dye:bp-DNA ratio of 1:2.<sup>[xii,xiv]</sup> Compound solutions were prepared as a DMSO stock with a concentration of 250  $\mu\text{M}$  and 1 mM. These stock solutions were irradiated for 10 s at 405 nm to measure the *trans*-derivative or 2 min at 520 nm to measure the *cis*-derivative. Netropsin was prepared as DMSO stocks with the same concentrations, but not irradiated. Solutions were kept in the dark and the measurement performed in the absence of light. Small aliquots of the compound stocks were stepwise added and the fluorescence spectra recorded after an incubation time of 3 min. The corresponding spectra are buffer subtracted and show

the mean out of three independent measurements. The maximum at 530 nm was plotted against the added amount of compound. In the plot of the fluorescence intensity against the added compound concentration, the mean value and its standard deviation was calculated out of three independent measurements. The binding affinity was calculated using the program HypSpec and setting the number of reagents to 3, using the non-corrected measured spectra.

The following figures show the recorded mean fluorescence spectra of the FID titrations of TO and dsDNA<sub>RAT</sub> with  $F_4$ Azo-(PyDp)(PyOMe) (**3**) and  $F_4$ Azo-(PyDp)<sub>2</sub> (**2**) each in the *trans*- and *cis*-conformation and netropsin.

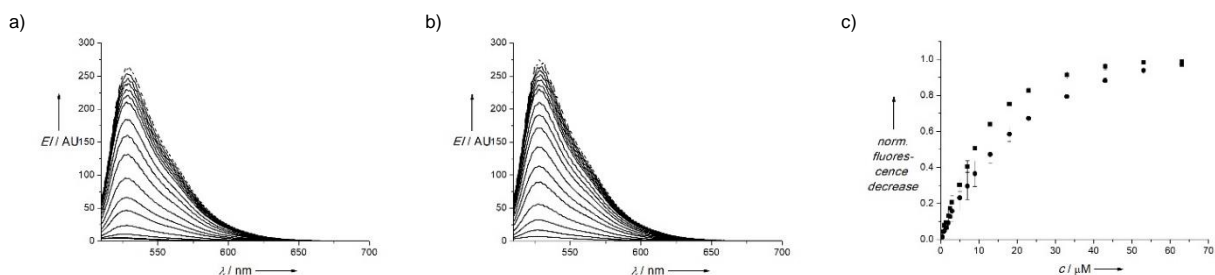


**Figure S26:** dashed line: mean fluorescence emission spectra of a 1  $\mu$ M TO and 6  $\mu$ M dsDNA<sub>RAT</sub> solution in 20 mM NaH<sub>2</sub>PO<sub>4</sub> pH 7.4, 100 mM NaCl. Solid lines: mean fluorescence emission spectra of solutions of a 6  $\mu$ M TO and 1  $\mu$ M dsDNA<sub>RAT</sub> solution in 20 mM NaH<sub>2</sub>PO<sub>4</sub> pH 7.4, 100 mM NaCl and increasing amounts of  $F_4$ Azo-(PyDp)(PyOMe) (**3**) in A) *trans*- conformation and B) *cis*- conformation. C) Fluorescence intensity maximum at 530 nm plotted against the concentration of added compound. Represented data are mean values and their standard deviation calculated from three independent experiments. Squares show the plot of  $F_4$ Azo-(PyDp)(PyOMe) (**3**) in the *trans*- conformation and circles in the *cis*- conformation.

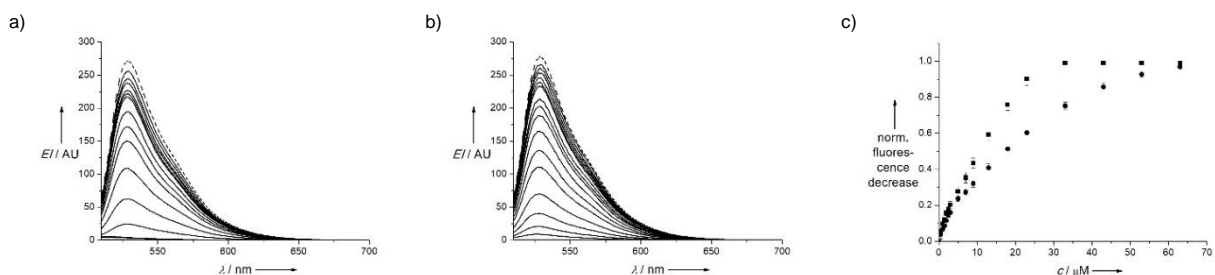


**Figure S27:** dashed line: mean fluorescence emission spectra of a 1  $\mu$ M TO and 6  $\mu$ M dsDNA<sub>RAT</sub> solution in 20 mM NaH<sub>2</sub>PO<sub>4</sub> pH 7.4, 100 mM NaCl. Solid lines: mean fluorescence emission spectra of solutions of a 6  $\mu$ M TO and 1  $\mu$ M dsDNA<sub>RAT</sub> solution in 20 mM NaH<sub>2</sub>PO<sub>4</sub> pH 7.4, 100 mM NaCl and increasing amounts of  $F_4$ Azo-(PyDp)<sub>2</sub> (**2**) in A) *trans*- conformation and B) *cis*-conformation. C) Fluorescence intensity maximum at 530 nm plotted against the concentration of added compound. Represented data are mean values and their standard deviation calculated from three independent experiments. Squares show the plot of  $F_4$ Azo-(PyDp)<sub>2</sub> (**2**) in the *trans*-conformation and circles in the *cis*- conformation.

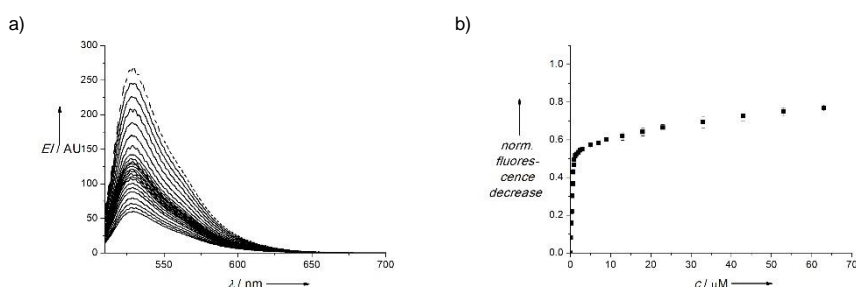


**Figure S28:** A) dashed line: mean fluorescence emission spectra of a 1  $\mu$ M TO and 6  $\mu$ M dsDNA<sub>RAT</sub> solution in 20 mM NaH<sub>2</sub>PO<sub>4</sub> pH 7.4, 100 mM NaCl. Solid lines: mean fluorescence emission spectra of solutions of a 6  $\mu$ M TO and 1  $\mu$ M dsDNA<sub>RAT</sub> solution in 20 mM NaH<sub>2</sub>PO<sub>4</sub> pH 7.4, 100 mM NaCl and increasing amounts of netropsin. B) Fluorescence intensity maximum at 530 nm plotted against the concentration of added compound. Represented data are mean values and their standard deviation calculated from three independent experiments.



Using the program HypSpec the corresponding binding affinities were calculated out of the non-corrected measured spectra and summarized in table S6 (Section Binding Affinity Calculation by HypSpec).

To check for the selectivity of the binder,  $F_4\text{Azo}-(\text{PyDp})_2$  (**2**) in the *trans*-conformation and netropsin were used in a FID titration with  $\text{dsDNA}_{\text{hGC}}$ . The following figures show the recorded mean fluorescence spectra.

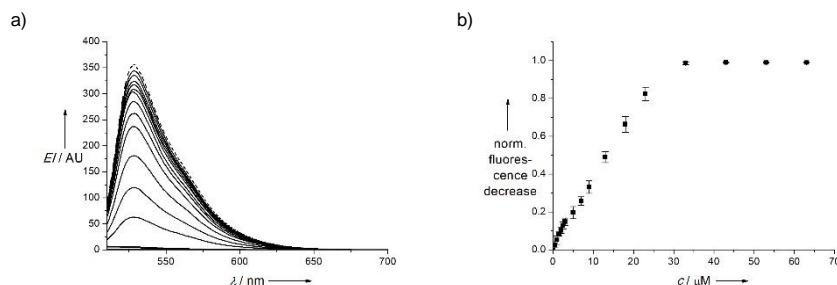


**Figure S29:** A) dashed line: mean fluorescence emission spectra of a  $1 \mu\text{M}$  TO and  $6 \mu\text{M}$   $\text{dsDNA}_{\text{hGC}}$  solution in  $20 \text{ mM NaH}_2\text{PO}_4$  pH 7.4,  $100 \text{ mM NaCl}$ . Solid lines: mean fluorescence emission spectra of solutions of a  $6 \mu\text{M}$  TO and  $1 \mu\text{M}$   $\text{dsDNA}_{\text{hGC}}$  solution in  $20 \text{ mM NaH}_2\text{PO}_4$  pH 7.4,  $100 \text{ mM NaCl}$  and increasing amounts of *trans*- $F_4\text{Azo}-(\text{PyDp})_2$ . B) Fluorescence intensity maximum at  $530 \text{ nm}$  plotted against the concentration of added compound. Represented data are mean values and their standard deviation calculated from three independent experiments.

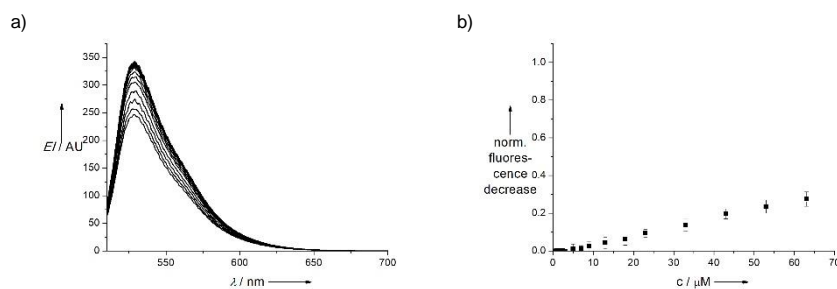


**Figure S30:** A) dashed line: mean fluorescence emission spectra of a  $1 \mu\text{M}$  TO and  $6 \mu\text{M}$   $\text{dsDNA}_{\text{hGC}}$  solution in  $20 \text{ mM NaH}_2\text{PO}_4$  pH 7.4,  $100 \text{ mM NaCl}$ . Solid lines: mean fluorescence emission spectra of solutions of a  $6 \mu\text{M}$  TO and  $1 \mu\text{M}$   $\text{dsDNA}_{\text{hGC}}$  solution in  $20 \text{ mM NaH}_2\text{PO}_4$  pH 7.4,  $100 \text{ mM NaCl}$  and increasing amounts of netropsin. B) Fluorescence intensity maximum at  $530 \text{ nm}$  plotted against the concentration of added compound. Represented data are mean values and their standard deviation calculated from three independent experiments.

Using the program HypSpec the corresponding binding affinities were calculated out of the non-corrected measured spectra and summarized in table S7 (Section Binding Affinity Calculation by HypSpec).

### Complex Formation Calculation by HySS2009

To have reliable results from the FID assays, all intercalation sites must be occupied with the minimal presence of free molecule in solution to maintain background fluorescence low and fluorescence decrease sufficiently large to give an adequate dynamic range.<sup>[xiv]</sup> To validate whether the used conditions during the FID are appropriated, we simulated how much percentage of TO-DNA complex is formed at the initial point of our FID assays by using the software Hyperquad Simulation and Speciation, HySS2009 (Protonic Software).<sup>[xv]</sup> We analyzed *calif thymus* DNA and DNA hairpins. The simulation mode was used, the number of reagents was set to 3 (TO, DNA, analyzed compound) and protons set to be absent. The input of the program was the concentration of the species and the binding constant of the TO-DNA complex, which was set to be constant. The binding affinity of the TO-DNA complex for the hairpin DNAs was determined experimentally (see table S3) and the one

for *calif thymus* DNA was  $K_D = 3.16 \mu\text{M}$ .<sup>[xvi]</sup> The percentage of formed complex was obtained from simulated graph. Table S3 shows the percentage of the *calif thymus* DNA-TO complex at different concentrations and ratios of both. We were not able to find suitable low micromolar concentrations resulting in a complex formation >95%. For the DNA hairpins, which are classically used in FID assays<sup>[xii]</sup> we were able to reach complex formations >95% with the conditions which were later applied. The complex percentages with the hairpin DNAs are shown in table S4.

**Table S3:** Simulated *calif thymus* DNA-TO complex percentages with different concentrations and ratios of *calif thymus* DNA and TO. The given percentages were simulated by using the program HySS2009.

DNA concentration [ $\mu\text{M}$ ]	TO concentration [ $\mu\text{M}$ ]	TO-DNA-complex
1	1	20%
	2	34%
	5	42%
	10	74%
	20	86%
5	1	11%
	2	22%
	5	46%
	10	68%
	20	83%
10	1	7%
	2	14%
	5	34%
	10	57%
	20	79%

**Table S4:** Simulated hairpin DNA-TO complex percentages with different concentrations and ratios of hairpin DNAs and TO. The given percentages were simulated by using the program HySS2009.

DNA concentration	TO concentration [ $\mu\text{M}$ ]	TO-DNA-complex
1 $\mu\text{M}$ <i>dsDNA</i> <sub>AT</sub>	1	78%
	6	>95%
1 $\mu\text{M}$ <i>dsDNA</i> <sub>GC</sub>	1	90%
	6	>95%

## Binding Affinity Calculation by HypSpec

Binding affinities were calculated by using the software HypSpec2014 (Protonic Software).<sup>[xvii]</sup> For the calculation of the binding affinities of TO to the hairpin DNAs, the number of reagents was set to 2 (TO and DNA), assuming a 1:1 binding mode. The fluorescence spectra of TO alone under the same conditions as described above was measured and due to its low intensity (see figure S31) only the spectra of the TO-DNA-complex was set to have a fluorescence spectra. All other spectra were assumed to be none. pH readings were set to be absent. The spectra of the fluorescence measurements, including the concentration of each reagent at each measurement point was prepared in an extra file and loaded into the program. The binding affinity of the TO-DNA-complex was refined, aiming the lowest sigma value, assuring that the molar absorbances are positive and the percentage of the formed complexes and free reagents make sense. Represented data are mean values calculated from three independent experiments. Figure S32 shows exemplary one out of the three binding affinity determination fits of HypSpec at a wavelength of the maximum of 530 nm. Table S5 summarized the determined binding affinities.

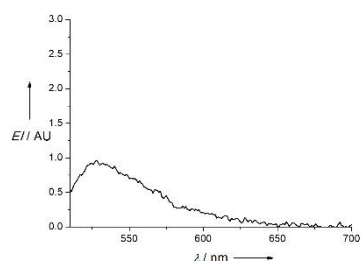


**Figure S31:** Mean fluorescence spectra of a 1  $\mu\text{M}$  solution of TO in 20 mM  $\text{NaH}_2\text{PO}_4$  100 mM NaCl pH 7.4.

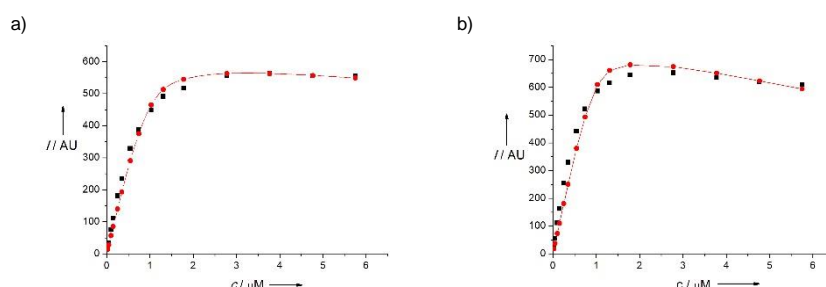


**Figure S32:** Representative plots of the binding affinity determination of TO to A)  $\text{dsDNA}_{\text{hAT}}$  and B)  $\text{dsDNA}_{\text{hGC}}$  at the wavelength of the maximum of 530 nm. Shown are in black the intensities experimentally determined at different concentrations of  $\text{dsDNA}$  and in red the corresponding fit performed by HypSpec.

**Table S5:** Determined mean  $K_D$ -values and standard deviations of TO to  $\text{dsDNA}_{\text{hAT}}$  and  $\text{dsDNA}_{\text{hGC}}$ .

	TO to $\text{dsDNA}_{\text{hAT}}$	TO to $\text{dsDNA}_{\text{hGC}}$
Mean $K_D$ value	$59.8 \pm 13.1$ nM	$11.6 \pm 3.8$ nM

For the calculation of the binding affinities of  $F_4\text{Azo}-(\text{PyDp})(\text{PyOme})$  (**3**) and  $F_4\text{Azo}-(\text{PyDp})_2$  (**2**) in the *trans*- and *cis*-conformation it was proceeded like described above, but the number of reagents was set to 3 (TO, DNA and compound **2** or **3**). Only the spectra of the TO-DNA-complex was set to have a fluorescence spectra, as the spectrum of TO alone is very low compared to the recorded ones (see fig. S321). The binding affinity of the TO-DNA complex was set to constant using the constant value, which was calculated above (table S5). The binding affinity of the binder-DNA complex was refined like

described above. For the case of the netropsin (**1**) the best fit was obtained using the data up to 2  $\mu\text{M}$  concentration; higher concentrations suggest different binding modes.

Represented data are mean values calculated from three independent experiments Figure S33 shows exemplary one out of the three binding affinity determination fits of HypSpec at a wavelength of the maximum of 530 nm. Table S6 and S7 summarized the determined binding affinities.

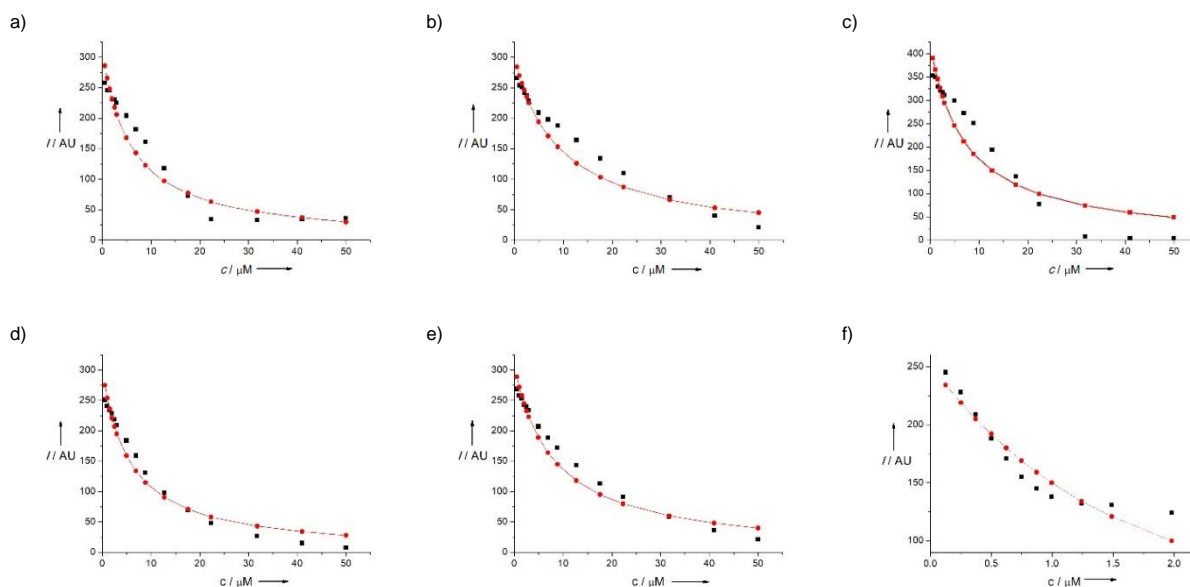


**Figure S33:** Representative plots of the FID binding affinity determination of A) *trans*- $F_4\text{Azo}-(\text{PyDp})_2$  to  $ds\text{DNA}_{\text{hAT}}$ , B) *cis*- $F_4\text{Azo}-(\text{PyDp})_2$  to  $ds\text{DNA}_{\text{hAT}}$ , C) *trans*- $F_4\text{Azo}-(\text{PyDp})_2$  to  $ds\text{DNA}_{\text{hGC}}$ , D) *trans*- $F_4\text{Azo}-(\text{PyDp})(\text{PyOMe})$  to  $ds\text{DNA}_{\text{hAT}}$ , E) *cis*- $F_4\text{Azo}-(\text{PyDp})(\text{PyOMe})$  to  $ds\text{DNA}_{\text{hAT}}$  and F) netropsin to  $ds\text{DNA}_{\text{hAT}}$ , at the wavelength of the maximum of 530 nm. Shown are in black the intensities experimentally determined at different concentrations of DNA and in red the corresponding fit performed by HypSpec.

**Table S6:** Determined mean  $K_D$ -values and standard deviations of  $F_4\text{Azo}-(\text{PyDp})_2$  (**2**) and  $F_4\text{Azo}-(\text{PyDp})(\text{PyOMe})$  (**3**) as their *trans*- and *cis*-isomer and netropsin to  $ds\text{DNA}_{\text{hAT}}$ . Binding affinities were calculated using the program HypSpec.

	$F_4\text{Azo}-(\text{PyDp})(\text{PyOMe})$ ( <b>3</b> )		$F_4\text{Azo}-(\text{PyDp})_2$ ( <b>2</b> )		netropsin
	<i>trans</i>	<i>cis</i>	<i>trans</i>	<i>cis</i>	
Mean $K_D$ value	$53.6 \pm 2.8$ nM	$81.5 \pm 6.6$ nM	$59.9 \pm 1.2$ nM	$108.3 \pm 14.9$ nM	$9.9 \pm 0.6$ nM

**Table S7:** Determined mean  $K_D$ -values and standard deviations of  $F_4\text{Azo}-(\text{PyDp})_2$  (**2**) and  $F_4\text{Azo}-(\text{PyDp})(\text{PyOMe})$  (**3**) in their *trans*- and *cis*-conformation to  $ds\text{DNA}_{\text{hGC}}$ . n.c. stands for non-calculated.

	$F_4\text{Azo}-(\text{PyDp})_2$ <i>trans</i>	netropsin
Mean $K_D$ -value	$13.3 \pm 0.6$ nM	n.c.

## Control Experiments with $F_4\text{Azo}-(\text{PyDp})_2$ (**2**)

To ensure the stability of the *trans*- and the *cis*-state of  $F_4\text{Azo}-(\text{PyDp})_2$  (**2**) during the measurements, we further performed several control experiments.

To show the stability of the isomers of the compound  $F_4\text{Azo}-(\text{PyDp})_2$  (**2**) during the FID measurement, a solution of 50  $\mu\text{M}$  of **2** in 20 mM  $\text{NaH}_2\text{PO}_4$  pH 7.4, 100 mM NaCl and DMSO (95:5) (total volume 500  $\mu\text{L}$ ) was irradiated in a cuvette for 10 s at 405 nm or 2 min at 520 nm to achieve the maximum *cis/trans* or *trans/cis* conversion. All solutions were kept in the dark and the measurements performed in the absence of light. The cuvette was placed into the fluorimeter and the temperature adjusted to 20  $^\circ\text{C}$ . One sample was taken and 30  $\mu\text{L}$  injected into the HPLC. The cuvette was placed back in the fluorimeter, which is used in the FID measurements. 5 fluorescence measurement points were performed and a new 30  $\mu\text{L}$  sample was taken to inject into the HPLC. The same procedure was repeated after 10 and 15 measurement points. Figure S34 illustrates the chromatograms, which show the stability of the *trans*- and the *cis*-state during the FID measurement.

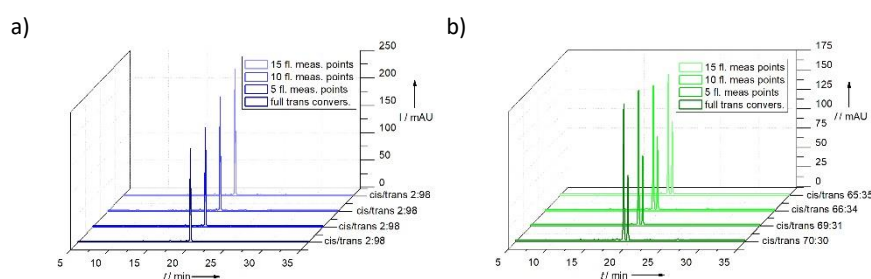


**Figure S34:** RP-HPLC chromatogram of  $F_4\text{Azo}-(\text{PyDp})_2$  (**2**) show the stability after irradiation at A) 405 nm for 10 s and B) 520 nm for 2 min and their corresponding *trans/cis*-ratio during the FID measurements. Samples were taken before the measurement and after 5, 10 and 15 measurement points. Represented data are a representative one of three measurements from independent experiments

To analyze the stability of both isomers of  $F_4\text{Azo}-(\text{PyDp})_2$  (**2**) during the gel mobility shift assay, a solution of 50  $\mu\text{M}$  of  $F_4\text{Azo}-(\text{PyDp})_2$  (**2**) 1X SDB (10 mM Tris, 1 mM EDTA pH 8.0, 50 mM NaCl) and DMSO (95:5) was irradiated for 10 s at 405 nm or 2 min at 520 nm to achieve the maximum *cis/trans* or *trans/cis* conversion. Afterwards it was stored in total darkness at r.t. and RP-HPLC chromatograms, under the same conditions as before were recorded after different time periods (figure S35).

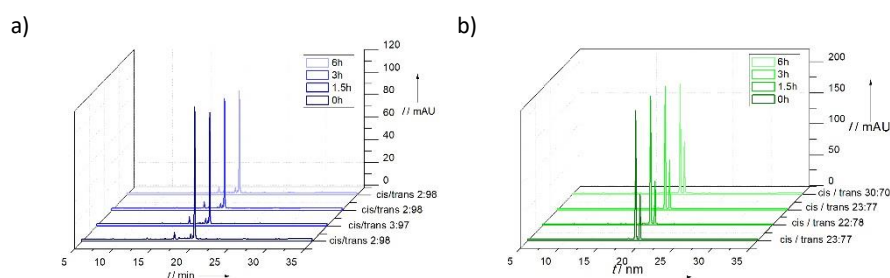


**Figure S35:** RP-HPLC chromatogram of  $F_4\text{Azo}-(\text{PyDp})_2$  (**2**) under mobility shift assay conditions show the dark stability after irradiation at A) 405 nm for 10 s and B) 520 nm for 2 min and their corresponding *trans/cis*-ratio after several time points. Represented data are a representative one of three measurements from independent experiments

To analyze the thermal stability of  $F_4\text{Azo}-(\text{PyDp})_2$  (**2**), a solution of 50  $\mu\text{M}$  of  $F_4\text{Azo}-(\text{PyDp})_2$  (**2**) in 10 mM Tris pH 7.4, 10 mM NaCl and DMSO (95:5) was irradiated for 30 s at 405 nm to achieve the maximum *cis/trans* conversion. Afterwards the temperature was increased with 0.5 $^\circ\text{C}/\text{min}$  and RP-HPLC chromatograms, under the same conditions as before, were recorded after different temperature points (figure S36).

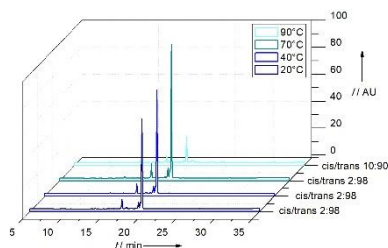


**Figure S36:** RP-HPLC chromatogram of  $F_4\text{Azo}-(\text{PyDp})_2$  (**2**) after several temperature points. Represented data are a representative one of three measurements from independent experiments

To check how much the DMSO influences the FID measurements, a FID measurement, like described above was performed, but adding DMSO instead of the DMSO stocks of the compounds to the solution of  $6\ \mu\text{M}$  of TO and a  $1\ \mu\text{M}$  of  $ds\text{DNA}_{\text{hAT}}$  in  $20\ \text{mM}\ \text{NaH}_2\text{PO}_4$  pH 7.4,  $100\ \text{mM}\ \text{NaCl}$  (total volume  $1\ \text{mL}$ ). The maximum at  $530\ \text{nm}$  was plotted against the added amount of compound, which equals the added DMSO amount. In the plot of the fluorescence intensity against the added compound concentration, the mean value and its standard deviation was calculated out of three independent measurements. The plots are shown in figure S37.

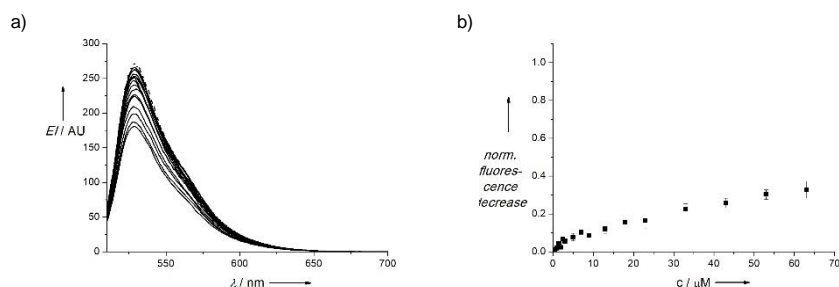


**Figure S37:** A) dashed line: mean fluorescence emission spectra of a  $1\ \mu\text{M}$  TO and  $6\ \mu\text{M}$   $ds\text{DNA}_{\text{hAT}}$  solution in  $20\ \text{mM}\ \text{NaH}_2\text{PO}_4$  pH 7.4,  $100\ \text{mM}\ \text{NaCl}$ . Solid lines: mean fluorescence emission spectra of solutions of a  $6\ \mu\text{M}$  TO and  $1\ \mu\text{M}$   $ds\text{DNA}_{\text{hAT}}$  solution in  $20\ \text{mM}\ \text{NaH}_2\text{PO}_4$  pH 7.4,  $100\ \text{mM}\ \text{NaCl}$  and increasing amounts of DMSO. B) Fluorescence intensity maximum at  $530\ \text{nm}$  plotted against the concentration of added compound, which equal the added amount of DMSO. Mean values with their standard deviation are shown. Represented data and standard deviations are calculated from three independent experiments

To rule out quenching effects, the influence of the added  $F_4\text{Azo}-(\text{COOH})_2$  (**5**) was checked, by following the same procedure like described for the FID titrations. The plots are shown in figure S38.

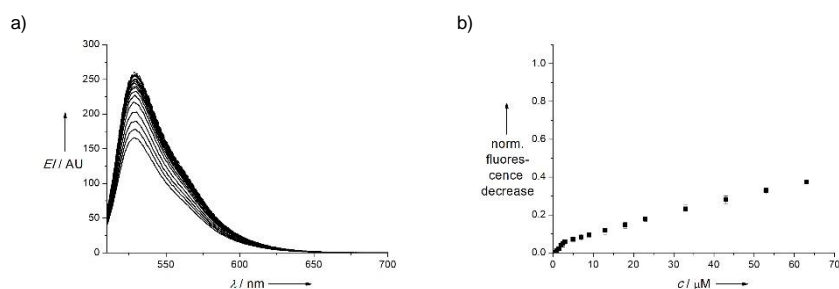


**Figure S38:** A) dashed line: mean fluorescence emission spectra of a  $1\ \mu\text{M}$  TO and  $6\ \mu\text{M}$   $ds\text{DNA}_{\text{hAT}}$  solution in  $20\ \text{mM}\ \text{NaH}_2\text{PO}_4$  pH 7.4,  $100\ \text{mM}\ \text{NaCl}$ . Solid lines: mean fluorescence emission spectra of solutions of a  $6\ \mu\text{M}$  TO and  $1\ \mu\text{M}$   $ds\text{DNA}_{\text{hAT}}$  solution in  $20\ \text{mM}\ \text{NaH}_2\text{PO}_4$  pH 7.4,  $100\ \text{mM}\ \text{NaCl}$  and increasing amounts of  $F_4\text{Azo}-(\text{COOH})_2$  (**5**). B) Fluorescence intensity maximum at  $530\ \text{nm}$  plotted against the concentration of added compound. Mean values with their standard deviation are shown. Represented data and standard deviations are calculated from three independent experiments.

## CD Experiments

For the characterization of the binding of compound  $F_4\text{Azo}-(\text{PyDp})_2$  (**2**) via circular dichroism, a solution of  $50\ \mu\text{M}$   $\text{dsDNA}_{\text{CT}}$  in  $20\ \text{mM}$   $\text{NaH}_2\text{PO}_4$  pH 7.4,  $100\ \text{mM}$   $\text{NaCl}$  was prepared in the corresponding cuvette and measured. Solutions of  $F_4\text{Azo}-(\text{PyDp})_2$  were prepared as a DMSO stock with a concentration of either  $250\ \mu\text{M}$  or  $1\ \text{mM}$ . These stock solutions were irradiated for  $10\ \text{s}$  at  $405\ \text{nm}$  to measure the *cis*-derivative or  $2\ \text{min}$  at  $520\ \text{nm}$  to measure the *trans*-derivative. Solutions were kept in the dark and the measurement performed in the absence of light. Small aliquots of the compound stocks were stepwise added and the fluorescence spectra recorded after an incubation time of  $3\ \text{min}$ . The corresponding spectra are buffer subtracted and show the mean out of two measurements. Figure S39 shows the CD spectra of the *calf thymus* DNA after buffer subtraction. Represented data are mean values calculated from two independent experiments.

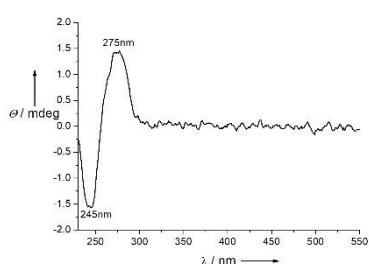


**Figure S39:** Buffer subtracted CD spectra of a  $50\ \mu\text{M}$  solution  $\text{dsDNA}_{\text{CT}}$  in  $20\ \text{mM}$   $\text{NaH}_2\text{PO}_4$  pH 7.4,  $100\ \text{mM}$   $\text{NaCl}$ . Represented data are mean values calculated from two independent experiments.

We further recorded the CD spectra of a solution of  $5\ \mu\text{M}$   $\text{dsDNA}_{\text{AT}}$  and  $\text{dsDNA}_{\text{GC}}$  in  $20\ \text{mM}$   $\text{NaH}_2\text{PO}_4$  pH 7.4,  $100\ \text{mM}$   $\text{NaCl}$ . The procedure were equal the described above. The corresponding spectra are buffer subtracted. Represented data are mean values calculated from two independent experiments (figure S40).

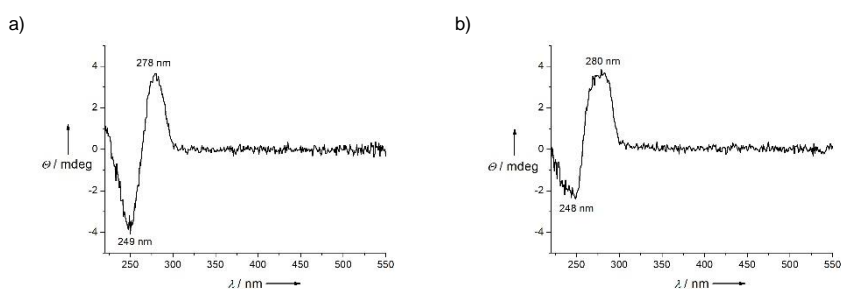


**Figure S40:** Buffer subtracted CD spectra of a  $5\ \mu\text{M}$  solution of A)  $\text{dsDNA}_{\text{AT}}$  and B)  $\text{dsDNA}_{\text{GC}}$  in  $20\ \text{mM}$   $\text{NaH}_2\text{PO}_4$  pH 7.4,  $100\ \text{mM}$   $\text{NaCl}$ . Represented data are mean values calculated from two independent experiments

We further titrated the DNA with increasing amount of spermine. The procedure and concentrations were equal the described above. The spectra were buffer subtracted (figure S41).

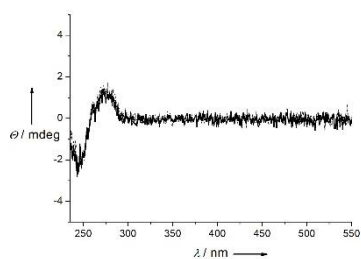


**Figure S41:** Buffer subtracted CD spectra of the titrations of a 50  $\mu\text{M}$  solution  $\text{dsDNA}_{\text{CT}}$  in 20 mM  $\text{NaH}_2\text{PO}_4$  pH 7.4, 100 mM NaCl with increasing amounts of spermine where the added equivalents are 0, 0.16, 0.5, 1.1 and 2.8 per mol of  $\text{dsDNA}_{\text{CT}}$ . Represented data are mean values calculated from two independent experiments.

## DLS Experiments

In order to study the effect of  $\text{trans-F}_4(\text{PyDp})_2$  (*trans-2*) and netropsin on the hydrodynamic diameter of the nucleosome and the nucleosomal DNA we performed DLS measurements. 100  $\mu\text{L}$  of a 2.00  $\mu\text{M}$  nucleosome stock or nucleosomal DNA in 10 mM Tris 1 mM EDTA pH 8.0 and 50 mM NaCl was prepared in the corresponding cuvette and measured. Stocks of  $\text{trans-F}_4(\text{PyDp})_2$  (*trans-2*, 1.41 mM, 2.94 mM and 5.88 mM) and netropsin (5.88 mM and 11.76 mM) in DMSO were prepared. For every addition, stock volumes of 1.25  $\mu\text{L}$  were stepwise added and the spectra recorded after an incubation time of 3 min. Represented data are a representative one of two measurements from independent experiments. Figure S42 shows the DLS signals of the nucleosome and the free nucleosomal DNA after incubation with different concentrations of netropsin.

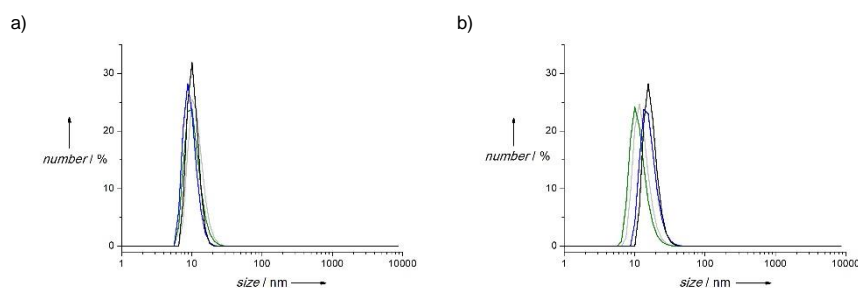


**Figure S42:** DLS signals of a solution of a) 2  $\mu\text{M}$  nucleosome and b) 2  $\mu\text{M}$  nucleosomal DNA in 10 mM Tris 1 mM EDTA pH 8.0 and 50 mM NaCl with increasing amounts of netropsin, where the equivalents in bp are 0 (grey), 0.25 (green), 0.5 (blue) and 1.0 (black) eq. Represented data are a representative one of two measurements from independent experiments.

For the precipitation by  $\text{MgCl}_2$ , the nucleosome stock was prepared in 3.5 mM Tris 0.35 mM EDTA pH 8.0. For every addition,  $\text{MgCl}_2$  stock volumes (62.5 mM and 125 mM) in MilliQ water of 1.25  $\mu\text{L}$  were stepwise added and the spectra recorded after an incubation time of 3 min.

To find out at which  $\text{MgCl}_2$  concentration the nucleosome precipitates, the solutions were analyzed before spectroscopically on a NanoDrop 2000 spectrometer (Thermo Scientific) by measuring the absorbance at 260 nm. Different amounts of  $\text{MgCl}_2$  were added, the samples incubated for 20 min at r.t. and centrifuged for 20 min at 14000 rpm at r.t. The absorbance at 260 nm of the supernatant was determined. Figure S43 shows the plot of the absorbance against the  $\text{MgCl}_2$  concentration.



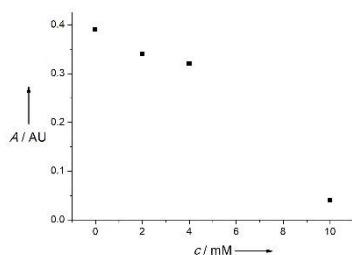


**Figure S43:** Determined absorbance at 260 nm of the nucleosome in 3.5 mM Tris 0.35 mM EDTA pH 8.0 after addition of different amounts of  $MgCl_2$ .

## Nucleosome Assays

For the nucleosome assays nucleosomal DNA was produced by polymerase chain reaction (PCR) or in a large scale by alkaline lysis and the histone octamers extracted from chicken blood. Both were assembled to nucleosomes using salt gradient dialysis. To study the effect of our molecules to the nucleosome, Mobility Shift Assays were performed.

### Nucleosomal DNA

The nucleosomal DNA (dsDNA<sub>601</sub>) was obtained in two different ways either in a small scale by PCR, which was used for the assembly of nucleosomes and the EMSA studies or in a big scale by a large scale plasmid preparation and further EcoRV-digest for the assembly of higher concentrated nucleosomes, which was used for the DLS experiments.

#### **Small scale:**

The Plasmid pGEM-3z/601 (Addgene plasmid # 26656, deposited by Jonathan Widom) was used as nucleosomal DNA template. This plasmid was replicated in DH5 alpha cells to facilitate long-term storage and sequencing, Thus, this plasmid was diluted from an initial concentration of 1.1  $\mu\text{g}/\mu\text{L}$  to a final one of 0.1  $\mu\text{g}/\mu\text{L}$ . 0.5  $\mu\text{L}$  of this solution (containing 50 ng of the plasmid) was added to 50  $\mu\text{L}$  of competent cells (*E. coli* DH5 alpha). The cells were then transferred into a 2 mm-gap cuvette for electroporation at 2.5 kV with a 5.8 ms pulse. 1 mL of LB medium (10 g/L tryptone, 5 g/L yeast extract, 10 g/L NaCl) was added to the cells immediately, and the cells were recovered by incubation at 37°C and 800 rpm for 1 h. Afterwards, cells were plated onto ampicillin containing agar, and grown overnight at 37°C. A streak of bacteria was transferred into 5 mL of LB medium containing ampicillin, and grown for 24 h at 37°C and 200 rpm. For long-term storage, 300  $\mu\text{L}$  glycerol (80%) was added to 700  $\mu\text{L}$  of the bacterial culture, mixed and shock-frozen in liquid nitrogen, after which the glycerol stock was stored at -80°C. The plasmid for amplification was performed from 4 mL of bacterial culture with a GenElute HP Plasmid Miniprep Kit (Sigma Aldrich) by following the manufacturer's instructions. The plasmid was eluted in 50  $\mu\text{L}$  millipore water. Afterwards, the plasmid was amplified by polymerase chain reaction (PCR). The reagents described in table S8 were mixed and the PCR run with the temperature program indicated in table S9. After finishing the PCR cycles, the products were purified using a GenElute PCR CleanUp Kit (Sigma Aldrich) and eluted with water. The DNA concentration was determined by NanoDrop. The yield from a 1 mL reaction volume was 24.2  $\mu\text{g}$  of DNA.

**Table S8:** List of reagents used for the polymerase chain reaction of Widom 601 DNA.

reagent	amount
HF buffer	1X
DMSO	3%
dNTPs	200 $\mu$ M each
forward primer	0.5 $\mu$ M
reverse primer	0.5 $\mu$ M
plasmid pGEM-3z/601	1 ng/ $\mu$ L
phusion polymerase	1 U / 50 $\mu$ L

**Table S9:** Temperature program for the polymerase chain reaction of Widom 601 DNA.

initial denaturation	98 °C / 30 s
denaturation	98 °C / 8 s
annealing	60 °C / 20 s
elongation	72 °C / 10 s
number of cycles	30
final elongation	72 °C / 4 min
	4 °C / hold

**Table S10:** primer sequences used in the polymerase chain reaction of Widom 601 DNA.

primer	sequence
forward primer	CCTGGAGAATCCCGGTGC
reverse primer	CAGGATGTATATATCTGACACGTGCC

### **Large scale:**

The Plasmid pUC-19/16x601 (deposited by Ji-Joon Song) was used as nucleosomal DNA template. This plasmid was replicated in DH5 alpha cells and grown on agar plates as described above. A streak of bacteria was transferred into 6 mL of LB medium containing ampicillin, and grown for o/n at 37°C and 200 rpm. 1 mL each was transferred into 1 L of LB medium containing ampicillin, and grown for o/n at 37°C and 200 rpm. The alkaline lysis plasmid preparation was performed following a protocol of Luger *et al.*<sup>[xviii]</sup> For the purification of the insert, 5.44 mg plasmid at a concentration of 1.0 µg/mL in 10 mM Tris HCl pH 8.5 10 mM MgCl<sub>2</sub> 100 mM KCl and 0.1 mg/mL BSA was treated with 700 U EcoRV (Thermo Fisher) at 37°C o/n and additional 70 U EcoRV for 7 h at 37°C. The purification was performed following the same protocol as described above. As a final purification step, gel filtration was included. SEC was performed on an Äkta FPLC system (Amersham Biosciences) equipped with pump P-920, mixer M-925, sample injection valve INV-907, fraction collector Frac-950, monitor UPC-900 and remote connector CU-950, controlled via Unicorn V5.0 software, using a Superdex 200 10/300 GL-column by GE Healthcare with a flow of 0.5 mL/min in 10 mM Tris 1 mM EDTA pH 8.0 and 150 mM NaCl. Detection was executed at a wavelength of 254 nm. The final product fractions were concentrated using a 10000 MWCO Amicon Ultra-15 Centrifugal Filter (Merck).

### **Native Polyacrylamide Gel Electrophoresis**

To analyze molecular weights of DNA and nucleosomes and to perform the EMSA, native polyacrylamide gel electrophoresis (native PAGE) was performed. Polyacrylamide gels were prepared as 5% gels in 0.5X TBE (10 mM Tris, 45 mM borate, 1 mM EDTA). Therefore, 1.875 µL 40% acrylamide solution (19 : 1, acrylamide : bisacrylamide) was diluted in 0.5X TBE to a total volume of 15 mL. The reaction was started by addition of 150 µL of an APS solution (10% in water) and 7.5 µL TEMED. The mixture was immediately poured into commercially available gel cassettes (glas, 1.00 mm, Biorad) placed in a Tetra Cell Casting Stand (Biorad), where wells were created by comb insertion. After complete polymerization (approximately 40 min), the comb was removed, the glass plates and wells washed with MilliQ water and the cassette placed into an electrophoresis chamber filled with 0.5X TBE. The wells were flushed with the running buffer by pipette. After adding 0.1 volumes glycerol to the samples, 20 µL containing 0.06 µM DNA or 0.27µM nucleosomes were loaded into the wells. The gel was run at 90 V for 40 min in a Ready Gel Cell (Biorad) using a Power Pac 300 (Biorad). The gel was poststained for 15 min in an ethidium bromide solution (50 µL of 0.1% solution in 100 mL 0.5X TBE buffer) and visualized under UV-light using a ChemiDoc MP Imaging System (BioRad).

### **Histone Octamer Extraction**

Chicken erythrocyte histone octamers were extracted from chicken blood, following a procedure of Smale *et al.*<sup>[xix]</sup> Divergent to the protocol, the lysis of the chicken erythrocyte nuclei and the final removal of the DNA was modified. The lysis of the chicken erythrocyte nuclei was performed by sonication 5 times 30 s at 30% with a Sonopuls Ultrasonic Homogenizer HD 2200 (Bandelin) with 2 min rest in between on ice until all clumps were converted into a homogeneous solution. To remove remaining DNA from the chicken histones, purification by hydroxyapatite chromatography did not yield in sufficiently pure histone octamers, but remaining DNA. For further purification, the solution was concentrated to 3.5 mg/mL and treated 3 times with 5 mL HT Gel (Biorad). Before use, the HT Gel was washed with wash buffer and then added to the histone solution. After incubation for 3 h at 4°C, the HT Gel was centrifuged and the supernatant collected. Purity was checked by 6% stacking and 15% running SDS-PAGE. Staining was performed with coomassie. To verify the absence of DNA, a gel performed in the same way was stained with EtBr. Figure S44 shows the SDS-PAGE of the final histone octamers.

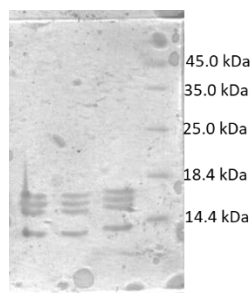


**Figure S44:** SDS-PAGE of the purified histone octamers.

### *Reconstitution of Nucleosome Core Particles*

Nucleosome core particles were reconstituted by salt gradient dialysis.<sup>[xix]</sup> A test assembly to experimentally verify the amount of chicken histones necessary. to nucleosome reconstitution was performed in a final concentration of 1  $\mu\text{g}$  DNA per 30  $\mu\text{L}$  reaction volume. Such DNA amount was mixed in 1X SDB (10 mM Tris, 1 mM EDTA pH 8.0 and 2 M NaCl) with chicken histone octamers at different concentrations: volumes between 9.75  $\mu\text{L}$  and 11.25  $\mu\text{L}$  in 0.25  $\mu\text{L}$  steps of a histone octamer stock of 47  $\mu\text{g}/\text{mL}$  were added. These solutions were given in dialysis cells (Nadir-dialysis tubing, cellulosehydrate, molecular weight cut-off: 10 – 20 kDa, Carl Roth) and dialyzed in 1X SDB for 1 h. The NaCl concentration was step-wise reduced (2 M  $\rightarrow$  1 M  $\rightarrow$  500 mM  $\rightarrow$  50 mM; dialysis time each 1 h) while keeping the other buffer components constant. The final dialysis step was performed for 16 h. The nucleosomes were taken out of the dialysis chamber, centrifuged at 10000 rpm for 2 min and the supernatant analyzed by EMSA. Figure S45 shows the native PAGE gel electrophoresis mobility shift assay (EMSA) analyzed by EtBr-staining of the test assembly, were conditions 3 were found to be the ideal conditions.

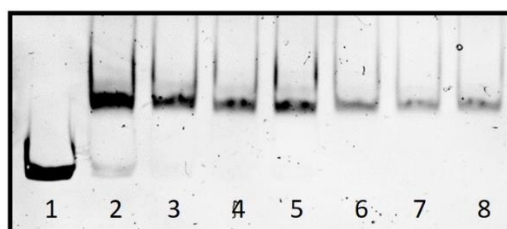


**Figure S45:** EMSA results showing the test assembly of the nucleosome. Experiments were carried out with 0.06  $\mu\text{M}$  of free DNA or 0.27  $\mu\text{M}$  of nucleosome. All experiments were carried out in the following buffer solution: 10 mM Tris, 1 mM EDTA pH 8.0 and 50 mM NaCl. 1 marks the free DNA, 2-8 mark the test assembly conditions of 1  $\mu\text{g}$  DNA mixed with 9.25, 9.50, 9.75, 10.00, 10.25, 10.50, 10.75  $\mu\text{L}$  of a histone octamer stock of 47  $\mu\text{g}/\text{mL}$ .

For the large scale nucleosome assembly, the optimal conditions from above were used to assemble enough nucleosomes. The assembly was performed under the same concentrations and conditions, but in a reaction volume of 600  $\mu\text{L}$ . Purity of the reconstituted nucleosome core particles was checked by EMSA.

For higher concentrated nucleosomes, which were necessary for DLS, nucleosomes were reconstituted at a concentration of 10  $\mu\text{g}$  DNA per 30  $\mu\text{L}$  reaction volume. The procedure matches the above described one.

## Gel Electrophoresis Mobility Shift Assay (EMSA)

To verify nucleosome stability after incubation with  $F_4\text{Azo-(PyDp)}_2$  (**2**) and  $F_4\text{Azo-(PyDp)(PyOMe)}$  (**3**) EMSA was performed. To 20  $\mu\text{L}$  of a 0.3  $\mu\text{M}$  solution of nucleosomes (40  $\mu\text{M}$  bp after DMSO stock addition) in 10 mM Tris pH 8.0, 1 mM EDTA and 50mM NaCl, stock solutions of the compound (**2**) or (**3**) were added in the dark. Stock solutions were prepared in DMSO and irradiated for 10 s at 405 nm or 2 min at 520 nm to obtain the *trans*- or *cis*-isomer. Solutions were kept in the dark and the measurement performed in the absence of daylight. Dilution rows were prepared and 2  $\mu\text{L}$  of these stocks added to the nucleosomes. The DMSO stocks had an end concentration of 1.76, 0.88, 0.44, 0.22, 0.11, 0.055, 0.028, 0.014 mM (this equals 4, 2, 1, 0.5, 0.25, 0.13, 0.06, 0.03 eq in bp). As controls, 55 nM free DNA (8  $\mu\text{M}$  bp) and 0.27  $\mu\text{M}$  nucleosome (40  $\mu\text{M}$  bp) in 10 mM Tris, 1 mM EDTA pH 8.0 and 50mM NaCl and DMSO (90:10) were prepared. The solutions were incubated for 3 h at r.t., 2  $\mu\text{L}$  glycerol added and the samples loaded on the native PAGE gel, run and stained with EtBr.

We further incubated the nucleosome with netropsin under the same conditions and same concentrations but without irradiation as well as using higher concentrations of netropsin with the DMSO stocks having an end concentration of 14.1, 7.04, 3.52, 1.76, 0.88 mM (this equals 32, 16, 8, 4, 2 eq in bp).

We further performed the nucleosome binding assays with in situ irradiation. For this purpose we chose conditions with a clear difference in nucleosome stability for the *trans*- and *cis*-isomer of  $F_4\text{Azo-(PyDp)}_2$  (**2**). Following the procedure described above we incubated two reference samples of 40  $\mu\text{M}$  bp nucleosome with 0.5 and 0.25 eq of  $F_4\text{Azo-(PyDp)}_2$  (**2**) in *trans*- and *cis*-conformation for 3 h. Another three nucleosome samples were incubated with 0.5, 0.25 and 0.13 eq of  $F_4\text{Azo-(PyDp)}_2$  (**2**) in *cis*-conformation for 1 h, irradiated these samples for 10 s at 405 nm and incubated for another 2 h.

To validate the influence of the irradiation during the in situ irradiation experiment on the nucleosome binding, we prepared samples of 40  $\mu\text{M}$  bp nucleosome in 20  $\mu\text{L}$  10 mM Tris, 1 mM EDTA pH 8.0 and 50mM NaCl and added 2  $\mu\text{L}$  of DMSO. The samples were irradiated for 1 s / 5 s / 10 s / 30 s / 1 min / 5 min at 405 nm and the EMSA performed.

## EMSA Controls of the DLS

During the measurements of the DLS, aliquots of each concentration steps were taken, to analyze them by EMSA. 2  $\mu$ L of the 2  $\mu$ M solution were mixed with 0.5  $\mu$ L of glycerol and loaded on a 5% native PAGE 0.5X TBE. The gel was performed like described above. Analysis after EtBr revealed the results presented in figure S46.

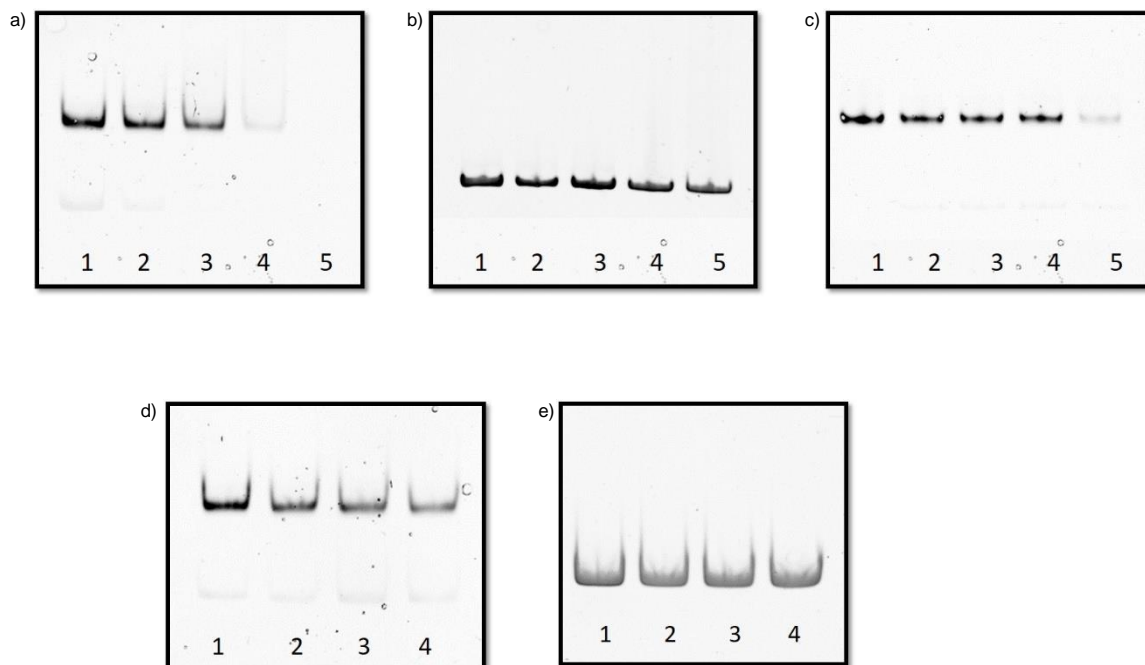


**Figure S46:** EMSA results showing the NCP after incubation with a) *trans*-F<sub>4</sub>(PyDp)<sub>2</sub>, c) MgCl<sub>2</sub> and d) netropsin at different concentrations and the free nucleosomal DNA after incubation with b) *trans*-F<sub>4</sub>(PyDp)<sub>2</sub> and e) netropsin at different concentrations. Molar equivalents of the compounds per mol bp are in a and b) 0, 0.06, 0.13, 0.25 and 0.50 eq; in d) and e) 0, 0.25, 0.50, 1.0 eq. MgCl<sub>2</sub> concentrations in c) are 0, 2.5, 3.75, 5.0, 10.0 mM. 2  $\mu$ L aliquots of the sample were taken during the DLS measurement, mixed with 0.5  $\mu$ L glycerol, run on a 5% native PAGE 0.5X TBE and stained with EtBr.

## References

---

- [i] H. E. Gottlieb, V. Kotlyar, A. Nudelman, *J. Org. Chem.* **1997**, *62*, 7512–7515.
- [ii] D. Bléger, J. Schwarz, A.M. Brouwer, S. Hecht, *J. Am. Chem. Soc.* **2012**, *134*, 20597-20600.
- [iii] C. Knie, M. Utecht, F. Zhao, H. Kulla, S. Kovalenko, A.M. Brouwer, P. Saalfrank, S. Hecht, D. Bléger, *Chem. Eur. J.* **2014**, *20*, 16492-16501.
- [iv] E. E. Baird, P. B. Dervan *J. Am. Chem. Soc.* **1996**, *118*, 6141-6146.
- [v] J.W. Lown, K. Krowicki, *J. Org. Chem.* **1985**, *50*, 3774 – 3779.
- [vi] C. Hotzel, A. Marotto, U. Pindur, *Eur. J. Med. Chem.* **2002**, *37*, 367 – 378.
- [vii] D. F. Swinehart, *J. Chem. Educ.* **1962**, *39*, 333–335.
- [viii] C.C. Trevithick-Sutton, L. Mikelsons, V. Filippenko, J.C. Scaiano, *Photochem. and Photobiol.* **2007**, *83*, 556-562.
- [ix] G. Kallansrud, B. Ward, *Anal. Biochem.* **1996**, *236*, 134–138.
- [x] <http://www.thermofisher.com/order/catalog/product/ND-2000>, 15.09.2018.
- [xi] Y.-W. Han, Y. Tsunaka, H. Yokota, T. Matsumoto, G. Kashiwazaki, H. Morinaga, K. Hashiya, T. Bando, H. Sugiyama, Y. Harada, *Biomater. Sci.* **2014**, *2*, 297-307.
- [xii] W.C. Tse, D.L. Boger, *Acc. Chem. Res.* **2004**, *37*, 61-69.
- [xiii] D.L. Boger, W.C. Tse, *Bioorg. Med. Chem.* **2001**, *9*, 2511.
- [xiv] D.L. Boger, B.E. Fink, S.R. Brunette, W.C. Tse, M.P. Hedrick *J. Am. Chem. Soc.* **2001**, *123*, 5878-5891.
- [xv] L. Alderighi, P.Gans, A. Ienco, D. Peters, A. Sabatini, A. Vacca, *Coord. Chem. Rev.* **1999**, *184*, 311-318.
- [xvi] J. Nygren, N. Svanvik, M. Kubista, *Biopolymers* **1998**, *46*, 39-51.
- [xvii] P. Gans, A. Sabatini, A. Vacca, *Talanta* **1996**, *43*, 1739-1753.
- [xviii] P.N. Pamela, N. Dyer, R.S. Edayathumangalam, C.L. White, Y. Bao, S. Chakravarthy, U.M. Muthurajan, K. Luger, *Methods Enzymol.* **2004**, *375*, 23-44.
- [xix] Transcriptional regulation in eukaryotes: concepts, strategies, and techniques, M.F. Carey, C.L. Peterson, S.T. Smale **2009**, CSHL Press, pp. 539-620.

## 4. Cumulative Part

### 4.2.1 Conclusion

In this chapter we described the synthesis and study of a novel photoswitchable DNA binder. The interaction of this *ortho*-tetra-fluoroazobenzene derivative with dsDNA as well as the nucleosome is visible-light controllable. To the best of our knowledge, it is the first example of a visible-light mediated nucleosome binder. Such compound may lay the ground for the development of new approaches to externally control epigenetic processes. However, the unspecific DNA binding of our compound would likely alter cell functions randomly. Therefore, future directions aim the design and study of sequence specific photocontrollable DNA and nucleosome binders to add specificity to our initial external control mechanism.

### 4.2.2 Further Developments and Outlook

After the photoswitchable nucleic-acid binder  $F_4\text{Azo}-(\text{PyDp})_2$  was analyzed towards its photophysical and DNA-binding properties, further studies were performed to gain a deeper insight into the process of nucleosome disassembly. Additional dynamic light scattering (DLS), size exclusion chromatography (SEC) measurements and gel electrophoresis were accomplished with  $F_4\text{Azo}-(\text{PyDp})_2$ , EtBr and netropsin. In the case of EtBr, the addition of increasing amounts of compound to the nucleosome resulted in a shift of the size distribution to larger particles (Figure 4.2.1 A). Still, these particles were smaller than the formed ones upon addition of  $F_4\text{Azo}-(\text{PyDp})_2$ . This is consistent with previous gel electrophoresis studies,<sup>[1,2]</sup> which suggested that the intercalation of EtBr into the DNA led to a structural distortion and, in turn, disassembly of the nucleosomes. In contrast to our new photoswitchable compound, EtBr formed smaller aggregates. Whereas addition of 0.5 eq of our described compound in the *trans*-form to 2  $\mu\text{M}$  nucleosome in 10 mM Tris 1 mM EDTA pH 8.0 and 50 mM NaCl formed particles >1000 nm, addition of EtBr under the same conditions, resulted in particles <100 nm. Addition of EtBr to free nucleosomal DNA (Figure 4.2.1 B) did not lead to differences in the DLS, as the induced structural distortion did not result in a detectable difference in the particle size. However, loading the DLS samples on a control electrophoresis gel, demonstrated increased smearing of the band upon higher EtBr concentrations which was congruent with the described structural distortion and formation of many different species through unspecific electrostatic interaction.<sup>[4]</sup> Subsequent addition of stoichiometric amount of histone octamers to the EtBr-DNA particles formed larger particles of 1000 nm. It was additionally tested, to reproduce the large agglomerates induced by the addition of  $F_4\text{Azo}-(\text{PyDp})_2$  to nucleosomes. By final addition of histones to  $F_4\text{Azo}-(\text{PyDp})_2$ -treated free DNA this could be proven. As seen in Figure 4.2.1 C, the difference upon histone addition to the DNA aggregates at the highest  $F_4\text{Azo}-(\text{PyDp})_2$  concentration of 1  $\mu\text{M}$ , did not show a significant difference. The reason might be that already dsDNA alone formed large aggregates at this binder concentration. Addition of  $F_4\text{Azo}-(\text{PyDp})_2$  in the *cis*-form, led to slightly smaller agglomerates than the one induced by the *trans* isomer. Irradiation of this samples for 10 s at 405 nm formed the *trans* isomer in situ and led to slightly higher aggregates than



## 4. Cumulative Part

before (Figure 4.2.1 D). This behavior is in agreement with the azobenzene trimethylammonium bromide surfactant AzoTAB, which compacts DNA ten times more in its *trans*-form than in its *cis*-form.<sup>[4]</sup>

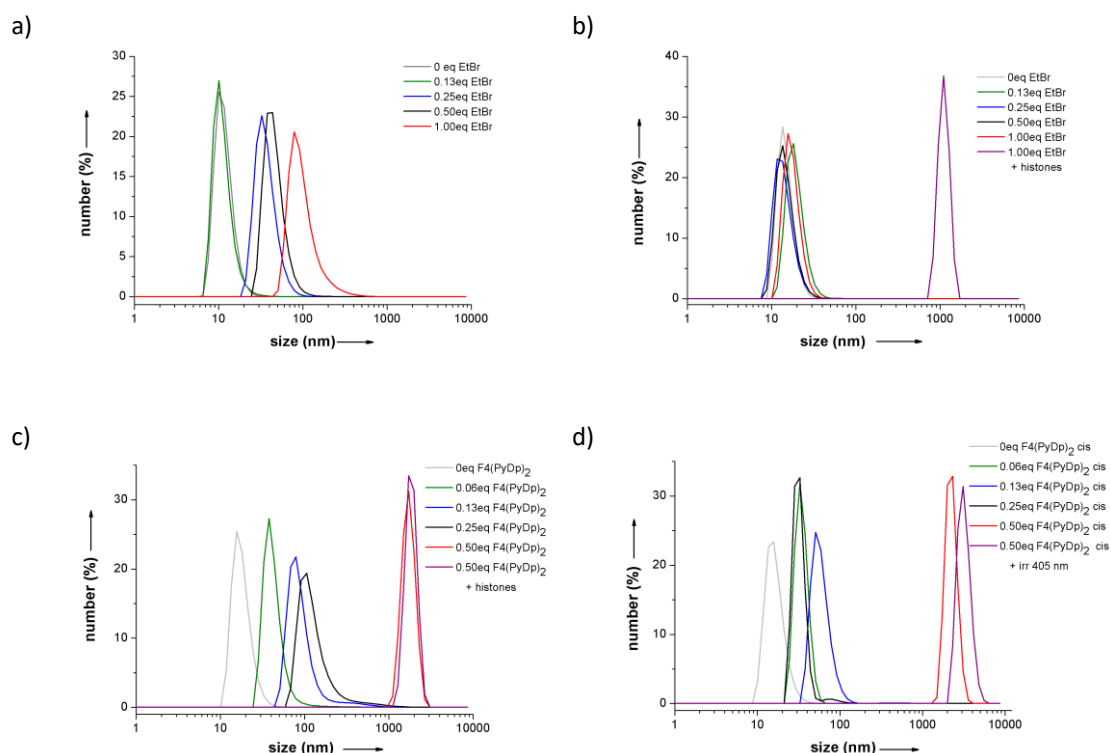


**Figure 4.2.1.** DLS signals of a solution of a) 2 μM nucleosome and b-d) 2 μM nucleosomal DNA in 10 mM Tris 1 mM EDTA pH 8.0 and 50 mM NaCl with in a and b) increasing amounts of EtBr, where the equivalents in bp are 0 (grey), 0.13 (green), 0.25 (blue), 0.50 (black) and 1.0 (red). In b) subsequently 1.0 eq histone octamer was added (violet). In c) increasing amounts of F<sub>4</sub>Azo-(PyDp)<sub>2</sub> as the *trans* isomer and in d) increasing amounts of F<sub>4</sub>Azo-(PyDp)<sub>2</sub> as the *cis* isomer were added, where the equivalents in bp are 0 (grey), 0.06 (green), 0.13 (blue), 0.25 (black) and 0.5 (red). In c) subsequently 1.0 eq histone octamer was added (violet) and in d) the sample was subsequently irradiated for 10 s at 405 nm (violet).

Moreover, size exclusion chromatography (SEC) measurements with nucleosomes after addition of F<sub>4</sub>Azo-(PyDp)<sub>2</sub>, EtBr and netropsin were recorded as an attempt for detecting the free nucleosomal DNA after addition of F<sub>4</sub>Azo-(PyDp)<sub>2</sub> to nucleosomes, and consequently verify the disassembly instead of simple precipitation. Whereas in the case of EtBr, the disassembly could be visualized by gel electrophoresis, this could not be shown for F<sub>4</sub>Azo-(PyDp)<sub>2</sub>. For SEC measurements, nucleosomes at a concentration of 2 μM in 10 mM Tris 1 mM EDTA pH 8.0 and 150 mM NaCl were centrifuged after one hour of addition of the corresponding compound to remove precipitated particles and the supernatant injected. After verifying that aprotinin has no effect on the nucleosomes, it was used as size standard by addition before the centrifugation. Before, it was shown experimentally that aprotinin has no effect on the nucleosomes. As seen in Figure 4.2.2, SEC is a less sensitive detection method than gel electrophoresis and DLS. Only traces of free DNA could be detected for the EtBr treated samples at a ratio of 0.50 eq. For all the other samples no free DNA could be detected, and in the case of F<sub>4</sub>Azo-(PyDp)<sub>2</sub> the difference between the *cis* and the *trans* isomer could not even be visualized. However, the

## 4. Cumulative Part

general trend of increasing aggregation, which led to precipitation, could be confirmed by the decreasing signal of the nucleosome in SEC and the increasing pellet size after centrifugation.

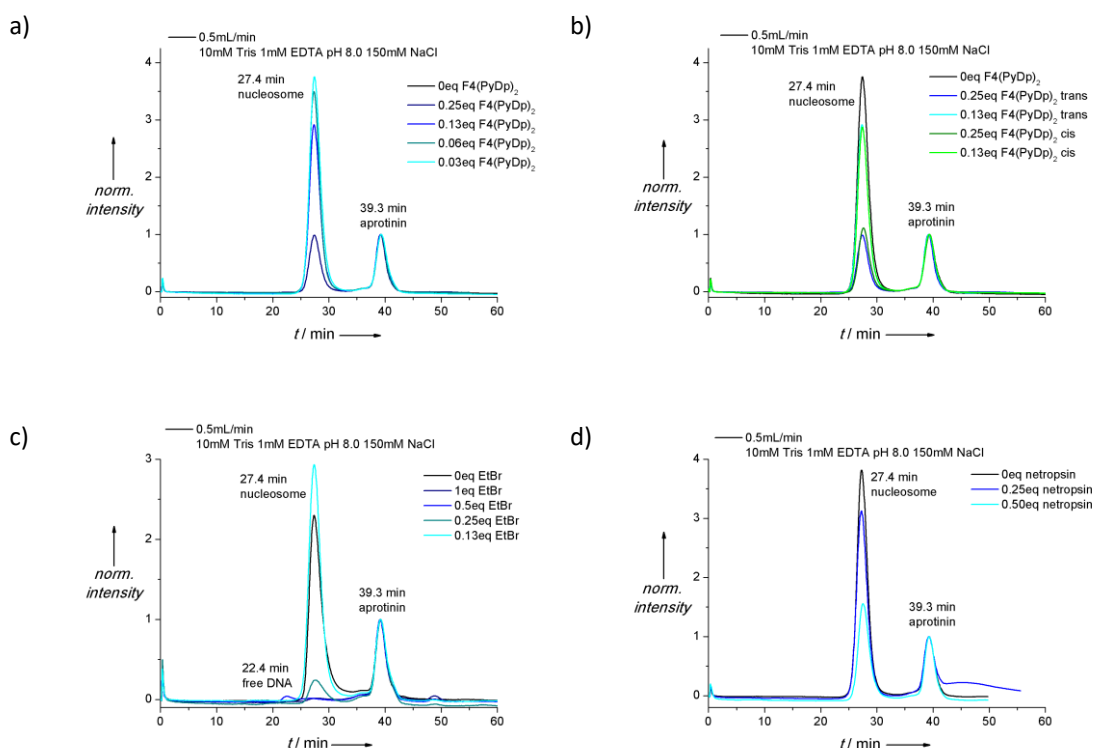


**Figure 4.2.2.** SEC chromatograms of a solution of 2  $\mu\text{M}$  nucleosome and 1 mg/mL aprotinin in 10 mM Tris 1 mM EDTA pH 8.0 and 150 mM NaCl after addition of increasing amounts of a and b)  $F_4\text{Azo}(\text{PyDp})_2$ , c) EtBr and d) netropsin, an incubation time of 1 h and subsequent injection of the supernatant after centrifugation. Added equivalents and the addition of the trans or cis isomer in a and b) are indicated in the corresponding chromatograms.

This additional development of the photoswitchable DNA binder points at visible-light mediated dynamic control of sequence-specific DNA binders. However, the Fmoc-approach based solid phase synthesis of pyrrole and imidazole polyamide hairpins is not compatible with base labile compounds such as *ortho*-fluoroazobenzene. It was possible to develop a compatible solid phase based procedure to access photoswitchable polyamide hairpins. The next chapter of this thesis presents the synthesis of new Mtt-protected monomers and their application in polyamide synthesis.

### 4.2.3 Author Contribution

The idea for this article resulted from the attempt to introduce real-time manipulation and dynamic control in pyrrole-imidazole (Pylm) polyamide hairpins. Due to low yields in solid phase approaches after introduction of *ortho*-fluoroazobenzene, and the need of intensive optimization, we decided to synthesize photoswitchable-netropsin derivatives in solution as a contingent plan. We foresaw that these molecules should be interesting *per se*. Therefore, I planned and synthesized different photoswitchable molecules based on the minor groove binder netropsin. The solution-synthesis approach provided us with sufficient amount to fully characterize the DNA binding. I planned and conducted all experiments

#### 4. Cumulative Part

myself. I analyzed the switching behavior of the new molecules by RP-HPLC, UV-vis spectroscopy and NMR. I improved and performed dsDNA binding studies, such as melting temperature analysis, fluorescence intercalation displacement measurements, circular dichroism titrations and UV-vis spectroscopy titrations. The binding affinities, I analyzed with the programs HypSpec and HySS. To conduct the experiments on the nucleosome, I optimized and performed the extraction of chicken erythrocyte histone octamers from chicken blood. Literature based protocols had to be modified and sharpened at different stages to yield sufficient amount of histones. The DNA, which wraps around the histone proteins to form the nucleosome, I initially produced in small scale by PCR and afterwards I conducted a large scale preparation by employing plasmids with multiple repeats of the Widom 601 sequence. Nucleosomes were assembled after being introduced by Dr. Karim Bouazoune (Institute of Molecular Biology and Tumor Research, Marburg). He supported us with fruitful discussions on biological issues during the manuscript preparation. I carried out all the electromobility shift assays and dynamic light scattering (DLS) measurements once instructed by Mathias Wojcik and Prof. Dr. Udo Bakowsky. Jun.-Prof. Dr. Olalla Vázquez had the role of corresponding author, was leading or involved in all the 14-role taxonomy for author-contribution assignment.<sup>[5]</sup>

Marburg,

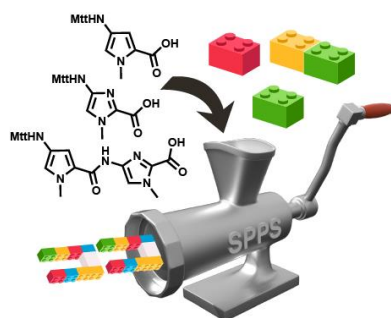
Jun. Prof. Dr. Olalla Vázquez

Benedikt Heinrich

#### 4.2.4 References

- [1] McMurray, C. T.; van Holde, K. E. Binding of Ethidium to the Nucleosome Core Particle. 1. Binding and Dissociation Reactions. *Biochemistry* **1991**, *30*, 23, 5631-5643.
- [2] McMurray, C. T.; van Holde, K. E. Binding of ethidium bromide causes dissociation of the nucleosome core particle. *Proc. Natl. Acad. Sci. U. S. A.* **1986**, *83*, 22, 8472-8476.
- [3] Liebler, E. K.; Diederichsen, U. From IHF Protein to Design and Synthesis of a Sequence-Specific DNA Bending Peptide. *Org. Lett.* **2004**, *6*, 17, 2893-2896.
- [4] Le Ny, A.-L. M.; Lee, C. T. Photoreversible DNA Condensation Using Light-Responsive Surfactants. *J. Am. Chem. Soc.* **2006**, *128*, 19, 6400-6408.
- [5] Allen, L.; Scott, J.; Brand, A.; Hlava, M.; Altman, M. Publishing: Credit where credit is due. *Nature* **2014**, *508*, 7496, 312-313.

### 4.3 4-Methyltrityl (Mtt)-Protected Pyrrole and Imidazole Building Blocks for Solid Phase Synthesis of DNA-Binding Polyamides



DNA-binding polyamides are synthetic oligomers consisting of the repetition of pyrrole/imidazole units with high specificity and affinity for double-stranded (ds)DNA. To increase the synthetic diversity of these compounds and their conjugates, we report a novel methodology based on 4-Methyltrityl (Mtt)-solid-phase peptide synthesis (SPPS), which is milder than the conventional Fmoc- and Boc-SPPS. Also, our building blocks are more synthetic accessible than the standard ones. We demonstrate the robustness of this approach by the preparation and study of a hairpin containing all precursors. Importantly, our strategy is orthogonal to Fmoc-SPPS, compatible with sensitive molecules and it could be readily automatized.

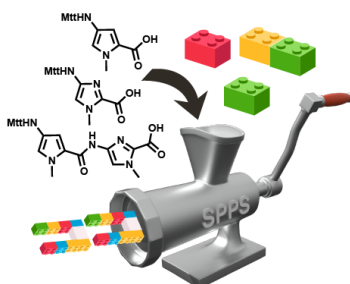
This chapter was submitted as: [Heinrich, B.;](#) Vázquez, O.\* 4-Methyltrityl (Mtt) Protected Pyrrole and Imidazole Building Blocks for Solid Phase Synthesis of DNA-Binding Polyamides. *Org. Lett.* **2019**, *manuscript under revision*. Upon acceptance of the article: Copyright American Chemical Society 2019. Material in this chapter was reproduced from the above mentioned reference with permission from the American Chemical Society.

# 4-Methyltrityl (Mtt)-Protected Pyrrole and Imidazole Building Blocks for Solid Phase Synthesis of DNA-Binding Polyamides

Benedikt Heinrich and Olalla Vázquez\*

Fachbereich Chemie, Philipps-Universität Marburg, Hans-Meerwein-Straße 4, 35043 Marburg

Supporting Information Placeholder



**ABSTRACT:** DNA-binding polyamides are synthetic oligomers consisting of the repetition of pyrrole/imidazole units with high specificity and affinity for double-stranded (ds)DNA. To increase the synthetic diversity of these compounds and their conjugates, we report a novel methodology based on 4-methyltrityl (Mtt)-solid-phase peptide synthesis (SPPS), which is milder than the conventional Fmoc- and Boc-SPPS. Also, our building blocks are more synthetic accessible than the standard ones. We demonstrate the robustness of this approach by the preparation and study of a hairpin containing all precursors. Importantly, our strategy is orthogonal to Fmoc-SPPS, compatible with sensitive molecules and it could be readily automatized.

The discovery of the dimeric interaction of distamycin A in the DNA minor groove<sup>1</sup> paved Dervan's way for the development of programmable hairpin pyrrole-imidazole (Py-Im) polyamides capable of specifically targeting double-stranded (ds) DNA sequences.<sup>2-7</sup> During the last two decades, the vast repertoire of synthesized polyamides has demonstrated the implementation of the Dervan hairpins as a powerful tool to interfere with DNA-dependent processes and their potential in medicine as therapeutics. Thus, these modular probes have been involved in gene expression,<sup>8-10</sup> epigenetic control,<sup>11-14</sup> DNA replication,<sup>15</sup> DNA overwinding/underwinding.<sup>16</sup> Furthermore, polyamides have been conjugated to fluorophores for screenings and diagnosis.<sup>17-20</sup> Currently, more complex functionalization has been reported to improve or diversify the use of these molecules<sup>10, 14, 21-22</sup>

Nowadays solid-phase peptide synthesis (SPPS) is the method of choice for the preparation of Py-Im polyamides. To date, the strategies have been restricted to the use of *tert*-butyloxycarbonyl (Boc)<sup>23-25</sup> and fluorenylmethyloxycarbonyl (Fmoc)<sup>24, 26</sup> protecting groups for the *N*-methyl pyrrole and *N*-methyl imidazole amino acids. However, the increasing complexity of the polyamide conjugates demands alternative approaches to expand the scope of the reactions as well as the functionalities used in the synthesis of hairpin batteries. For this purpose, we envisaged using the 4-methyl trityl (Mtt) group as the amino-protecting group of the pyrrole/imidazole building blocks (Figure 1). Indeed, Mtt-protecting group does not only allow milder deprotection procedures as the ones involved in Boc chemistry (2% TFA/DCM for Mtt versus 80% TFA/DCM/0.5M PhSH for Boc), but also it is orthogonal to the Fmoc-based synthesis as well as compatible with a broad palette of building reactions.<sup>27</sup>

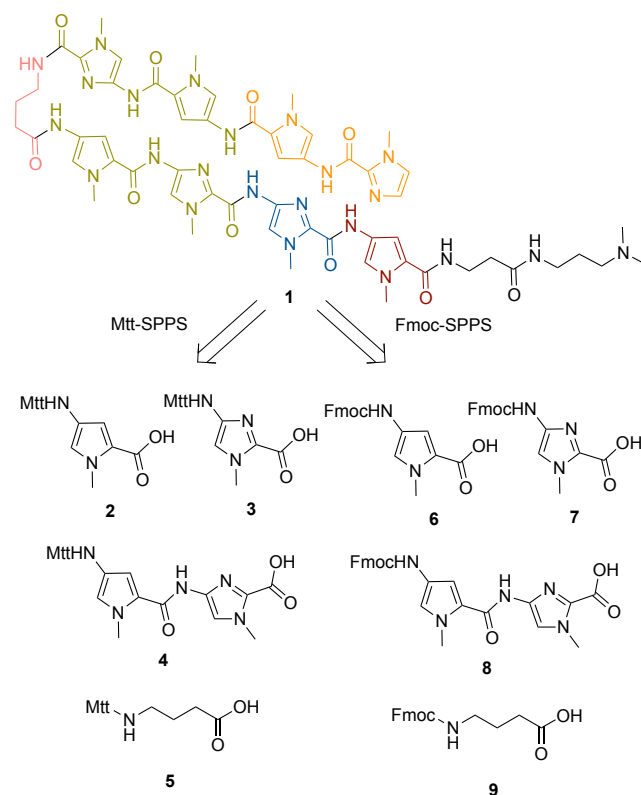
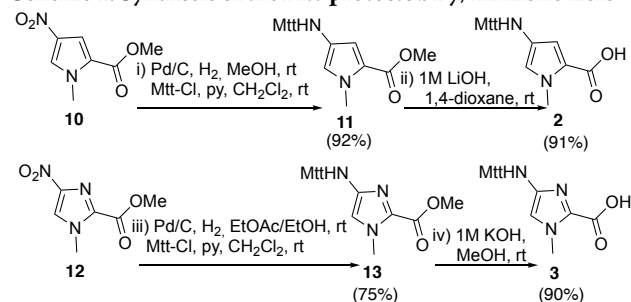


**Figure 1.** ImPyPyIm- $\gamma$ -PyImImPy- $\beta$ -Dp (**1**) prepared from Mtt-SPPS and Fmoc-SPPS. The colors highlight the different building blocks incorporated during the synthesis.

Herein, we describe the preparation of Mtt-protected pyrrole (**2**) and imidazole (**3**) monomers for Py-Im polyamide SPPS. Our straightforward synthesis results in higher yields than those used for the Fmoc- and Boc-analogues. In addition, we report the procedure to yield the dimeric Mtt-protected Py-Im building block (**4**) to counter the synthetic difficulty from the electron-deficient nucleophilic imidazole amine.<sup>28</sup> The Mtt-protected  $\gamma$ -aminobutyric acid (**5**) as a turn unit of the hairpin was synthesized too. We exemplified our approach with the synthesis of a Py-Im polyamide containing all our new Mtt-protected compounds: ImPyPyIm- $\gamma$ -PyImImPy- $\beta$ -Dp (**1**) and compared the synthetic efficiency of this methodology to that of the “conventional” Fmoc-SPPS.

The synthesis of the Mtt-protected precursors is shown in Scheme 1. The transformation of the corresponding commercially available NO<sub>2</sub>-Py/Im-OMe compounds (**10** and **12**, respectively) into the desired Mtt-protected Py/Im amino acids (**2** and **3**, respectively) was carried out in a two-step procedure. Thus, palladium-catalyzed reductive chemistry followed by in situ protection of the resulting amine with Mtt-Cl, and subsequent ester hydrolysis afforded the Mtt-protected monomers with excellent yields: 84% for Mtt-Py-OH (**2**) and 68% for Mtt-Im-OH (**3**). Comparing the synthetic accessibility of our Mtt-protected Py/Im monomers to that of the previous reported, ours have higher yield than the Boc- and Fmoc-protected analogues<sup>23,26</sup> (64% for Boc-Py-OH and 42% for Boc-Im-OH; 58% for Fmoc-Py-OH and 30% for Fmoc-Im-OH). Furthermore, both the Mtt-PyIm-OH dimer and Mtt- $\gamma$ -OH turn motif were prepared following the same reaction sequence from the previous reported NO<sub>2</sub>-PyIm-OMe<sup>23</sup> and the commercial available methyl  $\gamma$ -aminobutyrate hydrochloride (Scheme S4).

### Scheme 1. Synthesis of the Mtt-protected Py/Im monomers



The different  $\pi$ -electron density of the *N*-heterocycles entails a distinct reactivity towards the Mtt deprotection by using TFA. As expected, in the case of the electron-rich pyrrole the Mtt group was more acid-labile. Thus, in presence of 0.1% TFA for 3 min the removal of the protecting group of Mtt-Py-OMe was almost complete while the electron-deficient imidazole analogue required 2.0% TFA for 3 min for the efficient cleavage. In figure 2, a zoom-in of the <sup>1</sup>H-NMR spectra of the Mtt-methyl group in its bound and free form is shown at different TFA concentrations in CDCl<sub>3</sub>. At higher TFA concentrations, the signals are low-field shifted, which is in agreement with our observations of the <sup>1</sup>H-NMR spectra of Mtt-Cl under the same conditions (Figure S50) as well as reported trityl derivatives.<sup>29-30</sup> The two different peaks for the free Mtt-methyl group can be reasoned by an equilibrium with TFA (Figure 2a), which was described previously.<sup>31-32</sup>

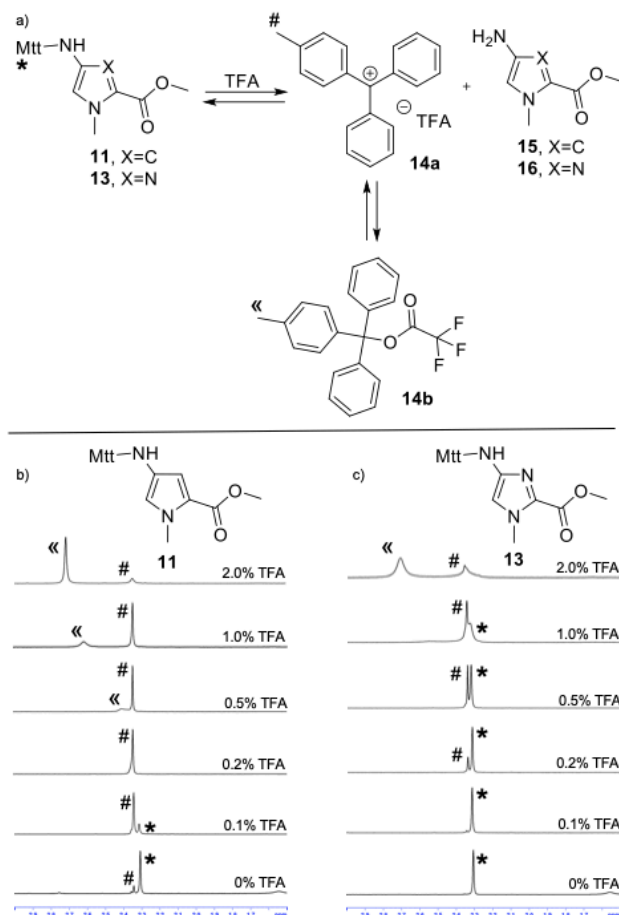


**Figure 2.** a) Reaction scheme of the Mtt deprotection; b) zoom-in of the aliphatic region of the <sup>1</sup>H-NMR spectra of Mtt-Py-OMe (**11**) and c) Mtt-Im-OMe (**13**) in CDCl<sub>3</sub> at 25°C after addition of different amounts of TFA and incubation for 3 min. The signals of the methyl of the Mtt-protecting group are marked in the scheme and the corresponding NMR spectra. The small free Mtt signal in b) at 0% TFA is due to acid traces in CDCl<sub>3</sub>.

For testing the applicability of our Mtt-protected compounds for Py-Im SPPS, we next synthesized a Dervan hairpin (ImPyPyIm- $\gamma$ -PyImImPy- $\beta$ -Dp, **1**) containing all of them (Figure 1). For comparison we prepared the same sequence using the Fmoc-protected compounds too. Our strategy offers a mild alternative to the current protocols, which must be particularly interesting for basic-sensitive conjugates and those susceptible to strong acidic conditions or nucleophilic attack. Along these lines, the conventional *N,N*-dimethylaminopropylamine (Dp) aminolysis used as final cleavage<sup>26</sup> (68 eq, 55 °C, 18 h) was exchange for a controlled amide bond formation in solution in both synthesis. The implementation of Mtt-SPPS was straightforward using the same coupling and capping conditions as the ones described in the Fmoc-SPPS<sup>9</sup> except the deprotection step. Thus, 2% TFA in CH<sub>2</sub>Cl<sub>2</sub> for 20 min served as a base-free alternative to release the reactive amine, instead of the 20% piperidine in DMF used in Fmoc-SPPS. The aromatic amine and the color of the pyrrole and imidazole prevent the use of both the ninhydrin<sup>33</sup> and the TNBS test<sup>34</sup> to monitoring the progress of the coupling reactions. However, stepwise cleavage of a sample of resin and reverse phase (RP)-HPLC analysis verified high yields till the incorporation of the turn amino acid (>95%) (Figure S64). We observed that, unlike the Fmoc- $\gamma$ -OH, the coupling of the Mtt- $\gamma$ -OH did not occur under the standard conditions: 4 eq Mtt- $\gamma$ -OH, 4 eq HATU, 12



eq DIPEA. NMR experiments revealed that the electron-rich protecting group Mtt increased the nucleophilicity of the secondary amine yielding the corresponding deactivated Mtt-butylolactam (Scheme S6, Figure S58-S63) in presence of HATU and DIPEA ( $pK_a = 10.75$ ).<sup>35</sup> Indeed, the acetylated polyamide starting material was the only product detected in the HPLC chromatogram (Figure S65a). However, the use of weaker bases such as NMM ( $pK_a = 7.38$ )<sup>36</sup> and pyridine ( $pK_a = 5.21$ )<sup>36</sup> reduced the intramolecular deactivation and allowed the successful coupling obtaining the desired product with 10% and 65% yield, respectively (Table 1, Entry B & C). Coupling with PyBOP increased the amount of desired product up-to 75% (Table 1, Entry G) and corroborated the general tendency observed with the different bases. Importantly, due to the Mtt orthogonality to Fmoc synthesis, the co-synthesis with Fmoc- $\gamma$ -OH was possible too.

**Table 1.** Tested conditions for the Mtt- $\gamma$ -OH (**5**) incorporation.<sup>a</sup>

#	coupling reagent	base	yield/%
A	4 eq HATU	12 eq DIPEA	<5
B	4 eq HATU	12 eq NMM	10
C	4 eq HATU	12 eq pyridine	65
D	4 eq HATU	8 eq pyridine	63
E	4 eq PyBOP	12 eq NMM	42
F	4 eq PyBOP	8 eq NMM	52
G	4 eq PyBOP	8 eq pyridine	75

<sup>a</sup> Reaction conditions: 4 eq Mtt- $\gamma$ -OH (0.3M in NMP), 4 eq coupling reagent and 8 or 12 eq base were pre-incubated for 3 min and coupled for 1 h. After capping, cleavage and HPLC analysis, yields were calculated by integration of the peak areas with an intensity >10% related to the highest peak in the chromatogram.

After the incorporation of the turn motif, the rest of the couplings proceeded as expected for both protocols. Once all the synthesis steps were completed, the Py-Im polyamide was cleaved from the resin, which resulted in a single peak in the RP-HPLC chromatogram (Figure S43 & S44). ImPyPyIm- $\gamma$ -PyImImPy- $\beta$ -COOH **35** yields were comparable via both methodologies. Dp was placed in solution at the C-terminus of the polyamide to increase the affinity (Scheme S5).<sup>25</sup>

Finally, we tested the affinity and specificity of ImPyPyIm- $\gamma$ -PyImImPy- $\beta$ -Dp (**1**) by thermal denaturation analysis. These spectroscopic measurements were performed on

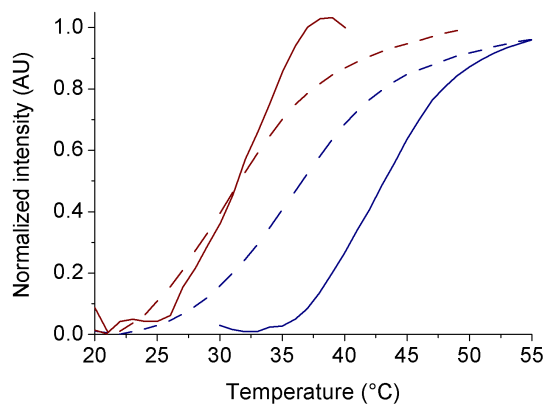


**Figure 3.** Melting curves of a 1  $\mu$ M duplex dsDNA solution in 10 mM  $\text{NaH}_2\text{PO}_4$  pH 7.4: 5'-GGTAGCCGTACC-3' (blue) or 5'-GGTAGCTGTACC-3' (red) in presence (straight) and absence (dotted) of 1.2  $\mu$ M ImPyPyIm- $\gamma$ -PyImImPy- $\beta$ -Dp (**1**).

12-mer dsDNA duplexes with the sequences 5' - GGTAGCCGTACC -3' and 5' - GGTAGCTGTACC -3', which contain the target and a single mismatch binding site, respectively. Satisfactorily, our Py-Im polyamide (**1**) has higher thermal stabilization value in the presence of the target dsDNA than the mismatched one ( $\Delta T_m$  of 6.6  $^\circ\text{C}$  versus  $\Delta T_m$  of 1  $^\circ\text{C}$ ).

In conclusion, this work represents the first report of Mtt-protected pyrrole and imidazole building blocks for DNA-binding polyamides. Our monomers are accessible with the higher yields than those use in the conventional Boc- and Fmoc-SPPS. We demonstrate the utility of this methodology by the synthesis and study of a DNA-binding hairpin bearing all types of Mtt-protected compounds needed. This approach is both orthogonal to Fmoc-SPPS and compatible to sensitive groups. Therefore, we foresee that our Mtt-SPPS will increase the synthetic diversity in Py-Im polyamide chemistry affording novel bifunctional polyamide conjugates. In addition, it could be readily adapted to automated synthesis.

## ASSOCIATED CONTENT

### Supporting Information

Experimental procedures, spectroscopic and analytical data of all new compounds are provided as well as additional experiments. The Supporting Information is available free of charge on the ACS Publications website.

## AUTHOR INFORMATION

### Corresponding Author

\* E-mail: [olalla.vazquez@staff.uni-marburg.de](mailto:olalla.vazquez@staff.uni-marburg.de)

### ORCID

Benedikt Heinrich: 0000-0002-9074-5983

Olalla Vázquez: 0000-0002-7555-1865

### Notes

The authors declare no competing financial interest.

## ACKNOWLEDGMENT

We thank Abbas Sajediabkenar for his contribution in the synthesis of several starting materials. We further thank Prof. Dr. Armin Geyer and Dr. Xiulan Xie for the helpful NMR discussions. We acknowledge the Deutsche Forschungsgemeinschaft (DFG) for co-financing the AccuTOF GCv 4G (JEOL) Time of Flight (TOF) mass spectrometer (grant: INST 160/622-1 FUGG to U. Linne).

## REFERENCE

1. Pelton, J. G.; Wemmer, D. E., *Proc Natl Acad Sci US A* **1989**, *86* (15), 5723-7.
2. Dervan, P. B., *Bioorg Med Chem* **2001**, *9* (9), 2215-35.
3. Dervan, P. B.; Burli, R. W., *Curr Opin Chem Biol* **1999**, *3* (6), 688-93.
4. White, S.; Szewczyk, J. W.; Turner, J. M.; Baird, E. E.; Dervan, P. B., *Nature* **1998**, *391* (6666), 468-71.
5. Yu, Z.; Pandian, G. N.; Hidaka, T.; Sugiyama, H., *Adv Drug Deliv Rev* **2019**, *147*, 66-85
6. Kawamoto, Y.; Bando, T.; Sugiyama, H., *Bioorg Med Chem* **2018**, *26* (8), 1393-1411.
7. Blackledge, M. S.; Melander, C., *Bioorg Med Chem* **2013**, *21* (20), 6101-14.
8. Hargrove, A. E.; Martinez, T. F.; Hare, A. A.; Kurmis, A. A.; Phillips, J. W.; Sud, S.; Pienta, K. J.; Dervan, P. B., *PLoS One* **2015**, *10* (11), e0143161.

9. Yang, F.; Nickols, N. G.; Li, B. C.; Marinov, G. K.; Said, J. W.; Dervan, P. B., *Proc Natl Acad Sci U S A* **2013**, *110* (5), 1863-8.
10. Yu, Z.; Guo, C.; Wei, Y.; Hashiya, K.; Bando, T.; Sugiyama, H., *J Am Chem Soc* **2018**, *140* (7), 2426-2429.
11. Taniguchi, J.; Feng, Y.; Pandian, G. N.; Hashiya, F.; Hidaka, T.; Hashiya, K.; Park, S.; Bando, T.; Ito, S.; Sugiyama, H., *J Am Chem Soc* **2018**, *140* (23), 7108-7115.
12. Pandian, G. N.; Taniguchi, J.; Junetha, S.; Sato, S.; Han, L.; Saha, A.; AnandhaKumar, C.; Bando, T.; Nagase, H.; Vaijyanthi, T.; Taylor, R. D.; Sugiyama, H., *Sci Rep* **2014**, *4*, 3843.
13. Patel, S.; Pongkulapa, T.; Yin, P. T.; Pandian, G. N.; Rathnam, C.; Bando, T.; Vaijyanthi, T.; Sugiyama, H.; Lee, K. B., *J Am Chem Soc* **2015**, *137* (14), 4598-601.
14. Pandian, G. N.; Shinohara, K.; Ohtsuki, A.; Nakano, Y.; Masafumi, M.; Bando, T.; Nagase, H.; Yamada, Y.; Watanabe, A.; Terada, N.; Sato, S.; Morinaga, H.; Sugiyama, H., *ChemBiochem* **2011**, *12* (18), 2822-8.
15. Martinez, T. F.; Phillips, J. W.; Karanja, K. K.; Polaczek, P.; Wang, C. M.; Li, B. C.; Campbell, J. L.; Dervan, P. B., *Nucleic Acids Res* **2014**, *42* (18), 11546-59.
16. Wang, C. C.; Dervan, P. B., *J Am Chem Soc* **2001**, *123* (36), 8657-61.
17. Olenyuk, B. Z.; Zhang, G. J.; Klco, J. M.; Nickols, N. G.; Kaelin, W. G., Jr.; Dervan, P. B., *Proc Natl Acad Sci U S A* **2004**, *101* (48), 16768-73.
18. Han, Y. W.; Sugiyama, H.; Harada, Y., *Biomater Sci* **2016**, *4* (3), 391-9.
19. Chenoweth, D. M.; Viger, A.; Dervan, P. B., *J Am Chem Soc* **2007**, *129* (8), 2216-7.
20. Bando, T.; Fujimoto, J.; Minoshima, M.; Shinohara, K.; Sasaki, S.; Kashiwazaki, G.; Mizumura, M.; Sugiyama, H., *Bioorg Med Chem* **2007**, *15* (22), 6937-42.
21. Han, Y.-W.; Tsunaka, Y.; Yokota, H.; Matsumoto, T.; Kashiwazaki, G.; Morinaga, H.; Hashiya, K.; Bando, T.; Sugiyama, H.; Harada, Y., *Biomaterials Science* **2014**, *2* (3), 297-307.
22. Minoshima, M.; Bando, T.; Shinohara, K.; Sugiyama, H., *Nucleic Acids Symp Ser (Oxf)* **2009**, (53), 69-70.
23. Baird, E. E.; Dervan, P. B., *Journal of the American Chemical Society* **1996**, *118* (26), 6141-6146.
24. Fang, L.; Yao, G.; Pan, Z.; Wu, C.; Wang, H. S.; Burley, G. A.; Su, W., *Org Lett* **2015**, *17* (1), 158-61.
25. Belitsky, J. M.; Nguyen, D. H.; Wurtz, N. R.; Dervan, P. B., *Bioorg Med Chem* **2002**, *10* (8), 2767-74.
26. Wurtz, N. R.; Turner, J. M.; Baird, E. E.; Dervan, P. B., *Org Lett* **2001**, *3* (8), 1201-3.
27. Chouikhi, D.; Ciobanu, M.; Zambaldo, C.; Duplan, V.; Barluenga, S.; Winssinger, N., *Chemistry* **2012**, *18* (40), 12698-704.
28. Wetzler, M.; Wemmer, D. E., *Org Lett* **2010**, *12* (15), 3488-90.
29. Hojo, M.; Ueda, T.; Yamasaki, M., *J Org Chem* **1999**, *64* (13), 4939-4942.
30. Kobayashi, N., *B Chem Soc Jpn* **2002**, *75* (1), 1-19.
31. Shahsavari, S. C., J.; Wigstrom, T.; Gooding, J.; Gauronskas, A.; Fang, S., *Tetrahedron Lett.* **2016**, *57* (34), 3877-80.
32. Feigel, M. K., H., *Angew. Chem. Int. Ed. Engl.* **1977**, *16* (4), 256-7.
33. Sarin, V. K.; Kent, S. B. H.; Tam, J. P.; Merrifield, R. B., *Anal Biochem* **1981**, *117* (1), 147-157.
34. Hancock, W. S.; Battersby, J. E., *Anal Biochem* **1976**, *71* (1), 260-4.
35. Boncel, S. S., K.; Hefczyc, Barbara; Walczak, K. Z., *Beilstein J. Org. Chem.* **2011**, *7*, 173-8.
36. Carpino, L. A. E.-F., A., *Tetrahedron* **1999**, *55* (22), 6813-30.



**4-Methyltrityl (Mtt)-Protected Pyrrole and Imidazole Building Blocks for Solid Phase Synthesis of DNA-Binding Polyamides**

Benedikt Heinrich and Olalla Vázquez

## TABLE OF CONTENT

<b>ABBREVIATIONS</b> .....	169
<b>General Methods and Materials</b> .....	171
<i>Nuclear Magnetic Resonance Spectroscopy (NMR)</i> .....	171
<i>High Performance Liquid Chromatography (HPLC)</i> .....	171
<i>Mass Spectrometry</i> .....	172
<i>UV-Vis Spectroscopy</i> .....	172
<i>FT-IR Spectroscopy</i> .....	172
<b>Synthesis in Solution</b> .....	173
<i>Synthesis of Pyrrole Monomers Nitro-Py-OMe (10), Fmoc-Py-OH (6) and Fmoc-PyIm-OH(8)</i> .....	173
<i>Synthesis of Imidazole Monomer Fmoc-Im-OH (7)</i> .....	176
<i>Synthesis of ImPy-OH (31) and Fmoc-<math>\gamma</math>-OH (9)</i> .....	179
<i>Synthesis of Mtt-building blocks</i> .....	181
<b>NMR and IR spectra of new compounds</b> .....	185
<b>Solid Phase Peptide Synthesis</b> .....	206
<i>Manual Solid Phase Protocol for Peptide Synthesis</i> .....	206
<i>Synthesis and Characterization Data of the Polyamides</i> .....	207
<b>Concentration Determination</b> .....	209
<b>Thermal Melting Analysis</b> .....	210
<b>Stability of the Mtt-building blocks</b> .....	211
<b>Additional Experiments</b> .....	217
<i>Synthesis of Mtt-butyrolactam (36)</i> .....	217
<i>Test Implementation of Mtt-<math>\gamma</math>-OH</i> .....	221
<b>References</b> .....	222

## ABBREVIATIONS

A	adenine, absorbance
aq	aqueous
arom	aromatic
AU	arbitrary units
Boc	<i>tert</i> -butyloxycarbonyl
br	broad
<i>c</i>	concentration
C	cytosine
calcd	calculated
CI	chemical ionization
COSY	correlation spectroscopy
d	doublet
DCC	<i>N,N'</i> -dicyclohexylcarbodiimide
DIC	<i>N,N'</i> -diisopropylcarbodiimide
DIPEA	<i>N,N'</i> -diisopropylethylamine
DMAP	4-(dimethylamino)pyridine
Dp	<i>N,N</i> -dimethyl-1,3-diaminopropane
dsDNA	double-stranded DNA
EI	electron ionization
ESI	electrospray ionization
Fmoc	fluorenylmethyloxycarbonyl
FT-IR	fourier-transform infrared spectroscopy
G	guanine
HATU	hexafluorophosphate azobenzotriazole tetramethyl uronium
HMBC	heteronuclear multiple bond correlation spectroscopy
HOBt	1-hydroxybenzotriazole
HPLC	high performance liquid chromatography
HRMS	high resolution mass spectrometry
HSQC	heteronuclear single quantum correlation spectroscopy
Im	imidazole
<i>J</i>	coupling constant

l	length
m	multiplet, medium
Mtt	4-methyltrityl
NMM	4-methylmorpholine
NMR	nuclear magnetic resonance
OSU	<i>N</i> -hydroxysuccinimide
PHB	4-hydroxybenzyl
PhSH	thiophenol
ppm	parts per million
Py	pyrrole
PyBOP	(benzotriazol-1-yloxy)tripyrrolidinophosphonium hexafluorophosphate
q	quartet
$R_f$	retention factor
RP	reverse-phase
s	singlet, strong
SPPS	solid phase peptide synthesis
ss	single stranded
t	triplet
T	thymine
TG	tentagel
$T_m$	melting temperature
TMS	trimethylsilyl
$t_R$	retention time
UV	ultraviolet
Vis	visible
w	weak
$\beta$	$\beta$ -alanine
$\gamma$	$\gamma$ -aminobutyric acid
$\delta$	chemical shift
$\varepsilon$	extinction coefficient

## General Methods and Materials

All commercially purchased reagents were used from the following companies without further purification: trichloroacetyl chloride, *N*-methylimidazole, fuming nitric acid, thiophenol, 1-hydroxybenzotriazole hydrate, PyBOP, DMSO for molecular biology and ssDNAs from Sigma Aldrich (USA); sodium hydroxide, potassium hydroxide and concentrated nitric acid from Merck (Germany); DMF peptide grade, HATU, piperidine and NMP from Iris Biotech (Germany); DIPEA, acetic anhydride and Fmoc-Cl from Carl Roth (Germany); Pd/C, 4-methylmorpholine, 4-aminobutanoic acid and *N,N*-dimethyl-1,3-diaminopropane from Alfa Aesar (USA); pyridine, triethylamine, cesium carbonate, acetonitrile and sodium chloride from VWR (USA); 4-methyltrityl chloride, FmocOSu and (Boc)<sub>2</sub>O from Fluorochem (UK); OxymaPure and DIC from Carbolution (Germany); *N*-methyl pyrrole and benzyl bromide from Acros Organics (Belgium); trifluoroacetic acid from abcr (Germany); dimethylamino pyridine and *N,N'*-dicyclohexylcarbodiimide from Fluka (USA); sodium bicarbonate from PanReac AppliChem (Germany), reverse phase filter cartridges Oasis HLB 20cc from Waters (Germany) and TG R PHB resin from Rapp Polymere (Germany). Water was purified with a milli-Q Ultra Pure Water Purification System (TKA, Germany). For aqueous solutions for reaction deionized water was used. The buffer for thermal melting analysis was prepared with milli-Q water.

### *Nuclear Magnetic Resonance Spectroscopy (NMR)*

All NMR spectra were automatically measured at 300 K either in a Bruker AV III HD 300 MHz at a frequency of 300 MHz (<sup>1</sup>H) or 75 MHz (<sup>13</sup>C) or in a Bruker AV III HD 500 MHz at a frequency of 500 MHz (<sup>1</sup>H) or 125 MHz (<sup>13</sup>C). All chemical shifts ( $\delta$ ) are given in ppm and are relative to tetramethylsilane (TMS), i.e.  $\delta(\text{TMS}) = 0$  ppm. As internal standards, deuterated chloroform (CDCl<sub>3</sub>), deuterated methanol (CD<sub>3</sub>OD), dimethyl sulfoxide (DMSO) with TMS were used. Solvent shifts (ppm):  $\delta(\text{CHCl}_3) = 7.26$  ppm (<sup>1</sup>H),  $\delta(\text{CHCl}_3) = 77.16$  ppm (<sup>13</sup>C),  $\delta(\text{CH}_3\text{OH}) = 3.31$  ppm (<sup>1</sup>H),  $\delta(\text{CH}_3\text{OH}) = 49.00$  ppm (<sup>13</sup>C),  $\delta(\text{DMSO}) = 2.50$  ppm (<sup>1</sup>H),  $\delta(\text{DMSO}) = 39.52$  ppm (<sup>13</sup>C).<sup>[i]</sup> The assignment of each signal was based on two-dimensional nuclear magnetic resonance spectroscopy (2D NMR), i.e. heteronuclear single quantum coherence (HSQC) and heteronuclear multiple bond correlation spectroscopy (HMBC). TopSpin was used to analyze the spectra.

### *High Performance Liquid Chromatography (HPLC)*

For preparative purposes, a PLC 2020 Personal Purification System (Gilson) with a preparative Nucleodur C18 HTec-column (5  $\mu\text{m}$ , 250 x 16 mm; Macherey & Nagel) using an isocratic regime during the first five minutes, for column equilibration, followed by a linear gradient 5% to 50% B in 30 min with a flow rate of 10 mL/min at 25 °C was used. The detection was carried out by measuring the absorption at wavelengths: 220 nm and 304 nm. Milli-Q water (A) and MeCN (B) were employed as eluents with an addition of 0.1% of TFA in both solvents.

For analytical purposes, an Agilent 1260 Infinity II HPLC-System (Agilent Technologies) was used with an eclipse XDB-C18 column (5  $\mu\text{m}$ , 4.6 x 150 mm, Agilent). The flow rate was 1.0 mL/min using an isocratic regime of 5% B during the first five minutes, for column equilibration, followed by the linear in 30 min at 55 °C. The isocratic regime and the linear gradient are:

- 1) isocratic: 5% B, gradient 5-75% B.
- 2) isocratic: 5% B, gradient 5-95% B.

For purity determination, the integrals of the corresponding peaks were set into comparison. Only peaks with a signal intensity >10% to the highest peak were taken into consideration.

### ***Mass Spectrometry***

High resolution electrospray ionization mass spectrometry (HR-ESI-MS) was performed on a Finnigan LTQ-FT (Thermo Fischer Scientific). The resolution was set to 100.000. HR-EI-MS and HR-CI-MS was performed on an AccuTOF GCv 4G (JEOL) Time of Flight (TOF) mass spectrometer. An internal or external standard was used for drift time correction.

### ***UV-Vis Spectroscopy***

UV-Vis measurements for concentration determinations were performed on a Tecan 20M at room temperature using a quartz cuvette (Hellma Analytics; 104-QS) with a pathlength of 1 cm in a volume of 1 mL.

Thermal melting analysis was performed on a Jasco V-650 UV-Vis spectrophotometer equipped with a Jasco PAC-743 temperature controlled cell holder and a Julabo F250 cooling system. The measurements were performed in a 1 mL quartz cuvette (Hellma Analytics; 104-QS) with a pathlength of 1 cm, a concentration of 1.0  $\mu\text{M}$  of duplex DNA with and without 1.2  $\mu\text{M}$  of polyamide in 10 mM  $\text{NaH}_2\text{PO}_4$  pH 7.4. It was measured at 260 nm, with a medium response, a band width of 20 nm, from 20-95  $^\circ\text{C}$  and a slope of 0.5  $^\circ\text{C}/\text{min}$ . Three independent measurements were recorded and the intensity normalized.

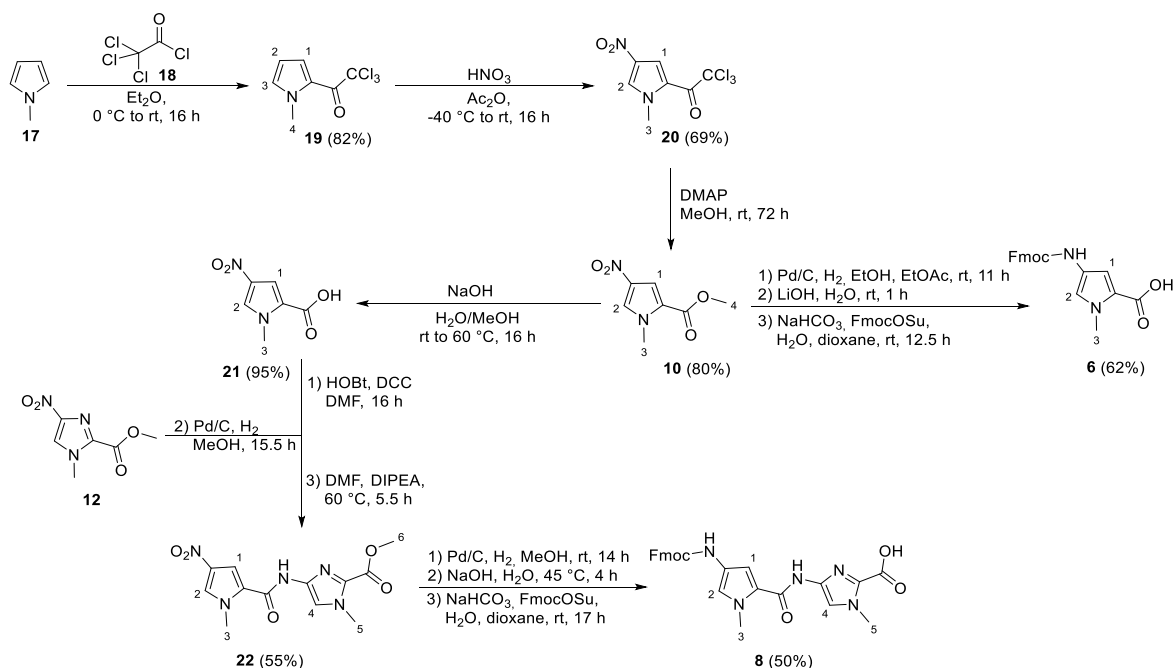
### ***FT-IR Spectroscopy***

IR measurements were performed on a Bruker Alpha II Platinum ATR FTIR spectrometer. The absorption bands are given in  $\text{cm}^{-1}$ , intensities are reported as s = strong, m = medium, w = weak.

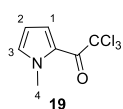
## Synthesis in Solution

### Synthesis of Pyrrole Monomers Nitro-Py-OMe (10), Fmoc-Py-OH (6) and Fmoc-PyIm-OH (8)

This synthesis was reported before by Dervan *et al.*,<sup>[ii]</sup> Sugiyama *et al.*,<sup>[iii]</sup> Lown *et al.*,<sup>[iv]</sup> Pindur *et al.*,<sup>[v]</sup> and König *et al.*<sup>[vi]</sup> Such procedure is based in the preparation of the nitro pyrrole methylester **10**.<sup>[iii]</sup> We followed the same approach with minor modifications.

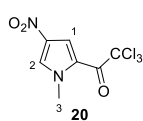


**Scheme S1:** Synthesis route of nitro-Py-OMe (**10**) and Fmoc-Py-OH (**6**) and Fmoc-PyIm-OH (**8**) starting from *N*-methylpyrrole (**17**).



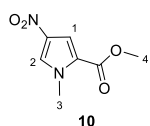
**2,2,2-trichloro-1-(1-methyl-1H-pyrrol-2-yl)ethan-1-one (19):** Under inert atmosphere, a solution of *N*-methylpyrrole (2.20 mL, 25.0 mmol) in Et<sub>2</sub>O (5.0 mL) was added to a solution of trichloroacetyl chloride (2.80 mL, 25.0 mmol) in Et<sub>2</sub>O (5.0 mL) at 0 °C over 1 h.

The reaction mixture was stirred for 16 h at rt and neutralized with K<sub>2</sub>CO<sub>3</sub> solution (aq). It was extracted with Et<sub>2</sub>O (4 x 200 mL), dried over MgSO<sub>4</sub> and the solvent removed under reduced pressure to yield the desired product (**19**, 4.67 g, 20.6 mmol, 82%) as brown solid. The characterization is in agreement with the literature.<sup>[vii]</sup> **R<sub>f</sub>** = 0.60 (*n*-pentane/EtOAc 1:1). **<sup>1</sup>H-NMR** (300 MHz, DMSO-*d*<sub>6</sub>, δ): 7.46 - 7.42 (m, 2H, *CH*-1 and *CH*-3), 6.30 (dd, 1H, *J* = 4.3 Hz, *J* = 2.5 Hz, *CH*-2), 3.91 (s, 3H, *CH*-4). **<sup>13</sup>C-NMR** (75 MHz, DMSO-*d*<sub>6</sub>, δ): 171.8 (C=O), 135.3 (CH), 123.6 (CH), 120.7 (C<sub>q</sub>), 109.1 (CH), 96.0 (CCl<sub>3</sub>), 36.2 (CH<sub>3</sub>). **HRMS-Cl<sup>+</sup>** (*m/z*): [M+H]<sup>+</sup> calcd for C<sub>7</sub>H<sub>6</sub>Cl<sub>3</sub>NOH, 225.95932; found, 225.95978.

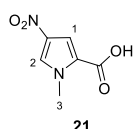


**2,2,2-trichloro-1-(1-methyl-4-nitro-1H-pyrrol-2-yl)ethan-1-one (20):** Under inert atmosphere, to a solution of 2,2,2-trichloro-1-(1-methyl-1H-pyrrol-2-yl)ethan-1-one (1.50 g, 6.62 mmol) in Ac<sub>2</sub>O (8.00 mL, 84.6 mmol), conc. HNO<sub>3</sub> (0.60 mL, 14.4 mmol) was added at -40 °C over 30 min. The reaction mixture was slowly warmed up to rt and stirred for 16 h. It was neutralized with Na<sub>2</sub>CO<sub>3</sub> solution (aq), extracted with EtOAc (4 x 150 mL), washed with brine (3 x 100 mL), the organic phases dried over MgSO<sub>4</sub> and the solvent removed under

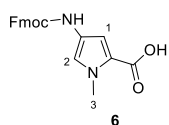
reduced pressure to yield the desired product (**20**, 1.24 g, 4.56 mmol, 69%) as brown solid. The characterization is in agreement with the literature.<sup>[ii]</sup>  $R_f = 0.16$  (*n*-pentane/EtOAc 10:1). <sup>1</sup>H-NMR (300 MHz, DMSO-*d*<sub>6</sub>, δ): 8.56 (d, 1H, *J* = 1.6 Hz, *CH*-2), 7.80 (d, 1H, *J* = 1.6 Hz, *CH*-1), 4.00 (s, 3H, *CH*-3). <sup>13</sup>C-NMR (75 MHz, DMSO-*d*<sub>6</sub>, δ): 172.8 (C=O), 134.2 (C<sub>q</sub>), 132.5 (CH), 120.6 (C<sub>q</sub>), 116.3 (CH), 94.5 (CCl<sub>3</sub>), 50.0 (CH<sub>3</sub>). HRMS-**CI**<sup>+</sup> (*m/z*): [M+H]<sup>+</sup> calcd for C<sub>7</sub>H<sub>5</sub>Cl<sub>3</sub>N<sub>2</sub>O<sub>3</sub>H, 270.94440; found, 270.94291.



**methyl 1-methyl-4-nitro-1H-pyrrole-2-carboxylate (10):** To a solution of 2,2,2-trichloro-1-(1-methyl-4-nitro-1H-pyrrol-2-yl)ethan-1-one (**20**, 4.72 g, 17.4 mmol) in MeOH (58 mL), DMAP (212 mg, 1.74 mmol) was added and the reaction mixture stirred at rt for 72 h. The solvent was removed and the crude product purified by column chromatography (silica, *n*-pentane/EtOAc 4:1 → 1:1) to yield the desired product (**10**, 2.57 g, 14.0 mmol, 80%) as yellow solid. The characterization is in agreement with the literature.<sup>[iii]</sup>  $R_f = 0.16$  (*n*-pentane/EtOAc 10:1). <sup>1</sup>H-NMR (300 MHz, DMSO-*d*<sub>6</sub>, δ): 8.27 (d, 1H, *J* = 2.0 Hz, *CH*-2), 7.30 (d, 1H, *J* = 2.0 Hz, *CH*-1), 3.92 (s, 3H, *CH*-3), 3.80 (s, 3H, *CH*-4). <sup>13</sup>C-NMR (75 MHz, DMSO-*d*<sub>6</sub>, δ): 159.8 (C=O), 134.2 (C<sub>q</sub>), 129.4 (CH), 122.6 (C<sub>q</sub>), 111.5 (CH), 51.7 (CH<sub>3</sub>), 37.4 (CH<sub>3</sub>). HRMS-**ESI**<sup>+</sup> (*m/z*): [M+H]<sup>+</sup> calcd for C<sub>7</sub>H<sub>8</sub>N<sub>2</sub>O<sub>4</sub>H, 185.05623; found, 185.05665.



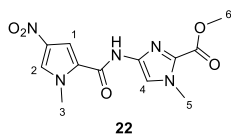
**1-methyl-4-nitro-1H-pyrrole-2-carboxylic acid (21):** To a solution of methyl 1-methyl-4-nitro-1H-pyrrole-2-carboxylate (**10**, 2.00 g, 10.9 mmol) in MeOH (25.0 mL) 1 M NaOH (aq, 15 mL) was added and the reaction mixture stirred at rt for 16 h and heated at 60 °C for 1 h. Afterwards, it was extracted with EtOAc (3 x 100 mL) and washed with saturated NaHCO<sub>3</sub> (aq, 3 x 100 mL). The aqueous phases were acidified with 2 M HCl (aq), extracted with EtOAc (4 x 200 mL), the organic phases dried over MgSO<sub>4</sub>, filtered and the solvent removed under reduced pressure to yield the desired product (**22**, 1.77 g, 10.4 mmol, 95%) as pale yellow solid. The characterization is in agreement with the literature.<sup>[viii]</sup>  $R_f = 0.33$  (EtOAc/formic acid 1:0.02). <sup>1</sup>H-NMR (300 MHz, DMSO-*d*<sub>6</sub>, δ): 13.11 (s, 1H, COOH), 8.21 (d, 1H, *J* = 2.1 Hz, *CH*-2), 7.25 (d, 1H, *J* = 2.1 Hz, *CH*-1), 3.91 (s, 3H, *CH*-3). <sup>13</sup>C-NMR (75 MHz, DMSO-*d*<sub>6</sub>, δ): 160.9 (C=O), 134.0 (C<sub>q</sub>), 129.1 (CH), 123.8 (C<sub>q</sub>), 111.4 (CH), 37.4 (CH<sub>3</sub>). HRMS-**ESI**<sup>-</sup> (*m/z*): [M]<sup>-</sup> calcd for C<sub>6</sub>H<sub>5</sub>N<sub>2</sub>O<sub>4</sub>, 169.0255; found, 169.0257.



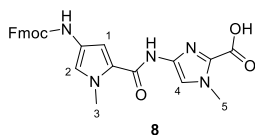
**4-(((9H-fluoren-9-yl)methoxy)carbonyl)amino)-1-methyl-1H-pyrrole-2-carboxylic acid (6):** Nitro-Py-OMe (**10**, 2.56 g, 13.9 mmol) was dissolved in EtOH (15 mL) and EtOAc (15 mL). Pd/C (10% dry, 500 mg, 20% w/w) was added and the reaction mixture stirred under hydrogen atmosphere. After 3 h and 4 h Pd/C (10% dry, 500 mg, 20% w/w) was added and the reaction mixture stirred under hydrogen atmosphere. After another 4 h it was filtered over celite and the solvent removed. The crude was suspended in 2 M LiOH (aq, 35 mL) and stirred at rt for 1 h. It was neutralized with 4 M HCl (aq), the solvent reduced, the crude dissolved in H<sub>2</sub>O (15 mL) and 1,4-dioxane (15 mL), NaHCO<sub>3</sub> (5.86 g, 69.6 mmol) and FmocOSu (5.63 g, 16.7 mmol) added. The reaction mixture was stirred under nitrogen atmosphere for 12.5 h at rt. It was diluted with water and acidified with 2 M HCl (aq). The product was extracted with EtOAc (4 x 200 mL), the organic phases dried over MgSO<sub>4</sub>, filtered and the solvent removed under reduced pressure. It was purified by column chromatography (silica, CH<sub>2</sub>Cl<sub>2</sub>/MeOH 100:1 → 20:1 → 10:1 → 10:1 including 1% formic acid) to yield the desired product (**6**, 3.12 g, 8.61 mmol, 62%) as brown solid. The characterization is in agreement with the literature.<sup>[vi]</sup>  $R_f = 0.25$  (CH<sub>2</sub>Cl<sub>2</sub>/MeOH 20:1). <sup>1</sup>H-NMR (300 MHz, DMSO-*d*<sub>6</sub>, δ): 12.11 (s, 1H, COOH), 9.41 (s, 1H, NH), 7.90 (d, 2H, *J* = 7.4 Hz, *CH*<sub>arom.</sub>), 7.72 (d, 2H, *J* = 7.1 Hz, *CH*<sub>arom.</sub>), 7.42 (d, 2H, *J* = 7.1 Hz, *CH*<sub>arom.</sub>), 7.34 (d, 2H, *J* = 7.4 Hz, *CH*<sub>arom.</sub>), 7.03 (s, 1H, *CH*-2), 6.62 (s, 1H, *CH*-1), 4.44 (d, 2H, *J* = 6.5 Hz, *CH*<sub>2</sub>-Fmoc), 4.28 (t, 1H, *J* = 6.5 Hz,



CH-Fmoc), 3.78 (s, 3H, CH<sub>3</sub>-3). <sup>13</sup>C-NMR (75 MHz, DMSO-*d*<sub>6</sub>, δ): 162.0 (C=O), 153.3 (C=O), 143.8 (2C, C<sub>q</sub>), 140.8 (2C, C<sub>q</sub>), 127.6 (2C, CH), 127.1 (2C, CH), 125.0 (2C, CH), 122.3 (C<sub>q</sub>), 120.2 (C<sub>q</sub>), 120.1 (2C, CH), 118.6 (CH), 107.5 (CH), 65.4 (CH<sub>2</sub>), 46.7 (CH), 36.0 (CH<sub>3</sub>). **HRMS-ESI<sup>+</sup>** (*m/z*): [M+Na]<sup>+</sup> calcd for C<sub>21</sub>H<sub>18</sub>N<sub>2</sub>O<sub>4</sub>Na, 385.1159; found, 385.1154.



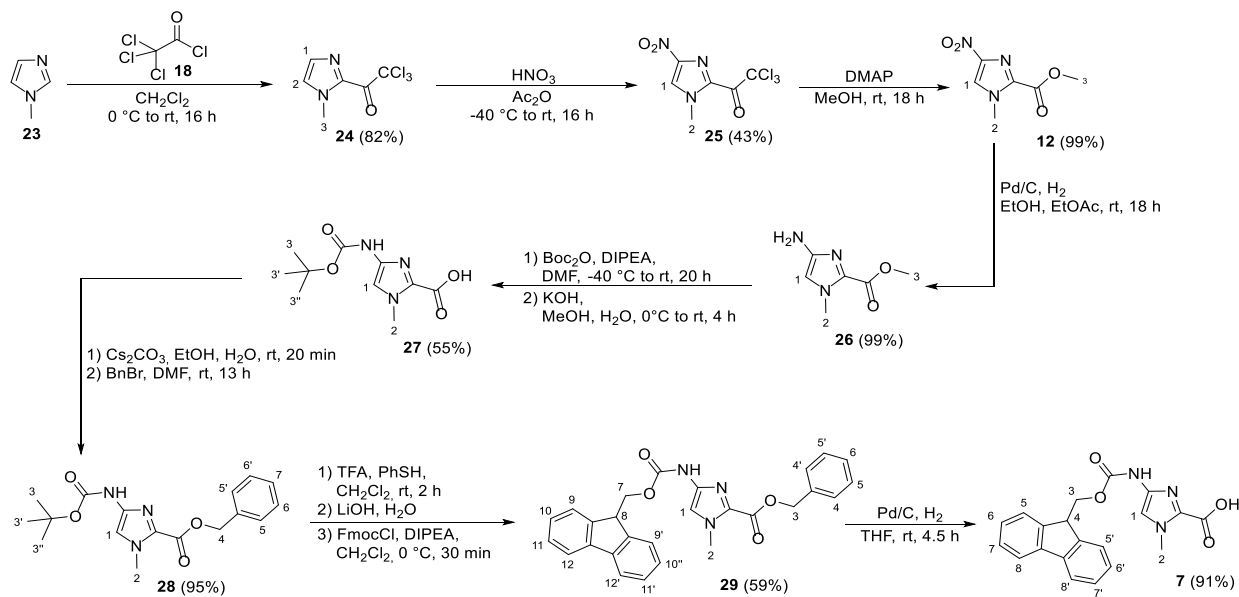
**methyl 1-methyl-4-(1-methyl-4-nitro-1H-pyrrole-2-carboxamido)-1H-imidazole-2-carboxylate (22):** To a solution of nitro-Py-OH (1.04 g, 6.14 mmol) in DMF (10.0 mL) it was added HOBT x H<sub>2</sub>O (1.13 g, 7.41 mmol) followed by DCC (1.53 g, 7.41 mmol). The solution was stirred for 16 h and the urea side product removed by filtration. Separately, to a solution of nitro-Im-OMe (1.20 g, 6.48 mmol) in MeOH (11.0 mL) Pd/C (10% dry, 240 mg, 20% *w/w*) was added and the reaction mixture stirred under hydrogen atmosphere for 15.5 h. The catalyst was removed by filtration through celite, the solvent removed and the OBt ester solution directly added. DIPEA (1.90 mL, 10.9 mmol) was added and the solution stirred at 60 °C for 5.5 h. The DMF was removed under reduced pressure and deionized water added to the crude. The formed precipitate was filtered and washed with 1 M HCl (aq, 5 x 50 mL) and water (7 x 50 mL). After freeze drying the precipitate, it was purified by column chromatography (silica, EtOAc/NEt<sub>3</sub> 100:1) to yield the desired product (**22**, 1.04 g, 3.38 mmol, 55%) as pale brown solid. The characterization is in agreement with the literature.<sup>[ix]</sup> **R<sub>f</sub>** = 0.21 (*n*-pentane/EtOAc 1:1). **<sup>1</sup>H-NMR** (300 MHz, DMSO-*d*<sub>6</sub>, δ): 11.15 (s, 1H, NH), 8.20 (d, 1H, *J* = 2.0 Hz, CH-2), 7.81 (d, 1H, *J* = 2.0 Hz, CH-1), 7.69 (s, 1H, CH-4), 3.96 (s, 3H, CH<sub>3</sub>-3), 3.94 (s, 3H, CH<sub>3</sub>-5), 3.82 (s, 3H, CH<sub>3</sub>-6). **<sup>13</sup>C-NMR** (75 MHz, DMSO-*d*<sub>6</sub>, δ): 158.9 (C=O), 157.3 (C=O), 137.1 (C<sub>q</sub>), 133.9 (C<sub>q</sub>), 131.0 (C<sub>q</sub>), 128.8 (CH), 125.2 (C<sub>q</sub>), 115.7 (CH), 108.8 (CH), 51.9 (CH<sub>3</sub>), 37.8 (CH<sub>3</sub>), 35.5 (CH<sub>3</sub>). **HRMS-ESI<sup>+</sup>** (*m/z*): [M+Na]<sup>+</sup> calcd for C<sub>12</sub>H<sub>13</sub>N<sub>5</sub>O<sub>5</sub>Na, 330.0809; found, 330.0810.



**4-(4-(((9H-fluoren-9-yl)methoxy)carbonyl)amino)-1-methyl-1H-pyrrole-2-carboxamido)-1-methyl-1H-imidazole-2-carboxylic acid (8):** To a solution of nitro-PyIm-OMe (929 mg, 3.02 mmol) in MeOH (10.0 mL), Pd/C (10% dry, 549 mg, 60% *w/w*) was added and the mixture stirred under hydrogen atmosphere for 14 h. The catalyst was removed by filtration through celite, the solvent removed and 1 M NaOH (aq, 10.0 mL) added. After 3 h at 45 °C, 1 M NaOH (aq, 5.00 mL) was added and the solution stirred for another 1 h. 1 M HCl (aq) was added until pH 7 was reached. The water was removed under reduced pressure, the residue dissolved in H<sub>2</sub>O (8.00 mL) and 1,4-dioxane (5.00 mL) and NaHCO<sub>3</sub> (1.27 g, 15.1 mmol) and FmocOSu (1.02 g, 3.02 mmol) added. The solution was stirred under nitrogen atmosphere at rt for 16 h. H<sub>2</sub>O (5.00 mL) and 1,4-dioxane (5.00 mL) were added and the solution stirred for another 40 min. The dioxane was removed under reduced pressure and the formed precipitate filtered and washed with water (6 x 50 mL). The residue was freeze dried and purified by column chromatography (silica, CH<sub>2</sub>Cl<sub>2</sub>/MeOH 100:1 → 20:1 including 1% formic acid) to yield the desired product (**8**, 734 mg, 1.51 mmol, 50%) as pale brown solid. The characterization is in agreement with the literature.<sup>[iii]</sup> **R<sub>f</sub>** = 0.33 (EtOAc). **<sup>1</sup>H-NMR** (300 MHz, DMSO-*d*<sub>6</sub>, δ): 10.57 (s, 1H, COOH), 9.46 (s, 1H, NH), 8.15 (s, 1H, NH), 7.91 (d, 2H, *J* = 7.3 Hz, CH<sub>arom.</sub>), 7.74 (d, 2H, *J* = 6.5 Hz, CH<sub>arom.</sub>), 7.57 (s, 1H, CH-4), 7.47 – 7.31 (m, 4H, CH<sub>arom.</sub>), 7.01 (s, 1H, CH-2), 6.95 (s, 1H, CH-1), 4.47 – 4.37 (m, 2H, CH<sub>2</sub>-Fmoc), 4.33 – 4.24 (m, 1H, CH-Fmoc), 3.91 (s, 3H, CH<sub>3</sub>-3), 3.82 (s, 3H, CH<sub>3</sub>-5). **<sup>13</sup>C-NMR** (125 MHz, DMSO-*d*<sub>6</sub>, δ): 172.8 (C=O), 163.2 (C=O), 153.5 (C=O), 143.9 (2C, C<sub>q</sub>), 140.8 (2C, C<sub>q</sub>), 137.2 (C<sub>q</sub>), 132.6 (C<sub>q</sub>), 127.7 (2C, CH), 127.1 (2C, CH), 125.2 (2C, CH), 122.6 (C<sub>q</sub>), 122.1 (C<sub>q</sub>), 120.2 (2C, CH), 118.1 (CH), 114.6 (CH), 105.0 (CH), 65.5 (CH<sub>2</sub>), 46.7 (CH), 36.3 (CH<sub>3</sub>), 35.4 (CH<sub>3</sub>). **HRMS-ESI<sup>+</sup>** (*m/z*): [M+H]<sup>+</sup> calcd for C<sub>26</sub>H<sub>23</sub>N<sub>5</sub>O<sub>5</sub>H, 486.1777; found, 486.1772.

## Synthesis of Imidazole Monomer Fmoc-Im-OH (7)

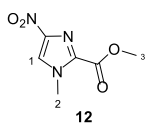
This synthesis was reported before by Dervan *et al.*,<sup>[iii,x]</sup> and Shibuya *et al.*,<sup>[xi]</sup> Such procedure is based in the preparation of the nitro imidazole methylester **12**. We followed the same approach with minor modifications.



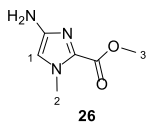
**Scheme S2:** Synthesis route of nitro-Im-OMe (**12**) and Fmoc-Im-OH (**7**) starting from *N*-methylimidazole (**23**).

**2,2,2-trichloro-1-(1-methyl-1H-imidazol-2-yl)ethan-1-one (24):** Under inert atmosphere, a solution of *N*-methylimidazole (5.58 mL, 70.0 mmol) in CH<sub>2</sub>Cl<sub>2</sub> (30 mL) was added to a solution of trichloroacetyl chloride (7.88 mL, 70.2 mmol) in CH<sub>2</sub>Cl<sub>2</sub> (50 mL) at 0 °C over 1.5 h. The reaction mixture was stirred for 16 h at rt, CH<sub>2</sub>Cl<sub>2</sub> (40 mL) and triethylamine (9.75 mL, 70.2 mmol) were added at 0 °C over 30 min. The crude was purified by flash column chromatography (silica, *n*-pentane/EtOAc 1:1) to yield the desired product (**24**, 13.0 g, 57.2 mmol, 82%) as yellow solid. The characterization is in agreement with the literature.<sup>[xii]</sup> *R<sub>f</sub>* = 0.72 (*n*-pentane/EtOAc 1:1). <sup>1</sup>H-NMR (300 MHz, CD<sub>3</sub>OD, δ): 7.31 (s, 1H, CH-2), 7.08 (s, 1H, CH-1), 4.01 (s, 3H, CH<sub>3</sub>-3). <sup>13</sup>C-NMR (75 MHz, CD<sub>3</sub>OD, δ): 160.3 (C=O), 137.8 (C<sub>q</sub>), 129.4 (CH), 128.1 (CH), 119.5 (CCl<sub>3</sub>), 36.2 (CH<sub>3</sub>). HRMS-Cl<sup>+</sup> (*m/z*): [M+H]<sup>+</sup> calcd for C<sub>6</sub>H<sub>5</sub>Cl<sub>3</sub>N<sub>2</sub>O<sub>1</sub>H, 226.95457; found, 226.95069.

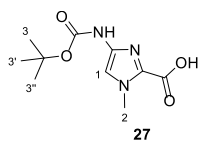
**2,2,2-trichloro-1-(1-methyl-4-nitro-1H-imidazol-2-yl)ethan-1-one (25):** Under inert atmosphere, Im-CCl<sub>3</sub> (**24**, 12.7 g, 56.0 mmol) was dissolved in Ac<sub>2</sub>O (72.6 mL, 768 mmol) and cooled to -40 °C. Fuming HNO<sub>3</sub> (15.2 mL, 364 mmol) was added carefully dropwise over 1.5 h. The reaction mixture was slowly warmed it up to rt and stirred with the flask placed in a water bath for 16 h. Afterwards the reaction was neutralized with saturated Na<sub>2</sub>CO<sub>3</sub> (aq), at 0 °C, extracted with CH<sub>2</sub>Cl<sub>2</sub> (4 x 200 mL) and dried over MgSO<sub>4</sub>. The solvent was removed to yield the desired product (**25**, 6.52 g, 23.9 mmol, 43%) as pale brown solid. The characterization is in agreement with the literature.<sup>[xii]</sup> *R<sub>f</sub>* = 0.55 (*n*-pentane/EtOAc 1:1). <sup>1</sup>H-NMR (300 MHz, CDCl<sub>3</sub>, δ): 7.95 (s, 1H, CH-1), 4.16 (s, 3H, CH<sub>3</sub>-2). <sup>13</sup>C-NMR (75 MHz, CDCl<sub>3</sub>, δ): 173.0 (C=O), 146.0 (C<sub>q</sub>), 133.8 (C<sub>q</sub>), 126.1 (CH), 93.7 (CCl<sub>3</sub>), 38.4 (CH<sub>3</sub>). HRMS-Cl<sup>+</sup> (*m/z*): [M+H]<sup>+</sup> calcd for C<sub>6</sub>H<sub>4</sub>Cl<sub>3</sub>N<sub>3</sub>O<sub>3</sub>H, 271.93965; found, 271.94021.



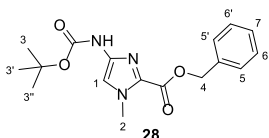
**methyl 1-methyl-4-nitro-1H-imidazole-2-carboxylate (12):** Nitro-Im-CCl<sub>3</sub> (7.17 g, 26.3 mmol) was suspended in MeOH (145 mL), followed by DMAP (437 mg, 3.58 mmol) addition. The resulting reaction mixture stirred for 18 h at rt. The crude was purified by flash column chromatography (silica, *n*-pentane/EtOAc: 4:1 → 1:1 → 1:2) to yield the desired product (**12**, 4.87 g, 26.3 mmol, >99%) as pale yellow solid. The characterization is in agreement with the literature.<sup>[xiii]</sup>  $R_f = 0.33$  (*n*-pentane/EtOAc 1:1). <sup>1</sup>H-NMR (300 MHz, CD<sub>3</sub>OD,  $\delta$ ): 8.29 (s, 1H, CH-1), 4.08 (s, 3H, CH<sub>3</sub>-2), 3.96 (s, 3H, CH<sub>3</sub>-3). <sup>13</sup>C-NMR (75 MHz, CD<sub>3</sub>OD,  $\delta$ ): 159.6 (C=O), 142.9 (C<sub>q</sub>), 136.6 (C<sub>q</sub>), 126.9 (CH), 53.2 (CH<sub>3</sub>), 37.5 (CH<sub>3</sub>). HRMS-ESI<sup>+</sup> (*m/z*): [M+Na]<sup>+</sup> calcd for C<sub>6</sub>H<sub>7</sub>N<sub>3</sub>O<sub>4</sub>Na, 208.0329; found, 208.0328.



**methyl 4-amino-1-methyl-1H-imidazole-2-carboxylate (26):** Nitro-Im-OMe (4.83 g, 26.1 mmol) was suspended in EtOH (75 mL). EtOAc (75 mL) and Pd/C 10%, 50% wet (0.1 w/w%) in a slurry of EtOAc (15 mL) was added and the mixture stirred in the dark under hydrogen atmosphere for 18 h. The crude was filtered over celite and the solvent removed under reduced pressure to yield the desired product (**26**, 4.01 g, 25.8 mmol, 99%) as pale yellow solid. The characterization is in agreement with the literature.<sup>[x]</sup>  $R_f = 0.07$  (EtOAc). <sup>1</sup>H-NMR (300 MHz, CD<sub>3</sub>OD,  $\delta$ ): 6.55 (s, 1H, CH-1), 4.83 (s, 2H, NH<sub>2</sub>), 3.90 (s, 3H, CH<sub>3</sub>-2), 3.86 (s, 3H, CH<sub>3</sub>-3). <sup>13</sup>C-NMR (75 MHz, CD<sub>3</sub>OD,  $\delta$ ): 160.1 (C=O), 147.3 (C<sub>q</sub>), 132.2 (C<sub>q</sub>), 111.0 (CH), 52.2 (CH<sub>3</sub>), 36.0 (CH<sub>3</sub>). HRMS-ESI<sup>+</sup> (*m/z*): [M+Na]<sup>+</sup> calcd for C<sub>6</sub>H<sub>9</sub>N<sub>3</sub>O<sub>2</sub>Na, 178.0587; found, 178.0588.

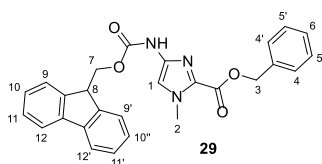


**4-((tert-butoxycarbonyl)amino)-1-methyl-1H-imidazole-2-carboxylic acid (27):** NH<sub>2</sub>-Im-OMe (3.97 g, 25.6 mmol) was dissolved in DMF (30 mL). Afterwards DIPEA (7.52 mL, 44.3 mmol) and Boc<sub>2</sub>O (10.9 g, 50.0 mmol) were added. The mixture was stirred in the dark for 18 h at rt and heated at 40 °C for other 2 h. The reaction mixture was extracted with Et<sub>2</sub>O (4 x 200 mL) and washed with brine (aq, 3 x 100 mL), 10% citric acid (aq, 3 x 100 mL), brine (aq, 3 x 100 mL), saturated NaHCO<sub>3</sub> (aq, 3 x 100 mL) and brine (aq, 3 x 100 mL). The organic phases were dried over MgSO<sub>4</sub> and the solvent removed under reduced pressure. The crude was dissolved in MeOH (80 mL) and 1 M KOH (aq, 50 mL) was added at 0 °C and stirred in the dark for 30 min and another 3.5 h at rt. The reaction mixture was extracted with Et<sub>2</sub>O (3 x 150 mL), the aqueous phase cooled to 0 °C and 10% NaHSO<sub>4</sub>(aq) added until pH 3. The mixture was extracted with EtOAc (4 x 200 mL), the organic phases dried over MgSO<sub>4</sub> and the solvent removed under reduced pressure to yield the desired product (**27**, 3.38 g, 14.0 mmol, 55%) as pale brown solid. The characterization is in agreement with the literature.<sup>[xii]</sup>  $R_f = 0.02$  (*n*-pentane/EtOAc 1:1). <sup>1</sup>H-NMR (300 MHz, CD<sub>3</sub>OD,  $\delta$ ): 7.20 (s, 1H, CH-1), 4.00 (s, 3H, CH<sub>3</sub>-2), 1.51 (s, 9H, CH<sub>3</sub>-3). <sup>13</sup>C-NMR (75 MHz, CD<sub>3</sub>OD,  $\delta$ ): 160.9 (C=O), 152.9 (C=O), 137.5 (C<sub>q</sub>), 134.5 (C<sub>q</sub>), 112.4 (CH), 79.5 (C<sub>q</sub>), 35.7 (CH<sub>3</sub>), 28.6 (3C, CH<sub>3</sub>). HRMS-ESI<sup>+</sup> (*m/z*): [M+Na]<sup>+</sup> calcd for C<sub>10</sub>H<sub>15</sub>N<sub>3</sub>O<sub>4</sub>Na, 264.0955; found, 264.0955.



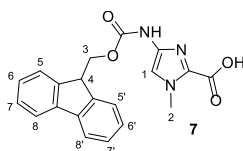
**benzyl 4-((tert-butoxycarbonyl)amino)-1-methyl-1H-imidazole-2-carboxylate (28):** Boc-Im-OH (3.34 g, 10.1 mmol) was suspended in 66% EtOH (67 mL) and Cs<sub>2</sub>CO<sub>3</sub> (3.34 g, 10.3 mmol) added. After stirring for 20 min at rt, the suspension was filtered over glass wool and the solvent removed under reduced pressure. The crude was dissolved in DMF (180 mL), BnBr (1.75 mL, 14.6 mmol) added and the mixture stirred for 13 h. Deionized water was added. It was extracted with EtOAc (4 x 200 mL), washed with water (3 x 100 mL) and the organic phases dried over MgSO<sub>4</sub>. The crude was purified by flash column chromatography (silica, *n*-pentane/EtOAc: 10:1 → 5:1 → 1:1) to yield the desired product (**28**, 3.17 g, 9.57 mmol, 95%) as pale brown solid. The characterization is in agreement with the literature.<sup>[xiii]</sup>  $R_f = 0.65$  (*n*-pentane/EtOAc 1:1). <sup>1</sup>H-NMR (300 MHz, CD<sub>3</sub>OD,  $\delta$ ): 7.49-7.42 (m, 2H, CH<sub>arom.</sub>), 7.40-7.32 (m, 3H, CH<sub>arom.</sub>), 7.25 (s, 1H, CH-1), 5.35 (s, 2H, CH<sub>2</sub>-4), 3.96 (s,

3H,  $CH_3$ -2), 1.50 (s, 9H,  $CH_3$ -3).  $^{13}C$ -NMR (75 MHz,  $CD_3OD$ ,  $\delta$ ): 159.5 (C=O), 154.8 (C=O), 139.3 ( $C_q$ ), 137.2 ( $C_q$ ), 135.5 ( $C_q$ ), 129.6 (2C, CH), 129.5 (2C, CH), 129.4 (CH), 115.6 (CH), 81.3 ( $C_q$ ), 67.9 ( $CH_2$ ), 36.5 ( $CH_3$ ), 28.6 (3C,  $CH_3$ ). **HRMS-ESI<sup>+</sup>** ( $m/z$ ):  $[M+Na]^+$  calcd for  $C_{17}H_{21}N_3O_4Na$ , 354.1424; found, 354.1425.



**benzyl 4-(((9H-fluoren-9-yl)methoxy)carbonyl)amino)-1-methyl-1H-imidazole-2-carboxylate (29):** Boc-Im-OBn (3.13 g, 9.45 mmol) was dissolved in  $CH_2Cl_2$  (12.5 mL) and a mixture of TFA (8.2 mL),  $CH_2Cl_2$  (4.4 mL) and PhSH (960  $\mu$ L) was added. After stirring for 2 h in the dark, the reaction mixture was added dropwise at 0 °C to 2 M LiOH

(aq, 100 mL). It was extracted with  $Et_2O$  (4 x 100 mL), washed with 2 M LiOH (aq, 3 x 80 mL) and the organic phases dried over  $MgSO_4$ . The solvent was removed under reduced pressure. The crude, under inert atmosphere, was dissolved in  $CH_2Cl_2$  (20 mL) and DIPEA (6.4 mL, 36.8 mmol) and Fmoc-Cl (2.46 g, 9.52 mmol) were added at 0 °C. It was stirred in the dark for 30 min at 0 °C. It was acidified with 1 M HCl (aq), extracted with  $CH_2Cl_2$  (4 x 150 mL), the organic phases dried over  $MgSO_4$  and the solvent removed under reduced pressure. The crude was purified by flash column chromatography (silica, *n*-pentane/ $EtOAc$ : 10:1  $\rightarrow$  4:1  $\rightarrow$  0:1) to yield the desired product (**29**, 2.52 g, 5.56 mmol, 59%) as a colorless solid. The characterization is in agreement with the literature.<sup>[x]</sup>  $R_f$  = 0.73 (*n*-pentane/ $EtOAc$  1:1).  $^1H$ -NMR (300 MHz,  $DMSO-d_6$ ,  $\delta$ ): 10.36 (s, 1H, NH), 7.90 (d, 2H,  $J$  = 7.5 Hz,  $CH_{arom.}$ ), 7.76 (d, 2H,  $J$  = 7.0 Hz,  $CH_{arom.}$ ), 7.47-7.30 (m, 10H,  $CH_{arom.}$  and  $CH$ -1), 5.30 (s, 2H,  $CH_2$ -3), 4.36-4.23 (m, 3H,  $CH_2$ -7 and  $CH$ -8), 3.92 (s, 3H,  $CH_3$ -2).  $^{13}C$ -NMR (75 MHz,  $DMSO-d_6$ ,  $\delta$ ): 158.1 (C=O), 153.2 (C=O), 143.7 (2C,  $C_q$ ), 140.7 (2C,  $C_q$ ), 137.9 ( $C_q$ ), 135.7 ( $C_q$ ), 130.8 ( $C_q$ ), 128.4 (2C, CH), 128.3 (2C, CH), 128.2 (CH), 127.6 (2C, CH), 127.0 (2C, CH), 125.3 (2C, CH), 120.0 (2C, CH), 113.9 (CH), 66.1 ( $CH_2$ ), 66.0 ( $CH_2$ ), 46.4 (CH), 35.4 ( $CH_3$ ). **HRMS-ESI<sup>+</sup>** ( $m/z$ ):  $[M+Na]^+$  calcd for  $C_{27}H_{23}N_3O_4Na$ , 476.1581; found, 476.1582.

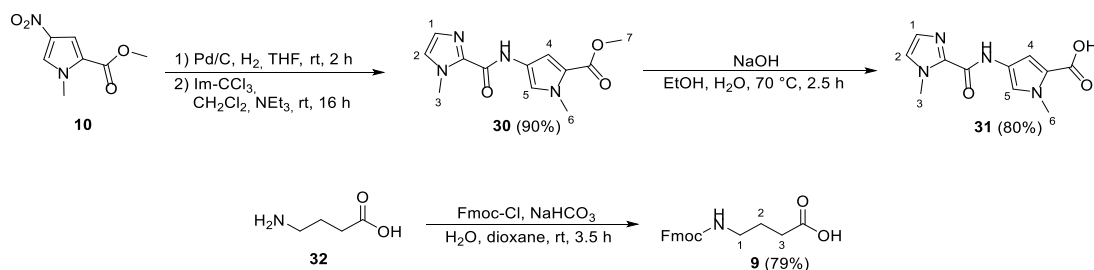


**4-(((9H-fluoren-9-yl)methoxy)carbonyl)amino)-1-methyl-1H-imidazole-2-carboxylic acid (7):** Fmoc-Im-OBn (100 mg, 0.22 mmol) was dissolved in THF (2.0 mL) and Pd/C 10% dry (0.25 w/w%) was added. The reaction mixture was stirred under hydrogen atmosphere for 4.5 h at rt. The reaction mixture was filtered over celite and the solvent removed under reduced pressure to yield the

desired product (**7**, 72.7 mg, 0.20 mmol, 91%) as a pale grey solid. The characterization is in agreement with the literature.<sup>[xiv]</sup>  $R_f$  = 0.32 ( $CH_2Cl_2$ / $MeOH$ /formic acid 100:10:1).  $^1H$ -NMR (500 MHz,  $DMSO-d_6$ ,  $\delta$ ): 11.71 (s, 1H, COOH), 10.30 (s, 1H, NH), 7.91 (d, 2H,  $J$  = 7.4 Hz,  $CH_{arom.}$ ), 7.77 (d, 2H,  $J$  = 7.4 Hz,  $CH_{arom.}$ ), 7.43 (dd, 2H,  $J$  = 7.4 Hz,  $J$  = 7.4 Hz,  $CH_{arom.}$ ), 7.34 (dd, 2H,  $J$  = 7.4 Hz,  $J$  = 7.4 Hz,  $CH_{arom.}$ ), 7.28 (s, 1H,  $CH$ -1), 4.36-4.24 (m, 3H,  $CH_2$ -3 and  $CH$ -4), 3.88 (s, 3H,  $CH_3$ -2).  $^{13}C$ -NMR (125 MHz,  $DMSO-d_6$ ,  $\delta$ ): 160.1 (C=O), 153.4 (C=O), 143.7 (2C,  $C_q$ ), 140.8 (2C,  $C_q$ ), 137.4 ( $C_q$ ), 132.3 ( $C_q$ ), 127.7 (2C, CH), 127.2 (2C, CH), 125.5 (2C, CH), 120.2 (2C, CH), 113.3 (CH), 66.2 ( $CH_2$ ), 46.5 (CH), 35.5 ( $CH_3$ ). **HRMS-ESI<sup>+</sup>** ( $m/z$ ):  $[M+H]^+$  calcd for  $C_{20}H_{17}N_3O_4H$ , 364.1292; found, 364.1284.

## Synthesis of ImPy-OH (31) and Fmoc- $\gamma$ -OH (9)

This synthesis was reported before by Sekine *et al.*,<sup>[xv]</sup> and Herdewijn *et al.*<sup>[xvi]</sup>. We followed the same approach with minor modifications.



Scheme S3: Synthesis route of ImPy-OH (31) and Fmoc- $\gamma$ -OH (9).

**methyl 1-methyl-4-(1-methyl-1H-imidazole-2-carboxamido)-1H-pyrrole-2-carboxylate (30):** Pd/C (10% dry, 400 mg, 40% w/w) was added to a solution of nitro-Py-OMe (1.00 g, 5.43 mmol) in THF (10.0 mL). The mixture was stirred under hydrogen atmosphere for 2 h. The catalyst was removed by filtration through celite and the solvent removed under reduced pressure. The residue was dissolved in CH<sub>2</sub>Cl<sub>2</sub> (15 mL) and Im-CCl<sub>3</sub> (**24**, 1.24 g, 5.43 mmol) and NEt<sub>3</sub> (2.27 mL, 16.3 mmol) added. The reaction was stirred for 16 h, the solvent removed and the crude purified by column chromatography (silica, CH<sub>2</sub>Cl<sub>2</sub>/MeOH 100:0 → 100:1 → 50:1) to yield the desired product (**30**, 1.29 g, 4.91 mmol, 90%) as pale brown solid. The characterization is in agreement with the literature.<sup>[xviii]</sup> **R<sub>f</sub>** = 0.27 (*n*-pentane/EtOAc 1:1). **<sup>1</sup>H-NMR** (300 MHz, CDCl<sub>3</sub>,  $\delta$ ): 9.12 (s, 1H, NH), 7.40 (d, 1H, *J* = 2.0 Hz, CH-2), 7.03 (d, 1H, *J* = 0.9 Hz, CH-5), 6.98 (d, 1H, *J* = 0.9 Hz, CH-4), 6.80 (d, 1H, *J* = 2.0 Hz, CH-1), 4.09 (s, 3H, CH<sub>3</sub>-6), 3.90 (s, 3H, CH<sub>3</sub>-3), 3.80 (s, 3H, CH<sub>3</sub>-7). **<sup>13</sup>C-NMR** (75 MHz, CDCl<sub>3</sub>,  $\delta$ ): 161.6 (C=O), 156.4 (C=O), 139.0 (C<sub>q</sub>), 127.9 (CH), 125.9 (CH), 121.4 (C<sub>q</sub>), 120.7 (CH), 120.2 (C<sub>q</sub>), 108.4 (CH), 51.2 (CH<sub>3</sub>), 36.9 (CH<sub>3</sub>), 35.8 (CH<sub>3</sub>). **HRMS-ESI<sup>+</sup>** (*m/z*): [M+H]<sup>+</sup> calcd for C<sub>12</sub>H<sub>14</sub>N<sub>4</sub>O<sub>3</sub>H, 263.1144; found, 263.1139.

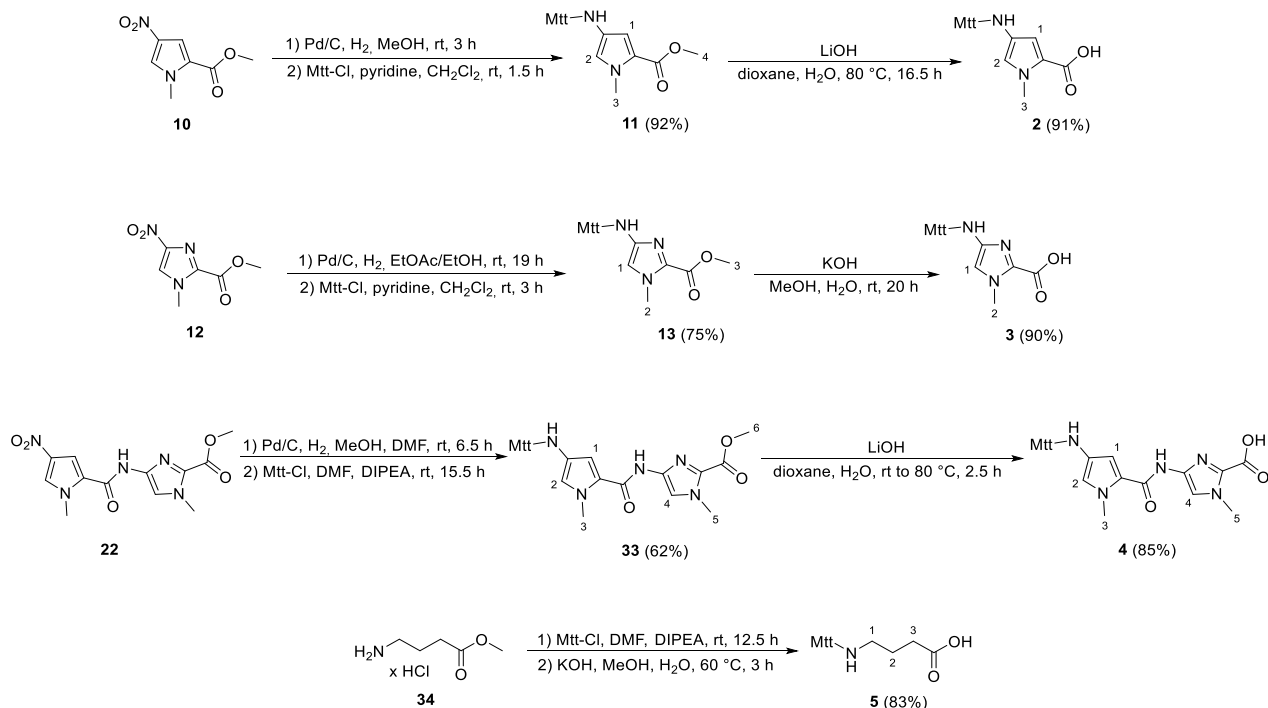
**1-methyl-4-(1-methyl-1H-imidazole-2-carboxamido)-1H-pyrrole-2-carboxylic acid (31):** ImPy-OMe (723 mg, 2.75 mmol) was dissolved in EtOH (3.0 mL) and 0.6 M NaOH (aq, 5.0 mL) and stirred at 70 °C for 2.5 h. The EtOH was removed under reduced pressure and the aqueous phase extracted with CH<sub>2</sub>Cl<sub>2</sub>. The aqueous layers were acidified with 1 M HCl (aq) to pH 3, filtered, washed with deionized H<sub>2</sub>O and freeze dried to yield the desired product (**31**, 544 mg, 2.19 mmol, 80%) as grey solid. The characterization is in agreement with the literature.<sup>[xvi]</sup> **R<sub>f</sub>** = 0.42 (EtOAc). **<sup>1</sup>H-NMR** (300 MHz, DMSO-*d*<sub>6</sub>,  $\delta$ ): 12.20 (br s, 1H, COOH), 10.47 (s, 1H, NH), 7.47 (s, 1H, CH-2), 7.39 (s, 1H, CH-5), 7.04 (s, 1H, CH-4), 6.98 (s, 1H, CH-1), 3.98 (s, 3H, CH<sub>3</sub>-6), 3.82 (s, 3H, CH<sub>3</sub>-3). **<sup>13</sup>C-NMR** (75 MHz, DMSO-*d*<sub>6</sub>,  $\delta$ ): 161.9 (C=O), 156.0 (C=O), 138.6 (C<sub>q</sub>), 126.9 (CH), 126.3 (CH), 121.9 (C<sub>q</sub>), 120.4 (CH), 119.7 (C<sub>q</sub>), 108.9 (CH), 36.1 (CH<sub>3</sub>), 35.1 (CH<sub>3</sub>). **HRMS-ESI<sup>+</sup>** (*m/z*): [M+H]<sup>+</sup> calcd for C<sub>11</sub>H<sub>12</sub>N<sub>4</sub>O<sub>3</sub>H, 249.0982; found, 249.0978.

**4-(((9H-fluoren-9-yl)methoxy)carbonyl)amino)butanoic acid (9):** 4-Aminobutanoic acid (502 mg, 4.87 mmol) was dissolved in deionized water (24 mL) and 1,4-dioxane (12 mL). Fmoc-Cl (1.38 g, 5.33 mmol) and NaHCO<sub>3</sub> (1.92 g, 22.9 mmol) were added and the mixture stirred at rt for 3.5 h. The mixture was poured into deionized water (50 mL) and extracted with Et<sub>2</sub>O (3 x 50 mL). The aqueous layer was acidified with 2 M HCl (aq) to pH 3 and the remaining precipitate filtered and dried in vacuo to yield the desired product (**9**, 1.25 g,

3.85 mmol, 79%) as white solid. The characterization is in agreement with the literature.<sup>[xviii]</sup>  $R_f = 0.83$  ( $\text{CH}_2\text{Cl}_2/\text{MeOH}$  1:1).  **$^1\text{H-NMR}$**  (300 MHz,  $\text{DMSO-}d_6$ ,  $\delta$ ): 11.62 (br s, 1H, COOH), 7.88 (d, 2H,  $J = 7.3$  Hz,  $\text{CH}_{\text{arom.}}$ ), 7.69 (d, 2H,  $J = 7.3$  Hz,  $\text{CH}_{\text{arom.}}$ ), 7.45 – 7.37 (m, 2H,  $\text{CH}_{\text{arom.}}$ ), 7.36 – 7.29 (m, 3H,  $\text{CH}_{\text{arom.}}$ , NH), 4.29 (d, 2H,  $J = 6.7$  Hz,  $\text{CH}_2\text{-Fmoc}$ ), 4.25 – 4.16 (m, 1H,  $\text{CH-Fmoc}$ ), 3.04 – 2.95 (m, 2H,  $\text{CH}_2\text{-1}$ ), 2.20 (t, 2H,  $J = 7.4$  Hz,  $\text{CH}_2\text{-3}$ ), 1.69 – 1.55 (m, 2H,  $\text{CH}_2\text{-2}$ ).  **$^{13}\text{C-NMR}$**  (75 MHz,  $\text{DMSO-}d_6$ ,  $\delta$ ): 174.2 (C=O), 156.1 (C=O), 143.9 (2C,  $\text{C}_q$ ), 140.7 (2C,  $\text{C}_q$ ), 127.5 (2C, CH), 127.0 (2C, CH), 125.1 (2C, CH), 120.1 (2C, CH), 65.2 ( $\text{CH}_2$ ), 46.7 (CH), 39.7 ( $\text{CH}_2$ ), 31.1 ( $\text{CH}_2$ ), 29.9 ( $\text{CH}_2$ ). **HRMS-ESI<sup>+</sup>** ( $m/z$ ):  $[\text{M}+\text{Na}]^+$  calcd for  $\text{C}_{19}\text{H}_{19}\text{N}_1\text{O}_4\text{Na}$ , 348.1206; found, 348.1201.

## Synthesis of Mtt-building blocks

This synthesis is based in the preparation of the Mtt-protected methyl esters to yield the final Mtt-building blocks **2**, **3**, **4**, and **5**, which are used in the solid phase synthesis.

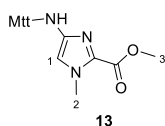


**Scheme S4:** Synthesis route of Mtt-Py-OH (**2**), Mtt-Im-OH (**3**), Mtt-PyIm-OH (**4**) and Mtt-γ-OH (**5**).

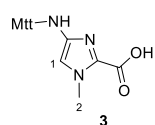
**methyl 4-((diphenyl(p-tolyl)methyl)amino)-1-methyl-1H-pyrrole-2-carboxylate (11):** Nitro-Py-OMe (**10**, 300 mg, 1.63 mmol) was dissolved in MeOH (7.0 mL). Pd/C (10% dry, 75 mg, 25% w/w) was added and the reaction mixture stirred under hydrogen atmosphere. After 3 h, it was filtered over celite and the solvent removed. Under inert atmosphere, the residue was dissolved in CH<sub>2</sub>Cl<sub>2</sub> (2.4 mL) and pyridine (2.0 mL). At 0 °C, MttCl (477 mg, 1.63 mmol) dissolved in CH<sub>2</sub>Cl<sub>2</sub> (1.2 mL) and pyridine (1.0 mL) was added dropwise for 30 min. After 1 h at rt, the solvent was removed under reduced pressure, the crude co-evaporated with EtOAc (3 x 10 mL) and purified via flash column chromatography (silica, CH<sub>2</sub>Cl<sub>2</sub>/NEt<sub>3</sub> 100:2). Mtt-Py-OMe (**11**, 616 mg, 1.50 mmol, 92%) was obtained as pale yellow solid. *R<sub>f</sub>* = 0.52 (CH<sub>2</sub>Cl<sub>2</sub>/NEt<sub>3</sub> 100:1). <sup>1</sup>H-NMR (300 MHz, CD<sub>3</sub>OD, δ): 7.41 - 7.36 (m, 4H, CH<sub>arom.</sub>), 7.28 - 7.14 (m, 8H, CH<sub>arom.</sub>), 7.08 - 7.02 (m, 2H, CH<sub>arom.</sub>), 6.12 (d, 1H, *J* = 2.1 Hz, CH-2), 5.83 (d, 1H, *J* = 2.1 Hz, CH-1), 3.65 (s, 3H, CH<sub>3</sub>-4), 3.55 (s, 3H, CH<sub>3</sub>-3), 2.28 (s, 3H, CH<sub>3</sub>-Mtt). <sup>13</sup>C-NMR (75 MHz, CD<sub>3</sub>OD, δ): 163.2 (C=O), 147.6 (2C, C<sub>q</sub>), 144.4 (C<sub>q</sub>), 137.1 (C<sub>q</sub>), 133.3 (C<sub>q</sub>), 130.3 (4C, CH), 130.3 (2C, CH), 129.2 (2C, CH), 128.5 (4C, CH), 127.4 (2C, CH), 120.9 (CH), 119.9 (C<sub>q</sub>), 111.1 (CH), 73.1 (C<sub>q</sub>), 51.1 (CH<sub>3</sub>), 36.4 (CH<sub>3</sub>), 21.0 (CH<sub>3</sub>). **HRMS-ESI<sup>+</sup>** (*m/z*): [M+H]<sup>+</sup> calcd for C<sub>27</sub>H<sub>26</sub>N<sub>2</sub>O<sub>2</sub>H, 411.2067; found, 411.2062. **FT-IR** (neat)  $\tilde{\nu}$  = 3055 (w), 3022 (w), 2945 (w), 1698 (m), 1571 (w), 1507 (w), 1490 (w), 1443 (s), 1404 (w), 1368 (w), 1255 (m), 1209 (w), 1185 (w), 1151 (w), 1099 (s), 1054 (w), 1028 (w), 962 (w), 901 (w), 814 (m), 762 (m), 701 (s), 629 (w), 590 (w), 574 (w), 511 (w), 472 (w), 439 (w).

**4-((diphenyl(p-tolyl)methyl)amino)-1-methyl-1H-pyrrole-2-carboxylic acid (2):** Mtt-Py-OMe (**11**, 275 mg, 0.67 mmol) was dissolved in 1,4-dioxane (18 mL), 1 M LiOH (aq, 5 mL) added and the reaction mixture stirred for 16.5 h at 80 °C. The solvent

was removed and the crude purified over reverse phase silica column chromatography (Oasis HLB cc Vac Cartridge, 30  $\mu\text{m}$  particle size, Waters, USA;  $\text{H}_2\text{O}/\text{MeCN}/\text{NEt}_3$  100:0:0.1%  $\rightarrow$  90:10:0.1%  $\rightarrow$  75:25:0.1%  $\rightarrow$  50:50:0.1%  $\rightarrow$  0:100:0.1%) to yield Mtt-Py-OH (**2**, 241 mg, 0.61 mmol, 91%) as pale yellow solid.  $R_f = 0.54$  ( $\text{CH}_2\text{Cl}_2/\text{MeOH}/\text{NEt}_3$  100:10:1).  $^1\text{H-NMR}$  (500 MHz,  $\text{DMSO-}d_6$ ,  $\delta$ ): 7.37 -7.34 (m, 4H,  $\text{CH}_{\text{arom.}}$ ), 7.25 - 7.21 (m, 6H,  $\text{CH}_{\text{arom.}}$ ), 7.16 - 7.12 (m, 2H,  $\text{CH}_{\text{arom.}}$ ), 7.05 - 7.02 (m, 2H,  $\text{CH}_{\text{arom.}}$ ), 5.69 (d, 1H,  $J = 2.1$  Hz,  $\text{CH-2}$ ), 5.39 (d, 1H,  $J = 2.1$  Hz,  $\text{CH-1}$ ), 5.13 (s, 1H,  $\text{NH}$ ), 3.49 (s, 3H,  $\text{CH}_3$ -3), 2.24 (s, 3H,  $\text{CH}_3$ -Mtt).  $^{13}\text{C-NMR}$  (125 MHz,  $\text{DMSO-}d_6$ ,  $\delta$ ): 166.1 (C=O), 146.6 (2C,  $\text{C}_q$ ), 143.5 ( $\text{C}_q$ ), 134.8 ( $\text{C}_q$ ), 129.6 ( $\text{C}_q$ ), 129.0 ( $\text{C}_q$ ), 128.8 (6C, CH), 127.9 (2C, CH), 127.2 (4C, CH), 125.9 (2C, CH), 112.4 (CH), 106.0 (CH), 71.0 ( $\text{C}_q$ ), 35.2 ( $\text{CH}_3$ ), 20.5 ( $\text{CH}_3$ ). **HRMS-ESI**<sup>+</sup> ( $m/z$ ):  $[\text{M}+\text{Na}]^+$  calcd for  $\text{C}_{26}\text{H}_{24}\text{N}_2\text{O}_2\text{Na}$ , 419.1730; found, 419.1725. **FT-IR** (neat)  $\tilde{\nu} = 3345$  (w), 3081 (w), 3056 (w), 3022 (w), 2975 (w), 2921 (w), 2172 (w), 1562 (m), 1489 (w), 1438 (s), 1402 (w), 1364 (w), 1326 (w), 1284 (w), 1207 (w), 1185 (w), 1152 (w), 1119 (w), 1030 (w), 901 (w), 814 (w), 771 (m), 700 (s), 626 (w), 576 (w), 511 (w), 492 (w), 472 (w), 450 (w).

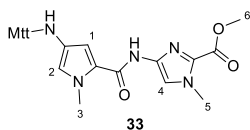


**methyl 4-((diphenyl(p-tolyl)methyl)amino)-1-methyl-1H-imidazole-2-carboxylate (13):** Nitro-Im-OMe (**12**, 506 mg, 2.96 mmol) was dissolved in EtOH/EtOAc 1:1 (10 mL). Pd/C (10% dry, 38 mg, 8% w/w) was added and the reaction mixture stirred under hydrogen atmosphere. After 19 h, it was filtered over celite and the solvent removed. Under inert atmosphere, the residue was dissolved in  $\text{CH}_2\text{Cl}_2$  (3.6 mL) and pyridine (2.4 mL) and MttCl (867 mg, 2.96 mmol) was added. After 3 h at rt, the solvent was removed under reduced pressure, the crude coevaporated with EtOAc (3 x 10 mL) and purified via flash column chromatography (silica,  $\text{CH}_2\text{Cl}_2/\text{MeOH}/\text{NEt}_3$  100:0:1  $\rightarrow$  100:1:1  $\rightarrow$  10:1:1). Mtt-Im-OMe (**13**, 908 mg, 2.21 mmol, 75%) was preserved as pale yellow solid.  $R_f = 0.24$  ( $\text{CH}_2\text{Cl}_2/\text{NEt}_3$  100:1).  $^1\text{H-NMR}$  (300 MHz,  $\text{CD}_3\text{OD}$ ,  $\delta$ ): 7.40 -7.33 (m, 4H,  $\text{CH}_{\text{arom.}}$ ), 7.29 - 7.15 (m, 8H,  $\text{CH}_{\text{arom.}}$ ), 7.11 - 7.04 (m, 2H,  $\text{CH}_{\text{arom.}}$ ), 5.46 (s, 1H,  $\text{CH-1}$ ), 3.81 (s, 3H,  $\text{CH}_3$ -3), 3.59 (s, 3H,  $\text{CH}_3$ -2), 2.28 (s, 3H,  $\text{CH}_3$ -Mtt).  $^{13}\text{C-NMR}$  (75 MHz,  $\text{CD}_3\text{OD}$ ,  $\delta$ ): 160.0 (C=O), 147.1 ( $\text{C}_q$ ), 146.7 (2C,  $\text{C}_q$ ), 143.5 ( $\text{C}_q$ ), 137.7 ( $\text{C}_q$ ), 131.6 ( $\text{C}_q$ ), 130.0 (6C, CH), 129.5 (2C, CH), 128.9 (4C, CH), 127.9 (2C, CH), 111.7 (CH), 72.1 ( $\text{C}_q$ ), 52.3 ( $\text{CH}_3$ ), 35.8 ( $\text{CH}_3$ ), 20.9 ( $\text{CH}_3$ ). **HRMS-ESI**<sup>+</sup> ( $m/z$ ):  $[\text{M}+\text{H}]^+$  calcd for  $\text{C}_{26}\text{H}_{25}\text{N}_3\text{O}_2\text{H}$ , 412.2031; found, 412.2023. **FT-IR** (neat)  $\tilde{\nu} = 3252$  (w), 3055 (w), 3022 (w), 2947 (w), 1704 (s), 1560 (m), 1485 (w), 1443 (s), 1412 (w), 1271 (m), 1199 (m), 1121 (s), 1067 (w), 1052 (w), 1014 (w), 966 (w), 928 (w), 900 (w), 843 (w), 816 (m), 788 (w), 749 (w), 701 (s), 629 (m), 575 (w), 538 (w), 513 (w), 474 (w), 438 (w).



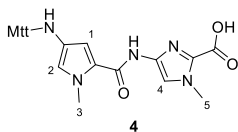
**4-((diphenyl(p-tolyl)methyl)amino)-1-methyl-1H-imidazole-2-carboxylic acid (3):** Mtt-Im-OMe (**13**, 423 mg, 1.03 mmol) was dissolved in MeOH (3.4 mL), 1 M KOH (aq, 1.7 mL) added and the reaction mixture stirred for 20 h at rt. At 0  $^\circ\text{C}$ , it was acidified until pH 4 with 10% AcOH (aq). The product was extracted with  $\text{CHCl}_3$  (4 x 50 mL), washed with 10% AcOH (3 x 50 mL) and the combined organic layers dried over  $\text{MgSO}_4$ . The solvent was removed to yield Mtt-Im-OH (**3**, 368 mg, 0.93 mmol, 90%) as pale yellow solid.  $R_f = 0.51$  ( $\text{CH}_2\text{Cl}_2/\text{MeOH} / \text{NEt}_3$  100:10:1).  $^1\text{H-NMR}$  (300 MHz,  $\text{CDCl}_3$ ,  $\delta$ ): 8.43 (br s, 1H,  $\text{NH}$ ), 7.41 -7.34 (m, 4H,  $\text{CH}_{\text{arom.}}$ ), 7.27 - 7.16 (m, 8H,  $\text{CH}_{\text{arom.}}$ ), 7.07 - 7.00 (m, 2H,  $\text{CH}_{\text{arom.}}$ ), 4.87 (s, 1H,  $\text{CH-1}$ ), 3.65 (s, 3H,  $\text{CH}_3$ -2), 2.28 (s, 3H,  $\text{CH}_3$ -Mtt).  $^{13}\text{C-NMR}$  (75 MHz,  $\text{CDCl}_3$ ,  $\delta$ ): 158.9 (C=O), 144.7 (2C,  $\text{C}_q$ ), 141.4 ( $\text{C}_q$ ), 139.6 ( $\text{C}_q$ ), 136.5 ( $\text{C}_q$ ), 133.7 ( $\text{C}_q$ ), 129.3 (6C, CH), 128.6 (2C, CH), 127.8 (4C, CH), 126.9 (2C, CH), 104.0 (CH), 71.6 ( $\text{C}_q$ ), 34.9 ( $\text{CH}_3$ ), 21.1 ( $\text{CH}_3$ ). **HRMS-ESI**<sup>+</sup> ( $m/z$ ):  $[\text{M}+\text{H}]^+$  calcd for  $\text{C}_{25}\text{H}_{23}\text{N}_3\text{O}_2\text{H}$ , 398.1863; found, 398.1865. **FT-IR** (neat)  $\tilde{\nu} = 3167$  (w), 2921 (w), 1628 (m), 1534 (w), 1511 (w), 1492 (w), 1444 (w), 1322 (m), 1186 (w), 1159 (w), 1123 (w), 1094 (w), 1070 (w), 1031 (w), 1001 (w), 941 (w), 900 (w), 815 (m), 798 (w), 758 (w), 701 (s), 629 (m), 576 (w), 541 (w), 502 (w), 438 (w).





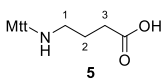
**methyl 4-((diphenyl(p-tolyl)methyl)amino)-1-methyl-1H-pyrrole-2-carboxamido)-1-methyl-1H-imidazole-2-carboxylate (33):** To a solution of nitro-PyIm-OMe (300 mg, 0.98 mmol) in MeOH (7.0 mL) and DMF (0.5 mL), Pd/C (10% dry, 100 mg, 33% w/w) was added and the mixture stirred under hydrogen atmosphere for 6.5 h. The catalyst was removed by filtration through

celite and the solvent removed under reduced pressure. The residue was dissolved in DMF (1.8 mL), and DIPEA (268  $\mu$ L, 1.54 mmol) was added. At 0  $^{\circ}$ C, Mtt-Cl (220 mg, 0.75 mmol) dissolved in DMF (1.2 mL) and DIPEA (137  $\mu$ L, 0.79 mmol) was added dropwise over 10 min. The reaction was stirred at rt for 15.5 h and the solvent removed under reduced pressure. The crude was purified by column chromatography (silica, CH<sub>2</sub>Cl<sub>2</sub>/NEt<sub>3</sub> 100:1) to yield the desired product (**33**, 323 mg, 0.61 mmol, 62%) as pale yellow solid.  $R_f$  = 0.33 (*n*-pentane/EtOAc 1:1). <sup>1</sup>H-NMR (300 MHz, CDCl<sub>3</sub>,  $\delta$ ): 7.44 (s, 1H, CH-4), 7.43 - 7.39 (m, 4H, CH<sub>arom.</sub>), 7.31 - 7.27 (m, 2H, CH<sub>arom.</sub>), 7.25 - 7.20 (m, 4H, CH<sub>arom.</sub>), 7.17 - 7.13 (m, 2H, CH<sub>arom.</sub>), 7.07 - 7.03 (m, 2H, CH<sub>arom.</sub>), 6.21 (d, 1H, *J* = 2.0 Hz, CH-2), 5.72 (d, 1H, *J* = 2.0 Hz, CH-1), 3.95 (s, 3H, CH<sub>3</sub>-5), 3.88 (s, 3H, CH<sub>3</sub>-6), 3.56 (s, 3H, CH<sub>3</sub>-3), 2.28 (s, 3H, CH<sub>3</sub>-Mtt). <sup>13</sup>C-NMR (75 MHz, CDCl<sub>3</sub>,  $\delta$ ): 161.0 (C=O), 160.2 (C=O), 147.6 (2C, C<sub>q</sub>), 144.4 (C<sub>q</sub>), 138.6 (C<sub>q</sub>), 137.1 (C<sub>q</sub>), 133.2 (C<sub>q</sub>), 132.8 (C<sub>q</sub>), 130.3 (6C, CH), 129.2 (2C, CH), 128.5 (4C, CH), 127.4 (2C, CH), 122.4 (C<sub>q</sub>), 119.9 (CH), 116.7 (CH), 107.4 (CH), 73.2 (C<sub>q</sub>), 52.6 (CH<sub>3</sub>), 36.4 (2C, CH<sub>3</sub>), 21.0 (CH<sub>3</sub>). HRMS-ESI<sup>+</sup> (*m/z*): [M+Na]<sup>+</sup> calcd for C<sub>32</sub>H<sub>31</sub>N<sub>5</sub>O<sub>3</sub>Na, 556.2319; found, 556.2317. FT-IR (neat)  $\tilde{\nu}$  = 3322 (w), 3054 (w), 3022 (w), 2927 (w), 2851 (w), 1711 (m), 1650 (m), 1559 (w), 1528 (m), 1456 (w), 1431 (s), 1401 (w), 1368 (w), 1301 (w), 1274 (m), 1247 (w), 1215 (w), 1187 (w), 1124 (s), 1104 (w), 1055 (w), 1017 (w), 895 (w), 839 (w), 817 (w), 753 (m), 701 (s), 658 (w), 629 (w), 589 (w), 511 (w), 442 (w).



**4-((diphenyl(p-tolyl)methyl)amino)-1-methyl-1H-pyrrole-2-carboxamido)-1-methyl-1H-imidazole-2-carboxylic acid (4):** Mtt-PyIm-OMe (287 mg, 0.55 mmol) was dissolved in 1,4-dioxane (14 mL) and 1 M LiOH (aq, 7 mL) and stirred for 1 h at 80  $^{\circ}$ C and 1.5 h at rt. The dioxane was removed under reduced pressure and the crude purified over reverse phase silica column

chromatography (Oasis HLB cc Vac Cartridge, 30  $\mu$ m particle size, Waters, USA; H<sub>2</sub>O/MeCN/NEt<sub>3</sub> 100:0:0.1%  $\rightarrow$  50:50:0.1%). The product fractions were freeze dried to yield the desired product (**4**, 242 mg, 0.47 mmol, 85%) as pale yellow solid.  $R_f$  = 0.25 (CH<sub>2</sub>Cl<sub>2</sub>/MeOH/NEt<sub>3</sub> 100:10:1). <sup>1</sup>H-NMR (300 MHz, DMSO-*d*<sub>6</sub>,  $\delta$ ): 10.09 (s, 1H, NH), 7.43 - 7.36 (m, 4H, CH<sub>arom.</sub>), 7.31 - 7.24 (m, 6H, CH<sub>arom.</sub>), 7.20 - 7.14 (m, 2H, CH<sub>arom.</sub>), 7.11 - 7.06 (m, 3H, CH<sub>arom.</sub>, CH-4), 7.00 (s, 1H, CH-2), 5.40 (s, 1H, CH-1), 5.24 (s, 1H, NH), 3.90 (s, 3H, CH<sub>3</sub>-5), 3.50 (s, 3H, CH<sub>3</sub>-3), 2.25 (s, 3H, CH<sub>3</sub>-Mtt). <sup>13</sup>C-NMR (75 MHz, DMSO-*d*<sub>6</sub>,  $\delta$ ): 161.7 (C=O), 158.2 (C=O), 146.1 (2C, C<sub>q</sub>), 143.0 (C<sub>q</sub>), 140.4 (C<sub>q</sub>), 135.2 (2C, C<sub>q</sub>), 131.0 (C<sub>q</sub>), 128.8 (4C, CH), 128.7 (2C, CH), 128.2 (2C, CH), 127.5 (4C, CH), 126.2 (2C, CH), 121.4 (C<sub>q</sub>), 116.0 (CH), 109.8 (CH), 106.5 (CH), 71.0 (C<sub>q</sub>), 35.7 (CH<sub>3</sub>), 34.2 (CH<sub>3</sub>), 20.5 (CH<sub>3</sub>). HRMS-ESI<sup>+</sup> (*m/z*): [M+Li]<sup>+</sup> calcd. for C<sub>31</sub>H<sub>29</sub>N<sub>5</sub>O<sub>3</sub>Li, 526.2426; found, 526.2423. FT-IR (neat)  $\tilde{\nu}$  = 3324 (w), 3054 (w), 3022 (w), 2928 (w), 1622 (w), 1574 (w), 1538 (w), 1461 (w), 1427 (s), 1404 (w), 1345 (m), 1309 (w), 1253 (w), 1217 (w), 1185 (w), 1156 (w), 1105 (w), 1054 (w), 1029 (w), 898 (w), 846 (w), 813 (w), 753 (m), 702 (s), 663 (w), 632 (w), 587 (w), 508 (w).



**4-((diphenyl(p-tolyl)methyl)amino)butanoic acid (5):** Methyl 4-aminobutyrate hydrochloride (300 mg, 1.95 mmol) was suspended in DMF (4.5 mL) and DIPEA (678  $\mu$ L, 3.89 mmol). At 0  $^{\circ}$ C, Mtt-Cl (520 mg, 1.78 mmol) dissolved in DMF

(1.5 mL) and DIPEA (618  $\mu$ L, 3.55 mmol) was added dropwise over 5 min. After 12.5 h at rt, the solvent was removed under reduced pressure and the crude purified by column chromatography (silica, CH<sub>2</sub>Cl<sub>2</sub>/NEt<sub>3</sub> 100:1). The product was dissolved MeOH (6.0 mL) and 1 M KOH (aq, 3 mL) and stirred at 60  $^{\circ}$ C for 3 h. The reaction mixture was extracted with *n*-pentane (3 x 50 mL), MeOH was removed from the aqueous phase under reduced pressure and this phase acidified with 20% AcOH (aq) until pH 4. It was extracted with EtOAc (6 x 50 mL), washed with brine and dried over MgSO<sub>4</sub>. The solvent was

removed to yield the desired product (**5**, 581 mg, 1.62 mmol, 83%) as colourless solid.  $R_f = 0.18$  (*n*-pentane/EtOAc 1:1). **<sup>1</sup>H-NMR** (300 MHz, CD<sub>3</sub>OD,  $\delta$ ): 7.42 -7.32 (m, 10H,  $CH_{\text{arom.}}$ ), 7.29 – 7.20 (m, 4H,  $CH_{\text{arom.}}$ ), 2.73 (t, 2H,  $J = 6.3$  Hz,  $CH_2$ -1), 2.45 – 2.38 (m, 2H,  $CH_2$ -3), 2.35 (s, 3H,  $CH_3$ -Mtt), 1.90 – 1.80 (m, 2H,  $CH_2$ -2). **<sup>13</sup>C-NMR** (75 MHz, CD<sub>3</sub>OD,  $\delta$ ): 179.5 (C=O), 142.9 (2C, C<sub>q</sub>), 139.6 (C<sub>q</sub>), 139.3 (C<sub>q</sub>), 130.1 (2C, CH), 130.0 (2C, CH), 129.8 (4C, CH), 129.5 (4C, CH), 129.1 (2C, CH), 74.8 (C<sub>q</sub>), 46.2 (CH<sub>2</sub>), 35.4 (CH<sub>2</sub>), 24.3 (CH<sub>2</sub>), 21.0 (CH<sub>3</sub>). **HRMS-ESI<sup>+</sup>** ( $m/z$ ): [M+Na]<sup>+</sup> calcd for C<sub>24</sub>H<sub>25</sub>NO<sub>2</sub>Na, 382.1778; found, 382.1787. **FT-IR** (neat)  $\tilde{\nu} = 3022$  (w), 2920 (w), 2852 (w), 1707 (w), 1562 (w), 1490 (w), 1446 (m), 1403 (w), 1311 (w), 1190 (w), 1158 (w), 1103 (w), 1031 (w), 1002 (w), 905 (w), 813 (w), 751 (m), 702 (s), 637 (w), 613 (m), 571 (w), 533 (w), 496 (w).

## NMR and IR spectra of new compounds

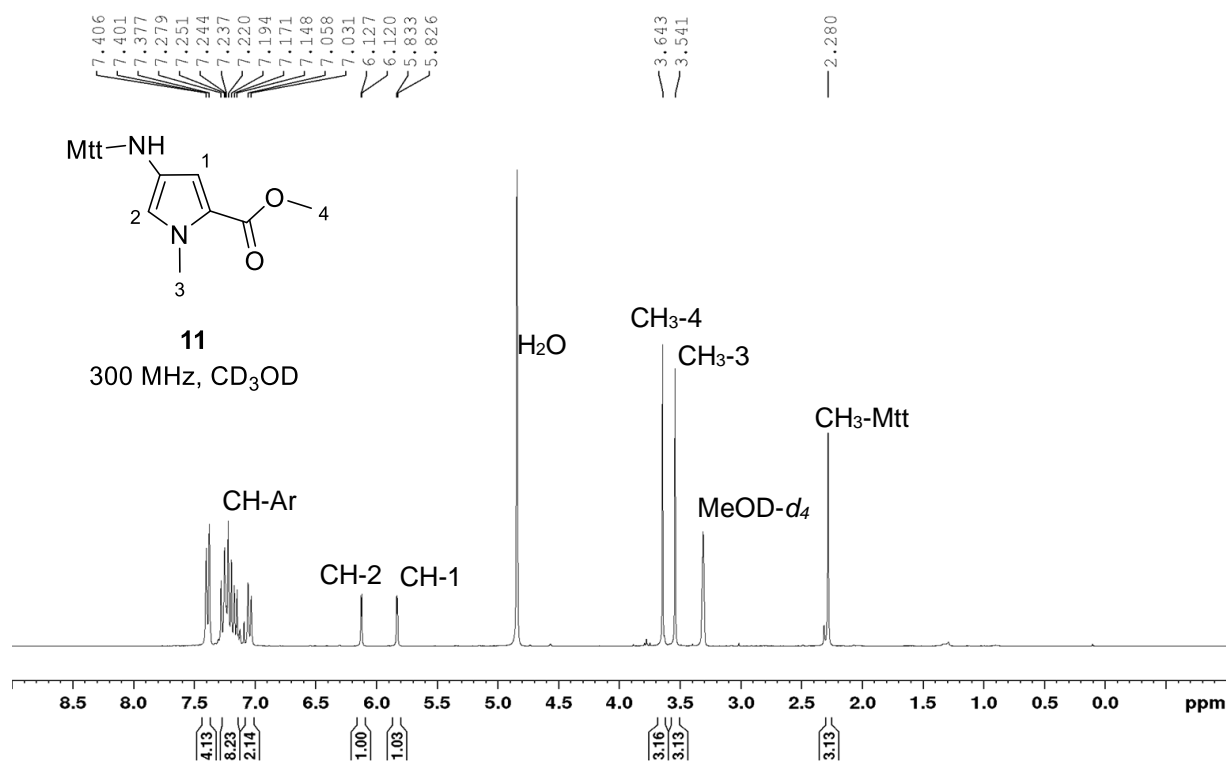


Figure S1: <sup>1</sup>H-NMR (300 MHz) spectrum of Mtt-Py-OMe (**11**).

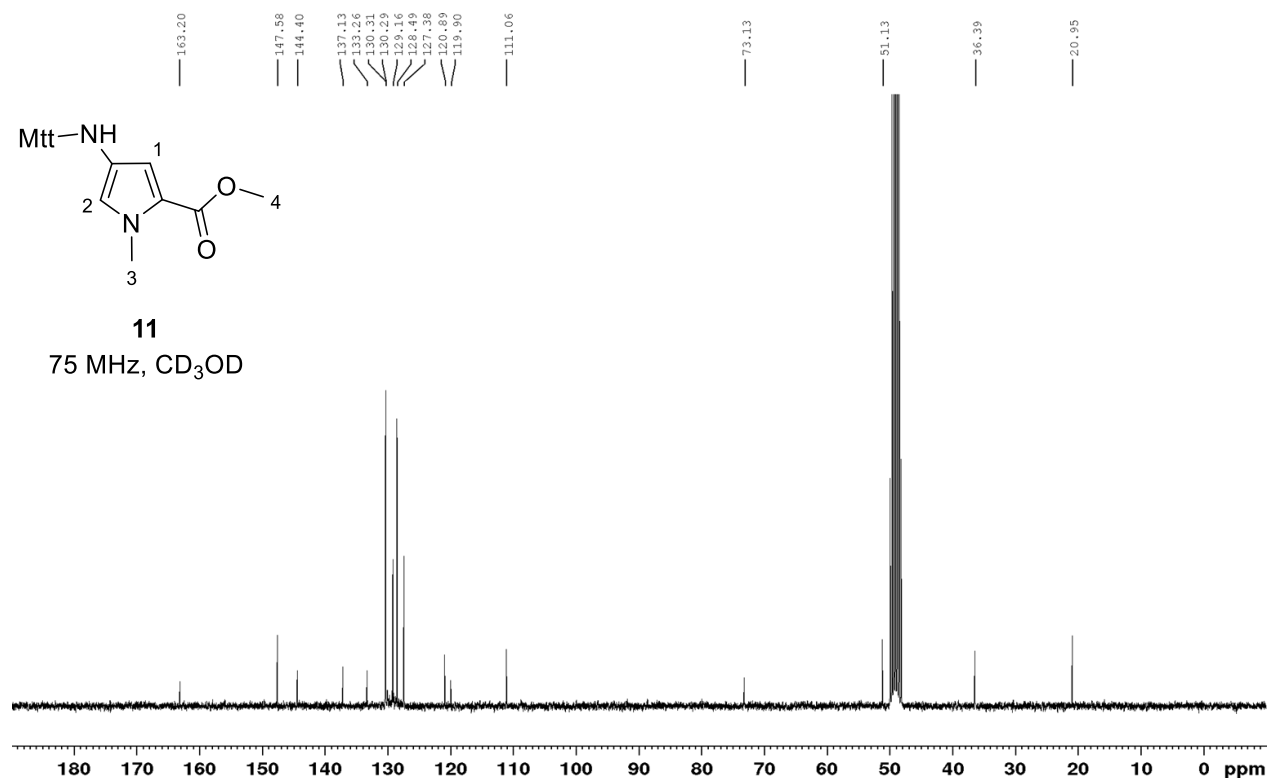


Figure S2: <sup>13</sup>C-NMR (75 MHz) spectrum of Mtt-Py-OMe (**11**).

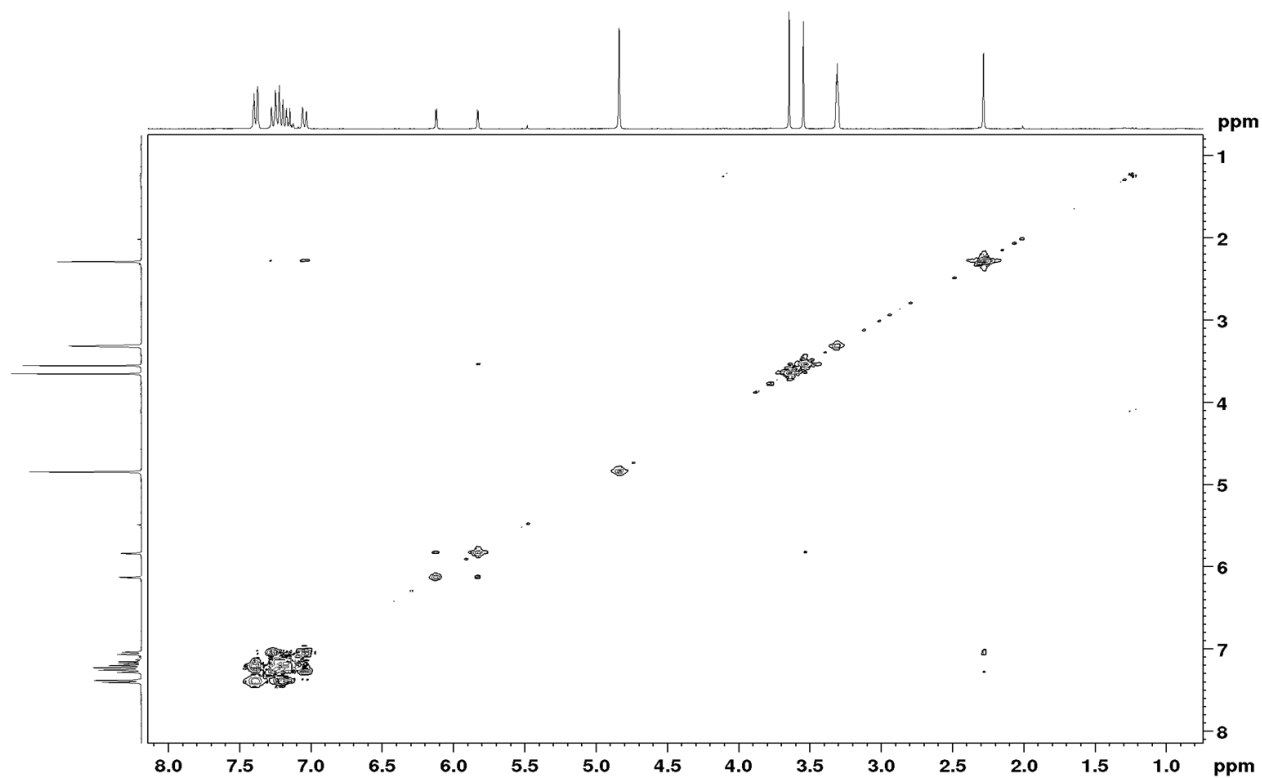


Figure S3: COSY-NMR (300 MHz) spectrum of Mtt-Py-OMe (**11**).

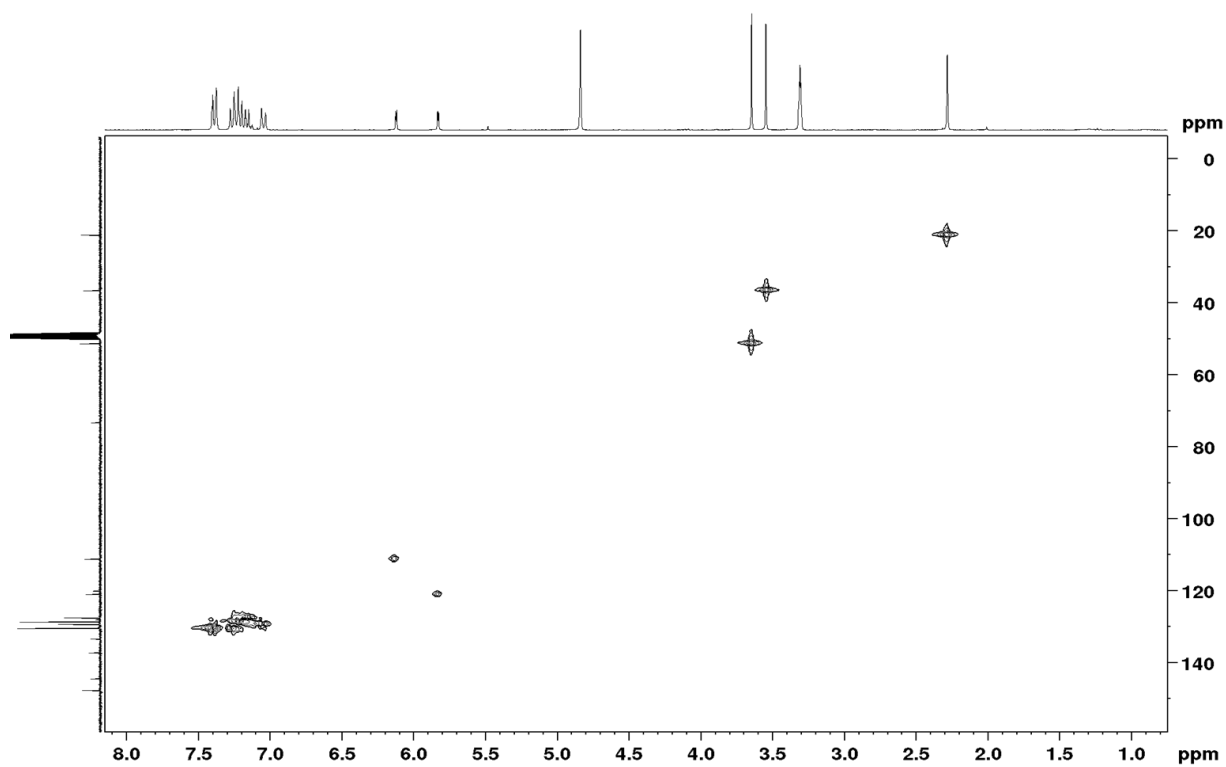


Figure S4: HSQC-NMR (300 MHz, 75 MHz) spectrum of Mtt-Py-OMe (**11**).

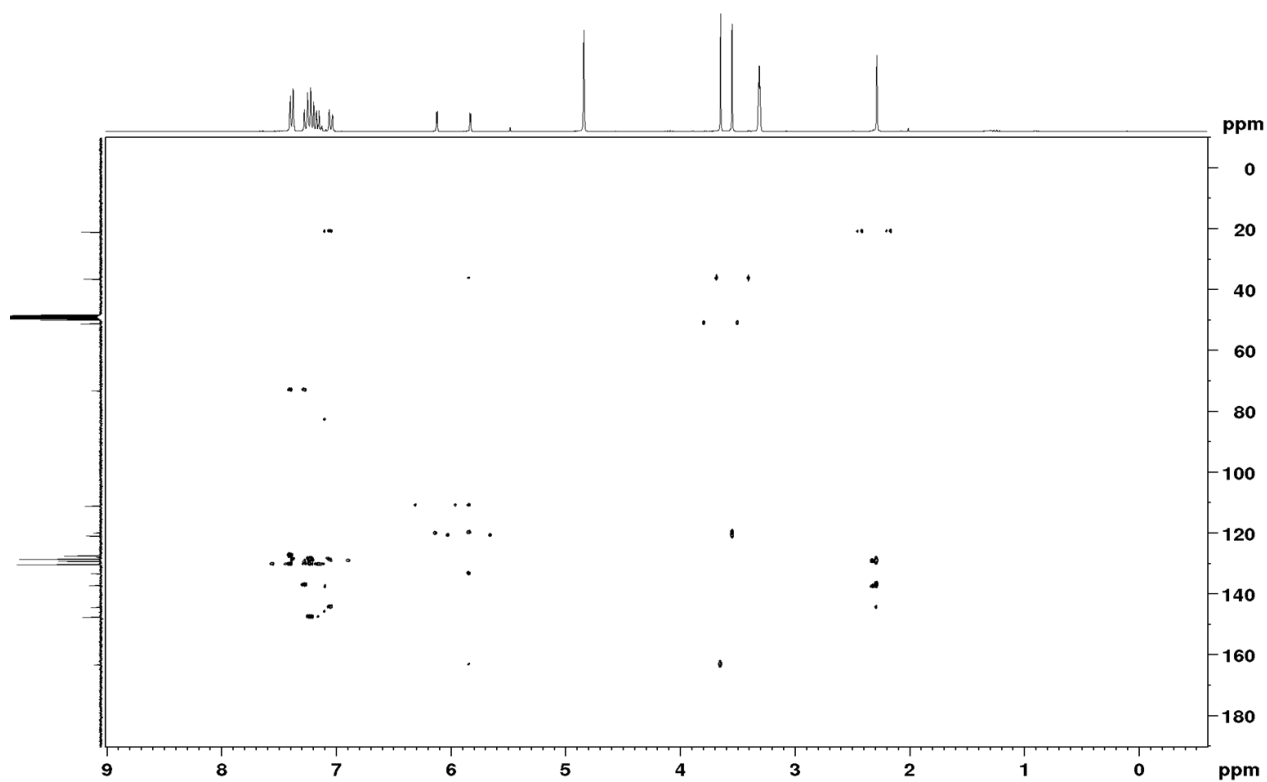


Figure S5: HMBC-NMR (500 MHz, 125 MHz) spectrum of Mtt-Py-OMe (11).

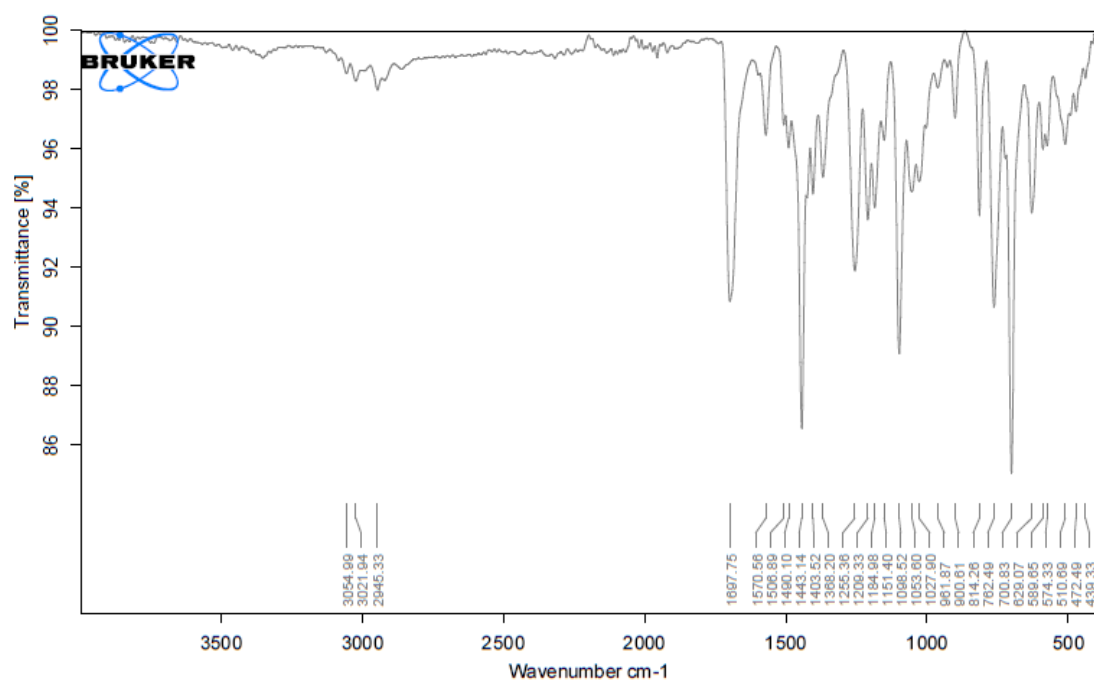


Figure S6: IR spectrum of Mtt-Py-OMe (11).

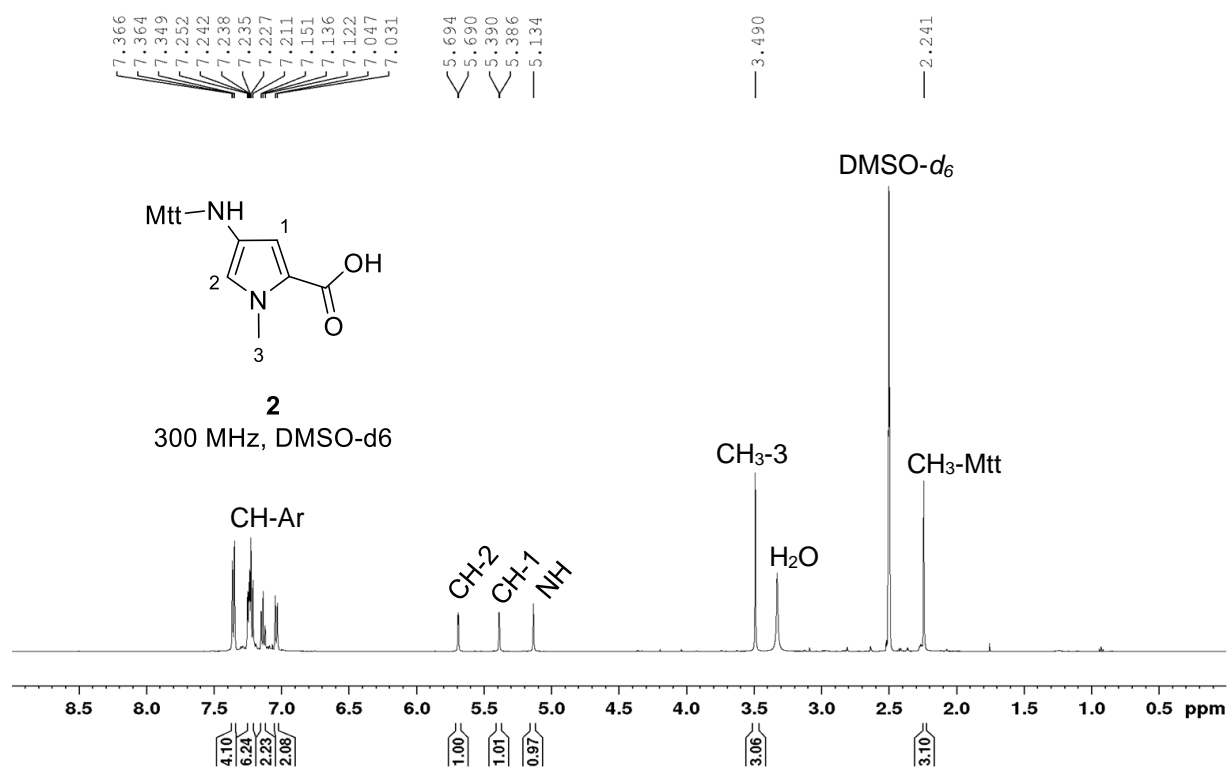


Figure S7: <sup>1</sup>H-NMR (300 MHz) spectrum of Mtt-Py-OH (**2**).

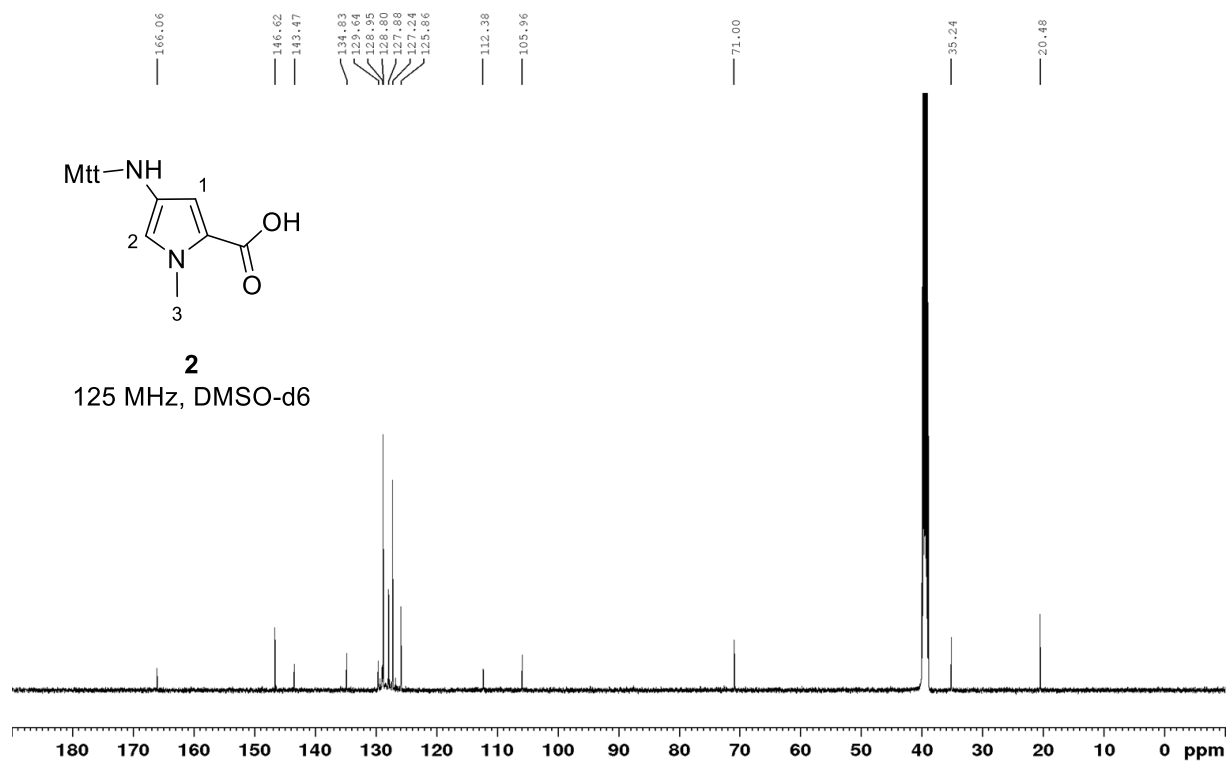
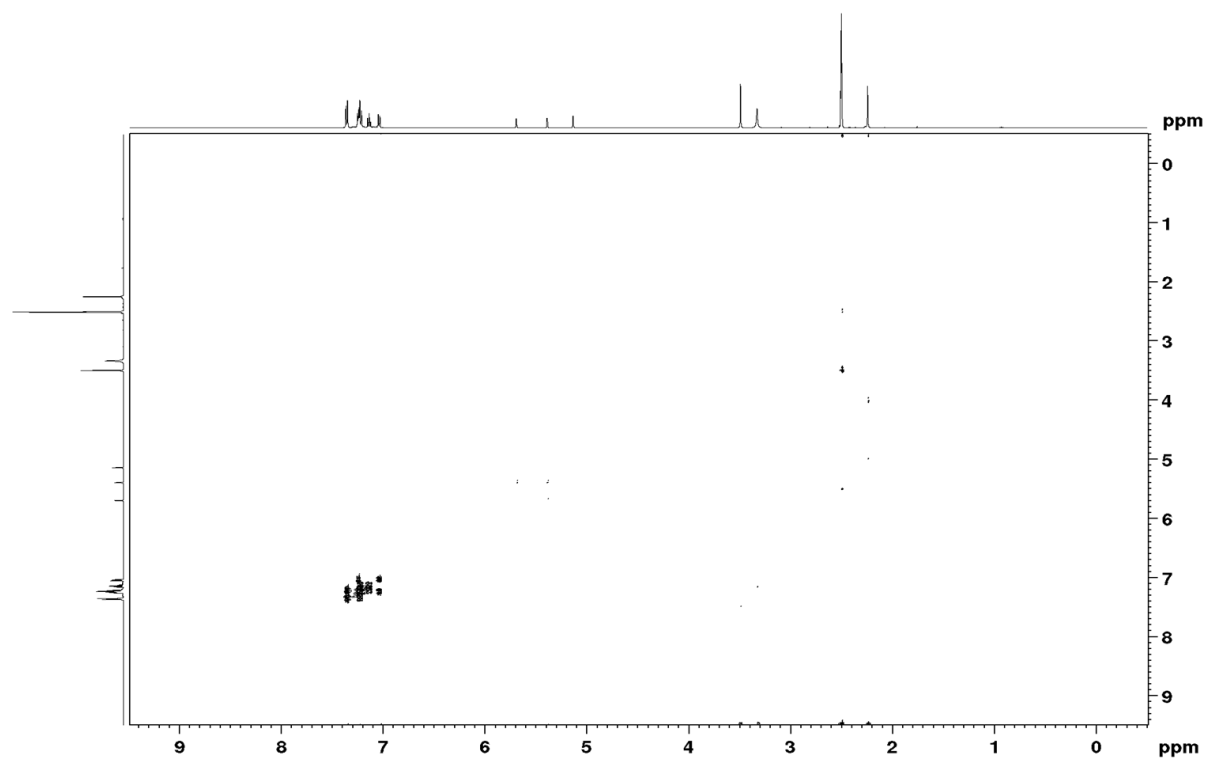
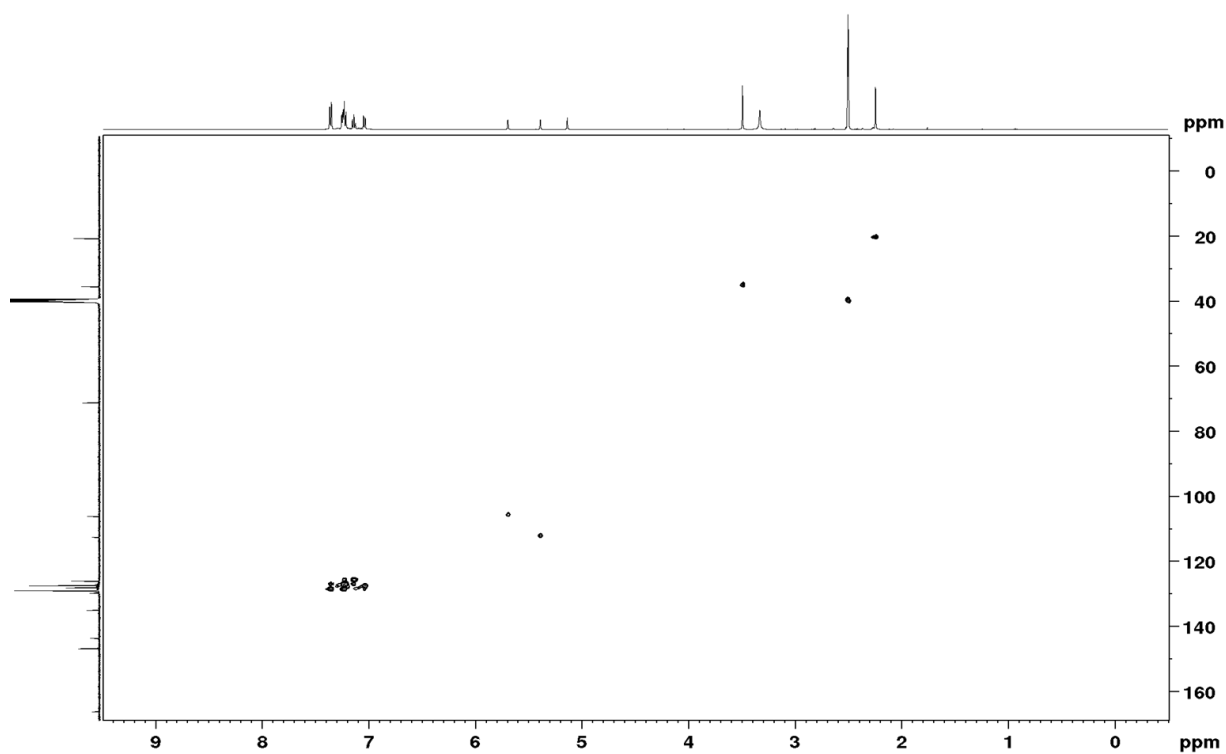


Figure S8: <sup>13</sup>C-NMR (125 MHz) spectrum of Mtt-Py-OH (**2**).



**Figure S9:** COSY-NMR (500 MHz) spectrum of Mtt-Py-OH (**2**).



**Figure S10:** HSQC-NMR (500 MHz, 125 MHz) spectrum of Mtt-Py-OH (**2**).

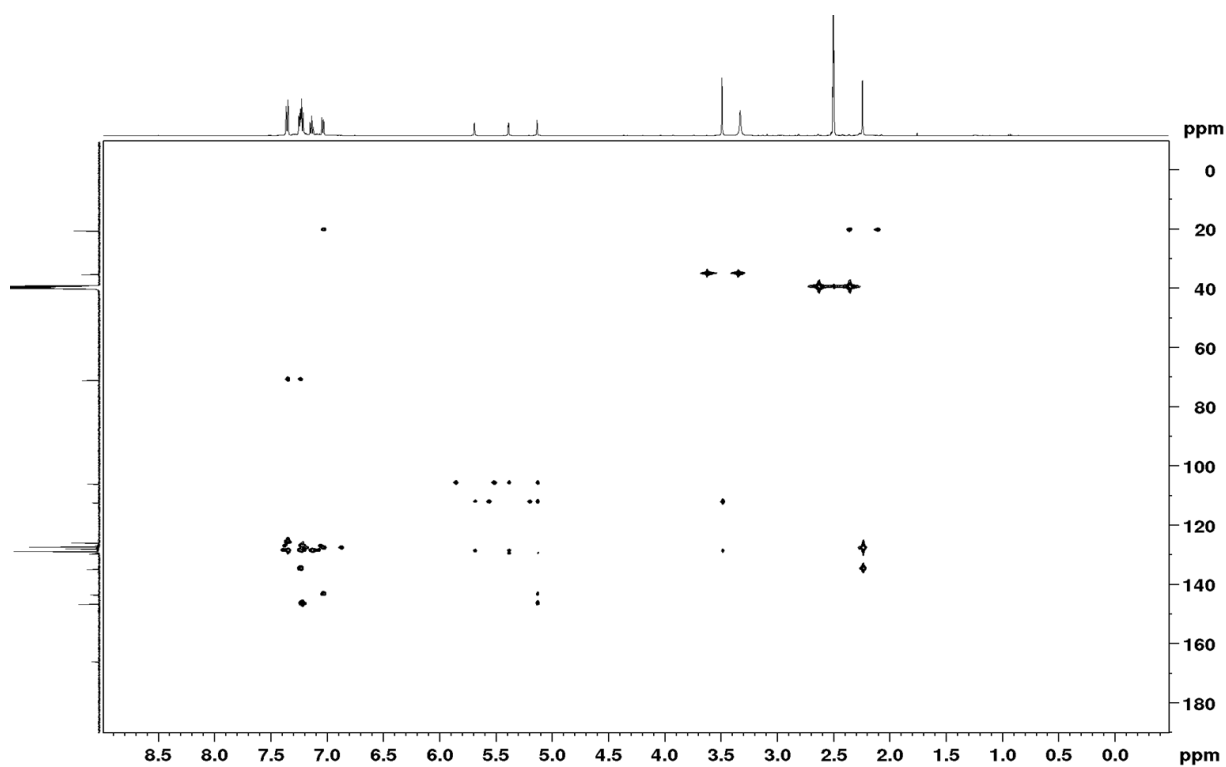


Figure S11: HMBC-NMR (500 MHz, 125 MHz) spectrum of Mtt-Py-OH (2).

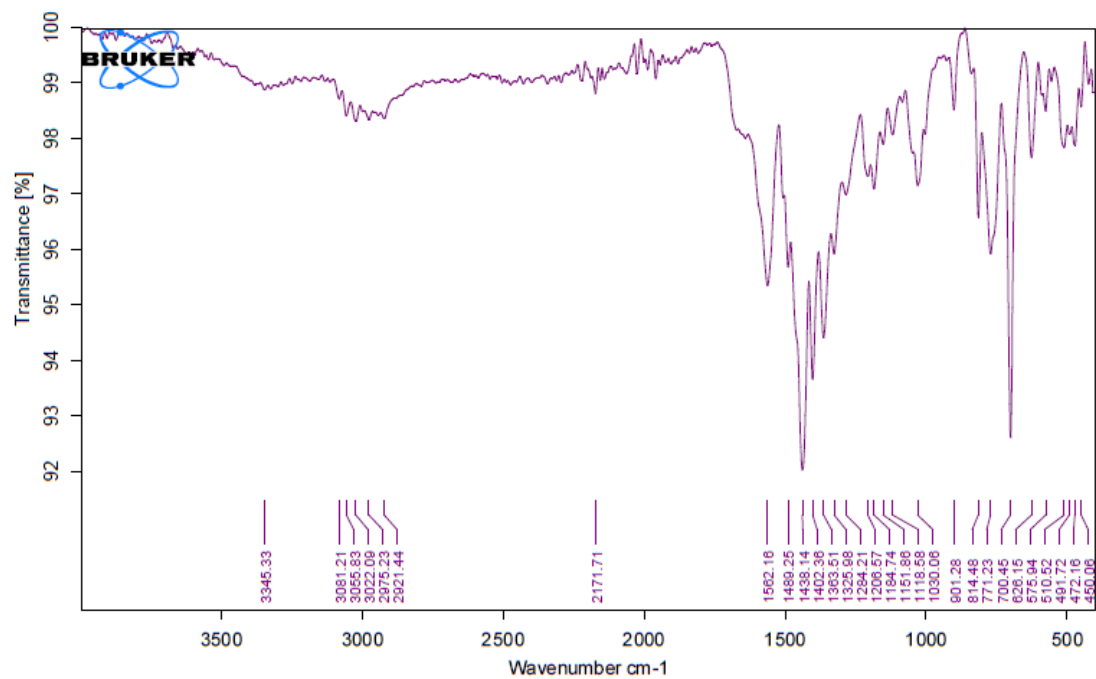
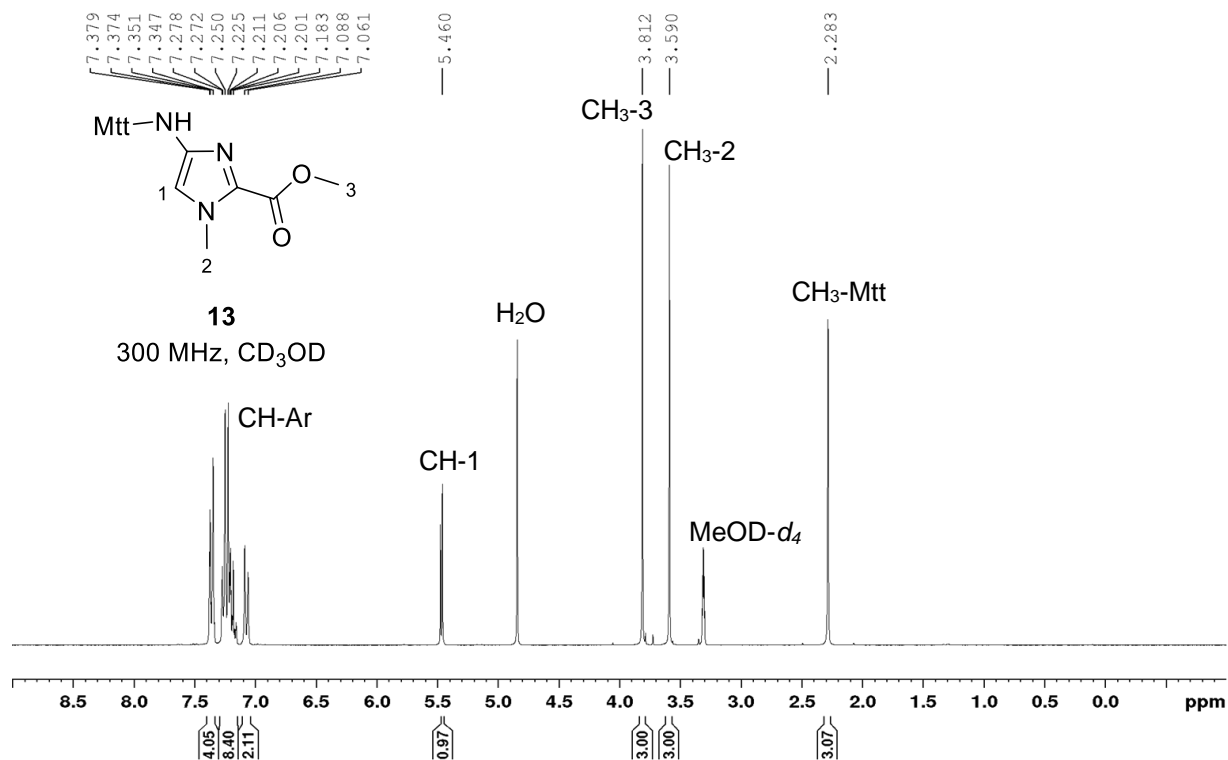
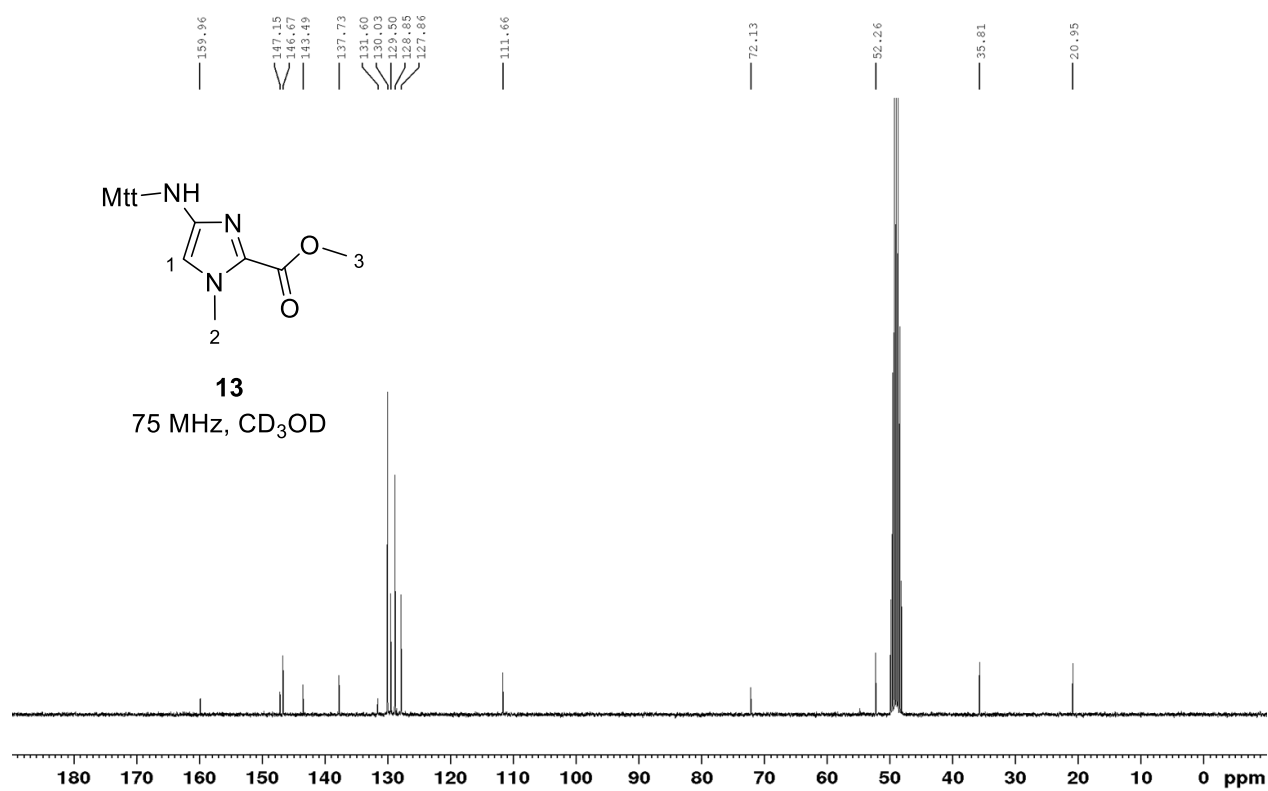


Figure S12: IR spectrum of Mtt-Py-OH (2).





**Figure S13:** <sup>1</sup>H-NMR (300 MHz) spectrum of Mtt-Im-OMe (**13**).



**Figure S14:** <sup>13</sup>C-NMR (75 MHz) spectrum of Mtt-Im-OMe (**13**).

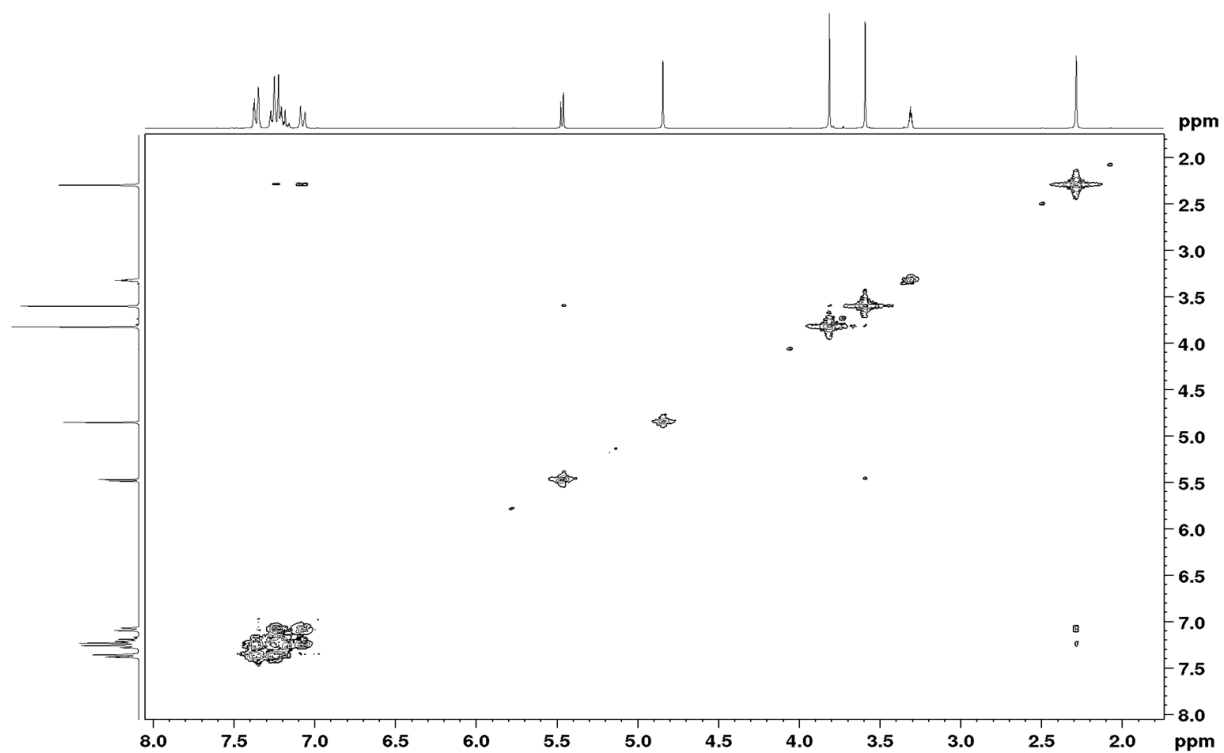


**Figure S15:** COSY-NMR (300 MHz) spectrum of Mtt-Im-OMe (**13**).

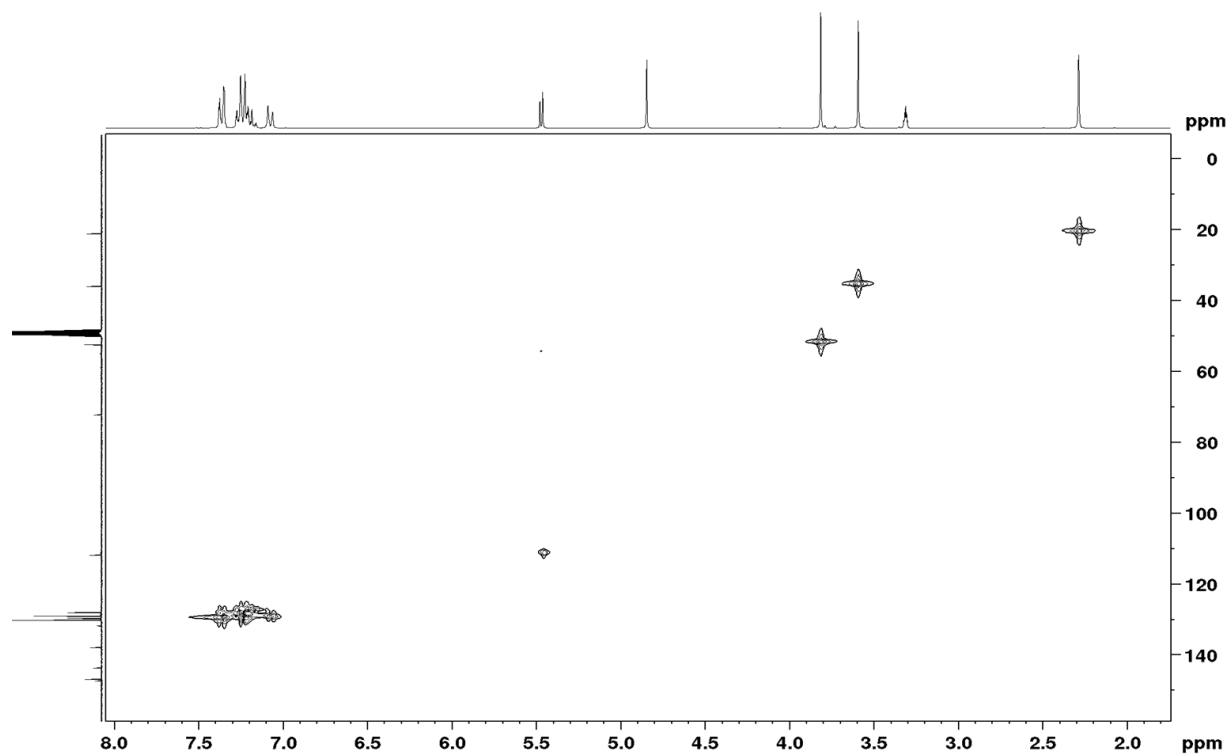


**Figure S16:** HSQC-NMR (300 MHz, 75 MHz) spectrum of Mtt-Im-OMe (**13**).

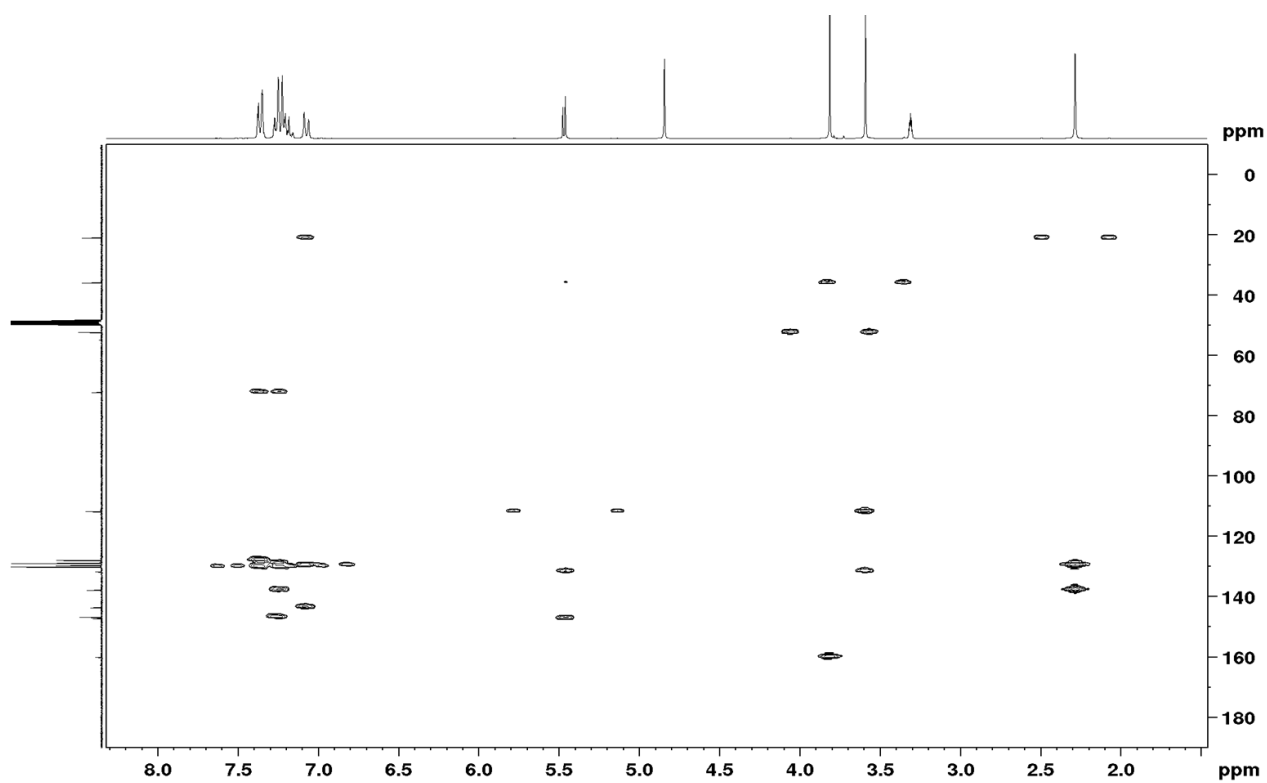


Figure S17: HMBC-NMR (500 MHz, 125 MHz) spectrum of Mtt-Im-OMe (13).

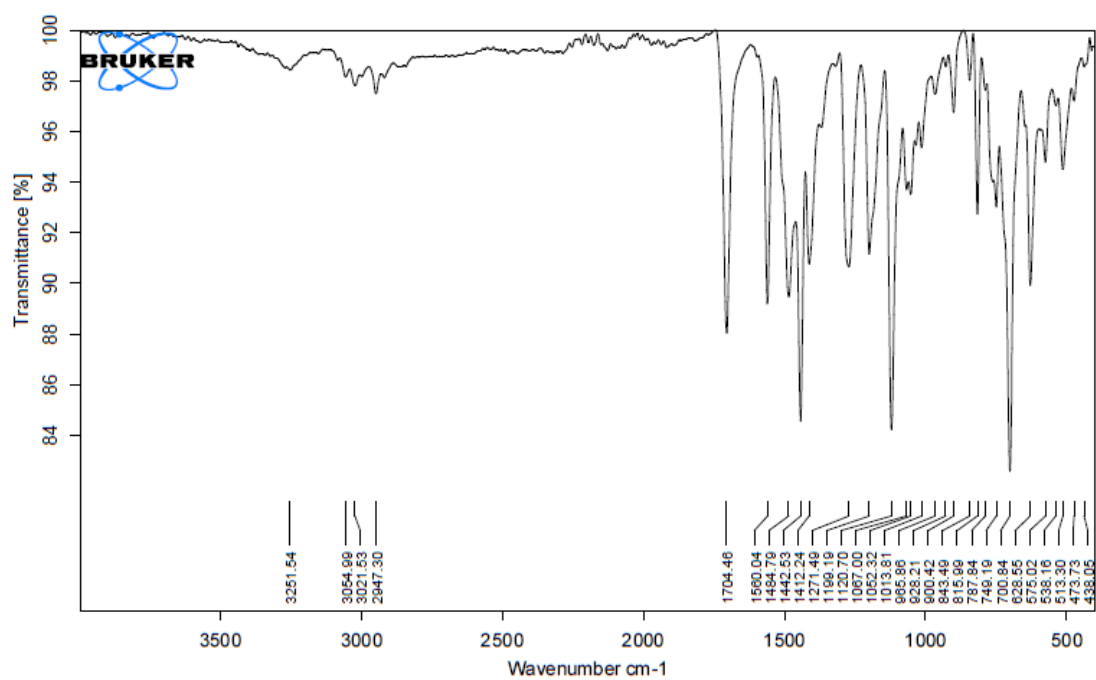
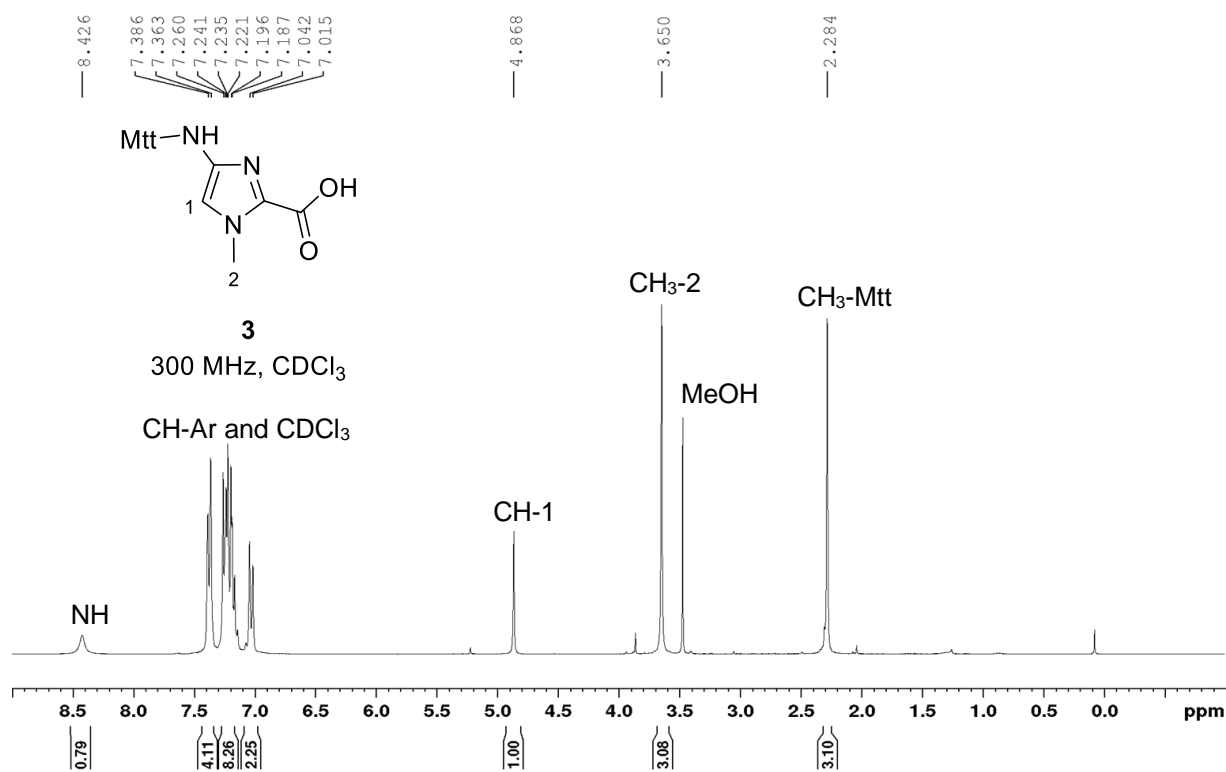
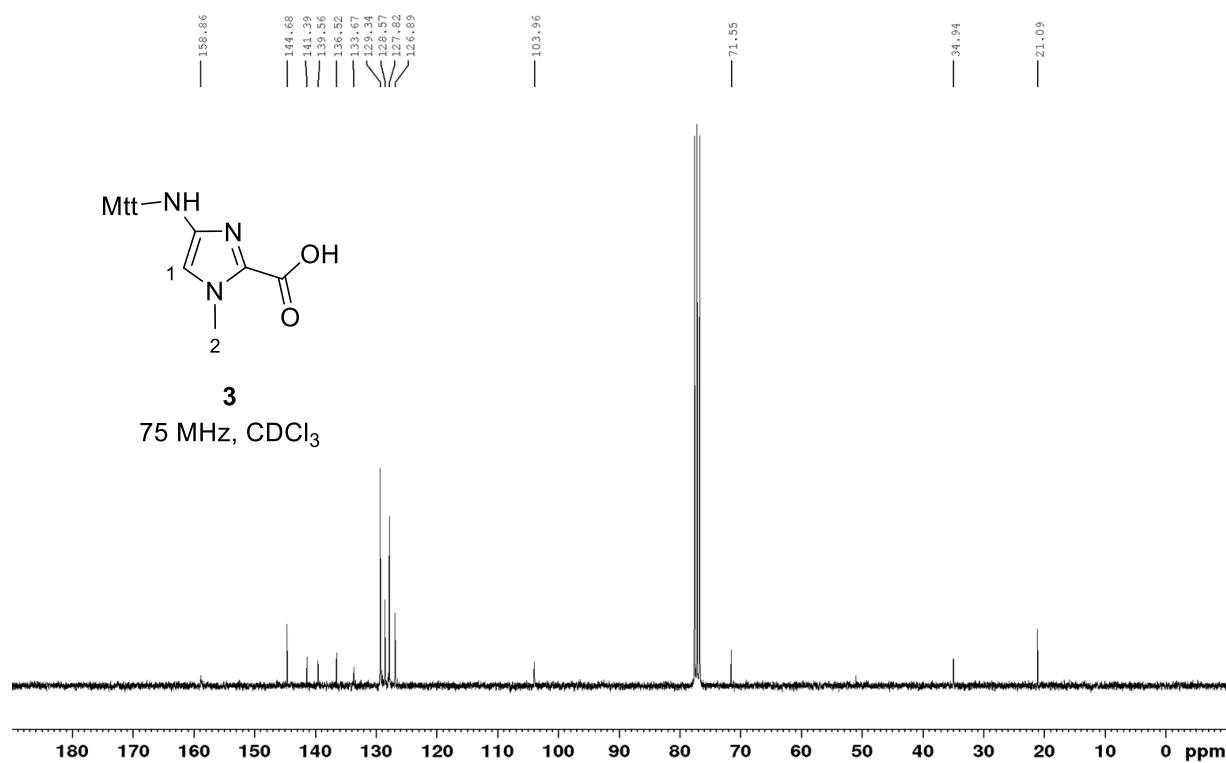


Figure S18: IR spectrum of Mtt-Im-OMe (13).



**Figure S19:** <sup>1</sup>H-NMR (300 MHz) spectrum of Mtt-Im-OH (**3**).



**Figure S20:** <sup>13</sup>C-NMR (75 MHz) spectrum of Mtt-Im-OH (**3**).

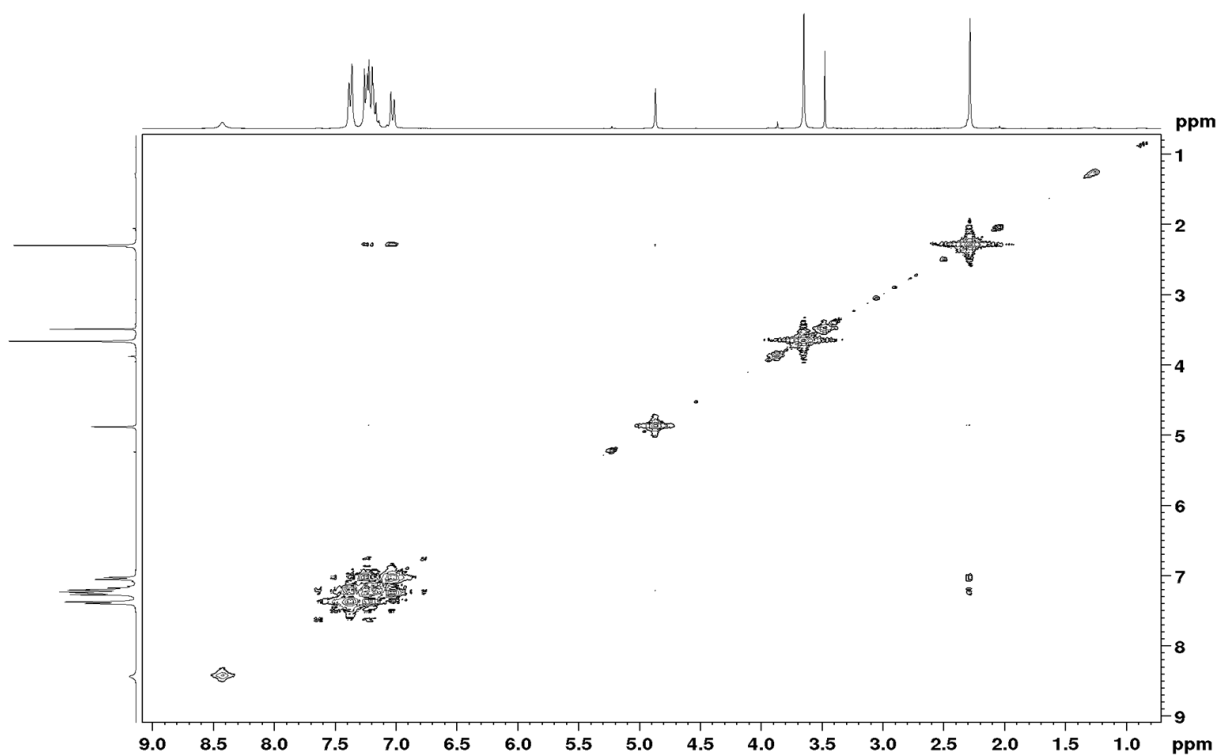


**Figure S21:** COSY-NMR (300 MHz) spectrum of Mtt-Im-OH (3).

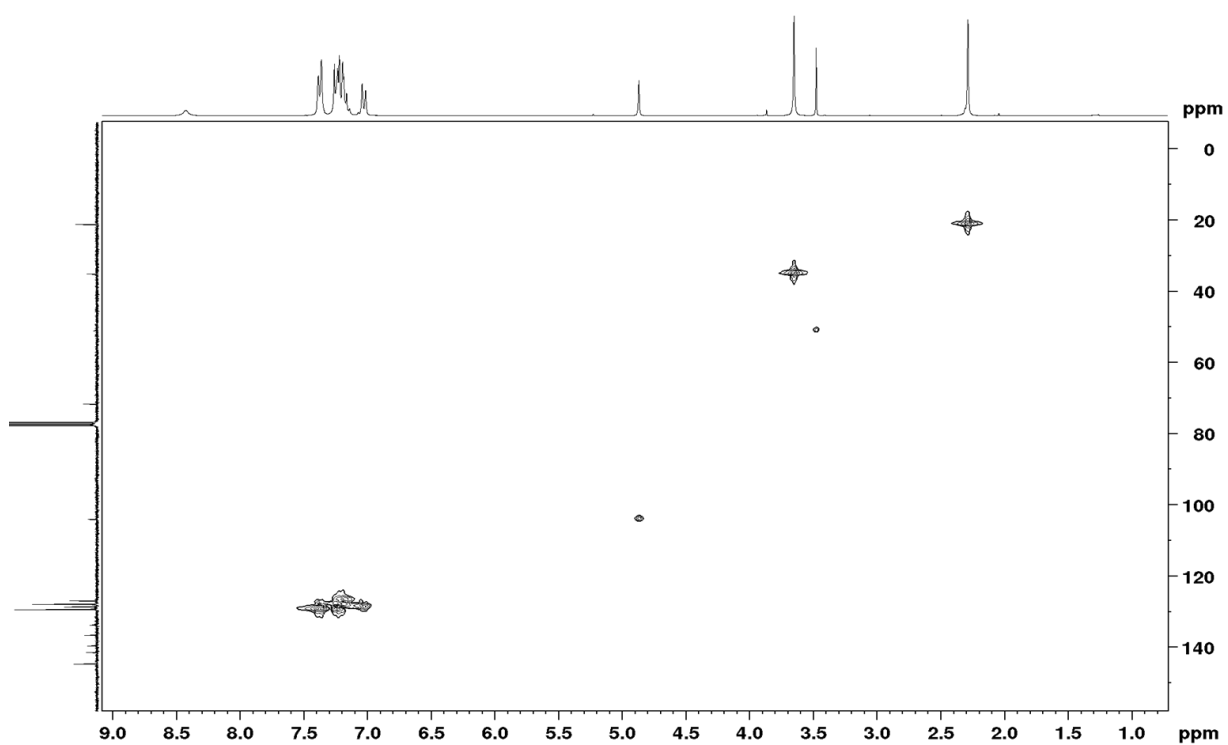


**Figure S22:** HSQC-NMR (300 MHz, 75 MHz) spectrum of Mtt-Im-OH (3).

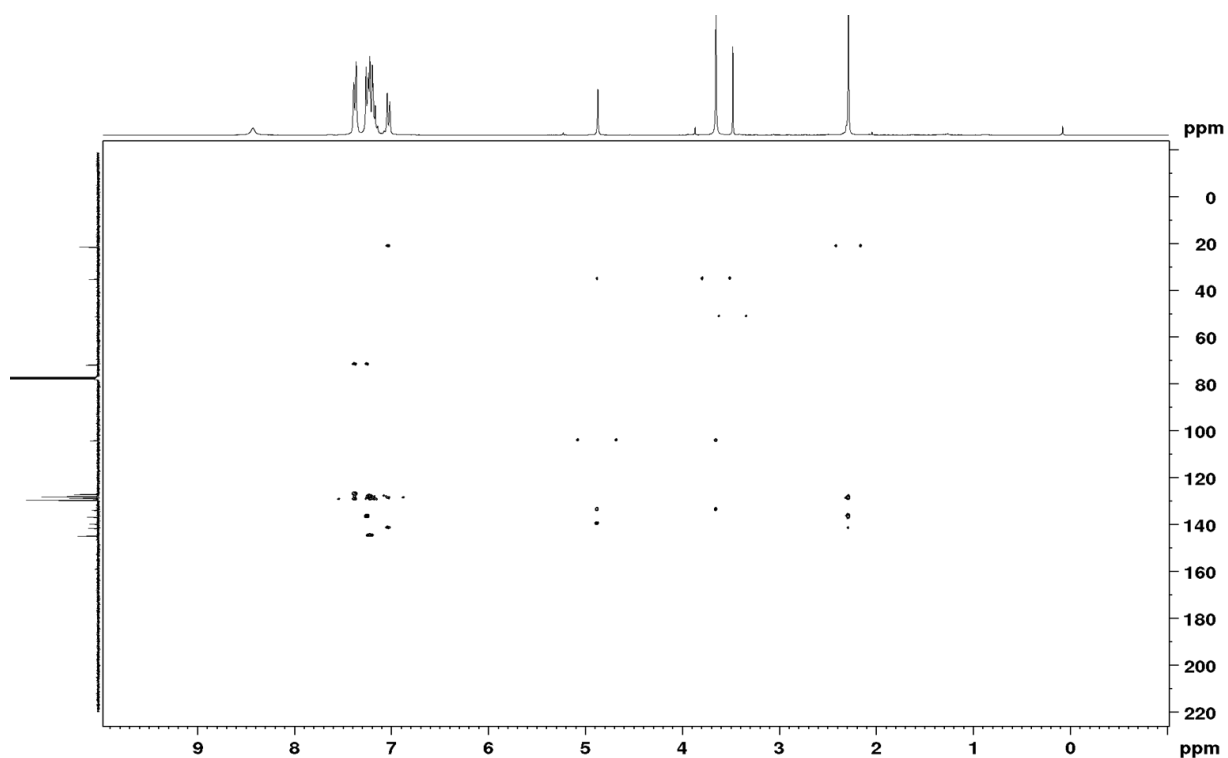


Figure S23: HMBC-NMR (500 MHz, 125 MHz) spectrum of Mtt-Im-OH (3).

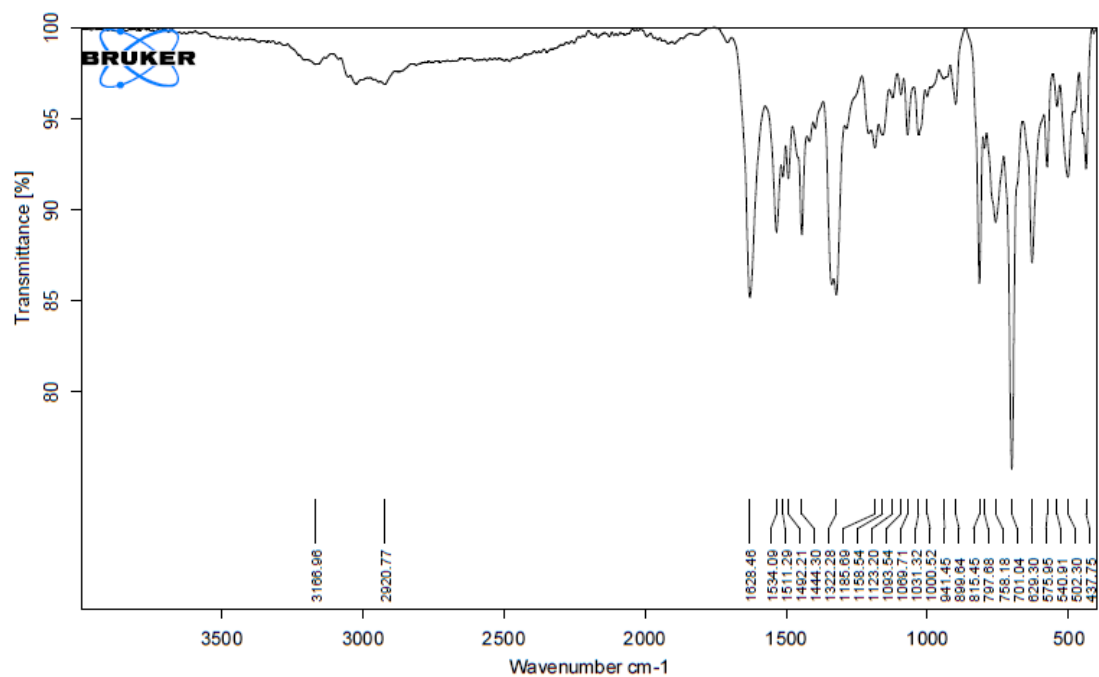


Figure S24: IR spectrum of Mtt-Im-OH (3).

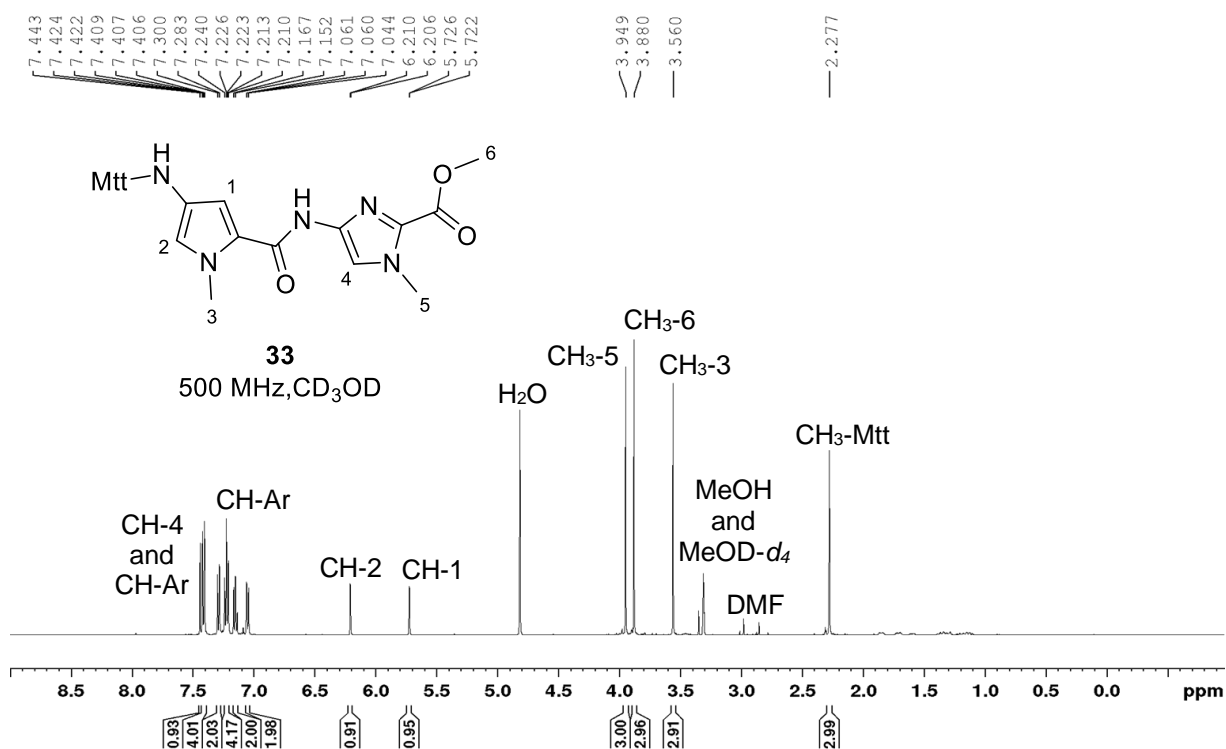


Figure S25: <sup>1</sup>H-NMR (500 MHz) spectrum of Mtt-PyIm-OMe (**33**).

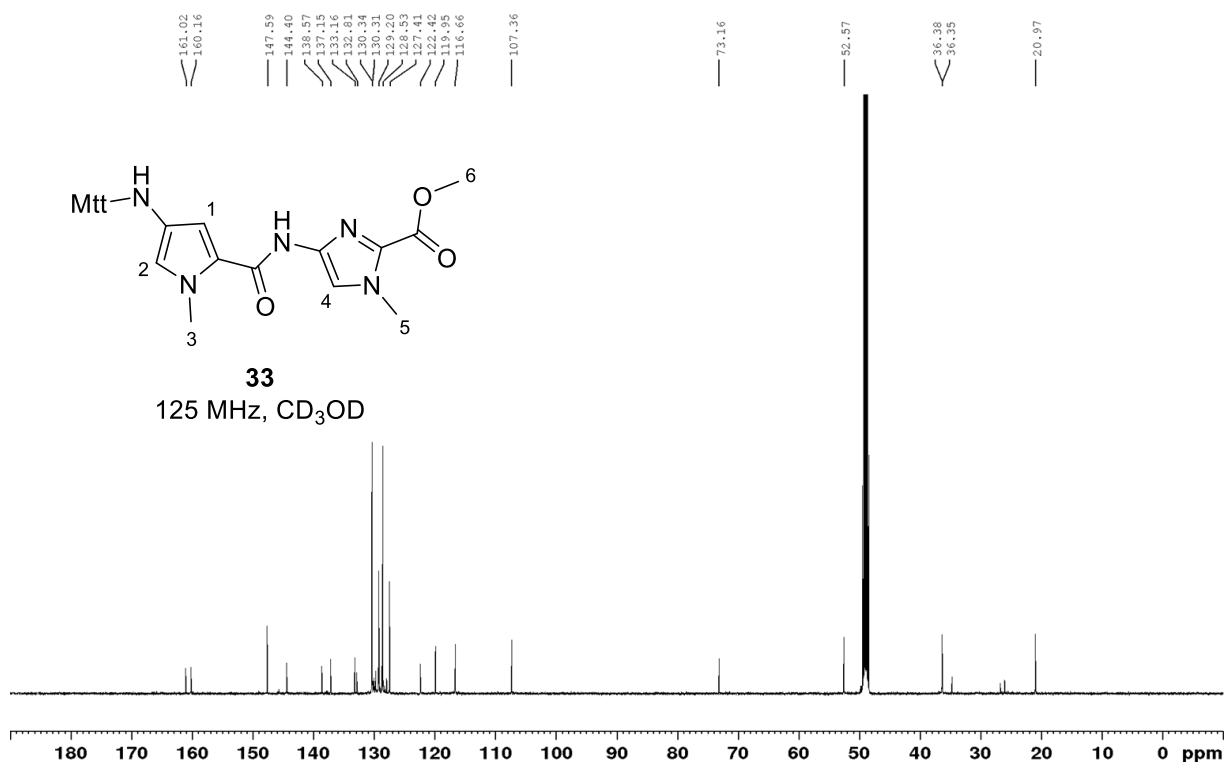
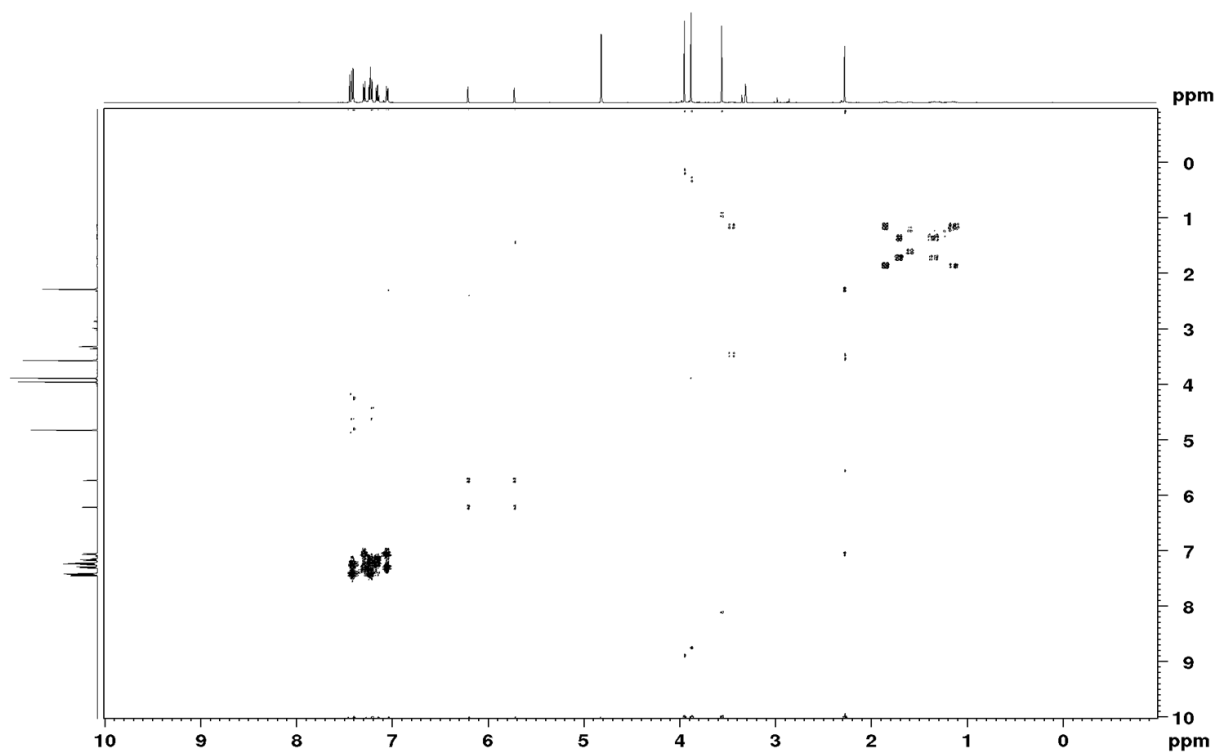
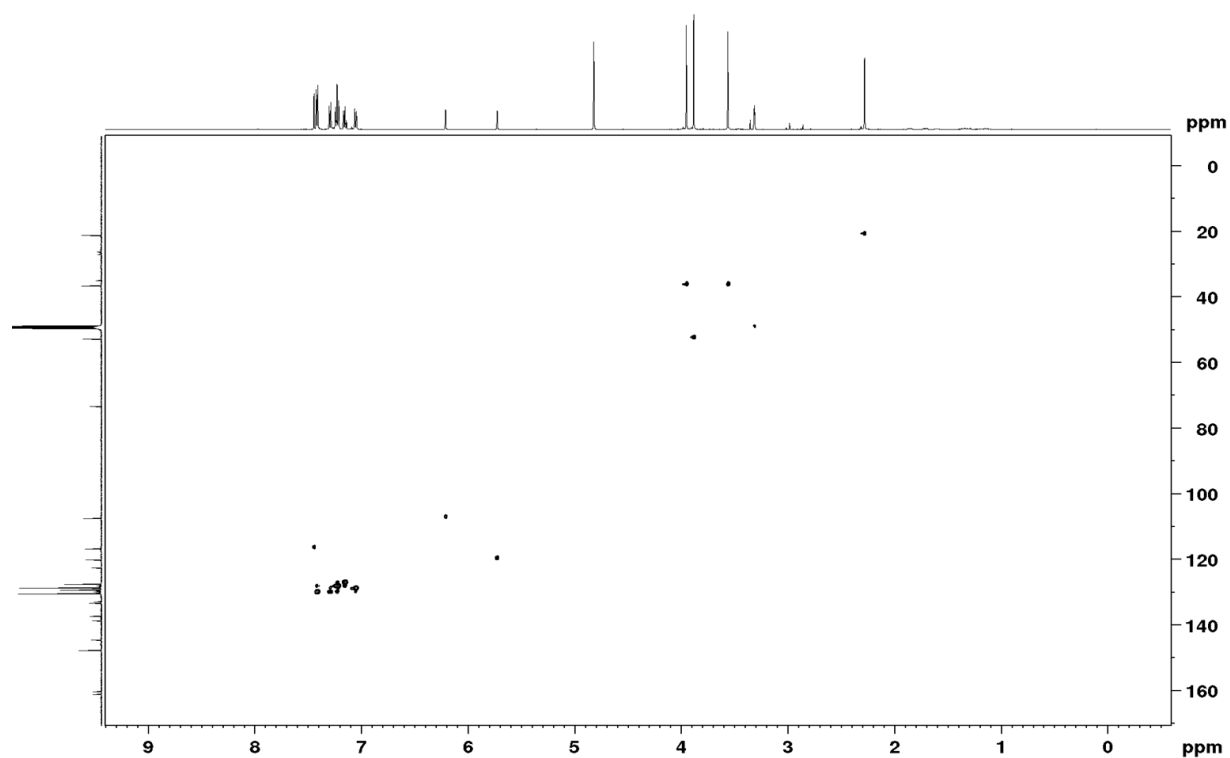


Figure S26: <sup>13</sup>C-NMR (125 MHz) spectrum of Mtt-PyIm-OMe (**33**).



**Figure S27:** COSY-NMR (500 MHz) spectrum of Mtt-PyIm-OMe (**33**).



**Figure S28:** HSQC-NMR (500 MHz, 1255 MHz) spectrum of Mtt-PyIm-OMe (**33**).



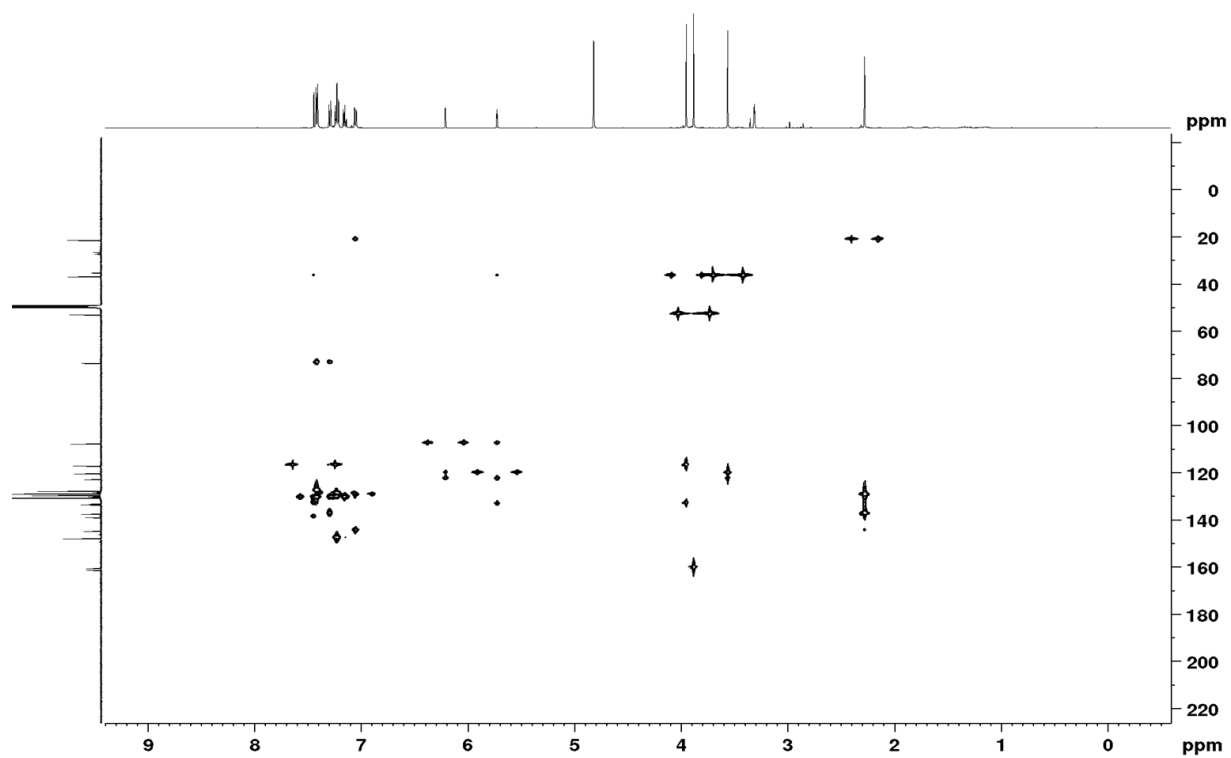


Figure S29: HMBC-NMR (500 MHz, 125 MHz) spectrum of Mtt-PyIm-OMe (33).

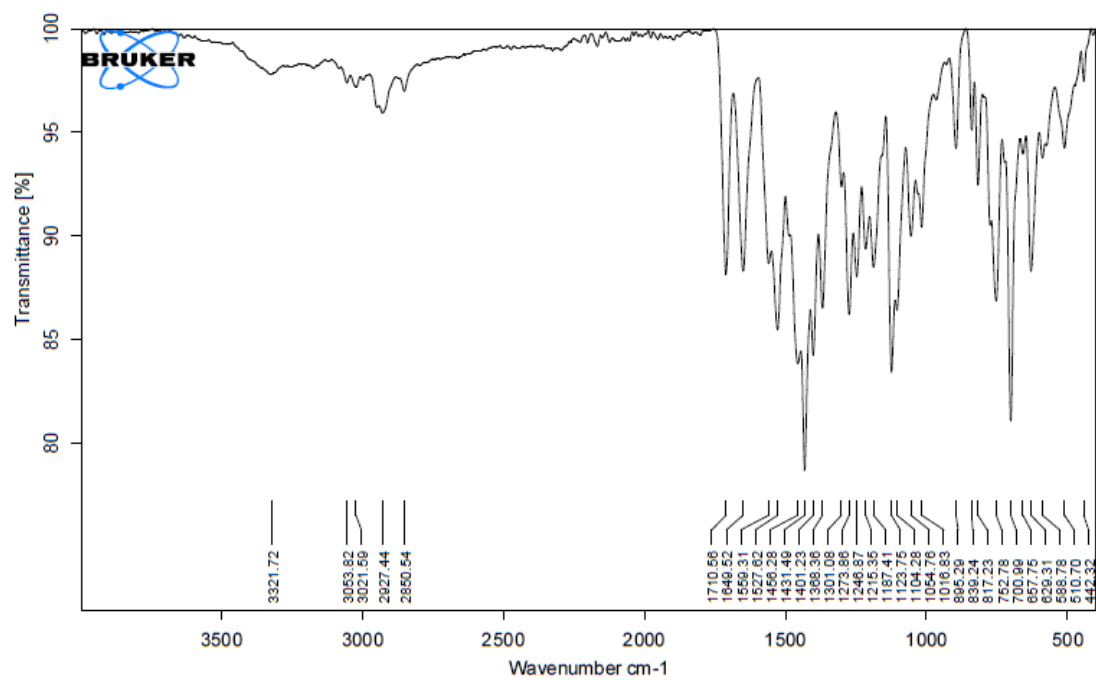


Figure S30: IR spectrum of Mtt-PyIm-OMe (33).

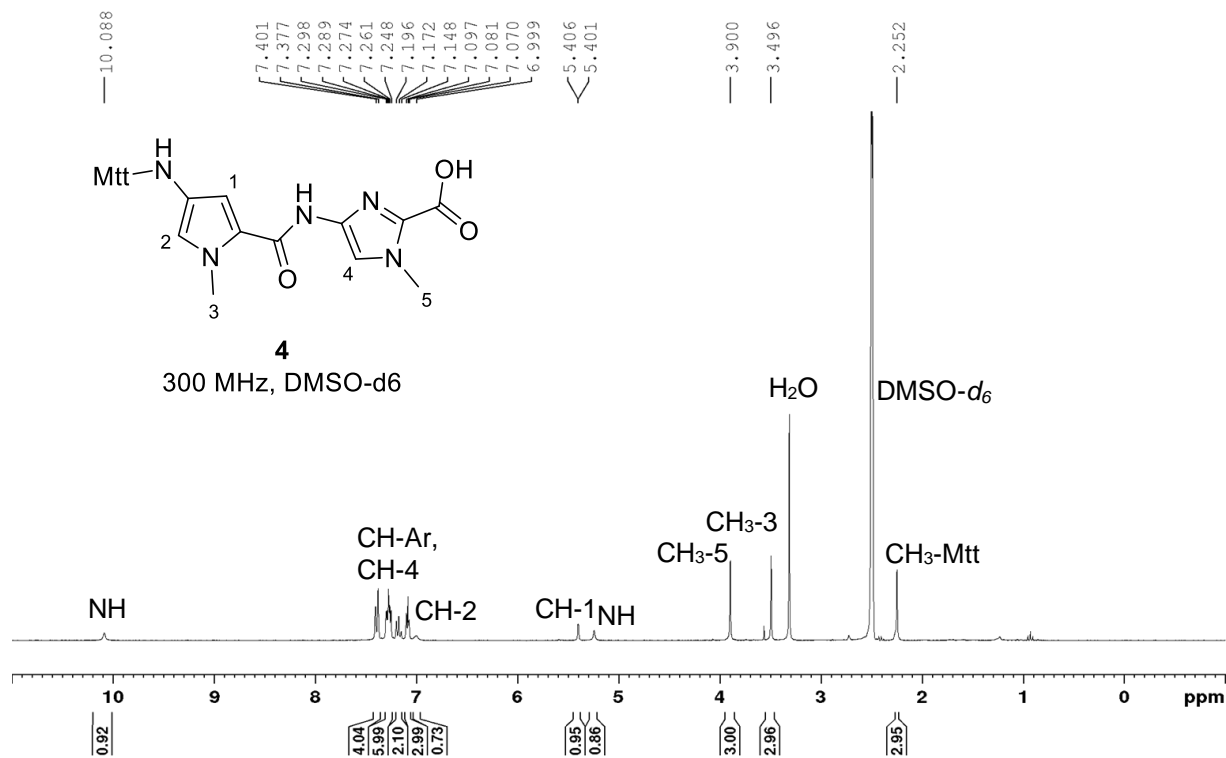


Figure S31:  $^1\text{H-NMR}$  (300 MHz) spectrum of Mtt-PyIm-OH (**4**).

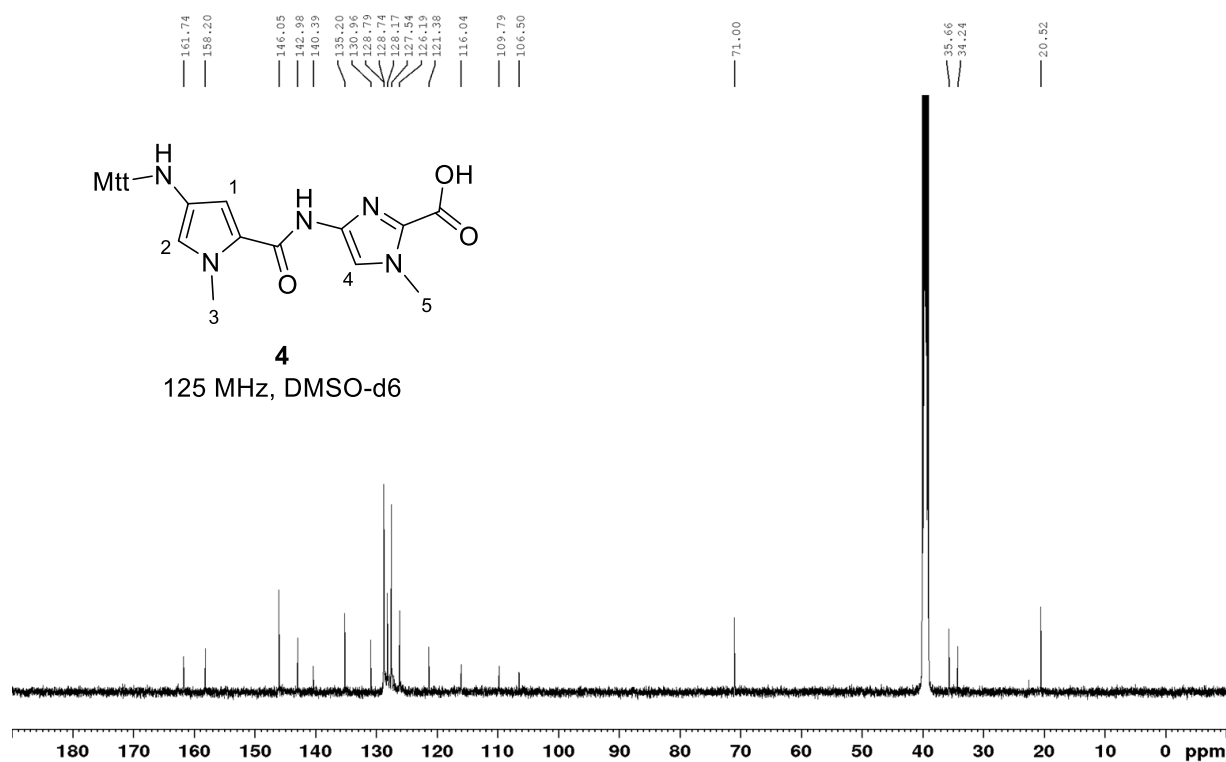


Figure S32:  $^{13}\text{C-NMR}$  (125 MHz) spectrum of Mtt-PyIm-OH (**4**).

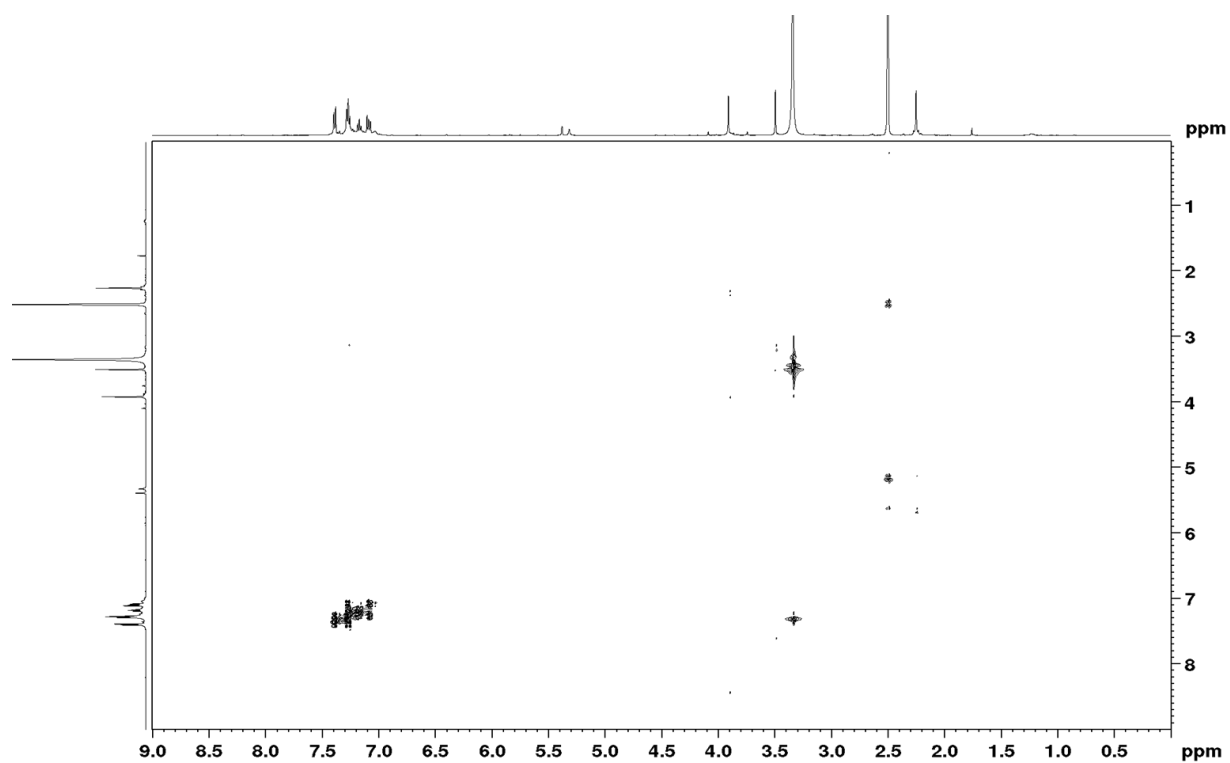


Figure S33: COSY-NMR (500 MHz) spectrum of Mtt-PyIm-OH (4).

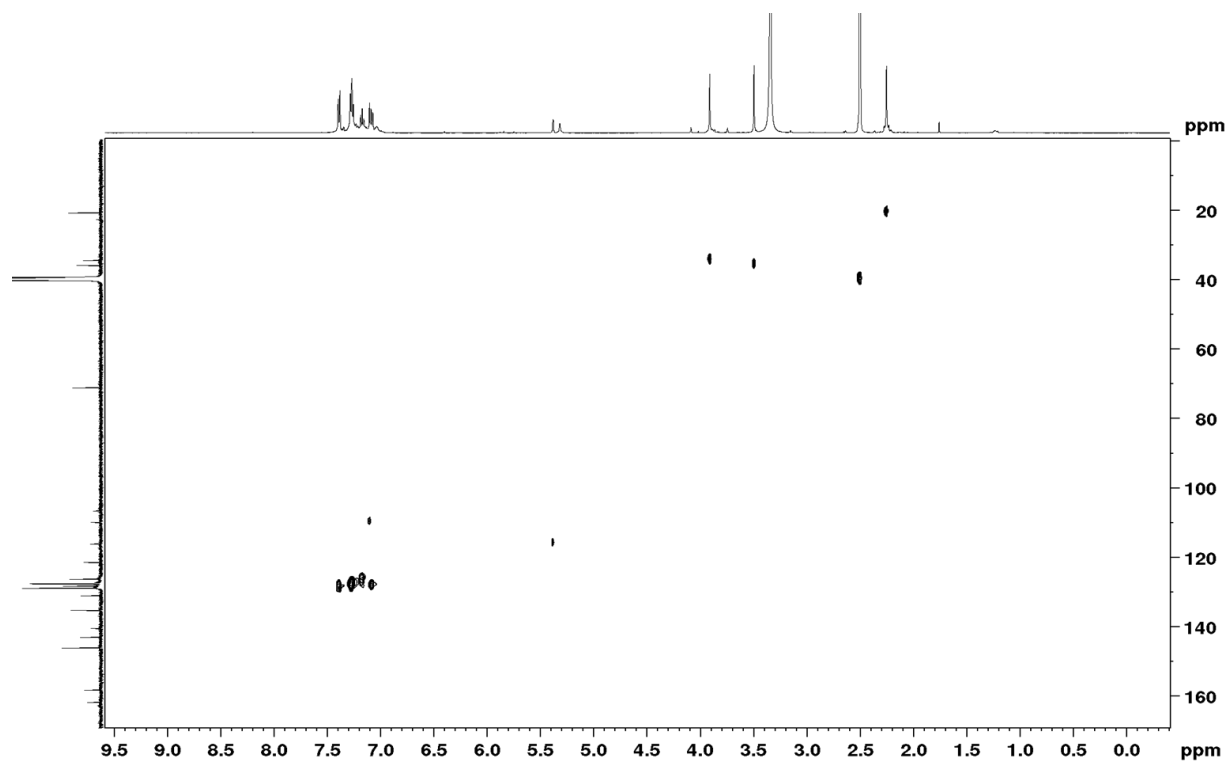


Figure S34: HSQC-NMR (500 MHz, 125 MHz) spectrum of Mtt-PyIm-OH (4).

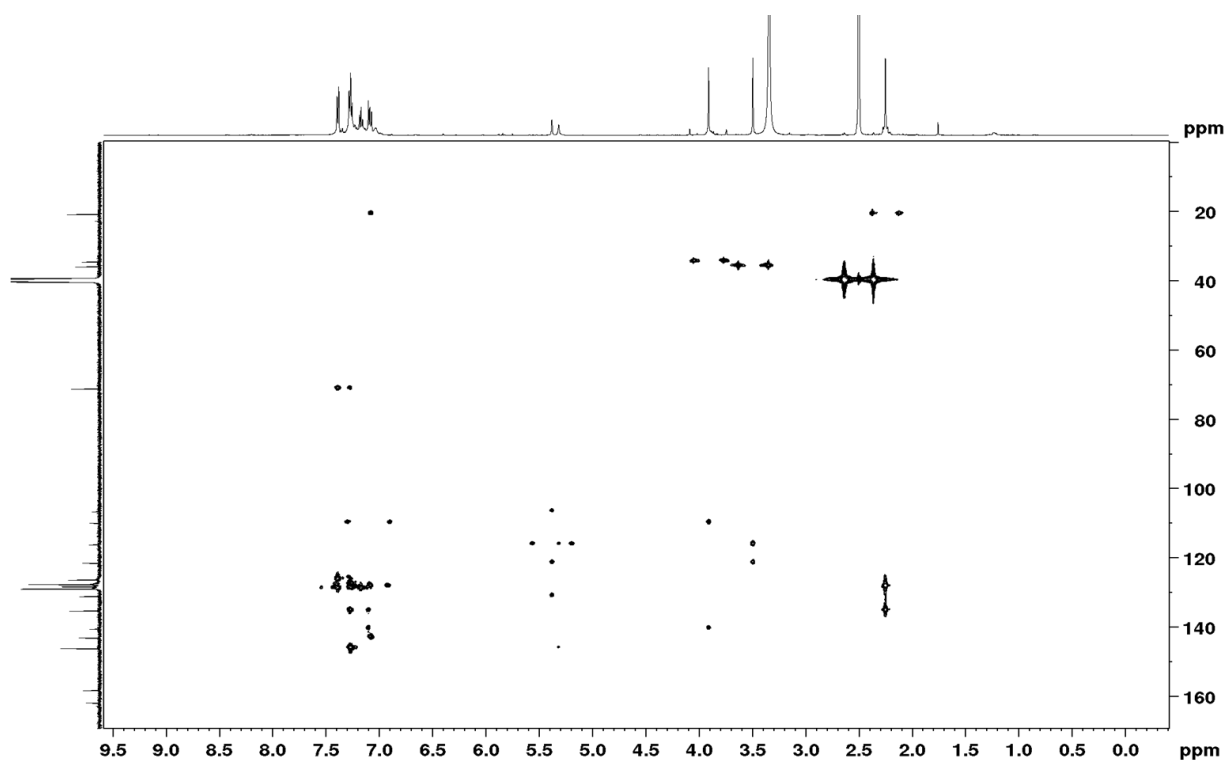


Figure S35: HMBC-NMR (500 MHz, 125 MHz) spectrum of Mtt-PyIm-OH (4).

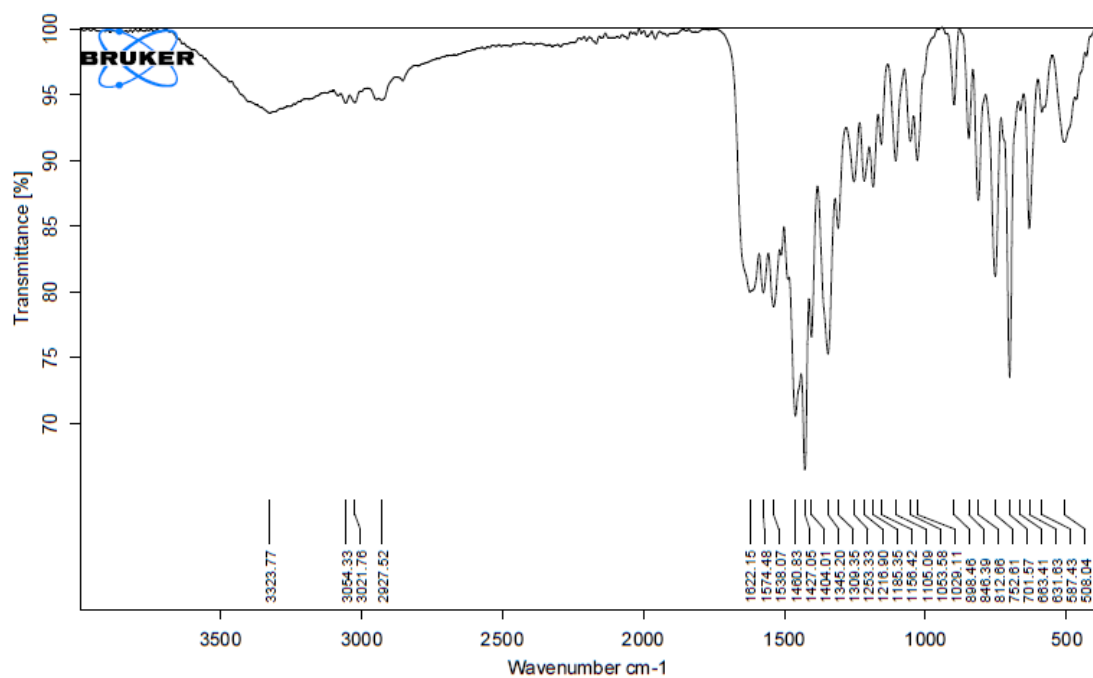


Figure S36: IR spectrum of Mtt-PyIm-OH (4).

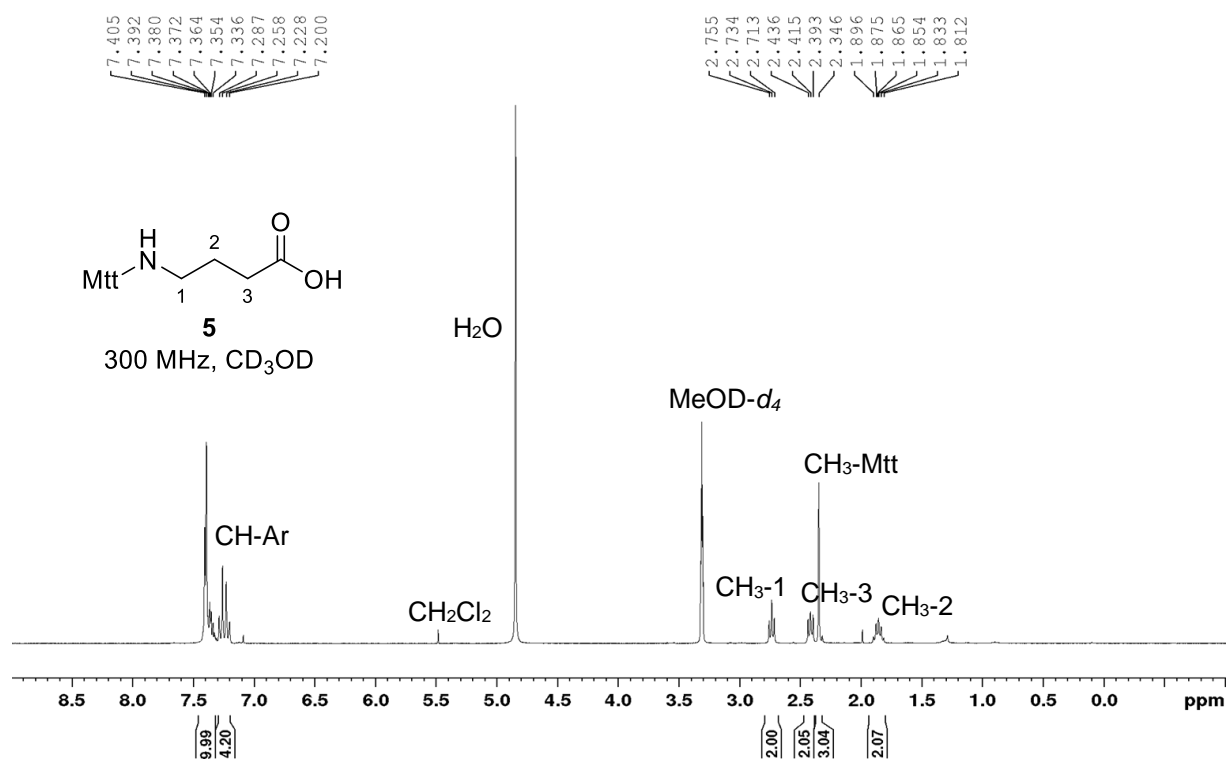


Figure S37:  $^1\text{H-NMR}$  (300 MHz) spectra of Mtt- $\gamma$ -OH (**5**).

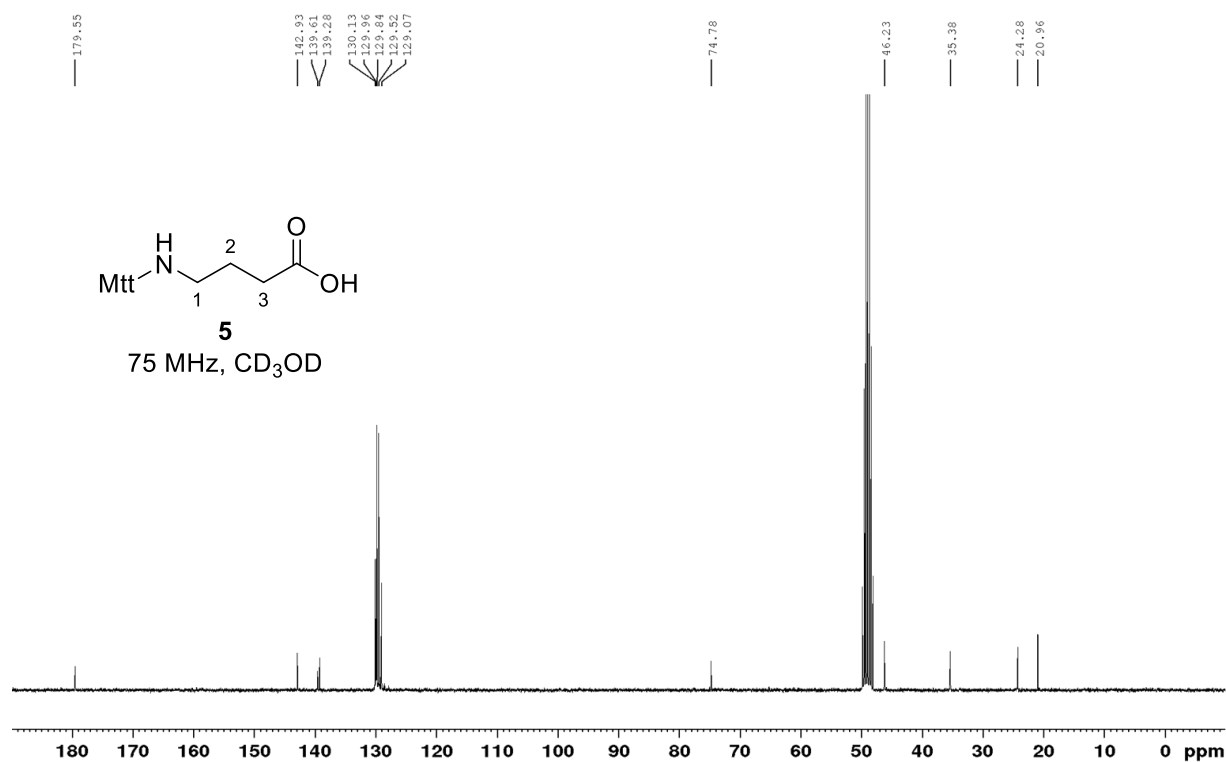
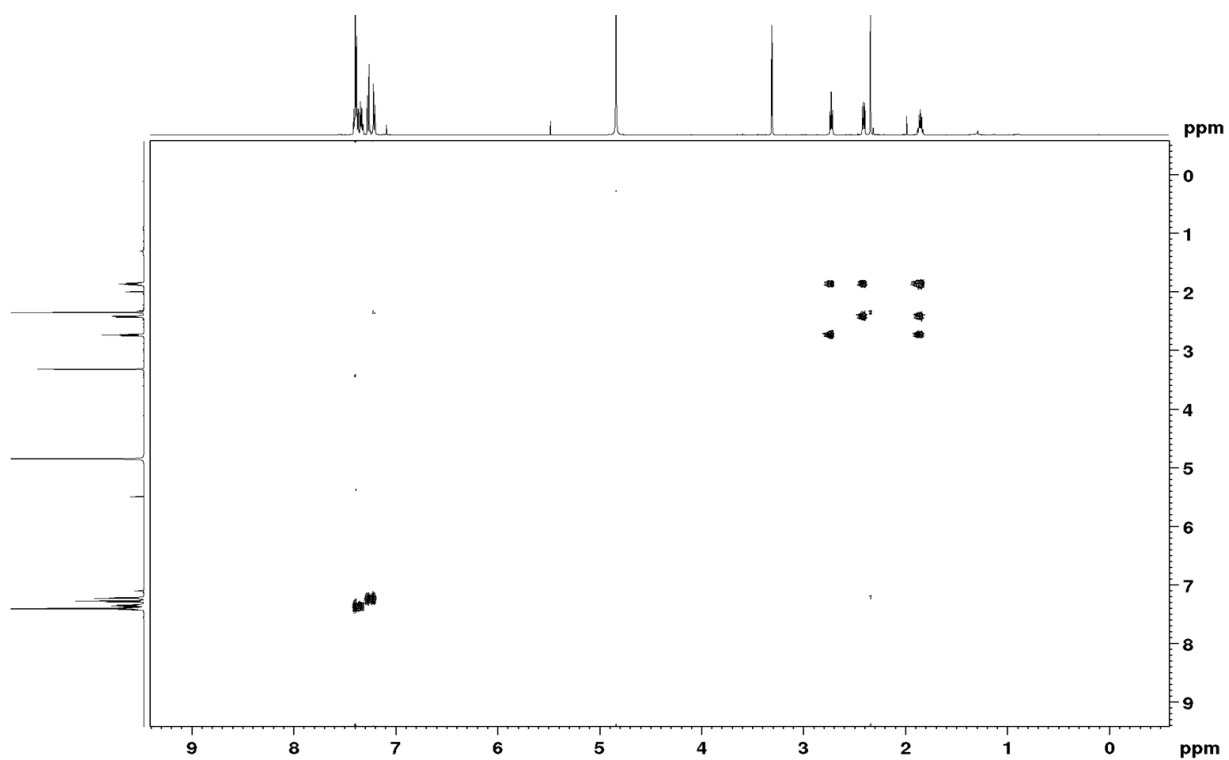
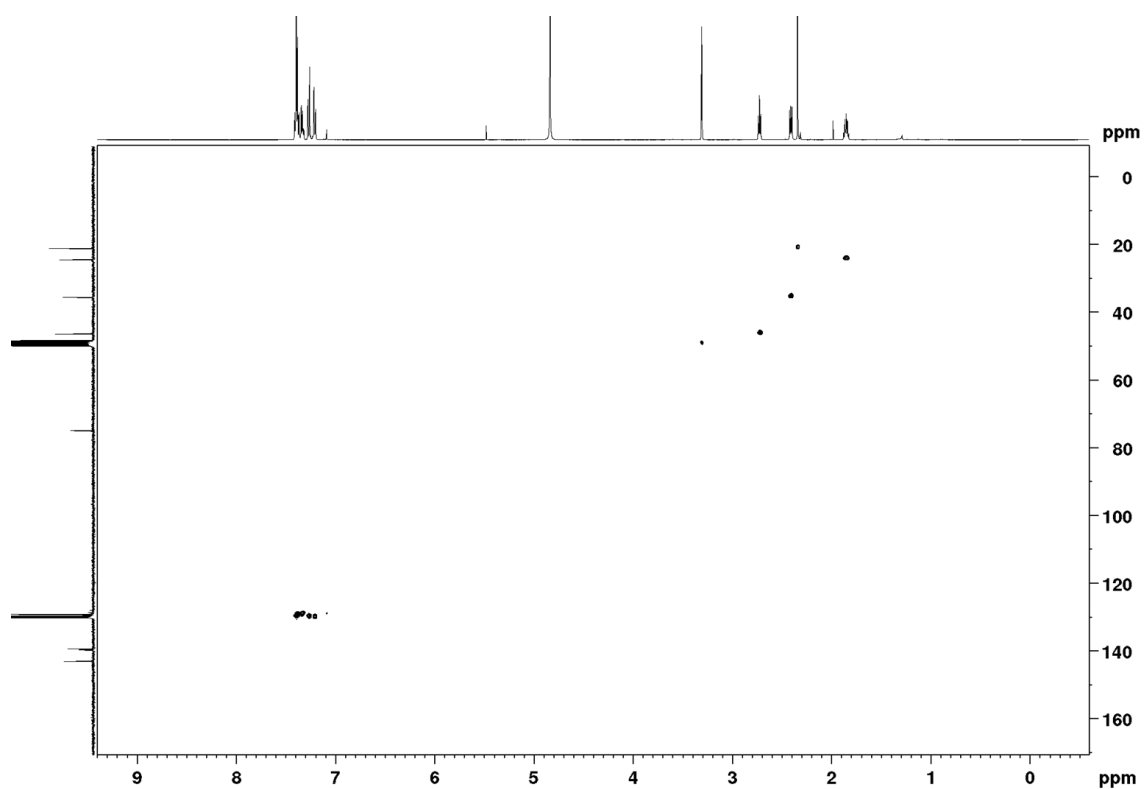


Figure S38:  $^{13}\text{C-NMR}$  (75 MHz) spectrum of Mtt- $\gamma$ -OH (**5**).



**Figure S39:** COSY-NMR (500 MHz) spectrum of Mtt- $\gamma$ -OH (5).



**Figure S40:** HSQC-NMR (500 MHz, 75 MHz) spectrum of Mtt- $\gamma$ -OH (5).

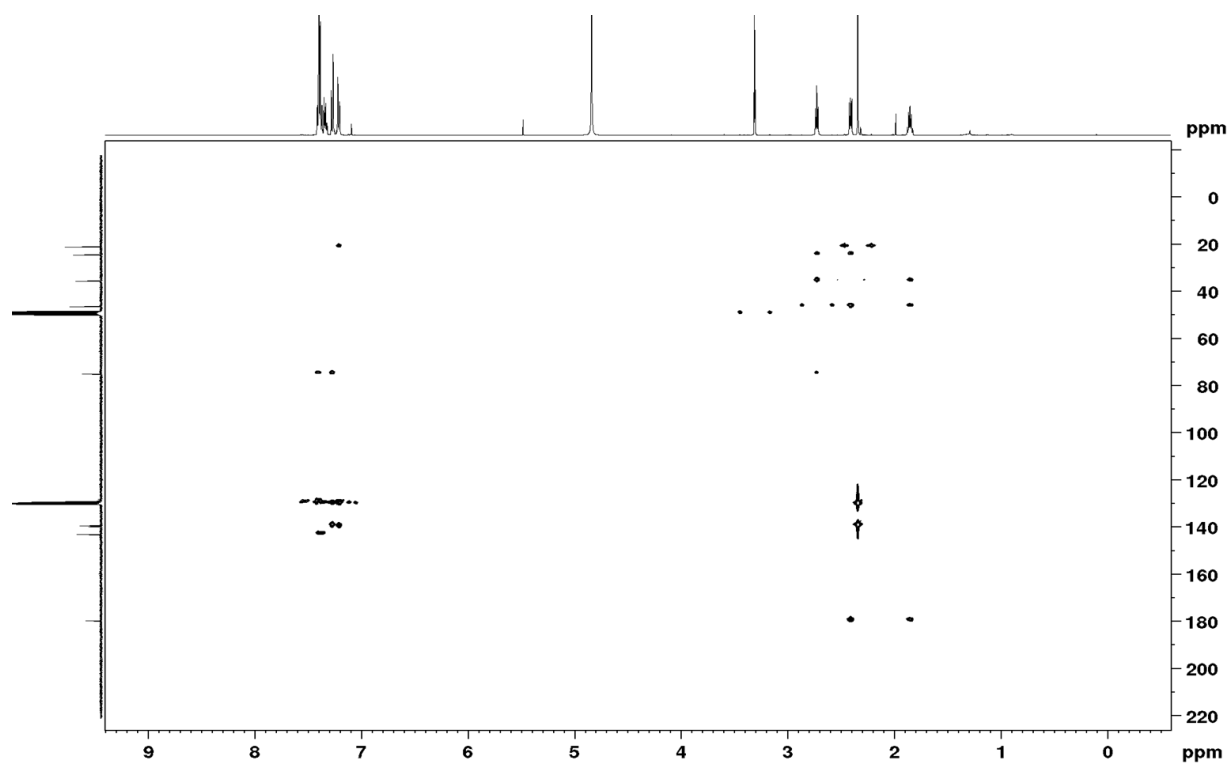


Figure S41: HMBC-NMR (500 MHz, 75 MHz) spectrum of Mtt- $\gamma$ -OH (5).

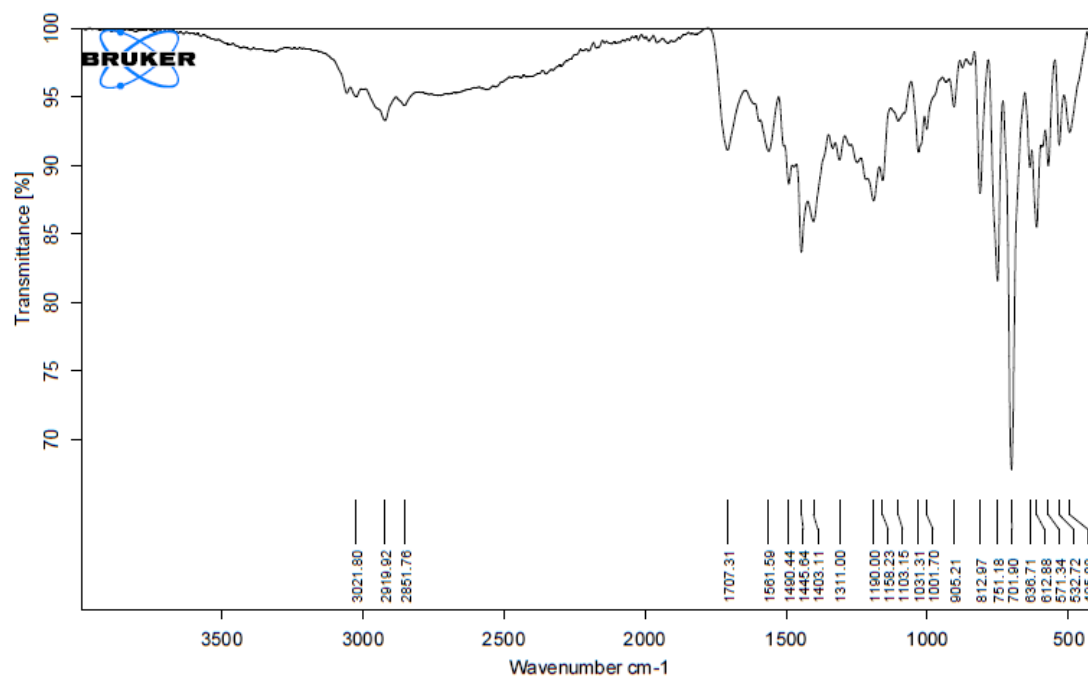


Figure S42: IR spectrum of Mtt- $\gamma$ -OH (5).

## Solid Phase Peptide Synthesis

Both, Fmoc-SPPS and Mtt-SPPS, follow the same protocol, except the deprotection step. Further modifications are described below.

The polyamide hairpins were synthesized manually in 2 mL polypropylene reactors with plunger and frit, (pore size 25  $\mu\text{m}$ , MultiSynTech GmbH; Germany). TG R PHB resin was preloaded with Fmoc- $\beta\text{Ala-OH}$  and the loading determined before further couplings.

*Loading of the first amino acid:*<sup>[xix]</sup> Under inert atmosphere, TG R PHB resin (500 mg, 0.18 - 0.23 mmol/g) was placed in a flask, covered with DMF (3.0 mL) and swelled for 30 min. In a second flask, under inert atmosphere, Fmoc- $\beta\text{Ala-OH}$  (358 mg, 1.15 mmol) was dissolved in  $\text{CH}_2\text{Cl}_2$  (5.0 mL) and DMF (100  $\mu\text{L}$ ) and the solution cooled to 0  $^\circ\text{C}$  before adding DIC (89.0  $\mu\text{L}$ , 575  $\mu\text{mol}$ ). After 20 min, the solvent was removed, the residue dissolved in DMF (3.0 mL) and added to the swelled resin. DMAP (14.0 mg, 115  $\mu\text{mol}$ ) dissolved in DMF (50  $\mu\text{L}$ ) was added and the mixture was shaken under inert atmosphere for 1 h. The resin was filtered off and washed with DMF (5 x 0.5 mL),  $\text{CH}_2\text{Cl}_2$  (10 x 0.5 mL) and DMF (5 x 0.5 mL). Lutidine/ $\text{Ac}_2\text{O}$ /DMF 6:5:89 (2.0 mL) was added for 5 min. The resin was filtered off and washed with DMF (5 x 0.5 mL) and  $\text{CH}_2\text{Cl}_2$  (10 x 0.5 mL). It was dried under reduced pressure and the loading determined.

*Determination of the resin loading:* The Fmoc-group of a weighted amount of resin (~5.00 mg), previously loaded with the first amino acid, Fmoc- $\beta\text{Ala-OH}$ , was deprotected by adding twice a solution of 20% piperidine in DMF (500  $\mu\text{L}$ ) for 5 min. The filtrates were collected and the absorbance measured at 300 nm ( $\epsilon_{300\text{nm}}(\text{Fmoc}) = 7800 \text{ M}^{-1}\text{cm}^{-1}$ )<sup>[xx]</sup> on a Tecan 20M Spark plate reader and the loading was calculated.

### Manual Solid Phase Protocol for Peptide Synthesis

The amounts of reagents of the following synthesis protocol correspond to 10  $\mu\text{mol}$  scale. For higher scales, the reagents were scaled up correspondingly. For shaking an Edmund Bühler Swip shaker was used.

*Swelling:* 10  $\mu\text{mol}$  of resin was swollen in 0.5 mL DMF for 30 min.

*Deprotection of the temporal Fmoc group:* Piperidine (20% in DMF, 250  $\mu\text{L}$ ) was added to the resin and shaken for 5 min. This step was repeated, the resin filtered off and washed with DMF (5 x 0.5 mL),  $\text{CH}_2\text{Cl}_2$  (5 x 0.5 mL) and DMF (5 x 0.5 mL).

*Deprotection of the temporal Mtt-group:* TFA (2% in  $\text{CH}_2\text{Cl}_2$ , 250  $\mu\text{L}$ ) was added to the resin and shaken for 20 min. The resin was filtered off and washed with TFA (2% in  $\text{CH}_2\text{Cl}_2$ , 0.5 mL) until the washing solution was no longer coloured yellow. It was washed with  $\text{CH}_2\text{Cl}_2$  (8 x 0.5 mL), DMF (8 x 0.5 mL) and the resin incubated with DIPEA (10% in DMF, 250  $\mu\text{L}$ ) for 5 min to neutralize remaining acid.

*Coupling of amino acids:* The amino acid (4.00 eq) was dissolved in NMP (134  $\mu\text{L}$ ) and DIPEA (8.00 eq for Fmoc-amino acids and 12.0 eq for Mtt-amino acids), and HATU (4.00 eq) was added. The resulting solution was activated for 3 min and added to the resin. This mixture was shaken for 1 h in the case of Fmoc-Py-OH, Mtt-Py-OH, Fmoc- $\gamma$ -OH and Mtt- $\gamma$ -OH and 2 h in the case of Fmoc-Im-OH, Mtt-Im-OH, Fmoc-PyIm-OH, Mtt-PyIm-OH and ImPy-OH. For the introduction of the amino acids after the  $\gamma$ -turn, DMSO/NMP 1:1 (50  $\mu\text{L}$ ) was directly added to the coupling mixture after the corresponding coupling time for 30 min. The resin was filtered off and washed with DMF (5 x 0.5 mL),  $\text{CH}_2\text{Cl}_2$  (5 x 0.5 mL) and DMF (5 x 0.5 mL).

*Capping:* After coupling of each amino acid, a solution of  $\text{Ac}_2\text{O}$ /pyridine/DMF 5:5:90 (250  $\mu\text{L}$ ) was added to the resin and it was shaken for 5 min. The resin was filtered off and washed with DMF (5 x 0.5 mL),  $\text{CH}_2\text{Cl}_2$  (5 x 0.5 mL) and DMF (5 x 0.5 mL).



*Cleavage of the polyamide hairpins:* The dried resin was treated with TFA/H<sub>2</sub>O 9:1 (1.0 mL) for 2 h. The resin was filtered off and the filtrate was added to dry ice-cold Et<sub>2</sub>O (12.0 mL). After 30 min, the precipitated polyamide was centrifuged, washed once with dry ice-cold Et<sub>2</sub>O, centrifuged, the supernatant was discarded and the polyamide pellet was dissolved in H<sub>2</sub>O/MeCN 1:1 including 0.1% TFA and freeze-dried.

*Characterization:* The freeze-dried products were identified via analytical HPLC-MS on an Agilent 1260 Series HPLC-system (Agilent Technologies) as described before. Electrospray Ionization Mass Spectrometry (ESI-MS) was performed as described before.

### **Synthesis and Characterization Data of the Polyamides**

Unless otherwise noted, the synthesis of the polyamides was performed manually following the protocol described above. The purity of the polyamides was calculated from the integrated peak areas of the HPLC chromatograms, taken peaks with an >10% intensity to the highest peak in the chromatogram and is given as % for each polyamide.

**Im-Py-Py-Im- $\gamma$ -Py-Im-Im-Py- $\beta$ -COOH (35):** After precipitation and lyophilisation, the crude product was obtained from the Fmoc-approach (**35**, 2.80  $\mu$ mol, 28%) in form of a brown solid. The yield was determined spectroscopically.  $t_R = 19.5$  min (gradient 5-75% B). Purity 93%. **HRMS-ESI<sup>+</sup>** ( $m/z$ ): [M+2H]<sup>2+</sup> calcd for C<sub>51</sub>H<sub>57</sub>N<sub>21</sub>O<sub>11</sub>H<sub>2</sub>, 570.7346; found, 570.7359.

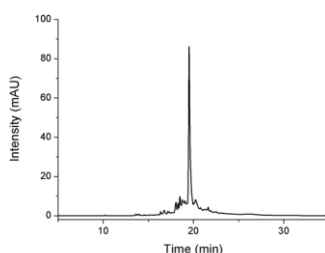


**Figure S43:** HPLC chromatogram of the crude polyamide hairpin **35** resulting from the Fmoc approach. Gradient 5-75% B.

**Im-Py-Py-Im- $\gamma$ -Py-Im-Im-Py- $\beta$ -COOH (35):** After precipitation and lyophilisation, the crude product was obtained from the Mtt-approach (**35**, 1.42  $\mu$ mol, 14%) in form of a brown solid. The yield was determined spectroscopically.  $t_R = 19.5$  min (gradient 5-75% B). Purity 83%. **HRMS-ESI<sup>+</sup>** ( $m/z$ ): [M+H]<sup>+</sup> calcd for C<sub>51</sub>H<sub>57</sub>N<sub>21</sub>O<sub>11</sub>H, 1140.4625; found, 1140.4688.

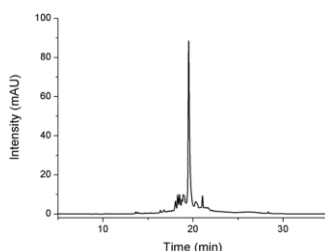
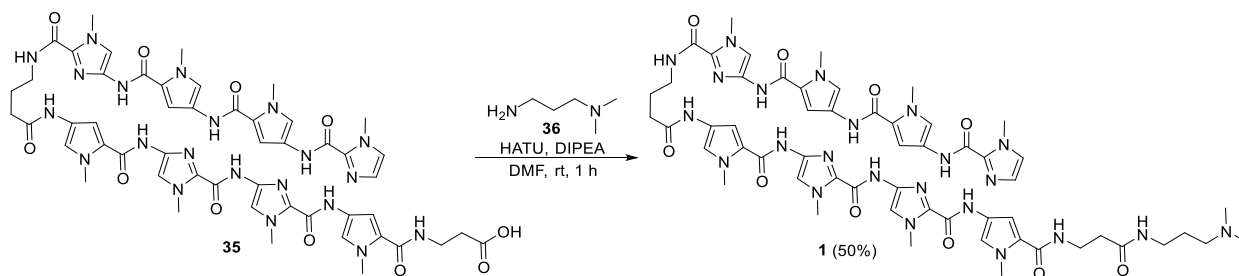


**Figure S44:** HPLC chromatogram of the crude polyamide hairpin **35** resulting from the Mtt approach. Gradient 5-75% B.

### Synthesis of Im-Py-Py-Im- $\gamma$ -Py-Im-Im-Py- $\beta$ -Dp (**1**):



**Scheme S5:** Reaction scheme for the formation Im-Py-Py-Im- $\gamma$ -Py-Im-Im-Py- $\beta$ -Dp (**1**) from Im-Py-Py-Im- $\gamma$ -Py-Im-Im-Py- $\beta$ -COOH (**35**).

Im-Py-Py-Im- $\gamma$ -Py-Im-Im-Py- $\beta$ -COOH (**35**, 2.2 mg, 1.93  $\mu$ mol) was dissolved in DMF (10  $\mu$ L) and HATU (2.9 mg, 7.72  $\mu$ mol) and DIPEA (2.69  $\mu$ L, 15.4  $\mu$ mol) were added. The mixture was shaken for 5 min before *N,N*-dimethyl-1,3-diaminopropane (0.97  $\mu$ L, 7.72  $\mu$ mol) was added. After shaking for 1 h at rt, H<sub>2</sub>O/MeCN (7:3, 1.0 mL) was added and the solution purified by preparative HPLC as described above. The fractions containing Im-Py-Py-Im- $\gamma$ -Py-Im-Im-Py- $\beta$ -Dp **1** were lyophilized to give the desired product (**1**, 0.97  $\mu$ mol, 50%) as pale-brown TFA salt. The yield was determined spectroscopically.  $t_R$  = 18.7 min (gradient 5-75% B). Purity >95%. **HRMS-ESI**<sup>+</sup> ( $m/z$ ): [M+2H]<sup>2+</sup> calcd for C<sub>56</sub>H<sub>69</sub>N<sub>23</sub>O<sub>10</sub>H<sub>2</sub>, 612.7872; found, 612.7885.

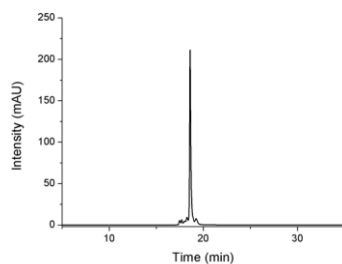


**Figure S45:** HPLC chromatogram of the purified polyamide hairpin **1**. Gradient 5-75% B.

## Concentration Determination

Concentrations were measured on a Tecan Spark 20M. Values were background-subtracted.

For the concentration determination of the ssDNAs, the purchased lyophilized DNA was dissolved in milli-Q water. Their molar extinction coefficients were determined by using the following formula:<sup>[xxi]</sup>

$$\epsilon_{260nm} = \{(8.8 * \#T) + (7.3 * \#C) + (11.7 * \#G) + (15.4 * \#A)\} * 0.9 * 10^3 M^{-1}cm^{-1} \quad (S1)$$

In the formula # = number of nucleobases determined throughout the DNA sequence, T = thymine, C = cytosine, G = guanine, A = adenine. Table S1 summarizes the sequences and the determined extinction coefficients of the ssDNAs.

To form the duplex DNAs, equimolar amounts of the complementary ssDNAs were heated to 95 °C for 10 min and slowly cooled down to room temperature. Hybridized duplex DNAs serve the target sequence (dsDNA<sub>AGCCGT</sub>) and a single mismatch duplex DNA (dsDNA<sub>AGCTGT</sub>). The mismatch is marked in bold and red.

**Table S1.** Binding sites, sequences and extinction coefficients of ssDNA, which were used as hybridized duplexes for thermal melting analysis.

DNA	binding site	sequence (5' – 3')	extinction coefficient at 260 nm
ssDNA <sub>AGCCGT</sub>	AGCCGT	GGTAGCCGTACC	111960 M <sup>-1</sup> cm <sup>-1</sup>
ssDNA <sub>ACGGCT</sub>	ACGGCT	GGTACGGCTACC	111960 M <sup>-1</sup> cm <sup>-1</sup>
ssDNA <sub>AGCTGT</sub>	AGCTGT	GGTAGCTGTACC	113310 M <sup>-1</sup> cm <sup>-1</sup>
ssDNA <sub>ACAAGCT</sub>	ACAAGCT	GGTACAAGCTACC	115290 M <sup>-1</sup> cm <sup>-1</sup>

For the polyamide hairpin we used an extinction coefficient from the literature:  $\epsilon_{310nm} = 69500 M^{-1}cm^{-1}$ <sup>[xxii]</sup>

## Thermal Melting Analysis

Thermal melting analysis was performed for duplex DNAs serving the target sequence of polyamide **1** and the target sequence with a single mismatch alone and together with the polyamides. The represented data in table S2 shows the calculated mean from three independent measurements and their corresponding standard deviations. To calculate the melting temperature, the plots of the thermal melting temperature from figure S46 were fitted by applying the Boltzmann equation in the plotting program Origin. The figure shows the corresponding normalized thermal melting curves with their standard deviations.

**Table S2.** Melting temperatures of DNA hairpins with and without polyamide hairpins. Represented data are mean values and their standard deviation calculated from three independent experiments.

DNA	polyamide	$T_m$	$\Delta T_m$
dsDNA <sub>AGCCGT</sub>	-	$36.2 \pm 0.3$ °C	
dsDNA <sub>AGCCGT</sub>	polyamide <b>1</b>	$42.8 \pm 0.6$ °C	6.6 °C
dsDNA <sub>AGCTGT</sub>	-	$30.9 \pm 0.2$ °C	
dsDNA <sub>AGCTGT</sub>	polyamide <b>1</b>	$31.9 \pm 0.7$ °C	1.0 °C

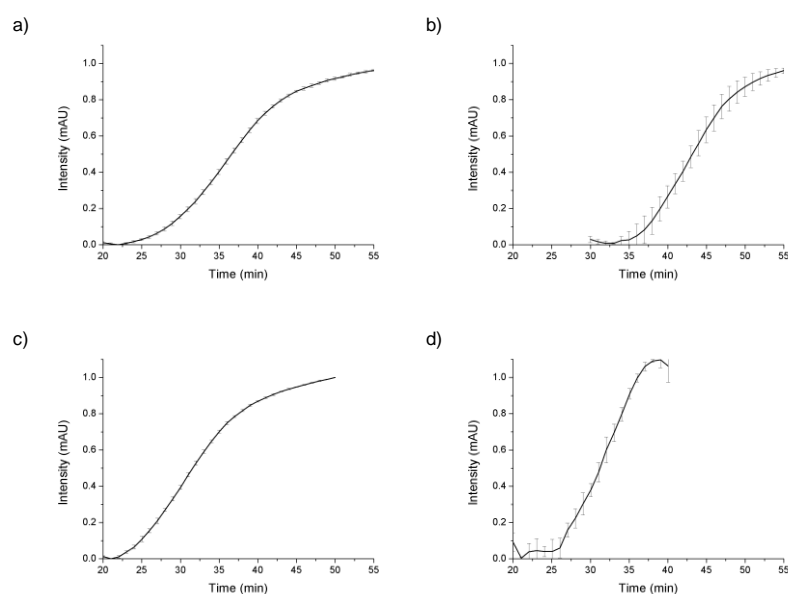


**Figure S46:** Melting curves of a 1  $\mu$ M duplex dsDNA solution in 10 mM NaH<sub>2</sub>PO<sub>4</sub> pH 7.4: 5'-GGTAGCCGTACC-3' without (a) and with (b) addition of 1.2  $\mu$ M polyamide **1** and 5'-GGTAGCTGTACC-3' without (c) and with (d) addition of polyamide **1**. Represented data is the mean of three independent measurements including their standard deviation.

## Stability of the Mtt-building blocks

For the study of the stability of the Mtt-building blocks via NMR, a solution of 5 mg of Mtt-Py-OMe (**11**) or Mtt-Im-OMe (**13**) was dissolved in 0.6 mL CDCl<sub>3</sub> containing different amounts of TFA to give a 12.6 mM solution. Their <sup>1</sup>H-NMR spectra was measured 3 min after dissolving the corresponding compound and the chemical shifts of the Mtt-methyl group were compared, as this signal shows the largest difference upon Mtt-deprotection. Figure 2, S47 and S48 show the comparison of the Mtt-lability between protected pyrrole and imidazole. Figure S49 presents the HSQC spectra of Mtt-Py-OMe (**11**) at 2% TFA to prove the presence of a methyl group for the new arising peak at higher TFA concentrations.

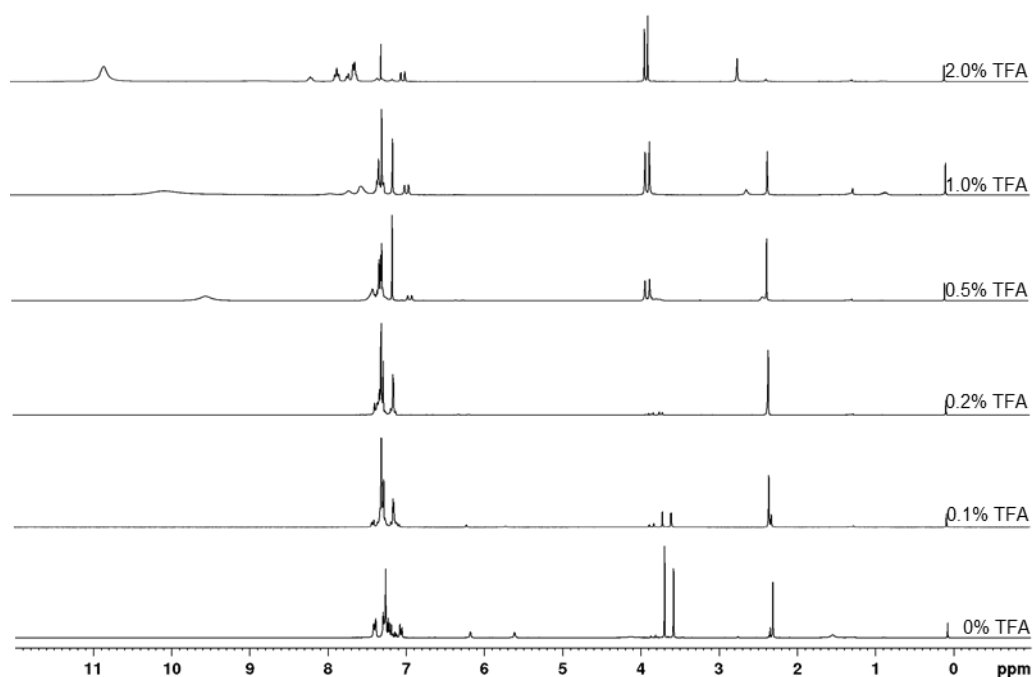


**Figure S47:** <sup>1</sup>H-NMR spectra (300 MHz) of Mtt-Py-OMe (**11**) in CDCl<sub>3</sub> at different TFA concentrations.

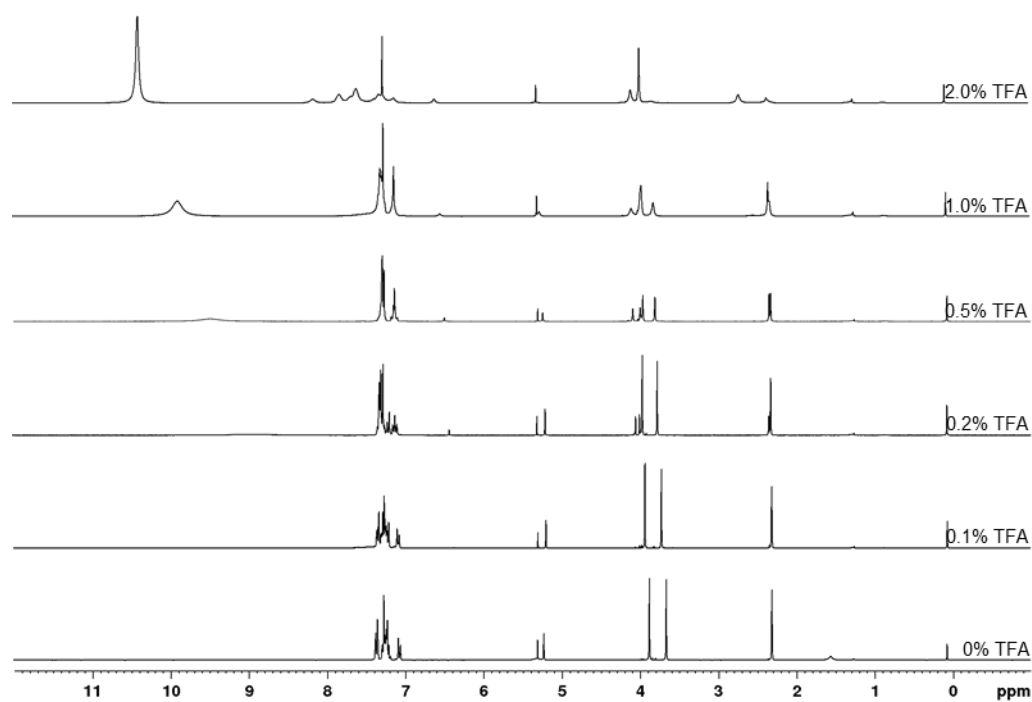


**Figure S48:**  $^1\text{H}$ -NMR spectra (300 MHz) of Mtt-Im-OMe (**13**) in  $\text{CDCl}_3$  at different TFA concentrations.

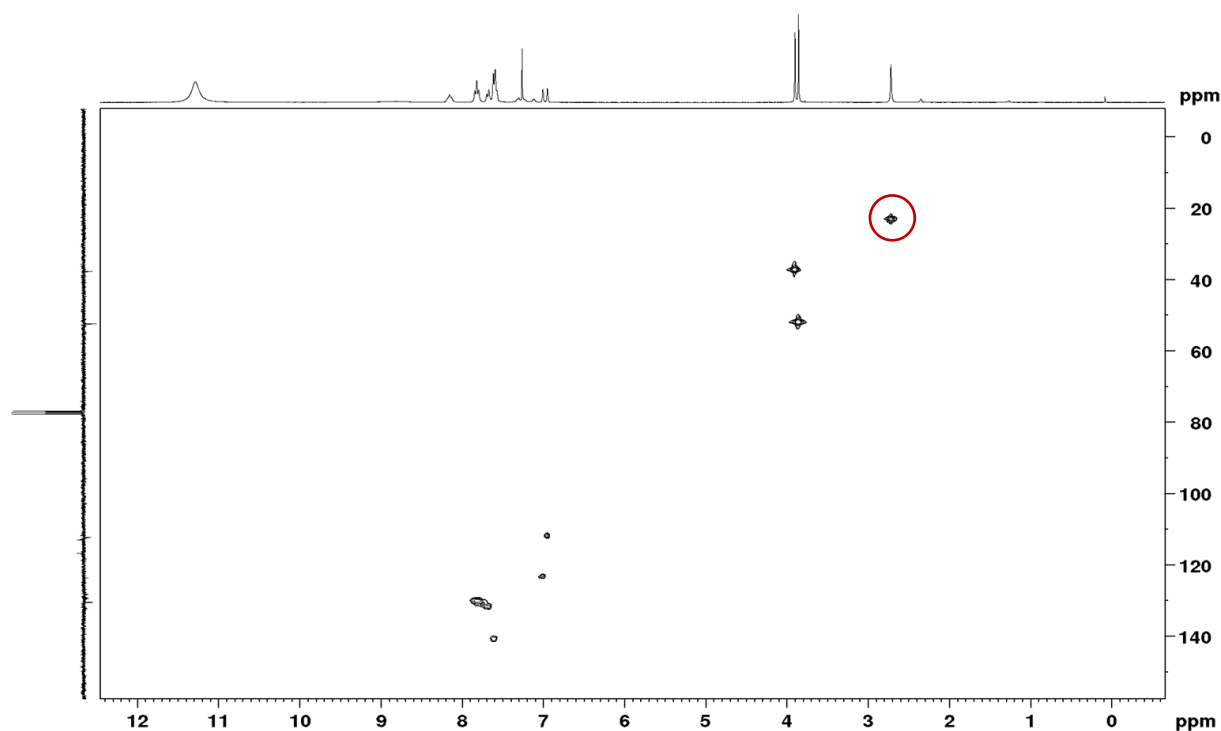


**Figure S49:** HSQC-spectra (300 MHz, 75 MHz) of Mtt-Py-OMe (**11**) in  $\text{CDCl}_3$  including 2% TFA. The methyl signal of the shifted Mtt peak is marked with a circle.

To explain the lowfield shift and the broadening of the signals, the  $^1\text{H}$ -NMR spectra of 5 mg Mtt-Cl as a reference compound in 0.6 mL  $\text{CDCl}_3$  and increasing amounts of TFA were recorded and are shown in figure S50. Figure S51 – S56 show the HSQC, HMBC and APT-spectra of 19 mg Mtt-Cl in 0.6 mL  $\text{CDCl}_3$  with and without addition of 5% TFA.

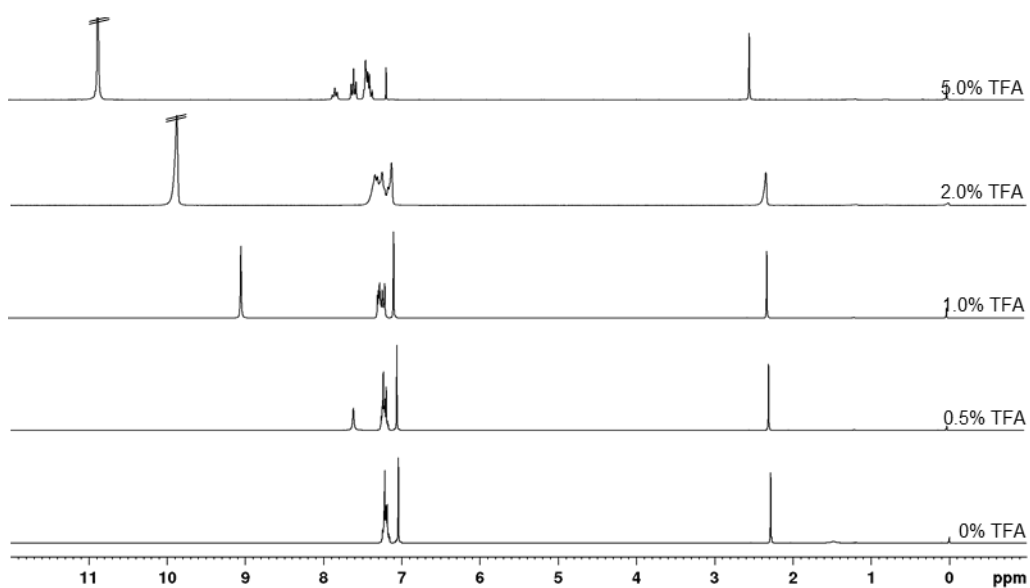


**Figure S50:**  $^1\text{H-NMR}$  spectra (300 MHz) of Mtt-Cl in  $\text{CDCl}_3$  at different TFA concentrations.

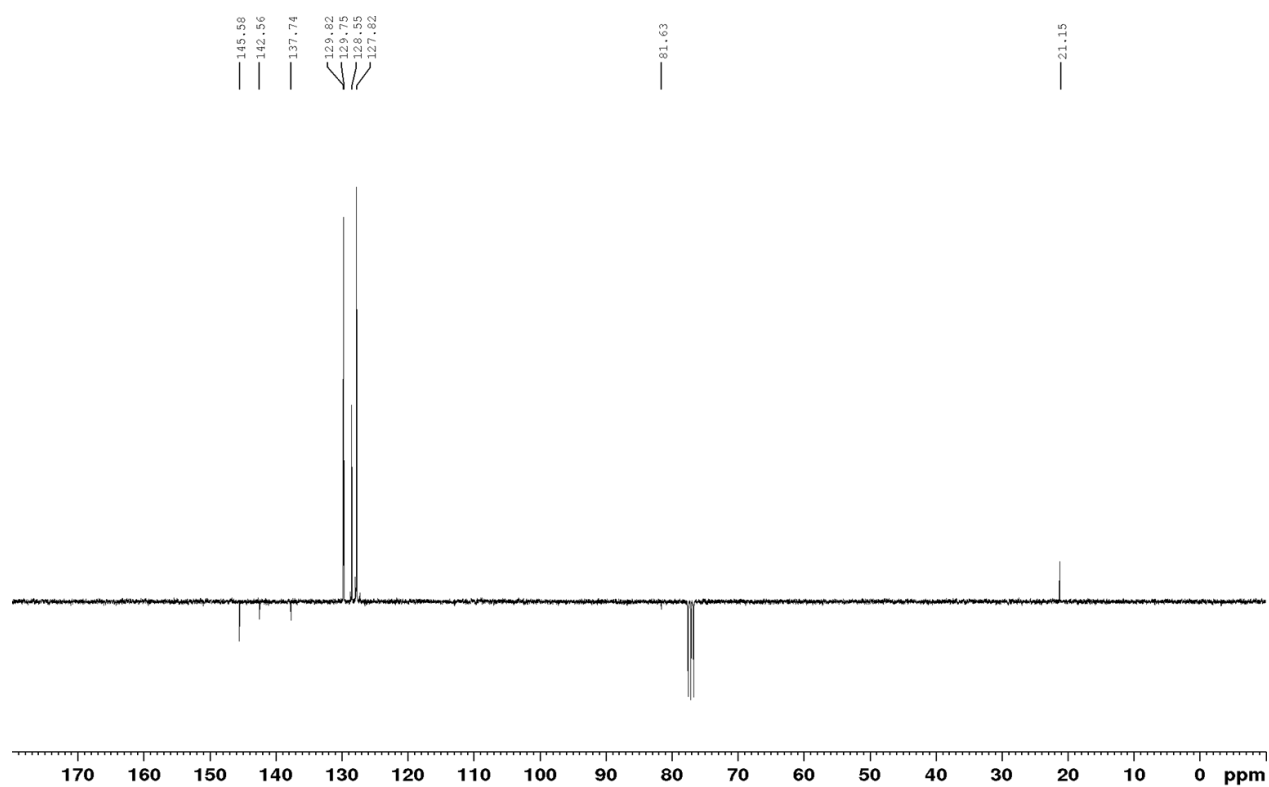


**Figure S51:** APT-NMR spectra (300 MHz) of Mtt-Cl in  $\text{CDCl}_3$  without addition of TFA.

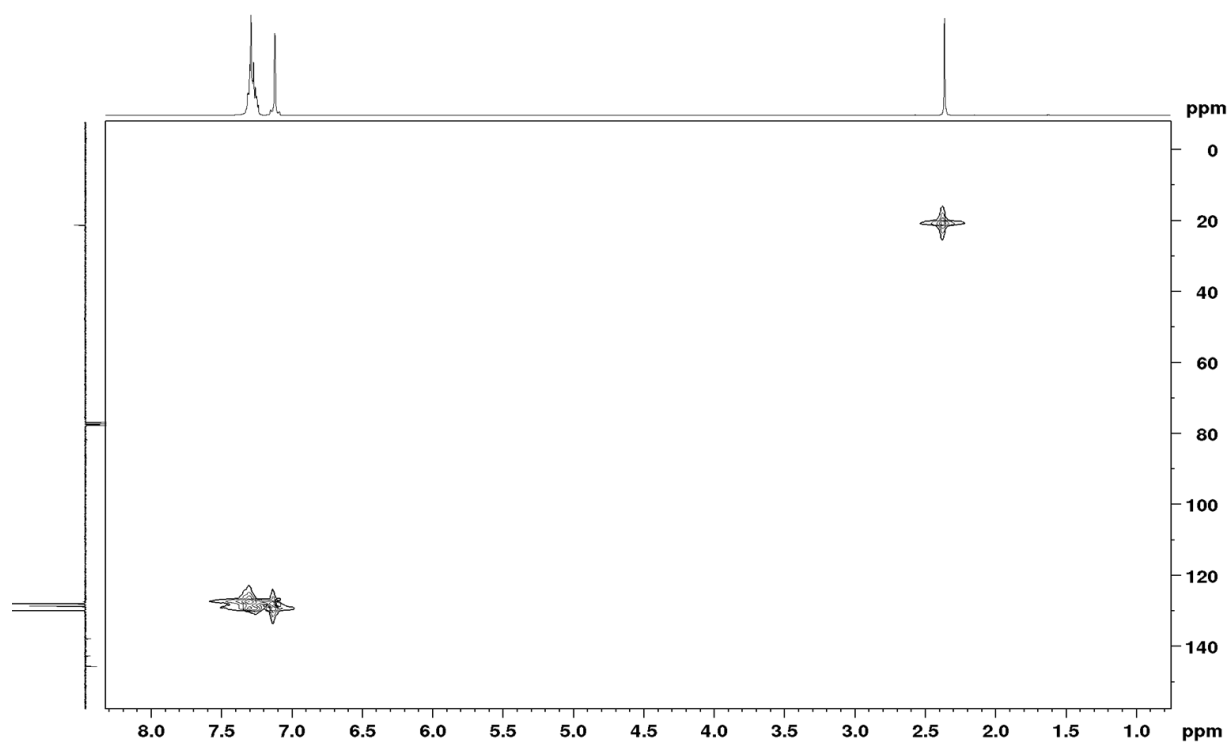


**Figure S52:** HSQC-NMR spectra (300 MHz) of Mtt-Cl in CDCl<sub>3</sub> without addition of TFA.

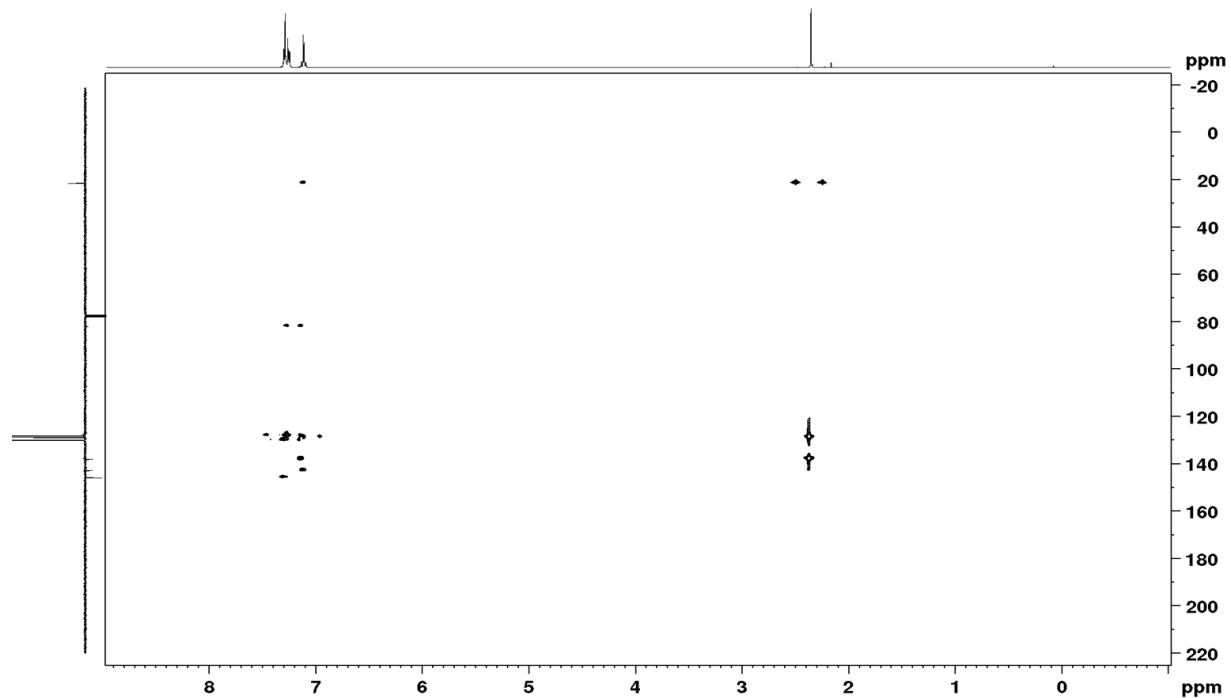


**Figure S53:** HMBC-NMR spectra (300 MHz) of Mtt-Cl in CDCl<sub>3</sub> without addition of TFA.



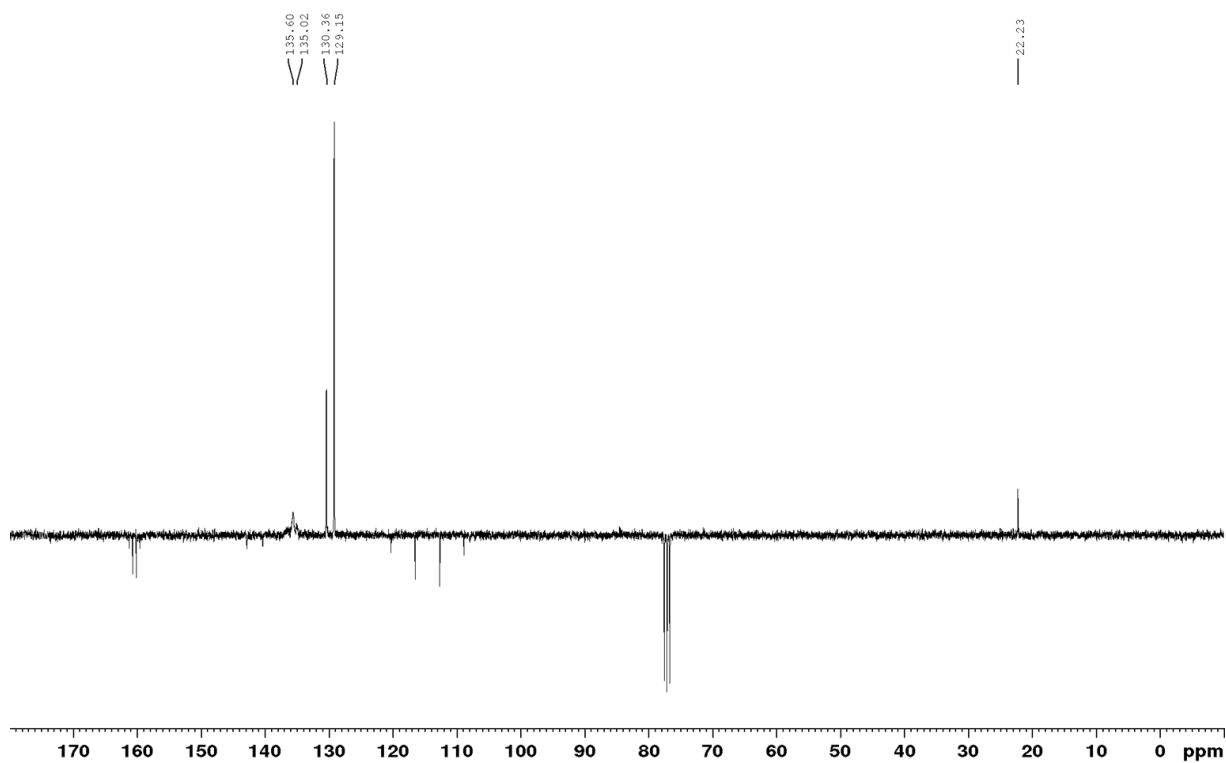


**Figure S54:** APT-NMR spectra (300 MHz) of Mtt-Cl in  $\text{CDCl}_3$  including 5% TFA.

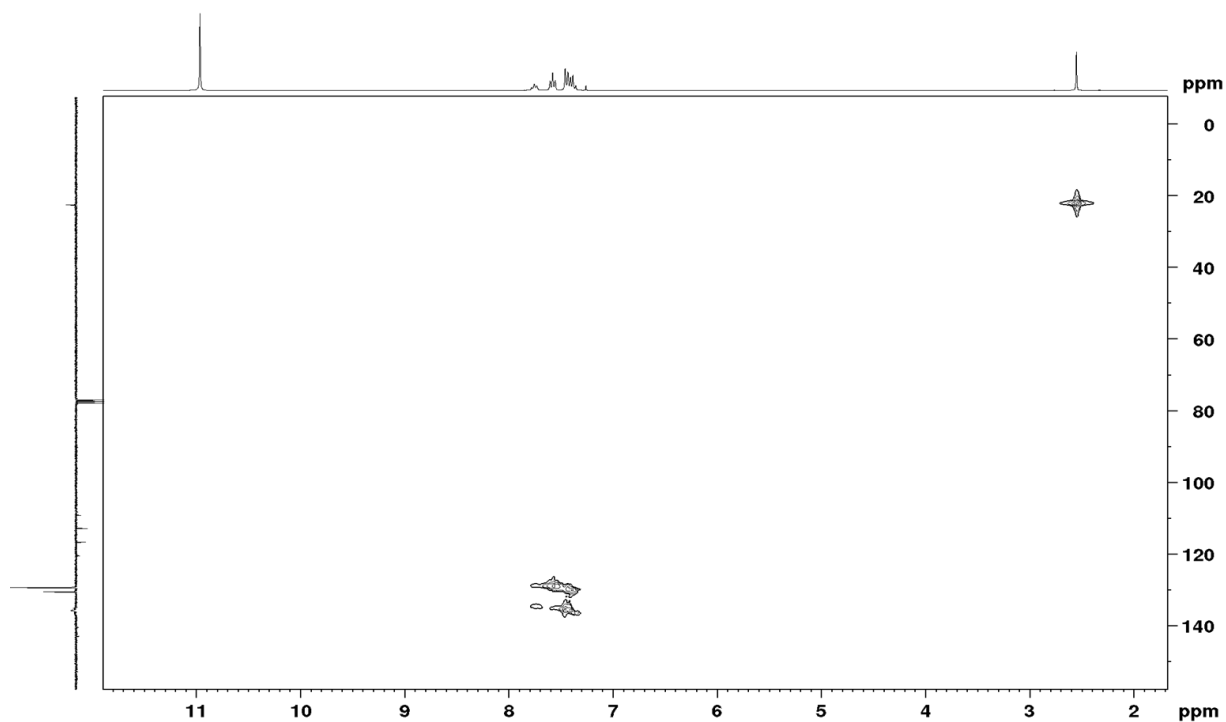


**Figure S55:** HSQC-NMR spectra (300 MHz) of Mtt-Cl in  $\text{CDCl}_3$  including 5% TFA.

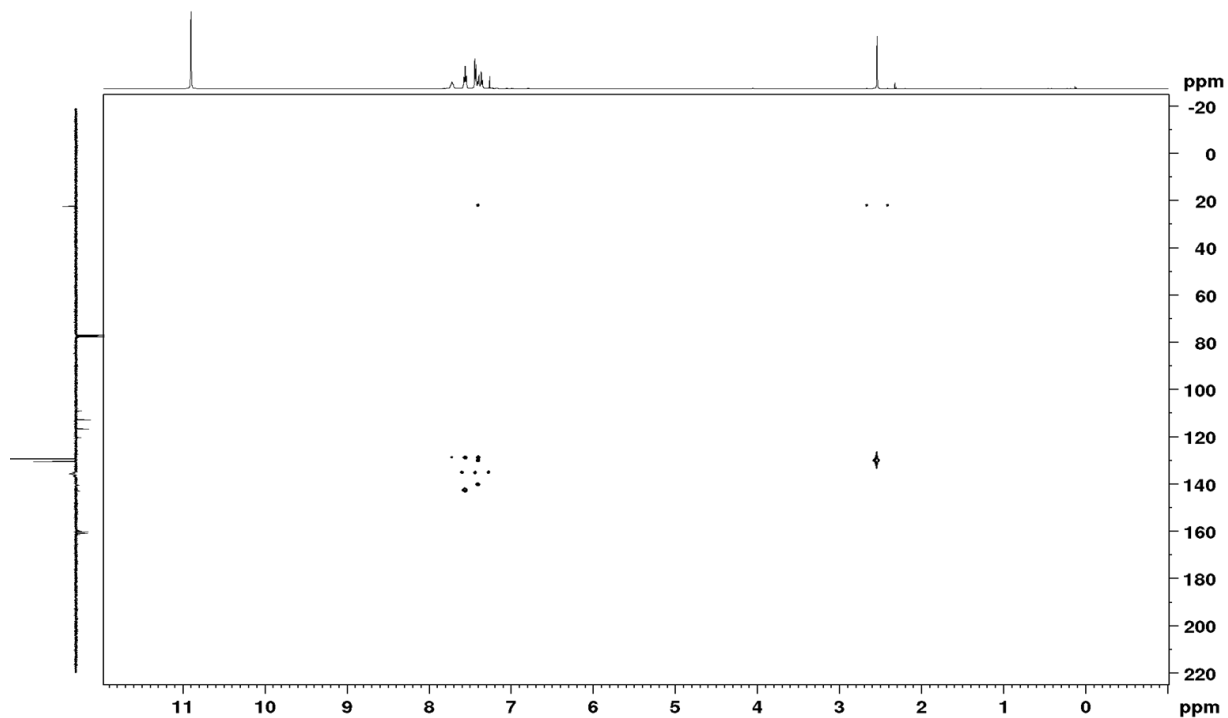


**Figure S56:** HMBC-NMR spectra (300 MHz) of Mtt-Cl in  $\text{CDCl}_3$  including 5% TFA.

Figure S57 represents the APT-spectra of a 5% TFA solution in  $\text{CDCl}_3$ .

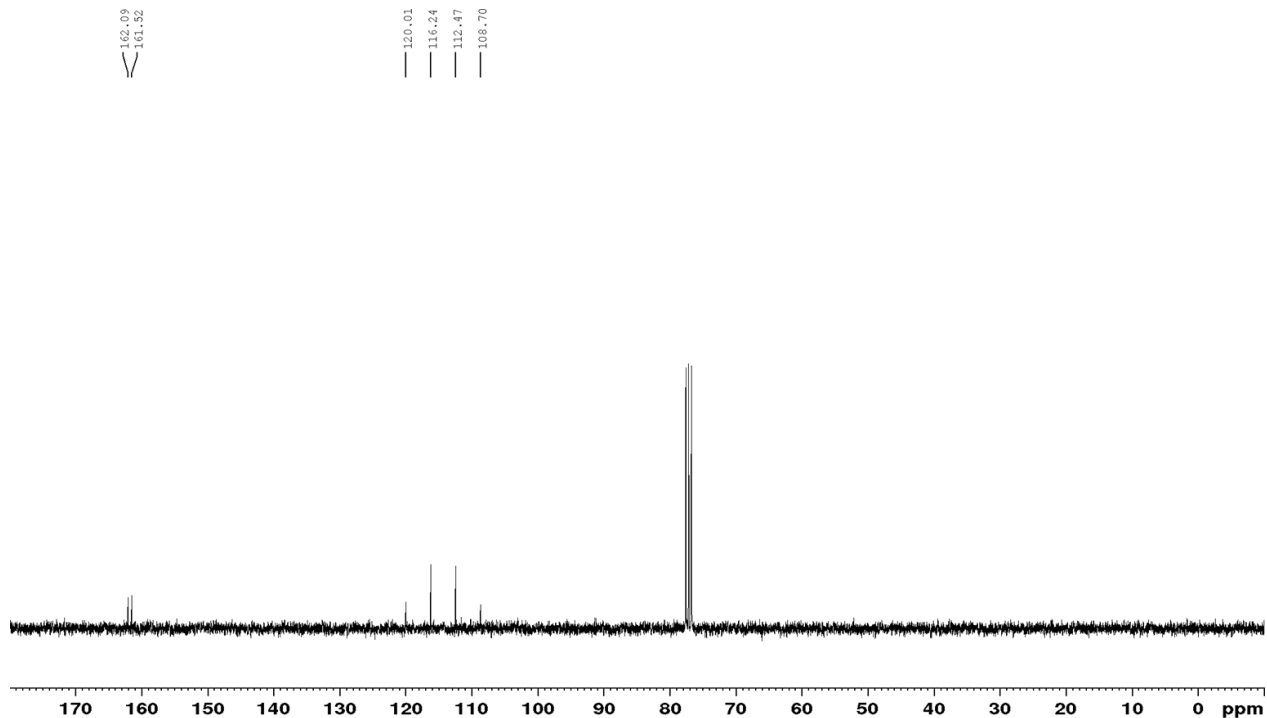
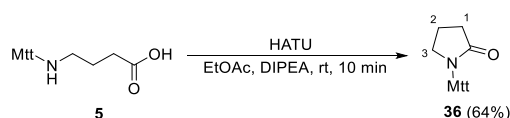


**Figure S57:** APT-NMR spectra (300 MHz) of 5% TFA in  $\text{CDCl}_3$ .

## Additional Experiments

Further experiments were performed to prove the formation of Mtt-butylrolactam (**36**) and optimize the coupling conditions to implement Mtt- $\gamma$ -OH (**5**).

### Synthesis of Mtt-butylrolactam (**36**)



**Scheme S6:** Reaction scheme for the formation of Mtt-butylrolactam (**36**) from Mtt- $\gamma$ -OH (**5**).

**1-(diphenyl(p-tolyl)methyl)pyrrolidin-2-one (**36**):** Mtt- $\gamma$ -OH (50.0 mg, 139 nmol) and HATU (52.9 mg, 139 nmol) were dissolved in EtOAc (500  $\mu$ L) and DIPEA (73  $\mu$ L, 419 nmol) added. After 10 min at rt, the solvent was removed under reduced pressure and the crude purified by column chromatography (silica, CH<sub>2</sub>Cl<sub>2</sub>/NEt<sub>3</sub> 100:1 and *n*-pentane/EtOAc 2:1) to yield the desired product (**36**, 30.2 mg, 88.4 nmol, 64%) as colourless solid. *R<sub>f</sub>* = 0.42 (*n*-pentane/EtOAc 1:1). **<sup>1</sup>H-NMR** (300 MHz, CDCl<sub>3</sub>,  $\delta$ ): 7.30–7.17 (m, 10H, CH<sub>arom.</sub>), 7.16–7.06 (m, 4H, CH<sub>arom.</sub>), 3.46 (t, 2H, *J* = 6.8 Hz, CH<sub>2</sub>-3), 2.37 (t, 2H, *J* = 8.0 Hz, CH<sub>2</sub>-1), 2.30 (s, 3H, CH<sub>3</sub>-Mtt), 2.11–1.97 (m, 2H, CH<sub>2</sub>-2). **<sup>13</sup>C-NMR** (75 MHz, CDCl<sub>3</sub>,  $\delta$ ): 178.2 (C=O), 144.3 (2C, C<sub>q</sub>), 141.3 (C<sub>q</sub>), 137.8 (C<sub>q</sub>), 130.8 (2C, CH), 130.7 (4C, CH), 129.1 (2C, CH), 128.5 (4C, CH), 127.8 (2C, CH), 75.0 (C<sub>q</sub>), 51.6 (CH<sub>2</sub>), 34.2 (CH<sub>2</sub>), 20.9 (CH<sub>3</sub>), 19.8 (CH<sub>2</sub>). **HRMS-ESI<sup>+</sup>** (*m/z*): [M+H]<sup>+</sup> calcd for C<sub>24</sub>H<sub>23</sub>NOH, 342.1852; found, 342.1862. **FT-IR** (neat)  $\tilde{\nu}$  = 3020 (w), 2966 (w), 2874 (w), 1692 (s), 1509 (w), 1491 (w), 1443 (w), 1389 (m), 1319 (w), 1282 (w), 1259 (m), 1190 (w), 1159 (w), 1121 (w), 1086 (w), 1022 (w), 945 (w), 929 (w), 906 (w), 804 (m), 761 (w), 740 (m), 698 (s), 664 (w), 635 (w), 581 (w), 546 (m), 519 (w), 498 (w), 482 (w).

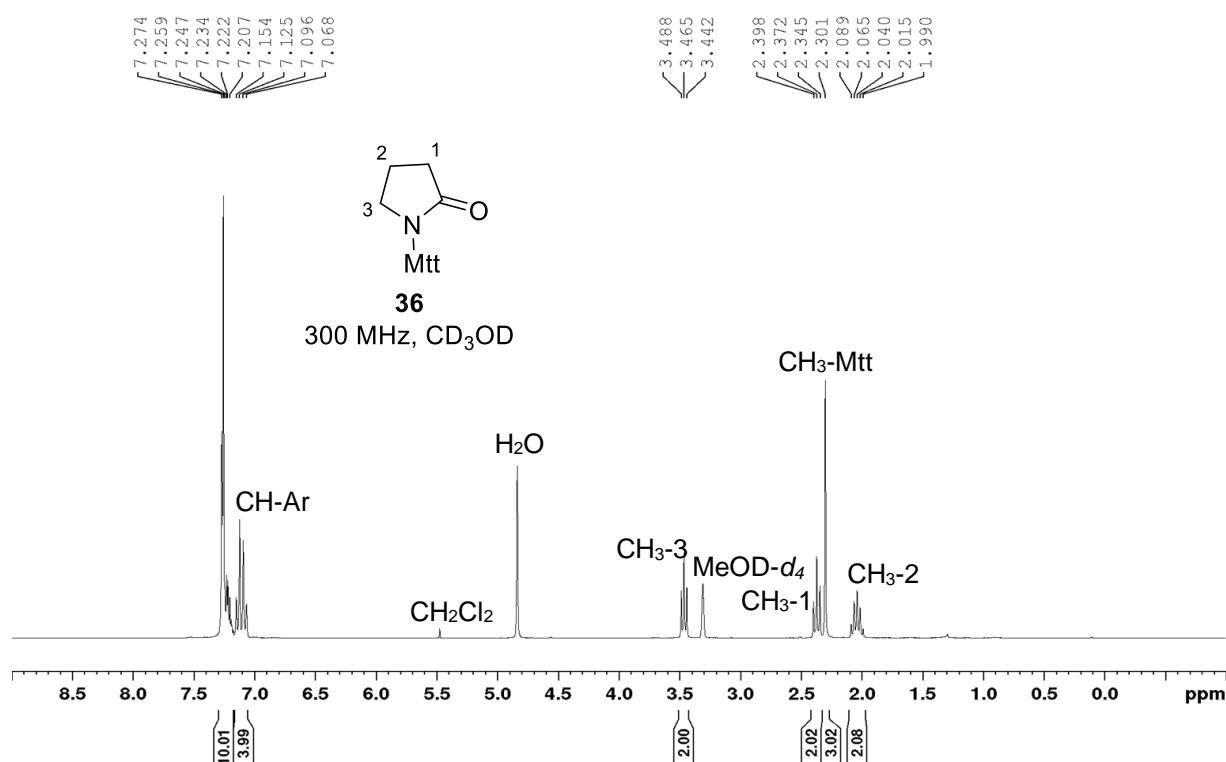


**Figure S58:**  $^1\text{H-NMR}$  (300 MHz) spectrum of Mtt-butylolactam (**36**).

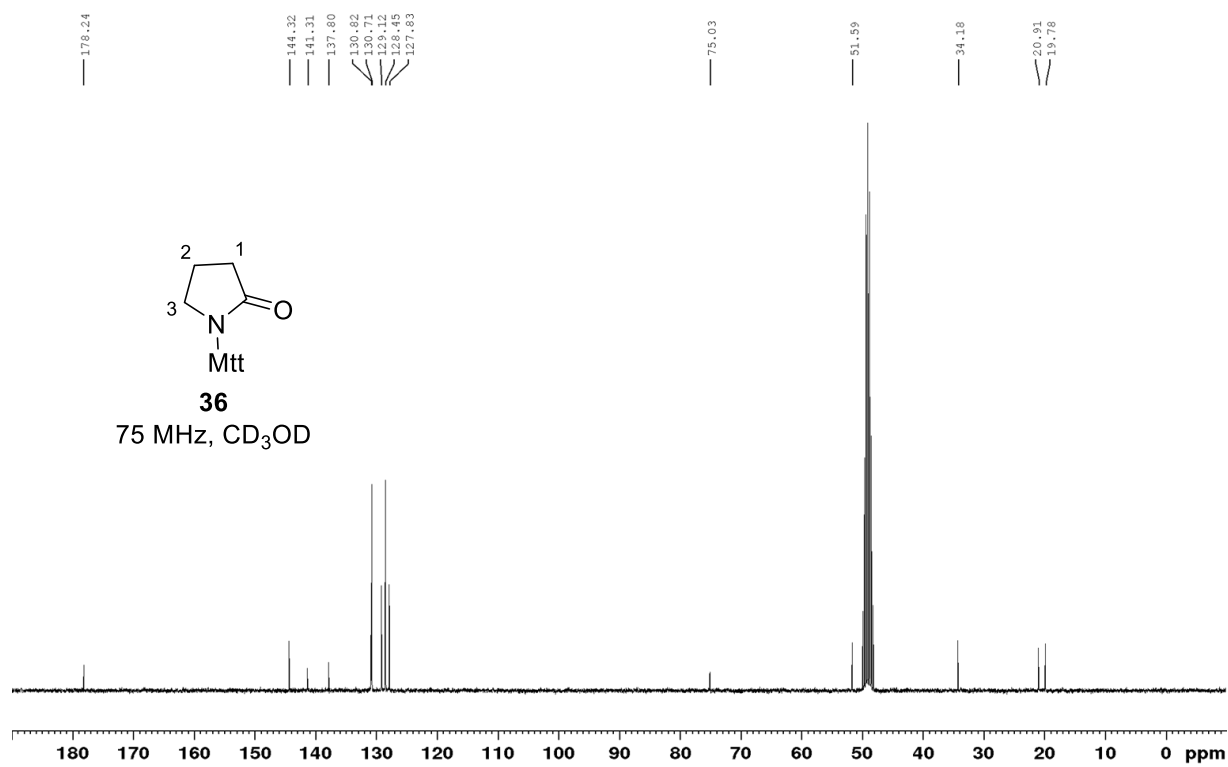


**Figure S59:**  $^1\text{H-NMR}$  (75 MHz) spectrum of Mtt-butylolactam (**36**).

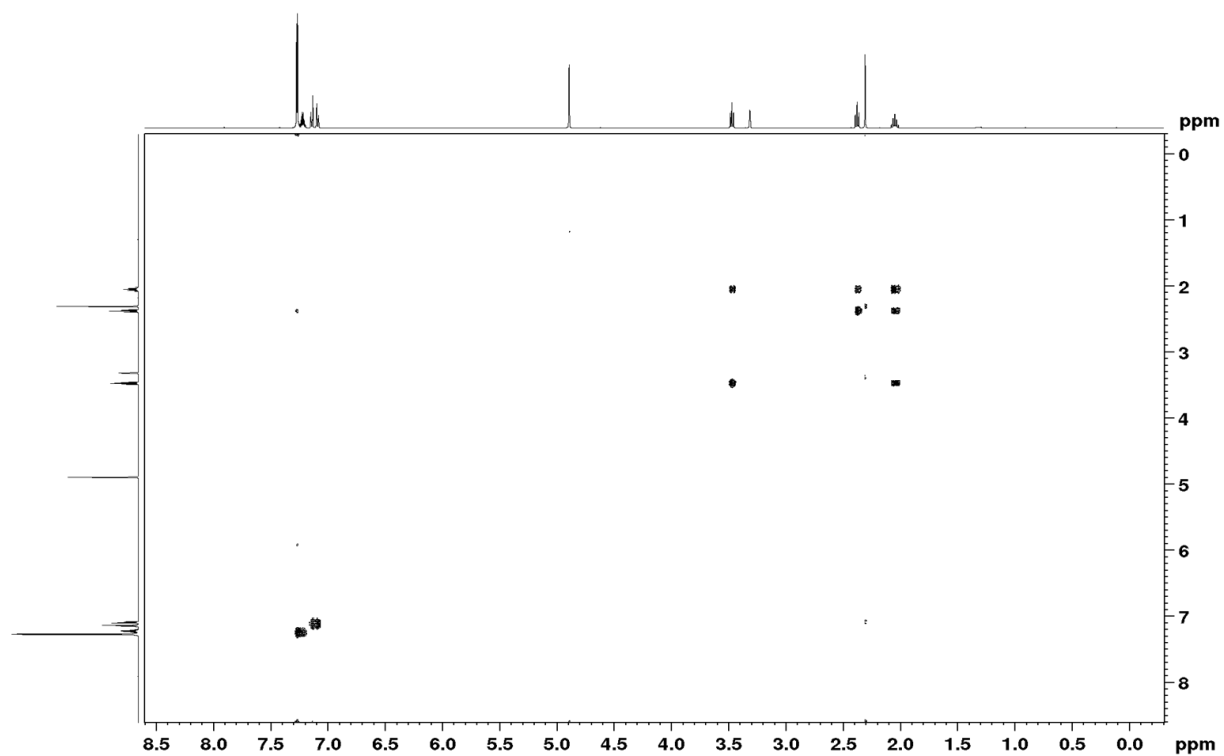


**Figure S60:** COSY-NMR (500 MHz) spectrum of Mtt-butylolactam (**36**).

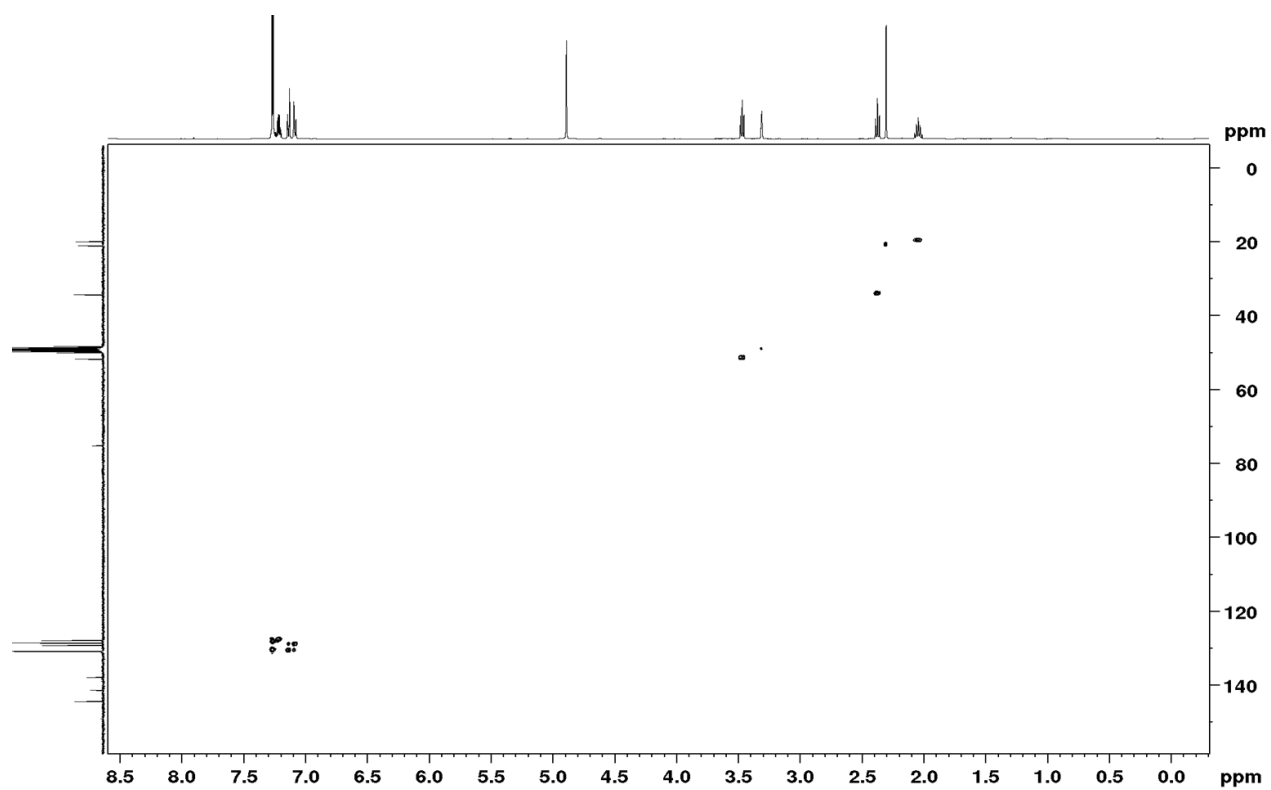


**Figure S61:** HSQC-NMR (500 MHz, 75 MHz) spectrum of Mtt-butylolactam (**36**).

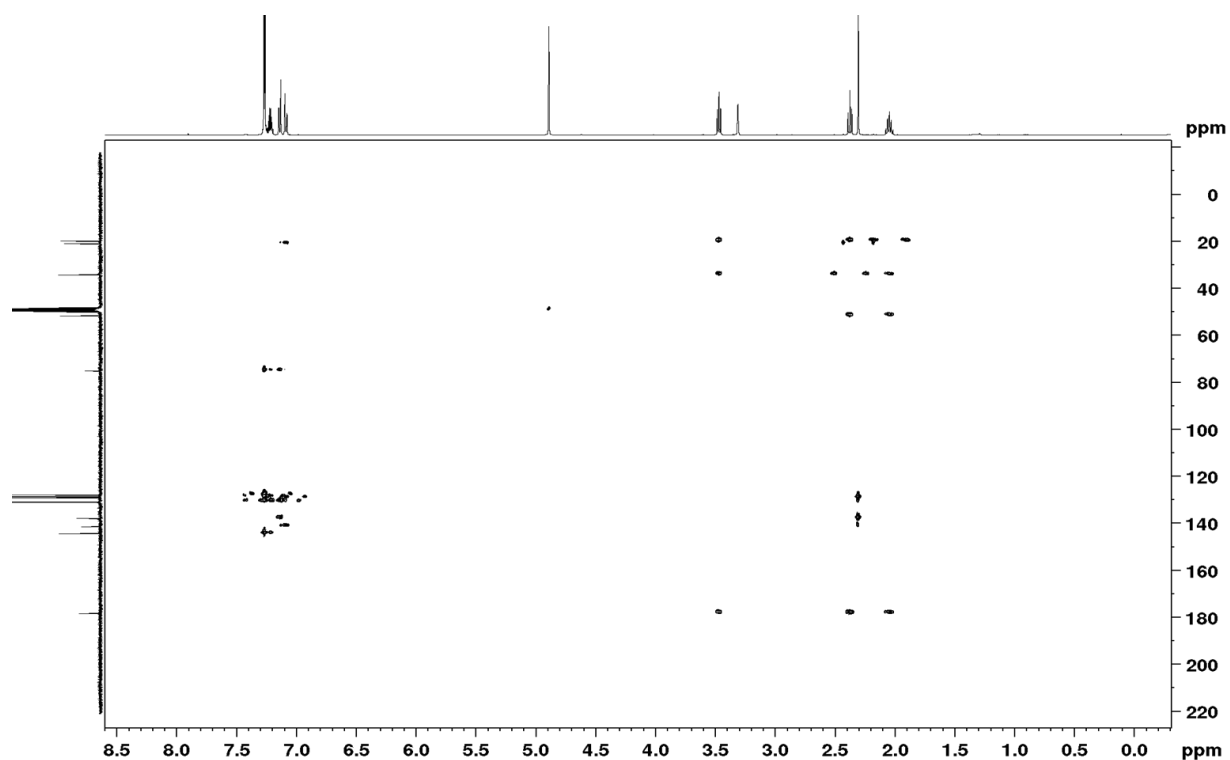


Figure S62: HMBC-NMR (500 MHz, 75 MHz) spectrum of Mtt-butyrolactam (**36**).

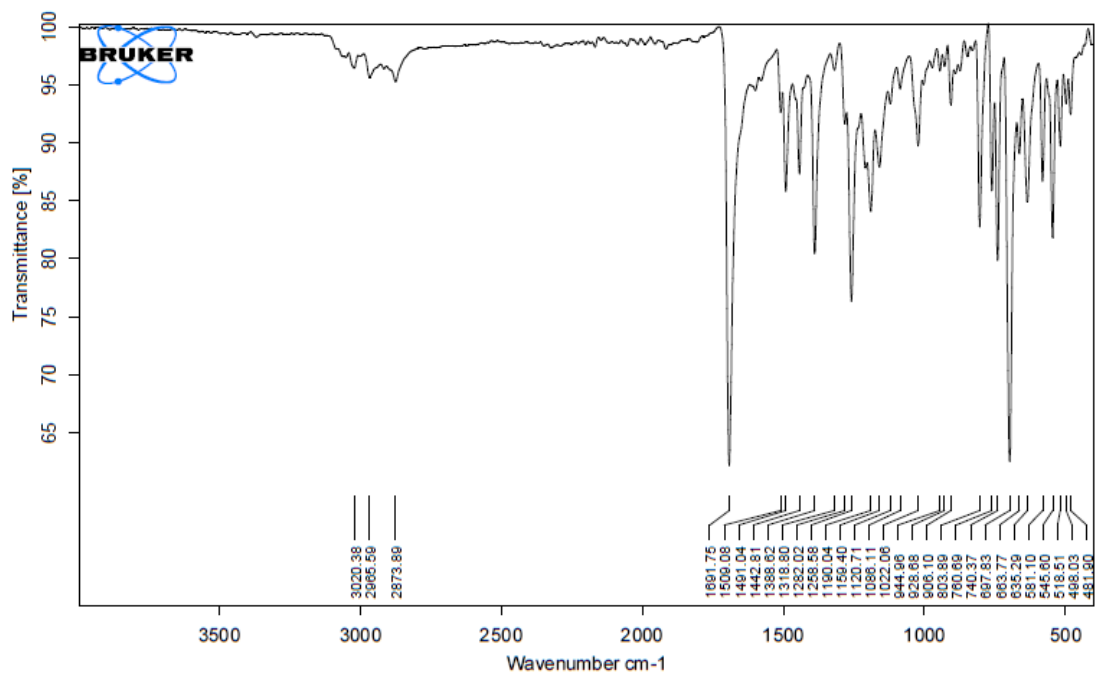
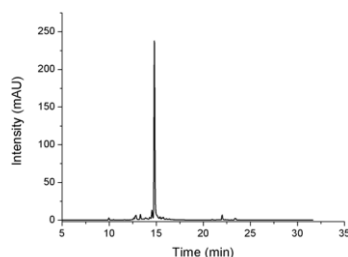


Figure S63: IR spectrum of Mtt-butyrolactam (**36**).

### Test Implementation of Mtt- $\gamma$ -OH

For the introduction of Mtt- $\gamma$ -OH, Mtt-Py-Im-Im-Py- $\beta$  was synthesized on solid support. Figure S63 shows the HPLC chromatogram of the successful coupling with a purity >95%.



**Figure S64:** HPLC chromatogram of the test cleavage of H<sub>2</sub>N-Py-Im-Im-Py- $\beta$ -COOH. Gradient 5-95% B.

In 3  $\mu$ mol scales, the Mtt group was deprotected as described above and Mtt- $\gamma$ -OH (**5**) coupled at 0.3M in NMP with different coupling conditions over one hour. After washing, capping and cleavage, HPLC analysis revealed the coupling efficiency. Integration of the product peak (H<sub>2</sub>N- $\gamma$ -Py-Im-Im-Py- $\beta$ -COOH,  $t_R$  = 17.3 min) in comparison to peaks with an >10% intensity to the highest peak in the chromatogram let to the described coupling yields. The corresponding HPLC-chromatograms are shown in figure S65.

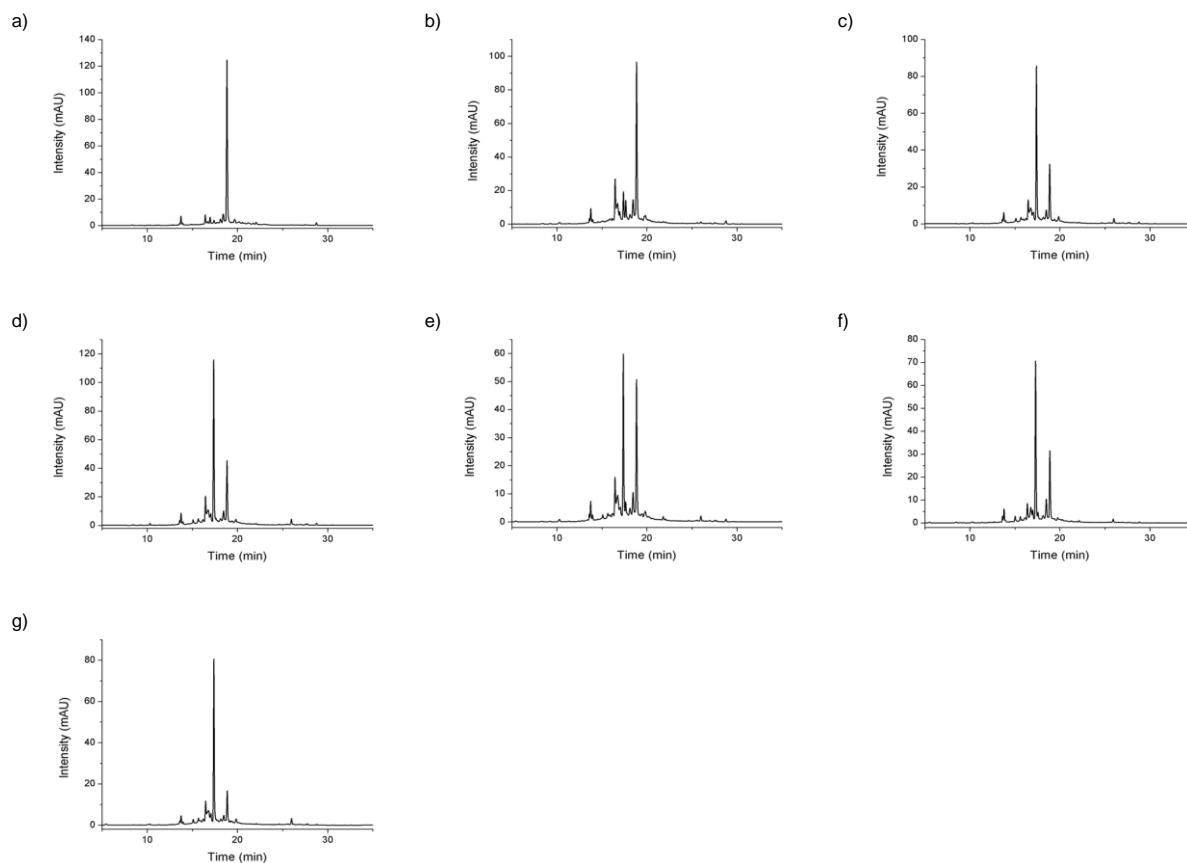


**Figure S65:** HPLC chromatograms of the test couplings for the introduction of Mtt- $\gamma$ -OH (**5**). Gradient 5-75% B. Coupling conditions were a) 4 eq Mtt- $\gamma$ -OH, 4 eq HATU, 12 eq DIPEA; b) 4 eq Mtt- $\gamma$ -OH, 4 eq HATU, 12 eq NMM; c) 4 eq Mtt- $\gamma$ -OH, 4 eq HATU, 12 eq pyridine; d) 4 eq Mtt- $\gamma$ -OH, 4 eq HATU, 8 eq pyridine; e) 4 eq Mtt- $\gamma$ -OH, 4 eq PyBOP, 12 eq NMM; f) 4 eq Mtt- $\gamma$ -OH, 4 eq PyBOP, 8 eq NMM; g) 4 eq Mtt- $\gamma$ -OH, 4 eq PyBOP, 8 eq pyridine.

## References

- 
- [i] H. E. Gottlieb, V. Kotlyar, A. Nudelman *J. Org. Chem.* **1997**, *62*, 7512–7515.
- [ii] E. E. Baird, P. B. Dervan *J. Am. Chem. Soc.* **1996**, *118*, 6141-6146.
- [iii] M. Minoshima, T. Bando, S. Sasaki, J. Fujimoto, H. Sugiyama *Nucleic Acids Res.* **2008**, *36*, 9, 2889-2894.
- [iv] J.W. Lown, K. Krowicki *J. Org. Chem.* **1985**, *50*, 3774 – 3779.
- [v] C. Hotzel, A. Marotto, U. Pindur *Eur. J. Med. Chem.* **2002**, *37*, 367 – 378.
- [vi] B. König, M. Rödel *Synth. Commun.* **1999**, *29*, 943-950.
- [vii] C. Hotzel, A. Marotto, U. Pindur *Eur. J. Med. Chem.* **2003**, *38*, 2, 189-197.
- [viii] B. Heinrich, K. Bouazoune, M. Wojcik, U. Bakowsky, O. Vázquez *Org. Biomol. Chem.* **2019**, *17*, 7, 1827-1833.
- [ix] A. Viger, P. B. Dervan *Bioorg. Med. Chem.* **2006**, *15*, 14, 8539-8549.
- [x] P.B. Dervan, E. E. Baird, Method for the synthesis of pyrrole and imidazole carboxamides on a solid support. U.S. Patent 6545162, April 8, 2003.
- [xi] E. Nishiwaki, S. Tanaka, H. Lee, M. Shibuya *Heterocycles* **1988**, *27*, 1945-1952.
- [xii] D. Jaramillo, Q. Liu, J. Aldrich-Wright, Y. Tor *J. Org. Chem.* **2004**, *46*, 3492-3497.
- [xiii] A. J. Fallows, I. Singh, R. Dondi, P. M. Cullis, G. A. Burley *Org. Lett.* **2014**, *16*, 17, 4654-4657.
- [xiv] N. R. Wurtz, J. M. Turner, E. E. Baird, P. B. Dervan *Org. Lett.* **2001**, *3*, 8, 1201-1203.
- [xv] K. Seio, M. Mizuta, T. Terada, M. Sekine *J. Org. Chem.* **2005**, *70*, 10311-10322.
- [xvi] T. Lescrinier, C. Hendrix, L. Kerremans, J. Rozenski, A. Link, B. Samyn, A. V. Aerschot, E. Lescrinier, R. Eritja, J. V. Beeumen, P. Herdewijn *Chem. Eur. J.* **1998**, *4*, 425-433.
- [xvii] N. Shiga, S. Takayanagi, R. Muramoto, T. Murakami, R. Qin, Y. Suzuki, K. Shinohara, A. Kenada, T. Nemoto *Bioorg. Med. Chem. Lett.* **2017**, *27*, 10, 2197-2200.
- [xviii] J. W. Drijfhout, W. Bloemhoff *Int. J. Pept. Protein Res.* **1991**, *37*, 1, 27-32.
- [xix] Merck KGaA, Novabiochem® Peptide Synthesis; Merck KGaA: Darmstadt, 2012, p 2.32.
- [xx] W.J. Fang, T. Yakovleva, J.V. Aldrich *Biopolymers* **2011**, *96*, 715-722.
- [xxi] G. Kallansrud, B. Ward *Anal. Biochem.* **1996**, *236*, 134–138.
- [xxii] J. L. Meier, A. S. Yu, I. Korf, D. J. Segal, P. B. Dervan *J. Am. Chem. Soc.* **2012**, *134*, 42, 17814-17822.



## 4. Cumulative Part

### 4.3.1 Conclusion

A new toolbox of 4-methyltrityl (Mtt)-monomers and dimers was introduced for the solid phase synthesis of DNA-binding pyrrole and imidazole polyamide hairpins. The synthesis of these new building blocks was straightforward with excellent yields over two steps: 84% for Mtt-Py-OH and 68% for Mtt-Im-OH. In contrast, the previously reported Boc- and Fmoc-building blocks are described with lower yields (64% for Boc-Py-OH and 42% for Boc-Im-OH; 58% for Fmoc-Py-OH and 30% for Fmoc-Im-OH).<sup>[1,2]</sup> The utility of the methodology was successfully shown by the synthesis and study of a DNA-binding polyamide employing all Mtt-building blocks. It is orthogonal to Fmoc and will allow the implementation of base labile compounds and other sensitive groups in Py-Im polyamide chemistry, affording novel bifunctional polyamide conjugates.

Interestingly, in the context of my thesis, whereas the *ortho*-fluoroazobenzene moiety is not stable under Fmoc-deprotection conditions,<sup>[3]</sup> our new monomers allowed the introduction of this photoswitchable compound into the polyamide-hairpin backbone. It will access the introduction of dynamic and spatial control in the level of sequence specific DNA binding in biological assays.

### 4.3.2 Further Developments and Outlook

Having the Mtt-monomers in hand, we aimed to apply this toolbox to expand the photoswitchable DNA binders based on netropsin (chapter 4.2) to sequence-specific polyamide hairpins. A sequence which targets the  $\alpha$ -satellite nucleosome was chosen to serve as a scaffold to introduce the *ortho*-fluoroazobenzene in the turn of the hairpin. Successful solid phase synthesis and purification yielded the polyamide hairpin represented in Figure 4.3.1.

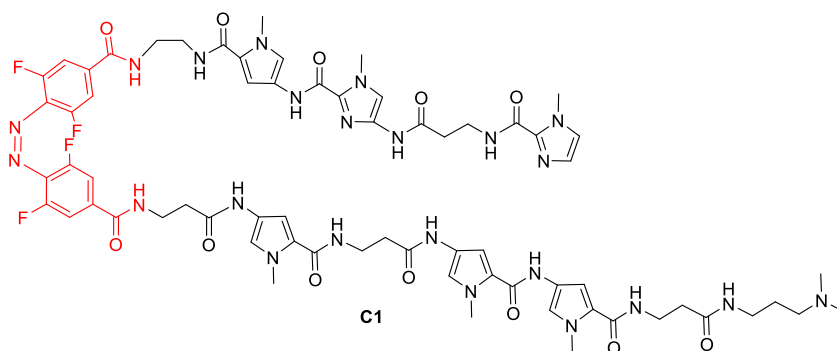


**Figure 4.3.1.** Structure of the first described photoswitchable polyamide hairpin **C1**. The sequence was chosen to target the  $\alpha$ -satellite nucleosome.

Analytical data and a Figure of the RP-HPLC chromatogram, including the mass spectra of the photoswitchable polyamide hairpin (Figure 4.3.2) are given below:

**HRMS-ESI<sup>+</sup> (*m/z*):** [M+2H]<sup>2+</sup> calcd for C<sub>67</sub>H<sub>77</sub>F<sub>4</sub>N<sub>23</sub>O<sub>12</sub>H<sub>2</sub>, 736.8107; found, 736.8107; **t<sub>R</sub>** = 13.6 min (trans), 15.2 min (cis) (gradient 25-40% B).

## 4. Cumulative Part

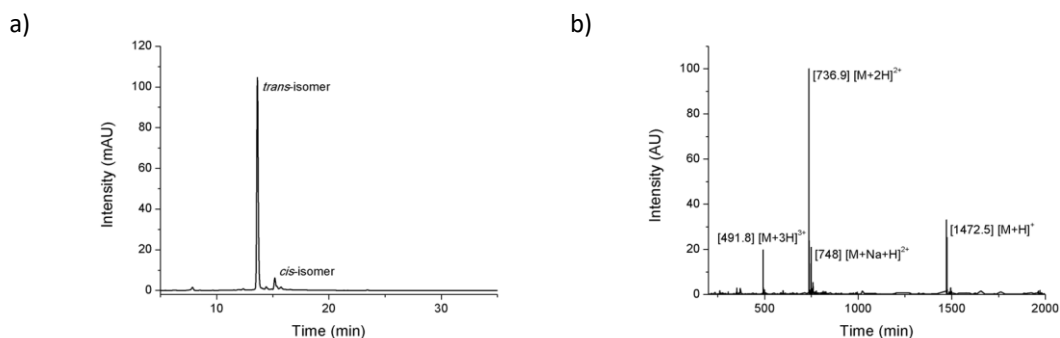


**Figure 4.3.2.** a) RP-HPLC chromatogram of photoswitchable polyamide hairpin **C1**. Gradient 25-40% B. b) ESI spectrum of **C1**.

The isomerization of the synthesized visible-light switch was studied in H<sub>2</sub>O / MeCN 1:1 via HPLC and UV-vis spectroscopy. Both techniques displayed that the photostationary state after 30 s irradiation at 405 nm for the *trans*-isomer and after 2 min irradiation at 520 nm for the *cis*-isomer was reached. HPLC analysis demonstrated the dark stability of both forms for up-to at least 11 h (Figure 4.3.3), which turns this compound into a suitable agent for a number of biological assays.

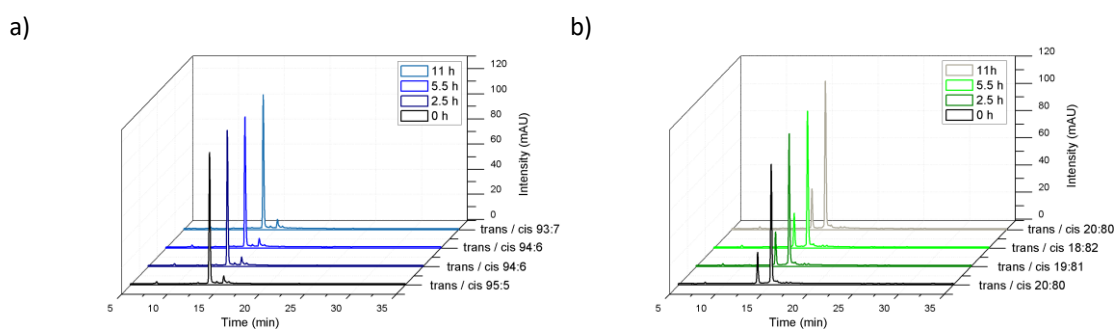


**Figure 4.3.3.** RP-HPLC chromatograms of F<sub>4</sub>Azo-polyamide hairpin (**C1**) showing the dark stability at 20 °C after irradiation at a) 405 nm for 30 s and b) 520 nm for 2 min and their corresponding *trans/cis*-ratio after several time points. Gradient 25 – 40% B. Represented data are a representative one of three measurements from independent experiments.

By UV-vis spectroscopy, the isobestic point at 272 nm could be determined (Figure 4.3.4 A) and the difference in the absorbance spectra of the two isomers could be shown, which are in agreement with the spectra of *ortho*-fluorazobenzenes from the literature.<sup>[4]</sup> Subsequent changes of the spectra were observed upon stepwise irradiation of the different wavelengths (Figure 4.3.4 B and C) and stability of at least 13 cycles could be verified (Figure 4.3.4 D).

#### 4. Cumulative Part

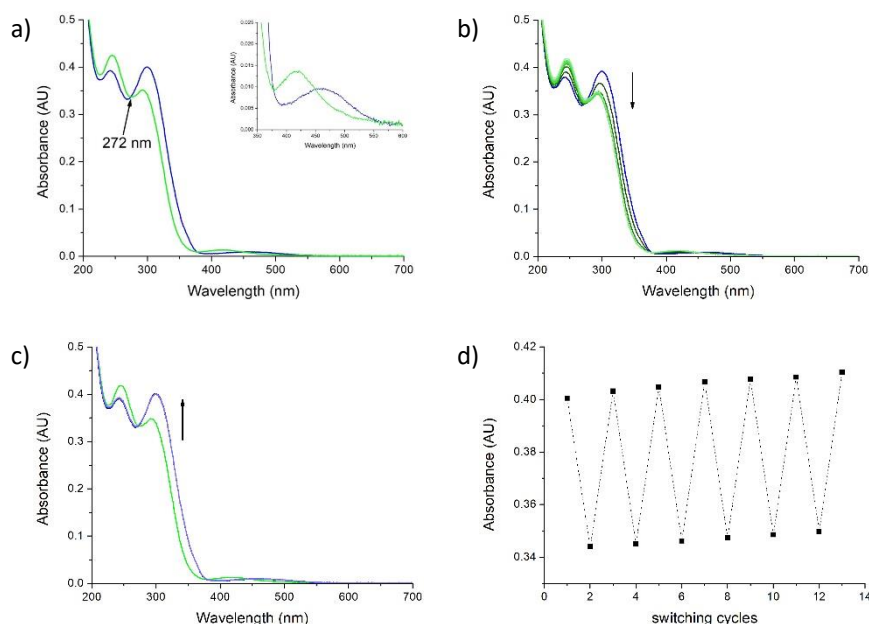


**Figure 4.3.4.** UV-vis spectra of a  $7.0 \mu M$  solution of  $F_4$ Azo-polyamide hairpin (**C1**) in  $H_2O/MeCN$  1:1 after irradiation at a) 405 nm for 30 s (blue) and 520 nm for 2 min (green), b) initially irradiated at 405 nm for 30 s and after successive irradiation times at 520 nm, c) initially irradiated at 520 nm for 10 min and after successive irradiation times at 405 nm, d) reversible photochromism upon altering irradiation at 520 nm and 405 nm measured at 299 nm. Represented data are the calculated mean from three measurements from independent experiments.

Additional developments will show the exact binding mode of both isomers and their difference in binding towards DNA targets. Within a collaboration with Gonzalo Jiménez-Osés and Claudio Navo Najera (CICbioGUNE, Spain), molecular dynamics (MD) simulations for the nucleosomal DNA sequence (5'-AAA AGTGTA TTT-3') in the absence and in the presence of several polyamide ligands were performed. The studied polyamides had the same sequence than compound **C1**, but bear different photoswitches in their turn-unit. As seen in Figure 4.3.5, it could be observed that the ligand without photoswitch (no photoswitch) would show the highest affinity without disturbing the native structure of DNA too much. The  $F_4$ Azo-derivative would display high affinity, but the DNA structure was not conserved, especially in the surrounding of the photoswitch due to steric hindrance. The hemithioindigo-derivative showed very few constructive interactions and low affinity, but disrupted the DNA structure. Finally, the diarylethene derivative shows a reasonable binding energy, but effects the native structure of the DNA.

## 4. Cumulative Part

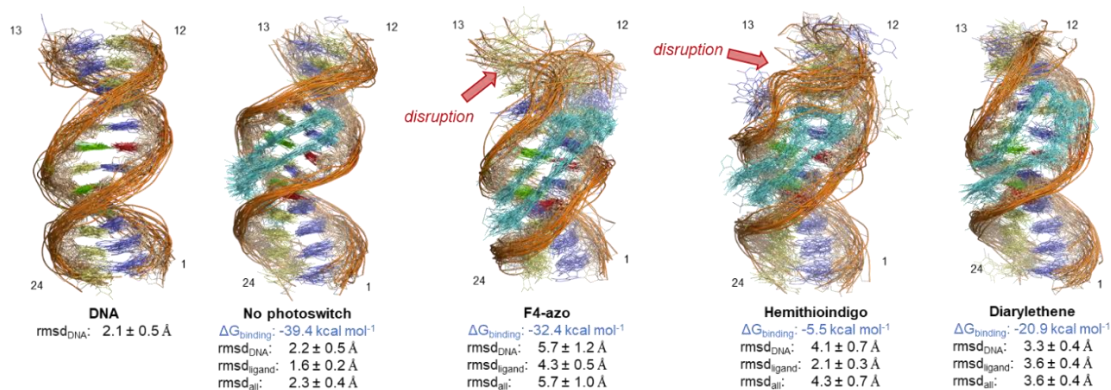


**Figure 4.3.5.** Conformational ensembles for each complex show 20 superimposed representative snapshots derived from the trajectories (1000 ns). DNA backbone and bases are shown as an orange cartoon and colored lines, respectively. A: blue, T: yellow, G: green, C: red. Ligand is shown as turquoise lines. Nonpolar hydrogens have been omitted for clarity. The binding energies ( $\Delta G_{\text{binding}}$ ) were estimated using Molecular Mechanics and the Generalized Born model with surface area continuum solvation (MM/GBSA).

New photoswitchable polyamide hairpins could allow specific real time manipulation of many DNA based processes such as replication, DNA repair or nucleosome based epigenetic phenomena. We envision to apply our system in the control of specific epigenetic processes.

### 4.3.3 Author Contribution

I synthesized all described Fmoc-monomers and dimers and established their use to access polyamide hairpins. The synthesis of the Mtt-building blocks and their stability studies in solution were conducted by myself. I could further demonstrate their applicability in solid phase synthesis and their orthogonality to Fmoc-SPPS towards the synthesis and study of a DNA-binding polyamide hairpin. I applied the Mtt-building blocks to synthesize a photoswitchable polyamide. Moreover, I purified and studied the photoisomerization of the polyamide by HPLC and UV-vis spectroscopy. Abbas Sajediabkenar (AK Vázquez) synthesized some starting materials during his master thesis under my guidance. Gonzalo Jiménez-Osés and Claudio Navo Najera performed MD-simulations. Jun.-Prof. Dr. Olalla Vázquez had the role of corresponding author, was leading or involved in all the 14-role taxonomy for author-contribution assignment.<sup>[5]</sup>

Marburg,

Jun. Prof. Dr. Olalla Vázquez

Benedikt Heinrich

#### 4.3.4 References

- [1] Baird, E. E.; Dervan, P. B. Solid Phase Synthesis of Polyamides Containing Imidazole and Pyrrole Amino Acids. *J. Am. Chem. Soc.* **1996**, *118*, 26, 6141-6146.
- [2] Wurtz, N. R.; Turner, J. M.; Baird, E. E.; Dervan, P. B. Fmoc Solid Phase Synthesis of Polyamide Containing Pyrrole and Imidazole Amino Acids. *Org. Lett.* **2001**, *3*, 8, 1201-1203.
- [3] Albert, L.; Penalver, A.; Djokovic, N.; Werel, L.; Hoffarth, M.; Ruzic, D.; Xu, J.; Essen, L. O.; Nikolic, K.; Dou, Y.; Vázquez, O. Modulating Protein-Protein Interactions with Visible-Light-Responsive Peptide Backbone Photoswitches. *ChemBioChem* **2019**, *20*, 11, 1417-1429.
- [4] Knie, C.; Utecht, M.; Zhao, F.; Kulla, H.; Kovalenko, S.; Brouwer, A. M.; Saalfrank, P.; Hecht, S.; Bléger, D. *ortho*-Fluoroazobenzenes: Visible Light Switches with Very Long-Lived Z Isomers. *Chem. Eur. J* **2014**, *20*, 50, 16492-16501.
- [5] Allen, L.; Scott, J.; Brand, A.; Hlava, M.; Altman, M. Publishing: Credit where credit is due. *Nature* **2014**, *508*, 7496, 312-313.

#### 4.4 Spicing up an Interdisciplinary Chemical Biology Course with the Authentic Big Picture of Epigenetic Research



We describe an integrative chemical biology course focused on epigenetics that strives to bring the research culture to chemistry and biology Master's students. The course combines three modules: lectures, discovery-based research lab and science communication. Importantly, the outline of our course design could be easily adapted to different fields, improving the synergy between research and teaching in other universities.

This chapter was submitted as: [Heinrich, B.](#); Graulich, N.; Vázquez, O.\* Spicing up an Interdisciplinary Chemical Biology Course with the Authentic Big Picture of Epigenetic Research. *J. Chem. Educ.* **2019**, *manuscript under replied revision*. Upon acceptance of the article: Copyright American Chemical Society 2019. Material in this chapter was reproduced from the above mentioned reference with permission from the American Chemical Society.

---

# Spicing up an Interdisciplinary Chemical Biology Course with the Authentic Big Picture of Epigenetic Research

Benedikt Heinrich,<sup>†</sup> Nicole Graulich,<sup>‡</sup> and Olalla Vázquez\*,<sup>†</sup>

5 † Departement of Chemistry, Philipps-University Marburg, Hans-Meerwein-Straße 4, 35043, Marburg, Germany.

‡ Institute of Chemistry Education, Justus-Liebig-University, Heinrich-Buff-Ring 17, 35392 Gießen, Germany.

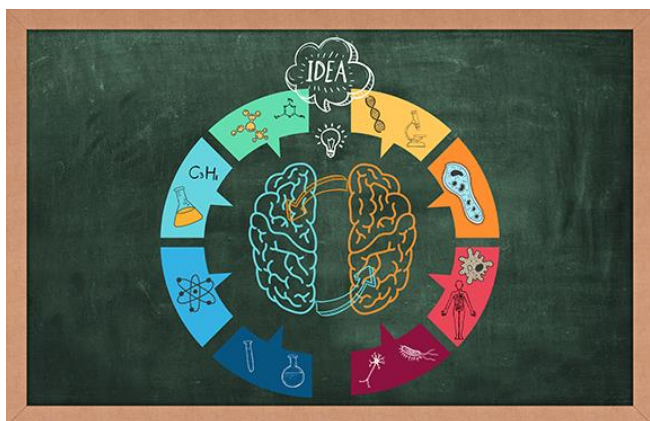
10

## ABSTRACT

The complexity of the world's current grand challenges demands interdisciplinary approaches. The education of future scientists must cross the silos of the traditional disciplines; however, there is still a strong reluctance to tear such walls down. Here, we describe an integrative chemical biology course focused on epigenetics that strives to bring research culture to chemistry and biology Master's students. The course, which has been successfully implemented for the past two years, combines three modules: lectures, discovery-based research lab and science communication. Importantly, the outline of our course design could be easily adapted to different fields, improving the synergy between research and teaching in our universities.

20

## GRAPHICAL ABSTRACT



## KEYWORDS

Cross-disciplinary teaching; cooperative learning; inquiry-based/discovery learning; interdisciplinary; chemical biology; epigenetics; organic chemistry; hands-on learning.

---

## INTRODUCTION

The study of chemistry is not only for learning chemical concepts, but using them as analytical and predictive tools in new situations. Such skills may become even more imperative in the interdisciplinary subjects, where contexts change, but the required techniques remain the same. Interdisciplinary teaching in STEM<sup>1,2,3,4,5,6</sup> has been demonstrated to be important for providing students with more authentic environments and preparing them for coping with their current global challenges.<sup>7,8</sup> Accordingly, the number of teaching lab experiments that highlight the interplay of multiple disciplines is increasing.<sup>9,10,11,12,13,14,15</sup> However, high-level chemistry education often remains bound to traditional disciplinary divisions. This lack of interdisciplinary interactions is evidenced by the relative absence of interdepartmental teaching collaborations, despite a wealth of cutting-edge research at the interface of scientific fields. Unfortunately, segregation also occurs in laboratory and lecture courses, which often are run independently from each other. Traditional laboratory courses are often based on classical “cookbook” experiments, usually without reference to interdisciplinary perspective.<sup>16</sup> However, educational research suggests the academic consequences may be severe.<sup>17</sup> For example, many students of discipline-segregated learning face significant difficulty in finding the connections between the disciplines, which prevents meaningful learning. These integrative abilities are crucial to achieving more in-depth understanding for tackling cross-interdisciplinary challenges. Students should, consequently, experience collaborative work between disciplines during their studies, and become equipped to recognize interdisciplinary links.<sup>18</sup>

By definition, chemical biology is an interdisciplinary pursuit toward the understanding of the interface of chemistry and biology. This inherently interconnected field<sup>19</sup> has significant potential as a vehicle for interdisciplinary teaching. However, chemical biology teaching is challenging and possesses unique problems for education as it requires, concurrently, both broad and in-depth knowledge.<sup>20,21</sup> Additionally, cultural differences between chemistry and biology departments create further challenges for chemical biology educational programs.<sup>22</sup>

Here, we report the development, implementation, and evaluation of an interdisciplinary chemical biology course in epigenetics between Master’s students from two different disciplines (chemistry and biology), that aims to promote the “authentic big picture” of research and the reality of scientific practice. We have emphasized interdisciplinary collaborative work and created a



---

research experience by the integration of lessons and experiments into a genuine research project, which culminates with both the writing of a scientific article and the defense of a joint research proposal. An overview of the themes taught during the lectures, the material for the discovery-based research lab implementation and the evaluation surveys are available in the Supporting Information. Importantly, this report is intended as a springboard for those who wish to adapt and implement interdisciplinary education in their courses.

## CONTEXT AND MOTIVATION

Our course offers a chemical biology approach to epigenetics. Epigenetics is broadly defined as the study of heritable or possibly-heritable variations in gene expression unrelated to changes in the DNA sequence. Thus, while the genome — the sequence of the DNA — is the blueprint for life, it is ultimately epigenetics that influences cell diversity and strongly controls gene expression. These changes occur by regulation of chromatin<sup>23</sup> via chemical modifications of the DNA and histone proteins (histone language<sup>24,25,26</sup>). Misregulation of epigenetic processes has been linked to many disease areas.<sup>27</sup> Traditionally, this field has been studied just from a purely biological perspective, but now its chemical potential has become evident, and consequently, it has emerged as a bountiful topic for chemical biologists.<sup>28</sup> The fundamental building block of chromatin is the nucleosome. This consists of an approximately 150 base pair (bp) DNA chain wrapped in 1.7 left-handed superhelical turns around a histone protein octamer. Beyond the structural and protective functions of the nucleosome, it also plays a dynamic role in epigenetic regulation.<sup>29</sup> Hence, the nucleosome represents an epigenetic target of great potential. In the last decade, a handful of small molecules have accessed and targeted the nucleosomal DNA successfully.<sup>30,31</sup> Particularly, the sequence-specific DNA binders: pyrrole-imidazole polyamides interact with the nucleosome<sup>32,33</sup> and can control epigenetic processes.<sup>34</sup> Apart of inhibition of DNA methylation<sup>35</sup> which causes major epigenetic changes, polyamide hairpins have been used as nucleosomal clamps<sup>32</sup> connecting two aligned minor grooves. They have further been used as cyanine dye-polyamide conjugates in fluorescence studies, such as Förster Resonance Energy Transfer (FRET) on the nucleosome.<sup>33</sup> Recently polyamides conjugated small-molecules like JQ-1<sup>36</sup> and acetyl lysine mimetics<sup>34</sup> have allowed to recruit epigenetic proteins.

Epigenetics was judiciously chosen as the course topic due to its appeal for both disciplines, and their differing approaches to the subject matter. Additionally, this topic has been under-researched

from both a chemistry and biology educational perspective.<sup>37,38,39</sup> This theme expediently marries our desired to foster reciprocal cross-talk with models that support (and reward) scientists who excel simultaneously in teaching and research.<sup>40</sup> Finally, the approach of DNA targeting with polyamides is applicable to numerous targets other than the nucleosome,<sup>41</sup> and to our knowledge, has never been explored in the context of education, despite its high potential.

## COURSE DESIGN

### Learning Objectives

The course was envisioned to engage students in authentic research environment. Therefore, upon its completion, they will have gained skills in chemical biology (solution / solid phase synthesis; spectroscopy; electrophoresis; PCR and HPLC) and combined their experimental results into a scientific article as well as designed their own research project in epigenetics. Furthermore, the students will gain appreciation for the importance of interdisciplinary research.

### Student population

This course was designed for chemistry and biology Master's students. The participants were all from different educational backgrounds and none participated in interdisciplinary discovery-based research or science communication courses before.

### Implementation

The newly-designed course was instituted at Philipps-Universität Marburg as part of the chemistry and biology curricula with two cohorts during the 2016/2017 and 2017/2018 winter semesters (Table 2).

**Table 2. Cohorts of students during the courses.**

Cohort	ETCS	Total students	m	f	chem	bio	ChemBio experience
2016	9	10	7	3	7	3	6
2017	9	11	3	8	4	7	4

*m = male, f = female, chem = chemistry Master's student, bio = biology Master's student; ECTS = European Credit Transfer System, 1 ECTS equaling 30 study hours; ChemBio experience = students who had participated in an introductory undergraduate chemical biology lecture.*

The shared structure, timeline specifying the face-to-face hours per week, assignment, outcomes, and evaluation of both cohorts are illustrated in Figure 1 and specified in Table S1-S4.

The course comprised three different types of teaching modules: 1) lectures, 2) discovery-based research lab, and 3) a scientific communication workshop, instructed by a lecturer and a teaching

assistant from the chemical biology division. In each week of the lab section and for the proposal, we always try to mix biologists and chemists in a group and formed new groups after each week. It lasted 14 weeks from which, the final 4 weeks were dedicated to the individual writing of the article and preparing the proposal poster in groups.

115

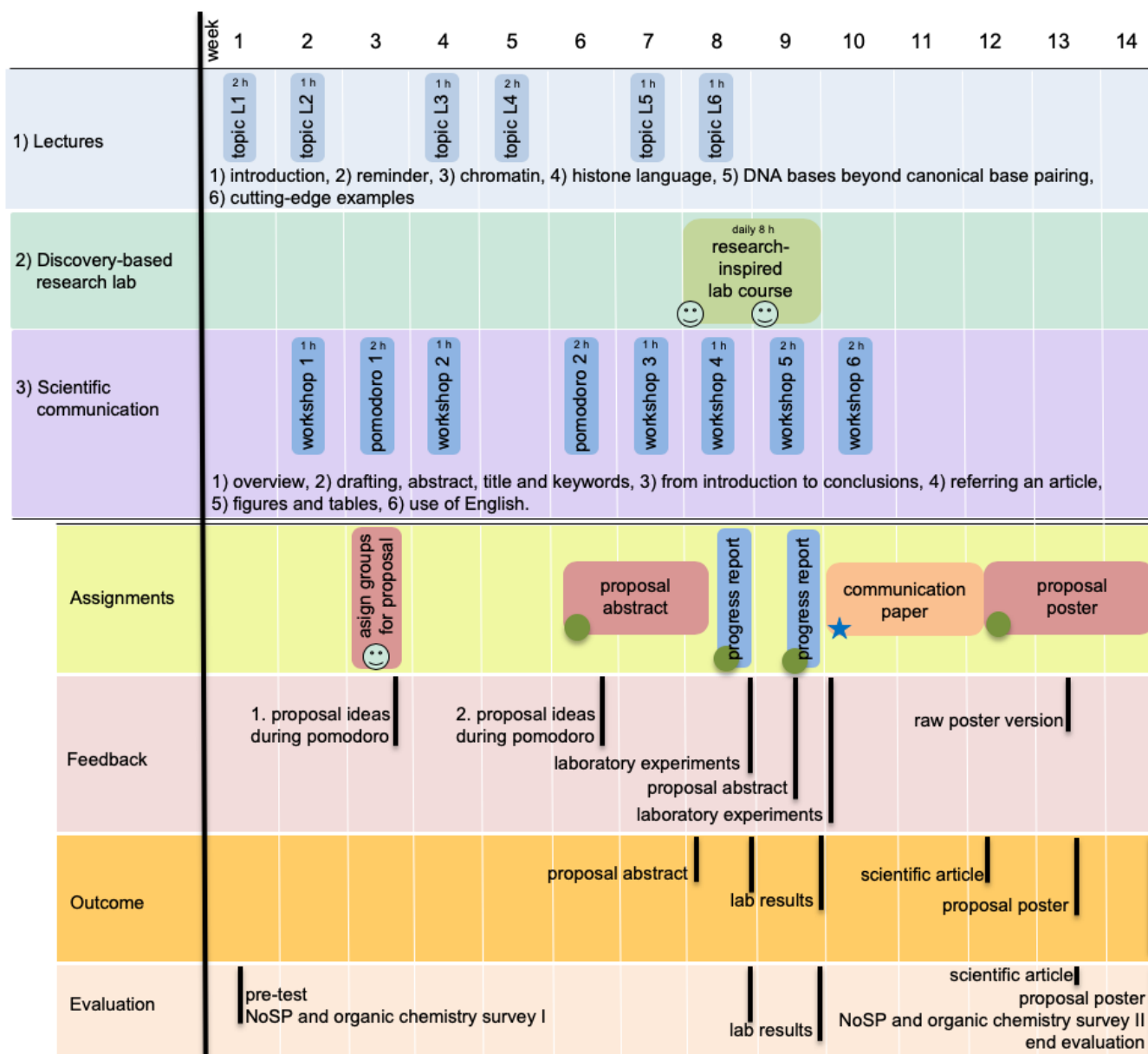


Figure 1. Timeline of the course divided in clusters of 1) lectures; 2) discovery-based research lab, and 3) scientific communication. The detailed topics of the lectures and workshop can be found in Box 1 and Table S2, respectively. In addition, assignments, outcomes and the time points where the students received feedback or were evaluated are included. NoSP = nature of the scientific practice. The smileys represent new group formations, the star indicates an individual assignment and green circles group assignment.

120

Lectures containing integrated technology<sup>37</sup> and supported by active learning pedagogies<sup>42</sup> (10% course time): initially, we started the course with a formative assessment of students' preconceptions in organic chemistry and their perspective of the nature of scientific practice to

125 tailor the lectures accordingly. During these first units, students were exposed to the basics of epigenetics and chemical biology concepts as listed in Box 1 (Fig 2) using a variety of direct interactive teaching resources and peer-instruction activities to maintain cooperation between students and increase team-working skills.

**Box 1. Course material covered during the lectures**

Topics:

L1: *Introduction*

- Chemical biology versus biochemistry
- Genetics versus epigenetics

L2: *Reminder*

- Basic concepts under a chemical biology perspective: resonance, specific biological interactions, tautomerism, PCR, DNA, proteins, nucleophilicity,  $pK_a$ , arrow pushing mechanisms

L3: *Chromatin*

- Chromatin architecture
- Tailored chromatin in the lab

L4: *Histone Language*

- Post-translational modifications
- Readers, writers and erasers

L5: *DNA Bases beyond canonical base pairing*

L6: *Cutting-edge Examples*

- Chemical biology approaches in epigenetics from the literature

130 Figure 2. Box containing the course material covered during the lectures.

*Discovery-based research lab (50% course time):* this research-inspired lab section was organized as a two-week block. Unlike typical laboratory courses, the idea was to explore an authentic research project with a clear overarching goal: “the design, synthesis, and study of pyrrole-imidazole polyamides as potential nucleosome binders” (Fig 3, Table S5). Thus, the first three steps of the Fmoc-building blocks were synthesized and the final pyrrole and imidazole monomers (supplied by the instructors) were then assembled in solid phase synthesis to yield polyamide hairpins. In parallel, nucleosomes were assembled from free DNA and histone octamers

135

by salt gradient dialysis method. The analysis of the DNA and nucleosomal binding properties were performed by fluorescence intercalation displacement (FID), CD measurements and footprinting combined with capillary electrophoresis.

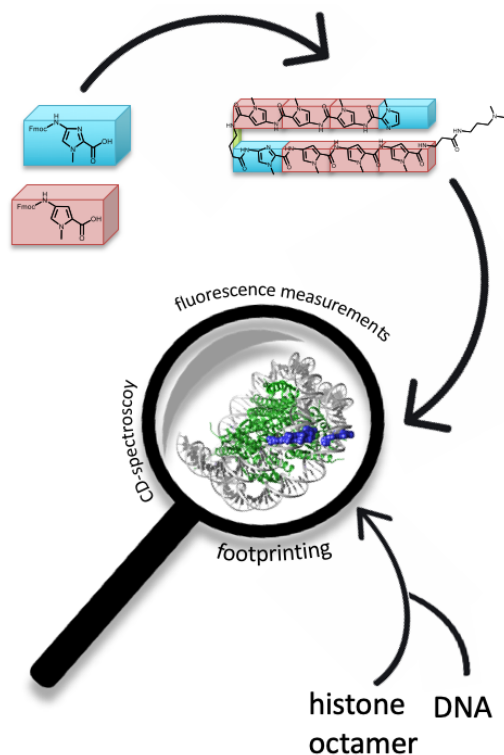


Figure 3. Concept figure of the discovery-based research lab course aiming at the design, synthesis, and study of pyrrole-imidazole polyamides as potential nucleosome binders. For the nucleosome representation pdb 1M18 was used.

145

Conducting a meaningful hands-on research project is central to the achievement of scientific literacy.<sup>43</sup> Thus, the students worked in small groups in the laboratory (biologist/chemist pairs) in a project divided in two major parts per week: 1) material preparation and 2) binding analysis (Fig. 4).

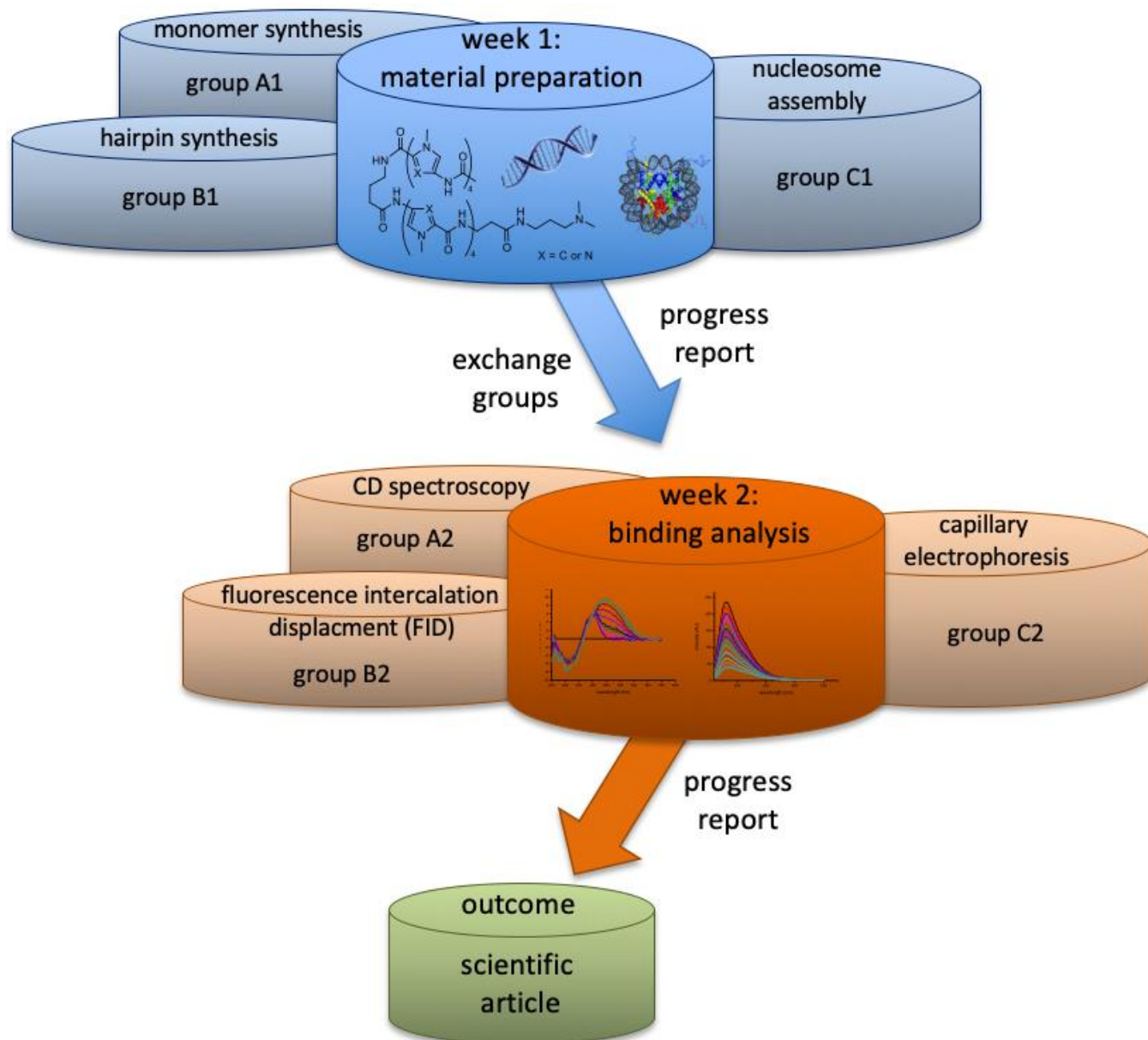


Figure 4. Overview of the research-inspired laboratory module, which is divided in two main sections by week: week 1) material preparation and week 2) binding analysis. The students were divided in three different groups (A1, B1 and C1), which were formed new after one week (A2, B2 and C2). Each student relied on the results of all groups to individually write a scientific article.

150

155 During the first week, group A1 (week 1, group A1; SI) synthesized in solution the first three steps of the building blocks needed for the solid-phase peptide synthesis (SPPS) of the polyamides. Due to time and safety restrictions, the final steps of the monomers were performed by the instructors and provided. Following a literature described synthesis,<sup>44,45</sup> the chemistry students could deepen their knowledge in synthesis by performing, for instance, reactions under inert atmosphere,

160 whereas the biology students gained their first hands-on experience in basic experimental techniques in organic synthesis, including column chromatography purification, extraction, rotary

---

evaporation, etc. Group B1 (week 1, group B1; SI) was in charge of SPPS of the polyamide hairpins.<sup>45</sup> The chemistry and biology students developed two novel polyamide hairpins, which were characterized by high-performance liquid chromatography (HPLC) and electrospray ionization mass spectrometry (ESI-MS). Products were purified by preparative HPLC. The reagents and monomers needed were supplied by the instructors (Table S5; SI). Group C1 (week 1, group C1; SI) was responsible for the preparation of fluorescein (FAM)-labeled DNA by polymerase chain reaction (PCR) and used this to assemble nucleosomes.<sup>46</sup> Progress and purity were controlled by gel electrophoresis. Afterwards, the students reported their results and difficulties in a joint seminar, which simulated the regular progress reports of ongoing investigations in research institutions. In addition, each student was required to keep a lab notebook throughout. During the second week, we altered the composition of the groups, to maximize the student interactions and increase the collaboration experience.<sup>47</sup> All students were introduced to both circular dichroism (CD) and fluorescence intercalation displacement (FID) spectroscopy. Then groups A2 and B2 (week 2, group A2 and B2; SI) analyzed the binding of the synthesized polyamide hairpins to the target DNA sequence with these techniques, while group C2 (week 2, group C2; SI) assisted the instructors to advance in the development of a new method to study sequence-specific DNA binding on nucleosomes<sup>A,48,49</sup> (further details in SI). Finally, all groups from week 2 participated in another progress-report presentation. All data were made available online to aid writing individual scientific articles, instead of using the typical university protocols. Here, it is important to highlight that the results of each individual group were essential to obtain the overall picture of the topic and improve precision in the paper after the laboratory course. Notably, the obtained results were new to both students and instructors. Student's lab course outcomes with examples from individual students, as well as an exemplary scientific article are provided (Fig. 5 and "Example of a Student's Scientific Article", SI)

---

<sup>A</sup> Due to non-published data, the protocol for group C2 is not detailed. Alternative useful references are added in the SI.



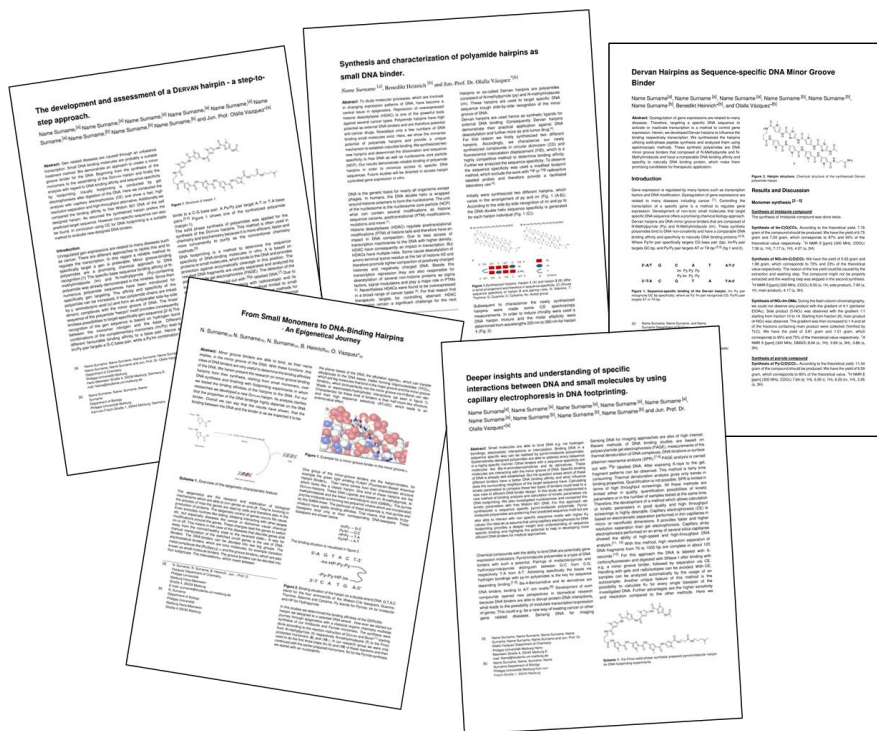


Figure 5. Front pages of exemplary articles written by students of the course (authors copy).

Scientific communication workshop (40% course time): documenting data, publishing research, scientific argumentation, and grant writing standard are authentic practices that researchers are typically engaged in. Throughout this course, the students were exposed to all these different types of scientific communication. Basic notions of scientific writing (Table S2; SI) were introduced in the course to enable the students to identify different communication styles and develop their skills and confidence to write a research article. This learning was conducted as an interactive, practical workshop using epigenetic research papers as guiding frameworks and which led to a scientific article from the discovery-based research lab. Since in both industrial and academic scientific research a permanent day-to-day record of work is established via laboratory notebooks, which are even considered legal documents, we consequently trained the students in best practices to keep complete and accurate laboratory notebooks (Fig. 6)



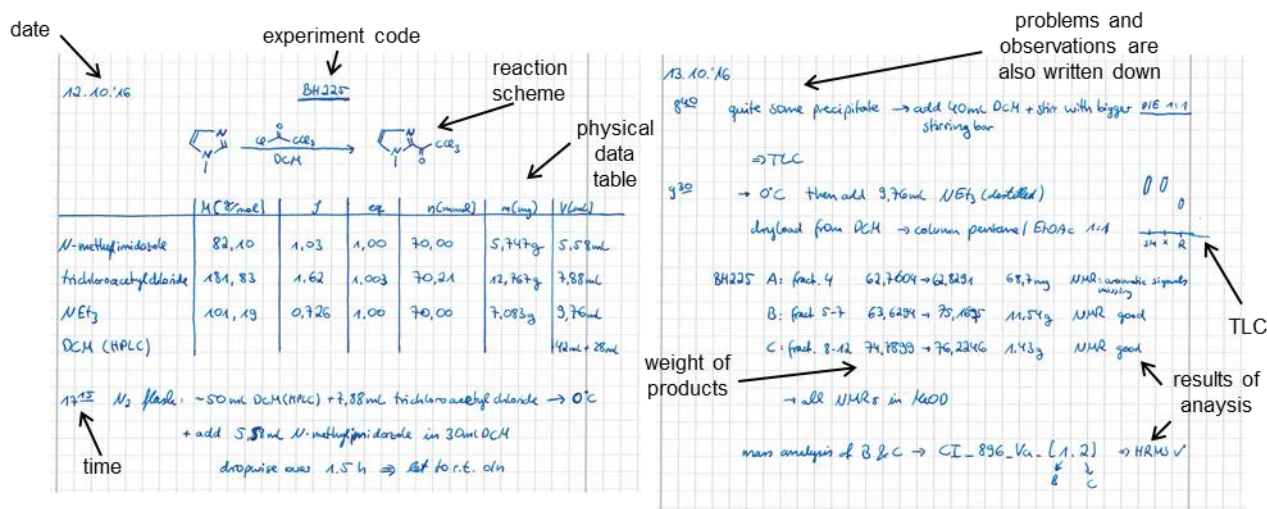


Figure 6. Sample of a laboratory notebook, highlighting the content (authors copy).

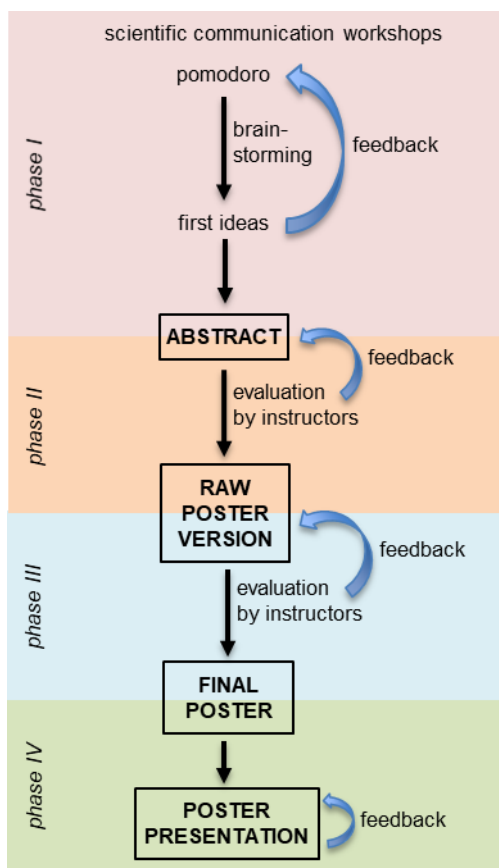
200

205

210

215

The students were divided into small groups of three to four students to design and defend their own research project. To maximize the interactions, groups were altered from the discovery-based research lab task, where possible. Bearing their Master's theses in mind but with total freedom in the specific research direction (so long as it involved epigenetics) the groups developed proposals. During this process they needed to 1) state the general idea they wished to address; 2) narrow the problem down to the specific aspect to solve (literature research); 3) state the idea (hypothesis); 4) design and plan the experiments. Initially, to find the research gap,<sup>50</sup> an interactive session based on the Pomodoro technique<sup>51,52</sup> and under questionnaire guidance ("Questions to start the proposal"; SI) was performed. The Pomodoro technique is a time management technique, where 25 min working sections are strictly interrupted by short five min breaks. The method is based on the idea that regular breaks help to work more efficient and creative. In the beginning, the students compared research interests and started the literature search using standard academic databases such as *Scifinder*, over four intervals of 25 min followed by five min break. We used these five-minute interruptions to brainstorm the findings, providing feedback from both peers and instructors.<sup>53</sup> We strategically introduced two of these sessions (Fig. 7). Despite the students were not familiarized with the technique, they adapted fast and appreciated the outcomes.



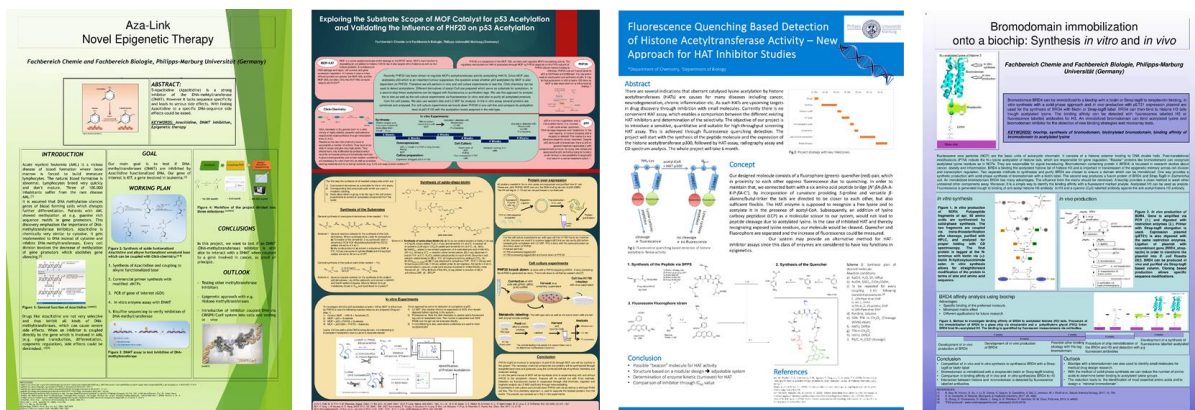
220

Figure 7. Research proposal development workflow for a poster format. Each milestones of the students: abstract, raw poster version, final poster and poster presentation are highlighted. Each of these milestones were evaluated by the instructors, and feedback was provided.

225

Afterwards, each group summarized their initial ideas in an abstract-like draft. This draft underwent several iterative feedback rounds from the instructors, and then served as a basis for a research proposal. At the end of the course, each group presented their results as a poster (Fig. 8; “Poster Template”; SI and “Example of a Student’s Research Proposal Poster”; SI), followed by a short 15-min explanation and a longer discussion (~30 min), where other professors from different disciplines were invited as referees to select the best proposal. This approach gave the groups the opportunity to hear about the projects of the other groups, exchange ideas and defend their own views. This was an excellent way to train and develop student’s oral and written communication skills.

230



235 Figure 8. Example of research proposal posters designed and presented during the course (authors copy).

As part of the course grade, the students submitted an individual scientific article for the research-inspired lab, and an abstract and poster for the joint scientific proposal. Furthermore, they were also assessed on the practical work, and oral presentations during both the progress report  
 240 seminars and poster defense.

#### Instructor's assessment of the student outcomes

To assess the outcomes of the students, different criteria were used. For the laboratory part, reported data from the literature or analytical measures were accessible for the assessment ("Evaluation Criteria for Discovery-based Research Lab"; SI). For the scientific paper and the

245 proposal poster, we used criteria such as the scientific content, structure, language ("Evaluation Criteria for the Scientific Communication"; SI). In addition to the examples of the student's outcomes provided (Fig. 5 and Fig. 8) we include lab course outcomes ("Outcomes of the Discovery-Based Research Lab"; SI) a student's article ("Example of a Student's Scientific Article"; SI), a students' proposal poster ("Example of a Student's Research Proposal Poster"; SI) and the survey  
 250 results ("Nature of Scientific Practice Survey Results"; "Organic Chemistry Survey Results"; SI).

#### FITTING OUR COURSE INTO THE COURSE-BASED RESEARCH EXPERIENCE MODEL (CRE)

The benefits of embedding research experiences into formal laboratory courses has been demonstrated by the implementation of course-based research experiences (CREs) in both undergraduate (CURE)<sup>54</sup> and graduate level.<sup>55</sup> Along these lines, our course fulfills the five  
 255 dimensions of a C(U)RE: science practice, discovery, broader relevance, collaboration, and iteration (Table 1).<sup>56</sup>

**Table 1. Dimensions of a CRE and Connection to our Course.**

<i>Item</i>	<i>CRE dimension</i>	<i>How it is addressed</i>
1	Science practice	Introduction into new topic, open inquiry, collecting and analyzing data, using instruments, reporting results, scientific writing and oral skills (communication, abstract, argumentation, presentation), designing the research proposal.
2	Discovery	Synthesis of new molecules, analysis of properties, finding a research gap
3	Broader relevance	Application in a wider biological context.
4	Collaboration	Joint perspectives and approaches from different disciplines, interdisciplinary answer to research questions and data interpretation, students sharing all data for an individual assignment.
5	Iteration	Repeatedly analysis, different analysis validation methods, similar compound synthesis procedures, several rounds of feedback during the proposal writing.

## EVALUATION OF THE OVERALL COURSE EXPERIENCE

260 According to our assessment criteria and the presented students' outputs (Fig. 5; Fig. 8; "Student's Outcome"; SI) the overall result was positive. Furthermore, to gain a deeper understanding of students' experience in the class, we used a survey with open-ended and Likert scale questions to rate both the overall experience and each teaching module ("Evaluation Results"; SI). All students from both cohorts who volunteered for this study were provided with information  
265 about their rights and the handling of the data beforehand; informed consent was obtained from all participants. IRB (Institutional Review Board) approval is not required for studies in education at German universities, but the recruitment process followed ethical guideline. We ensured that students could opt out at any time during data collection and that their privacy and rights were protected at any time. Students' consent included the use of their data (survey answers, interview  
270 transcripts), including their written work, for research and publication purposes. Interviews were conducted in German and consequently, translated for this publication. Since nothing was

changed between the courses, we combined the evaluations of both cohorts to provide a more realistic impression.

The survey's results showed that the course was evaluated very positively (Fig. 9): 86% of the students rated our new interdisciplinary course as "excellent", "very good", or "good". Notably, no students rated the course as "very poor". A deeper analysis of each separate course module ("Evaluation Results"; SI) revealed an overall positive impression throughout all the sections. Engagement was deemed particularly high: all students rated it as "excellent", "very good" or "good". The lab sessions (76%), the assignments (81%), the communication (86%), the proposal project work (81%), the poster presentation (86%) and the lectures (91%) were also rated highly positive in the three highest categories.

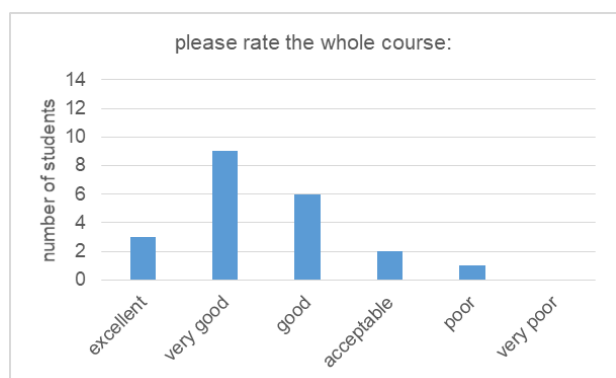


Figure 9. Students' opinions of the whole course.

### 285 Student perception of the course

In addition to the above evaluation of the course, the positive outcomes were further highlighted by answers to open-ended questions ("Evaluation Results"; SI), and post-course interviews with some student volunteers. The students described all sections of the course as having a positive learning effect. Compared to standard courses, our students appreciated the possibility to include their own ideas and felt their effort was valuable. By performing a "real-world project" ("Evaluation Results", 14g; SI) they described feeling like an actual scientist. Furthermore, the focus on collaboration served as a basis for a productive and friendly working environment. Many students highlighted the interaction with students from a different discipline, especially during the research proposal. The "power of interdisciplinary" ("Evaluation Results", 12b; SI) and the synergistical integration of biology and chemistry was found to be valuable for future scientific approaches. This overall positive impression of interdisciplinary work was, additionally highlighted

---

in the three post interviews that we conducted with three students from the 2016 cohort. In particular, the students emphasized the positive and open culture between students and instructors. Even the biology students, who were sometimes felt overwhelmed by synthesis during the lab section, experienced an open-minded collaborative group work that helped them to become confident in their skills, as shown in the following explanation of a biology student, talking about her most valuable moment of the course:

305 *“Organic synthesis is a bit dirtier than normal synthesis (laughs). I was not prepared for this. I thought it might be easier for me to adapt to this situation, because lab is lab, but it wasn’t like that. (pause) But the good thing was that I had a chemist in my group and I was just asking him a lot of questions [...] at the end, the last few days, I could do it on my own. When I was unsure, I could always ask [...] That was different to what I was used to. But now I know that in the future, I could do a synthesis, and if I have problems, I can just ask somebody who knows it better (laughs).”*

This collaborative interdisciplinary aspect and the value of having biologists and chemists together in a group became apparent when in students’ open-ended answer in the survey, when they described their process of collecting ideas and writing their proposal. The students valued learning about the structure of scientific publications, the use of keywords, and the methodology to present their work. Some of them stated that the course improved their self-confidence (“Evaluation Results”, 13; SI). Time management was mentioned by some of the students as the most 315 challenging part of the course. Importantly, this was not negatively evaluated. On the contrary, students realized the importance of the cooperative work (“Evaluation Results”, 11g, 16i+k; SI) and that the course assignments resemble the real-world research (“Evaluation results”, 11g, 14g; SI). This process of exchanging ideas and using what is most suitable for the scientific publications is further highlighted in one of the interviews by a biology student who struggled slightly in the lab, but 320 could provide her insight into biological processes during the proposal writing process. The quote illustrates how each discipline contributed their perspective and knowledge to approach the problem solution:

One biology student:

325 *“Beside the lab, I think when we did the poster I could use my biology background, because we picked a rather biological topic and I had more to contribute. Basically, I had the most ideas at the beginning; I mean we started with an idea and so this was biological. And then we searched how we*

---

*can use chemical methods, at least in, to combine it. So, we had a synthesis and overexpression and protein...something, we used a method to analyze the proteins chemically. And so, this helped a lot. I had no idea about the analytical methods, but I knew better how proteins may behave and what would*

330 *work or not.”*

These examples, survey results and personal experiences expressed in the interview, during the course underpins the overall good impression that the structure and design of the course was well-received by the students.

### **PRACTICAL ADVICE FOR FUTURE INSTRUCTORS: CHALLENGES AND BENEFITS**

335 A primary challenge is the time commitment required from the students and the organization of the integrated lab sections. On the one hand, traditional lectures and laboratory courses might seem to require less effort. On the other hand, in the traditional learning the research output is always the same. Our course design, however, advanced our own research and increased our visibility in our own and in a different department. From a student's perspective, the course enables experience and

340 learning of genuine science, allows visualizing the advantages of collaborative work, and promotes innovative and critical thinking, which will not only be advantageous during their studies but also in later life. Our interdisciplinary approach allows learners to tackle broad scope research questions, which are not solvable by one discipline alone. Students finishing the course can bring a new collaborative spirit into the conservative university system to lower the barriers to interdisciplinary

345 collaborations. We envision that the whole concept of the course could be adapted for several interdisciplinary fields as long as the discovery-based research lab is planned in stages. For instance, we foresee feasible adaptability in fields like material science and nanotechnology in which physicists and chemists could learn together or in biophysics for biologists and mathematicians or neuroscience for chemists and biologists, or drug discovery for chemists and medicine students, etc.

350 A challenge from an instructor's perspective is the difference in prior knowledge. In an interdisciplinary course, each group of students should be able to equally contribute their knowledge to the overall objective, e.g. during the lab section or in the lecture. We tried to involve and support all students by teaching highly interdisciplinary topics in the lectures, covering basic concepts of both disciplines. In our case, we believe that we succeeded at managing the issue of differing student

355 backgrounds because they did not report feeling outperformed by students of the other disciplines. The reason may be that we carefully mixed biology and chemistry students together and regularly



---

changed the groupings to stimulate idea exchange and support from each discipline. This consequently strengthened the collaborative aspect.

Sine we were aware that the number of new methods and tasks were challenging, we envisioned  
360 a small-group course with two fully committed instructors from the chemical biology division. As an anecdotic point, in the first cohort we were also considering to leave the research project proposal to give more time for the communication. We discussed it with the students but gratifyingly for us, the students were the ones who asked us for doing the research proposal too. The overall design and the implementation of this course in a teaching lab would allow a scale up of this course for larger cohorts  
365 if the number of methods and required equipment would be reduced. Although further planning and organization beforehand will be necessary, the research-inspired lab might especially profit from larger and mixed cohorts, enabling broader topics and a more screening-oriented approach.

## **CONCLUSION**

This course brings the framework of real-world research into a chemical biology course with a  
370 focus on epigenetics. This interdisciplinary experience for biology and chemistry Master's students combines a discovery-based research lab course with scientific communication. Although the time investments of students and instructors are relatively high, our output outcompetes traditional lecture courses, which was demonstrated by the student's outcomes, surveys and the positive perspective described in course evaluations. Furthermore, a high proportion of group work promoted  
375 collaborative approaches during the course.

In conclusion, with the growing need for interdisciplinary approaches across scientific research, our presented course design can easily be applied to many different fields of science, to empower more students to confront the complex societal problems with innovative and collaborative ideas. Future approaches will target the long-term impact of these practices, the interdisciplinary  
380 experience and the involvement in collaborative work.

## **ASSOCIATED CONTENT**

### **Supporting Information**

The Supporting Information containing the organizational material (course timetables and topic  
description, list of reagents used, hazards, questions to start the proposal, poster template, criteria  
385 for assessments and experimental procedures) student's outcomes, and survey's results is available on the ACS Publications website at DOI: 10.1021/acs.jchemed.



---

## AUTHOR INFORMATION

Corresponding Author

\*E-mail: olalla.vazquez@staff.uni-marburg.de

## 390 ACKNOWLEDGMENTS

We would like to thank the students of the course; Robert Giessmann for introducing us and the students into the Pomodoro technique; Dr. Fabienne Quennet for giving us deeper insights into the world of English writing during the course; Lisa-Marie Koch and Dr. Cornelia Brendel (UKGM) for measuring the capillary electrophoresis samples. We gratefully acknowledge Prof. Dr. Rory  
395 Waterman (University of Vermont) and Prof. Dr. Andrew Feig (Wayne State Chemistry) for their constructive feedback of the manuscript. This work was financially supported by the Fulbright Commission (Fulbright-Cottrell Award 2016, to O.V.).

## REFERENCES

---

1. Charkoudian, L. K.; Sampson, N. S.; Kumar, K.; Kritzer, J. A. Designing convergent chemistry curricula. *Nat. Chem. Biol.* **2016**, *12*, 6, 382-386.
2. Feig, A. L. Challenge your teaching. *Nat. Struct. Mol. Biol.* **2004**, *11*, 16-19.
3. Vogel Taylor, E. M.; Mitchell, R.; Drennan, C. L. Creating an Interdisciplinary Introductory Chemistry Course *without* Time-Intensive Curriculum Changes. *ACS Chem. Biol.* **2009**, *4*, 12, 979-982.
4. McGill, T. L.; Williams, L. C.; Mulford, D. R.; Blakey, S. B.; Harris, R. J.; Kindt, J. T.; Lynn, D. G.; Marsteller, P. A.; McDonald F. E.; Powell, N. L. Chemistry Unbound: Designing a New Four-Year Undergraduate Curriculum. *J. Chem. Educ.* **2019**, *96*, 1, 35-46.
5. Madden, M. E.; Baxter, M.; Beauchamp, H.; Bouchard, K.; Habermas, D.; Huff, M.; Ladd, B.; Pearson, J.; Plague, G. Rethinking STEM Education: An Interdisciplinary STEAM Curriculum. *Procedia Comput. Sci.* **2013**, *20*, 541-546.
6. Tripp, B.; Shortlidge, E. E. A Framework to Guide Undergraduate Education in Interdisciplinary Science. *CBE Life Sci. Educ.* **2019**, *18*, 3, 1-12.
7. Ledford, H. How to solve the world's biggest problems. *Nature* **2015**, *525*, 7569, 308-311.
8. Fischman, J. Arizona's big bet: The research rethink. *Nature* **2014**, *514*, 7522, 292-294.
9. Smith, M. R.; McAllister, R.; Newkirk, K.; Basing, A.; Wang, L. Development of an Interdisciplinary Experimental Series for the Laboratory Courses of Cell and Molecular Biology and Advance Inorganic Chemistry. *J. Chem. Educ.* **2012**, *89*, 1, 150-155.
10. Hormann, J.; Streller, S.; Kulak, N. Synthesis and Evaluation of Artificial DNA Scissors: An Interdisciplinary Undergraduate Experiment. *J. Chem. Educ.* **2018**, *95*, 10, 1848-1855.

- 
11. Felton, D. E.; Ederer, M.; Steffens, T.; Hartzell, P. L.; Waynant, K. V. UV-Vis Spectrophotometric Analysis and Quantification of Glyphosate for an Interdisciplinary Undergraduate Laboratory. *J. Chem. Educ.* **2018**, *95*, 1, 136-140.
  12. Bazley, I. J.; Erie, E. A.; Feiereisel, G. M.; LeWarne, C. J.; Peterson, J. M.; Sandquist, K. L.; Oshin, K. D.; Zeller, M. X-ray Crystallography Analysis of Complexes Synthesized with Tris(2-pyridylmethyl)amine: A Laboratory Experiment for Undergraduate Students Integrating Interdisciplinary Concepts and Techniques. *J. Chem. Educ.* **2018**, *95*, 5, 876-881.
  13. Cresswell, S. L.; Loughlin, W. A. A Case-Based Scenario with Interdisciplinary Guided-Inquiry in Chemistry and Biology: Experiences of First Year Forensic Science Students. *J. Chem. Educ.* **2017**, *94*, 8, 1074-1082.
  14. Hooker, P. D.; Deutschmann, W. A.; Avery, B. J. The Biology and Chemistry of Brewing: An Interdisciplinary Course. *J. Chem. Educ.* **2014**, *91*, 3, 336-339.
  15. Dillner, D. K.; Ferrante, R. F.; Fitzgerald, J. P.; Schroeder, M. J. Integrated Laboratories: Laying the Foundation for Undergraduate Research Experiences. *J. Chem. Educ.* **2011**, *88*, 12, 1623-1629.
  16. Reid, N.; Shah, I. The role of laboratory work in university chemistry. *Chem. Educ. Res. Pract.* **2007**, *8*, 172-185.
  17. Hofstein, A.; Mamlok-Naaman, R. The laboratory in science education: the state of the art. *Chem. Educ. Res. Pract.* **2007**, *8*, 2, 105-107.
  18. Ebenezer, J. V. Making chemistry learning more meaningful. *J. Chem. Educ.* **1992**, *69*, 6, 464.
  19. Altmann K. H.; Buchner, J.; Kessler, H.; Diederich, F.; Kräutler, B.; Lippard, S.; Liskamp, R.; Müller, K.; Nolan, E. M.; Samori, B.; Schneider, G.; Schreiber, S. L.; Schwalbe, H.; Toniolo, C.; van Boeckel, C. A. A.; Waldmann, H.; Walsh, C. T. The State of the Art of Chemical Biology. *ChemBioChem.* **2009**, *10*, 1, 16-29.
  20. Kritzer, J. A. When Undergraduates Ask “Why”, Chemical Biology Answers. *ACS Chem. Biol.* **2006**, *1*, 7, 411-413.
  21. Godwin, H. A.; Davis, B. L. Teaching undergraduates at the interface of chemistry and biology: challenges and opportunities. *Nat. Chem. Biol.* **2005**, *1*, 176-179.
  22. Back to school. *Nat. Chem. Biol.* **2005**, *1*, 4, 175.
  23. He, C.; Cole, P. Introduction: Epigenetics. *Chem. Rev.* **2015**, *115*, 6, 2223-2224.
  24. Strahl, B. D.; Allis C. D. The language of covalent histone modifications. *Nature* **2000**, *403*, 6765, 41-45.
  25. Soshnev, A. A.; Josefowicz, S. Z.; Allis, C. D. Greater Than the Sum of Parts: Complexity of the Dynamic Epigenome. *Mol. Cell* **2016**, *62*, 5, 681-694.
  26. Lee, J.-S.; Smith, E.; Shilatifard, A. The Language of Histone Crosstalk. *Cell* **2010**, *142*, 5, 682-685.

- 
27. Chi, P.; Allis, C. D.; Wang, G. G. Covalent histone modifications—miswritten, misinterpreted and mis-erased in human cancers. *Nat. Rev. Cancer* **2010**, *10*, 7, 457-469.
  28. Allis, C. D.; Muir, T. W. Spreading Chromatin into Chemical Biology. *ChemBioChem* **2011**, *12*, 264-279.
  29. Voigt, P.; Reinberg, D. Histone Tails: Ideal Motifs for Probing Epigenetics through Chemical Biology Approaches. *ChemBioChem* **2011**, *12*, 236-252.
  30. Trzuppek, J. D.; Gottesfield, J. M.; Boger, D. L. Alkylation of duplex DNA in nucleosome core particles by duocarmycin SA and yatakemycin. *Nat. Chem. Biol.* **2006**, *2*, 79-82.
  31. Chua, E. Y.; Davey, G. E.; Chin, C. F.; Dröge, P.; Ang, W. H.; Davey, C. A. Stereochemical control of nucleosome targeting by platinum-intercalator antitumor agents. *Nucleic Acids Res.* **2015**, *43*, 11, 5284-5296.
  32. Edayathumangalam, R. S.; Weyermann, P.; Gottesfield, J. M.; Dervan, P. B.; Luger, K. Molecular recognition of the nucleosomal “super groove”. *Proc. Natl. Acad. Sci. U. S. A.* **2004**, *101*, 18, 6864-6869.
  33. Han, Y.-W.; Tsunaka, Y.; Yokota, H.; Matsumoto, T.; Kashiwazaki, G.; Morinaga, H.; Hashiya, K.; Bando, T.; Sugiyama, H.; Harada, Y. Construction and characterization of Cy3- or Cy5-conjugated hairpin pyrrole-imidazole polyamides binding to DNA in the nucleosome. *Biomater. Sci.* **2014**, *2*, 297-307.
  34. Taniguchi, J.; Feng, Y.; Pandian, G. N.; Hashiya, F.; Hidaka, T.; Hashiya, K.; Park, S.; Bando, T.; Ito, S.; Sugiyama, H. Biomimetic Artificial Epigenetic Code for Targeted Acetylation of Histones. *J. Am. Chem. Soc.* **2018**, *140*, 23, 7108-7115.
  35. Shinohara, K.; Yoda, N.; Takane, K.; Watanabe, T.; Fukuyo, M.; Fujiwara, K.; Kita, K.; Nagase, H.; Nemoto, T.; Kaneda, A. Inhibition of DNA Methylation at the *MLH1* Promoter Region Using Pyrrole-Imidazole Polyamide. *ACS Omega* **2016**, *1*, 6, 1164-1172.
  36. Erwin, G. S.; Grieshop, M. P.; Ali, A.; Qi, J.; Lawlor, M.; Kumar, D.; Ahmad, I.; McNally, A.; Teider, N.; Worringer, K.; Sivasankaran, R.; Syed, D. N. Eguchi, A.; Ashraf, M.; Jefferey, J.; Xu, M.; Park, P. M. C.; Mukhtar, H.; Srivastava, A. K.; Faruq, M.; Bradner, J. E.; Ansari, A. Z. Synthetic transcription elongation factors license transcription across repressive chromatin. *Science*
  37. Stark, L. A. Epigenetics Online: Multimedia Teaching Resources. *CBE Life Sci. Educ.* **2010**, *9*, 1, 6-9.
  38. Drets-Esser, D.; Bass, K. M.; Stark, L. A. Using Small-Scale Randomized Controlled Trials to Evaluate the Efficacy of New Curricular Materials. *CBE Life Sci. Educ.* **2014**, *13*, 4, 593-601.
  39. Reinagel, A.; Speth, E. B. Beyond the Central Dogma: Model-Based Learning of How Genes Determine Phenotypes. *CBE Life Sci. Educ.* **2016**, *15*, 1, 1-13.
  40. Bradforth, S. E.; Miller, E. R.; Dichtel, W. R.; Leibovich, A. K.; Feig, A. L.; Martin, J. D.; Bjorkman, K. S.; Schultz, Z. D.; Smith, T. L. University learning : Improve undergraduate science education. *Nature* **2015**, *523*, 7560, 282-284.

- 
41. Dervan, P. B.; Bürli, R. W. Sequence-specific DNA recognition by polyamides. *Curr. Opin. Chem. Biol.* **1993**, 3, 6, 688-693.
  42. Armbruster, P.; Patel, M.; Johnson, E.; Weiss, M. Active Learning and Student-centered Pedagogy Improve Student Attitudes and Performance in Introductory Biology. *CBE Life Sci. Educ.* **2009**, 8, 3, 203-213.
  43. National Research Council. *National Science Education Standards*. The National Academies Press: Washington, DC, 1996.
  44. Baird, E. E.; Dervan, P. B. Solid Phase Synthesis of Polyamides Containing Imidazole and Pyrrole Amino Acids. *J. Am. Chem. Soc.* **1996**, 118, 6141-6146.
  45. Wurtz, N. R.; Turner, J. M.; Baird, E. E.; Dervan, P. B. Fmoc Solid Phase Synthesis of Polyamides Containing Pyrrole and Imidazole Amino Acids. *Org. Lett.* **2001**, 3, 8, 1201-1203.
  46. Heinrich, B.; Bouazoune, K.; Wojcik, M.; Bakowsky, U.; Vázquez, O. *ortho*-Fluoroazobenzene derivatives as DNA intercalators for photocontrol of DNA and nucleosome binding by visible light. *Org. Biol. Chem.* **2019**, 17, 1827-1833.
  47. Doymus, K.; Teaching Chemical Equilibrium with the Jigsaw Technique. *Res. Sci. Educ.* **2008**, 38, 2, 249-260.
  48. Heinrich, B.; Bouazoune, K.; Wojcik, M.; Bakowsky, U.; Vázquez, O. *ortho*-Fluoroazobenzene derivatives as DNA intercalators for photocontrol of DNA and nucleosome binding by visible light. *Org. Biol. Chem.* **2019**, 17, 1827-1833.
  49. Zou, T.; Kizaki, S.; Sugiyama, H. Investigating Nucleosome Accessibility for MNase, Fe<sup>II</sup> Peplomycin, and Duocarmycin B<sub>2</sub> by Using Capillary Electrophoresis. *ChemBioChem* **2018**, 19, 664-668.
  50. Robinson, K. A.; Akinyede, O.; Dutta, T.; Sawin, V. I.; Li, T.; Spencer, M. R.; Turkelson, C. M.; Weston, C. *Framework for Determining Research Gaps During Systematic Review: Evaluation [Internet]*. Agency for Healthcare Research and Quality (US): Rockville, 2013.
  51. Cirillo, F. *The Pomodoro Technique: The Acclaimed Time-Management System That Has Transformed How We Work*. Penguin Random House LLC: New York, 2006; p. 149.
  52. Chemjobber. Chemjobber shares his tips on overcoming procrastination. *Chem. Eng. News* **2018**, 96, 3, 21.
  53. Harrington, K. Harness the power of groups to beat the 'PhD blues'. *Nature* **2018**, 559, 7712, 143-144.
  54. *Expanding the CURE Model: Course-Based Undergraduate Research Experience*; Waterman, R., Heemstra, J., Eds.; Research Corporation for Science Advancement: Tucson, 2018.
  55. Cooper, K. M.; Brownell, S. E. Developing Course-Based Research Experiences in Discipline-Based Education Research: Lessons Learned and Recommendations. *J. Microbiol. Biol. Educ.* **2018**, 19, 2, 1-6.
  56. Auchincloss, L. C.; Laursen, S. L.; Branchaw, J. L.; Eagan, K.; Graham, M.; Hanauer, D. I.; Lawrie, G.; McLinn, C. M.; Pelaez, N.; Rowland, S.; Towns, M.; Trautmann, N. M.; Varma-

---

Nelson, P.; Weston, T. J.; Dolan, E. L. Assessment of Course-Based Undergraduate Research Experiences: A Meeting Report. *CBE-Life Sciences Education* **2014**, *13*, 29-40.

## **Spicing up an Interdisciplinary Chemical Biology Course with the Authentic Big Picture of Epigenetic Research**

5 Benedikt Heinrich,<sup>†</sup> Nicole Graulich,<sup>‡</sup> and Olalla Vázquez\*,<sup>†</sup>

<sup>†</sup> Department of Chemistry, Philipps-University Marburg, Hans-Meerwein-Straße 4, 35043, Marburg, Germany.

<sup>‡</sup> Institute of Chemistry Education, Justus-Liebig University, Heinrich-Buff-Ring 17, 35392 Gießen, Germany.

10

---

## TABLE OF CONTENT

15	<b>Abbreviations.....</b>	<b>254</b>
	<b>Course Timetables and Topic Descriptions .....</b>	<b>255</b>
	<b>Discovery-Based Research Lab Design .....</b>	<b>256</b>
	<b>List of Reagents.....</b>	<b>258</b>
	<b>Hazards .....</b>	<b>259</b>
20	<b>Primer Sequences and DNA Preparation.....</b>	<b>259</b>
	<b>Experimental Description for each Group .....</b>	<b>260</b>
	<i>Week 1, group A1 – Pyrrole (Py) and imidazole (Im) monomer synthesis: .....</i>	<i>260</i>
	<i>Week 1, group B1 - Polyamide Hairpin Synthesis: .....</i>	<i>263</i>
	<i>Week 1, group C1 - Nucleosome Assembly:.....</i>	<i>267</i>
25	<i>Week 2, group A2 - Analysis of the New DNA Binder by Circular Dichroism (CD): .....</i>	<i>270</i>
	<i>Week 2, group B2 - Analysis of the New DNA Binder by Fluorescence Intercalation     Displacement (FID): .....</i>	<i>272</i>
	<i>Week 2, group C2 - Analysis of the New DNA binder by Footprinting Combined with     Capillary Electrophoresis (CE): .....</i>	<i>273</i>
30	<b>Questions to Start the Proposal .....</b>	<b>274</b>
	<b>Poster Template .....</b>	<b>275</b>
	<b>Evaluation Criteria for Discovery-Based Research Lab .....</b>	<b>276</b>
	<b>Evaluation Criteria for the Scientific Communication.....</b>	<b>278</b>
	<b>Student's Outcome .....</b>	<b>279</b>
35	<i>Outcomes of the Discovery-Based Research Lab.....</i>	<i>279</i>
	<i>Example of a Student's Scientific Article .....</i>	<i>284</i>
	<i>Example of a Student's Research Proposal Poster.....</i>	<i>288</i>
	<b>Evaluation Results.....</b>	<b>289</b>
	<b>Nature of Scientific Practice Survey Results.....</b>	<b>297</b>
40	<b>Organic Chemistry Survey Results .....</b>	<b>299</b>
	<b>References.....</b>	<b>302</b>

---

## ABBREVIATIONS

APS	ammoniumperoxodisulfate
bp	base pair
CD	circular dichroism
CE	capillary electrophoresis
ddH <sub>2</sub> O	double distilled water
dNTP	nucleoside triphosphate
EDTA	ethylenediaminetetraacetic acid
FAM	fluorescein
FID	fluorescence intercalation displacement
Fmoc	fluorenylmethoxycarbonyl
HATU	[4,5-b]pyridinium 3-oxid hexafluorophosphate
HF	high fidelity
ICD	induced circular dichroism
Im	imidazole
K <sub>D</sub>	binding constant
NoSP	nature of scientific writing
OD	optical density
PAGE	polyacrylamide gel electrophoresis
PCR	polymerase chain reaction
Py	pyrrole
RP-HPLC	reverse phase high performance liquid chromatography
SDB	salt dialysis buffer
SPPS	solid phase peptide synthesis
TBE	Tris-Borate-EDTA buffer
TEMED	tetramethylethylenediamine
test cl.	test cleavage
TO	thiazole orange
W601	Widom 601 DNA



## COURSE TIMETABLES AND TOPIC DESCRIPTIONS

The timetables show the plan of the whole course (Table S1) and the specific topics covered during the scientific communication workshop (Table S2). The lecture topics are shown in the manuscript in Box 1 (Figure 2).

50 **Table S1.** General course timetable.

<i>time</i>	<i>duration</i>	<i>event</i>	<i>description</i>	<i>assignment(s) (outcome/observation)</i>
week -10	1h	information meeting	basic description of the course to interested master students from chemistry and biology	
week -3		sign up deadline	students had to sign up for the course	signing in
week 1	2h	lecture 1	topic L1	
week 2	2h	lecture 2, workshop 1	topic L2, topic W1	
week 3	2h	Pomodoro 1	group formation for research proposal, rounds of brainstorming and group feedback I	brainstorming and topic idea finding in groups
week 4	2h	lecture 3, workshop 2	topic L3, topic W2	
week 5	2h	lecture 4	topic L4	
week 6	2h	Pomodoro 2	rounds of brainstorming and group feedback II	group work on proposal abstract
week 7	2h	lecture 5, workshop 3	topic L5, topic W3	
week 8	full days	lab course week 1	introduction, security introduction, lab exercises (see extra lab course plan)	hand in proposal abstract
week 9	2h	lecture 6, workshop 4	topic L6, topic W4	
	full days	lab course week 2	lab exercises (see extra lab course plan)	
	2h	workshop 5	topic W5	
	1h	scientific writing	students received group feedback about submitted proposal abstract	
week 10	2h	workshop 6	topic W6 by an Scientific English expert	
week 10	flexible	scientific writing	communication	individual writing of communication
week 11	flexible	scientific writing	communication	individual writing of communication
week 12	flexible	scientific writing	poster of proposal	hand in communication, group design of poster about proposal
week 13	flexible	scientific writing	poster of proposal, group feedback on draft poster version	hand in draft of the poster version, group work on final poster about proposal
week 14	2h	final presentation	poster presentation and individual feedback by external referees	group poster presentation
	flexible	feedback	feedback of the communication	

55 **Table S2.** Course material covered during the scientific communication workshops.

<i>topic</i>	<i>topic description</i>
topic W1	Overview: types of scientific writing; structure; writing elements by analyzing articles
topic W2	Drafting: importance of the outline; practical exercises abstract, title and keywords; practical exercises
topic W3	From introduction to conclusions
topic W4	Referring an article and in-class writing exercises
topic W5	Effective use of figures and tables
topic W6	Use of English by a Scientific English expert

### DISCOVERY-BASED RESEARCH LAB DESIGN

Tables S3 and S4 summarize a detailed plan for each day of the discovery-based research lab. Table S5 shows the parameters, which were on the research question and experimental techniques to answer them.

60

**Table S3.** Plan of the first week for the discovery-based research lab.

<i>group</i>	<i>Monday</i>	<i>Tuesday</i>	<i>Wednesday</i>	<i>Thursday</i>	<i>Friday</i>
A1: monomer	get glassware, start acetylation of Py + Im	purify acetylation of Py + Im start nitration of Py + Im	purify nitration of Py + Im start esterification of Py + Im	purify esterification of Py	purify esterification of Im
B1: hairpin	get glassware, learn SPPS start hairpin synthesis	continue hairpin synthesis, test cleavage	analyze test cl. continue hairpin synthesis, test cleavage	analyze test cl. continue hairpin synthesis, test cleavage	analyze test cl. final cleavage and purification
C1: nucleosome	get glassware , prepare buffers	PCR W601, gel for purity	start nucleosome test assembly	check nucleosome purity, nucleosome big scale assembly	check nucleosome purity

65

**Table S4.** Plan of the second week for discovery-based research lab.

<i>group</i>	<i>Monday</i>	<i>Tuesday</i>	<i>Wednesday</i>	<i>Thursday</i>	<i>Friday</i>
A2: analysis of hairpins by CD	presentation meeting 1 finish rest of 1. week introduction in all new devices	CD measurement	CD measurement	analysis of data	presentation meeting 2 finish rest, clean all give glassware back
B2: analysis of hairpins by FID	presentation meeting 1 finish rest of 1. week introduction in all new devices	fluorescence displacement measurement	fluorescence displacement measurement	analysis of data	presentation meeting 2 finish rest, clean all give glassware back
C2: analysis of sequence specific nucleosome binding (footprinting)	presentation meeting 1 finish rest of 1. week introduction in all new devices	prepare sample	CE measurement	analysis of data	presentation meeting 2 finish rest, clean all give glassware back

**Table S5.** Parameters, which were on the research question and experimental techniques to answer them.

<i>Parameter (research question)</i>	<i>Experimental technique (answer)</i>
Binding affinity to free DNA	CD spectroscopy (induced circular dichroism) fluorescence spectroscopy (fluorescence intercalation displacement) capillary electrophoresis
Binding affinity to nucleosomes	capillary electrophoresis

## LIST OF REAGENTS

Table S6 summarizes the used reagents, including its corresponding CAS-number and the used supplier. For non-commercial reagents, procedures and references for preparations are given.

**Table S6.** List of used reagents including their CAS-number and the used supplier.

<i>Chemical</i>	<i>CAS-number</i>	<i>supplier</i>
trichloroacetyl chloride	76-02-8	Sigma Aldrich (USA)
N-methylpyrrole	96-54-8	Acros Organics (Belgium)
potassium carbonate	584-08-7	Carl Roth (Germany)
magnesium sulfate anhydrous	7487-88-9	Carl Roth (Germany)
acetic anhydride	108-24-7	Carl Roth (Germany)
conc. Nitric acid	7697-37-2	Merck (Germany)
sodium carbonate	497-19-8	Carl Roth (Germany)
sodium chloride	7647-14-5	VWR (USA)
4-dimethylaminopyridine (DMAP)	1122-58-3	Fluka (USA)
N-methylimidazole	616-47-7	Sigma Aldrich (USA)
triethylamine	121-44-8	VWR (USA)
sodium hydrogen carbonate	144-55-8	Carl Roth (Germany)
dimethylformamid (DMF)	68-12-2	Iris Biotech (Germany)
N-methyl-2-pyrrolidone (NMP)	872-50-4	Iris Biotech (Germany)
N,N-diisopropylethylamine (DIPEA)	7087-68-5	Carl Roth (Germany)
1-[Bis(dimethylamino)methylene]-1H-1,2,3-triazolo- [4,5-b]pyridinium 3-oxid hexafluorophosphate (HATU)	148893-10-1	Iris Biotech (Germany)
Rink amide (RAM) MBHA-resin	431041-83-7	Fluorochem (UK)
Fmoc-βAla-OH	35737-10-1	TCI (Japan)
Fmoc-γ-OH	116821-47-7	Iris Biotech (Germany)
piperidine	110-89-4	Iris Biotech (Germany)
pyridine	110-86-1	VWR (USA)
DMSO biomolecular grade	67-68-5	Sigma Aldrich (USA)
triisopropylsilane (TIS)	6485-79-6	Sigma Aldrich (USA)
trifluoroacetic acid (TFA)	76-05-1	abcr (Germany)
5XHF buffer	-	New England Biolabs (USA)
dNTPs	-	Invitrogen (USA)
primers	-	Sigma Aldrich (USA)
phusion polymerase	-	New England Biolabs (USA)
40% 19:1 acrylamide : bisacrylamide	-	Carl Roth (Germany)
tetramethylethylenediamine (TEMED)	110-18-9	Carl Roth (Germany)
ammoniumperoxodisulfate (APS)	7727-54-0	Carl Roth (Germany)
tris(hydroxymethyl)aminomethane (Tris)	77-86-1	Carl Roth (Germany)
ethylenediaminetetraacetic acid (EDTA)	60-00-4	Merck (Germany)
boric acid	10043-35-3	Carl Roth (Germany)
sodium dihydrogen phosphate monohydrate	10049-21-5	Merck (Germany)
thiazole orange (TO)	107091-89-4	Sigma Aldrich (USA)
hairpin DNAs	-	Sigma Aldrich (USA)
Fmoc-βAla-RAM resin	Load RAM-MBHA-resin following reference [1]	
Fmoc-Py-OH	Synthesized following reference [2,3]	

Fmoc-Im-OH	Synthesized following reference [2,3,4]
Fmoc-Im-Py-OH	Synthesized following reference [5]
plasmid pGEM-3z/601	Addgene plasmid #26656, deposited by Jonathan Widom
chicken erythrocyte histone octamers	Prepared following reference [6]

## 75 HAZARDS

Within each lab assignment the hazards varied. Especially in the synthesis stations, the most common hazards were flammable liquids and toxic reagents, which were reduced to a minimum amount and replaced when alternatives were possible. All hazardous work was performed in fume hoods and protective coats and goggles were compulsory during the whole two weeks of the practical course. Before the course, all students received a basic security introduction considering the inexperience of the biologists. The main security issues were highlighted and hazardous steps were mentioned and discussed during the course too.

## PRIMER SEQUENCES AND DNA PREPARATION

Table S7 shows the primer sequences that were used in the polymerase chain reaction of Widom 601 DNA.

**Table S7.** Primer sequences used in the polymerase chain reaction of Widom 601 DNA.

<i>primer</i>	<i>Sequence 5'-3'</i>
forward primer FAM601_F	[6FAM] CCT GGA GAA TCC CGG TGC
reverse primer 601_R	CAG GAT GTA TAT ATC TGA CAC GTG CC

The DNA hairpins for the CD-spectroscopy and fluorescence intercalation displacement (FID) were prepared prior to the laboratory course. The two DNA strands from Table S8 were dissolved in ddH<sub>2</sub>O and each mixture was heated to 95 °C for 10 min and then slowly cooled to r.t. Their concentration was determined spectroscopically on a Tecan Spark 20M. Their molar extinction coefficients were determined by using the following formula:<sup>7</sup>

$$\epsilon_{260nm} = \{(8.8 * \#T) + (7.3 * \#C) + (11.7 * \#G) + (15.4 * \#A)\} * 0.8 * 10^3 M^{-1}cm^{-1} \quad (S1)$$

In the formula # = number of nucleobases determined throughout the DNA sequence, T = thymine, C = cytosine, G = guanine, A = adenine.

**Table S8.** DNA sequences used for the CD and FID analysis.

<i>DNA name</i>	<i>DNA sequence 5'-3'</i>
Nucleosome_1	GGC AGTGTA CGC TTTT GCG TACTACT GCC
Nucleosome_2	GGC AGACTA CGC TTTT GCG TAGTCT GCC

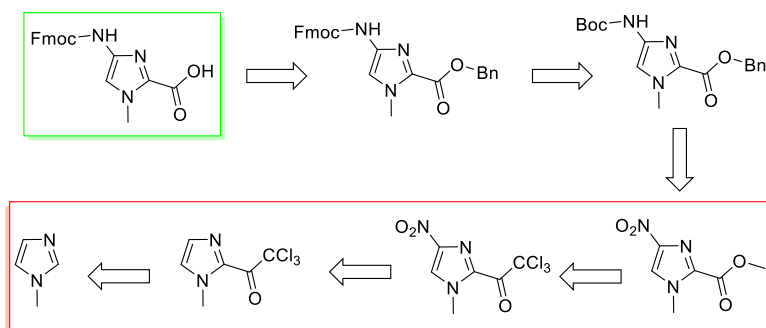
## EXPERIMENTAL DESCRIPTION FOR EACH GROUP

Week 1, group A1 – Pyrrole (Py) and imidazole (Im) monomer synthesis:

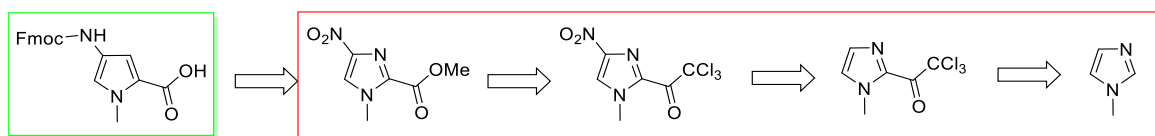
References: *Proc. Natl. Acad. Sci. USA* **2004**, 101, 6864.; *Org. Lett.* **2001**, 3, 1201.; *J. Am. Chem. Soc.* **1996**, 118, 6141.; *J. Am. Chem. Soc.* **2006**, 8766.; *Heterocycles* **1988**, 27, 1945.;  
Patent  
WO 199703975 A2.

Questions: Why do we need to go two different ways of synthesis for the imidazole and the pyrrole monomer? What do we need all the chemicals in each reaction for? What are the mechanisms of the reactions? With which chemicals do we need to work carefully?

Retrosynthetic pathway of the monomer synthesis:



**Scheme S1.** Retrosynthetic pathway for the imidazole monomer. Synthesis steps which were performed by the students are highlighted with a red box. The final green-highlighted Fmoc-monomer was previously prepared and supplied by the instructors.

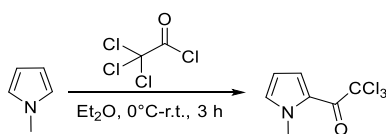


**Scheme S2.** Retrosynthetic pathway for the pyrrole monomer. Synthesis steps which were performed by the students are marked with a red box. The final green-highlighted Fmoc-monomer was previously prepared and supplied by the lab instructors.

Below, the detailed synthetic procedures for the synthesis steps which were performed by the students is shown. The remaining steps until the final Fmoc-building blocks were conducted and supplied by the instructors, due to time restrictions and dangerous and complicated synthesis steps.

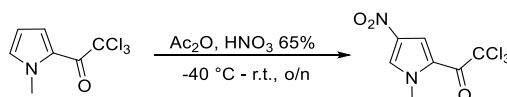
The references which were used to prepare the final monomers are summarized in Table S6.

### Synthesis of Py-C(O)CCl<sub>3</sub>



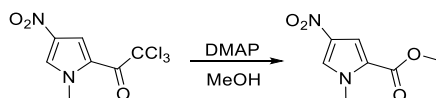
130 Under nitrogen atmosphere, trichloroacetylchlorid (50.0 mmol) was dissolved in Et<sub>2</sub>O (10 mL) and cooled to 0 °C. *N*-Methylpyrrole (50.0 mmol) was dissolved in Et<sub>2</sub>O (10 mL) and added dropwise over 30 min. The reaction mixture was warmed up to r.t. and stirred for another 3 h. At 0 °C, the reaction was quenched with K<sub>2</sub>CO<sub>3</sub> (26 mmol) dissolved in H<sub>2</sub>O (14 mL). It was extracted with Et<sub>2</sub>O, dried over MgSO<sub>4</sub>, filtered and the solvent removed. Analysis was performed (<sup>1</sup>H, <sup>13</sup>C, Cl).

### 135 Synthesis of NO<sub>2</sub>-Py-C(O)CCl<sub>3</sub>



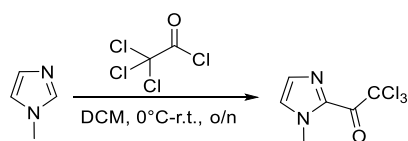
140 Under nitrogen atmosphere, Py-C(O)CCl<sub>3</sub> (1 eq) was dissolved in Ac<sub>2</sub>O (13 eq) and cooled down to -40 °C. 65% HNO<sub>3</sub> (2.2 eq) was added dropwise. The reaction mixture was slowly warmed up to r.t. and stirred overnight. At 0 °C, the reaction mixture was carefully neutralized with Na<sub>2</sub>CO<sub>3</sub> (sat.) to pH 7. It was extracted 4 x with EtOAc and washed 3 x with brine. The organic layers were dried over MgSO<sub>4</sub>, filtered and the solvent removed. Analysis was performed (<sup>1</sup>H, <sup>13</sup>C, Cl).

### Synthesis of NO<sub>2</sub>-Py-OMe

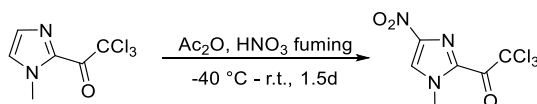


145 NO<sub>2</sub>-Py-C(O)CCl<sub>3</sub> (1 eq) was dissolved in MeOH to give a 0.3 M solution. DMAP (0.1 eq) was added and the solution stirred overnight. The solvent was removed in a dryload and the crude purified by flash column chromatography (pentane/EtOAc 4:1 → 1:1). Analysis was performed (<sup>1</sup>H, <sup>13</sup>C, ESI<sup>+</sup>).

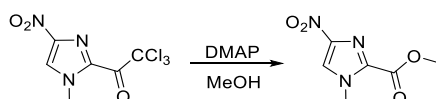
150

155 Synthesis of Im-C(O)CCl<sub>3</sub>

Under nitrogen atmosphere, trichloroacetylchlorid (35.1 mmol) was dissolved in CH<sub>2</sub>Cl<sub>2</sub> (25 mL) and cooled to 0 °C. *N*-Methylimidazole (35.0 mmol) was dissolved in CH<sub>2</sub>Cl<sub>2</sub> (15 mL) and added dropwise over 1.5 h. The reaction mixture was warmed up to r.t. and stirred until full conversion (at least 3 h).  
160 At 0 °C, freshly distilled NEt<sub>3</sub> (35.1 mmol) was added dropwise over 30 min. The solvent was removed in a dryload and the crude purified by flash column chromatography (pentane/EtOAc 1:1). Analysis was performed (<sup>1</sup>H, <sup>13</sup>C in CDCl<sub>3</sub>, CI).

Synthesis of NO<sub>2</sub>-Im-C(O)CCl<sub>3</sub>

Under nitrogen atmosphere, Im-C(O)CCl<sub>3</sub> (1 eq) was dissolved in Ac<sub>2</sub>O (13 eq) and cooled down to -40 °C. Fuming HNO<sub>3</sub> (6.5 eq) was added dropwise over 1.5 h. The reaction mixture was slowly warmed up to r.t. and stirred overnight. The reaction mixture was neutralized carefully with saturated NaHCO<sub>3</sub> under cooling and extracted with CH<sub>2</sub>Cl<sub>2</sub>, dried over MgSO<sub>4</sub>, filtered and the  
170 solvent removed. Analysis was performed (<sup>1</sup>H, <sup>13</sup>C in CDCl<sub>3</sub>, CI).

Synthesis of NO<sub>2</sub>-Im-OMe

Under nitrogen atmosphere, NO<sub>2</sub>-Im-C(O)CCl<sub>3</sub> (1 eq) was dissolved in MeOH to give a 0.3 M solution.  
175 DMAP (0.1 eq) was added and the solution stirred overnight. The solvent was removed in a dryload and the crude purified by flash column chromatography (pentane/EtOAc 4:1 → 1:1 → 1:4). The gradient was not increased too fast, as with this column the 4-NO<sub>2</sub>- and 5-NO<sub>2</sub>-isomer were separated. Analysis was performed (<sup>1</sup>H, <sup>13</sup>C in DMSO, ESI<sup>+</sup>).



---

180 Week 1, group B1 - Polyamide Hairpin Synthesis:

General procedure for the polyamide hairpin coupling

185 The hairpins were synthesised manually in a 20  $\mu\text{mol}$  scale in 2 mL polypropylene syringes equipped with a filter and plunger (pore size 25  $\mu\text{m}$ , MultiSynTech GmbH; Germany). All solutions needed were freshly prepared in the morning of use.

The needed amount of preloaded Fmoc- $\beta$ Ala-RAM-resin (loading = 0.54 mmol/g) was weighted into a filter-syringe and the resin swelled in 1.5 mL DMF for 30 min.

Solutions were prepared in 50 mL falcon tubes and refilled to 1.5 mL reaction tubes:

190 deprotection solution: 20% piperidine in DMF, 500  $\mu\text{L}$  (24x) / 1.5 mL reaction tubes (12 mL in total)

capping solution: 5%  $\text{Ac}_2\text{O}$ , 5% pyridine in DMF, 500  $\mu\text{L}$  (12x) / 1.5 mL reaction tubes (6 mL in total)

It was followed the procedure of the table at the end of this protocol:

195 deprotection: Deprotection was performed twice for 5 min.

coupling: Coupling of **Fmoc-Py-OH** was performed with 4 eq of the amino acid and 4 eq HATU dissolved in **DMF** to give a 0.3 M solution. DIPEA (8 eq) was added and the mixture preincubated for 3 min before addition to the resin. Coupling was performed for 1 h. After introduction of Fmoc- $\gamma$ -OH, after 1 h of coupling, DMSO/DMF 1:1 (100  $\mu\text{L}$ ) was added for 30 min.

200 Coupling of **Fmoc-Im-Py-OH** and **Fmoc-Im-OH** was performed with 4 eq of the amino acid and 4 eq HATU dissolved in **NMP** to give a 0.3 M solution. DIPEA (12 eq) was added and the mixture preincubated for 3 min before addition to the resin. Coupling was performed for 2 h. After introduction of Fmoc- $\gamma$ -OH, after 2 h of coupling, DMSO/DMF 1:1 (100  $\mu\text{L}$ ) was added for 30 min.

205 capping: Capping was performed once for 5 min.

test cleavage: After the capping step, a little sample of resin, which was washed with  $\text{CH}_2\text{Cl}_2$  last, was transferred to an 1.5 mL reaction tubes and 180  $\mu\text{L}$  cleavage mixture (TFA/ $\text{CH}_2\text{Cl}_2$ / $\text{H}_2\text{O}$ /TIS 90/5/2.5/2.5) were added and shaken at r.t. for 1.5 to 2 h. The solvent was transferred into another 1.5 mL reaction tube without the resin balls, the solvent was removed under nitrogen flow, and the crude dried under vacuum for 10 min. The sample was re-dissolved in  $\text{H}_2\text{O}$ /MeCN 7/3 0.1% TFA and the  $\text{OD}_{304}$  was determined on the nanodrop and the sample injected in the HPLC to verify the successful couplings. The injected amount was calculated by  $V = 3.6 \mu\text{L} / \text{OD}_{304}$ .

---

215 final cleavage: To the resin, cleavage mixture (1 mL / 10  $\mu$ mol, TFA/CH<sub>2</sub>Cl<sub>2</sub>/H<sub>2</sub>O/TIS 90/5/2.5/2.5) was added and stirred at r.t. for 2 h. The solvent was transferred into a filter syringe, filtered and washed once with 1 mL TFA, to remove the resin balls. The solvent was removed under nitrogen flow and the crude dried under vacuum for 10 min. The crude was dissolved in H<sub>2</sub>O/MeCN (7/3) 0.1% TFA and purified on the preparative RP-HPLC.



## Pairing rules for Dervan-polyamide hairpins

Pairing rules for polyamides, which bind sequence-specific to the DNA, were nicely summarized by Dervan and Bürli.<sup>8</sup> By designing the right polyamide, many different sequences can be addressed. For the design of a sequence, some rules need to be followed: a pyrrole opposite of an imidazole (Py/Im) targets a C-G basepair, whereas an imidazole opposite of a pyrrole (Im/Py) targets a G-C basepair. A pyrrole pyrrole pair (Py/Py) targets both, A-T and T-A. The C-terminal  $\beta$ -alanine linker and the  $\gamma$ -turn both are specific for an A/T or T/A pair on the flanking sides of the polyamide.  $\beta$ -alanine can be introduced instead of pyrrole and reveals the same binding selectivity's. However, their introduction gives a less rigid polyamide hairpin, which results in less truncations during coupling and therefore higher yields. The orientation of the polyamide upon binding to the DNA orientates the  $N \rightarrow C$  of the polyamide in the 5'  $\rightarrow$  3' direction of the DNA. The table below summarizes the pairing rules of all building block combinations. The example polyamide in the figure below illustrates its pairing rules to a 6-bp DNA.

**Table S9.** Pairing rules of all building block combinations for the synthesis of polyamides.

pair	G-C	C-G	T-A	A-T
Im/Py	+	-	-	-
Py/Im	-	+	-	-
Py/Py	-	-	+	+
Im/Im	-	-	-	-
Im/ $\beta$	+	-	-	-
$\beta$ /Im	-	+	-	-
Py/ $\beta$	-	-	+	+
$\beta$ /Py	-	-	+	+
$\beta$ / $\beta$	-	-	+	+

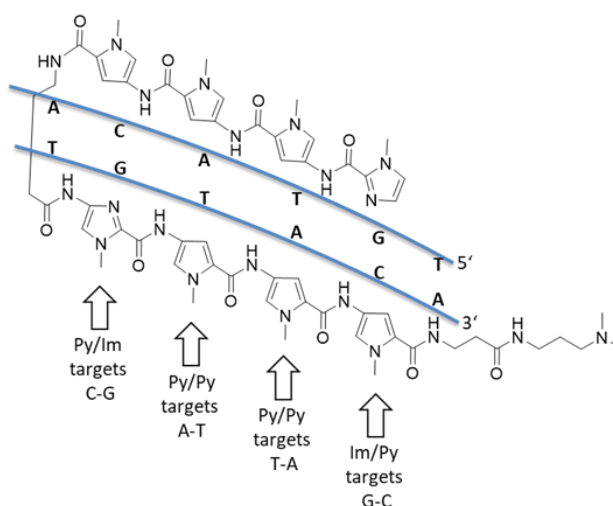


**Figure S1.** Example of polyamide hairpin binding to a 6 bp DNA to visualize the pairing rules.

245

Week 1, group C1 - Nucleosome Assembly:

**PCR for DNA601 and FAM-DNA601:**

250 Questions: What does PCR stands for? How does PCR works? What do we need each component of the PCR for? How does the purification of the produced DNA work?

Procedure for W601-DNA:

During the PCR, all components were **always** stored on ice. The phusion polymerase was stored in the cooling block and only shortly taken out of the freezer when needed.

	amount [ $\mu$ L]	final concentration
ddH <sub>2</sub> O	532.2	
5xHF	160	1X
DMSO 100%	24	3%
dNTP(10 mM)	16 each	200 $\mu$ M each
primer 601_R (HPLC, 100 $\mu$ M)	4	0.5 $\mu$ M
primer FAM601_F (100 $\mu$ M)	4	0.5 $\mu$ M
plasmid pGEM-601 (211 ng/ $\mu$ L)	3.8	1 ng/ $\mu$ L
phusion polymerase (2 U/ $\mu$ L)	8	1 U/ 50 $\mu$ L

255 The mixtures were prepared twice. All components except the phusion polymerase were combined and mixed gently with a pipette. The mixture was stored on ice and it was checked for the free PCR cyclers. At last, the phusion polymerase was added, mixed again gently and portions of 50  $\mu$ L were filled in each PCR tube. All the liquid was shortly spinned down and placed into the PCR cyclers. The program of the table below was started:

98 °C	30 s
98 °C	8 s
60 °C	20 s
72 °C	10 s
72 °C	4 min
4 °C	hold

260

After the program was finished, two PCR tubes were combined in one 1.5 mL reaction tubes and the procedure of the *PCR & DNA Clean Up Kit* (New England Biolabs) provided was followed, but 600  $\mu$ L loading buffer used and the columns loaded twice. 5 columns in total were used.

265 The DNA was eluted from the column with 10  $\mu$ L ddH<sub>2</sub>O and all eluents collected in one 1.5 mL reaction tube. It was re-eluted with 25  $\mu$ L elution buffer. Afterwards, the DNA concentration was determined on the nanodrop.

---

### **Determination of DNA purity**

270 To determine the purity of prepared DNA, a 2% agarose gel was run. To prepare the gel, 1.2 g of agarose was added to 60 g of 1X TBE buffer in an Erlenmeyer flask. The mixture was heated until all particles were completely dissolved and the solution was gently boiling. The solution was cooled down for 3 min and 2  $\mu\text{L}$  of midori green were added. It was shaken again gently, poured into a gel caster and the comb placed into it. After polymerisation was finished the comb was removed carefully and the gel transferred into the running chamber filled with 1X TBE and the pockets were filled with:

- 275 1) 5  $\mu\text{L}$  of DNA ladder CSL 1kb  
2) 0.3  $\mu\text{g}$  of the prepared DNA in a total volume of 6  $\mu\text{L}$  TBE buffer and 1  $\mu\text{L}$  6x DNA loading dye

The gel was run for 40 min at 90 V. The gel was analyzed with a ChemiDoc MP by Biorad.

### **Nucleosome assembly:<sup>9</sup>**

280 Questions: Which of the used chemicals are dangerous? Are all nucleosomes the same? – check for alpha-satellite, widom601 and the composition of the histone core. What are PTMs? How does the reconstitution of nucleosomes work?

### **Buffer preparation**

285 Nucleosome Core Particles (NCPs) were reconstituted by the salt-gradient-dialysis method. Different buffers were prepared:

1 L 20X TE buffer: 200 mM Tris, 20 mM EDTA, pH 8.0

1 L 10X TBE buffer: 40 mL 0.5 M EDTA pH 8.0, 108 g Tris, 55g boric acid → filled up to 1 L

290 250 mL SDB buffer (“salt dialysis buffer”): 10 mM Tris, 1 mM EDTA, 2 M NaCl, pH 8.0  
(12.5 mL 20X TE, 29.22g NaCl → filled up to 125 mL, took out 1 mL and filled up to a total volume of 250 mL)

1L of 1X TE-buffer (10 mM Tris, 1 mM EDTA, pH 8.0)

All buffers were stored at 4°C

### **Reconstitution of NCPs**

295 It was reconstituted in a volume of 30  $\mu\text{L}$ , which contained 1  $\mu\text{g}$  of DNA (90876 Da) and varying amounts of histone octamers prepared from chicken erythrocytes. To assemble this 1  $\mu\text{g}$  of DNA, about 2.4  $\mu\text{L}$  of the 1:10 glycerol stock of histones in 1X SDB were needed. It was planned to prepare a titration row with 11.0 / 11.5 / 12.0 / 12.5  $\mu\text{L}$  of the 1:50 stock to determine the exact ratio needed.

The dialysis membrane was placed in 1X SDB+2M NaCl for at least 20 min.

300

---

The used histone dilution in low binding tubes was: 1:50 glycerol stock in 1X SDB  
Histone and DNA mixtures were prepared in low binding tubes by adding 1.0 µg DNA and the volumes given above of the 1:50 histone stock into a total volume of 30 µL SDB

305 Dialysis chambers: Samples were pipetted into cut 1.5 ml reaction tube caps and a small membrane was added (The membrane was placed in water before and shortly put into the beaker (2 M NaCl). The membranes were separated from each other, put with the inside face onto the cap rim and the other part stored) and the chamber closed with the cut tube piece. The dialysis cells were put into the beaker filled with 250 mL 1X SDB (2 M NaCl) and shaken in a way that the liquid came into  
310 contact with the membrane. All solutions were kept at 4 °C all the time. It was stirred for 1 h at about 60 rpm. After 1 h 250 mL TE were added → 1 M NaCl. After 1 h 250 mL were discarded from the beaker and 250 mL TE were added → 500 mM NaCl. After 1 h all but 50 mL were discarded and 450 mL TE were added → 50 mM NaCl. Stirring was continued for at least 1 h. The dialysis cells were removed from the beaker and dried on top with a pipette tip. The samples were pipetted from  
315 the dialysis cells by perforating the membrane on the non-liquid side, then sucked up and transferred into a low binding tube. A gel was poured to check the purity and the best conditions. As a reference 100 ng free DNA and half of the amount of each nucleosome titration was loaded.

To pour the 5% native PAGE gel 0.5X TBE, 1.875 mL 40% acrylamide and 750 µL 10X TBE were added into a 50 mL falcon tube. It was filled up to 15 mL with water, mixed and 150 µL 10% APS  
320 and 7.5 µL TEMED were added. It was mixed again, the gel poured into the cassette, the comb inserted and polymerized for about 40 min. After polymerization the chamber was rinsed to remove all SDS, the comb removed and the chambers washed with Millipore water. The gel was placed into the chamber and filled up with 0.5X TBE. For sample preparation, half of the nucleosome amount was mixed with 2 µL glycerol (cut tip end) and the chambers loaded. A 100 ng DNA sample as  
325 reference was also loaded. The gel was run at 90 V for 40 min. DNA bands in the gels were visualized using post-staining by allowing the gel to float in 100 mL 0.5X TBE and 10 µL SYBR Safe DNA Gel Stain (10000X) for 30 min. The bands were visualized with Chemidoc instruments.

For large scale assembly a reaction volume of 50 µL was used.

330

### **CD measurements**

References: *Curr. Protein Pept. Sci.* **2000**, 1, 349.; *Biochemistry*, **1999**, 38, 2143.; *Bioconjugate Chem.* **2015**, 26, 2054.

335 Questions: What does CD stands for? How does a CD measurement works? What do we use CD measurements for? Why do we get a CD signal, although or molecule is not chiral? What is an ICD?

### How the CD spectrometer was turned on and off:

#### *Turn on:*

- 340
- the nitrogen flow was turned on
  - the nitrogen monitor (Afristo) was turned on and the gas flow checked (at least >2.5 L/min; best 5-10 L/min)
  - the computer and screen were turned on
  - the water bath (Haake WKL 26) and peltier controller (CDF426) were turned on

345

  - the CD-spectrometer JASCO J810s was turned on
  - the software SpectraManager was started: spectrum measurement was chosen from the list on the right
  - It was waited for at least 20 min before the first measurement, to let the lamp heat up and stabilize

350

  - it was proceeded by clicking measurement – accessory – Temperature: Jasco Peltier Controller – ok
  - it was proceeded by clicking control – accessory – put the desired temperature – apply – close
  - it was proceeded by clicking measurement – parameters – put the desired settings

355

#### *Turn off:*

- all data were saved (also as.txt file) and downloaded onto an USB-stick
- the software was closed and in the Spectra Manager “Instrument STOP” was chosen
- the JASCO J810s, water bath and peltier controller were shut down

360

- the nitrogen gas was turned off
- the nitrogen monitor was turned off
- the computer and the screen was shut down

### How concentrations of a stock solution were determined:



---

365 A little bit of the polyamide hairpin sample was dissolved in 100  $\mu\text{L}$  ddH<sub>2</sub>O. It was vortexed well and all centrifuged down.

On the photometer, a 500  $\mu\text{L}$  absorbance cuvette was filled with 500  $\mu\text{L}$  of ddH<sub>2</sub>O and a blank measured. 3  $\mu\text{L}$  of the stock was added, well mixed and the absorbance at the wavelength given measured. Three data point between an absorbance between 0.3 and 1.0 were recorded. The solution  
370 was kept from the cuvette and from the stock and freeze dried on the lysophylizer after finishing with the measurements. The concentration of the stock was calculated with the equation:<sup>10</sup>

$$c(\text{stock}) = \frac{A}{\varepsilon} * \frac{V_{\text{total}}}{V_{\text{sample}}}$$

It was used:<sup>11</sup>  $\varepsilon_{310\text{nm}}$ (unmodified polyamide hairpin) in ddH<sub>2</sub>O = 69200 M<sup>-1</sup>cm<sup>-1</sup>

375

#### How CD measurements were performed:

The following settings were used: 20°C, 0.2 cm pathlength, start: 380 nm, end: 220 nm, scanning speed 100 nm/min, response 0.25 s, data pitch 1 nm, accumulations 3, bandwidth 2 nm, sensitivity: high, scanning mode: continuous.

380 To have a 10  $\mu\text{M}$  DNA solution in the end, it was calculated how much of the DNA stock was needed to get this final concentration in a volume of 500  $\mu\text{L}$ . The 0.2 cm pathlength CD cuvette was filled with (500  $\mu\text{L}$  – V (DNA stock)) 20 mM NaH<sub>2</sub>PO<sub>4</sub> 100 mM NaCl pH 7.4, the cuvette placed in the spectrometer, 5 min waited and the blank measured. The calculated DNA amount was added, carefully mixed while avoiding to produce bubbles in the cuvette, 3 min waited and measured.  
385 Increasing amounts (250  $\mu\text{M}$ ) of polyamide hairpin stock were added, carefully mixed while avoiding to produce bubbles in the cuvette, 3 min waited and measured. It was continued until the recorded spectra reached a saturation.

The data was exported from the CD-spectrometer and plotted in  $\theta \times 10^{-4}$  [deg/M\*cm] versus the  
390 wavelength. The maxima of the ICD signal was plotted against the concentration of polyamide hairpin and the K<sub>D</sub> calculated by using the program DynaFit.<sup>12</sup>

---

Week 2, group B2 - Analysis of the New DNA Binder by Fluorescence Intercalation Displacement (FID):

395

References: *Org. Lett.* **2010**, *12*, 216.; *Acc. Chem. Res.* **2004**, *37*, 61-69.

400

Questions: What is fluorescence? Why do we need two different types of cuvettes when we measure absorbance and fluorescence? What is a Stokes shift? What is an absorbance, emission and excitation spectra? Why do we expect a change of fluorescence when we increase the concentration of DNA in our fluorophore stock? Why do we expect a decrease in fluorescence when we add our polyamide hairpin to the mixture?

How concentrations of a stock solution were determined:

It was followed the protocols of the CD measurements.

405

How the spectrometer settings were set:

To use the fluorimeter, first the computer was turned on, then the fluorimeter and the water bath. When all sounds of the fluorimeter were finished, the program was started and then the lamps turned on by using the program. It was waited for at least 20 min before the first measurement to let the lamp stabilize. Then only the emission lamp was turned on and auto scale pressed. Then only the excitation lamp was turned on and auto scale pressed. In the end, only the emission lamp was turned on. For measurements it was proceeded by clicking on file – properties and the setting typed in. Ok was pressed, the measurement started and the results saved. Then, it was continued with the next measurement.

415

How the polyamide hairpin titrations were performed:

Measurements were performed in a volume of 1 ml at a concentration of 6  $\mu$ M thiazole orange and 1  $\mu$ M DNA duplex with the right target sequence in 20 mM  $\text{NaH}_2\text{PO}_4$  100 mM NaCl pH 7.4 with increasing amounts of polyamide hairpin.

420

The following settings were used: 20°C, excitation wavelength: 490 nm, excitation slidth: 3 nm, emission wavelength: 510 - 700 nm, emission slidth: 3 nm, scanning speed 500 nm/min, response 0.2 s, sensitivity: medium, data pitch: 1 nm.

425

To have a 6  $\mu$ M thiazole orange and 1  $\mu$ M DNA hairpin solution in the end, it was calculated how much of the stocks were need, to achieve this final concentration in a volume of 1 mL. The cuvette was filled with (1 mL – V (DNA stock) – V (thiazole orange stock)) 20 mM  $\text{NaH}_2\text{PO}_4$  100 mM NaCl pH 7.4 buffer, the cuvette placed into the spectrometer, 5 min waited and the blank measured. The

---

430 calculated thiazole orange amount was added, carefully mixed while avoiding to produce bubbles in  
the cuvette, 1 min waited and measured. The calculated DNA amount was added, carefully mixed  
while avoiding to produce bubbles in the cuvette, 3 min waited and measured. Increasing amounts  
(250  $\mu$ M and 1 mM) of polyamide hairpin stock were added, carefully mixed while avoiding to produce  
bubbles in the cuvette, 3 min waited and measured. It was continued until the recorded spectra were  
nearly absent.

435

To plot the fluorescence intensity versus the wavelength the data from the spectrometer was  
exported. The maxima of the fluorescence signal was plotted against the concentration of polyamide  
hairpin and the  $K_D$  calculated by using the program DynaFit.<sup>12</sup>

440

Week 2, group C2 - Analysis of the New DNA binder by Footprinting Combined with Capillary  
Electrophoresis (CE):

445 *For this methodology only references, questions and the procedure and data of the final sample  
preparation are given due to non-published data.*

References: *ChemBioChem* **2018**, 19, 664-668.; *Org. Biol. Chem.* **2019**, 17, 1827-1833.

450 Questions: What is capillary electrophoresis? On which methods is it based on? Which are the  
most common applications? How can a nucleosome disassemble? Why do we use different reagents for  
CE of free DNA and nucleosomes? Can potential minor groove binders bind at any position of the  
nucleosome? How does the common footprinting methodology works? What are advantages and  
disadvantages?

455 How concentrations of a stock solution were determined:

It was followed the protocols of the CD measurements.

Sample preparation:

460 The freeze-dried DNA amount was dissolved in 12  $\mu$ L Formamid and 0.5  $\mu$ L size standard (550 BTO,  
Biotype).

The CE samples were run on an *ABI PRISM 310* genetic analyzer by *Applied Biosystems*. All samples  
were separated on denaturing POP-4 polymer (*Applied Biosystems*) in a capillary with a length of  
47 cm (36 cm well-to-read) and a diameter of 50  $\mu$ m. After an electrokinetical injection of 5 s at 15 kV  
the samples were run for 28 min at 60 °C and 15 kV.

465

---

## QUESTIONS TO START THE PROPOSAL

Before starting with the Pomodoro-technique, the students filled in a questionnaire to guide their own ideas and facilitate initial introduction among students. The questions in the questionnaire were:<sup>13</sup>

470

- What are your research interests?
- What are the problems in your interested fields? Why are they important?
- With what sources of data can you validate the importance of the proposed project?
- How is the existing knowledge inadequate?

475

- Why are your ideas better?
- What makes your project new / unique / different?
- What will it contribute and who will benefit from it?

## POSTER TEMPLATE

480 For the proposal poster, the students were supplied with the poster template below as a guide. They were free to choose the template or use other approaches to present their idea.

<h1>TITLE OF THE NEW RESEARCH PROJECT</h1>		
Name surname, name surname, <i>Fachbereich Chemie and Fachbereich Biologie, Philipps-Marburg Universität (Germany)</i> e-mail: xxx@.cn; e-mail: xxx@.de		
<i>Picture explaining clearly the main idea of the research project</i>	<b>ABSTRACT:</b> Summary of your research project. At the end, include the keywords.  <b>KEYWORDS:</b>	
<b>INTRODUCTION</b> Explain briefly the basic concepts in order to understand the research project.  Identify challenges and possible problems of the chosen topic.  Please, do it with a visual approach: use schemes and figures whenever possible.  Use captions to explain your figures or schemes: <b>Figure 1.</b> XXXXX; <b>Scheme 1.</b> XXXXX.  The extent of the three sections can be adapted for your specific needs. However, be aware that the working plan together with subordinate sections is likely the most extensive one.	<b>GOAL</b> Explain the specific goal and how it will contribute to the solution of the described problems and challenges.  Please, do it with a visual approach: use schemes and figures whenever possible.  Use captions to explain your figures or schemes: <b>Figure 1.</b> XXXXX; <b>Scheme 1.</b> XXXXX.  <b>WORKING PLAN</b> Provide a detailed strategy on how to achieve your goal.  Use subordinate sections. Again, do it as visual as possible.	<b>CONCLUSIONS</b> Summarize the most important points.
<b>REFERENCES:</b> [1] Meunier, B.; de Visser, S. P.; Shaik, S. <i>Chem. Rev.</i> <b>2004</b> , <i>104</i> , 3947–3980. [2] Binder, W. H. <i>Angew. Chem., Int. Ed.</i> <b>2005</b> , <i>44</i> , 5172–5175. [3] ... Please use the ACS citation format for journals. For more information see <a href="http://pubs.acs.org/doi/abs/10.1021/bk-2006-STYG.ch014">http://pubs.acs.org/doi/abs/10.1021/bk-2006-STYG.ch014</a> from within the university network.		

**Figure S1:** Poster template, which was provided for the students.

---

## EVALUATION CRITERIA FOR DISCOVERY-BASED RESEARCH LAB

485 To assess the outcome of the students, different criteria for each experimental technique were used (below).

### **Synthesis:**

490 All synthesized monomer precursors were literature described.<sup>[3]</sup> Therefore, the access of the molecules, yields and characterization by <sup>1</sup>H and <sup>13</sup>C NMR spectroscopy and CI or ESI mass spectrometry can be easily evaluated.

The synthesized polyamide hairpins were novel. To judge the success of the synthesis HPLC-MS analysis was performed. The number of peaks revealed how many truncations and other side products were formed and mass analysis helped to assign the chromatograms. In the ideal case, the  
495 HPLC-chromatogram would show a single peak and a mass spectra containing only masses, which belong to the product polyamide.

### **PCR and nucleosome assembly**

The success of the PCR and nucleosome assembly as well as their purity was tested by native  
500 polyacrylamide gel electrophoresis (PAGE). Supplying free DNA and nucleosome reference samples and/or the addition of DNA ladder validated the size of the bands in the gel and allowed the assessment of the results.

### **CD measurements**

505 To assess the results of the CD measurements we compared the observed signals with the literature reported of known similar compounds. After addition of dsDNA hairpin to the buffer the typical bands for B-DNA: minimum at 250 nm and a maximum at 280 nm were expected.<sup>[9]</sup> Addition of increasing amounts of polyamide resulted in an induced CD signal at the absorbance range of the polyamide (300-360 nm).<sup>[14]</sup> Absence of contamination by the students could be evaluated by initial  
510 measurements of the buffer in which no distinct signal was expected. Overlay of the buffer- and DNA-spectra with previous ones, performed by the instructors helped to assess the results.

Final calculation of the binding constant allowed the students and the instructors to compare their results to known literature values in the nM-region<sup>[14]</sup> and judge their measurements.

### **FID measurements**

515 FID measurements were performed with 6-TramTO-3.<sup>[15]</sup> In the first cohort we used this fluorescent dye, which was developed in our own laboratory. After finding out with the help of the students that it was not a suitable dye for FID measurements, we changed to thiazole orange for the second cohort. To assess the results of the FID measurements it was checked, if the observed signals align with the  
520 expectations in comparison to known compounds. Fluorescence measurements of the buffer alone and of the buffer and the dye gave the expected weak fluorescence intensity signals. After addition of the DNA to the dye solution, the typical strong fluorescence signals at 645 nm for 6-TramTO-3<sup>[15]</sup>

---

and 530 nm for TO<sup>[16,17]</sup> was anticipated. Addition of subsequent amounts of polyamide resulted in a decreasing fluorescence signal.<sup>[16,17]</sup> Absence of contamination by the students could be evaluated  
525 by initial measurements of the buffer in which no distinct signal was expected.

Final calculation of the binding constant allowed the students and the instructors to compare their results to known literature values in the nM-region<sup>[16]</sup> and judge their measurements.

### **General evaluation**

530 The discovery-based research lab was evaluated following the criteria given below:

- Did the students achieve the synthesis/PCR and nucleosome assembly/CD measurements/FID measurements?
- How do the students work in the lab?
- 535 • Does the analysis data of the synthesis fit the reported ones from the literature?
- How are the yields and the purity?
- Do the measurements look as expected?
- Do the calculated data fit the region from the literature?
- Are the students able to evaluate and interpret their data?

540

---

## EVALUTATION CRITERIA FOR THE SCIENTIFIC COMMUNICATION

The scientific article and the research proposal poster, including the presentation were evaluated following the given guidelines:

545

### **Scientific article:**

- Was the communication prepared using the journal template?
- How is the general / first impression?
- Does the communication follow the general structure and addresses each content appropriately?  
550
  - Title: does the title suits to the content?
  - Abstract: appropriated structured and summarizing the relevant content?
  - Introduction: scope of background info? Connection between precedents and new results?
  - 555
    - Is there a scientific gap to highlight the importance of the article?
    - Discussion: well discussed results? Importance of bigger picture?
    - Methods: clear and complete?
    - References: complete and following the right style?
- What data were used?
- 560
  - Does it have scientific rigor?
  - Is the used language clear and understandable?
  - Are the figures coherent with the data?

### **Research Proposal Poster:**

565

- Is it well structured?
- How is the general / first impression?
- Does the topic cover the field of epigenetics?
- Is it a novel project?
- Is the timeline and methodology feasible?
- 570
  - Is it visual and understandable?
  - How do the students present their poster:
    - Did they understand the topic and the precedents?
    - Do they present their poster well?
    - Are all students taking part equally?
    - 575
      - Are they able to answer (defence) questions?



## STUDENT'S OUTCOME

In this section, examples of student's outcomes for the lab course, the scientific article and the poster are given. Tables which describe the criteria, which were used to evaluate and rate the outcomes, are further supplied.

580

## OUTCOMES OF THE DISCOVERY-BASED RESEARCH LAB

### Synthesis:

Below, students' results of the  $^1\text{H-NMR}$ ,  $^{13}\text{C-NMR}$  and HRMS are noted and exemplary a figure of the corresponding  $^1\text{H-NMR}$  spectra is shown.

585

### Py-CCl<sub>3</sub>:

**$^1\text{H-NMR}$**  (300 MHz, DMSO-*d*<sub>6</sub>,  $\delta$ ): 7.46 - 7.42 (m, 2H, CH-1 and CH-3), 6.30 (dd, 1H,  $J = 4.3$  Hz,  $J = 2.5$  Hz, CH-2), 3.91 (s, 3H, CH-4).

590

**$^{13}\text{C-NMR}$**  (75 MHz, DMSO-*d*<sub>6</sub>,  $\delta$ ): 171.8 (C=O), 135.3 (CH), 123.6 (CH), 120.7 (C<sub>q</sub>), 109.1 (CH), 96.0 (CCl<sub>3</sub>), 36.2 (CH<sub>3</sub>).

**HRMS-CI<sup>+</sup>** ( $m/z$ ): [M+H]<sup>+</sup> calcd for C<sub>7</sub>H<sub>6</sub>Cl<sub>3</sub>NOH, 225.95932; found, 225.95978.

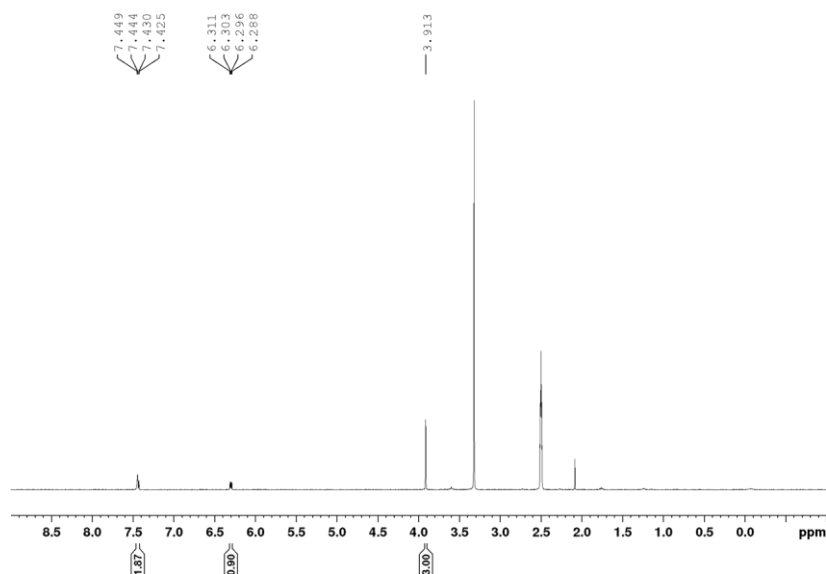


**Figure S3.**  $^1\text{H-NMR}$  spectra of Py-CCl<sub>3</sub>.

595

### NO<sub>2</sub>-Py-CCl<sub>3</sub>:

**$^1\text{H-NMR}$**  (300 MHz, DMSO-*d*<sub>6</sub>,  $\delta$ ): 8.56 (d, 1H,  $J = 1.6$  Hz, CH-2), 7.80 (d, 1H,  $J = 1.6$  Hz, CH-1), 4.00 (s, 3H, CH-3).

600

**$^{13}\text{C-NMR}$**  (75 MHz, DMSO-*d*<sub>6</sub>,  $\delta$ ): 172.8 (C=O), 134.2 (C<sub>q</sub>), 132.5 (CH), 120.6 (C<sub>q</sub>), 116.3 (CH), 94.5 (CCl<sub>3</sub>), 50.0 (CH<sub>3</sub>).

**HRMS-CI<sup>+</sup>** ( $m/z$ ): [M+H]<sup>+</sup> calcd for C<sub>7</sub>H<sub>5</sub>Cl<sub>3</sub>N<sub>2</sub>O<sub>3</sub>H, 270.94440; found, 270.94291.

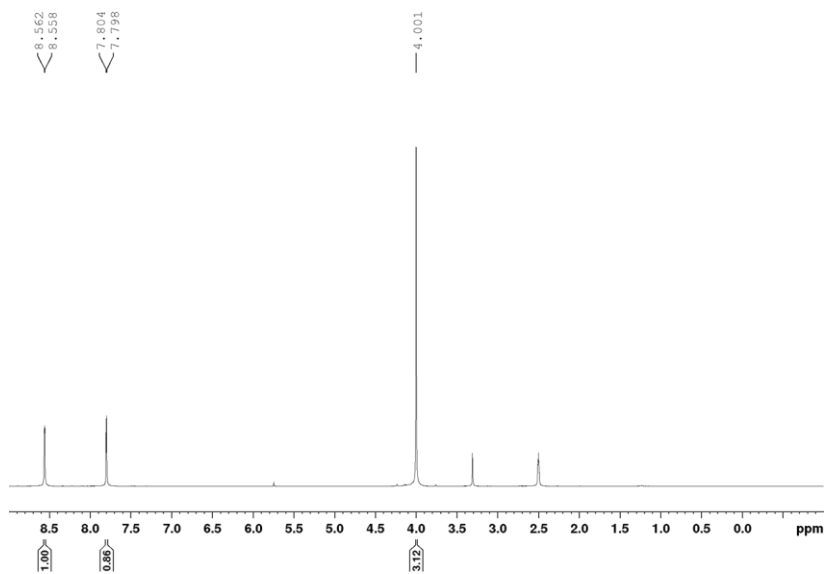


**Figure S4.**  $^1\text{H-NMR}$  spectra of  $\text{NO}_2\text{-Py-CCl}_3$ .

605  $\text{NO}_2\text{-Py-OMe}$ :

**$^1\text{H-NMR}$**  (300 MHz,  $\text{DMSO-}d_6$ ,  $\delta$ ): 8.27 (d, 1H,  $J = 2.0$  Hz,  $\text{CH-2}$ ), 7.30 (d, 1H,  $J = 2.0$  Hz,  $\text{CH-1}$ ), 3.92 (s, 3H,  $\text{CH-3}$ ), 3.80 (s, 3H,  $\text{CH-4}$ ).

**$^{13}\text{C-NMR}$**  (75 MHz,  $\text{DMSO-}d_6$ ,  $\delta$ ): 159.8 (C=O), 134.2 ( $\text{C}_q$ ), 129.4 (CH), 122.6 ( $\text{C}_q$ ), 111.5 (CH), 51.7 ( $\text{CH}_3$ ), 37.4 ( $\text{CH}_3$ ).

610 **HRMS-ESI $^+$**  ( $m/z$ ):  $[\text{M}+\text{H}]^+$  calcd for  $\text{C}_7\text{H}_8\text{N}_2\text{O}_4\text{H}$ , 185.05623; found, 185.05665.

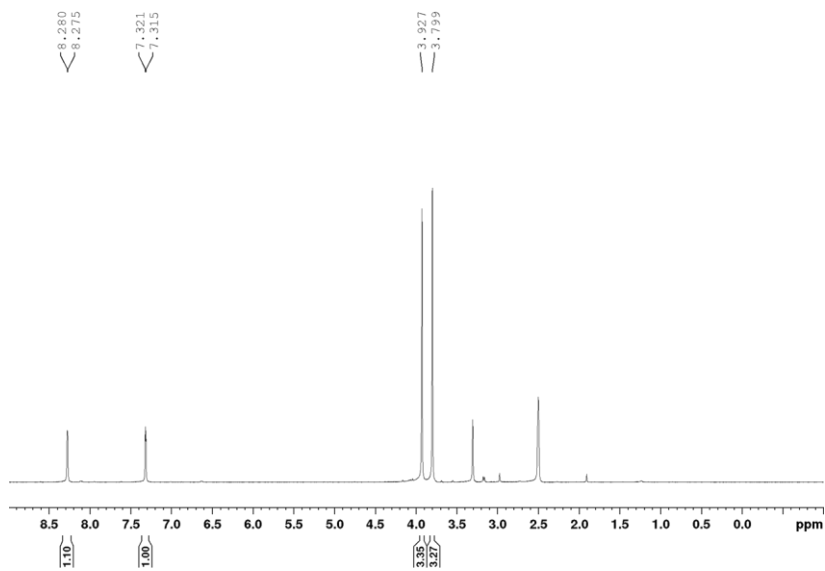


**Figure S5.**  $^1\text{H-NMR}$  spectra of  $\text{NO}_2\text{-Py-OMe}$ .

615

620

Im-CCl<sub>3</sub>:

**<sup>1</sup>H-NMR** (300 MHz, CD<sub>3</sub>OD, δ): 7.31 (s, 1H, CH-2), 7.08 (s, 1H, CH-1), 4.01 (s, 3H, CH<sub>3</sub>-3).

**<sup>13</sup>C-NMR** (75 MHz, CD<sub>3</sub>OD, δ): 160.3 (C=O), 137.8 (C<sub>q</sub>), 129.4 (CH), 128.1 (CH), 119.5 (CCl<sub>3</sub>), 36.2 (CH<sub>3</sub>).

625 **HRMS-Cl<sup>+</sup>** (*m/z*): [M+H]<sup>+</sup> calcd for C<sub>6</sub>H<sub>5</sub>Cl<sub>3</sub>N<sub>2</sub>O<sub>1</sub>H, 226.95457; found, 226.95069.

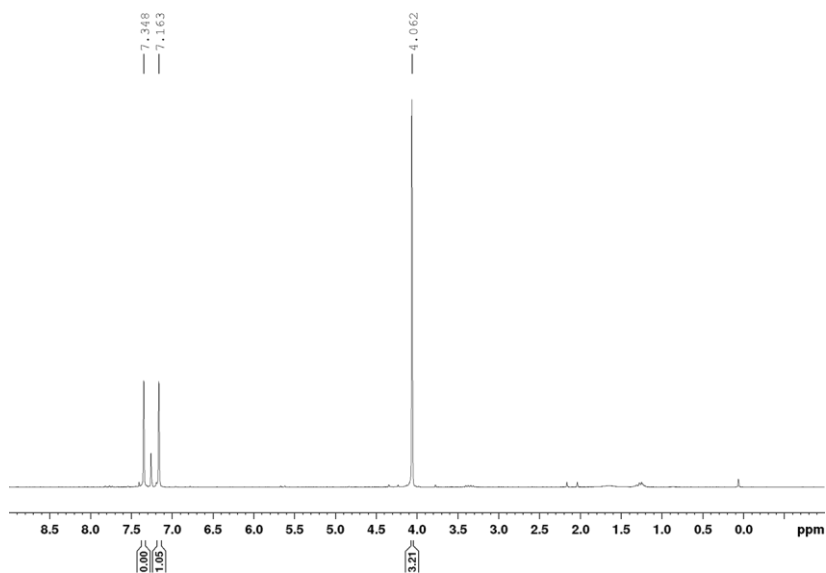


**Figure S6.** <sup>1</sup>H-NMR spectra of Im-CCl<sub>3</sub>.

NO<sub>2</sub>-Im-CCl<sub>3</sub>:

630 **<sup>1</sup>H-NMR** (300 MHz, CDCl<sub>3</sub>, δ): 7.95 (s, 1H, CH-1), 4.16 (s, 3H, CH<sub>3</sub>-2).

**<sup>13</sup>C-NMR** (75 MHz, CDCl<sub>3</sub>, δ): 173.0 (C=O), 146.0 (C<sub>q</sub>), 133.8 (C<sub>q</sub>), 126.1 (CH), 93.7 (CCl<sub>3</sub>), 38.4 (CH<sub>3</sub>).

**HRMS-Cl<sup>+</sup>** (*m/z*): [M+H]<sup>+</sup> calcd for C<sub>6</sub>H<sub>4</sub>Cl<sub>3</sub>N<sub>3</sub>O<sub>3</sub>H, 271.93965; found, 271.94021.

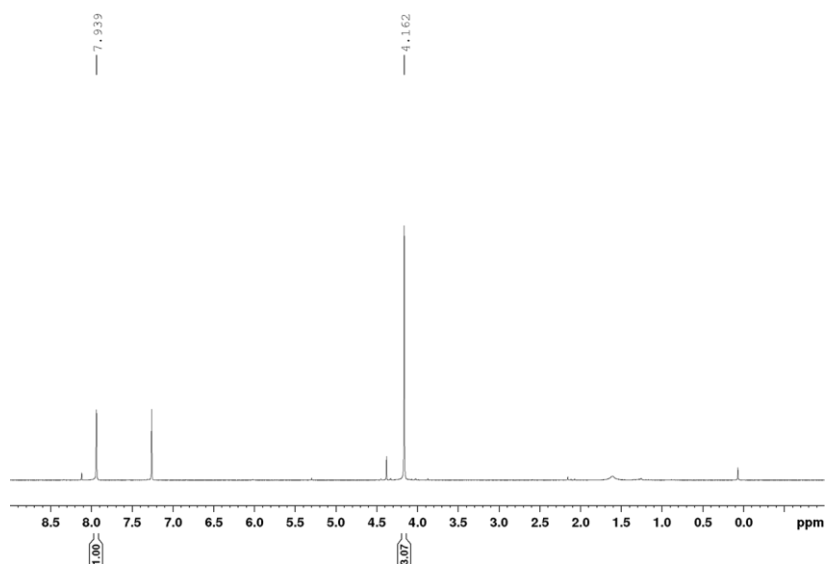


**Figure S7.** <sup>1</sup>H-NMR spectra of NO<sub>2</sub>-Im-CCl<sub>3</sub>.

635

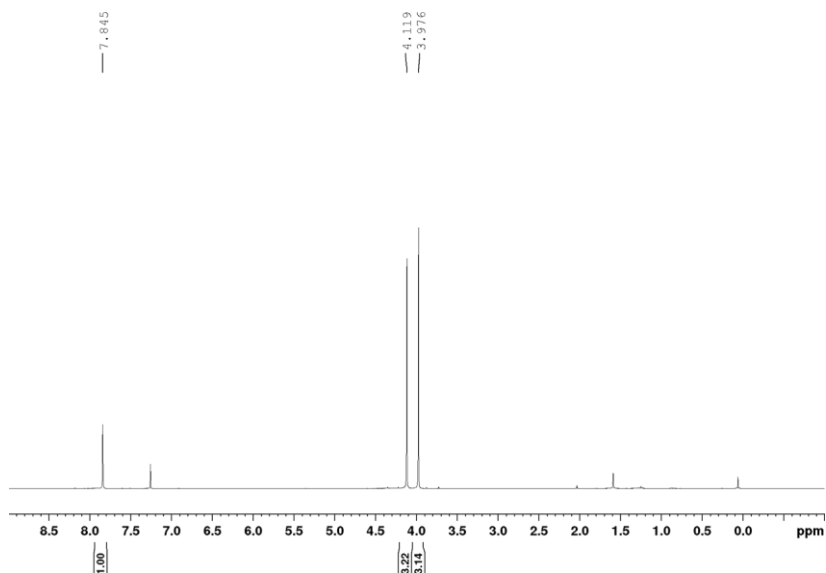
NO<sub>2</sub>-Im-OMe:

640

**<sup>1</sup>H-NMR** (300 MHz, CD<sub>3</sub>OD, δ): 8.29 (s, 1H, CH-1), 4.08 (s, 3H, CH<sub>3</sub>-2), 3.96 (s, 3H, CH<sub>3</sub>-3).

**<sup>13</sup>C-NMR** (75 MHz, CD<sub>3</sub>OD, δ): 159.6 (C=O), 142.9 (C<sub>q</sub>), 136.6 (C<sub>q</sub>), 126.9 (CH), 53.2 (CH<sub>3</sub>), 37.5 (CH<sub>3</sub>).

**HRMS-ESI<sup>+</sup>** (*m/z*): [M+Na]<sup>+</sup> calcd for C<sub>6</sub>H<sub>7</sub>N<sub>3</sub>O<sub>4</sub>Na, 208.0329; found, 208.0328.



645

**Figure S8.** <sup>1</sup>H-NMR spectra of NO<sub>2</sub>-Im-OMe.

Polyamide Hairpin Synthesis:

Figure S9 shows an exemplary HPLC-chromatogram of polyamide 1 after 4 couplings from the students' progress report.

650

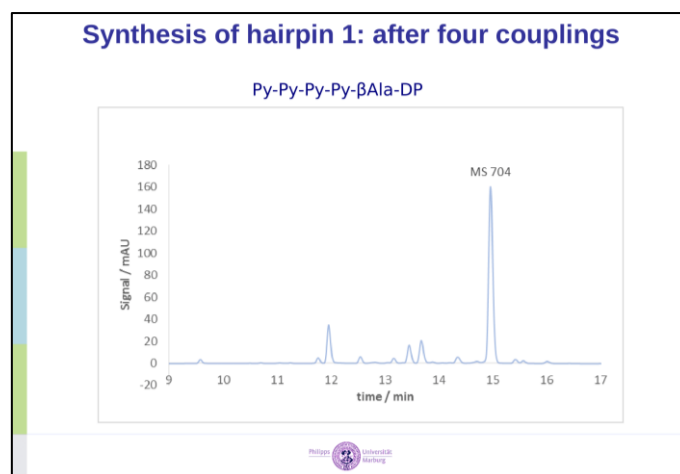
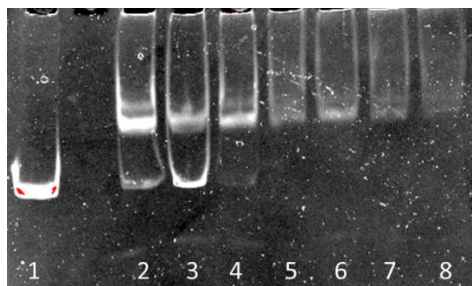


**Figure S9.** HPLC chromatogram of a test cleavage of polyamide 1 after 4 couplings with marked mass, which was found in the product peak. The figure represents a slide of the students' progress report seminar.

655

660 **PCR and nucleosome assembly**

In the figure below, lane-1 shows the free DNA-W601 from the PCR. Lane 2-8 are the results of nucleosome test assemblies with increasing amounts of histone octamers while keeping the DNA amount constant.

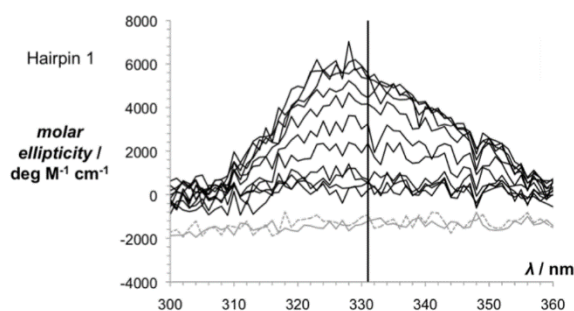


665

**Figure S10.** Native PAGE analysis of free DNA-W601 in lane-1 and nucleosome test assemblies in lane 2-8 with increasing amounts of histone octamers.

**CD-measurements**

670 Figure S11 shows an exemplary CD titration with polyamide **1** taken from a student's communication.

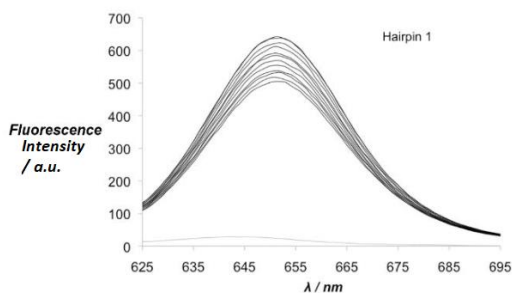


675

**Figure S11.** Exemplary CD titration of DNA with polyamide hairpin **1**. CD signal increase upon addition of more polyamide.

**FID-measurements**

Figure S12 presents an example of a student's result of the FID titration of polyamide **1** with 6-TramTO-3.



680

**Figure S12.** Exemplary FID titration of 6-TramTO-3 and DNA. Subsequent addition of polyamide resulted in a decrease of fluorescence signal intensity.

## Synthesis and characterization of polyamide hairpins as small DNA binder.

Name Surname <sup>[a]</sup>, Benedikt Heinrich <sup>[b]</sup> and Jun.-Prof. Dr. Olalla Vázquez <sup>\*[b]</sup>

**Abstract:** To study molecular processes, which are involved in changing expression patterns of DNA, have become a central issue in epigenetics. Repression of overexpressed histone deacetylases (HDAC) is one of the powerful tools against several cancer types. Polyamide hairpins have high potential as external DNA binders and are therefore potential anti-cancer drugs. Nowadays only a few numbers of DNA binding small molecules exist. Here, we show the immense potential of polyamide hairpins and provide a unique mechanism to establish inducible binding. We synthesized two new hairpins and determined the dissociation and sequence specificity to free DNA as well as nucleosome core particle (NCP). Our results demonstrate reliable binding of polyamide hairpins in order to minimize access to specific DNA sequences. Future studies will be directed in access hairpin controlled gene expression *in vitro*.

DNA is the genetic basis for nearly all organisms except phages. In humans, the DNA double helix is wrapped around histone octamers to form the nucleosome. The unit of the nucleosome is the nucleosome core particle (NCP) what can contain several modifications as histone sequence variants, posttranslational (PTM) modifications, mutations and more <sup>[1]</sup>.

Histone deacetylases (HDAC) regulate posttranslational modifications (PTM) of histone tails and therefore have an impact in DNA compaction. Due to less access of transcription machineries to the DNA with higher density, HDAC have consequently an impact in transcription. But HDACs have multiple roles. Some cause deacetylation of amino-terminal lysine residue at the tail of histone H3 and therefore promote tighter compaction of positively charged histones and negatively charged DNA. Beside this transcription repression they are also responsible for deacetylation of several non-histone proteins as sigma factors, signal modulators and play a major role in PTMs <sup>[2]</sup>. Nevertheless HDACs were found to be overexpressed in a broad range of cancer types <sup>[3]</sup>. For that reason find therapeutic targets for controlling aberrant HDAC expression remain a significant challenge for the next decades.

Hairpins or so-called Dervan hairpins are polyamides consist of *N*-methylpyrrole (py) and *N*-methylimidazole (im). These hairpins are used to target specific DNA sequence trough side-by-side recognition of the minor groove of DNA.

Dervan hairpins are used hence as synthetic ligands for external DNA binding. Consequently Dervan hairpins demonstrate their practical application against DNA deacetylation and further more as anti-tumor drug <sup>[4]</sup>.

For that reason we firstly synthesized two different hairpins. Accordingly, we characterize our newly synthesized compounds in circular dichroism (CD) and fluorescence intercalation displacement (FID), which is a highly competitive method to determine binding affinity. Further we analyzed the sequence specificity. To observe the sequence specificity was used a modified footprint method, which exclude the work with <sup>32</sup>P or <sup>33</sup>P radioactive labelled probes and therefore provide a facilitated laboratory use <sup>[5]</sup>.

Initially were synthesized two different hairpins, which varies in the arrangement of py and im (Fig. 1 (A-B)). According to the side-by-side recognition of im and py to the DNA double helix sequence specificity is generated for each hairpin individual (Fig. 1 (C)).

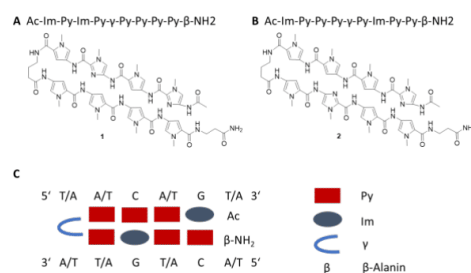


**Figure 1.** Synthesized hairpins. Hairpin 1 (A) and hairpin 2 (B) differ in amid arrangement and therefore in sequence specificity. (C) Shows sequence specificity of hairpin 2 and pairing rules. A: Adenine; T: Thymine; G: Guanine; C: Cytosine; Ac: Acetyl group.

Subsequent to characterize the newly synthesized hairpins were made some CD spectroscopy measurements. In order to induce chirality were used a DNA hairpin mixture and the molar ellipticity were determined from wavelengths 220 nm to 380 nm for hairpin 1 (Fig. 2).

As we can see from figure 2, hairpin 1 bound to the DNA and therefore an increasing molar ellipticity is observed around 325 nm. The general ability of hairpin 1 to bind to DNA could be hereby observed. As also indicated, that the

[a] Name Surname  
Faculty  
Philipps-University-Marburg  
Adress  
email: NAME@students.uni-marburg.de

[b] Jun.-Prof. Dr. O. Vázquez, B. Heinrich  
Chemical Biology  
Philipps-University Marburg  
Hans-Meerwein Strasse 4, 35032 Marburg, Germany  
email: vazquezv@chemie.uni-marburg.de

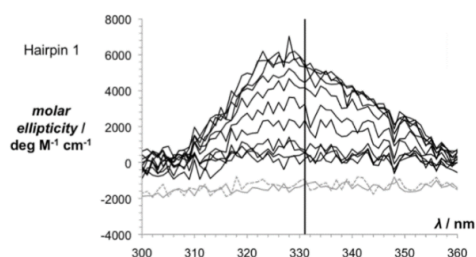


**Figure 2.** Induced CD spectroscopy of hairpin 1. In grey are measurements without addition of DNA or hairpin (discontinuous) and the second one without hairpin and with the addition of DNA (grey). In black are added increasing hairpin concentrations to DNA. The hairpin concentrations varies from 0,7  $\mu\text{M}$  to 33  $\mu\text{M}$ .

increasing ellipticity is coupled to an increasing amount of the hairpin. The lowest hairpin concentration causes the lowest shift as well as the highest hairpin concentration causes the highest shift as visible in figure 3. To further characterize the binding intensity of hairpin 1 the dissociation constant ( $K_D$ ) was calculated (Fig. 3).

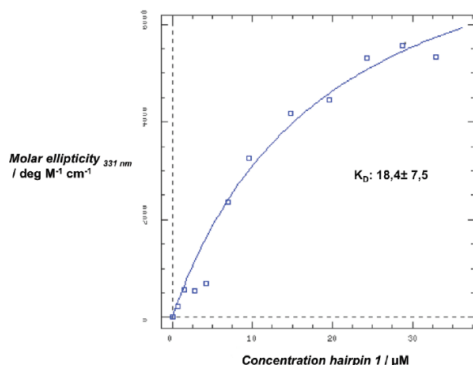


**Figure 3.** Molar ellipticity at 331 nm wavelength with various concentrations of hairpin 1 from 0,7  $\mu\text{M}$  to 33  $\mu\text{M}$ .  $K_D$  of 18,4  $\mu\text{M} \pm 7,5$   $\mu\text{M}$  was determined with DynaFit.

The  $K_D$  values correlate to already published constants that are in a range between 1,1 $\pm$ 0,3  $\mu\text{M}$  and 5,9 $\pm$ 0,7 nM for comparable polyamides [6]. Nevertheless the  $K_D$  value for hairpin 1 could be determined, according to the high standard deviation it is indicated that the measurements were less than ideal (Fig. 3).

To extend the characterization of hairpin 1 further fluorescence spectroscopy were performed to analyze the binding. It was chosen a competitive test. To test the binding affinity was used 6-TramTO-3 [7] cyanine dye triazole to label the DNA via fluorescence around 650 nm wavelengths. The dye is only detectable when intercalated into DNA. DNA and dye itself have no fluorescence (Fig. 4). With increasing concentrations of DNA binder (hairpin 1) the dye should be displaced and the fluorescence decreasing.

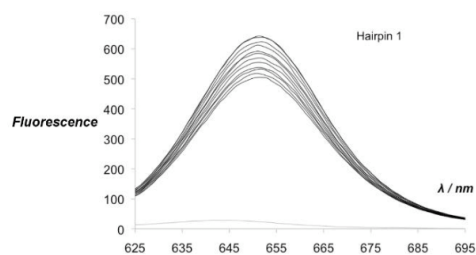


**Figure 4.** Fluorescence displacement with 6-TramTO-3 cyanine dye triazole. Detection of the binding of DNA to hairpin 1. In grey (discontinuous) was only added DNA; in grey was only added 6-TramTO-3 cyanine dye triazole. In black were used increasing amounts of hairpin 1 from 1  $\mu\text{L}$  to 10  $\mu\text{L}$  in addition to DNA and 6-TramTO-3 cyanine dye triazole. Stock concentration hairpin 1 was 216  $\mu\text{M}$ . Fluorescence intensities were followed from 625 nm to 700 nm.

As can be seen from figure 4 that hairpin 1 can successfully displace, with increasing concentration, the cyanine dye. According to previous CD spectroscopy measurements, were these results expected. It is confirmed that hairpin 1 could serve as small molecule binder. Even the conditions were not that precise and the measurements should be repeated.

After we showed that our hairpin bind DNA, it is important to prove the sequence specificity of hairpins in order to ensure an accurate gene repression. Therefore was used a footprint method. The method was modified. Instead of radioactive labeling was used 6-carboxyfluorescein (6-FAM). Free DNA (W601) and DNA (W601) coupled to histone octamers (NCP) were tested. According to amid arrangement (Fig. 1 (C)) of hairpin 2 were one potential binding site predicted (Fig. 6, red entangled). Footprint method is based on DNase fragmentation. Potential binders prevent specific sequence from disruption. Capillary electrophoresis generates afterwards a specific fragment pattern where each peak contains fragments with

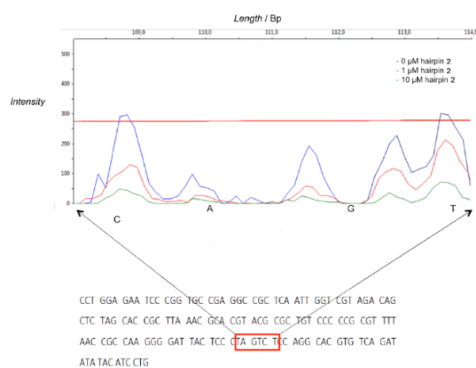


**Figure 5.** Detail of the predicted binder site. Top: Intensity of fragments with lengths between 108 bp and 114 bp. Hairpin 2 was used in two concentrations (0  $\mu\text{M}$  and 10  $\mu\text{M}$ ) with free DNA (50  $\mu\text{M}$ ). Bottom: DNA sequence of DNA W601. Red entangled: Predicted binder site. It was used 4 mU DNase I.



specific base pair (bp) length. The higher the intensity of the peaks the more fragments are developed. Fragment pattern of the potential binding site is shown in figure 5. At the predicted binding site were the results remarkable good. It is clearly visible that with increasing hairpin 2 concentrations the intensity of these fragments is decreasing. Because of the binding of hairpin 2 is the access for the DNase I limited. Consequently the fewer fragments were cut at this position the less fragments arise with this specific length.

It is suggested that hairpins can bind the minor groove of DNA. When DNA is associated to histone octamers for compaction seven minor grooves are potential binding sites. To characterize the hairpin further, it is most important to determine the sequence specificity to the NCP. The potential binding site was again investigated through footprint method (Fig. 6).

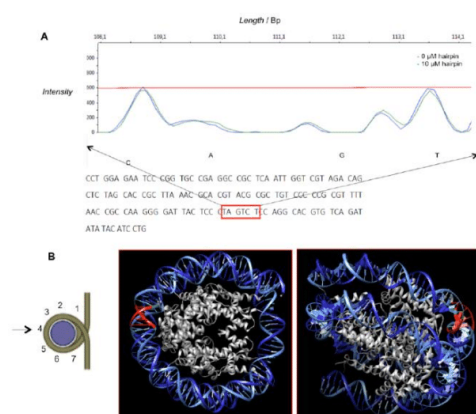


**Figure 6.** Potential binding site of hairpin 2 to DNA of NCP. It was used 0 μM and 10 μM hairpin 2 and 100 μM NCP. DNase I concentration was used 400 U (A). (B) Predicted binding site is located in the 4th minor groove of DNA (indicated in red). Blue: DNA double helix; Grey: Histone octamers [9] images were modulated with the help of UCSF chimera.

For the predicted binding site is no difference with or without hairpin 2 visible in fragment pattern intensity. In this case we cannot confirm the binding affinity of hairpin 2 to the NCP. More or less have to be checked further the potential binding site in context of the structural assembly. It might that there are steric hindrance problems due to interactions with the NCP that restrict the binding ability. Nevertheless the binding site seems free of histone tails or other visible elements (Fig. 6 (B)). Despite this, the experiments should be repeated to come to a final conclusion. Although the binding was not obtained experimentally, it can be assumed to be possible. These dates are not representative.

In conclusion it could be proved the general ability of polyamide hairpins as small DNA binding molecules. Furthermore the new synthesized hairpin 1 could be

characterized in binding to DNA via induced CD spectrometry and trough fluorescence displacement via fluorescence spectroscopy. Also for hairpin 2 the DNA binding was proven trough footprint. Reasonable results were also shown in sequence specificity of hairpin 2 to free DNA even when the binding to the NCP was not detectable. It is evident from the results the immense potential of polyamide hairpins as DNA binder. For investigations we also provide a modified footprint method to analyze specific binding sites, which ease the laboratory daily routine and showed a great application for fluorescence displacement.

As discussed previously are polyamides grateful tools to target specific sequences and interrupt the DNA-protein interaction as observed for DNase I. This might be transferred also to the interaction between transcription machinery and DNA. Finally it is possible to control the expression of specific DNA regions such as HDACs in order to limit the expression of these genes. Due to the nearly unlimited arrangement of the py and im monomers, this system offers a bright repertoire of targetable sequence. According to the pleiotropic role and relevance of HDAC in multiple completely different but essential cell processes, it remains a high risk of several unknown reaction in a potential in vivo application. This project opens a starting point for a new lineage of polyamide modifications and couplings. As outlined in the introduction are next steps to determine the efficiency of gene repression in vitro. But the non-natural small molecules, which bind DNA specifically, are potentially dynamic tools in human medicine.

## Experimental Section

### Hairpin synthesis, purification and analysis

Hairpins were prepared by solid-phase synthesis using *N*-Fmoc protected intermediate steps. Concentration and isolation were done and determined by HPLC [9].

### CD Spectrometry

For the CD measurements were used JASCO J810s CD spectrometer and Software SpectraManager. 5 μM DNA, 10 mM sodium phosphate 100 mM NaCl pH 7,5 were used to induce chirality.  $K_D$  was calculated through the program DynaFit. Spectra were measured from 220 nm to 380 nm.

### Fluorescence displacement

1 μM cyanine dye 6-TramTO-3 and 6 μM DNA in 10 mM Tris 50 mM KCl pH 7,6 with increasing amount of hairpin were used.  $K_D$  were calculated using the program DynaFit. Fluorescence were measured using a fluorimeter. Excitation wavelengths were used 610 nm and emission wavelength 625 nm-750 nm.



#### Footprint experiments

To reconstitute NCP were used 1 µg W601 DNA and histone octamers prepared from chicken erythrocytes. For assembly were performed NaCl from 2M to 50 mM salt gradient dialyses. It was used 50 ng DNA (W601) and 100 ng NCP601 with different concentrations of hairpin 2. For free DNA (W601) were used 4 mU DNase I and for NCP 400 U DNase I. Incubation time was 60s. To analyze the footprint pattern were used capillary electrophoresis.

## Acknowledgements

*Name Surname* was supported by the master course: interdisciplinary chemical biology approach to epigenetics, Philipps-University Marburg, Germany. I would thank Benedikt Heinrich for synthesizing the final Fmoc building blocks. Furthermore we would like to thank the complete AG Vázquez for their founding and support in all research stages.

*Conflict of interest statement.* Non declared.

**Keywords:** Amides • DNA recognition • Drug design

- [1] A. K. Shaytan, G. A. Armeev, A. Goncareenco, V. B. Zhurkin, D. Landsman, A. R. Panchenko *J. Mol. Biol.* **2016**, *1*, 221-237.
- [2] E. J. Noonan, R. F. Place, D. Pookot, S. Basak, J. M. Whitson, H. Hirata, C. Giardina, R. Dahiya *Oncogene* **2009**, *28*, 1714-172.
- [3] S. Yoon, H. Eom *Chronam Med. J.* **2016**, *52*, 1-11.
- [4] G. Kashiwazaki, T. Bando, T. Yoshidome, S. Masui, T. Takagaki, K. Hashiya, G. N. Pandian, J. Yasuoka, K. Akiyoshi, H. Sugiyama *J. Am. Chem. Soc.* **2012**, *55*, 2057-2066.
- [5] B. Ying, D- Fourmy, S. Yoshizawa *RNA* **2007**, *11*, 2042-2050.
- [6] L. N. Schulte, B. Heinrich, H. Janga, B. T. Schmeck, O. Vázquez *Angew. Chem. Int. Ed.* **2018**, *57*, 11564-11568.
- [7] M. Minoshima, T. Bando, S. Sasaki, J. Fujimoto, H. Sugiyama *Nucleic Acids Res.* **2008**, *9*, 2889-2894.
- [8] D. Vasudevan, E. Y. D. Chua, C. A. Davey *J. Mol. Biol.* **2010**, *1*, 1-10.
- [9] E. E. Baird, P. B. Dervan, *J. Am. Chem. Soc.* 1996, *118*, 6141-6146.

# Exploring the Substrate Scope of MOF Catalyst for p53 Acetylation and Validating the Influence of PHF20 on p53 Acetylation

Fachbereich Chemie und Fachbereich Biologie, Philipps-Universität Marburg (Germany)

## MOF-KAT

MOF is a lysine acetyltransferase which belongs to the MYST family. MOFs main function is depositing an acetylation to histone H4K16, but it also targets other histones as well as non-histone proteins. It contributes to DNA damage and repair, cell survival and gene expression regulation. In humans it occurs in two different protein complexes, the MOF-NSL and the MOF-MSL complex. Only the MOF-NSL complex targets p53 K120.<sup>[1]</sup>

## Click-Chemistry

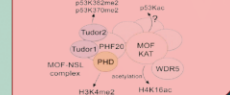
Click-chemistry is the generic term for a wide variety of highly reliable, powerful and selective reactions for rapid synthesis through heteroatom links (C-X-C). Reactions that are click-chemistry have to be in scope and give very high yields. They should have only unreactive by-products which must be removable without chromatographic methods. A good stereospecificity and simple reaction conditions are necessary for click-chemistry as well as available starting materials and no or benign solvents (e.g. H<sub>2</sub>O) and easy product isolation.<sup>[1]</sup>

Recently PHF20 has been shown to regulate MOFs acetyltransferase activity acetylating H4K16. Since MOF also acetylates p53 which is an important tumour suppressor, the question arose whether p53 acetylation by MOF is also dependent on PHF20. Therefore we will perform in vitro and cell culture experiments to test this. Click chemistry can be used to detect acetylations. Different derivatives of acetyl-CoA are prepared which serve as substrate for acetylation. In a second step these acetylations can be tagged with fluorescence or purification tags. We use this approach to analyse the in vitro as well as the cell culture experiments via fluorescence (in vitro) and also to purify all acetylated products from the cell lysates. We also use western blot and LC-MS<sup>n</sup> for analysis. In the in vitro assay several proteins are combined and analysed. For cell culture experiments we knock down PHF20 in one cell line and compare its acetylation level at p53 K120 with the acetylation levels acquired in the wild type.

PHF20 is a component of the MOF-NSL complex and regulates MOFs acetylating activity. The regulatory mechanism for H4K16 acetylation through MOF by PHF20 depends on the PHD subunit of PHF20 (shown below) binding to H3K4me3. PHF20 subunit Tudor2 binds to p53 at K370me2 and K382me2, this interaction leads to stabilization and activation of p53. It may be that acetylation of p53 at lysine 120 done by MOF is also dependent on or influenced by PHF20.<sup>[2]</sup>

## PHF20

PHF20 is a component of the MOF-NSL complex and regulates MOFs acetylating activity. The regulatory mechanism for H4K16 acetylation through MOF by PHF20 depends on the PHD subunit of PHF20 (shown below) binding to H3K4me3. PHF20 subunit Tudor2 binds to p53 at K370me2 and K382me2, this interaction leads to stabilization and activation of p53. It may be that acetylation of p53 at lysine 120 done by MOF is also dependent on or influenced by PHF20.<sup>[2]</sup>



p53 is a tumour suppressor and a transcription factor. It is involved in cell cycle arrest, apoptosis, DNA damage response and metabolism. In the vast majority of tumour diseases p53 is mutated or deleted. This makes it a very attractive target for cancer treatment. Despite p53 being well characterized, there is still no general treatment applicable in p53 compromised tumours. So every new compound associated to p53 and influencing its function could harbour a new possibility to target p53 and result in a cancer treatment option.<sup>[3]</sup>

## p53

## Synthesis:

-Sodium acetate salts

-Coenzyme A derivatives

-Azido-diazo-biotin

-H4 tail 1-19 aa

## In vitro Experiments:

Different protein combinations with MOF

Acetylation detection with:

-Western blot

-LC-MS<sup>n</sup>

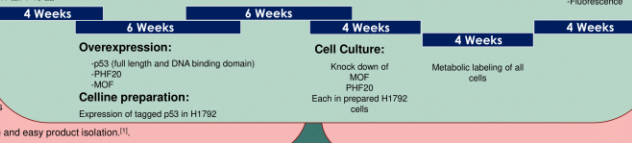
-Fluorescence

Acetylation detection with:

-Western blot

-LC-MS<sup>n</sup>

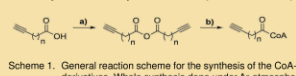
-Fluorescence



- The first step the synthesis of all needed compounds which are:
- 1) Coenzyme A derivatives as substrates for the in vitro assay
  - 2) Corresponding Sodium-acetate salts which are used in metabolic labeling
  - 3) Azido-diazo-biotin is going to be the tag in the cell culture experiments to extract all acetylated compounds from the lysate

## Synthesis of the Substrates

General synthesis of coenzyme A derivatives (time needed: ~ 5 h):

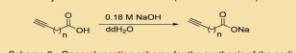


Scheme 1. General reaction scheme for the synthesis of the CoA-derivatives. Whole synthesis done under Ar-atmosphere

a) Formation of the anhydride: 2 eq carboxylic acid in anhydrous DCM, N,N'-dicyclohexylcarbodiimide (DCC) added, stirred for 4 h at r.t.

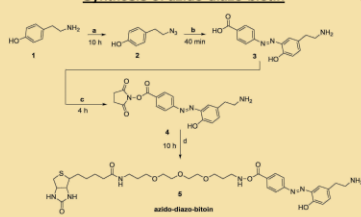
b) dry crude product of a) solved in anhydrous DMF at 0°C, 0.2 eq coenzyme A hydrate (CoA) and 0.6 eq Et<sub>3</sub>N added, stirred for 30 min at 0°C.<sup>[4]</sup>

General synthesis of the sodium salts (time needed: ~ 1h):



Scheme 2. General reaction scheme for the synthesis of the sodium salt derivatives. 1 eq of the carboxylic acid solved in ddH<sub>2</sub>O and NaOH added dropwise. Mixture filtered through membrane, frozen in N<sub>2</sub> and lyophilized to dryness.<sup>[4]</sup>

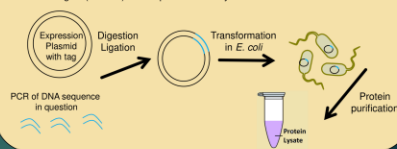
## Synthesis of azido-diazo-biotin



Scheme 3. Synthesis of azido-diazo-biotin (5): a) To an ice-cooled solution of NaN<sub>3</sub> (1.44 eq) in CH<sub>2</sub>Cl<sub>2</sub>, slowly added T<sub>1</sub>O<sub>2</sub> (1.2 eq) and stirred for 2 h at 0°C. A solution of tyramine (3.00 eq) in CH<sub>2</sub>Cl<sub>2</sub> added and stirred for 8 h at 0°C. (lit.: 96%) b) NaNO<sub>2</sub> added to ice-cooled suspension of 4-aminobenzoic acid in 6M HCl (40 mL), stirred at 0°C → reaction colour turned yellow. (2) (1 eq) dissolved in cooled THF at 0°C. K<sub>2</sub>CO<sub>3</sub> added subsequently to reach pH=8. Diazonium salt solution added slowly to (2) at 0°C. pH kept around 8 by adding K<sub>2</sub>CO<sub>3</sub>. (lit.: 45-55% over two steps) c) (3) (1 eq) dissolved in anhydrous THF. DCC (1.09 eq) and N-hydroxysuccinimide (1.09 eq) added under Ar-atmosphere. Stirred for 4 h at r.t., concentrated in vacuum, crude solid residue dissolved in chilled EtOAc. Urea filtered off. (lit.: 79%) d) Biotin-PEG-NH<sub>2</sub> (2 eq) added to solution of (4) in anhydrous DMF. (lit.: 80%)<sup>[4]</sup>

## Protein over expression

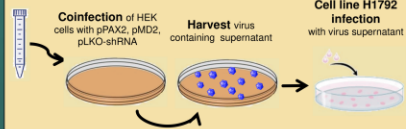
All proteins needed in the in vitro assay are expressed and purified from *E. coli*. These are: p53, PHF20, MOF and only the DNA binding domain of p53 (DBD). The H4 tail region (1-19 aa) can be purchased or synthesized.



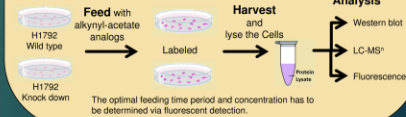
For the cell culture experiments our wild type cell line H1792 has to be modified at first, because we need it to express tagged p53 that we can purify p53 before analysing the acetylation with LC-MS<sup>n</sup>. This is done with the same procedure as the knock down of PHF20. Finished cell lines: H1792 expressing tagged p53, H1792 expressing tagged p53 and knock down of PHF20

## Cell culture experiments

PHF20 knock down: is done with a PHF20 targeting shRNA. A virus containing the shRNA is generated as vector. The knock down is verified by western blot [7]



Metabolic labeling: The wild type cells as well as the knock down cells are fed with alkynyl-acetate analogs



## Conclusion

PHF20 might be involved in acetylation of p53 K120 through MOF and will be clarified in this project. The necessary chemical compounds and proteins will be synthesized through straightforward routes and protocols using the combined skill set of synthetic chemistry and molecular biology. In vitro the performance of MOF will be monitored prior to experimenting with and without PHF20 in the acetylation mixture. Analysis will be carried out with three methods. Detection via fluorescence-marker in cooperation through click-chemistry, digestion and fragment analysis via LC-MS<sup>n</sup> and finally through immunoblotting. Experiments in cell culture use a knock-down PHF20 cell line as well as a wild type PHF20 cell line. The click-chemistry approach is used to separate the labeled proteins from the matrix. The analytic can proceed as in the in vitro experiments.

## In vitro Experiments

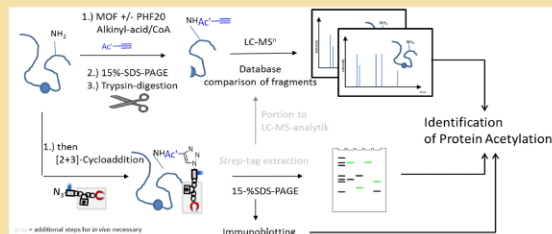
To investigate whether p53 acetylation at lysine 120 by MOF is influenced by PHF20 in vitro the following reaction mixtures are prepared (Diagram step 1):

- 1) Control: MOF + H4K16 + Substrate [7]
- 2) MOF + p53 + Substrate
- 3) MOF + p53 + PHF20 + Substrate
- 4) MOF + p53 DBD + PHF20 + Substrate

Lysine 120 lies within p53s DNA binding domain, it is interesting to investigate if acetylation occurs just on a separate domain

Three approaches serve for detection of acetylation of p53:

- 1) LC-MS<sup>n</sup> (the reaction mixture is separated via SDS, then trypsin digested before injecting to the system.)
- 2) Fluorescence: Here the click chemistry is used to add a fluorescent tag onto all acetylated sites. The mixture is separated over SDS PAGE and the gel can be analysed directly
- 3) Immunoblotting is also used where antibodies are used to mark acetylated p53

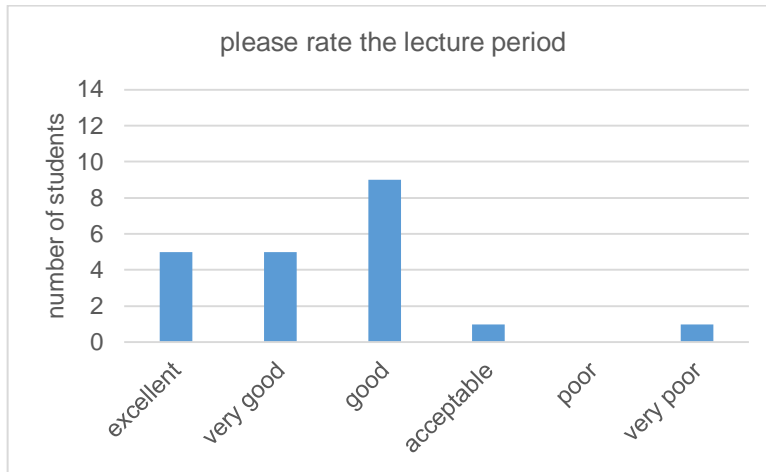


[1] H. C. Kott, M. G. Finn, K. B. Sharpless, *Angew. Chem. Int. Ed.* 2001, 40, 2004-2021 [2] D. P. Lane, *Nature*, 1992, 15-16 [3] S. M. Skyes, H. S. Mellert, M. A. Hober, K. L. R. Marmostein, W. S. Lane, S. B. McMahon, *Mol. Cell* 2006, 24, 841-851 [4] Y.-Y. Yang, J. M. Ascano, H. C. Hang, *JACS* 2010, 132, 3640-3644 [5] Z. Kaczmarek, E. Ortega, A. Goudarzi, H. Huang, S. Kim, J.A. Marquez, Y. Zhao, S. Khochbin, D. Panne, *Nat. Chem. Biol.* 2017, 13, 21-29 [6] 10.2210/pdb2zqz/pdb [7] Klein et al., *cell reports* 2016, 17(4), 1158-1170 [8] Q. Y. Chen, *AIMS Biophysics* 2015, 2(4), 555-569

## EVALUATION RESULTS

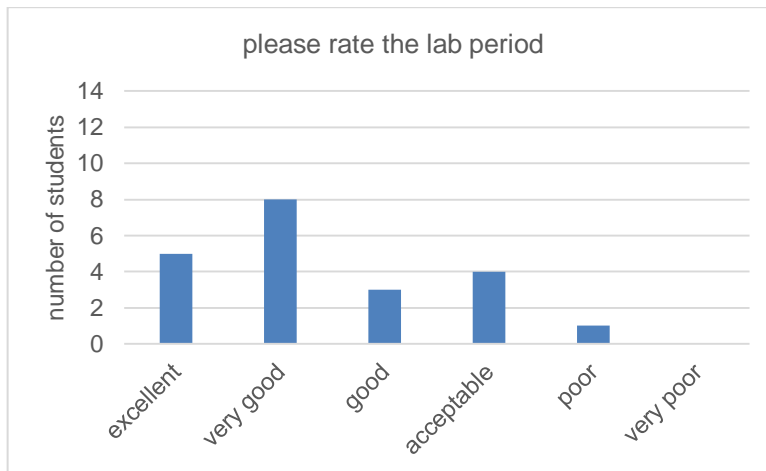
695 At the end of the course, the students were asked to evaluate the course. We used Likert scale and open-ended questions to collect the answers. The results and answers from the cohort in 2016/2017 and 2017/2018 were combined and are represented in the following. In the open-ended questions, the answers of the individual students were marked in italic from a to l.

### 1) Please rate the lecture period



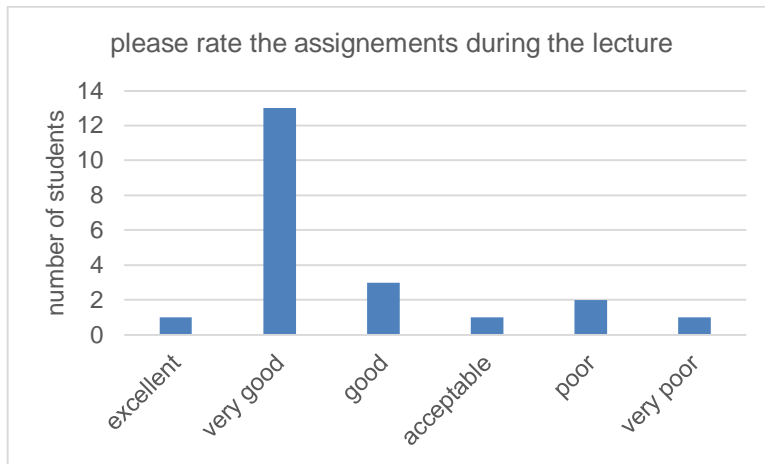
700

### 2) Please rate the lab period



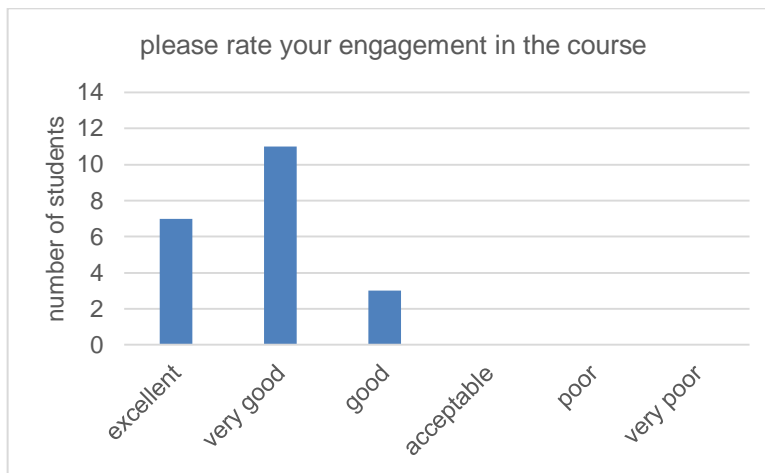
705

3) Please rate the assignments during the lecture

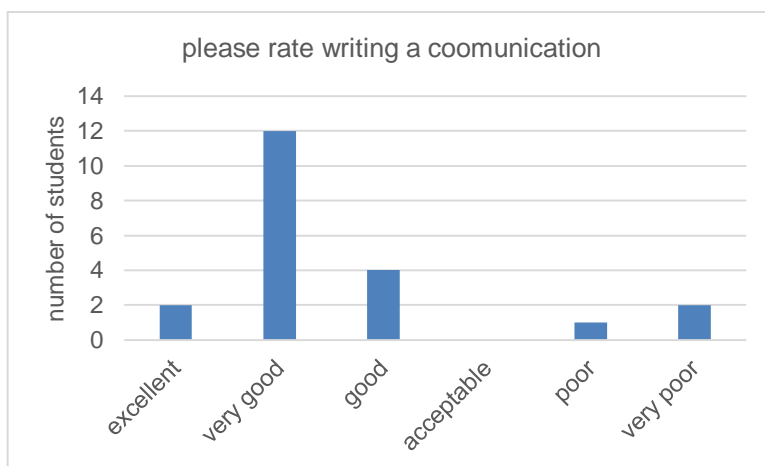


710

4) Please rate your engagement in the course

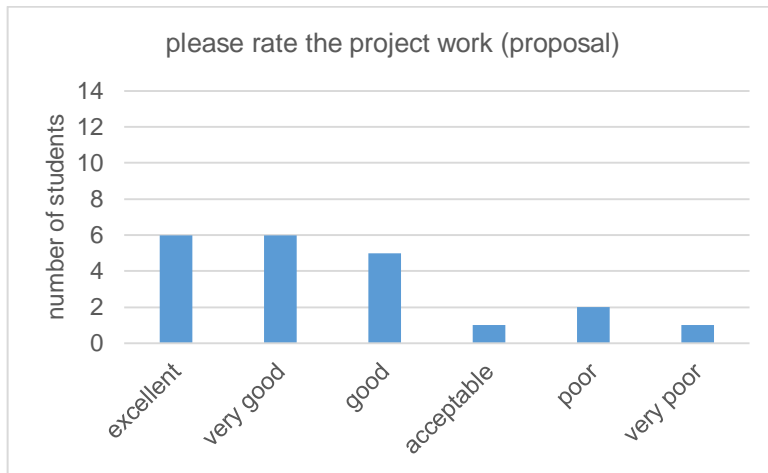


5) Please rate writing a communication



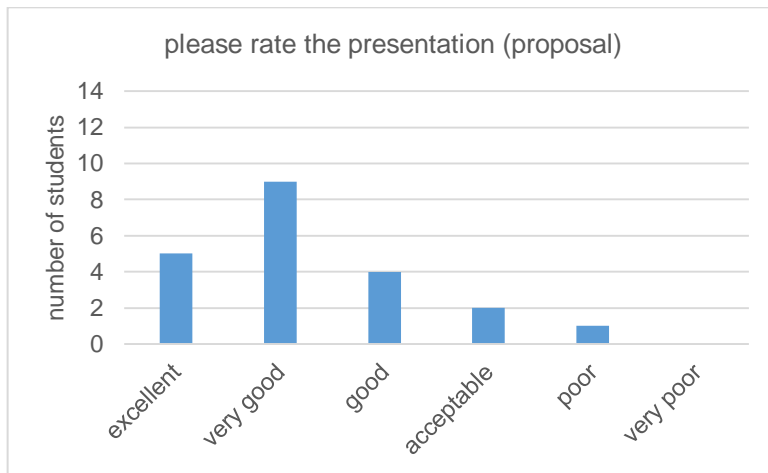
715

6) Please rate the project work (proposal)



720

7) Please rate the presentation (proposal)



8) What do you think was the most valuable part of the course for you personally?

725

- a. *Learn how to write scientifically and communicate.*
- b. *Doing the proposal.*
- c. *Communication.*
- d. *The lessons about the scientific writing.*
- e. *Interacting with students of other disciplines and the writing of a paper and a communication.*

730

- f. *To work interdisciplinary and to get to know a new research field.*
- g. *The whole course felt more like a group project, which is very nice. We got to learn how to work as a group on different topics in the lab course and designing the fictitious project was a fun and also very valuable experience, because finding a research gap is a very important skill of scientists that isn't really trained during other courses.*

- 
- 735 h. *I really like to have the interdisciplinary part of the course. Working together with chemists and biologists was really interesting and I got some new insights in some biologic work and thinking.*
- i. *This course really guide us to know how real research works (writing a paper, design experiment, developing ideas, create and present poster). Discussing ideas within an*
- 740 *interdisciplinary group was also a great experience.*
- j. *Refreshing some basic chemistry not used often in biological courses outside of mandatory chemistry lessons at the start of the bachelor. Additionally the use of language when writing scientific articles or protocols. It is expected of the students to write in English but the specific terminology is never focused on in any of the usual*
- 745 *courses.*

9) Can you describe your experience interacting with the other students?

- a. *Was a lot of teamwork, we wrote a lot, skyped, the others were fine. We helped us, was a good atmosphere.*
- 750 b. *Very good, one of the best thing of the course.*
- c. *Very productive and friendly working environment.*
- d. *Interaction was very valuable as well, because it felt like all students had different backgrounds and knowledge that could really come together in the proposal.*
- e. *It was really nice to work in groups and get new contacts and discuss also with other*
- 755 *students from another department and see their point of few to different themes.*
- f. *It was a really great experience to discuss the ideas, the project with the teammate. It really push us to think how we can make the project better, we really complete each other and managed to create a project for the poster.*
- g. *Everything went really well, everyone was helping each other to understand the*
- 760 *lectures, the lab work etc.*

10) What was the biggest challenge for you in the course?

- a. *Writing and formulating the thoughts about the research for everybody in the course understandable.*
- 765 b. *Making a somewhat complete story out of the course to write the communication about.*
- c. *Time.*

11) What would you recommend, what we should definitely keep in the future?

- 770 a. *The lab work and Poster session.*
- b. *Communication, Proposal, lab course and maybe theoretical lessons within the semester.*
- c. *The combination of writing a communication and presenting the proposal as a poster.*

- 
- 775
- d. *Mixing chemistry and biology students, since we see the things from "the other side".*
  - e. *The way that you interact with the pupils.*
  - f. *The writing part was good. Keep that.*
  - g. *Changing the groups - although it is sometimes hard, but this is how it's going to be in the future, we cannot always choose who we are working with, so it really close to reality. Also the poster - much work, but definitely worth it because I learnt so much*
- 780 *about the other discipline and chemical biology and had the chance to ask any question that came in my mind and discuss it in the group.*

12) To what extend do you think, did the course change your perspective on interdisciplinary research?

- 785
- a. *It reinforced my opinion on the importance of interdisciplinary research.*
  - b. *It will definitely. I saw the power of interdisciplinarity. Also it was very inspiring during the work on the proposal.*
  - c. *It changed it, I am now not as "afraid" as before to read a chemical paper and I learned and read about chemical methods which I didn't have in my head as helpful*
- 790 *for biology.*
- d. *Beside the benefits of different point of view as well as different methodology for the same research question, communications between the fields seem to be a bigger topic than I thought.*
  - e. *I would like to work in an interdisciplinary research field in the future.*
- 795
- f. *Interdisciplinary research is the future science.*
  - g. *The course got me really interested on the chemical biology and even more on the epigenetic topic and by designing our own project, we got to get an understanding of how you could apply knowledges from both disciplines.*
  - h. *I have learned new things and other ways of thinking.*
- 800
- i. *Before I didn't pay much attention to the application of chemical methods for biology but the course introduced me to the ideas of using small molecules and chemical reactions in biological systems.*

13) To what extend do you think, did the course change your perspective on scientific writing?

- 805
- a. *I really learned what "keywords" are useful in scientific writing. This helped a lot.*
  - b. *It has improved during the course a lot, because now I understand how is a paper structured and where to get the information. How to argue and present myself and my results.*
  - c. *It clarified the processes of writing and gave strategies not only for writing but also for*
- 810 *reading.*
- d. *A lot. It was always something I was scared of but now after finishing this course, I think that with practice it will get a lot better.*

- 
- e. *More self-confident.*
  - f. *No one has ever taught us the method of scientific writing. This is my first contact with and learning about science writing. Thank you very much.*

815

14) Do you think that this course is different from what you have done before? If yes, what are the main differences?

- a. *The overall system is way better than normal lab courses or lectures, especially the poster session is a new part, because one has the possibility of thinking about new ideas and not repeating old scripts.*
- b. *Yes. The interaction between students and the teachers were much more intensive. Somehow for me it was like giving a sense for what I am actually doing, it increased my motivation a lot. The combination of Theory, practical stuff and in the end the communication was in my point of view perfect.*
- c. *A lot of teamwork.*
- d. *Yes! More interactive working, learning of scientific writing, theoretical and practical work together with the same content.*
- e. *Yes, the active involvement of the students was bigger. The interconnection between practical course and lab was new.*
- f. *Yes it is. Different approaches with students from chemistry and biology working together and different theme (dealing with how to write scientific texts in a proper way).*
- g. *Yes, it felt more like a real world project, more like we are actual scientists. I really enjoyed actually using my knowledge and not just following instructions!*
- h. *It was different in that part that chemists and biologists work together in groups and see the different ways of thinking, which are varying between the two sciences.*
- i. *Yes. Before we only knew how to write protocol, which actually in real research we are not going to write protocol, but mostly paper, poster, and presentation.*
- j. *Yes, a lot more team work, a lot more support of the professors and supervisors.*
- k. *Yes, real improvement in skills and learning. In the process of completing the poster, I really understood how to do scientific research by discussing and reading the literature.*
- l. *Yes, usually in courses the students either work alone on a topic or in set groups that won't change during the course. The constant changing of groups allowed to work with different people throughout the course and related subjects.*

820

825

830

835

840

845

15) Does this course changed your perspective of biology and chemistry as separated disciplines? Why?

- a. *During the course I really experienced how colleagues from other departments contributed to the way of solving a problem. It was nice and inspiring to see their ways of approaching a problem with their methods.*

850



- 
- b. *Yes, it all depends more than I thought.*
- c. *Yes, a lot.*
- d. *I think they are very much connected and you can't look at them as separate disciplines.*
- 855
- e. *Yes, because you learn how to combine both.*
- f. *I don't think so. On the contrary, for the first time, I realized how interdisciplinary research links two different disciplines. Although the course was over, I continued to read the literature in the related field and the book the professor had recommended because it benefited a lot.*
- 860
- g. *No, before I also thought it is not a great gap between biology and chemistry.*

16) Do you think that both divisions (chemistry and biology) can work in a synergistic way?

Why?

- 865
- a. *Sure they can... biologist work with "living" systems they observe the whole organism, they have a broader view on things... but when it comes to molecular levels chemists can explain things a lot more in detail.*
- b. *Yes because they can complement each other really well.*
- c. *Of course, better overview of the whole subject, resulting in a better understanding.*
- 870
- d. *Yes, because there is a need of new perspectives to solve.*
- e. *I think the synergistic way is the only way for future.*
- f. *It feels like the biggest research topics are in medical science/biology. By applying chemical methods like synthesis or analysis methods, you can really help to solve problems that are not as easy from the biological standpoint.*
- 875
- g. *Yes, because the two disciplines are really close and can learn a lot from each other. Problems can be solved in the one discipline with the help of the other.*
- h. *Yes, because the challenges are seen from different ways.*
- i. *Of course they can, there is basically no real separation and if both parties are enthusiastic and able, the cooperation will bear rich scientific yield.*
- 880
- j. *Yes, it is proven already by our research proposal (poster) that we can solve problem with chemical biology approach.*
- k. *Yes, I think not only chemistry and biology can work together, but even more cross-cooperation with pharmacy or physics. For example, the intracellular binding sites can be better detected by different electron microscopy methods. Many problems in biochemical synergy research can solve pharmaceutical applications.*
- 885
- l. *Yes. During the development of the research proposal has shown that we often approached a task from different perspectives. The biologists were often focused on the 'bigger picture', which part of a biological system to target or which organism for example. The chemistry students however were very helpful in finding the specific molecule and the chemical processes required to target them.*
- 890

---

17) Do you have the feeling that interactions and problems solving between chemists and biologists went in both directions or just in one?

a. *In both directions.*

b. *In both.*

895

18) Do you think that writing the communication give you a better overview than the traditional separate protocols? Why?

a. *Yes, a communications gives one a "big picture" of a research project.*

b. *Yes! By writing a paper I learned a lot about the way of doing research, informed and get an overview of the recent research topic.*

c. *Yes because you were confronted to really make something out of the data we got and not just write it down and if something didn't work just write that also.*

d. *Yes because it's not just writing down the results, it is a kind of presenting the results.*

e. *Yes it does since one is forced to think a bit more about what was done in the course.*

f. *Yes, communication gives you an overview about the problem and how you solve it.*

g. *Yes. In separate protocols you only concentrate on the results you get and what they mean. In a communication you also have to combine everything in a bigger picture.*

900

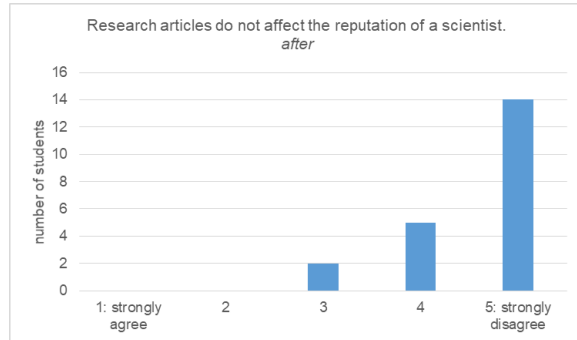
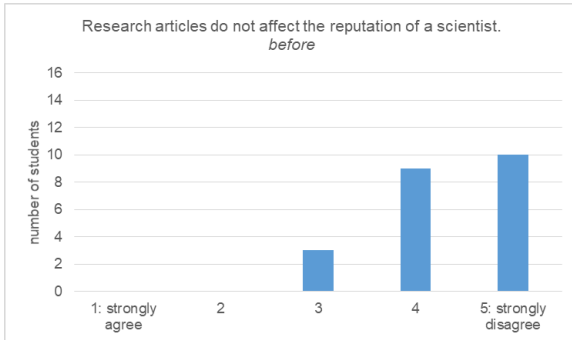
905

910

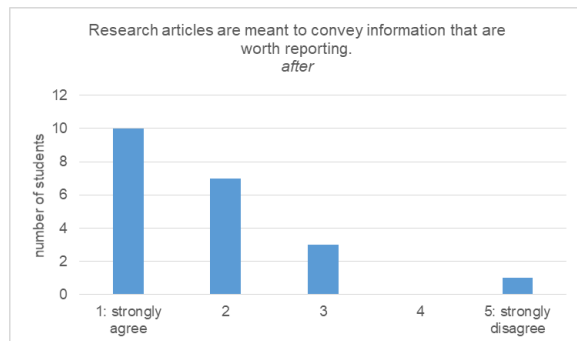
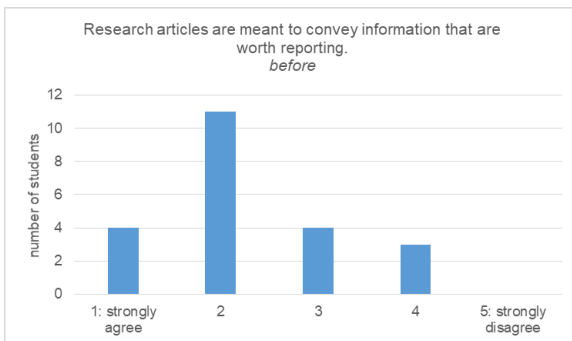
## NATURE OF SCIENTIFIC PRACTICE SURVEY RESULTS

The students performed a nature of scientific practise survey in the beginning and at the end of the course. The results from before and after the course are represented in the following:

915 1) Research articles do not affect the reputation of a scientist.

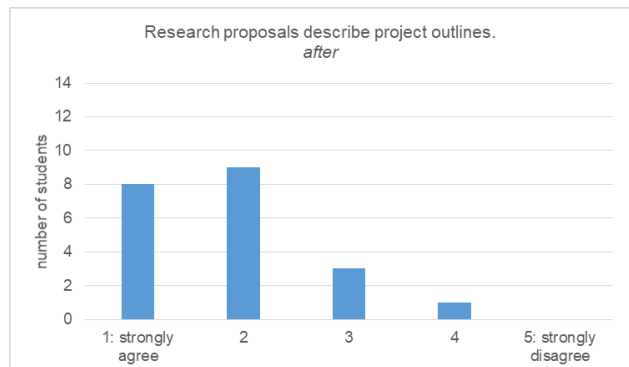
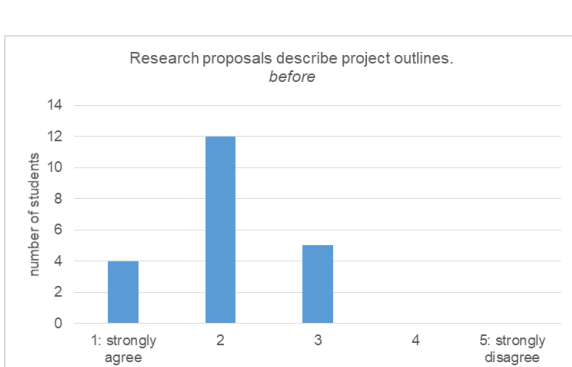


2) Research articles are meant to convey information that are worth reporting.

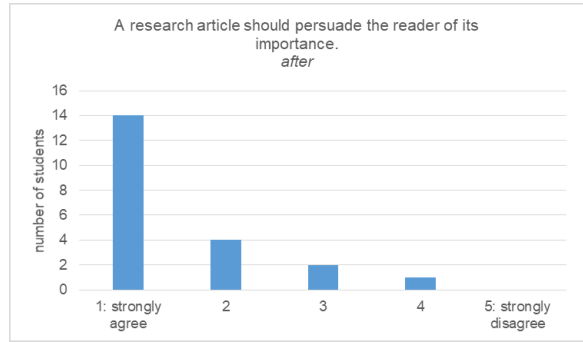
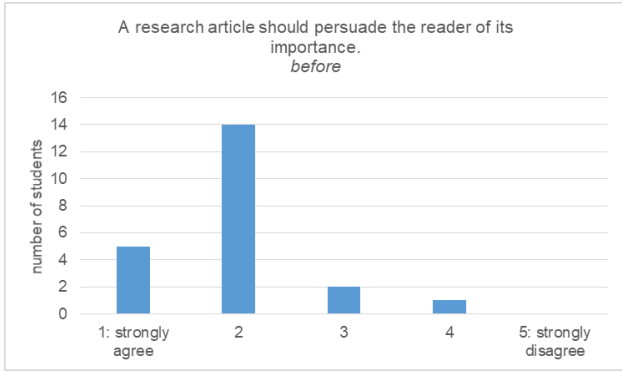


920

3) Research proposals describe project outlines.

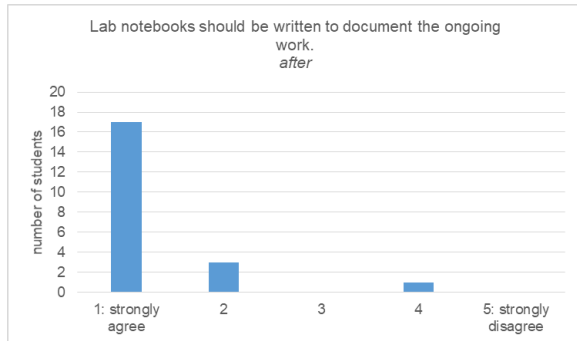
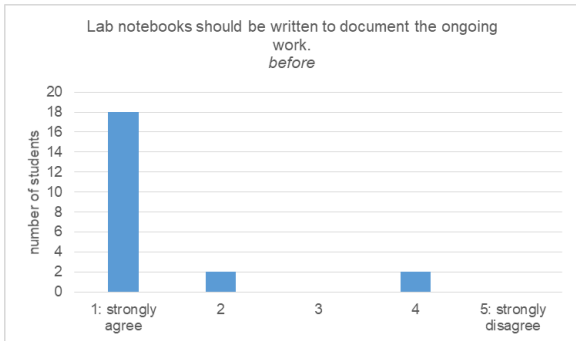


4) A research article should persuade the reader of its importance.

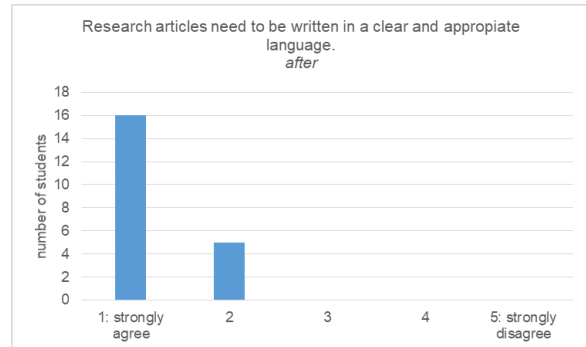


925

5) Lab notebooks should be written to document the ongoing work.



6) Research articles need to be written in a clear and appropriate language.

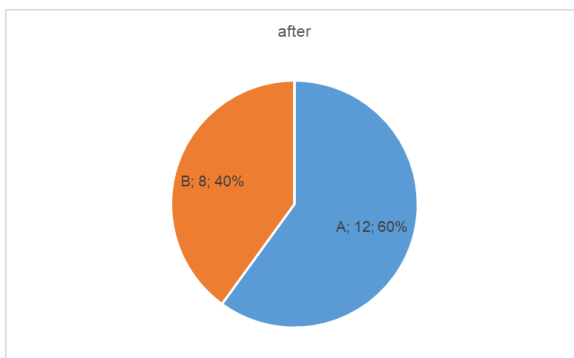
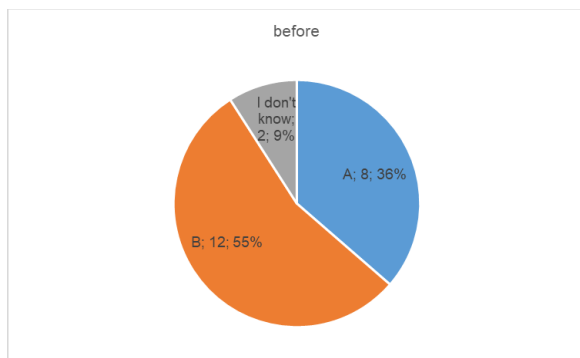
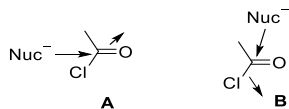


930

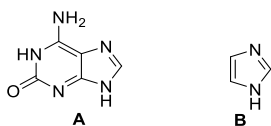
## ORGANIC CHEMISTRY SURVEY RESULTS

The students performed an organic chemistry survey in the beginning and at the end of the course. The results from before and after the course are represented in the following:

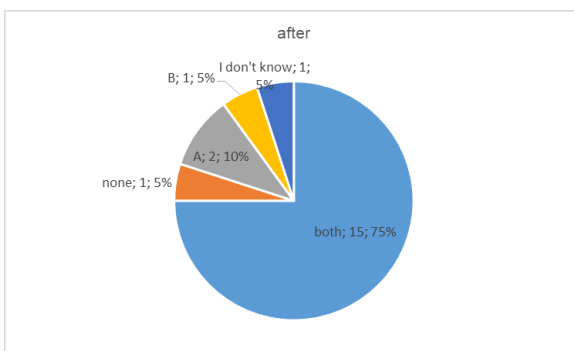
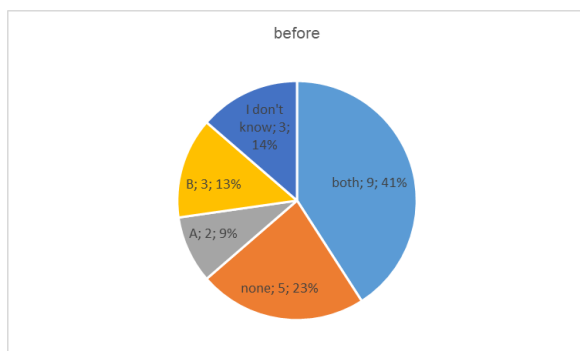
935 1) Indicate the direction of the reaction step.



2) Which molecule is aromatic?

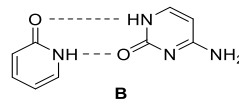
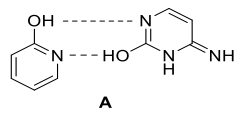


940

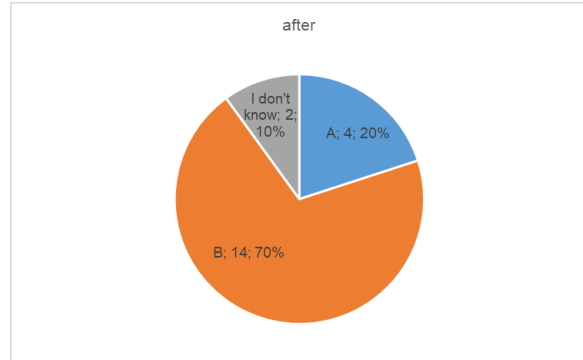
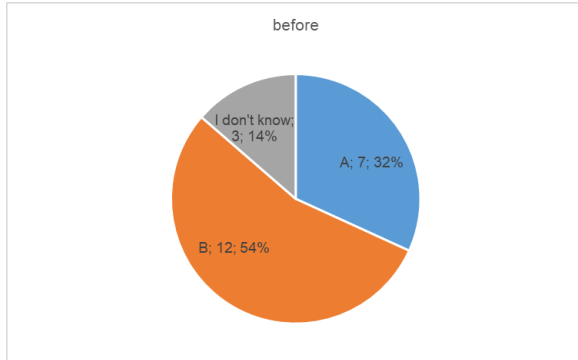


945

3) Which interaction is more favoured?



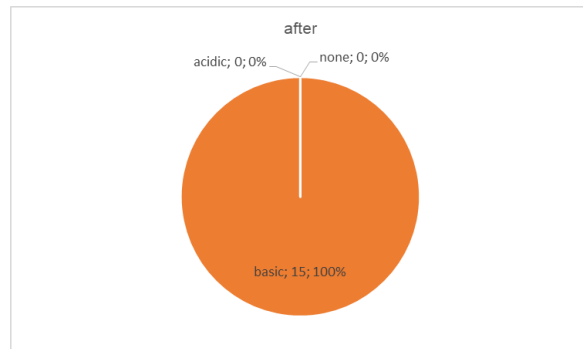
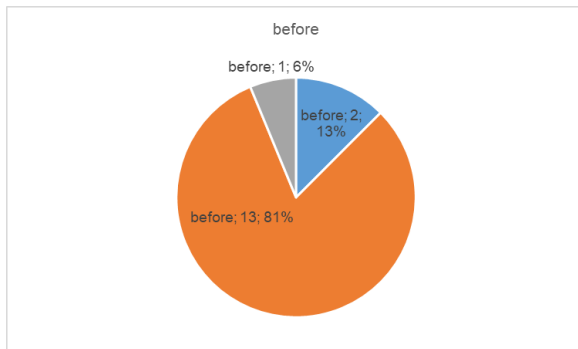
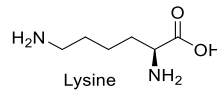
950



4) Which property are you expecting from the amino acid lysine?

- a. Acidic
- b. Basic
- c. Nonpolar (hydrophobic)
- d. Polar (uncharged)+
- e. Other

955

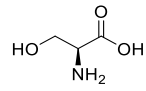


960

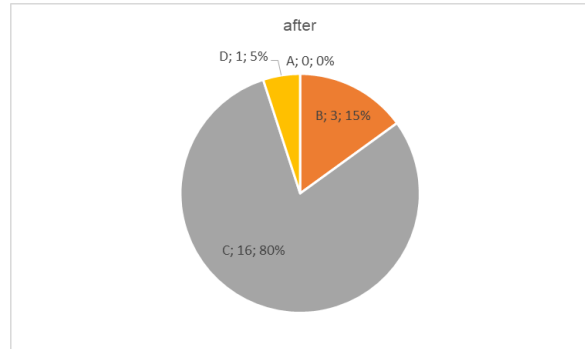
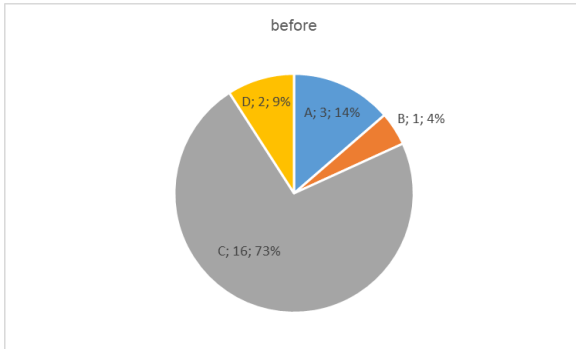
965

5) Which amino acid is shown in the picture?

- a. Cystein
- b. Methionine
- c. Serine
- d. Other



970



---

## REFERENCES

1. Albert, L.; Xu, J.; Wan, R.; Srinivasan, V.; Dou, Y.; Vázquez, O. Controlled inhibition of methyltransferases using photoswitchable peptidomimetics: towards an epigenetic regulation of leukemia. *Chem. Sci.* **2017**, *8*, 4612-4618.
2. Wurtz, N. R.; Turner, J. M.; Baird, E. E.; Dervan, P. B. Fmoc Solid Phase Synthesis of Polyamides Containing Pyrrole and Imidazole Amino Acids. *Org. Lett.* **2001**, *3*, 8, 1201-1203.
3. Baird, E. E.; Dervan, P. B. Solid Phase Synthesis of Polyamides Containing Imidazole and Pyrrole Amino Acids. *J. Am. Chem. Soc.* **1996**, *118*, 6141-6146.
4. Dervan, P. B.; Baird, E. E. Method for the synthesis of pyrrole and imidazole carboxamides on a solid support. U.S. Patent 6545162, April 8, 2003.
5. Minoshima, M.; Bando, T.; Sasaki, S.; Fujimoto, J.; Sugiyama, H. Pyrrole-imidazole hairpin polyamides with high affinity at 5'-CGCG-3' DNA sequence; influence of cytosine methylation on binding. *Nucleic Acids Res.* **2008**, *36*, 9, 2889-2894.
6. Carey, M. F., Peterson, C. L.; Smale, S. T. Transcriptional regulation in eukaryotes: concepts, strategies, and techniques. 2<sup>nd</sup> ed.; Cold Spring Harbor Laboratory Press: New York, USA, 2009; pp 539-620.
7. Kallansrud, G.; Ward, B. A Comparison of Measured and Calculated Single- and Double-Stranded Oligodeoxynucleotide Extinction Coefficients. *Anal. Biochem.* **1996**, *236*, 134-1, 138.
8. Dervan, P. B.; Bürli, R. W. Sequence-specific DNA recognition by polyamides. *Curr. Opin. Chem. Biol.* **1999**, *3*, 6, 688-693.
9. Heinrich, B.; Bouazoune, K.; Wojcik, M.; Bakowsky, U.; Vázquez, O. *ortho*-Fluoroazobenzene derivatives as DNA intercalators for photocontrol of DNA and nucleosome binding by visible light. *Org. Biol. Chem.* **2019**, *17*, 1827-1833.
10. Swinehart, D. F. The Beer-Lambert Law. *J. Chem. Educ.* **1962**, *39*, 333-335.
11. Dose, C.; Farkas, M. E.; Chenoweth, D. M.; Dervan, P. B. Next Generation Hairpin Polyamides with (*R*)-3,4-Diaminobutyric Acid Turn Unit. *J. Am. Chem. Soc.* **2008**, *130*, 6859-6866.
12. Kuzmic, P. Program DYNAFIT for the Analysis of Enzyme Kinetic Data: Application to HIV Proteinase. *Anal. Biochem.* **1996**, *237*, 2, 260-273.
13. <https://www.research.fsu.edu/media/1997/writing-successful-grants-exercises.pdf>, accessed July 18, 2019.
14. Pilch, D. S.; Poklar, N.; Baird, E. E.; Dervan, P. B.; Breslauer, K. J. The Thermodynamics of Polyamide-DNA Recognition: Hairpin Polyamide Binding in the Minor Groove of Duplex DNA. *Biochemistry* **1999**, *38*, 7, 2143-5151.
15. Schulte, L. N.; Heinrich, B.; Janga, H.; Schmeck, B. T.; Vázquez, O. A Far-Red Fluorescent DANN Binder for Interaction Studies of Live Multidrug-Resistant Pathogens and Host Cells. *Angew. Chem. Int. Ed.* **2018**, *57*, 36, 11564-11568.



- 
16. Tse, W. C.; Boger, D. L. A Fluorescent Intercalator Displacement Assay for Establishing DNA Binding Selectivity and Affinity. *Acc. Chem. Res.* **2004**, *37*, 1, 61-69.
  17. Boger, D. L.; Tse, W. C. Thiazole orange as the fluorescent intercalator in a high resolution fid assay for determining DNA binding affinity and sequence selectivity of small molecules. *Bioorg. Med. Chem.* **2001**, *9*, 9, 2511-2518.

## 4. Cumulative Part

### 4.4.1 Conclusion

The implementation of a new master course for chemistry and biology students with a focus on epigenetics brought the authentic big picture of research into the classroom and promoted collaborative work. The combination of lectures, a discovery-based research lab and scientific communication tried to break down the classical borders between disciplines, and also between traditionally separated course and lab structures. This course fosters cooperative research relationships between biology and chemistry students, provides a unique and genuine research experience and emphasizes the importance of science communication. Even though time investment of students and instructors was relatively high, evaluations and student outcomes clearly proved the aimed learning effect and the advance in our own research and, therefore, a successful implementation of the course and the overall positive outcomes. Future perspectives could target the long-term impact of these practices, the interdisciplinary approach and the collaborative work. Evaluations in two or three years could provide us with information about such issues.

In conclusion, following the need to tackle real-world problems, our course design and the interdisciplinary approach could easily be applied in many different fields of research, resulting in students with critical thinking minds and capable to solve the modern challenges with innovative and collaborative solutions.

### 4.4.2 Author Contribution

The overall design of the innovative master course, which serves the basis to this manuscript, was developed by Jun.-Prof. Dr. Olalla Vázquez as awarded proposal for the Cottrell-Fulbright Prize in 2016. In 2016 and 2017, we implemented the course together. I was designing and conducting the discovery-based research lab following my current research achievements under Jun.-Prof. Dr. Olalla Vázquez supervision. I prepared all necessary material (experimental procedures as hand-outs) and guided the students during the research lab. Moreover, I helped to correct and evaluate the outcoming of the articles elaborated by the students. As part of the scientific communication section of this course, I was leading the Pomodoro technique and guided the students to find their own research gap. Afterwards, I contributed in the correction, feedback and evaluation of the proposal products. The evaluation assessments were designed by Olalla Vázquez and Nicole Graulich (JLU, Gießen), but I also analyzed the surveys of the students. I contributed to write the manuscript and prepared several of the figures. Jun.-Prof. Dr. Olalla Vázquez had the role of corresponding author, was leading or involved in all the 14-role taxonomy for author-contribution assignment.<sup>[1]</sup>

Marburg,

Jun. Prof. Dr. Olalla Vázquez

Benedikt Heinrich

## 4. Cumulative Part

### 4.4.3 References

- [1] Allen, L.; Scott, J.; Brand, A.; Hlava, M.; Altman, M. Publishing: Credit where credit is due. *Nature* **2014**, *508*, 7496, 312-313.

## A List of Publications

- 4) Heinrich, B.; Vázquez, O.\* 4-Methyltrityl (Mtt) Protected Pyrrole and Imidazole Building Blocks for Solid Phase Synthesis of DNA-Binding Polyamides. *Org. Lett.* **2019**, *manuscript under revision*.
  
- 3) Heinrich, B.; Graulich, N.; Vázquez, O.\* Spicing up an Interdisciplinary Chemical Biology Course with the Authentic Big Picture of Epigenetic Research. *J. Chem. Educ.* **2019**, *manuscript under replied revision*.
  
- 2) Heinrich, B.; Bouazoune, K.; Wojcik, M.; Bakowsky, U.; Vázquez, O.\* *ortho*-Fluoroazobenzene derivatives as DNA intercalators for photocontrol of DNA and nucleosome binding by visible light. *Org. Biomol. Chem.* **2019**, *17*, 1827-1833.
  
- 1) Schulte, L. N.<sup>†</sup>; Heinrich, B.<sup>†</sup>; Janga, H.; Schmeck, B. T.; Vazquez, O.\* A Far-Red Fluorescent DNA Binder for Interaction Studies of Live Multidrug-Resistant Pathogens and Host Cells, *Angew. Chem. Int. Ed.* **2018**, *57*, 36, 11564-11568; and *Angew. Chem.* **2018**, *130*, 36, 11738-11742.

<sup>†</sup> these authors contributed equally.

## B Curriculum Vitae

### Academic Career

- Present – 11/2015      **PhD in Chemical Biology** at *Philipps-Universität, Marburg* (Germany)  
Supervisor: Jun. Prof. Dr. Olalla Vázquez  
*„Chemical Biology Applications of Photoresponsive DNA-Binding Agents“*
- 09/2015 – 04/2013      **Master Degree (1.0) in Chemistry** at *Philipps-Universität, Marburg* (Germany)  
Master thesis under the supervision of Jun.-Prof. Dr. Olalla Vázquez (1.0)  
*„Development of a multivalent library of nucleosome sensors“*
- 03/2013 – 04/2010      **Bachelor Degree (1.9) in Chemistry** at *Philipps-Universität, Marburg* (Germany)  
Bachelor thesis under the supervision of Prof.Dr. Armin Geyer (1.0)  
*„Synthese cyclischer Enaminpeptide und die Untersuchung des cis/trans-Verhältnisses in Prolin-Tripeptiden“*
- 06/2009 – 08/2002      **Secondary School** Felix-Klein Gymnasium, Göttingen (Germany)  
Graduation with Abitur (1.8)

### Experience Abroad

- 09/2016      **Summer School** “Selectivity as a Key for Sustainable Chemistry”, Shanghai (China)
- 06/2014 – 08/2013      **ERASMUS-semester** at Lund University (Sweden)  
Internship in the working group of Prof. Dr. Ulf Nielson

### Publications

- 2019      *Ortho*-Fluoroazobenzene Derivatives as DNA Intercalators for Photocontrol of DNA and Nucleosome Binding by Visible Light.  
  
B. Heinrich, K. Bouazoune, M. Wojcik, U. Bakowsky, O. Vázquez, *Org. Biomol. Chem.* **2019**, *17*, 1827-1833.
- 2018      A Far-Red Fluorescent DNA Binder for Interaction Studies of Live Multidrug-Resistant Pathogens and Host Cells  
  
L.N. Schulte<sup>+</sup>, B. Heinrich<sup>+</sup>, H. Janga, B.T. Schmeck, O. Vázquez, *Angew. Chem. Int. Ed.* **2018**, *57*, 11564-11568.

<sup>+</sup> both authors contributed equally to this work



## B. Curriculum Vitae

Biology *Interdisciplinary Chemical Biology Approach to Epigenetics CB3/CB4*, (WiSe 2016/2017, WiSe 2017/2018, WiSe 2018/2019), main teaching assistant of a new master practical course initiated by Jun.-Prof. Olalla Vázquez, interdisciplinary course for chemistry and biology master students

*Chemie für Biologen und Humanbiologen*, (SoSe 2017)

Medicine *Chemie für Humanmediziner, Zahnheilkundler und Lehramtsbiologen*, (SoSe 2016)

### **Student Supervision:**

Since 2015 I have supervised **17 internship students**, **1 Master Thesis**, **1 Bachelor Thesis** and **3 international guest students**.

### **Skills and Expertise**

Managerial Demonstrated to work reliable and independently in an international and interdisciplinary team of chemical biologists with close collaborations to microbiologists, medical and pharmaceutical scientists.

Experience of working on multiple projects simultaneously.

Technical MS Office, databases (SciFinder, Reaxys, PubMed), ChemDraw, Topspin, Origin, HypSpec, HySS, Dynafit.

Laboratory Organic Synthesis (solution and solid phase synthesis); Analytical HPLC-MS (Agilent), Preparative HPLC (Agilent, Gilson, Varian), UV-Vis Spectroscopy (Tecan, Jasco, Beckman Coulter), Circular Dichroism Spectroscopy (Jasco), Fluorescence Spectroscopy (Jasco), Dynamic Light Scattering (Malvern Instruments Zetasizer), Size-Exclusion Chromatography (ÄKTA), Capillary Electrophoresis (ABI PRISM), biochemical techniques (agarose and PAGE, PCR, expression, purification, growth curve analysis).

## C Permissions for the Reprint of Publications

*Angew. Chem. Int. Ed.* **2018**, *57*, 36, 11564-11568

This Agreement between Philipps-University Marburg -- Benedikt Heinrich ("You") and John Wiley and Sons ("John Wiley and Sons") consists of your license details and the terms and conditions provided by John Wiley and Sons and Copyright Clearance Center.

License Number	4635761382760
License date	Jul 25, 2019
Licensed Content Publisher	John Wiley and Sons
Licensed Content Publication	Angewandte Chemie International Edition
Licensed Content Title	A Far-Red Fluorescent DNA Binder for Interaction Studies of Live Multidrug-Resistant Pathogens and Host Cells
Licensed Content Author	Leon N. Schulte, Benedikt Heinrich, Harshavardhan Janga, et al
Licensed Content Date	Aug 6, 2018
Licensed Content Volume	57
Licensed Content Issue	36
Licensed Content Pages	5
Type of use	Dissertation/Thesis
Requestor type	Author of this Wiley article
Format	Print and electronic
Portion	Full article
Will you be translating?	No
Title of your thesis / dissertation	Nucleic Acid-Targeting Photosensitive Molecules for the Study and Control of Biological Processes
Expected completion date	Aug 2019
Expected size (number of pages)	300
Requestor Location	Philipps-University Marburg Hans-Meerwein-Strasse 4
	Marburg, 35032 Germany Attn: Philipps-University Marburg
Publisher Tax ID	EU826007151
Total	0.00 EUR

*Org. Biomol. Chem.* **2019**, *17*, 1827-1833.

Referring to the Royal Society of Chemistry, authors accepting the standard license to publish, have the sharing rights to use the accepted manuscript in submissions of grant applications, or academic requirements such as thesis or dissertations. (<https://www.rsc.org/journals-books-databases/journal-authors-reviewers/licences-copyright-permissions/#deposition-sharing>, last accessed 25.07.2019)



### C. Permissions for the Reprint of Publications

#### Org. Lett. 2019, manuscript under revision

Referring to the permission and license rights of ACS Publications, upon acceptance of this article, it is reprinted with permission from *Org. Lett.* **2019**, *manuscript under revision*. Copyright 2019 American Chemical Society.

#### J. Chem. Educ. 2019, manuscript under replied revision

Referring to the permission and license rights of ACS Publications, upon acceptance of this article, it is reprinted with permission from *J. Chem. Educ.* **2019**, *manuscript under replied revision*. Copyright 2019 American Chemical Society.